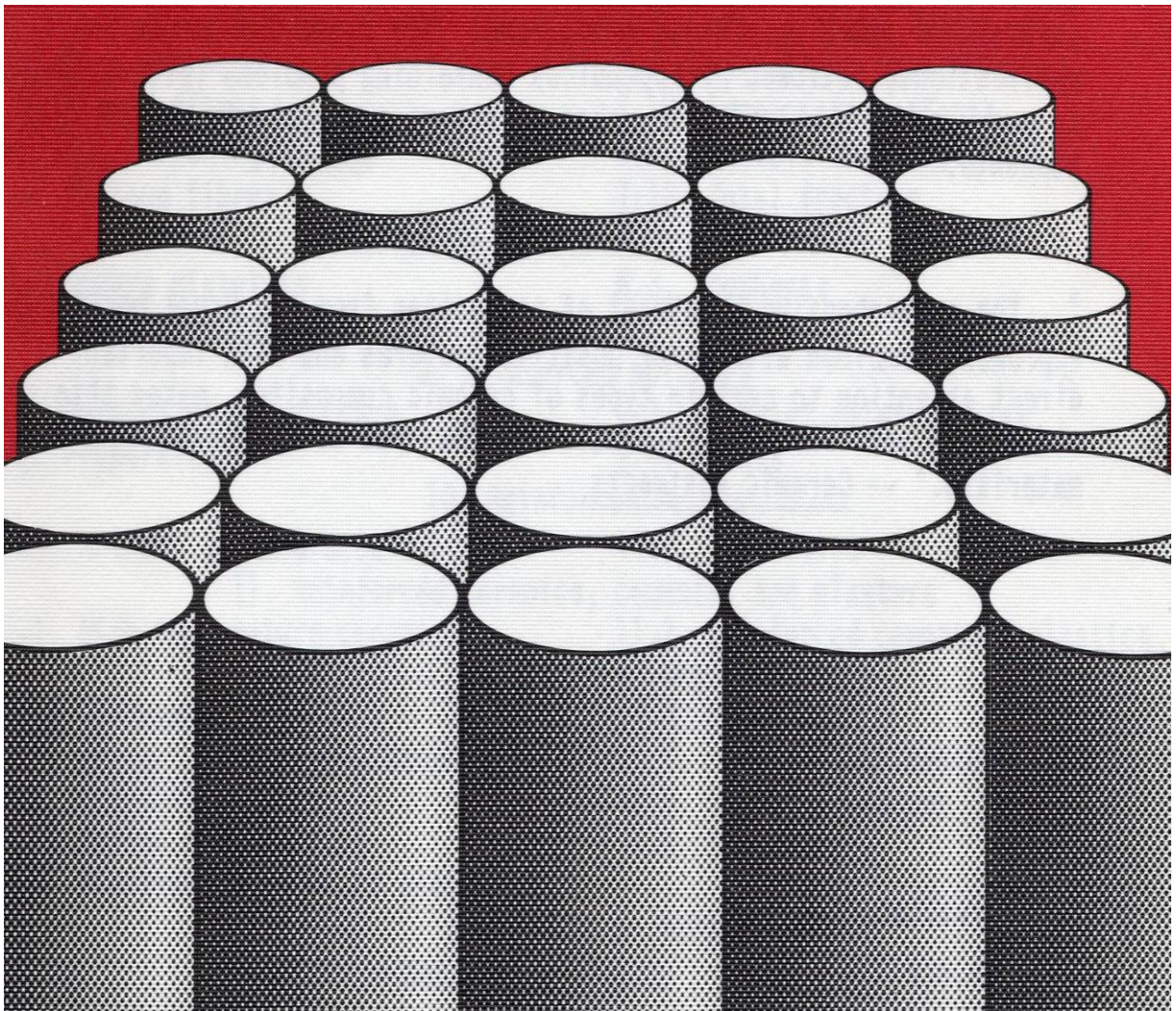


Load Bearing Fibre Composites

Second Edition: Web Version

Michael R. Piggott
Chemical Engineering and Applied Chemistry,
University of Toronto, Canada.





Frontispiece: A notable application of the first glass-polymer: the 107m tall radome that resides at the top of the Toronto 550m CN Tower. (Courtesy CN Tower Ltd.)

LOAD BEARING FIBRE COMPOSITES

Second Edition: Web version

MICHAEL R. PIGGOTT

**Ph.D., ARCS, DIC
SAMPE Fellow**

**Professor Emeritus
Department of Chemical Engineering & Applied Chemistry
University of Toronto, Ontario, Canada, M5S 3E5**

**Website
http://individual.utoronto.ca/michael_piggott/**

Copyright © Michael R. Piggott

1442 Sunset Drive, South Bruce Peninsula, Ontario N0H 2T0, Canada

PREFACE: WEB EDITION

This on-line edition, with free access, is prepared for those still interested in my contribution to, and discussion of the work of others, on the subject of fibre composites. The twelve chapters are word for word the same as the second edition of Load Bearing Fibre Composites, but hopefully with fewer typos and glitches. I have put some of the tables and illustrations into more appropriate locations and left out the index because it is unnecessary for the web version. (But note that, when you look up key words, you have to allow for pages i to vi of the title pages and prefaces and the three pages of the contents. That is ~10 pages in total.)

Michael R. Piggott
April 2016

PREFACE: SECOND EDITION

The subject of fibre composites has grown much since the first edition appeared. Now there is a conference on the subject, somewhere in the world, every week. There are more than twenty journals devoted to the subject. Specialist areas, such as the fibre-matrix interface and composite structures, have become subjects in their own right, with meetings devoted to them, and in the case of the interface, an international journal.

It is not the author's intention that this book should grow to match the prodigious amount of research in this subject area. However, there have been significant changes, largely because recent experimental work casts doubt on some of the basic ideas. These experiments were initiated largely because, in writing the first edition, I noticed that some ideas lacked convincing experimental support. Hence, I set out to do the (hopefully) appropriate tests.

Firstly, the theoretical compressive strengths seemed to be wide of the mark. Rosen's predictions were too high while the Argon suggestion gave a result which was independent of fibre volume fraction. The problem with Rosen was the assumption of a perfect composite. This has been resolved by the introduction of mesostructures, as described in Chapter 6. Ways of quantifying these experimentally are described and it is shown that they also influence other properties which are dominated by the matrix. An example of this is fatigue, which is touched on in Chapter 6. It is dealt with in more detail in Chapter 10, since the work is presently available only in the Journal literature.

Another subject of widespread misunderstanding is transport properties. Here, mistakes were made in evaluating relatively simple integrals derived from a simplistic model. Since this work is also unavailable elsewhere in textbooks, it is given detailed treatment here, again in Chapter 10.

The well known Kelly-Tyson theory of benign sliding or yielding reinforcement, which was actually questioned early on by Cratchley (see Fig. 5.12), lacks any convincing experimental support. A necessary outcome is that short fibre unidirectional composites must have curved stress-strain plots. The evidence for this put forward by Kelly (see Fig. P.1b) does not bear close scrutiny when compared with the plot in the paper he quoted: see Fig. P.1a. The missing curve in Fig. P.1b was for unidirectional continuous silica fibre ("quartz") reinforced epoxy which, had an extensometer been used, should have been a straight line.

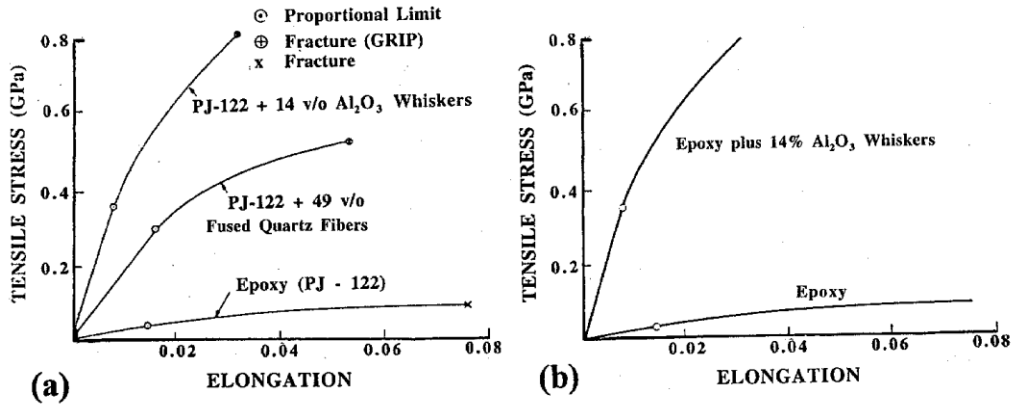


Fig. P.1. "Stress-strain curves". On the left is the original form of the plot. On the right the "redrawn" curves: note the missing curve. (After Sutton, W.H., Rosen, B.W. and Flom, D.G. 1964. SPE J. 20, 1203-9 and Kelly A., 1973, Strong Solids. second edition., p. 185 and third edition, 1986 with W.H. Macmillan, p.266. Clarendon Press, Oxford: ordinates metricized.)

Sutton et al cautioned against using the strain values shown in Fig. P.1a, since the cross head movement was used to estimate them. Moreover the concept of the critical aspect ratio first appeared in the pulp and paper industry and due recognition is given herein. A new way of looking at this is introduced in Chapter 5.

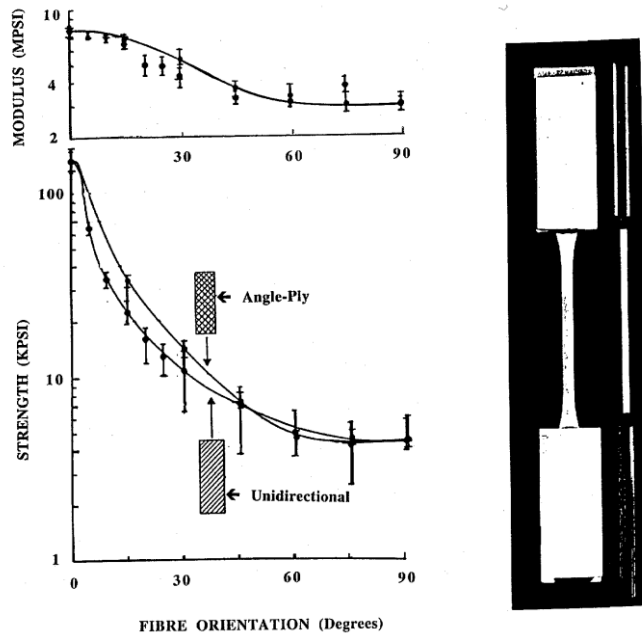


Fig. P.2. Superposition of oblique unidirectional and angle ply results from early experiments on glass-epoxy.

At right typical specimen dimensions are indicated. They were about 3.2 mm thick and had a gauge length of 63.5 mm and width of 4.6 mm, and were end tabbed. (After Tsai, S., 1965, NASA CR 224.)

Finally, perhaps most seriously, Stowell and Liu, in 1961, introduced the idea of three failure modes for laminates with oblique fibres. This was taken up by the composites community, both in the UK and the USA. They went so far as to design their test specimens so that they would fail according to the Stowell and Liu prescription - hence they were long and narrow.

Fig. P.2 shows some results for oblique unidirectional superposed on angle ply results. Note the very fast decrease of strength with ply angle, ϕ . A clue to the problem with this approach is indicated by the superposed modulus results. As we show in Chapter 4, the angle ply Young's modulus should be E_x while the oblique unidirectional modulus should be $1/\bar{S}_{11}$ with $E_x > 1/\bar{S}_{11}$ except for $\phi = 0^\circ$ or 90° . In Fig. P.2 the moduli "fits" are almost identical, showing that the fibres have not been adequately stressed. What we observe is an "edge softening" effect which reduces the modulus by up to 50%, and can reduce the strength by 90%. Both the early and more recent work on this are described in Chapter 4.

All those developments have been published in reputable refereed journals, and are referenced in the appropriate places in the book.

Other significant changes have been made. Platelet reinforcement has been omitted: it was not successful, as foreshadowed in the first edition's Chapter 8. (It was shown that strengthening could never be as great as with fibres.) Instead a new Chapter 8 describes interactions at the fibre-matrix interface in some detail. It is not generally realized that the polymers used for high performance composites have no shear failure process (see Chapter 6). This means that tensile methods should be used for investigating interface properties and axisymmetric tests, such as single fibre pull out, should be phased out. Practical ways for doing this are described.

Throughout the book, figures have been carefully chosen to draw attention to important relevant work, and the practice, started in the first edition, of giving full reference to the work in the subtitle, has been continued. It is hoped that the interested reader will follow up these references, and additional papers referenced in the papers quoted. The need to check the original work cannot be overemphasized. Many erroneous interpretations of original work have gained acceptance through constant repetition.

Reinforced polymers (highly successful) now have two Chapters (9 and 10) instead of one. Fibre reinforced metals, ceramics and cements (less successful) have been reduced to sharing a single chapter. Chapter 12 has been rewritten to ensure that only load bearing applications are included, and to take account of the more multifarious applications of fibre composites since the first edition. There are also many corrections of errors in the first edition, and I wish to thank readers and students for pointing out my mistakes.

I hope the reader will welcome some emphasis on our experimental work carried out at the University of Toronto. Without many dedicated students, this book would not have been possible. My students persevered at what must have seemed, at least in the beginning, to be unnecessary projects - rehashing things done two or three decades earlier, and taken as gospel in all the textbooks they could find. The more contentious issues (Kelly-Tyson and Stowell and Liu) were tested independently by three students each, in separate projects, sometimes years apart. Thank you for your hard work and dedication. I hope you learned something: I certainly did.

Moreover, I hope you, the reader, will follow our example. Take nothing for granted; do experiments to verify everybody's work, including ours. Undoubtedly we have not been able to find all the errors, omissions, wrong thinking etc. that has gone before. This presents a marvellous opportunity for eager young researchers with an innovative approach, coupled with the courage to question authority.

Finally, my thanks to Jenny Clifford, who looked after the affairs of my research group so well for more than 21 years. She provided a home base from which my students and I could operate, and helped us all through our problems. She has typed everything herein (and much, much more) scanned all the pictures, and set-up the equations. Her dedication has been exceptional and I am indeed grateful.

Any mistakes in the book are entirely mine.

Michael R. Piggott
March 2001

CONTENTS

Preface to the web Edition	iii
Preface to the second Edition.....	iii
1. Introduction - Properties of Materials	1
1.1 Conventional Materials	2
1.2 Elasticity Theory	14
Problems	30
2. Physical Factors Influencing Mechanical Properties	34
2.1 Strength of Solids Calculated from Bond Strengths	34
2.2 Dislocations.....	39
2.3 Notches and Cracks.....	42
2.4 Practical Limits for Strength	50
Problems	52
3. Fibres, Whiskers, and Platelets.....	55
3.1 Slender Forms of Material	55
3.2 Polymer Fibres and Metal Wires	58
3.3 Inorganic Fibres and Whiskers.....	61
3.4 Single Crystal Platelets	72
3.5 Forms of Reinforcement	72
Problems	78
4. Composite Mechanics: Long Fibres	80
4.1 Axial Modulus and Strength	80
4.2 Off Axis Properties	83
4.3 Laminae.....	88
4.4 Laminates	97
4.5 Random Fibre Structures	116
Problems	118
5. Composite Mechanics: Short Fibres	121
5.1 Elastic Stress Transfer.....	122
5.2 Elastic Stress-Strain Relationships	128
5.3 Composite Strength.....	131
5.4 Misorientation Effects.....	139
5.5 Variable Fibre Length	143
Problems	144

6.	Matrix Dominated Properties	146
	6.1 Shear Failure Processes in the Matrix.....	146
	6.2 Internal Structures in Composites: the Mesostructure	155
	6.3 Transverse Properties.....	158
	6.4 Shear Strengths	166
	6.5 Compressive Strengths.....	170
	6.6 Fatigue Endurance.....	185
	Problems	188
7.	Brittle Fracture Processes	191
	7.1 Fracture Mechanics	192
	7.2 Through Thickness Fracture	198
	7.3 Delamination Fracture.....	206
	7.4 Inhibition By Fibres of Matrix Plastic Work	208
	7.5 Impact Damage Evaluation	209
	Problems	213
8.	Interface Mechanics and Testing.....	216
	8.1 Properties Sensitive to Interface Strength	216
	8.2 Direct Measurement of Interface Strength	217
	8.3 Problems with Direct Interface Measurements	221
	8.4 Work of Fibre Pull Out in Composite Fracture	244
	8.5 Non Axisymmetric Tests	248
	8.6 Conclusions.....	255
	Problems	256
9.	Reinforcement of Polymers	259
	9.1 The Polymers	259
	9.2 The Interface	269
	9.3 Premixes.....	270
	9.4 Manufacturing Methods.....	272
	Problems	282
10.	Reinforced Polymer Properties.....	283
	10.1 Mechanical Properties.....	283
	10.2 Fatigue.....	290
	10.3 Creep	296
	10.4 Environment Effects	298
	10.5 Hybrid Composites	312
	10.6 Joints	316
	Problems	320
11	Other Fibre Composites	323
	11.1 The Thermal Contraction Problem	334
	11.2 Advantages and Drawbacks of Reinforced Metals	329

11.3	Manufacture of Reinforced Metals	330
11.4	Properties of Reinforced Metals	337
11.5	Joints	346
11.6	Reinforcement of Ceramics	347
11.7	Reinforced Ceramics Properties.....	353
11.8	Reinforced Cements and Plasters.....	359
	Problems	361
12	Applications	364
12.1	Aerospace Structures.....	365
12.2	Marine Structures.....	370
12.3	Ground Transport.....	372
12.4	Energy and Storage	375
12.5	Pipelines and Chemical Plant.....	376
12.6	Infrastructure	377
12.7	Medical Applications	378
12.8	Sports Equipment.....	381
12.9	Other Uses.....	382
	Problems	386
	Appendices	389
	A. Symbols used in Text.....	389
	B. Acronyms and Abbreviations	394
	C. SI Units.....	396

1. INTRODUCTION - PROPERTIES OF MATERIALS

This book describes the basic ideas in the relatively new field of fibre reinforced composites, and provides recent data on their load-bearing capabilities. In addition, selected data is given for more traditional materials, so that the reader can see where composite materials fit into the hierarchy of materials.

The discussion starts at a basic level, and such important properties as strength, creep resistance, and fatigue endurance are described. The connection between the chemical bond strength and the tensile strength is discussed, and the role of imperfections is shown to be of overwhelming importance.

The reasons for the good mechanical properties of fibres are set forth, and an account is given of the production of strong and stiff fibres. This is followed by a simplified description of the mechanics of the processes by which fibres can contribute strength, stiffness and toughness to weak matrices. Finally a brief sketch of the properties of composites is given, classified according to whether the matrix is polymeric, metallic, or ceramic (including cementitious). Emphasis is given, throughout the book, to load-bearing properties, and this is followed by a discussion of some of the diverse end uses of these materials.

The term composite has come to mean a material made by dispersing particles, of one or more materials in another material, which forms a substantially continuous network around them. The properties of the composite may bear little relation to those of the components, even though the components retain their integrity within the composite.

The components can be randomly arranged, or organized in some sort of pattern. Generally the arrangement will have a large effect on the properties. Further, they can have roughly spherical shapes, e.g. stones in concrete, or can have some very distinctive shape such as the iron carbide laminae found in some steels, or long thin fibres, such as the cellulose fibres in wood. The particle shape also has a very profound effect on the properties of the composite. Since this book is concerned with fibre-reinforced composites, it will largely restrict itself to the discussion of two-component composites, where one of the components is a long thin fibre or whisker (these are now defined by ASTM as filamentary composites) and where the composite has to have good load-carrying capacity.

Fibre-reinforced materials have been used by man for a very long time. The first to be used were naturally occurring composites, such as wood, but man also found out, long ago, that there were advantages to be gained from using artificial mixtures of materials with one component fibrous, such as straw in clay, for bricks, or horse hair in lime plaster for ceilings.

Recently, with the advent of cheap and strong glass fibres, and with the discovery of a number of new fibre-forming materials with better properties than anything available heretofore, the interest in fibre reinforced materials has increased rapidly, and is still accelerating. Fibre-reinforced polymers are replacing metals in a whole host of situations

where load-carrying capacity is important. More efficient aircraft, turbine engines, and cars, and more durable boats, can be produced with fibre composites, and worthwhile new applications for these materials are being found almost every day.

In order to appreciate the potential benefits to be gained from fibre reinforced materials, however, it is necessary first to be aware of what can be done with more traditional materials. The introductory section of this text therefore starts with a review of the important properties required for load-bearing materials, and discusses traditional materials in this context. Then follows a brief statement of the basic ideas of isotropic elasticity theory, and its extension to non-isotropic cases of interest for fibre reinforcement.

1.1 Conventional Materials

The important properties for load-bearing materials fall naturally into two groups: mechanical and non-mechanical. Mechanical properties include stiffness, strength, ductility, hardness, toughness, fatigue, and creep. These will be discussed first. Non-mechanical properties, which will be discussed later, include density, temperature resistance, corrosion resistance (including stress corrosion and hydrogen embrittlement), and cost.

1.1.1 Stiffness

The stiffness of a material, or its resistance to reversible deformation under load, is a very important mechanical property. In order to characterize the effect of the load on the material, it is normally converted to a stress, that is the force per unit area of cross-section acted on by the load. Expressed in these terms, it is then an indication of the forces experienced by the individual atoms in the material as a result of applying the load. The response of the atoms is to change their positions slightly. Hence, under a stretching, or tensile stress, the atoms move apart in the direction of the force. The distance moved, divided by the original distance, is called the strain.

The movement of the atoms under the action of applied loads can be observed and measured using X-ray diffraction or neutron diffraction. The combined movement of the atoms constituting the whole specimen being stressed can usually be measured quite easily using a sensitive displacement gauge.

A stiff material is one which deforms very little. Young's modulus is normally used as a measure of this, and is defined as the ratio of the tensile stress to the strain produced. The unit normally used for Young's modulus is the Pascal (Pa). (These units are described in Appendix C.) Other stiffness parameters will be discussed in the second part of this chapter.

Few materials are isotropic and so measurements of Young's modulus made in different directions will give different results. These differences are particularly marked with single crystals of non-metals. However, polycrystalline metals, polymers and ceramics are generally sufficiently isotropic that they can be assigned a single value for the Young's modulus.

Table 1.1. Strength and Stiffness of Various Materials

Material	Young's Modulus (GPa)	Tensile Strength (MPa)
Metals:		
Aluminium (pure, annealed)	71	60
High-strength aluminium alloy (Al-Zn-Cu-Mg)	71	650
Iron (cast)	152	360
High-strength iron alloy (maraging steel)	212	2000
Magnesium alloy (Mg-Zn-Zr)	45	340
Titanium alloy (Ti-Zn-Al-Mo-Si)	120	1400
Tungsten	411	1800
Zirconium alloy (zircaloy)	97	590
Stainless steel	215	900
Ceramics:		
Alumina (high density)	400	280
Concrete	50	3.5
Glass (sheet)	70	70
Polymers:		
Epoxy resin	2.5	60
Polycarbonate	2.5	65
Polyethylene (branched)	0.2	10
Rubber (natural)	0.018	32
Rubber (fluorocarbon)	0.002	7
Wood (Douglas fir)	14	34+
Wood (white pine)	7.6	16+

+ Parallel to the grain; long-term strength is half this.

Young's moduli range from about 1TPa for a favourable direction in a diamond crystal through 100GPa for a metal, 1GPa for a polymer, and 10MPa for a rubber. Table 1.1 gives the moduli of a representative selection for metals, ceramics, and polymers. The modulus of well-made specimens of crystalline elements or compounds is a measure of the deformability of the bonds between the atoms, and hence will be the same for different samples of the material. This is not quite the case with metal alloys, while with some polymers very large variations between the modulus of different specimens of chemically similar materials can be found.

1.1.2 Strength

The strength of a material is the stress required to break it. It differs markedly from the modulus, in being determined as much by the method of manufacture and previous history of the specimen, as by the nature of the atoms and their arrangement. Pure, annealed, metals, and non-fibrous polymers are weak in both tension and compression.

Ceramics and hard materials are generally much weaker in tension than in compression. Some polymer fibres are very strong in tension, while modern alloys, developed for use as structural members, are generally strong in both tension and compression. Typical tensile strengths are given in Table 1.1 for a variety of materials, excluding fibres and wires, some properties of which are given in Table 3.1.

1.1.3 Ductility, Hardness, and Toughness

Figure 1.1 shows the stress-strain curves obtained with two different metals. Here the stress is calculated using the initial cross-section of the material, and the strain is calculated directly from the change in length of the test section.

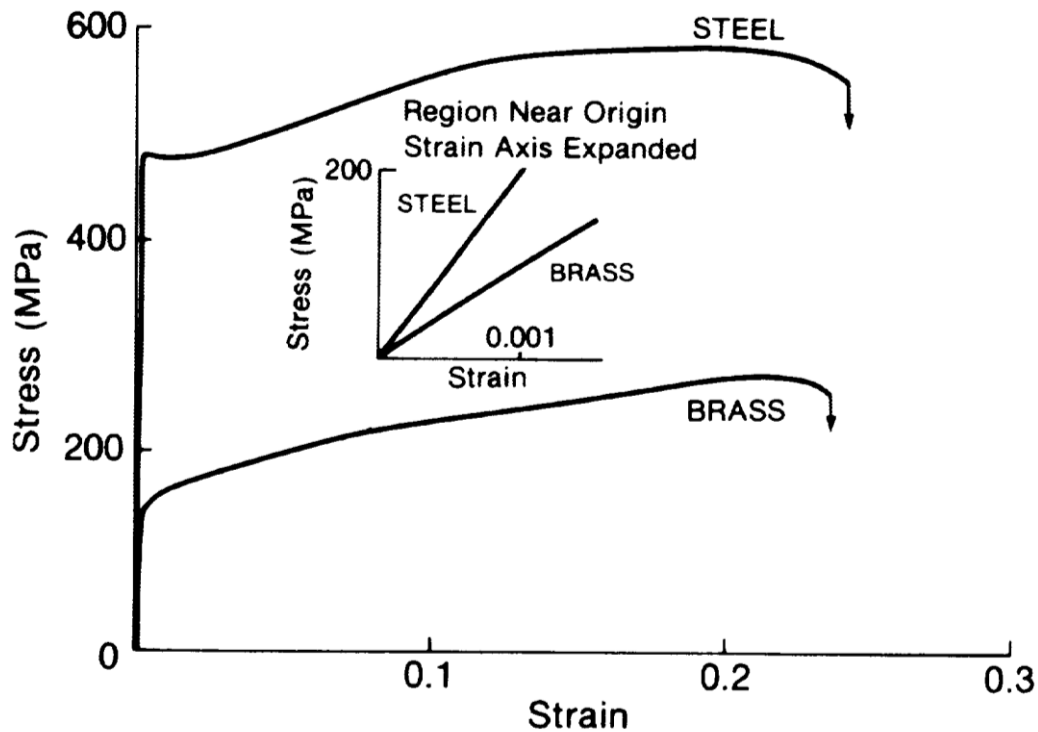


Fig. 1.1 Stress-strain curves for steel and brass.

With many metals the curve has three regions. First there is a linear region where the material is elastic, and on removal of the stress at any part of the line, the line is retraced back to the origin. The slope of the line gives the Young's modulus of the material.

The second part of the curve starts at the end of the linear region (this point is the yield point) and, except for a slight fall at the yield point in the case of some steels, the stress increases monotonically up to a maximum value, called the ultimate tensile strength.

In the third region the stress decreases monotonically with increasing strain until final failure occurs. In this region the specimen is not deforming uniformly; a region of reduced cross-section is formed (necking is occurring) and failure occurs at the neck.

(The maximum stress at the neck can be considerably greater than the stress in the rest of the material, so that the true stress at failure is much greater than that indicated by the stress axis. These two failure stresses are sometimes distinguished by calling the lower stress the engineering stress at failure, and the higher stress the true stress at failure. The true stress-true strain curve does not have a peak; the true stress increases monotonically to the failure point.)

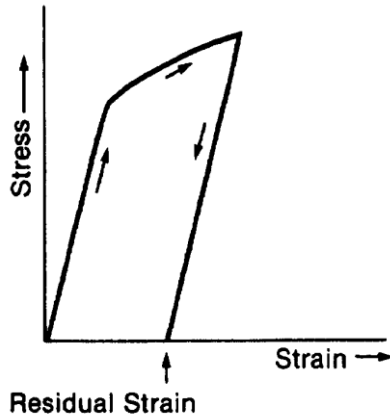


Fig. 1.2 Residual strain in a metal.

In the second and third regions of the stress-strain curve, removal of the stress does not result in the material retracing the curve back to the origin. Instead, with decreasing stress the strain decreases at a rate governed by the modulus of the material, i.e. the line has a slope which is the same as that near the origin (Fig. 1.2). When the stress has been reduced to zero, there is now still some strain remaining. This strain is the origin of ductility. A stress-strain curve which is entirely linear up to the breaking point, such as that obtained with a hard steel (e.g. razor blade steel) indicates very little ductility. A curve with a very long region after the yield point indicates a material with great ductility. With pure metals, the length of the specimen can sometimes be doubled before failure occurs.

Figure 1.3 shows the stress-strain curve for two polymers. It can be seen that they show similar features to those observed with metals, except that yielding is generally not so sharp, and the curve does not usually have a monotonically decreasing region. Some polymers (e.g. polyesters) have very little ductility. Note that the elastic limit occurs at much higher strains for plastics than it does for most metals. Furthermore, with polymers, the peak stress, rather than elastic limit, is taken as the yield stress.

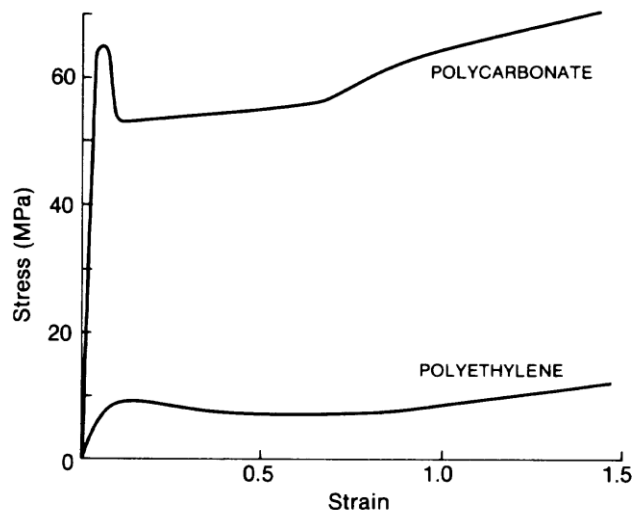


Fig. 1.3 Stress-strain curves for polyethylene and polycarbonate.

Hardness is a measure of the resistance of materials to plastic deformation, and hence ductile materials are usually not hard. It is determined by indenting the material with a hard ball, or a diamond with a pyramid-shaped tip, and measuring the size of indentation for a given load. Diamonds will leave indentations in glass, showing that plastic deformation, albeit small, is possible with glass. Table 1.2 gives some typical hardness values. They can be converted to roughly equivalent yield stresses in MPa by multiplying by three. Note, however, that with any metal or alloy, a wide range of hardness values can usually be obtained by heat treatment and cold working.

Toughness will be discussed in more detail later (section 2.3). It is often confused with ductility, and often erroneously equated with the area under the stress-strain curve. The measurement of toughness was put on a scientific footing with the advent of fracture mechanics. Fracture toughness or, more precisely, the work of fracture, is a measure of the work required to propagate a crack through unit area of material. Care is required in its measurement because, if a blunt crack is propagated into a specimen, an unrealistically high value for toughness is obtained. In addition, the impact methods of measuring toughness can give misleading results owing to the inclusion, in the result, of energy that has been dissipated as a result of processes unrelated to crack propagation, and to variations in notch sharpness.

Table 1.2 Approximate Values for the Hardness and Toughness of Some Materials

Material	Hardness (Kg/mm ²)	Work of Fracture (kJm ²)
Diamond	8400	-
Alumina	2600	0.02
Maraging steel	600	50
Hard tungsten	450	0.02
Glass	400	0.005
Titanium (99%)		200 30
High-strength aluminium alloy	180	10
Pure aluminium		20 >100
Polycarbonate	20	3
Epoxy resin	18	0.1
Wood, across the grain	6	20
Wood, parallel to the grain	3	0.015

There is some connection between ductility and toughness, since ductile materials are generally tough, and hard non-ductile materials are generally brittle. Table 1.2 gives some data on the work of fracture of some materials. The toughness of metals and alloys depends a great deal on heat treatment and work hardening, just as the hardness does. Thus toughness and hardness values are given for the metals and alloys in the same state.

1.1.4 Fatigue

Materials which are subject to alternating stresses sometimes fail at stresses which are surprisingly low compared with their failure strength when tested under conditions of monotonically increasing stress. This was already known to occur with steels. However, its seriousness was not fully appreciated until the disastrous failures of the first commercial jet passenger plane, the British Comet. This was made of what was considered to be an adequately strong aluminium alloy, yet the fuselage broke in two in mid-air. The failure started at the tip of a window, a crack propagating slowly therefrom under alternating loads, until it was so long that the material left was insufficient to support the load, so that complete failure of the whole fuselage suddenly occurred.

Nowadays materials are routinely tested for their fatigue resistance. The stressing regime used can be quite complicated, if it is desired to simulate service conditions. However, a good idea of the fatigue resistance can be obtained from a relatively simple test in which a piece of material is subjected to a sinusoidally varying stress (Fig. 1.4). The stress amplitude required to break the piece is plotted as a function of the logarithm of the number of cycles it can withstand at that stress amplitude.

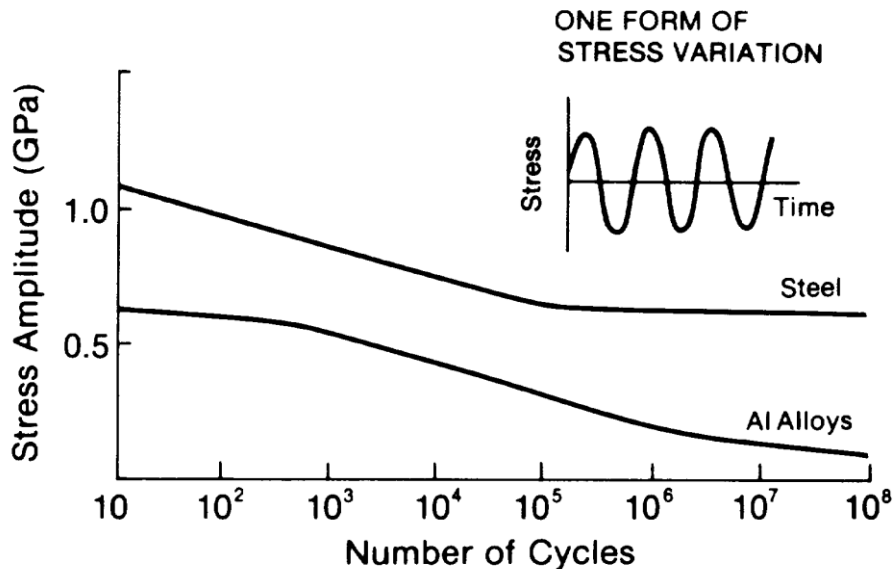


Fig. 1.4 Typical fatigue curves for aluminium alloys and steels.

When the test is carried out with aluminium alloys it is found that the breaking-stress decreases continuously as the number of cycles increases. Thus the material seems to have no strength after an infinite number of cycles. Iron alloys, on the other hand, still retain about half their strength after a very large number of cycles. The difference between the two is illustrated in Fig. 1.4. The fatigue or endurance limit is the stress amplitude of the plateau region observed after a large number of cycles.

Fatigue failure starts with plastic deformation at the surface of the specimen. Then very fine cracks begin to appear, and one of these gradually increases in length until it becomes big enough for the material to fail by the normal fracture process. The number of cycles to failure can vary greatly from specimen to specimen of the same material, even when great pains have been taken to make them identical. Once a fatigue crack has appeared, though, its further development follows simple laws.

1.1.5 Creep

Materials under constant stress can gradually extend by plastic deformation. The stress to cause this creep can be considerably less than the tensile strength. With metals the process is insignificant at temperatures less than about half the absolute melting-temperature. Thus the creep of the metals normally used for bridges and aircraft (steel and aluminium alloys), for example, is negligible at room temperature. Polymers, however, can creep significantly at room temperature.

Fig. 1.5 shows typical creep curves obtained with steel and an aluminium alloy. It may be seen that the curves have three regions. The first, primary creep region, has a relatively high creep rate. This decreases with time until a constant creep rate is achieved in the secondary creep region. Eventually the specimen has deformed to such an extent that necking starts, and the creep rate increases once again. This is the tertiary creep region, and it generally continues for a short period only, whereupon the specimen fails.

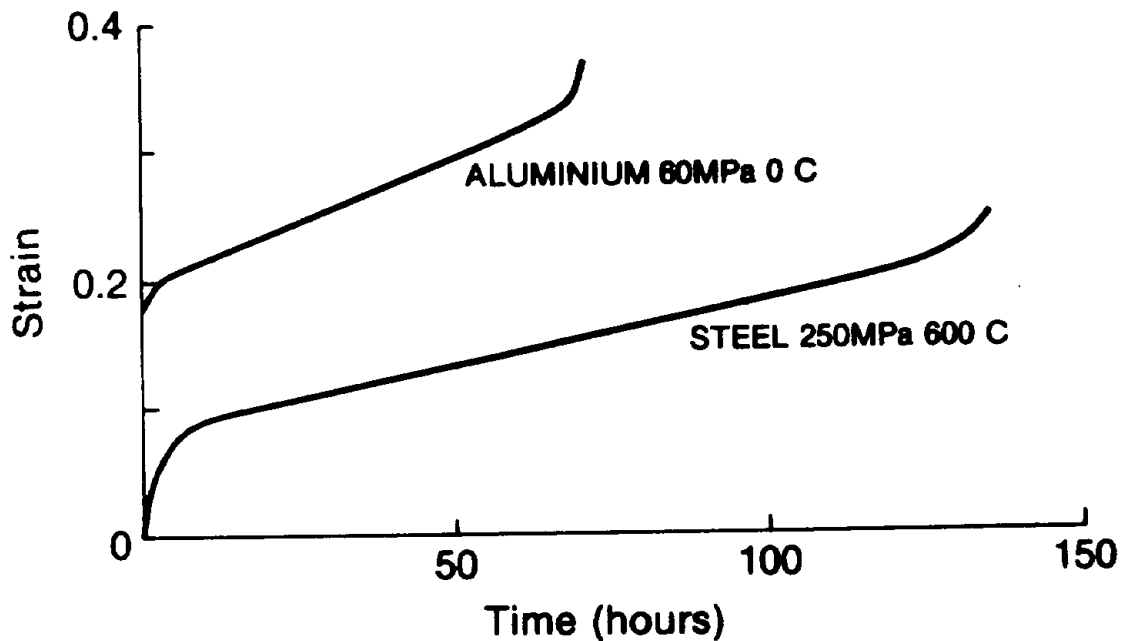


Fig. 1.5 Creep curves for aluminium at 0°C and steel at 600°C, at stresses indicated.

Polymers show similar behaviour: see Fig. 1.6.

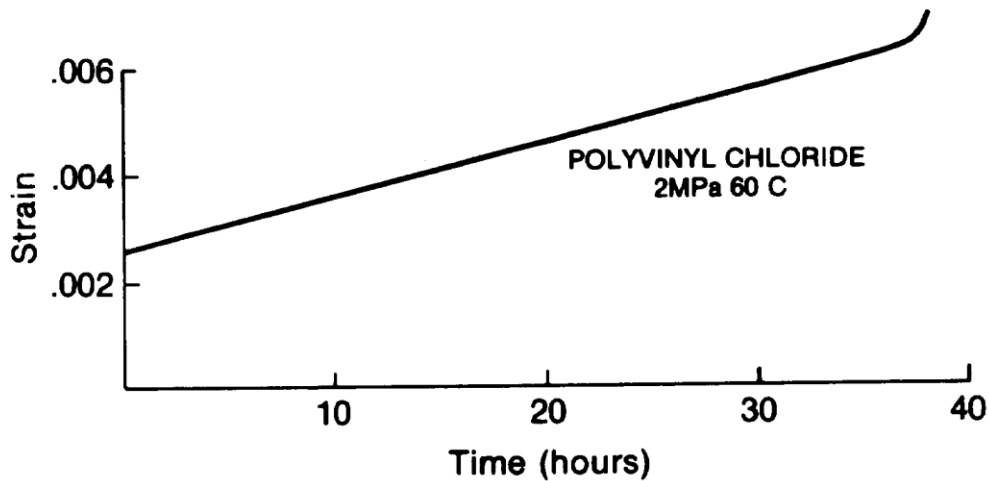


Fig. 1.6 Creep curve for polyvinyl chloride at 60°C under a stress of 2 MPa.

1.1.6 Density

A non-mechanical property of great importance is density. High density is an advantage for materials used for hammers, road rollers, flywheels, etc. These are exceptional cases, however. Generally, light materials have significant advantages. Aircraft and spacecraft are obvious examples of structures which need light materials, but any rapidly rotating part not used as an energy store is best made of light materials, since centrifugal forces are thereby reduced. Such parts as turbine rotors, for example, should be made of materials which are as light as possible, taking into account strength and deformation also. Cars used in cities would be more efficient, if lighter. In addition, since a large part of the strength of the members supporting bridges is used up sustaining the dead weight of the bridge structure, there would be benefits from using light materials for bridges, and other static load-bearing structures, again taking into account strength and stiffness as well.

In many applications, the density criterion should be combined with strength and stiffness, so that an efficiency criterion is obtained. For strength, the most obvious criterion is that the strength/density ratio should be as great as possible. Similarly for stiffness, the obvious criterion is that the modulus/density ratio should be as large as possible.

However, when account is taken of strength and stiffness, the role of density is not as great as might be expected. With metals, it is found that the modulus, which governs stiffness, and also to some extent controls the strength attainable (this will be discussed in the next chapter), is roughly proportional to the density, i.e. the modulus/density ratio is approximately constant. In the case of polymers the modulus, and hence stiffness, is far too low for their use in most structures, unless the polymer is reinforced. Thus the low density of unreinforced polymers has little significance for load-bearing structures which have to retain nearly their original shape when loaded. Ceramic materials show little relation between modulus and density. However, their extreme brittleness makes them

unsafe in tensile load-bearing applications, so they are only used in special circumstances, when some other property, such as resistance to high temperature, is of overriding importance.

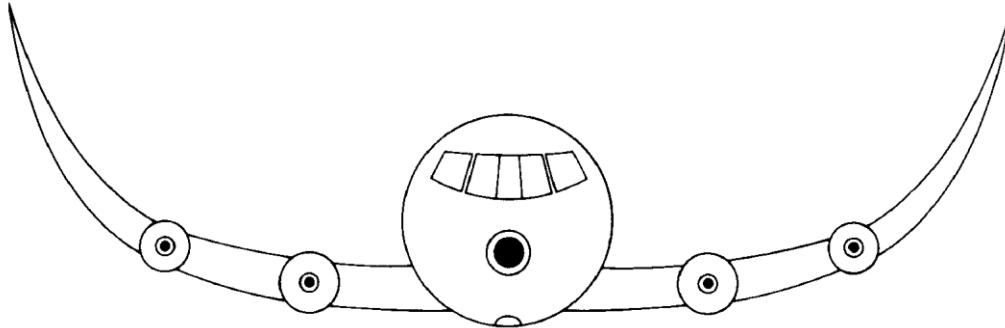


Fig. 1.7 Plane with strain of 0.016 in wing structure. (After Gordon, J.E., 1964, Proc. Roy. Soc. A282. 16-23.)

Why, then, is aluminium used for subsonic aircraft, and wood used for gliders? The reason is that many of the parts have to resist bending or buckling. Aircraft wings can only withstand a deformation under load of a few hundredths of a per cent before they lose the shape required to keep the craft aloft efficiently. Figure 1.7 shows what an aircraft would look like with 1.6% strain in the wing spar booms.

In the bending of a beam, the deformation results in curvature, of radius R , say. If the moment of forces causing the bending is M , then the basic formula for bending is

$$MR = EI \quad (1.1)$$

where E is the Young's Modulus of the beam and I is the moment of area of the beam, which for a beam of thickness d is $d^3/12$ per unit width. A beam with great resistance to bending has a high value of MR , and hence of EI , or $Ed^3/12$ (often called the flexural rigidity). The weight of beam per unit length and width is ρd . Now we can compare the weights of two materials having the same flexural rigidity. We will distinguish the materials by the subscripts 1 and 2. For the same flexural rigidity, they will have different thicknesses, related by the expression.

$$E_1 d_1^3 = E_2 d_2^3 \quad (1.2)$$

The ratio of their weights will be

$$\frac{W_1}{W_2} = \frac{\rho_1 d_1}{\rho_2 d_2} \quad (1.3)$$

and using equation (1.2) this comes to

$$\frac{W_1}{W_2} = \frac{\rho_1 / E_1^{1/3}}{\rho_2 E_2^{1/3}} \quad (1.4)$$

Clearly the most efficient material has the largest value of $E^{1/3}/\rho$

Table 1.3 Stiffness-Density Parameters for Some Materials

Material	Density ρ (Mg m ⁻³)	Young's Modulus, E (GPa)	E / ρ (MmNkg ⁻¹)	$E^{1/3}/\rho$
Aluminium	2.70	71	26.3	1.53
Epoxy	1.11-1.40	2.5	1.8-2.3	0.97-1.22
Magnesium	1.74	42	24.1	2.04
Polyethylene	0.93	0.2	0.22	0.63
Steel	7.87	212	26.9	0.76
Titanium	4.51	120	26.6	1.09
Tungsten	19.3	411	21.3	0.39
Wood (Sitka spruce)	0.39	13	33.3	6.03
Zirconium	6.49	94	14.5	0.70

The same result is obtained when we consider compressive failure of long thin beams, such as are used, for example, in aeroplane wings. These beams fail by buckling, and the compressive failure load is governed by the flexural rigidity.

Table 1.3 compares a number of structural materials on the basis of E/ρ and $E^{1/3}/\rho$. It will be seen that for most metals the values for E/ρ are close to 25, apart from zirconium. For wood the value is somewhat higher, while for polyethylene (and almost all other man made polymers) the value is very much less. However, the values for $E^{1/3}/\rho$ for the lighter materials such as wood, aluminium, and magnesium are much larger than for the heavier materials. Wood comes out best, and hence its use in the past for gliders. (Modern gliders, with refined aerodynamic surfaces, are made with fibreglass.) Aluminium alloys provide a good compromise for strength as well as $E^{1/3}/\rho$ and are more durable than wood, and hence are used for subsonic aircraft. (Some excellent small planes have been made with wood, however.)

1.1.7 Temperature Resistance

Another important non-mechanical property is resistance to extremes of temperature.

Polymers generally have a small range of temperatures over which they can be used. They tend to become brittle when cold, and soft when hot. Some nylons start to soften at as little as 60°C

Table 1.4 Some Thermal Properties of Polymers

Polymer	Temperature (°C)		
	Glass Transition	Melting	Processing
Polyethylene (low density)	-122	140	200
Polycarbonate	155	270	320
Polyetheretherketone (PEEK)	144	340	380
Polyetherketoneketone (PEKK)	156	338	370
Polyethersulphone (PES)	260	None	330
Polyimide (BMI)	258	None	180/227
Epoxy	206	None	177

Data for all resins except polyethylene and polycarbonate from I.Y. Chang and J.K. Lees, *J. Thermoplastic Comp. Mater* 1, (1988), 277-96.

Brittleness in polymers generally occurs at temperatures below the glass transition temperature, when the polymer changes from a rubbery state to a glass-like solid. For most amorphous polymers this occurs between +50 and -50°C. Even rubbers become brittle below about -70°C. The onset of brittleness means that these materials should be used with great care for tensile or flexural loads at low temperatures.

At the upper end of their temperature range polymers soften, then melt or decompose (or both). Even the best high temperature polymers (e.g. polyimides) do not last very long at 400°C. Table 1.4 lists some typical thermal properties of some polymers.

Some steels also become brittle below 0°C and until this danger was widely recognized, disastrous failures of large steel structures such as ships, bridges, and pressure vessels were not uncommon. Crystalline phase changes can also cause problems. The most striking case of this is tin, a solid piece of which can break up into a powder when taken repeatedly through the phase change that occurs at 13°C.

The problems at low temperatures can normally be avoided by suitable choice of materials. Materials to withstand high temperatures are much harder to find. Not only is there the danger of the material softening, but it can also suffer accelerated oxidation and corrosion, and creep rupture.

Conventional strong steels tend to lose their strength by changes in microstructure at temperatures in the range 200-300°C. Special steels for high temperatures use have been developed; one of the more notable type is the maraging steels which are useful up to 450-500°C. At higher temperatures, chromium must be added to impart corrosion resistance, and this enables temperatures up to 800°C to be reached, although at lower strength levels (about 350 MPa). For higher temperatures than this, cobalt based alloys are used, and such an alloy will withstand a stress of 150 MPa at 930°C. At still higher temperatures nickel based alloys may be used, strength levels of 150 MPa being achieved for 100 hours at 1000°C.

Aluminium alloys are only suitable for relatively low temperatures, and even aluminium alloys developed for high temperature use have short-term strengths of only about 50 MPa at 400°C. When light weight is important, titanium alloys are used. These can have short-term strengths of about 400 MPa at 700°C.

For temperatures above 1100°C ceramics have to be used. The loads that these can carry, however, are very limited. This is because they are extremely brittle, and the risk of catastrophic failure when under load at temperatures below the normal operating temperature is very great.

The production of more efficient engines for aircraft and land-based applications requires the development of better high-temperature materials. A significant portion of the research on new materials is devoted to this problem.

1.1.8 Corrosion Resistance

Even at moderate temperatures corrosion can be a serious problem. A familiar example of this is the rusting of the bodies of cars driven on the salty slush encountered in some cities with a heavy snowfall. Corrosion is a problem which is now well understood. It can often be solved by suitable choice of materials, avoidance of the use of combinations of metals which set up unfavourable electrochemical reactions under moist conditions, the use of sacrificial electrodes, and the protection of corrodible surfaces by such materials as paints. Since corrosion can cause total loss of fair-sized regions of load-bearing members, consideration of the corrosion conditions likely to be encountered is necessary when a load-bearing structure is being designed.

High temperature corrosion is a much more difficult problem, and provides an upper temperature limit to the usefulness of some metals and alloys. Protection of metal surfaces by coatings of various sorts is seldom a suitable remedy, except for use at moderate temperatures, since thermal expansion differences between the coating and the metal often results in fragmentation of the coating and spalling off, after a few cycles up to high temperature and back to room temperature. As mentioned in the previous section, if stainless steels, or nickel, chromium, and cobalt alloys are not sufficiently corrosion resistant for a high-temperature load-bearing structure, then ceramics normally have to be used, with their inherent disadvantage of very low load-bearing capacity at normal ambient temperatures.

When a material is stressed it is often more susceptible to corrosion than when unstressed. This phenomenon is called stress corrosion and is due to the greater chemical reactivity of a material when the atoms are not in their equilibrium positions in the structure. Hydrogen, often produced by corrosive attack, can enter the material as single atoms, and there form weak hydrides (e.g. in Zr), or collect in voids in the form of molecular hydrogen and weaken the material by exerting high pressures. Materials which are subject to these problems have to be provided with protective layers, if alternative materials are not available.

1.1.9 Cost

Probably the most important characteristic of a material is its cost. However, direct cost, on a weight or volume basis (i.e. dollars per kilogram or dollars per cubic metre) is seldom the operative criterion. In the building industry such a criterion may be important, since the most heavily used materials - steel, wood, bricks, plaster, and concrete, are the cheapest. They range in price from about \$0.01-0.1/kg for bricks, plaster, and concrete, to about \$0.1-1/kg for steel and wood. This clearly is not true, though, in aircraft, which require the use of relatively expensive materials such as aluminium. The more comprehensive concept of cost effectiveness is relevant in this case, and indeed for most uses of materials. For example, the use of the very expensive carbon fibre reinforced panels in the Boeing 747 Jumbo Jet is worth while because of the financial benefits that accrue from the resultant increase in the load-carrying capacity, and hence profitability, of the plane.

Cost effectiveness is a criterion which depends very greatly on the end use of the structure containing the material, and generalizations are difficult to make. It usually involves such factors as: cost per unit load supported, cost per unit of deformation permitted under load, fabrication cost, and general efficiency.

1.2 Elasticity Theory

In this section elasticity theory will be briefly introduced and the terminology used later for stresses and strains will be described. Two classes of stress are normally considered.

A body being pulled at each end by a force F (Fig. 1.8) is in uniaxial tension, and the **tensile stress**, σ , is equal to F , divided by the area over which it acts, i.e. the area of cross-section of the bar. The bar will become longer due to the stress, and the strain, ϵ , is the change in length divided by the original length, i.e. $\delta l/l$.

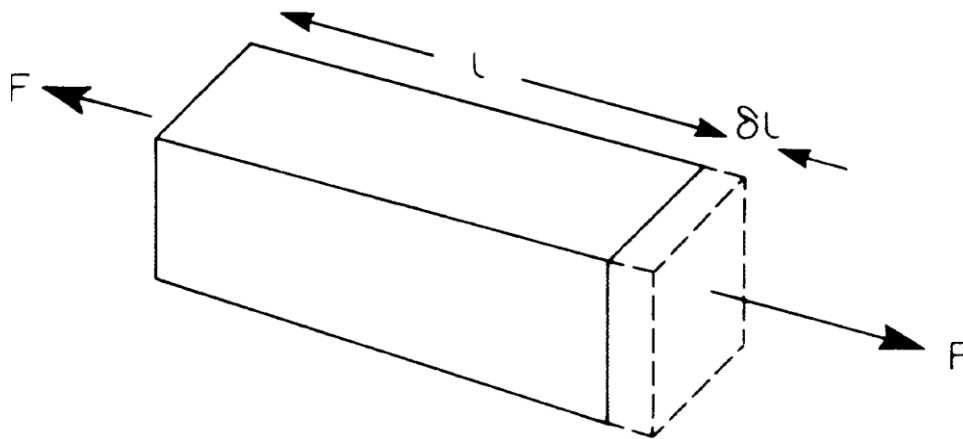


Fig. 1.8 Rod in uniaxial tension.

Figure 1.9 shows a rectangular body being sheared by a force F . The **shear stress**, τ , is equal to F , divided by the area of which it acts, i.e. the area of the top of rectangular box. The box will deform due to the stress, and the change in angle of the corners of the box, γ , is the shear strain.

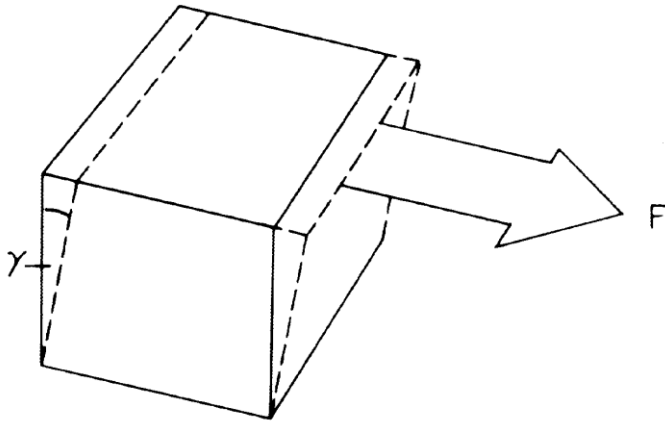


Fig. 1.9 Simple shear.

1.2.1 Stresses

We will now analyse bodies subject to more general stresses. Let us consider a small element of a solid body under stress. Any place in the body can be defined by Cartesian axes x , y , and z . Suppose the origin of these axes is at one corner of the small element of the body (Fig. 1.10).

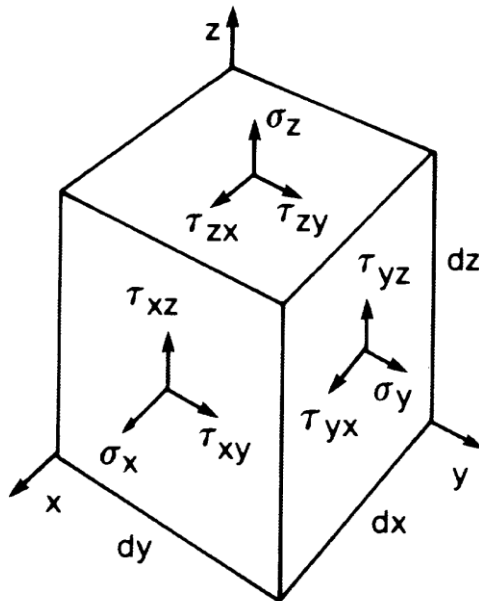


Fig. 1.10 Stresses on an elementary volume.

For simplicity we will consider a rectangular shaped element, whose sides have lengths, dx , dy , and dz as shown. The stresses in the body can be resolved into components in the three directions. Thus, we will have tensile stresses, σ_x , acting on the lower left face, and, in the opposite direction, on the opposite face of the body (not shown). Similarly there will be equal and opposite stresses, σ_y , acting on the faces normal to the y axis, and σ_z acting on the faces normal to the z axis.

The forces acting on each face in these directions are the product of the stress and the area of the face. For example, for the faces normal to the x axis they are $\sigma_x dy dz$.

Negative values for σ_x , σ_y , σ_z indicate compressive stresses.

In addition to the tensile stresses there will, in general, be shear stresses. The symbol τ will be used for the shear stress and the subscripts indicate the plane on which it acts, and the direction. Thus τ_{xy} is the shear stress in the plane normal to the x axis, acting in the y direction. (The first subscript is for the plane, the second for the direction.) Shears also act on the opposite faces to those shown, and again are in the opposite directions.

Although the subscripts suggest that there are six shears, in fact there are only three. This is apparent when we examine the tendency of the element to rotate under the action of the shears.

Consider the top and bottom faces of the element, together with faces normal to the y axis. Figure 1.11 shows the shears tending to rotate this.

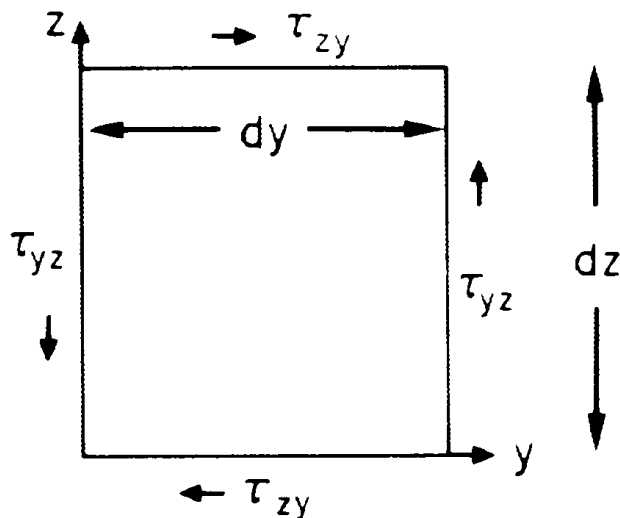


Fig. 1.11 Pure shear.

We will allow the dimensions of the element dz , dy (and dx) to go to zero, so that we can neglect body forces. (Body forces are forces that are not caused by externally applied loads. An example of a body force is the force arising from the action of the earth's gravitational field on the mass of the element.) The clockwise moment is given by the forces at top and bottom (Fig. 1.11), $\tau_{zy} dx dy$, multiplied by their distance apart, dz , i.e. τ_{zy}

$dx dy dz$. Similarly, the anticlockwise moment is $\tau_{yz} dx dz$ (the forces) multiplied by dy (the distance). For equilibrium (i.e. no rotation) the clockwise and anticlockwise moments must be equal

$$\tau_{zy} dx dy dz = \tau_{yz} dx dy dz \tag{1.5}$$

Thus $\tau_{zy} = \tau_{yz}$. Similarly $\tau_{xy} = \tau_{yx}$ and $\tau_{xz} = \tau_{zx}$.

We thus conclude that there are six components of stress: three tensile stresses, σ_x , σ_y and σ_z , and three shears τ_{xy} , τ_{yz} , τ_{xz} .

Only a limited number of problems have been solved when all six stresses have significant values, and all possible deformations resulting therefrom have to be considered. Fortunately, many systems reduce to the relatively simple planar form.

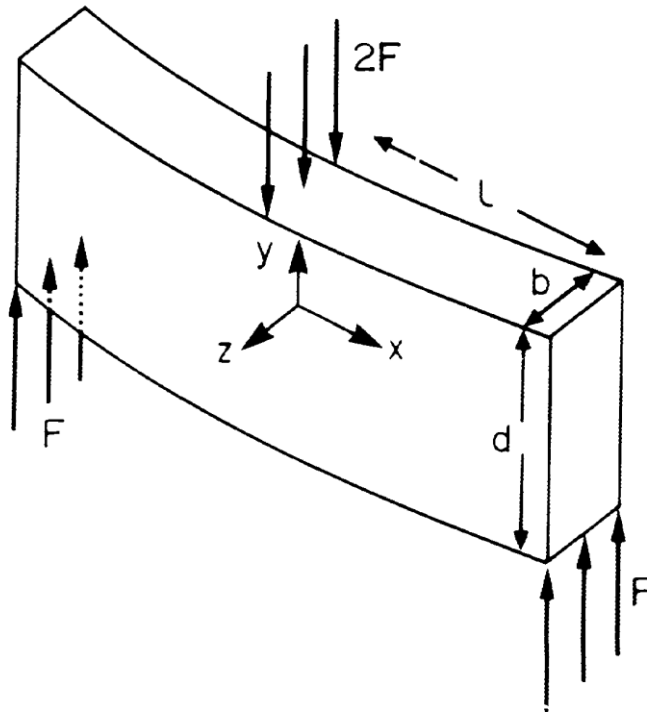


Fig. 1.12 Plane stress flexure.

For example, a very common problem is the bending of beams under a variety of loading systems. Very often it is possible to neglect the stresses in the direction of the thickness of the beam (the z direction for the orientation of axes shown in Fig. 1.12). This system is called Plane Stress, and in the case shown we can assume $\sigma_z \cong \tau_{xz} \cong \tau_{yz} \cong 0$. Stress analysis shows that the other stresses in the centrally loaded beam shown in Fig. 1.12 depend on the distance from the centre, as follows:

$$\sigma_x = F(l-x)y/I \tag{1.6}$$

$$\sigma_y = 0 \tag{1.7}$$

$$\tau_{xy} = F(d^2 - 4y^2)/[8I] \tag{1.8}$$

where

$$I = bd^3/12 \tag{1.9}$$

and in equation 1.6, the absolute value of x must be used.

1.2.2 Resolution of Stresses

Stresses acting on any plane can be calculated if the values of the six stresses are all known. For simplicity we will consider plane stress, with σ_z , τ_{yz} and τ_{xz} equal to zero. We will consider a small element of material of unit thickness in the z direction, with sides dx and dy , as shown in Fig. 1.13, so that $\tan \phi = dx/dy$. If we divide the element in two along the diagonal, the halves will only stay in position if held together by a stress σ and prevented from sliding by a shear τ . The values of σ and τ can be related to the stresses σ_x , σ_y , and τ_{xy} .

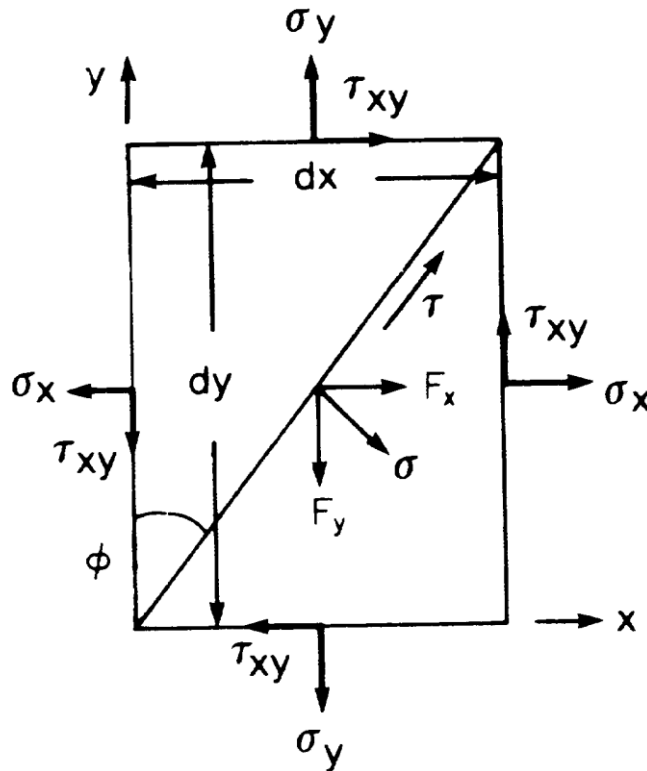


Fig. 1.13 Stresses and forces acting on a diagonal plane.

Let the forces acting across the plane be F_x and F_y (see Fig. 1.13). Equating forces in the x and y directions.

$$F_x = \sigma_x dy - \tau_{xy} dx \tag{1.10}$$

$$F_y = \sigma_y dx - \tau_{xy} dy \tag{1.11}$$

We can now resolve F_x and F_y along the normal to the plane to find σ . Thus

$$\sigma \sqrt{dx^2 + dy^2} = F_x \cos \phi + F_y \sin \phi \quad (1.12)$$

and using the equations for F_x and F_y (1.10) and (1.11) and noticing that

$$\cos \phi = dy / \sqrt{dx^2 + dy^2} \quad \text{and} \quad \sin \phi = dx / \sqrt{dx^2 + dy^2} \quad \text{we find that}$$

$$\sigma = \sigma_x^2 \cos^2 \phi + \sigma_y^2 \sin^2 \phi - 2\tau_{xy} \sin \phi \cos \phi \quad (1.13)$$

Resolving forces in the plane we obtain

$$\tau \sqrt{dx^2 + dy^2} = F_x \sin \phi + F_y \cos \phi \quad (1.14)$$

and making the same substitutions yields

$$\tau = (\sigma_x - \sigma_y) \sin \phi \cos \phi + \tau_{xy} (\cos^2 \phi - \sin^2 \phi) \quad (1.15)$$

We can choose ϕ so that $\tau = 0$. For this

$$\frac{\tau_{xy}}{\sigma_y - \sigma_x} = \frac{\sin \phi \cos \phi}{(\cos^2 \phi - \sin^2 \phi)} \quad (1.16)$$

This equation shows that the shears are zero in two directions. When the x and y axes are in these directions, they are called **Principal axes**.

A very important result of equation (1.15) is that when a piece of material is subject to uniaxial tension, e.g. $\tau_{xy} = \sigma_x = 0$ (so that σ_y is the only stress) then

$$\tau = \sigma_y \sin \phi \cos \phi \quad (1.17)$$

This shear has its maximum value when $\phi = \pi/4$, and is then $\tau = \sigma_y/2$. Thus, in a tensile test, very large shear forces can be produced, and ductile metals tested in this way normally start to fail by shearing at about 45° to the tensile axis. Final failure, however, usually involves tensile processes. Polymers do not normally fail in shear. Shear induced failure processes are discussed in Chapter 6.

(Note: this result is equivalent to the Tresca criterion, which is sometimes used to describe the yielding phenomenon in metals. However, it is more common to use the von Mises (octahedral) yielding criterion, which gives $\tau = \sigma_y/\sqrt{3}$ where σ_y is the uniaxial tensile stress needed to cause yielding.)

In the beam shown in Fig. 1.12 τ_{xy} has its maximum value in the central plane ($y = 0$). However, the maximum shear stresses are at the upper and lower surfaces under the load, and have the (absolute) value

$$\tau_{\max} = Fld/[4I] \quad (1.18)$$

1.2.3 Strains

In the same way that six stresses are needed to describe the state of stress of a body, six strains are needed to represent the state of deformation. The strains normally considered in elasticity theory are small, usually less than 0.001. It would be impractical to show such small strains in a diagram, so Fig. 1.14 shows a much exaggerated view of strains in the x - y plane. We again have an element with sides which were originally of lengths dx (OA) and dy (OB). As a result of the deformation O has moved to O', A to A' and B to B'. What was originally a right angle at O has become an angle $\pi/2 - \theta - \beta$, and the lengths OA and OB have both increased.

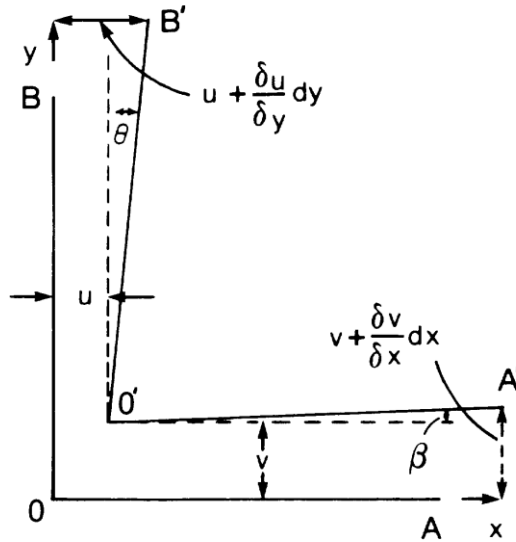


Fig. 1.14 Deformation of an L-shaped element.

If the displacements of O in the x and y directions are u and v respectively, then the corresponding displacements for A in these directions are $u + \frac{\partial u}{\partial x} dx$ and $v + \frac{\partial v}{\partial x} dx$ respectively. For B they are $v + \frac{\partial v}{\partial y} dy$ and $u + \frac{\partial u}{\partial y} dy$ respectively.

The change in length of OA (assuming $\beta \cong 0$) is the displacement of A in the x direction less the displacement of O in the x direction i.e. $u + \frac{\partial u}{\partial x} dx - u$. Thus the tensile strain (= change in length/original length) is $\partial u / \partial x$. Similarly, the strain in the y direction is $\partial v / \partial y$ and in the z direction (not shown) is $\partial w / \partial z$, for a displacement, w , of O in the z direction of w . If we write ϵ_x , ϵ_y , and ϵ_z for these strains, we therefore have

$$\epsilon_x = \partial u / \partial x \tag{1.19}$$

$$\epsilon_y = \partial v / \partial y \tag{1.20}$$

$$\epsilon_z = \partial w / \partial z \tag{1.21}$$

Compressive strains will be shown by negative values for ϵ_x , ϵ_y , or ϵ_z .

The rectangular element has also been sheared, so that the angle at O has decreased by $\theta + \beta$. In Fig. 1.14 it can immediately be seen that, for θ and β sufficiently small, we can write $\theta = \tan \theta$ and $\beta = \tan \beta$, so that $\theta = \partial u / \partial y$ and $\beta = \partial v / \partial x$. The total shear strain is $\theta + \beta$, so writing γ_{xy} for this, we have

$$\gamma_{xy} = \partial v / \partial x + \partial u / \partial y \tag{1.22}$$

and similarly

$$\gamma_{yz} = \partial w / \partial y + \partial v / \partial z \tag{1.23}$$

$$\gamma_{xz} = \partial w / \partial x + \partial u / \partial z \tag{1.24}$$

Plane strain, i.e. when all the strains normal to some plane in the body are zero, is analogous to plane stress. It is quite commonly assumed for the treatment of a stress problem, and often permits of relatively simple analysis.

1.2.4 Resolution of Strains

Strains can be resolved, just as stresses can. However, the process is purely geometric. We consider first the extension of the line OC, which corresponds to a strain ϵ_{x1} , Fig. 1.15. (For convenience we have a counter clockwise rotation, θ , in Fig. 1.15, whereas previously, for stress, we had a clockwise rotation ϕ : see Fig. 1.13. (This will be shown later to reverse some of the signs in the final equations.)

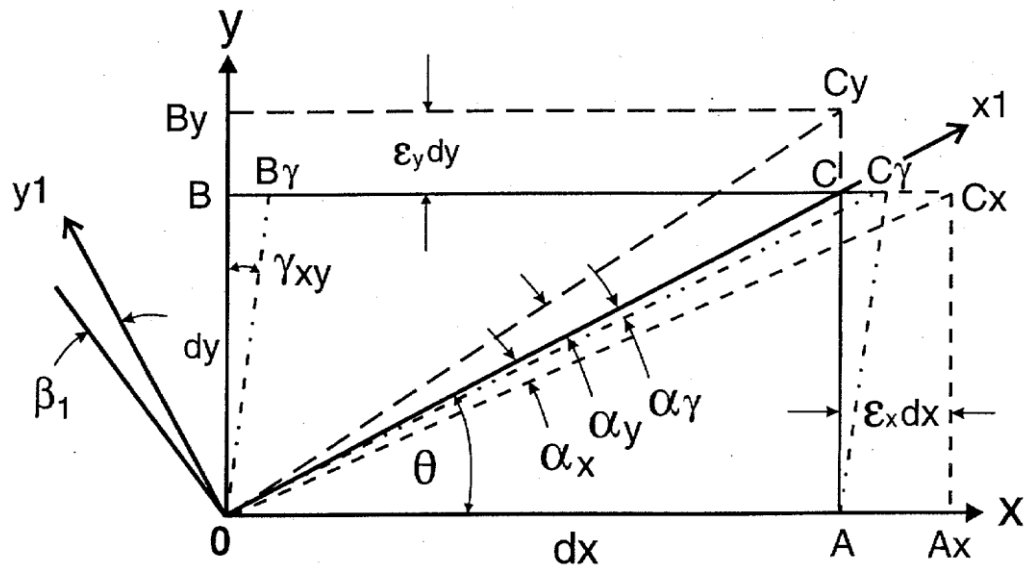


Fig. 1.15 Oblong OACB subject to extensions $\epsilon_x dx$ and $\epsilon_y dy$ and shear γ_{xy} .

We suppose that σ_x causes an elongation of the oblong with A moving to Ax and C to Cx, the extension being $\epsilon_x dx$. The extension of the diagonal, original length dl , is $\epsilon_x dx \cos \theta$ as can be seen from the expanded view of the region CCx in Fig. 1.16a.

Similarly, since the length $CC\gamma$ is $\gamma_{xy}dy$, the extension of the diagonal OC as C moves to $C\gamma$ due to shear τ_{xy} is $\gamma_{xy}dy\cos\theta$. Finally, the extension C to Cy by a similar development is $\varepsilon_y d y \sin\theta$.

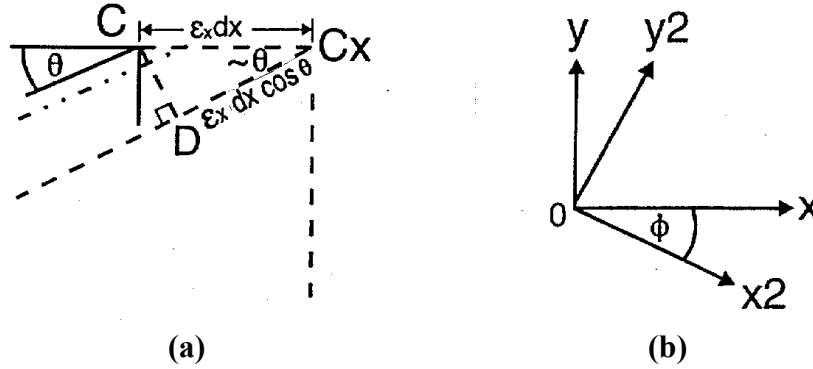


Fig. 1.16 (a) Details of region around point C in Fig. 1.15, and (b) clockwise rotation of axes by an amount ϕ .

We assume that we can sum these separate extensions. Thus the total change in the length of OC is the sum of the extensions. Since OC was originally $\sqrt{dx^2 + dy^2}$

$$\varepsilon_{x1} = (\varepsilon_x dx \cos\theta + \varepsilon_y dy \sin\theta + \gamma_{xy} dy \cos\theta) / \sqrt{dx^2 + dy^2} \quad (1.25)$$

Thus

$$\varepsilon_{x1} = \varepsilon_x \cos^2 \theta + \varepsilon_y \sin^2 \theta + \gamma_{xy} \sin\theta \cos\theta \quad (1.26)$$

since $\cos\theta = dx / \sqrt{dx^2 + dy^2}$ and $\sin\theta = dy / \sqrt{dx^2 + dy^2}$: see Fig. 1.15.

The shear strain will have two components, $\alpha 1$ and $\beta 1$. (Previously we had α and β ; see Fig. 1.14). $\alpha 1$ is the appropriate summation of α_x , α_y and α_γ shown in Fig. 1.15. Thus

$$\alpha 1 = \alpha_y - \alpha_x - \alpha_\gamma \quad (1.27)$$

In Fig. 1.16a, CD is shown as having a length of $\varepsilon_x dx \sin\theta$, so that for small α_x (i.e. $\sin\alpha_x \cong \alpha_x$), $\alpha_x = \varepsilon_x dx \sin\theta / \sqrt{dx^2 + dy^2}$. Similarly $\alpha_\gamma = \gamma_{xy} dy \sin\theta / \sqrt{dx^2 + dy^2}$ and $\alpha_y = \varepsilon_y \cos\theta / \sqrt{dx^2 + dy^2}$. Thus

$$\alpha 1 = (\varepsilon_y - \varepsilon_x) \sin\theta \cos\theta - \gamma_{xy} \sin^2 \theta \quad (1.28)$$

For $\beta 1$ we have angle $\pi/2 + \theta$ instead of θ . Substituting this into equation (1.28) gives

$$\beta 1 = (\varepsilon_y - \varepsilon_x) \cos\theta (-\sin\theta) - \gamma_{xy} \cos^2 \theta \quad (1.29)$$

Our shear strain $\gamma_{x1y1} = \alpha 1 - \beta 1$. Thus

$$\gamma_{11} = 2(\varepsilon_y - \varepsilon_x) \cos\theta \sin\theta - \gamma_{xy} (\cos^2 \theta - \sin^2 \theta) \quad (1.30)$$

Now, finally we let $\phi = -\theta$ so that we effect a clockwise rotation, ϕ , of our x and y axes, instead of the counterclockwise rotation shown at the left in Fig. 1.15. The new axes are x_2 and y_2 .

This gives, instead of equation (1.26)

$$\varepsilon_{x_2} = \varepsilon_x \cos^2 \phi + \varepsilon_y \sin^2 \phi - 2\gamma_{xy} \sin \phi \cos \phi \quad (1.31)$$

and instead of equation (1.30)

$$\gamma_{x_2 y_2} = 2(\varepsilon_x - \varepsilon_y) \sin \phi \cos \phi + \gamma_{xy} (\cos^2 \phi - \sin^2 \phi) \quad (1.32)$$

With our x_2 , axis directed along σ in Fig. 1.13, it can be seen that the tensile strain transformation, equation (1.31) is the same as the tensile stress equation (equation (1.13)) with respect to $\sin 2\theta$, $\cos 2\theta$ and $2\sin \theta \cos \theta$. The shear strain transformation, equation (1.32), is also the same, see equation (1.15), except for the 2 in front of $(\varepsilon_x - \varepsilon_y)$.

1.2.5 Elastic Constants

Only two constants are needed to describe the elastic behaviour of an isotropic material. For convenience, however, four are in common use. Each can be calculated if two of the others are known.

The most readily available elastic constant is Young's modulus, values of which have been given in Table 1.1. This is measured in a uniaxial tensile test, e.g. σ_x has a value, but all other stresses are zero. It is defined by an equation of the type

$$E = \sigma_x / \varepsilon_x \quad (1.33)$$

In a tensile test it is found that contractions occur normal to the direction of the applied stress. These may be used to determine another elastic constant, Poisson's ratio, ν , i.e.

$$\nu = -\varepsilon_y / \varepsilon_x = -\varepsilon_z / \varepsilon_x \quad (1.34)$$

for uniaxial tension in the x direction.

Since we only consider small stresses and strains, we can superpose stresses and strains arising from different applied loads by simple addition. Thus, for a system where σ_x , σ_y , σ_z , τ_{xy} , τ_{yz} , and τ_{zx} may all have values we can write, for the total tensile strains in each direction:

$$\varepsilon_x = \frac{1}{E} \{ \sigma_x - \nu(\sigma_y + \sigma_z) \} \quad (1.35)$$

$$\varepsilon_y = \frac{1}{E} \{ \sigma_y - \nu(\sigma_x + \sigma_z) \} \quad (1.36)$$

$$\varepsilon_z = \frac{1}{E} \{ \sigma_z - \nu(\sigma_x + \sigma_y) \} \quad (1.37)$$

For most metals ν is close to 0.3. However, for rubbers it is almost exactly 0.5 (this indicates no volume change when stressed in uniaxial tension) while for glass it is about 0.22.

The third elastic constant to be considered is the shear modulus G , defined by an expression of the type

$$G = \tau_{xy} / \gamma_{xy} \tag{1.38}$$

(i.e. shear modulus = shear stress/shear strain).

If we consider an element of a body of unit length in the z direction, subject to a tension in the y direction, and an equal but opposite compression in the x direction, and all other stresses zero, we can derive the relation between the shear modulus and the two preceding elastic constants. This state of stress is called **Pure Shear**. The body is deformed without any rotation. In contrast, a body sheared by a force parallel to one surface suffers deformation and rotation; this is called **Simple Shear**, and is illustrated in Fig. 1.9.

For our pure shear case we can write $\sigma_y = -\sigma_x = \sigma$, say.

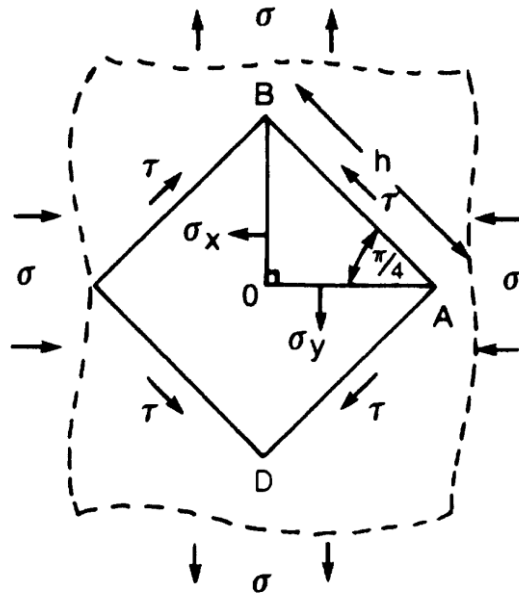


Fig. 1.17 Square element in pure shear.

We will consider a 45° isosceles triangle OAB, within our element of material Fig. 1.17. Let the hypotenuse have a length h . The forces acting on the triangle are as shown in Fig. 1.17. No stress has been shown acting across the hypotenuse. Suppose this were σ' , then equating forces normal to the hypotenuse we have,

$$h\sigma' = h \cos(\pi/4) \cdot \sigma_x \cos(\pi/4) + h \cos(\pi/4) \cdot \sigma_y \cos(\pi/4) \tag{1.39}$$

or

$$\sigma' = (\sigma_x + \sigma_y) \cos^2(\pi/4) = 0 \tag{1.40}$$

i.e. there is no stress acting across AB.

Equating forces parallel to the hypotenuse we obtain

$$h\tau = h \cos(\pi/4) \cdot \sigma_y \cos(\pi/4) - h \cos(\pi/4) \cdot \sigma_x \cos(\pi/4) \quad (1.41)$$

or

$$\tau = (\sigma_x - \sigma_y) \cos^2(\pi/4) = \sigma \quad (1.42)$$

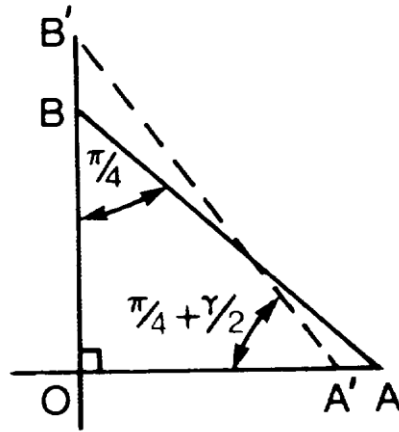


Fig. 1.18 Deformation of a sheared element.

Now consider the deformation. OA will be shortened to OA', and OB lengthened to OB', Fig. 1.18. The angle OAB will have changed by an amount $\gamma/2$, so that DAB, which was a right angle (Fig. 1.17), will have changed to $\pi/2 + \gamma$, i.e. γ is the total shear strain for the element. The relative changes in the lengths OA and OB are given by the strains ε_x and ε_y respectively, where, using equations (1.35) and (1.36):

$$\varepsilon_x = (\sigma_x - \nu\sigma_y) / E = -(1 + \nu)\sigma / E \quad (1.43)$$

and

$$\varepsilon_y = (\sigma_y - \nu\sigma_x) / E = +(1 + \nu)\sigma / E \quad (1.44)$$

Now $\tan \angle OAB'$ is OB'/OA' ; thus

$$\tan\left(\frac{\pi}{4} + \frac{\gamma}{2}\right) = \frac{OB'}{OA'} = \frac{1 + \varepsilon_y}{1 + \varepsilon_x} = \frac{1 + (1 + \nu)\sigma / E}{1 - (1 + \nu)\sigma / E} \quad (1.45)$$

(remembering that ε_x is negative and using equations (1.43) and (1.44)). The tangent can also be expanded; thus for small γ

$$\tan\left(\frac{\pi}{4} + \frac{\gamma}{2}\right) = \frac{\sin\left(\frac{\pi}{4} + \frac{\gamma}{2}\right)}{\cos\left(\frac{\pi}{4} + \frac{\gamma}{2}\right)} \cong \frac{\sin\frac{\pi}{4} + \frac{\gamma}{2} \cos\frac{\pi}{4}}{\cos\frac{\pi}{4} - \frac{\gamma}{2} \sin\frac{\pi}{4}} \quad (1.46)$$

therefore

$$\tan\left(\frac{\pi}{4} + \frac{\gamma}{2}\right) \cong \frac{1 + \gamma/2}{1 - \gamma/2} \quad (1.47)$$

Inspecting equations (1.45) and (1.47) we can see that

$$\gamma = 2(1 + \nu)\sigma/E \quad (1.48)$$

We now have both τ and γ in terms of the stress, σ , and the elastic constants. Thus, using equations (1.42) and (1.48), we have for the shear modulus, G .

$$G = \tau/\gamma = E/[2(1 + \nu)] \quad (1.49)$$

The fourth elastic constant to be considered is the resistance of the material to uniform compression, called the bulk modulus. The symbol K will be used for this. The modulus is defined by the expression

$$K = -P/e \quad (1.50)$$

where P is the pressure, which acts on all faces of an element of material, and e is the change in volume per unit of volume.

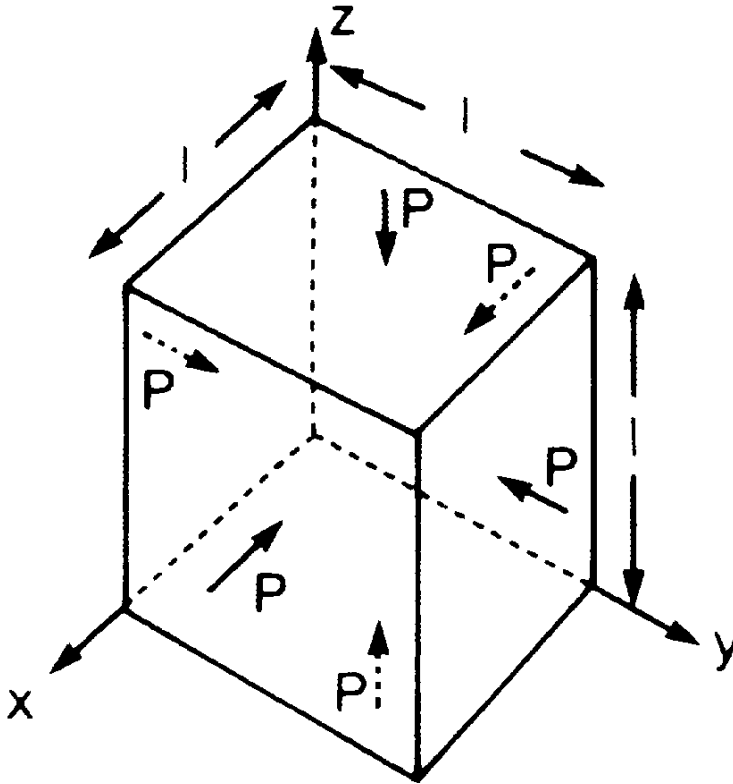


Fig. 1.19 Triaxial compression.

Let the element of material be a cube, with a pressure P acting on each face. If the side of the cube initially is l , and if the sides of the cube are parallel to the axes (Fig. 1.19), then the sides will be reduced to lengths $l(1 + \epsilon_x)$, $l(1 + \epsilon_y)$ and $l(1 + \epsilon_z)$ where

$$\varepsilon_x = \varepsilon_y = \varepsilon_z = -P(1 - 2\nu) / E \quad (1.51)$$

(using equations (1.35), (1.36), and (1.37) with $\sigma_x = \sigma_y = \sigma_z = -P$). The new volume of the cube is

$$(1 + e) l^3 = (1 + \varepsilon_x)(1 + \varepsilon_y)(1 + \varepsilon_z)l^3 \quad (1.52)$$

Expanding the right hand side of equation (1.52) and neglecting second and third orders products (e.g. $\varepsilon_x\varepsilon_y$ etc., and $\varepsilon_x\varepsilon_y\varepsilon_z$) and simplifying we find that the equation reduces to

$$e = \varepsilon_x + \varepsilon_y + \varepsilon_z \quad (1.53)$$

Using equation (1.51) therefore, we find that

$$e = -3P(1 - 2\nu) / E \quad (1.54)$$

so that the bulk modulus comes to

$$K = -P / e = E / [3(1 - 2\nu)] \quad (1.55)$$

We have thus derived expressions for the shear modulus and the bulk modulus in terms of Young's modulus and Poisson's ratio.

1.2.6 Anisotropic Materials

It was mentioned earlier that single crystals of materials are usually anisotropic. Fibre reinforced materials are often highly anisotropic. While two elastic constants are required to describe the elastic properties of isotropic materials, twenty-one are required for anisotropic materials with no planes of symmetry.

As with isotropic materials, there are normally six independent stresses and six independent strains for anisotropic materials. The tensile stresses are expressed thus: $\sigma_1, \sigma_2, \sigma_3$, while the shear stresses are expressed thus: $\tau_{23}, \tau_{31}, \tau_{12}$, and the strains are $\varepsilon_1 = \partial u / \partial x$ etc., and $\gamma_{23} = \partial v / \partial z + \partial w / \partial y$ etc. (i.e. the subscripts x, y, z used for isotropic materials are replaced by 1, 2, and 3). The stress-strain relations are best expressed in matrix form:

$$\begin{pmatrix} \sigma_1 \\ \sigma_2 \\ \sigma_3 \\ \tau_{23} \\ \tau_{31} \\ \tau_{12} \end{pmatrix} = \begin{pmatrix} C_{11} & C_{12} & C_{13} & C_{14} & C_{15} & C_{16} \\ C_{12} & C_{22} & C_{23} & C_{24} & C_{25} & C_{26} \\ C_{13} & C_{23} & C_{33} & C_{34} & C_{35} & C_{36} \\ C_{14} & C_{24} & C_{34} & C_{44} & C_{45} & C_{46} \\ C_{15} & C_{25} & C_{35} & C_{45} & C_{55} & C_{56} \\ C_{16} & C_{26} & C_{36} & C_{46} & C_{56} & C_{66} \end{pmatrix} \cdot \begin{pmatrix} \varepsilon_1 \\ \varepsilon_2 \\ \varepsilon_3 \\ \gamma_{23} \\ \gamma_{31} \\ \gamma_{12} \end{pmatrix} \quad (1.56)$$

The $[C_{ij}]$ matrix is the stiffness matrix. If it is required to calculate strains the compliance matrix, $[S_{ij}]$ is used as below (next page).

$$\begin{array}{c|c|cccccc|c}
 \varepsilon_1 & & S_{11} & S_{12} & S_{13} & S_{14} & S_{15} & S_{16} & \sigma_1 \\
 \varepsilon_2 & & S_{12} & S_{22} & S_{23} & S_{24} & S_{25} & S_{26} & \sigma_2 \\
 \varepsilon_3 & & S_{13} & S_{23} & S_{33} & S_{34} & S_{35} & S_{36} & \sigma_3 \\
 \gamma_{23} & = & S_{14} & S_{24} & S_{34} & S_{44} & S_{45} & S_{46} & \tau_{23} \\
 \gamma_{31} & & S_{15} & S_{25} & S_{35} & S_{45} & S_{55} & S_{56} & \tau_{31} \\
 \gamma_{12} & & S_{16} & S_{26} & S_{36} & S_{46} & S_{56} & S_{66} & \tau_{12}
 \end{array} \quad (1.57)$$

Notice that both these matrices are symmetric, i.e. $C_{ij} = C_{ji}$ and $S_{ij} = S_{ji}$.

The number of independent elastic constants is only nine for orthotropic materials. Laminae of fibre reinforced materials, with all the fibres parallel, are examples of orthotropic materials. These materials have three mutually orthogonal planes of symmetry for mechanical properties, and there are no interactions between normal stresses, σ_1 , σ_2 , and σ_3 , and shearing strains γ_{23} , γ_{31} , γ_{12} . Conversely there are no interactions between shearing stresses and normal strains. Thus equation (1.56) reduces to

$$\begin{array}{c|c|cccccc|c}
 \sigma_1 & & C_{11} & C_{12} & C_{13} & 0 & 0 & 0 & \varepsilon_1 \\
 \sigma_2 & & C_{12} & C_{22} & C_{23} & 0 & 0 & 0 & \varepsilon_2 \\
 \sigma_3 & & C_{13} & C_{23} & C_{33} & 0 & 0 & 0 & \varepsilon_3 \\
 \tau_{23} & = & 0 & 0 & 0 & C_{44} & 0 & 0 & \gamma_{23} \\
 \tau_{31} & & 0 & 0 & 0 & 0 & C_{55} & 0 & \gamma_{31} \\
 \tau_{12} & & 0 & 0 & 0 & 0 & 0 & C_{66} & \gamma_{12}
 \end{array} \quad (1.58)$$

and equation (1.57) reduces to

$$\begin{array}{c|c|cccccc|c}
 \varepsilon_1 & & S_{11} & S_{12} & S_{13} & 0 & 0 & 0 & \sigma_1 \\
 \varepsilon_2 & & S_{12} & S_{22} & S_{23} & 0 & 0 & 0 & \sigma_2 \\
 \varepsilon_3 & & S_{13} & S_{23} & S_{33} & 0 & 0 & 0 & \sigma_3 \\
 \gamma_{23} & = & 0 & 0 & 0 & S_{44} & 0 & 0 & \tau_{23} \\
 \gamma_{31} & & 0 & 0 & 0 & 0 & S_{55} & 0 & \tau_{31} \\
 \gamma_{12} & & 0 & 0 & 0 & 0 & 0 & S_{66} & \tau_{12}
 \end{array} \quad (1.59)$$

for axes taken parallel to the intersections of the symmetry planes.

Some materials are transversely isotropic. This is true for sheets of randomly oriented fibre composites. These materials have mechanical properties which are equal in all directions in a plane, and have only five independent elastic constants. Taking the 1-2 plane as the plane of isotropy, equations (1.58) and (1.59) reduce to

$$\begin{array}{c|ccc|cc|c}
 \sigma_1 & C_{11} & C_{12} & C_{13} & 0 & 0 & 0 \\
 \sigma_2 & C_{12} & C_{22} & C_{23} & 0 & 0 & 0 \\
 \sigma_3 & C_{13} & C_{23} & C_{33} & 0 & 0 & 0 \\
 \tau_{23} & 0 & 0 & 0 & C_{44} & 0 & 0 \\
 \tau_{31} & 0 & 0 & 0 & 0 & C_{55} & 0 \\
 \tau_{12} & 0 & 0 & 0 & 0 & 0 & C_{66}
 \end{array}
 =
 \begin{array}{c}
 \varepsilon_1 \\
 \varepsilon_2 \\
 \varepsilon_3 \\
 \gamma_{23} \\
 \gamma_{31} \\
 \gamma_{12}
 \end{array}
 \quad (1.60)$$

where $C_{66} = (C_{11} - C_{12}) / 2$, and

$$\begin{array}{c|ccc|cc|c}
 \varepsilon_1 & S_{11} & S_{12} & S_{13} & 0 & 0 & 0 \\
 \varepsilon_2 & S_{12} & S_{22} & S_{23} & 0 & 0 & 0 \\
 \varepsilon_3 & S_{13} & S_{23} & S_{33} & 0 & 0 & 0 \\
 \gamma_{23} & 0 & 0 & 0 & S_{44} & 0 & 0 \\
 \gamma_{31} & 0 & 0 & 0 & 0 & S_{55} & 0 \\
 \gamma_{12} & 0 & 0 & 0 & 0 & 0 & S_{66}
 \end{array}
 =
 \begin{array}{c}
 \sigma_1 \\
 \sigma_2 \\
 \sigma_3 \\
 \tau_{23} \\
 \tau_{31} \\
 \tau_{12}
 \end{array}
 \quad (1.61)$$

where $S_{66} = 2(S_{11} - S_{12})$

In practical tests on materials, it is usual to measure the tensile strain that results from a uniaxial tensile stress, so that a Young's modulus is obtained. If this is done in the three principal directions in an orthotropic material, three moduli would be obtained; E_1 , E_2 , and E_3 . In addition, the strains transverse to each stress should be measured, to obtain Poisson's ratios, ν_{ij} , where

$$\nu_{ij} = \varepsilon_j / \varepsilon_i \quad (1.62)$$

($i, j = 1, 2, 3, i \neq j$; the material is stressed in the i direction).

Only three Poisson's ratios are required, since

$$\nu_{ij} / E_i = \nu_{ij} / E_j \quad (1.63)$$

In addition, in order to determine all the elastic properties of the composite, shear tests should be performed to measure the three shear moduli G_{23} , G_{31} , and G_{12} . We can now express $[S]$ in terms of these *Engineering Constants*.

$$[S_{ij}] =
 \begin{array}{c|ccc|cc|c}
 1/E_1 & -\nu_{12}/E_1 & -\nu_{13}/E_1 & 0 & 0 & 0 \\
 -\nu_{12}/E_1 & 1/E_2 & -\nu_{23}/E_2 & 0 & 0 & 0 \\
 -\nu_{13}/E_1 & -\nu_{23}/E_2 & 1/E_3 & 0 & 0 & 0 \\
 0 & 0 & 0 & 1/G_{23} & 0 & 0 \\
 0 & 0 & 0 & 0 & 1/G_{31} & 0 \\
 0 & 0 & 0 & 0 & 0 & 1/G_{12}
 \end{array}
 \quad (1.64)$$

Relatively few elasticity problems have been solved for orthotropic materials, on account of the complexity of the stress-strain relations.

Further Reading

Timoshenko, S (1958) *Strength of Materials* Vols. 1 and 2 (D. Van Nostrand, New York)
 Smith, W.F., (1986) *Principles of Materials Science and Engineering* (McGraw Hill, New York)
 Gordon, J.E. (1976) *The New Science of Strong Materials* (Penguin Books Ltd., Harmondsworth, U.K.)

Chapter 1: Problems

You are strongly recommended to solve these problems in the order given. Data needed will be found in tables in this and other chapters of the book.

- 1.1 Calculate the breaking strains of pure aluminium, glass, concrete, epoxy resin and polycarbonate. Assume that all these materials are perfectly elastic.
- 1.2 Calculate the weight of a rod of maraging steel, and the weight of Douglas fir, both 30m long, and which, when hanging vertically, will just support a man weighing 75kg, hanging on the lower end. Assume the density of Douglas fir is the same as that of Sitka spruce.
- 1.3 A bar of metal has to withstand a large temperature decrease, to a minimum temperature of 20°C, while remaining the same length. What are the corresponding maximum temperatures for bars made from aluminium alloy and tungsten? (Thermal expansion coefficients are: Al, 23MK^{-1} and W, 4.3MK^{-1}).
- 1.4 A ship 165m long is moored against a quay by a steel hawser at the bow, and a nylon rope at the stern. Both moorings are at right angles to the quayside and have a length of 11m and a diameter of 0.127m. They are unstressed when the ship's side is in contact with the quay. An offshore wind springs up and exerts a force of 20MN on the ship normal to its side. What angle will the ship turn through as a result? How far will the stern section be from the quay? (Use data from Table. 3.1).
- 1.5 A steel girder, weighing 2.8 tonnes is supported at the centre by a vertical Kevlar rope 1.8cm diameter, and at the ends by vertical polyester ropes 1.3cm diameter, equal in length to the Kevlar rope. Calculate the stresses in the ropes. (Use data from Table 3.1)
- 1.6 A steel rod is held at 25° to the vertical by a vertical 0.50mm diameter nylon filament attached to its lower end. The upper end of the rod is held by a frictionless pivot at the same level as the upper end of the nylon filament. The rod has a

diameter of 3.8cm and a length of 1.7m. If a heavy weight is hung on the rod, so that the end is pulled down, and the rod becomes approximately vertical, will the nylon be stretched to such an extent that its stress, calculated assuming that the material behaves elastically, exceeds its ultimate tensile strength.

- 1.7 A load of 2.7 tonnes was to be supported by a strip of steel, fastened to another strip of steel by an overlapping joint, held together by steel rivets, 6.35mm diameter. However, the wrong steel was used for the rivets and in the riveting process, all but one of them broke. The strength of the steel was 190MPa, and it was too brittle. The only material that was available was white pine, cut from a local tree. How many wooden rods of the same diameter would have to be used in place of rivets to prevent the steel rivet from breaking when the load was applied. Would this number of rods make the steel rivet redundant? Assume that the failure shear stresses of the steel and wood are half their respective tensile strengths, and that the stress-strain curve of the steel is linear up to the fracture stress. The shear modulus of the wood is given with sufficient accuracy by dividing the Young's modulus by 2.6. The Poisson's ratio for steel is 0.29.
- 1.8 A sapphire crystal disc 3.18mm diameter and 1.00mm thick is sandwiched between two glass sheets 0.178m in diameter. The glass is also held apart by a 1.05mm thick natural rubber ring at the periphery of the sheets, and the space between is evacuated. What would the width of the ring have to be to prevent the air pressure on the glass from breaking the sapphire, assuming the compressive strength of the sapphire is the same as high density alumina, and that the glass does not break?
- 1.9 A circular bar has been made from a single crystal of tin with the basal plane only 3° out of alignment with the plane normal to the axis of the bar. If shear can occur on the basal plane at a stress 7.0MPa and cleavage can occur by separation at the basal plane at a stress of 60MPa, determine the mode of failure when the bar is tested in a tensile machine. Calculate both the stress required, and the load in kg, if the diameter of the bar is 0.62cm.

It can be shown by differentiation of equation 1.13 that the maximum and minimum tensile stresses are at angles ϕ to the y axis where $\tan 2\phi = 2\tau_{xy}/(\sigma_y - \sigma_x)$. Use this result to solve the following three problems.

- 1.10 A house near Bangkok was supported by four unreinforced concrete stilts. It was designed so that the concrete was under compression at a stress equal to its tensile strength. What would the speed of the wind in a typhoon have to be to cause failure of the stilts? The building presented an area of 42m^2 to the wind, and it weighed 35 tonnes. Neglect the moments of the wind forces, and consider the stilts as subject to shear from the wind force and compression from the building weight. You may assume that the pressure exerted by the wind is ρV^2 where V is the wind velocity and ρ is the density of the air, which has a value of 1.29kg m^{-3} .

- 1.11 A thin walled glass tube was used to connect a motor to a stirrer in a chemical plant. The shear stress in the glass was designed to be one quarter of its tensile failure stress. Due to a design fault the glass was also under a tensile stress along the length of the tube, and it broke. Calculate the minimum load that was needed to break the tube. The diameter of the tube was 3.0cm, and the wall thickness 1.2mm.
- 1.12 A link connecting a brake lever and the brake has a joint in it where two pieces of aluminium are held together by a 3.0mm diameter bolt. The bolt was brittle because of having had the wrong heat treatment, and fractured at a stress of 90MPa. The bolt was screwed up tightly so that the pieces of steel were held together with a force of 300N. If the coefficient of friction of the aluminium surfaces is 0.3, what would be the maximum force the joint could transmit?

It can be shown, by differentiation of equation 1.15 that the maximum and minimum shear stresses are at angle ϕ to the y axis where $\tan 2\phi = (\sigma_x - \sigma_y)/[2\tau_{xy}]$. Use this result to solve the following three problems.

- 1.13 The house near Bangkok (q. 10) had its concrete supports replaced by steel ones. The steel was ductile and had a compressive failure stress equal to its tensile failure stress of 150MPa. If the supports were designed to be under a compressive stress equal to one half of the material strength, what wind speed would be required to cause initiation of failure of the supports.
- 1.14 It was decided to use stainless steel with a tensile strength of 270MPa to replace the broken glass tube in the chemical plant. (q. 11). The shear stress in the steel was designed to be one half the apparent shear strength of the steel. What would be the minimum load needed to break this tube? (Note: you must first calculate the wall thickness of the tube: it had the same diameter as the glass one).
- 1.15 The bolt connecting the brake lever to the brake (q. 12) was replaced by one that was correctly heat treated, was ductile, and had a strength of 310MPa. What would be the maximum force the joint could transmit with the new bolt?

-
- 1.16 A car is travelling along a paved country road in the spring and has to stop suddenly at an intersection. The road has been damaged badly by the winter frosts, and the asphalt is broken up into pieces which are the same size as the area of contact of the car tire on the road. It being a cold spring morning the cracks are open near the surface, but closed further down: Determine whether the asphalt will fail beneath the car wheels, given the following data: weight of car = 1.7 tonnes; coefficient of friction of tires on road = 1.3; apparent shear strength of asphalt = 3.2MPa; tensile strength = 0.12MPa; thickness = 2.72cm. At the instant of stopping the tire pressure at the front is 2.2 bar, and the deceleration is sufficiently great that substantially all the car weight is supported by the front wheels. (1 bar = 100kPa.)

- 1.17 The materials to bridge a small ravine, 6.0m wide, in the mountains, have to be as light as possible in order to facilitate transport. Two horizontal, parallel, wide flange beams are to be used as the main supports, since this is the most efficient shape. They must each be 12m long and the cross-sectional area of material in them, A , and their depth, h , must be designed so that the maximum stress does not exceed one-half of the breaking strength, and they are stiff enough that under a maximum moment of 30 tonne-metres on each support (due to the passage of a loaded vehicle) the radius of curvature of the beams has a value of 60m. The moment of area of the beam is $I = 0.7 Ah^2$ and the maximum stress in the beam is $3M/Ah$. Develop equations for A and h , and compare the relative merits (so far as weight is concerned) of steel, aluminium alloy, and titanium alloy.
- 1.18 A fashionable designer decided that a water tank could be supported by three symmetrically disposed vertical pipes, one of which could also serve for the inlet water and the other two for the outflow. He used pewter (a lead-tin alloy) for tank and pipes, which had a strength of 40MPa. He made the pipes 10.2cm in diameter, and made the wall thickness 1.3mm. This, he calculated, was enough, with a 20% margin for safety, when the compressive stresses resulting from the weight of water in the tank were considered. He also checked to see if pipes with this wall thickness could withstand the tensile stresses due to the water pressure. In the inlet pipe this was 0.62MPa. (The circumferential stress, σ , due to pressure P in a thin walled tube is $\sigma = Pr/t$ where $2r$ is the tube diameter and t is the wall thickness). This was found to be more than adequate, so he did not check the effect of the combined compressive and tensile stresses. When tested, it was found that failure occurred before the tank had filled up. Explain why, and calculate the fraction filled at the instant of failure.

Chapter 1. Selected Answers

Answers are rounded off to the appropriate numbers of significant figures

- 1.1 0.85, 1.00, 0.070, 24 and 26 millistrain.
- 1.3 Aluminium alloy 420°C, tungsten 1040°C.
- 1.5 Terylene 0.99MPa, Kevlar 110MPa.
- 1.7 220 rods needed for steel with modulus of 212GPa; steel is redundant.
- 1.9 Cleavage, 60.2MPa, 18.2kg.
- 1.11 7.1kN.
- 1.13 267kmh⁻¹ (concrete stands up better; see q. 1.10)
- 1.15 1.2kN (the correct heat treatment more than doubles the maximum load, see question. 1.12)
- 1.17 $h = R \sigma_u^2 / E \rho$; $A = 25.2 ME / R \sigma_u^2$; figure of merit = $\sigma_u^2 / E \rho$; steel/aluminium alloy/titanian alloy = 2.4/2.2/2.6 (M = moment, R = radius, σ_u = strength.)

2. PHYSICAL FACTORS INFLUENCING MECHANICAL PROPERTIES

Composite materials make use of our knowledge of the influence of bond strength on materials strength, which is exerted through the internal structure of the material. Thus it is necessary first to understand the causes of the strengths and weaknesses of traditional materials.

It was only relatively recently realized that there is some connection between chemical bond strengths and the tensile strengths of materials. This is because the relationship is extremely indirect, and a given element or compound can have a great many different strengths according to how a sample of it is made, and the precise nature and distribution of the impurities within it.

A good example of this is iron. A small amount of carbon can greatly influence its strength, even when the carbon has no effect on the nature of predominant interatomic bonds. The effect of the carbon is strongly influenced by the heat treatment the iron (or steel) has undergone, and the strength of the material is also very sensitive to the prior mechanical treatment, again without any need to change the predominant bonding.

In this chapter, a rough estimate will be made of how strong a material could be, if perfect. This will be followed by a description of the two major sources of weakness in real materials and the practical effects of these.

2.1 Strength of Solids Calculated from Bond Strengths

A large number of attempts have been made to estimate the strength of materials from the strength of the chemical bonds within them. At first the results obtained seemed so high compared with the known strengths of materials, and varied in such an apparently random way from one material to another, that people were inclined to believe that the strength of solids had little to do with bond strengths.

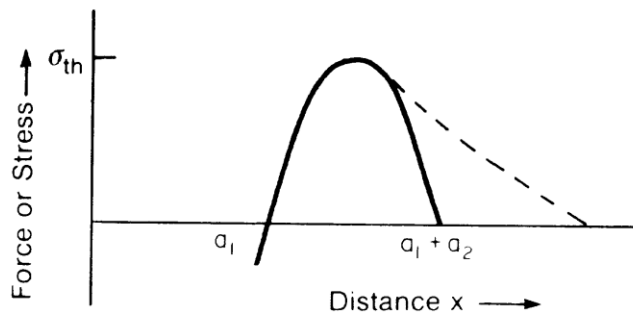


Fig. 2.1 Approximate force-distance relation for two atoms.

One of the simplest ways of obtaining a rough estimate of the theoretical strength of a solid is to assume that the variation of interatomic forces with distance can be approximated by a sine curve. Fig. 2.1 shows sine curve which crosses the axis at a_1 and at $a_1 + a_2$. Superimposed on this is a dashed line that indicates a typical force-distance relationship between two atoms, where this deviates significantly from the sine curve. At

$x = a_1$ there is no force, and this is the equilibrium position for the two atoms. Compression (negative force) is required to push the atoms closer together than the equilibrium value, and tensile forces are required to separate them.

If, instead of having two atoms, we have a solid crystal, consisting of vast numbers of atoms (a cubic mm of a solid contains $\sim 10^{20}$ atoms) arranged in some orderly way in rows and planes, we can assume that the force between two planes also follows the sine curve. If we apply a small stress (force per unit area), the distance between the planes will increase, and the rate of increase for increasing force is given by the modulus of elasticity, E (Young's modulus).

A plot of stress, σ , against distance will look the same as the force plot, and will have the equation

$$\sigma = k_1 \sin(\pi[x - a_1]/a_2) \quad (2.1)$$

where k_1 is a constant which can be determined from the slope of the curve at $x = a_1$, where the stress is zero. At $x = a_1 + dx$, the stress is $d\sigma$ and the strain is dx/a_1 . We can equate the modulus with the stress/strain ratio. Thus

$$E = a_1 \frac{d\sigma}{dx} \quad (2.2)$$

at $x = a_1$. From equation (2.1)

$$\frac{d\sigma}{dx} = \frac{k_1\pi}{a_2} \cos(\pi[x - a_1]/a_2) \quad (2.3)$$

so that

$$\frac{d\sigma}{dx} = \frac{k_1\pi}{a_2} \quad (2.4)$$

at $x = a_1$. Hence, substituting this into equation (2.2), we find that

$$k_1 = Ea_2/[\pi a_1] \quad (2.5)$$

If we now assume that $a_2 \cong a_1$,

$$k_1 \cong E/\pi \quad (2.6)$$

The breaking-strength of the material should be determined by the maximum stress. This is when $x = a_1 + a_2/2$, and has the value $\sigma_{th} = k_1$ (from equation (2.1)). So the theoretical strength, using equation (2.6) is

$$\sigma_{th} \cong E/\pi \quad (2.7)$$

If the strength were governed by this expression we would expect aluminium and glass to have roughly the same strength, of about 22GPa. However, macroscopic pieces of the best aluminium alloys have strengths of only 0.45GPa, and there seems to be little

potential for improving this figure, while the best glass sheets, rods, or tubes have a strength of only about 0.1GPa.

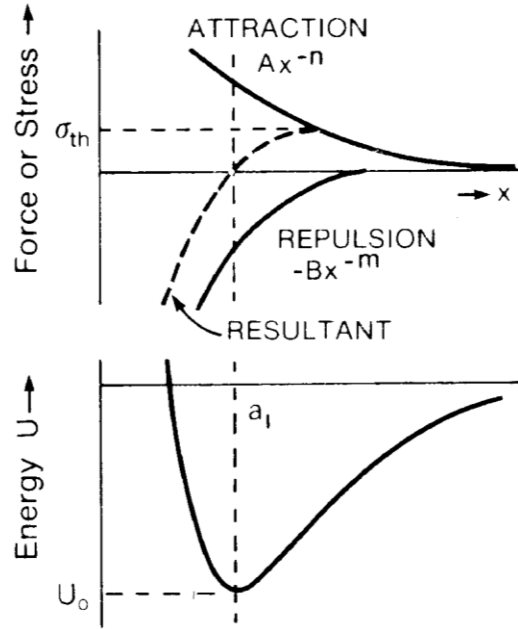


Fig. 2.2 Force-distance relation for two atoms, and associated energy.

A better approximation is obtained if we assume that the interactions between atoms are governed by two forces, one attractive and the other repulsive. The force of attraction originates from electrostatic forces (ionic solids), or covalent bonding forces (for elements like carbon or silicon), or metallic bonding forces, or Van der Waals forces. The repulsive force is a measure of the "squashability" of the atoms, and only becomes significant when the atoms are "touching". An expression used to describe these forces is

$$\sigma = Ax^{-n} - Bx^{-m} \quad (2.8)$$

and is shown schematically in Fig. 2.2. Integration of this equation gives an expression for the energy associated with these forces for $U = 0$ when $x \rightarrow \infty$:

$$U_0 = -\frac{A}{n-1}x^{-n+1} + \frac{B}{m-1}x^{-m+1} \quad (2.9)$$

This has a minimum value when $x = a_1$ of

$$U_0 = \frac{-A(m-n)}{(n-1)(m-1)}a_1^{-(n-1)} \quad (2.10)$$

where a_1 is the equilibrium separation of the atoms i.e. where the attraction and repulsion counterbalance each other, so that $\sigma = 0$. To dissociate the material we need to supply this energy U_0 . We can therefore obtain information about the constants in equation (2.8) by measuring the heat required to vaporize or sublime the material.

We can use equation (2.8) to estimate the theoretical strength, if we have values

for m , n , and the modulus of elasticity. As before, $E = x \frac{d\sigma}{dx}$ at $x = a_1$, and $\sigma = 0$ at this point. Thus

$$B = Aa_1^{m-n} \quad (2.11)$$

and

$$E = a_1 \left(-nAa_1^{-n-1} + mBa_1^{-m-1} \right) \quad (2.12)$$

which can be rearranged to give

$$A = \frac{Ea_1^n}{m-n} \quad (2.13)$$

We have now evaluated A and B in terms of E and a_1 together with m and n . The maximum strength will be when the stress reaches its maximum value, i.e. when $d\sigma/dx = 0$. This is when

$$x^{m-n} = mB/nA \quad (2.14)$$

Substituting for A and B using equations (2.12) and (2.11), and taking the $(m-n)$ th root gives

$$x = a_1 \left\{ \frac{m}{n} \right\}^{\frac{1}{m-n}} \quad (2.15)$$

At this value of x the stress (equation (2.8)) is σ_{th} where

$$\sigma_{th} = Aa_1^{-n} \left\{ \frac{n}{m} \right\}^{\frac{n}{m-n}} - Ba_1^{-m} \left\{ \frac{n}{m} \right\}^{\frac{m}{m-n}} \quad (2.16)$$

Substituting for B from equation (2.11) and for A from equation (2.12) we obtain

$$\sigma_{th} = \frac{E}{m-n} \left[\left\{ \frac{n}{m} \right\}^{\frac{n}{m-n}} - \left\{ \frac{n}{m} \right\}^{\frac{m}{m-n}} \right] \quad (2.17)$$

But $\frac{m}{m-n} = \frac{n}{m-n} + 1$, therefore

$$\sigma_{th} = \frac{E}{m-n} \left\{ \frac{n}{m} \right\}^{\frac{n}{m-n}} \left\{ 1 - \frac{n}{m} \right\} \quad (2.18)$$

and so finally,

$$\sigma_{th} = \frac{E}{m} \left\{ \frac{n}{m} \right\}^{\frac{n}{m-n}} \quad (2.19)$$

Thus, the theoretical strength can be calculated if E , m , and n are known.

For alkali halides $n = 2$ (electrostatic attraction falls off as the square of the distance) and m is about 10. So we would expect an alkali halide to have a theoretical strength of about one-fifteenth of its Young's modulus. The value for potassium chloride is 1.3GPa, which is vastly greater than the observed strength of a crystal of the material, which can be less than 1MPa. In the case of metals also, the values of m and n are such that the theoretical strength is about one-fifteenth of the Young's modulus. For iron, with $n = 4$ and $m = 7$ the value is 14GPa, which should be compared with 4.2GPa obtained with very strong steel wires.

The theoretical values calculated so far are for cleavage failure of the material. Failure by shear may also be possible and it is worth while examining the stress required for this, to determine whether shear failure could occur at a lower stress than tensile failure.

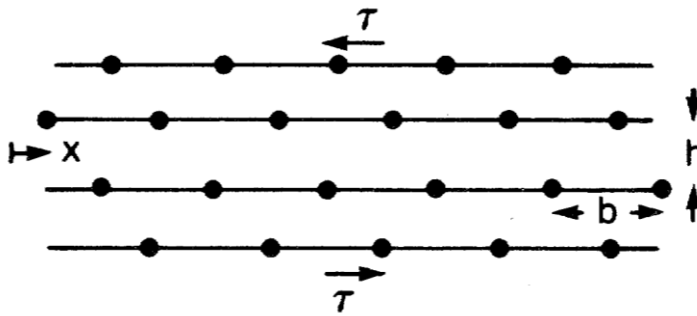


Fig. 2.3 Shear of planes of atoms over one another.

To calculate approximate values for the theoretical shear strength of materials, we will again assume a sine law variation of force with distance. We will consider two adjacent planes in a crystal, separated by a distance h , and containing atoms spaced at distance b (Fig. 2.3). As a shear displacement x occurs, the stress will be given by

$$\tau = k_2 \sin(2\pi x / b) \quad (2.20)$$

(We assume that the stress has a minimum when the atoms are opposite each other, as well as when they are in alternate positions as shown in Fig. 2.3). For small x the displacement will be governed by the shear modulus, G , i.e.

$$G = h \frac{d\tau}{dx} \quad (2.21)$$

for $x \cong 0$, but from equation (2.20),

$$\frac{d\tau}{dx} = \frac{2\pi k_2}{b} \cos(2\pi x / b) \quad (2.22)$$

so that

$$k_2 = Gb / [2\pi h] \quad (2.23)$$

The maximum force occurs when $x = b/4$ and then has the value k_2 . Thus the theoretical shear strength τ_{th} is

$$\tau_{th} = Gb / [2\pi h] \quad (2.24)$$

To estimate τ_{th} we need a realistic value of b/h . Face centred cubic metals, which are the most ductile metals, and hence of particular interest here, do not have simple shear displacements. Slip takes place most easily on (111) planes, which have the atom centres at the corners and centres of hexagons. Thus h is the distance between these planes i.e.

$a_0/\sqrt{3}$ where a_0 is the length of the cubic unit cell edge. b is the distance between nearest neighbour minimum energy positions on this plane, i.e. $a_0/\sqrt{6}$. We conclude, therefore, that

$$\tau_{th} \cong Gb/9 \quad (2.25)$$

If the material is in tension, this shear stress will be produced by a tensile stress of $2G/9$, assuming plane stress, and if the material is assumed to be isotropic, this comes to about $E/12$. Thus equation (2.24) gives a similar answer to equation (2.19). To determine whether shear failure or tensile failure is most likely to occur requires a much more detailed analysis. (This may be found in "Strong Solids": see the list of further reading at the end of the chapter.)

We conclude, finally, that the theoretical strength is some fraction of the modulus. A representative value, useful for comparison with practical strengths, is about $E/15$.

2.2 Dislocations

Although, as indicated in the previous section, the bonding forces between atoms should be able to impart very great strength to materials, the orderly arrangement of the atoms in solids makes deformation and failure possible at very low stresses. Within limits, the more perfect the structure is the weaker it is. This is particularly true with pure metals. The reason for this is that even the most regular arrangements still have occasional imperfections. In a crystal containing 10^{20} to 10^{22} atoms there will always be many places where atoms are missing, and other places where there are too many atoms. There will be still other places where impurity atoms distort the structure, even in the purest of materials.

These "point defects", however, are not the cause of the surprisingly easy deformation found with many pure metals. The main cause are lines of defects called dislocations.

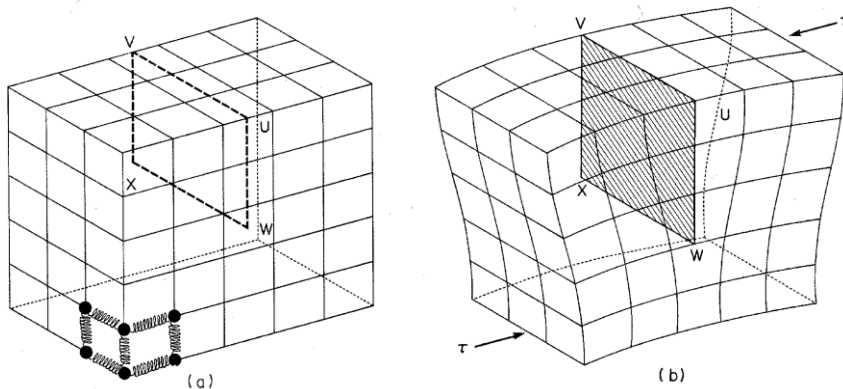


Fig. 2.4 Edge dislocation: (a) position of extra plane; (b) distortion resulting from the presence of the extra plane.

The simplest type of dislocation to visualize is the edge dislocation, shown in Fig. 2.4. The undistorted, or perfect structure, is shown at the left. The atoms are located at the crossing-points of the lines, and can be visualized as spheres, connected by springs to represent the bonding forces. The edge dislocation is equivalent to the insertion of an extra half-plane into the structure. This causes considerable distortion close to where the plane ends (WX) but relatively little elsewhere.

This extra half plane can move very easily across the crystal when there is a shear stress, τ , and results in the deformation shown in Fig. 2.5.

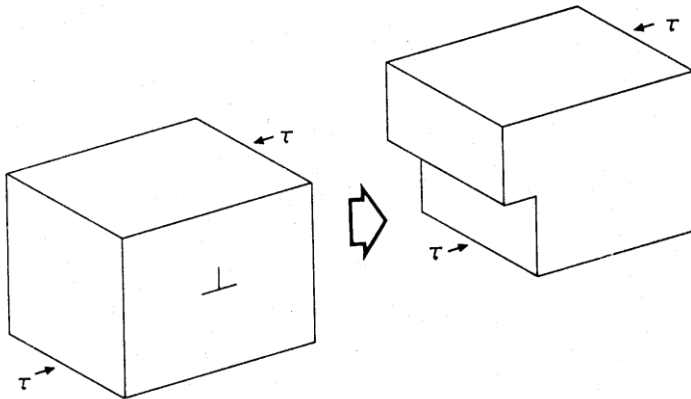


Fig. 2.5 Deformation due to the movement of an edge dislocation to the surface.

The inverted T symbolizes the dislocation. The horizontal part indicates the plane on which slip takes place (the slip plane), and the vertical part indicates the relative position of the extra plane of atoms. Figure 2.6 shows the deformation produced by the motion of many dislocations.

The calculation of the stress required for dislocation movement, the Peierl's stress, is rather difficult. The answer comes to zero for a straight dislocation unless terms of very small magnitude are included in the calculations (all the larger terms cancel out). Its value is very sensitive to the force-distance relation between neighbouring atoms.

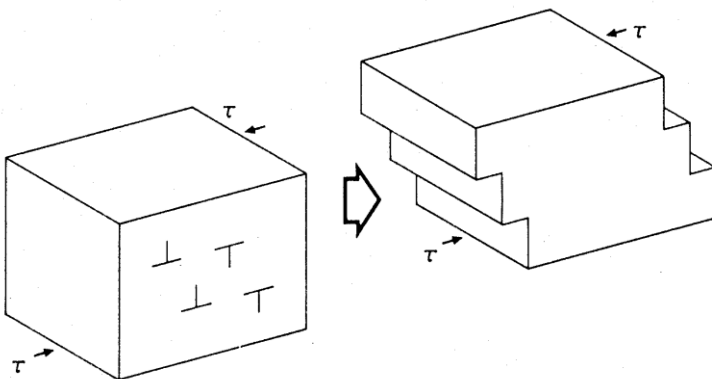


Fig. 2.6 Deformation due to the movement of many edge dislocations to the surface.

Figure 2.7 is a schematic drawing of the atomic positions around an ideal edge dislocation in a simple cubic lattice. If the dislocation width, W , is defined as the total distance in the slip direction, along the slip plane, over which the displacement of atoms

is greater than one-half of the maximum displacement, calculations suggest that the Peierl's stress depends very strongly upon W .

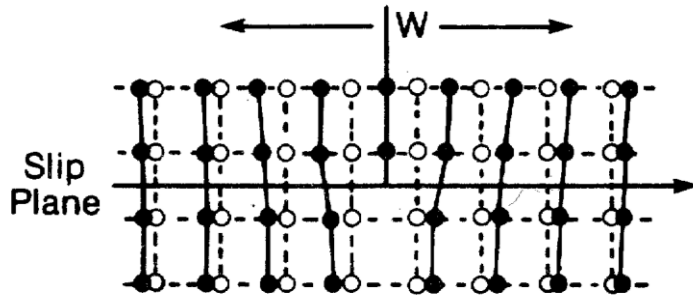


Fig. 2.7 Atomic positions around an edge dislocation.

For example, it has been suggested that

$$\tau = \frac{E}{1-\nu^2} e^{-2\pi W/b} \quad (2.26)$$

where b is the displacement associated with the dislocation, called the Burgers Vector. (Being a vector, it represents the direction as well as the magnitude of the dislocation.) It is usually the distance between neighbouring planes in the crystal lattice, or some fraction thereof. Equation (2.26) gives a very low result for metals. They have W roughly equal to three times b , so that $\tau \sim E/10^8$.

Unfortunately, although dislocations can be seen in the electron microscope, the exact positions of atoms around them cannot be determined, because even in images which appear to show atomic positions, the picture is a smeared-out one, with atoms in many planes (1000 or more) contributing to it.

Calculations of W have not been any more successful than direct observations, and since the Peierls stress is inversely proportional to an exponential function of W , even the order of magnitude of the Peierls stress is subject to considerable uncertainty. Experiments with very pure metals have shown that it can be very low; the more sensitive the apparatus, the lower the result obtained for the stress at which flow starts.

After a small amount of deformation has occurred the flow stress starts to increase. This is due to the generation of large numbers of new dislocations. They interfere with each other, making movement progressively more and more difficult. This process occurs with most metals and is called work hardening.

Dislocations may be regarded as units, or quanta, of slip. In real materials the displacements suffered by the atoms close to dislocations are much more complicated than the simple picture given here. Two limiting types of dislocation have been identified, the edge dislocation, which is the one already discussed, and the screw dislocation shown in Fig. 2.8. With the edge dislocation the slip or displacement is perpendicular to the dislocation line. With the screw it is parallel to the dislocation line.

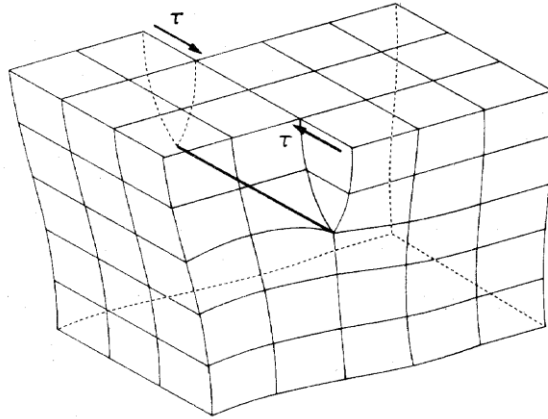


Fig. 2.8 A screw dislocation.

Normally dislocations are a mixture of edge and screw, and to make matters even more complicated, they often sub-divide themselves into partial dislocations. These involve smaller displacements of the atoms. In addition, the simple cubic structure pictured here does not adequately represent the arrangement of atoms in crystal lattices. The simplest crystals can be represented by cubic units, but with additional atoms at the centres of each face of the cube. The edge dislocation is thus not as simple as indicated in the drawings, and its movement is more tortuous than the linear movement indicated.

The complicated nature of dislocations, their generation and their interactions, has made quantitative predictions of mechanical properties very difficult. but they have been very useful in giving insight into the mechanical behaviour of materials, especially metals. They explain, in a qualitative fashion, why metals deform so easily; dislocations can be seen to move in the electron microscope under forces which are very small compared with atomic binding forces. The difficulty dislocations have in crossing crystal boundaries into neighbouring crystals explains why fine-grained materials usually have higher yield stresses than materials with large crystals. Their interactions with precipitates within metals helps to account for the improvements in mechanical properties that can be obtained by using alloys rather than pure metals, and suggests ways in which still better alloys may be developed.

Softening as well as hardening effects can be explained. Annealing causes the disappearance of large numbers of dislocations, as well as some recrystallization. Thus, when a work-hardened metal is annealed and subsequently deformed, the few dislocations remaining can move with relatively little interference from other dislocations.

These are just a few examples of the long list of effects which can be understood, or at least in which insight has been gained, by the use of explanations involving dislocations.

2.3 Notches and Cracks

To obtain strong metals it is necessary to interfere with dislocation motion so that plastic flow does not occur at low stresses. Our understanding of how to do this has

improved steadily in recent years, but it has been found that there is a limit to this method of improving materials. Aluminium alloys with yield strengths greater than 0.45GPa and steels with yield strengths greater than 1.4GPa have been known for more than 75 years. But they may only be used in a few carefully chosen applications and then only with great care. The reason for this is that when the ratio of the yield stress to the modulus reaches a certain value, the material no longer has sufficient ductility to make the necessary internal adjustments to alleviate the effect of the excess stresses that are to be found around the holes, notches, and cracks that are always present in most structures, even the most carefully built ones.

2.3.1 Stress Concentrations

Inglis originally showed in 1913 that the stresses close to the tips of cracks could be much higher than elsewhere in a piece of material. He did this by determining the stresses around elliptical holes. The ellipse is a particularly suitable shape for this purpose, because at one extreme value of the ellipticity (the ratio of major axis to minor axis) it is a circle, and at the other extreme it is an infinitely thin crack. Thus it can be used for cracks ranging from sharp ones of the utmost severity to mild cracks and round holes. In addition, the stresses and strains can be expressed completely in algebraic form (though they are rather cumbersome).

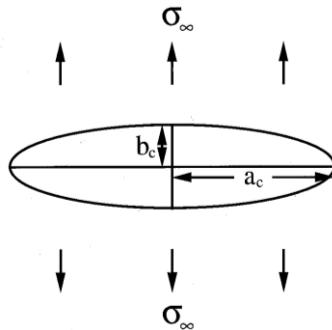


Fig. 2.9 An elliptic crack.

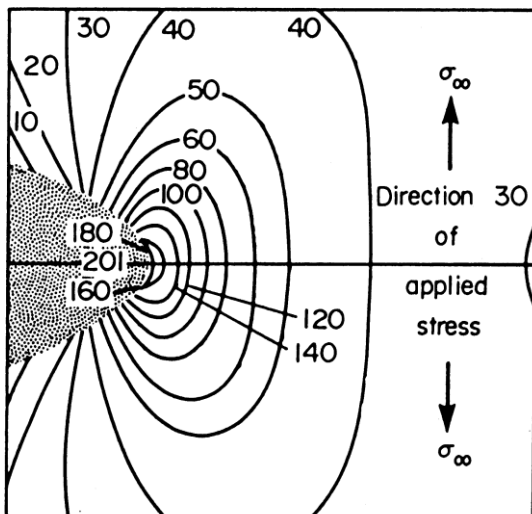


Fig. 2.10 Stresses near the tip of an elliptic crack. (After Gordon, J.E., 1964 Proc. Roy. Soc. A282. 508-520.)

Figure 2.9 represents an elliptic crack in a material under a stress σ_∞ normal to the crack plane. Figure 2.10 shows how the stresses are concentrated around the crack tip. The lines are loci of constant stress concentration, and the numbers indicate the amount by which the stress is multiplied. For such a sharp crack as this, where the ellipticity is 100 (i.e. the major axis of the ellipse is 100 times longer than the minor axis) the curvature at the crack tip is very sharp, and the stresses are correspondingly very high. At the crack tip the stress is 201 times greater than the applied stress.

In addition to the stresses in the same direction as the applied stress, there are stresses in directions at right angles to this. Figure 2.11 shows the stresses in the direction of the major axis of the ellipse.

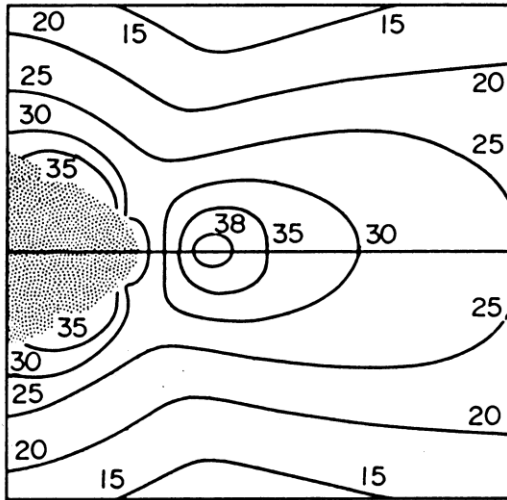


Fig. 2.11 Stresses at right angles to the stress applied to an elliptic crack. (After Gordon, J.E., 1964, Proc. Roy. Soc. A282, 508-520.)

The stresses in the crack plane are also shown in Figure 2.12. Here σ_y is the stress in the direction of the applied stress (σ_∞) and σ_x is the stress in the direction of the major axis of the ellipse. There are also stresses normal to the plane of the sheet.

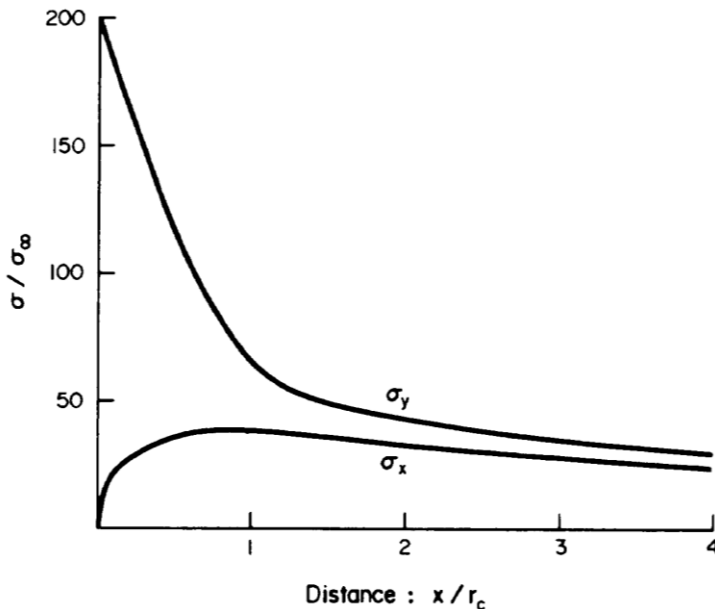


Fig. 2.12 Stresses near a crack tip. The applied stress (σ_∞) is in the same direction as σ_y ; $a_c/b_c = 100$. r_c is the radius of the crack tip.

Although the stresses at right angles to the applied stress are much smaller than those in the same direction as the applied stress, their effect is very important. The material close to the crack tip is subject to tensile forces in all directions, and this triaxial stress system inhibits shear flow. When the sheet is thin this is not very serious, the stress normal to the sheet being relatively small. Thus, if the material is ductile enough, some plastic flow can take place which will relieve the stresses and round off the crack tip. However, if the sheet is thick, and not particularly ductile, high stresses are developed normal to the sheet, stress relaxation is not so likely to take place, and brittle fracture is facilitated.

The maximum stress at the crack tip in a sheet, under tensile stress σ_x , along the direction of the minor axis of the ellipse (the stress being applied a long way away from the crack), is given by the equation

$$\sigma_{tip} = \sigma_{\infty} (1 + 2e) \tag{2.27}$$

where e is the ellipticity, a_c / b_c (see Figure 2.9). This formula only gives accurate values when the width of the sheet is very much greater than a_c , and the crack is not close to the edge of the sheet. If the radius of the crack tip is r_c , then the expression can also be written

$$\sigma_{tip} = \sigma_{\infty} (1 + 2\sqrt{a_c / r_c}) \tag{2.28}$$

This equation has been found to give about the correct answer for the stresses at the tips of cracks in the surfaces of materials if the 1 is neglected. It is not even necessary for the cracks to be elliptical. Figure 2.13 shows examples of cracks and steps to which this formula has been found to apply with reasonable accuracy.

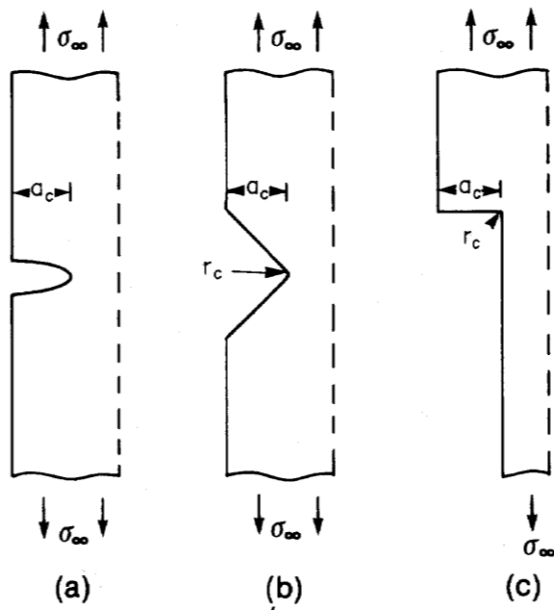


Fig. 2.13 Cracks and steps with stresses that obey the equation $\sigma_{tip} = \sigma_{\infty} (1 + 2\sqrt{a_c / r_c})$.

For very sharp cracks, or surface steps, very high stress concentrations are possible. If the crack or step has atomic dimensions at the tip, i.e. $r_c \sim 0.3$ nm, the height

of the step or depth of the crack only needs to be $0.75\mu\text{m}$ for a stress concentration factor of 100 to exist at the crack tip. Thus a material in which dislocations cannot move, or which contains no dislocations and so cannot yield under stress, is in danger of having the atomic bonds at the crack tip stressed to the breaking point when relatively small forces are applied to it.

This appears to be what happens in the case of glass. Glass does not have a regular structure, so dislocations cannot exist within it. It is very hard to produce any plastic effect in glass at room temperature; even a very sharp diamond, after being pressed into glass, leaves only a very tiny impression. The surface of ordinary glass is found to have millions of tiny cracks in it. These cracks form spontaneously, probably due to water vapour in the air, but are also caused by the surface coming into contact with hard materials during manufacture. Since glass has a theoretical strength of about $E/10$ or 7GPa, and yet its strength is normally only about 70MPa, we might conclude that the cracks need only have a length of about a micron if the tip has atomic dimensions. However, we also need to consider whether crack propagation is energetically favourable, since if no energy is released by the fracture process, it cannot occur spontaneously.

2.3.2 Energy Considerations

In 1920 A. A. Griffith explained why the tendency of a material to fracture does not depend only on the severity of the crack. There is a size effect also; thus for two notches having the same value of a_c / r_c but different sizes, the larger notch is much more likely to cause failure than the smaller one.

Griffith went on to show that energy must be continuously released for crack propagation to occur. Where this energy comes from appears to have been a much misunderstood matter by earlier exponents of the theory.

A cracked sheet, loaded by, for example, a hanging weight, has more elastic strain energy than a similar sheet without the crack. (The elastic strain energy of an element of material is one-half of the product of the stress, the strain, and the volume of the element.) The extra strain energy results from the stress concentration, which raises the average stress level, and also increases the strains. This extra energy is provided by the loading system, the hanging weight in our example. We find that the cracked sheet is more easily deformed (more compliant) than the uncracked one. Thus the weight moves further down when loading it, providing the extra energy needed, with an equal amount left over.

It was Griffith who showed that the potential energy of the system applying the forces (the weight) must decrease by exactly twice the extra energy due to the stress-concentrating effect of the crack. Thus the overall decrease in energy, i.e. the decrease in potential energy minus the increase in strain energy, is exactly equal to the increase in strain energy of the body due to the presence of the crack.

When other loading methods, such as fixed grip systems are used, the result is the same, but the analysis is slightly more complicated.

Some extra energy is required for the production of a crack, however. This is the work done in separating the atoms on one side of the crack face from those on the other side. In an ideal non-yielding solid, this work is equal to the surface energy of the solid ψ , multiplied by the total area of surface produced. The total extra energy per unit thickness due to a crack with vanishingly small width, b_c , in a thick sheet of the ideal solid is

$$U = 4a_c\psi - \pi\sigma_\infty^2(1 - \nu^2)a_c^2 / E \quad (2.29)$$

where ν is Poisson's ratio, and E the modulus of the solid. The first term is the energy absorbed in the production of new surface, and the second term is the energy released due to the loading system. (The second term is the same for a constant weight loading, and for fixed grip loading.)

For a crack to extend, the rate of release of elastic energy as a_c increases must exceed the rate of increase of the total surface energy for the same increase in a_c . The limiting case is when the two are equal. This is when $dU/da_c = 0$. Since

$$\frac{dU}{da_c} = 4\psi - \frac{2\pi\sigma_\infty^2(1 - \nu^2)a_c}{E} \quad (2.30)$$

this is when

$$\sigma_c^2 = \frac{2E\psi}{\pi(1 - \nu^2)a_c} \quad (2.31)$$

Equation (2.31) predicts that the failure stress should be inversely proportional to the square root of the crack length. Griffith showed that this relationship was obeyed by glass, and that an equation similar to (2.31) was quantitatively correct if ψ was equated with surface energy. We now know that there were some slight errors in his analysis, and that ψ calculated from fracture experiments with glass is three to ten times higher than the surface energy.

We can now calculate the crack length required for glass to fracture at its normal breaking strength, i.e. 70MPa. We use the value of E from Table 1.1 and half the work of fracture (Table 1.2) for ψ (ψ is only the work to fracture 1m^2 of material, since the fracture produces 2m^2 of new surface). Equation (2.31) produces the result $a_c = 50\mu\text{m}$.

At the end of section 2.3.1 we showed that if cracks in glass had atomically sharp tips, a crack only one micron long in a sheet stressed to 70 MPa would generate a stress equal to the theoretical strength at the tip. Clearly, if the crack has to be 50 microns long for failure to be energetically favourable, the crack tip radius must be several interatomic distances in order that the theoretical strength is not exceeded.

Since a crack in such a brittle material is not atomically sharp, we need to examine the concept of surface energy in more detail and see if it can indeed be used for ψ in the Griffith equation (equation (2.31)).

2.3.3 Surface Energy

The Griffith theory described above requires that the elastic energy released exceeds the surface energy required to produce the new fracture faces. The surface energy for solids, though larger than for liquids, is rather small, as can be shown by calculating it directly from the interatomic forces, as follows.

The surface energy is the energy associated with the unsatisfied interatomic bonds at the surface. These can be: (a) primary bonds, for example the electrostatic forces at the surface of a freshly cleaved sodium chloride crystal in a perfect vacuum; or (b) secondary bonds such as the hydrogen bonds that hold water molecules together, and create the surface tension that keeps the surface area of water droplets as small as possible.

We may calculate the surface energy of a solid by estimating the work needed to separate the atoms on either side of a plane in the solid. They must move sufficiently far apart that the interatomic forces have fallen to zero. The work required to do this is equal to the area under the force-distance curve in Fig. 2.2, between the equilibrium distance, a_1 , and infinity. For simplicity, we will consider unit area of cross-section. This will produce two surfaces. Thus

$$2\psi = \int_{a_1}^{\infty} \sigma dx \quad (2.32)$$

Substituting for σ using equation (2.8) and dividing both sides by 2 we obtain

$$\psi = \frac{1}{2} \int_{a_1}^{\infty} (Ax^{-n} - Bx^{-m}) dx \quad (2.33)$$

Integrating and evaluating this expression gives

$$\psi = \frac{1}{2} \left(\frac{Aa_1^{1-n}}{n-1} - \frac{Ba_1^{1-m}}{m-1} \right) \quad (2.34)$$

and substituting $B = Aa_1^{m-n}$ and $E = A(m-n)a_1^{-n}$ we find that

$$\psi = \frac{Ea_1}{2(m-1)(n-1)} \quad (2.35)$$

We can now estimate the values of ψ for materials for which m and n are known, together with E and a_1 .

For many materials the interatomic separation is roughly 0.25nm and $(m-1)(n-1)$ is of the order of 20. For metals and inorganic crystals E is in the range 10 to 1000GPa. Thus ψ should be in the range 0.05 to 5Jm⁻² for metals and inorganic materials, and somewhat less for polymers due to their lower moduli. Iron, for example, with $m = 7$ and $n = 4$ should have a surface energy of about 1.5Jm⁻².

These values are very low compared with most of the works of fracture given in Table 1.2. Maraging steel, which is mostly iron, has a result which is 40,000 times higher. Although 2ψ rather than ψ should be compared with the work of fracture, this still leaves a factor of 20,000 to account for.

2.3.4 Fracture Toughness

Nearly 30 years after Griffith published his work on glass, G.R. Irwin, observing that metals obeyed the same expression for fracture failure, i.e. $\sigma_\infty^2 a_c = \text{constant}$, used \mathcal{G} , the work of fracture, instead of 2ψ . Thus,

$$\sigma_\infty^2 = \frac{E\mathcal{G}}{\pi(1-\nu^2)a_c} \quad (2.36)$$

It is clear that \mathcal{G} is analogous to the surface energy. Since it is usually so much greater than 2ψ we conclude that fracture failure involves a great deal more than simply separating the appropriate atoms. That this is so can easily be demonstrated by examining the fracture surfaces of any fairly tough piece of material. It will be observed that a great deal of plastic work has been done on the metal near the new surface.

The fracture toughness for failure of the type we have described is defined by the expression:

$$\mathcal{K}_{Ic} = \sigma_\infty \sqrt{\pi a_c} \quad (2.37)$$

when the applied stress, σ_∞ , is sufficiently great to break a piece of the material, having a crack of length $2a_c$, in the centre, or of length a_c if it is at the edge. When σ_∞ is smaller than this,

$$\mathcal{K}_I = \sigma_\infty \sqrt{\pi a_c} \quad (2.38)$$

and \mathcal{K}_I is the stress intensity factor. \mathcal{K}_{Ic} is often referred to as the critical stress intensity factor. (There are also a \mathcal{K}_{IIc} and a \mathcal{K}_{IIIc} for cracks loaded in shear instead of in tension). \mathcal{K}_{Ic} and \mathcal{G} are thus related:

$$\mathcal{G} = (1-\nu^2)\mathcal{K}_{Ic}^2 / E \quad (2.39)$$

The fracture toughness is measured by determining the compliance of a specimen at the instant a crack of known size in it starts to propagate. Alternatively \mathcal{G} may be measured by determining the work required to propagate a crack slowly through a known distance in the material. The stress may be applied by tension, or flexure of the specimen. It is essential that the crack is extremely sharp, otherwise \mathcal{G} and \mathcal{K}_{Ic} are overestimated. This is ensured, in the case of metals, by notching the metal, and then fatiguing it so that the notch extends a few mm further. Corrections are made for notches that cut through a significant fraction of the cross section of the specimen, and precautions have to be taken to ensure that the specimen is sufficiently thick for the test to be valid. (The tougher the material, the thicker the specimen has to be.)

Older methods of measuring toughness are still widely used, especially for polymers and composites. Two important methods involve impact of a heavy hammer against a notched bar. The Charpy method uses a pendulum to strike a specimen in such a way that it is loaded in three-point bending. The energy lost by the pendulum is measured. For polymers and reinforced plastics the result is usually given as so many foot pounds of energy per inch width of notch. The specimen has a standard thickness in the direction of which it is struck (12.7mm), and a standard notch depth of 2.54mm. For 1-inch width of notch the broken surface has an area of $0.258 \times 10^{-3} \text{ m}^2$ (0.4 sq. inches), so 1 ft-lb/inch of notch is equivalent to 5.26 kJm^{-2} . For metals the specimen has a standard size of 10mm x 10mm and the notch depth is 2mm. Sub-size specimens (each dimension halved) are also sometimes used.

The Izod test operates on the same principle, except that the specimen has one end fixed in a clamp, and the pendulum breaks off the protruding end. The specimen dimensions are the same as for the Charpy test.

(Both tests are sometimes carried out on "unnotched" specimens. This is usually done with brittle materials, since otherwise the energy absorbed is too small to be measured accurately. With reinforced plastics this is done simply by reversing the notched specimen, so that the notch tip is under compression; with ceramics a round unnotched bar is used.)

Both tests can be improved by providing sensors to measure the forces exerted by the impacting hammer. These are called instrumented impact tests. A plot of force during impact vs. time is obtained using a fast recorder such as an oscilloscope. Use of these plots can eliminate some of the inaccuracies arising from the method, and \mathcal{K}_{Ic} values may be obtained directly.

Further improvement has resulted from making measurements at different notch depths and plotting the \mathcal{K}_{Ic} values obtained as a function of a_c . (\mathcal{K}_{Ic} , of course, has to be corrected for each a_c value, since a_c is a significant fraction of the total cross section in the tests). The plot normally has a plateau region where \mathcal{K}_{Ic} is independent of a_c . The value of \mathcal{K}_{Ic} in this region is the value required.

Another type of test is the Slow Bend Test. In this test the specimen is notched in such a way that the crack propagates slowly across the remainder of the cross-section. The work of fracture is calculated from the area under the force - distance curve. If unstable fracture occurs and the crack propagates quickly across the specimen the test is invalid, and a different shape of notch must be used.

2.4 Practical Limits for Strength

We have shown that the theoretical strength is very large and determined by the chemical bond strength. However, such high strengths are not normally achieved in

practice for one of two reasons. Either dislocations can move at low stress, leading to early failure by slip and plastic deformation, or the material is brittle, and can fail at very low stresses by the propagation of cracks which start at tiny imperfections, often too small to be seen except with powerful microscopes.

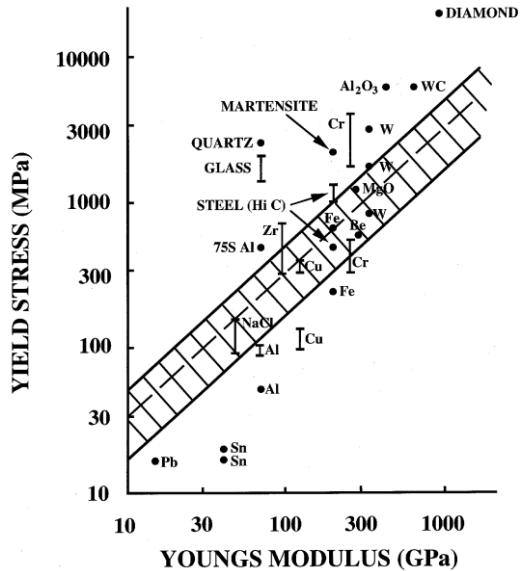


Fig. 2.14 Yield stress vs E indicating ductile-brittle transition. (After Piggott, M.R., 1975, *Int. J. Fracture* 11, 479-88.)

With metals it is possible to interfere with dislocation movement, and so increase the strength. However, this makes the materials more susceptible to brittle failure. This is illustrated in Fig. 2.14 which is a plot of yield stress vs. Young's modulus. A number of values have been plotted for metals to indicate the range of yield stresses that can be achieved. The hatched area indicates the transition region between ductile and brittle materials. Materials such as glass, quartz, and diamond are well in the brittle region. (They can be ductile at high temperature, however, since this decreases the yield stress.)

It is clear from Fig. 2.14 that if we want high strength coupled with adequate toughness we must use a material with a high modulus. The practical maximum strength of steel is about three times that of aluminium, and that of tungsten is higher still. In fact, a dimensional analysis predicts that serious brittleness occurs when the yield strain exceeds a constant value. Experience shows that it should not exceed about 0.007.

Also, we cannot allow the strains to become too high, as is graphically demonstrated in Fig. 1.7.

Usually we want a material that is light as well as strong and tough. Unfortunately, this does not appear to be possible with traditional load-bearing materials, since E/ρ is approximately constant for them (see Table 1.3).

A new approach is clearly needed. Fibre reinforced materials provide this.

Further Reading

- Hull, D, (1968), *Introduction to Dislocations*, (Pergamon Press, Oxford).
 Rolfe, S.T. and Barsom, J.M, (1977) *Fracture and Fatigue Control in Structures*, (Prentice-Hall, New Jersey).
 Kelly, A. and Macmillan, N.H. *Strong Solids* (Clarendon Press, Oxford, 3rd ed. 1986), Chpt. 1.

Chapter 2: Problems

You are strongly recommended to solve these problems in the order given. Data needed will be found in tables in this and other chapters of the book.

- 2.1 Calculate the theoretical cleavage strength for nickel, which has $m = 7$, $n = 4$ and $E = 200\text{GPa}$.
- 2.2 Calculate the strain in silicon at the onset of cleavage at the theoretical maximum stress, given that $m = 12$ and $n = 8$ for this material.
- 2.3 Copper is face-centred cubic with $E = 130\text{GPa}$ and the same values of m and n as nickel. At what stress does the theory indicate it should fail, and what would be the expected mode of failure?
- 2.4 Calculate the theoretical cleavage strength of iron, following the same reasoning as in section 2.1, but using a parabolic force-distance law, instead of the sine law given in equation 2.1. For iron $E = 212\text{GPa}$. (Note: you must first show that the parabolic law has the form $\sigma = (3a_1x - x^2 - 2a_1^2)$).
- 2.5 If we assume that the dislocation width can be calculated from the Peierl's stress, what would the value be for pure annealed aluminium yielding in tension at 57MPa , with $b = 0.25\text{nm}$?
- 2.6 Estimate the width of a dislocation in alumina from the hardness, assuming its Burgers vector is 0.475nm .
- 2.7 A specimen with a notch in its centre, 3.70cm long, was used for measuring the toughness of a magnesium alloy. The specimen was fatigued before testing, and the notch increased in length due to the formation of very sharp cracks at each end, 0.17cm long. When tested, the crack started to propagate when the stress was 63MPa . What was the work of fracture of the specimen?

- 2.8 A round tungsten bar, 2.51cm diameter, has a very sharp crack in it which is 1.1mm deep. If it is loaded up till it breaks, what weight would it be supporting at the moment of fracture?
- 2.9 If the rod described in question 2.8 was replaced by one of maraging steel with the same load carrying capacity when unnotched, what weight would it support if it had the same size of notch.
- 2.10 An oblong steel beam, used to support a small bridge, failed by brittle fracture. It was found to have been incorrectly heat treated, and had a work of fracture of only 10.1Jm^{-2} . Failure was initiated by a crack in the lower surface of the beam, 0.71mm deep and 1.31m from the centre. It was designed to bear a maximum stress of 220MPa. Compare the weight needed to cause failure and the design maximum weight. The weight is supported by loading the beam at its centre, the beam has a span of 4.8 m, a width (b_1) of 0.051m and a depth (d_1) of 0.21m, see Fig. 1.12. (Hint, to calculate the stress at the cracked section, calculate the internal bending moment, M , from the moment of the applied forces, and use $MR = EI$. The strain near the surface, and hence the stress, can be calculated from R ; you may assume that the region around the crack is at approximately constant stress; alternatively, the equations on p. 20 may be used.)
- 2.11 Estimate the depth of deformed zone at each crack surface for an aluminium alloy which has fractured with $\mathcal{G} = 260\text{kJm}^{-2}$. The yield strength of the material is 120MPa, and X-ray analysis showed that the plastic strain in the deformed zone was 0.98. Assume the material is perfectly plastic.
- 2.12 A rod 0.95mm diameter was used to support a 5.6kg load on a machine used to measure creep. The rod was made from brass, and was strong enough to support a load of 16.7kg. It was, however, brittle, and failure at the maximum load was caused by small surface flaws 7.6 μm deep. Because of this brittleness, care is needed when loading the machine, so that the 5.6kg weight is not released at a level much higher than its working position. What is the maximum height that the load can fall through without the wire breaking? For the brass $\nu = 0.350$ and $E = 101\text{GPa}$.
- 2.13 A ship's hatchway has a tiny crack at one of its corners where it is welded to the steel deck plates. If the crack extends into the plates for a distance of 0.80mm, and is oriented at right angles to the stress in the deck, what would the stress have to be if the work of fracture of the steel is 2.65kJm^{-2} ? The hatch is 4.00m square and has corners rounded to 25mm, and has one side parallel to the stress. If the stress concentration due to the hatchway falls off with distance from the hatch as the reciprocal of the square root of distance, so that it has fallen to one half of its maximum value at a distance of 12.5mm, determine the average stress required in the deck plates for the crack to extend right across the deck.

Chapter 2. Selected Answers

2.1 13.5GPa

2.3 8.8GPa; cleavage

2.5 0.32nm

2.7 5.12kJm⁻²

2.9 83tonnes

2.11 1.11mm

2.13 26.2 MPa and 13.0 MPa

3. FIBRES, WHISKERS AND PLATELETS

We have shown in Chapter 2 that there is a limit to how far we can go with traditional materials in the search for high strength with adequate toughness and low density. In this chapter we will show that slender forms of material provide an alternative of great potential.

3.1 Slender Forms of Material

If we make a piece of material small enough, we can suppress the weakening due to fracture, and that due to dislocation movement.

Consider fracture first. To achieve a strength of about the theoretical value, i.e. $E/15$, we must make the cross section of the material such that no diameter can contain a crack of length longer than a_c where

$$\left\{ \frac{E}{15} \right\}^2 = \frac{E\mathcal{G}}{\pi a_c (1 - \nu^2)} \quad (3.1)$$

(This is equation (2.36) with $E/15$ replacing σ_∞ ; \mathcal{G} is the work of fracture). For $\nu \cong 0.3$,

$$a_c \cong 80\mathcal{G}/E \quad (3.2)$$

For alumina this comes to about 4 nm using the data given in Chapter 1. Thus an alumina fibre of 4nm diameter should have the theoretical strength.

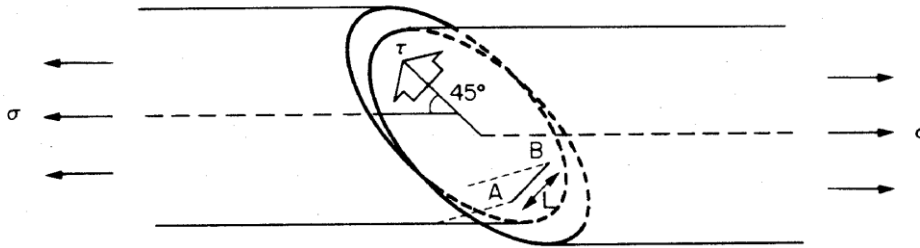


Fig. 3.1 Frank-Read source in a rod. Dislocation is fixed at A and B.

Now consider failure resulting from dislocation movement. Ductile failure does not result directly from the movement of dislocations initially present. Instead, a dislocation generator or multiplier is needed. The Frank-Read source is the most important of these, and consists of a dislocation which is held at its ends. (It can be held by other dislocations oblique to the slip plane, or by precipitates, etc.) Figure 3.1 shows a dislocation fixed at A and B. The stress required to generate dislocations depends on the length $AB (=L)$, and is given by

$$\tau = 2Gb / L \quad (3.3)$$

b being the Burgers vector and G the shear modulus.

Suppose this dislocation is in a slip plane at $\pi/4$ to the applied stress, as shown in Figure 3.1. It will then permit slip at the lowest possible stress, and we can write

$$\sigma = 2 \tau = 2Gb / L \quad (3.3)$$

Thus for $\sigma = E/15$, the theoretical strength, $L \sim 24b$ for materials with $G \cong E / 2.5$. Now $b \sim 0.25\text{nm}$, so a ductile fibre with a diameter of about 6nm should have the theoretical strength.

We, therefore, conclude that slender forms of material can achieve the theoretical strength. The dimensions required are somewhat impractical, though.

Fortunately, when we examine fine forms of material we find that they can be extremely strong. Fibres of glass with very smooth surfaces can be made quite easily. Although flaws are normally present, the strength of these fibres is very great: with pure silica it can reach 6GPa at 20°C and nearly 10GPa at -196°C, when free of flaws, while normal production glass fibres have strengths of 3GPa or more. When fine wires are made they are intensely worked. This causes a great deal of disorganization of the crystal structure, so that dislocations cannot multiply or move, except at very high stresses. At the same time the surface of the wire is quite smooth, so that fracture failure also is inhibited. Thus fine wires can also be made which are very strong indeed.

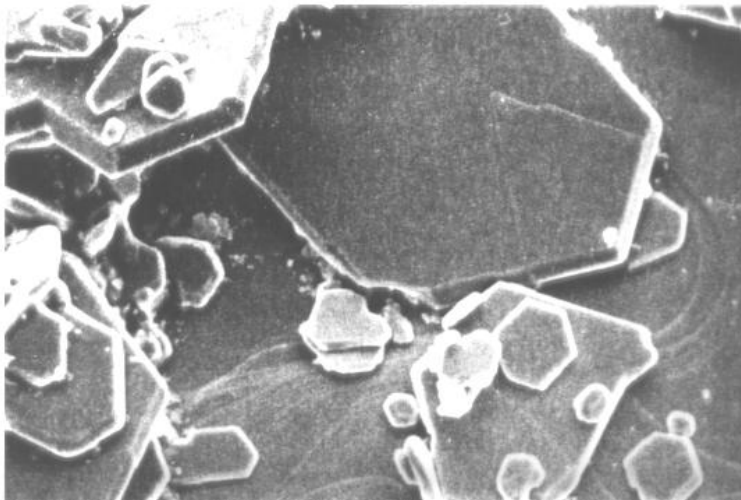


Fig. 3.2 Chromium oxide platelets. (Courtesy of R.T. Woodhams, University of Toronto.)

Potentially the most promising material for high strength, coupled with low density and high modulus, is the single crystal whisker. These are about 1 μm in diameter and have lengths of up to a few mm. Their faces are crystallographic planes, so that they have rectangular or diamond-shaped cross-sections. The surfaces are generally very smooth so that fracture is suppressed, and they usually contain just one screw dislocation, which is near the centre, and parallel to the fibre axis. Their strength can be quite close to the theoretical strength, and their stress-strain plots show slight curvature near the

breaking stress, even while they are still perfectly elastic. This is because the interatomic force-distance curve, Fig. 2.2, is linear only at low strains.

Still another form of strong material is the microplate, or platelet. Quite a number of compounds can be made to grow in laminar form, and mica is a well-known example. Figure 3.2 shows another example of this type of material. Although these compounds are potentially strong because dislocations are not usually mobile in them at 20°C, they must have smooth edges to have high strengths.

The importance of size and shape is illustrated in Fig. 3.3 which shows the strength of SiC in various forms.

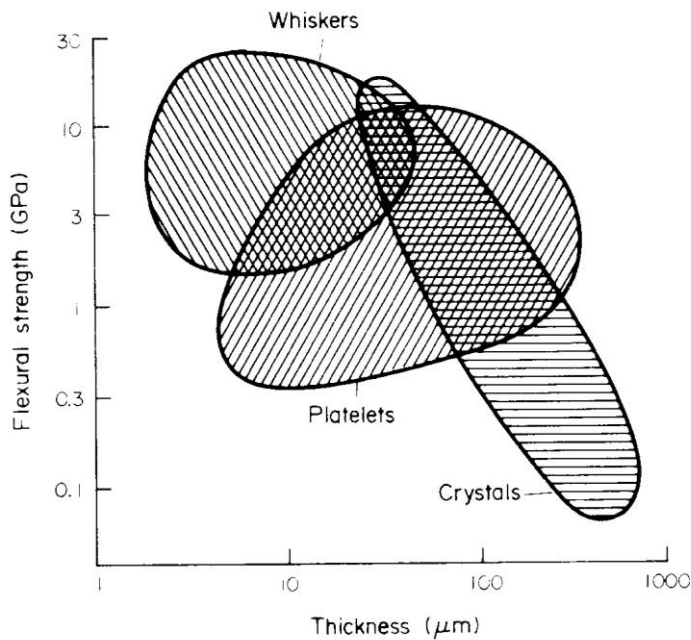


Fig. 3.3 Strength of various forms of silicon carbide.

3.1.1. Choice of Materials

Although slender forms of material can be very strong, to use them we shall need to put them into some type of matrix which will transfer the loads to them, and should ideally not allow them to transmit their inherent brittleness to the composite structure. If we assume for the moment that this can be done, we are free to choose our materials so that we can produce slender forms with maximum strength and modulus and minimum density.

For light weight we choose elements in the first two rows of the periodic table. We can use them either in elemental form, or as compounds. The elements or compounds should preferably be covalently bonded for the highest bond strengths in two or three dimensions.

Elemental carbon is one of the best examples. The three-dimensional covalently bonded structure of diamond has a very high modulus and a very low density. So does

the two-dimensional covalently bonded structure of graphite, though this is stiff and strong only in one plane. Some electrovalent compounds are also potentially very strong. Thus, as candidate materials we have Be, B, C, B₄C, B₁₃O₂, B₆Si, Al₄B₃, SiC, Si₃N₄, BeO, and Al₂O₃. These all have moduli in the range 400-1000GPa, and low densities. They also have very high melting (or sublimation) points.

While these elements and compounds are best in theory, in practice many other materials can be made in slender form, having excellent properties. An important consideration is the cost of making the fibres, and making high quality composites from them. In fact, a very wide range of fibres is available.

3.2. Polymer Fibres and Metal Wires

Polymer fibres and metal wires have been used by man for thousands of years. Many natural fibres have excellent properties, especially when their low densities are taken into account. Table 3.1 (p 60) lists the properties of some polymers and metals. It can be seen that the best natural polymers have strengths which are as much as one-fifth of the theoretical strength (assuming this is $E/15$).

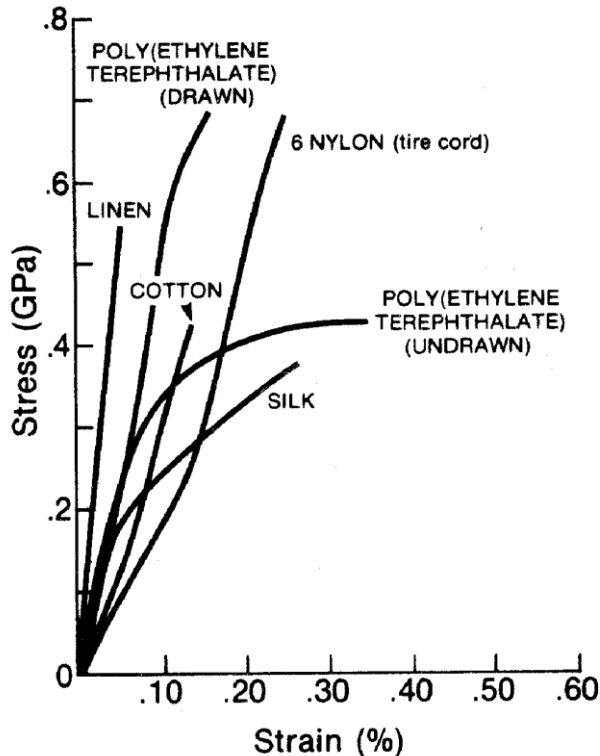


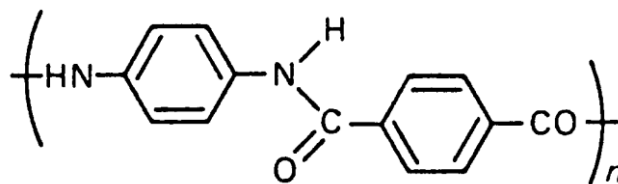
Fig. 3.4 Stress-strain curves for polymer fibres. (After Billmeyer, F.W., (1971), Textbook of Polymer Science, Wiley Interscience, New York, p. 516.)

The chief drawbacks of natural fibres are that they are affected by water, which reduces their strength and stiffness, and are subject to attack by fungi. Synthetic polymers were, until recently, characterized by very low moduli. Whereas flax and wood cellulose fibres have Young's moduli near 100GPa, nylon and polyester (polyethylene terephthalate) have moduli between 1 and 3GPa (see Table 3.1). The stress-strain curves

for most synthetic and natural polymers are far from linear. Figure 3.4 gives some examples. Both natural and synthetic polymers are very sensitive to heat. Few can withstand temperatures much in excess of 150°C, and marked loss in strength occurs with some of them (especially nylon) below 100°C.

Recent research however has shown that synthetic polymers can be made which have very high strengths and moduli. Furthermore, polyethylene, normally a very weak and low modulus material, can be drawn into high performance fibres when sufficiently high draw ratios are used.

Polyethylene fibres, marketed by Allied chemical with trade names Spectra 900 and 1000, are made from highly drawn ultra high molecular weight polyethylene. 53% of the theoretical Young's modulus (about 320MPa) is achieved by Spectra 1000, and the strength/density ratio is particularly notable (see Table 3.1). Their resistance to reactive chemicals and organic solvents is excellent, but their low melting point (147°C) makes them inadvisable for use above 100°C. Their transverse modulus is very low (1.49GPa) and their compressive strength is also low (~ 70MPa) and, as with normal polyethylene, they cannot easily be bonded to polymer matrices. Other manufacturers of high performance polyethylene fibres include Toyoba (Japan) and DSM (Netherlands).



Poly para-phenyleneterephthalamide

Polyaramid fibres, with structure shown above, have a lower theoretical modulus (250GPa), of which about 64% is achieved by Du Pont's Kevlar 149, see Table 3.1. (Other manufacturers, e.g Akzo-Enka and Teiju also produce polyaramids, but with lower properties.) Du Pont also produces Kevlar 29, which has a Young's modulus of about 70 GPa and Kevlar 49 with a modulus of 130GPa. Kevlar 49 is widely used as a reinforcement for polymers.

The stress-strain curve is concave up, i.e. the stiffness is relatively low at low stresses. While strong in tension, the fibres are rather weak in compression (0.3 to 0.5 GPa). The compressive modulus is also low (~ 65GPa) and the transverse modulus is very low (2.49GPa) and they tend to kink in compression, see Fig. 3.5. They are not quite so chemically resistant as polyethylene, but much more resistant to heat. Kevlar is completely stable at 150°C, but loses strength slowly at 200°C, while at 250°C, after 8 hours, its strength has decreased to about 70% of its initial value, and it continues to decline at a decreasing rate thereafter. It carbonizes at about 425°C. At liquid nitrogen temperature it retains full strength and toughness. Polyaramids are very resistant to most organic solvents, but they absorb some water without a significant effect on the strength.

Table 3.1 Properties of natural and high performance synthetic fibres and metal wires

	Material	Density (Mg m ⁻³)	Strength (GPa)	Young's Modulus (GPa)	Diameter (μ m)
Natural Polymers	Cotton	1.50	0.35	1.1	
	Flax		0.9	110	
	Silk	1.25	0.5	1.3	
	Wool	1.3	0.36	6	
	Wood (kraft paper)	~1.0	0.9	72	
Synthetic Polymers	Cellulose (Fortisan)	1.52	1.1	2.4	
	Polyester (thermoplastic)	1.38	0.6	1.2	
	Nylon	1.14	0.8	2.9	
	Spectra 900 TM	0.97	2.6	120+	38
	Spectra 1000 TM	0.97	3.0	170+	27
	Kevlar 49 TM ‡ TM	1.44	3.6	130*	12
	Kevlar 149‡ TM	1.47	2.41	160	12
	PBO	1.47	5.8	365	10
PBZT	1.47	4.2	330	10	
Metals	Beryllium	1.8	1.3	315	
	Molybdenum	10.3	2.1	343	
	Nickel alloy (Rene 41)	8.2	2.3		220
	Steel	7.9	4.2	210	
	Titanium alloy	4.6	2.2	120	
	Tungsten	19.3	3.9	411	

+ transverse modulus of polyethylene fibres is about 1.6GPa.

* transverse modulus of Kevlar 49 is 2.49GPa.

‡ there are equivalent grades of polyaramid fibres under the Twaron trade mark.

Polyaramid and polyethylene fibres have small negative axial coefficients of thermal expansion (-2.0 and -9 to 10MK⁻¹ respectively). Most polymers, however, have positive, and rather large, coefficients of thermal expansion in the range 30-100 MK⁻¹), and Kevlar's radial expansion is 59MK⁻¹, while Spectra's are 100-105MK⁻¹ (see Table 3.3 which lists radial and axial expansion coefficients).

Rigid rod polymers have also been synthesized and formed into fibres. These include PBO (polyphenylene benzobisoxazole) and PBZT (poly (paraphenylene benzo-bisthiazole)) with respective moduli of 365 and 330GPa and strengths 5.8 and 4.2GPa.

Their density is about the same as Kevlar 149 and so are their compressive strengths (0.4 GPa). The moduli exceed those of many metal wires (e.g. Table 3.1) and are about 58% of the theoretical.

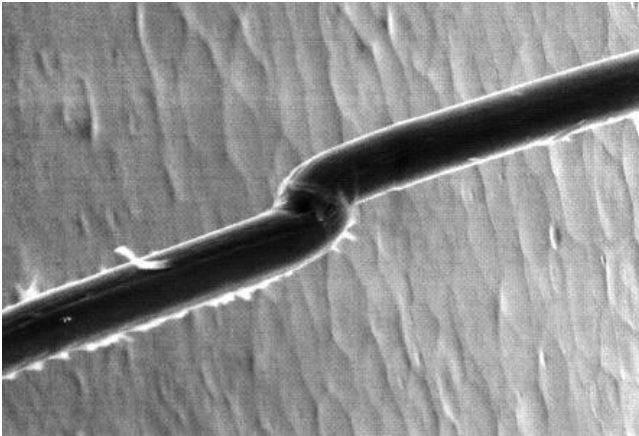


Fig. 3.5 Kevlar fibre which has been kinked in a peel test. Some defibrillation can also be seen at left. Fringe at bottom left is polyethylene matrix still adhering to the fibre.

Metal wires have relatively high strengths and moduli. Table 3.1 gives a few examples. Their densities are, of course, much greater than those of polymers so that the specific strengths (strength/density) are comparable with regular textile fibres such as nylon and polyester. Steel wires are much weakened by heat : for example, 30 minutes at 260°C decreases the strength of the steel in Table 3.1 to 75% of its 20°C value. The other wires are less affected, and tungsten is particularly stable in this respect. Steel wires cost about \$1/kg, and other metal wires can be quite expensive, i.e. as much as \$10/kg or more.

3.3 Inorganic Fibres and Whiskers

Inorganic materials in fibrous form have been widely used for many years. Asbestos retains its properties up to quite high temperatures, and has been widely used as an insulating material, and more recently, has been tried as a reinforcement for polymers. However, it has now fallen into disfavour because mining it and processing it is considered a hazard to health. Glass fibres are also used for insulation, at moderate temperatures. They also provide very useful reinforcement for polymers, and this so-called "fibreglass" is nowadays a very commonly used material.

Other inorganic fibrous materials have been developed recently, most notably, carbon and silicon carbide. In addition, the potentialities of inorganic whiskers have been appreciated in the last twenty years or so, and methods of making them in reasonable quantities for industrial use are being intensively developed. The various types of material will be discussed in turn.

3.3.1 Glass

Glass is a word which covers a wide range of materials, usually containing more than 50% of silica (SiO_2) with random structures. They are often regarded as super-cooled liquids, and this state is referred to as the vitreous state. Ordinary glass, used for

windows and bottles, typically contains 14% Na₂O, 10% CaO, 2.5% MgO, and 0.6% Al₂O₃, the remainder being SiO₂. It is relatively weak and has a high coefficient of thermal expansion compared with pure silica, coupled with very low thermal conductivity.

It is very brittle and it is easily broken into small pieces by rapid cooling. It softens at about 700°C and so is relatively easy to form, though care has to be taken to relieve stresses developed during the forming and cooling processes. Fibres are made from this glass, but they do not have very good properties, being comparatively weak and relatively easily attacked by water.

Borosilicate glasses contain a relatively large amount of B₂O₃ (typically 12.9%) together with Na₂O (3.8%), and Al₂O₃ (2.2%), are much stronger than soda-lime glass, more resistant to water and chemicals, and have much lower expansion coefficients. However, they are not easily drawn into fibres. The glass fibres used for textiles are of a different composition, and are the same as those used for reinforced polymers.

For reinforcement purposes, one of the most commonly used glasses is E-glass, developed originally for its good electrical properties. A typical composition is CaO 17.5%, Al₂O₃ 14.4%, B₂O₃ 8%, MgO 4.5%, most of the remainder (54.4%) being SiO₂.

The fibres are usually made by melting and stirring the ingredients, then allowing the liquid to fall through holes 1-2mm in diameter in a heated platinum dish. The glass is pulled away rapidly to draw the fibres down to about 10 microns diameter (Fig. 3.6). The platinum dish contains several hundred holes, and the fibres are all drawn together. To obtain strong fibres it is essential that the fibre surfaces do not touch anything, even another fibre. Consequently, they are coated, before being drawn together, with a "sizing". This is usually a starch-oil emulsion, or alternatively a special coating to ensure good adhesion between fibre and matrix when the fibres are later incorporated in a polymer.

The strongest known glass fibres are made from pure silica. At liquid nitrogen temperatures they can have a strength of 9.6GPa and break at a strain of nearly 14%. This strength is not affected by water very much at all, and the fibres are very resistant to acids (apart from HF, and H₃PO₄ at high temperatures) but they are weakened by alkaline solutions. A commercial silica fibre (Astroquartz) is available; see Table 3.2. Hollow glass fibres are also available. With S2 glass, for example, the density is reduced from 2.48 to 1.8, the modulus is reduced by about 23% and the strength about 27%.

All glass fibres are extremely sensitive to surface damage. Merely touching one fibre against another is sufficient to cause a crack which can reduce the strength to less than a half of the undamaged value. Handling the fibres is only possible if they have a protective layer on them, and even then considerable reduction in strength can occur unless great care is taken.

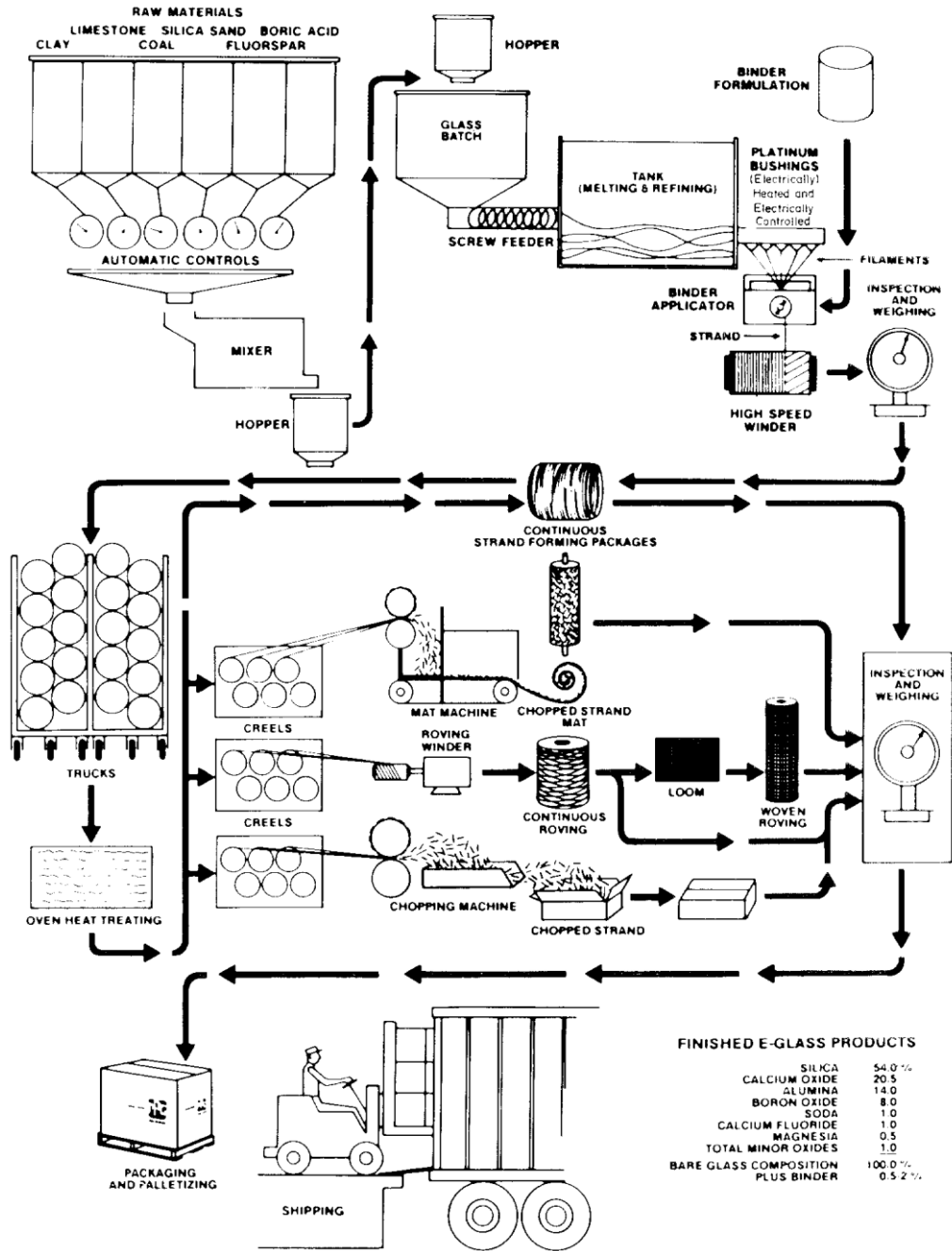


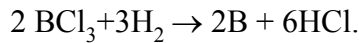
Fig. 3.6 Glass fibre production process. (Courtesy of PPG Industries Inc.)

Glass fibres are relatively cheap, about \$1/kg. while silica (Astroquartz) is quite expensive: \$40 /kg.

3.3.2 Boron

Boron fibres were developed in the 1960's for aerospace applications. Boron has a very low density (2.3Mgm^{-3}) and great potential strength, but is a very hard and brittle

material, not suitable for drawing down into the form of fine wire. It is, therefore, made by deposition onto a very fine tungsten wire (12.5 microns diameter) using the chemical reaction



Both reactants are gases, and other boron halides can be used instead of the chloride. A sketch of the apparatus used is shown in Fig. 3.7.

The tungsten wire is heated and strict temperature control is necessary to obtain consistent fibres having the optimum crystal size. Ideally, the crystals should be very small, about 2 to 3nm in diameter, so that the material is practically amorphous. The best results are obtained at about 1100°C. The diameter of fibres normally produced is about 0.1mm.

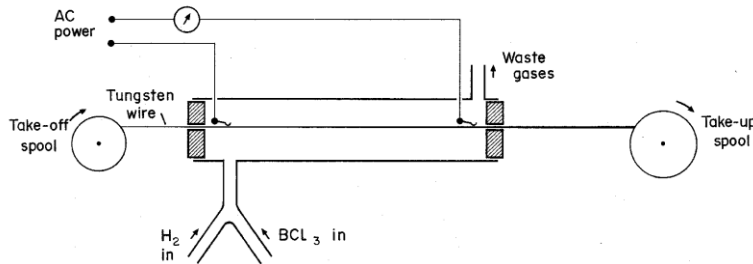


Fig. 3.7 Schematic drawing of chemical vapour deposition process used to make boron and large diameter silicon (SCS type) carbide fibres.

The fibres are extremely strong and stiff (Table 3.2), and retain their properties up to temperatures of about 500°C. For use above this temperature they must be coated with SiC or B₄C. This extends their usefulness up to 700°C (SiC) or 850°C (B₄C), and also provides protection from reactive metallic matrices, such as Al and Ti. They are also very hard, so are not easily damaged by careless handling (unlike glass). However, they are extremely expensive to manufacture and cost several hundred dollars per kg.

Attempts to reduce the cost by depositing the boron onto a heated carbon fibre substrate have not been very successful; the fibres thus produced were weaker. There appears to be less interest in these fibres now. They have been supplanted by silicon carbide.

3.3.3 Silicon Carbide and Silicon Nitride

These fibres are made using the same process as boron, namely, chemical vapour deposition, with tungsten wire or carbon fibre substrates. For silicon carbide chlorinated silanes are used, with hydrogen gas acting as a carrier. Decomposition occurs at high temperature to produce the silicon carbide. For example, with methylchlorosilane, the reaction is



The fibres produced are light, stiff, and strong (Table 3.2) but are easily damaged by abrasion. They are usually made with diameters of 0.10 - 0.14mm, but can be made

much thicker. Although silicon carbide itself is quite strong up to 1400°C, it reacts with the tungsten substrate at much lower temperatures, and so this type should not be used at temperatures above about 800°C. With the carbon substrate, some fibres can be used up to 1000°C or more.

Table 3.2 Values for Strength, Modulus and Maximum Use Temperature of Inorganic Fibres and Single Crystal Whiskers.

Representative values only are given. There is considerable variation in values reported for many of these materials. The temperatures are only intended as some indication of relative resistance to heating. In practice, maximum temperatures depend on stress and chemical environment.

Material	Density Temperature (Mg m ⁻³)	Strength (GPa)	Young's Modulus (GPa)	Diameter (µm)	(°C)
Chrysotile asbestos	2.5	5.5	160	10	500
E-glass	2.54	3.4	72	5-25	550
S-glass	2.48	4.8	85	5-15	650
Silica (Astroquartz)	2.2	3.45	69	9	1070
Boron	2.6	3.5	420	140	700 ⁺
SiC (SCS-6)	3.32	4.0	410	140	900
SiC (Nicalon)	2.8	2.7	185	10	1200
Si ₃ N ₄	2.5	2.5	300	10	1200
Carbon P120S (stiffest)	2.18	2.2	827	10	2500 ⁺
Carbon HMS (stiff)	1.9	2.3	377	5	2500 ⁺
Carbon (cheapest)	1.81	3.8	238	7.2	2500 ⁺
Carbon T40 (strongest)	1.81	5.6	290	5.1	2500 ⁺
Al ₂ O ₃ (Nextel 610))	3.88	1.9	373	10-12	1200
Al ₂ O ₃ (Nextel 312) [‡]	2.7	1.7	150	10-12	1200
Al ₂ O ₃ (Saffil)	3.0	2.0	300	3	1000
Al ₂ O ₃ whiskers	4.0	15	2250*	1	1200
SiC whiskers	3.2	21	840*	1	1600
BeO whiskers	3.0	6.9	720*	1	1500

* Maximum value, with most favourable crystallographic orientation

+ 500°C in oxidizing atmosphere

‡ contains 24% SiO₂ and 14% B₂O₃

The cost of making the fibres is similar to boron i.e. a few hundred dollars/kg. Several types, with different coatings or surface treatments are available. These will be

referred to in the text as CVD silicon carbide to distinguish them from the pyrolysed form described in the next paragraph.

Much finer fibres (about $10\mu\text{m}$ dia.) can be made directly from polycarbosilane polymer fibres by pyrolysis and subsequent heat treatment. The process is similar to that used to produce carbon fibres, discussed in the next section. There is free carbon present in the fibre which can result in serious corrosion when the fibre is used with aluminium.

Silicon nitride (Si_3N_4) fibres have also been made by the same process, using a perhydrosilazane precursor. Their properties are very similar to SiC (see Table 3.2).

3.3.4 Carbon

These are often called graphite fibres, and are usually made from polymer fibres by careful heat treatment. They can also be made from pitch.

Carbon can occur in three forms, diamond, graphite, and amorphous (or glassy). Only the crystalline forms have high modulus, and the only crystalline form of carbon that has been produced in fibre form resembles graphite. Amorphous carbon fibres can also be produced. They can be very strong (2.0GPa) but their low modulus (70GPa) renders them of little interest for high performance composites so they will not be considered any further here.

The polymer fibres (for example rayon or polyacrylonitrile) are first heated at relatively low temperature (about 220°C) in air under tension to oxidize the fibres and stabilize them so that they can be heated at higher temperatures without disintegrating. They are then heated at temperatures up to 2000°C , usually under tension. After the initial conversion to carbon, some recrystallization occurs, so that the graphite planes are oriented along the fibre axis, as shown in Fig. 3.8.

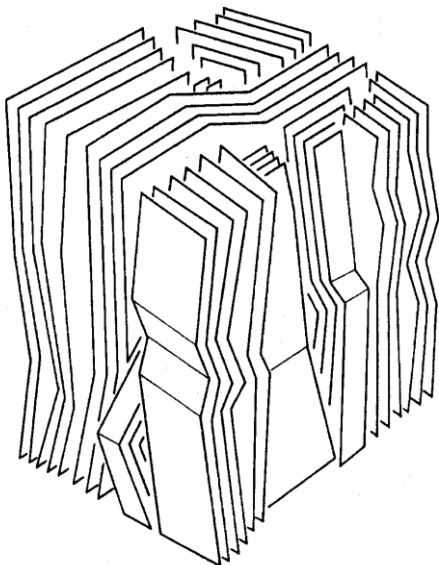


Fig. 3.8 Internal structure of a PAN precursor carbon fibre, showing the arrangement of planes of carbon atoms. (After Kelly, A. Strong Solids (2nd Edition: Clarendon Press, Oxford, 1973) p. 250.)

There is some advantage in having an oriented crystalline polymer as precursor, as this facilitates the production of high modulus fibres. Two types of fibre can be produced; a highly oriented high modulus type, and a less well oriented but slightly stronger variety (this requires less heating). Strengths and moduli of a cheap PAN based fibre is given in Table 3.2, together with values for a very high strength fibre, also PAN based.

High performance carbon fibres can also be made from pitch. Their internal structure is quite different from that shown in Fig. 3.8. A range of structures is in fact possible; see Fig. 3.9, depending on exact precursor and heat treatment. The process is similar to that used for the PAN precursor: after melt spinning to produce a fibre, then curing to solidify it, the fibre is pyrolysed and crystallised under tension.

A very wide range of fibres is possible: in the late 80's, no fewer than 40 varieties were being marketed by eight companies worldwide. Moduli (E_f) of up to 750GPa and strengths (σ_{fu}) up to 7GPa were available: but not with the same fibre; see Fig. 3.10. The line on the graph is

$$E_f \sigma_{fu} = 2000 \text{GPa}^2 \quad (3.5)$$

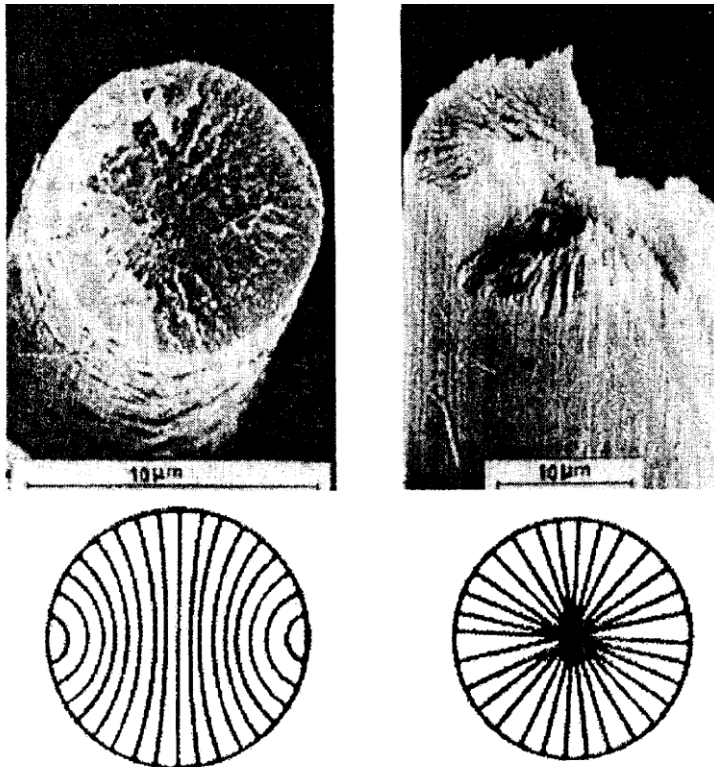


Fig. 3.9 Morphology of pitch precursor carbon fibres. (After Chuo, C.T., Gaur U. and Miller, B., 1993, *Comp. Sci. Tech*, **48**, 307-16.)

Pitch based fibres have the highest modulus and these can achieve more than 70% of the theoretical value for graphite. The very high strength fibres can be extremely thin - diameters can be as small as 5.1 μm . High strengths were achieved by care in the

processing so that the flaws are rare. Commercial realities have recently reduced the number of producers and of products but the number of varieties available is still great.

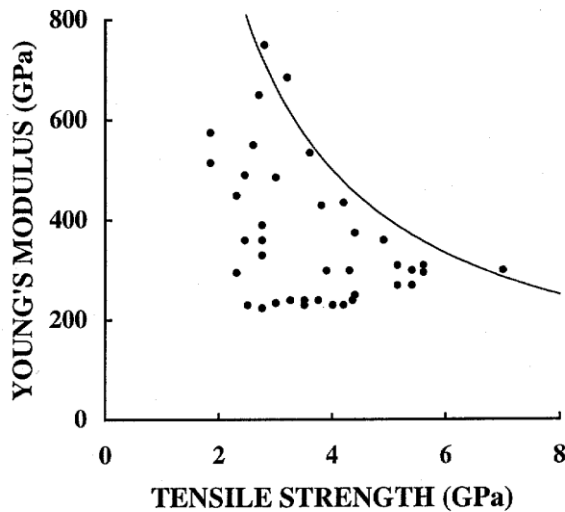


Fig. 3.10 Strength vs modulus for carbon fibres available in the late 1980's. (After Piggott, M.R., 1989, *Carbon* 27, 657-62.)

Although the fibres retain their properties at temperatures over 2000°C in vacuum, they are very easily oxidized at temperatures above about 500°C. The thermal conductivity of some carbon fibres are surprisingly high: P-100, P-120, and P-130X (Amoco Performance Products) being more conductive than copper, P-130X three times and HOPG six times more so. The electrical resistivities, however, are one to two hundred times greater than copper; see Fig. 3.11.

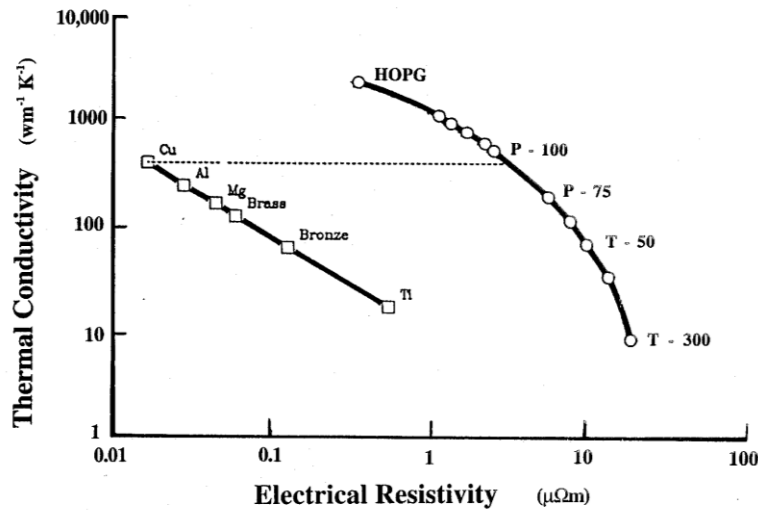


Fig. 3.11 Electrical resistivity vs thermal conductivity for metals and some carbon fibres (note that silver is about 6% more conductive than copper: from Amoco Performance Products data sheets.)

The external form of the fibres varies from extremely rough, as exemplified by some of the pitch precursor fibres, see Fig. 3.9, to extremely smooth, e.g. Hercules (now Hexcel) PAN precursor fibres. For example, Fig. 3.12 compares the appearance of glass, PAN precursor carbon, and silicon carbide, showing the carbon core.

Carbon fibre prices range about \$25/kg for the lower modulus and strength ones to over \$1000/kg for the ultra high modulus varieties.

Modulus and strength transverse to the fibres are much lower than in the axial direction; typically being about 5-8GPa; see Fig. 3.13.

3.3.5 Aluminium Oxide (Alumina) Fibres

Single crystal filaments with excellent properties can be produced by growth from pure molten Al_2O_3 (sapphire fibres). However it is more economical to produce polycrystalline impure Al_2O_3 fibres. These have properties which are comparable with the higher modulus carbons (see Table 3.2) but being fully oxidized are useful up to much higher temperatures in air. However, their density (3.9Mgm^{-3}) is somewhat high, while their cost is competitive with carbon and the thermal expansion is low at about 9MK^{-1} . As with carbon, the transverse modulus is low (about 13GPa).

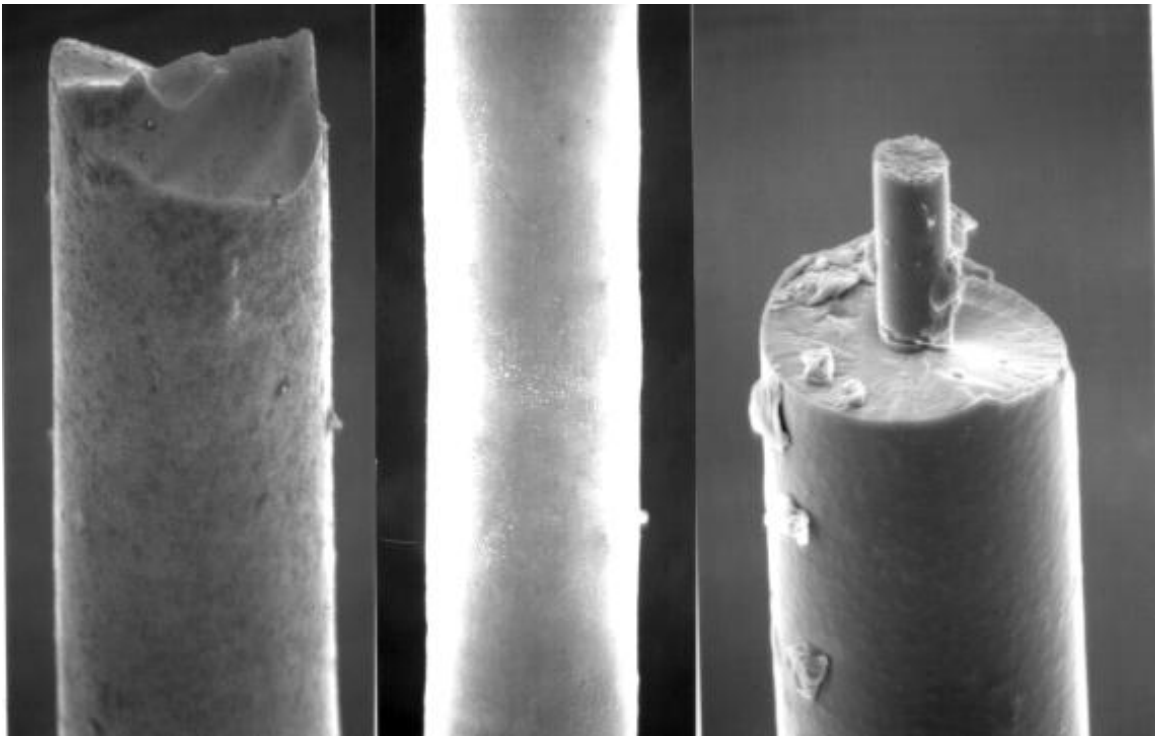


Fig. 3.12 Appearance of various fibres. Glass, $18\mu\text{m}$ diameter, at left, Hercules AS4 carbon, $8\mu\text{m}$, in centre, and silicon carbide, $140\mu\text{m}$.

Recently, a range of Al_2O_3 based fibres has been introduced under the trade name Nextel. Nextel 610 is $> 99\%$ Al_2O_3 and has the properties shown in Table 3.2. A grade containing 24% SiO_2 and 14% B_2O_3 (Nextel 312) has lower strength, density and modulus, Table 3.2, but also a much lower thermal expansion coefficient (3MK^{-1}).

Another form of Al_2O_3 fibres: "Saffil" (ICI), is in the form of a random mat of fine ($3\mu\text{m}$ diameter) short (few mm) filaments. Their density is a little lower than their bigger brothers, but otherwise their properties are very similar (see Table 3.2).

3.3.6 Inorganic Whiskers

These whiskers are the nearest approach we have to the perfect material. They are single crystals of about 1 micron in thickness, having lengths of up to 3 or 4mm. They have hexagonal, square, or parallelogram sections, the faces being crystal faces determined by the internal arrangement of atoms in the structure. They can be grown with only one dislocation, a screw dislocation along the whisker axis, which cannot move under an axial tensile stress. The surfaces are close to being atomically smooth, and thus free from cracks, and under suitable conditions, using pure materials, the internal structure is free of inclusions and cracks, or other faults.

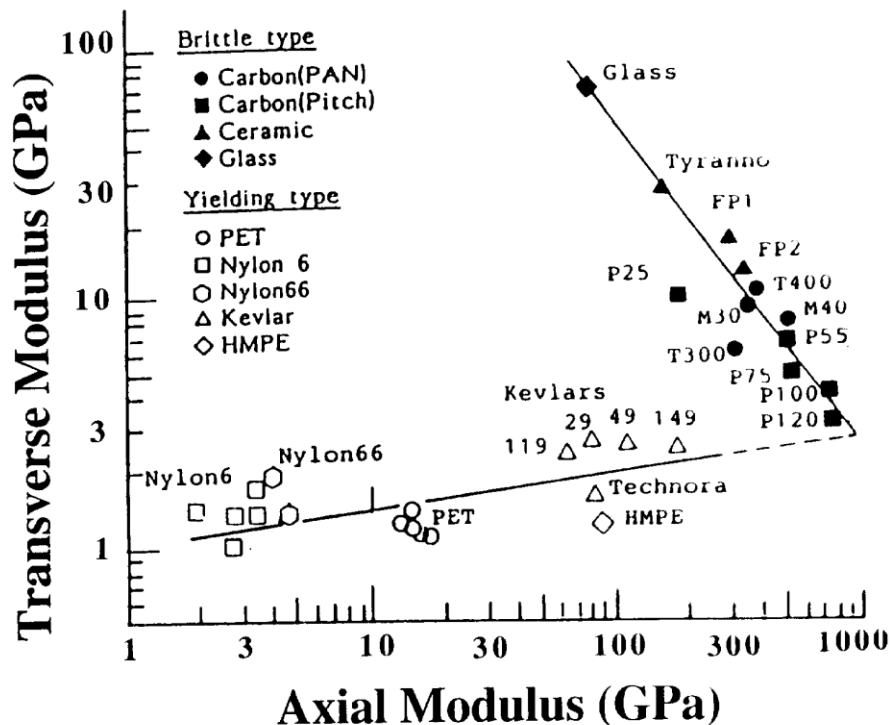


Fig. 3.13 Transverse axial moduli for glass, carbon, ceramic and polymer fibres. (After Kawabata, S., 1990, *J. Textile Inst.* **81**, 432-7.)

Whiskers can be made from a wide range of materials, and even alkali halides grown in this form have very high strengths. For example, whiskers of LiF have been produced which have a strength of 4.5GPa.

The properties of the whiskers depend a great deal on growth conditions, surface perfection, and diameter. Thick whiskers have many dislocations in them and are relatively weak. Growth steps also occur on the surface of thick whiskers, and act as stress raisers, lowering the strength. One micron is the maximum diameter normally suitable.

To produce kilogram quantities of high quality whiskers is extremely difficult, and so far, good whiskers have been very expensive (hundreds of dollars/kg). Their properties, however, far exceed those of the other forms of strong solids. Table 3.2 lists the properties of three types of whisker which resist high-temperature oxidation conditions. Whiskers produced in kilogram quantities, in commercial batch processes, do not come near to achieving the properties indicated in the table. Before being used in composites they have to be carefully sorted to remove large diameter fibres and very short ones. The final product then usually has to be aligned.

Table 3.3 Coefficients of Thermal Expansion (MK^{-1}) of Fibres

Fibre	Radial	Axial
Alumina (Nextel 610)	8.3	-
Alumina (Nextel 312)	3.0	-
Asbestos	9.2	-
Beryllium	12	+
Boron	6.3	+
Carbon (HMS)	8.0*	-0.5*
Glass (E-glass)	15.5	+
Glass (S-glass)	8.9	+
Glass (Astroquartz)	0.56	+
Kevlar	59	-2.0
Molybdenum	5.0	+
Polyethylene (Spectra 900)	100	-9
Polyethylene (Spectra 1000)	105	-10
Silicon carbide (CVD)	2.6	4.0
Silicon carbide (Nicalon)	3.1	+
Silicon nitride	1.5	+
Steel	12	+
Tungsten	4.3	+

+ These materials are assumed to be more or less isotropic, so the axial coefficient is approximately the same as the radial.

* The wide range of carbon fibres is accompanied by a range of thermal expansion coefficients. The above values are typical.

3.3.7 Thermal Conductivity and Expansion

The thermal conductivities of most fibres are very low. However, some carbon fibres have exceptionally high conductivities, as described earlier, see Fig. 3.11.

The thermal expansion coefficients of fibres are very important for reinforcement. With reinforced ceramics stress transfer between fibres and matrix requires that the matrix shrinks onto the fibres during manufacture. Since composites are usually made at elevated temperatures this requires that the matrix thermal expansion coefficient is larger

than that of the fibres. Unfortunately, however, differential thermal expansions can cause problems when composites are thermally cycled. These effects are discussed later.

Table 3.3 gives some thermal expansion coefficients for fibres at about 100°C. The coefficients for matrices are presented in the appropriate places in Chapters 10 and 11.

3.4 Single Crystal Platelets

Many materials grow naturally in platelet form, and though platelets are not normally as strong as whiskers, they can still have strengths of up to 10GPa. Figure 3.3 indicates the relative strengths of platelets and whiskers of SiC, compared with more equiaxed crystals. There is, however, tremendous scatter in the values, especially for platelets. There was some interest in using platelets as an alternative to fibres in the 1970's but there is little activity here now.



Fig. 3.14 Fibreglass roving.
(Courtesy of Fibreglas Canada Ltd.,
now Owens Corning.)

3.5 Forms of Reinforcement

In order to use the high strength of fibrous materials on a commercial scale, it is necessary to handle very large numbers of them at a time. In the case of glass fibres, a one millimetre diameter rod composed only of fibres tightly packed, would contain 10^4 fibres. Such rods, if made of chrysotile asbestos, would contain 10^9 fibrils. Methods

have been developed over a long period for the routine handling of large numbers of individual fibres.

The art of doing this was originally developed for the handling of textile fibres for the manufacture of clothing and of cellulose fibres for making paper and cardboard. These methods have recently been adapted for the handling of asbestos and glass, and very recently for the handling of single crystal whiskers.

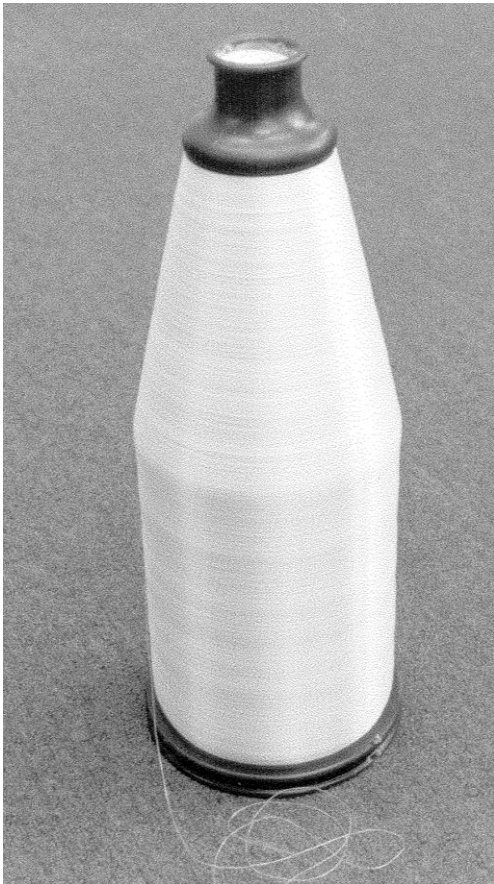


Fig. 3.15 Fibreglass yarn. (Courtesy of Fibreglas Canada Ltd., now Owens Corning.)

3.5.1 Random Mat

This is the sort of arrangement normally present in paper and cardboard. Single crystal whiskers, which grow as felt-like small cushions, of very low density, may be beaten down into a mat mechanically with some loss in aspect ratio (length/diameter) of the individual crystals. Asbestos fibres, after being broken up, can be settled into random mats. Glass fibres for use in reinforcement is manufactured in multiple, continuous fibre strands called roving - see Fig. 3.14., or twisted yarn, Fig. 3.15. To produce random arrangements the rovings are chopped into short lengths (3-50mm) and allowed to settle on a sheet. Fig. 3.16 shows an example of chopped strand mat of fibreglass.

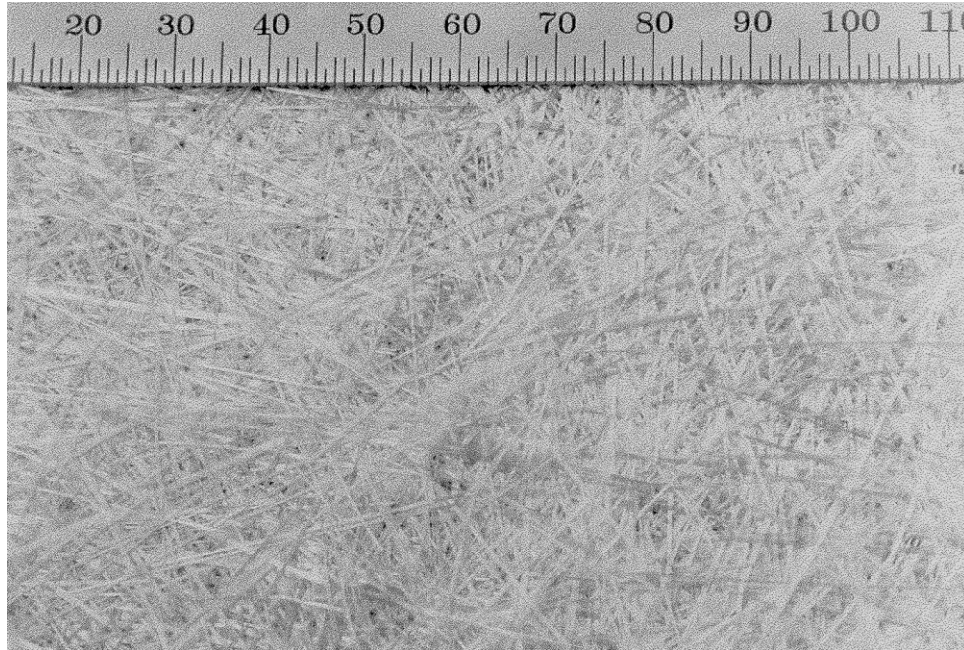


Fig. 3.16 Chopped strand mat; scale in mm. (Courtesy of Fiberglas Canada Ltd., now Owens Corning.)

Mats to be used for reinforcement are often made with some polymer present to hold the fibres in place. They are an inefficient form of reinforcement because it is impossible to pack large numbers of straight fibres tightly unless they are all parallel. The maximum volume fraction that can be obtained when they are random in a plane is about 0.4. For three-dimensional random arrangements the packing efficiency is much worse, especially for fibres and whiskers having large aspect ratios.

Continuous fibres can also be laid into mats. This arrangement has the same reinforcing potential as chopped strands, but has different handling and moulding characteristics. It can be moulded into more complicated shapes, and does not tear so easily.

When aligned fibres are required they can be prepared in the form of tapes. Then some type of binder is required to retain the shape.

3.5.2 Woven Fabrics

Yarns can be produced from a wide range of fibres and whiskers. In the case of short fibres and whiskers, the yarn must be spun (or twisted) to hold the fibres together. Continuous fibres require no spinning, but it is sometimes advantageous to do so. Fabrics are produced from these yarns by normal weaving processes. Figure 3.17 shows a typical glass fabric used to make a composite. When the fibres are not spun the fabrics are usually denser, and involve much less fibre flexure than with spun fibres.

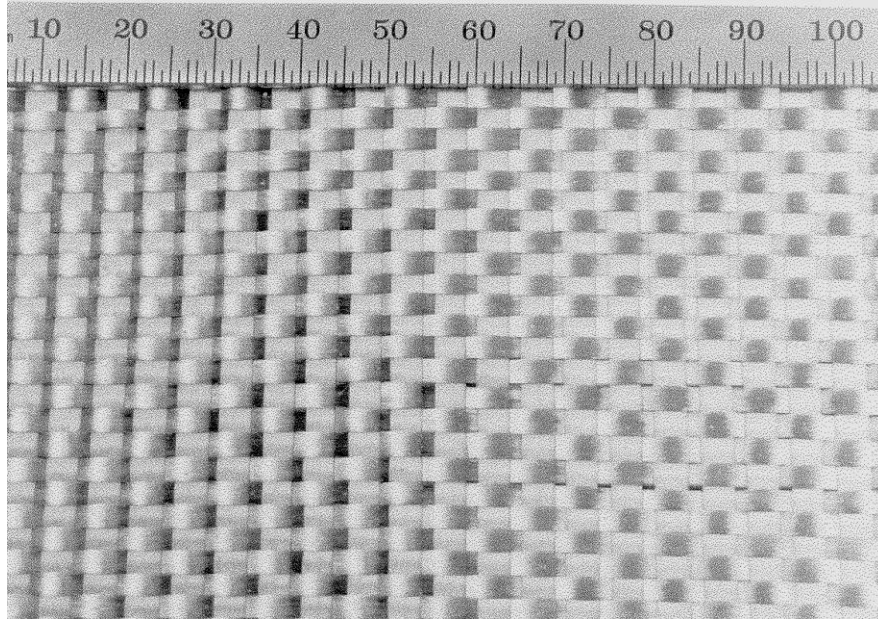


Fig. 3.17 Non-twisted glass fabric. (Courtesy of Fiberglass Canada Ltd., now Owens Corning.)

Since the fibres are highly flexed in fabrics made by conventional weaving processes, some fibre straightening can occur when the fabric is stretched. This results in a relatively low modulus composite, with similar properties in all directions. The modulus may be improved in one direction, with consequent loss of modulus and strength in the direction at right angles to it, if the fabric is made with the fibres completely straight in one direction, and with only a few fine threads in the other direction. This is a particularly useful method of weaving for very stiff fibres which can withstand relatively little flexure, for example the higher modulus carbons, Al_2O_3 , Si_3N_4 and CVD silicon carbide. Owing to their large diameters, CVD silicon carbide (and boron) fibres are extremely difficult to weave.

Woven fabrics should be used when high shear strengths are required in the plane of the reinforcing sheet (for example, when the sheet forms the side of a beam in flexure). The more unidirectional weaves generally have lower apparent shear strengths than conventional weaves. Special weaves, with good "drapeability" are available for use for complex curves. These can be used on double curvatures, and do not wrinkle easily.

There are also triaxial weaves which typically involve axial fibres accompanied by $+60^\circ$ and -60° fibres.

3.5.3 Braids and Knitted Fabrics

Typical braids are shown in Fig. 3.18. They are produced as tubes, and fibre densities and fibre angles relative to the tube axis can be varied. A wide range of different braids can be produced.

Knitted forms can be produced as flat pieces or tube and generally involve more circuitous fibre paths. Thus the fabric produced by this process is usually more flexible and drapeable.

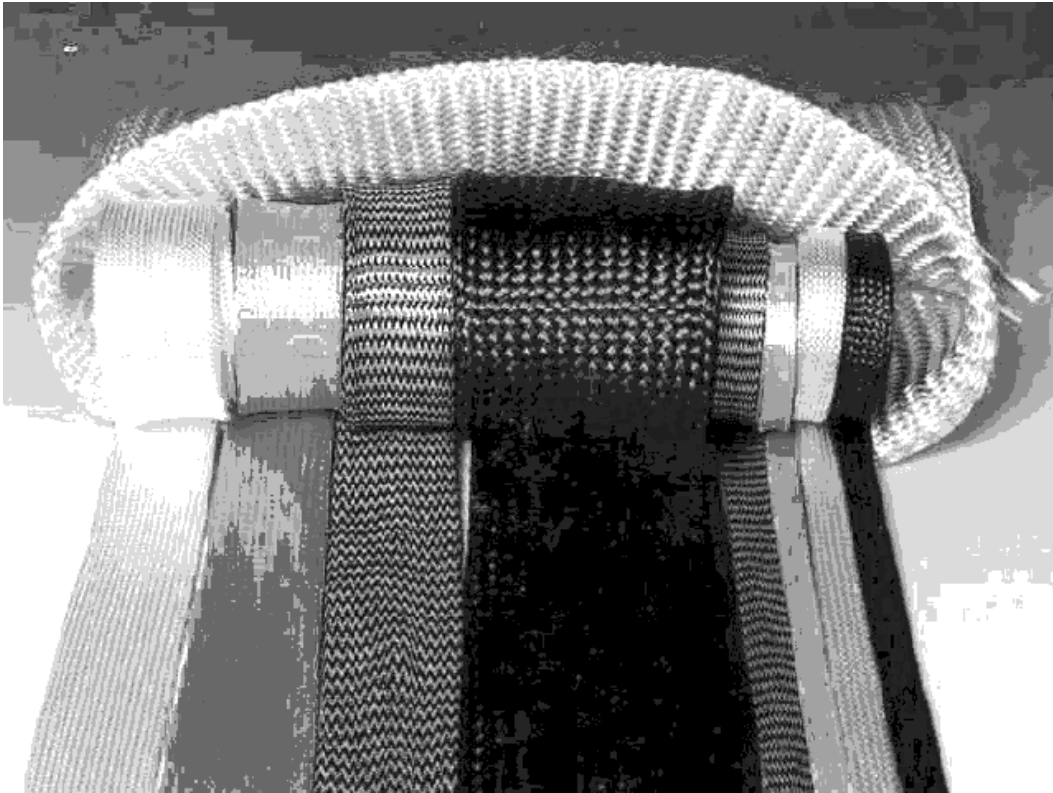


Fig. 3.18 Examples of braided forms. (Courtesy of A & P Technology.)

3.5.4 Three Dimensional Forms

Three dimensional woven forms have been developed for the aerospace industry. The fibres can be mutually orthogonal or else the fibres going through the thickness tows can be at an angle. Three dimensional fibre arrangements can also be produced by the braiding process. Braiding typically produces a cylindrical shape. It can be used in the cylindrical form or flattened to produce a planar, angle ply type of structure, with or without axial fibre tows. (Tows are the carbon fibre equivalent of glass fibre rovings: see Fig. 3.14) The braiding process can also be extended to make three dimensional structures with round, square or oblong profiles.

Some three dimensional forms are shown in Fig. 3.19 which also shows examples of woven, knitted and braided forms. Braids and weaves can also be prepared as "preforms" ready for impregnation in the actual shape required for a particular component: see Fig. 3.20

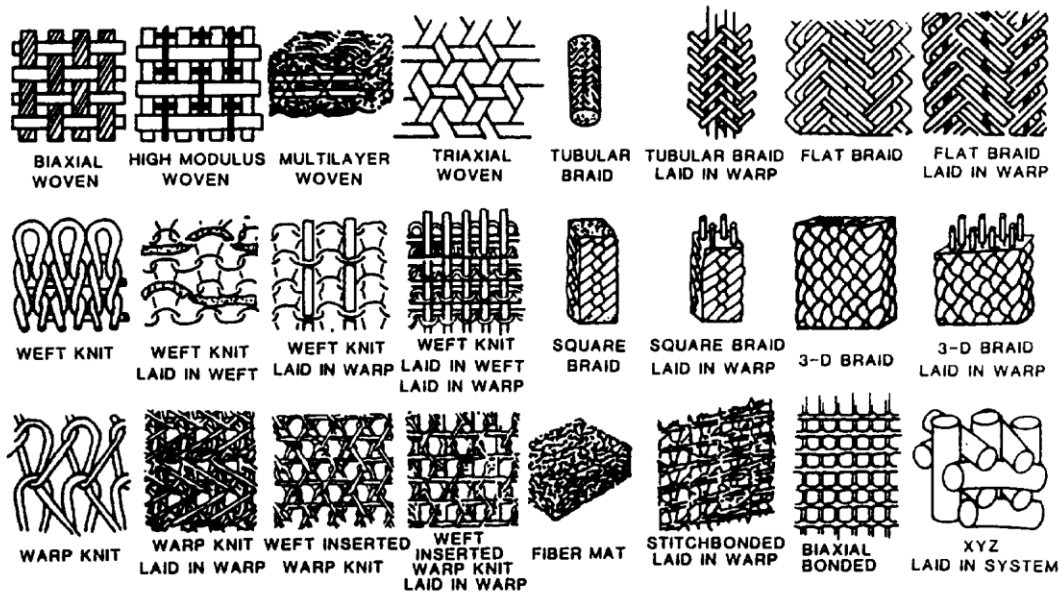


Fig. 3.19 Woven, knitted braided and other two dimensional and three dimensional fibre forms. (After Ko, F.K., 1989 Ceramic Bulletin 68, 401-14.)

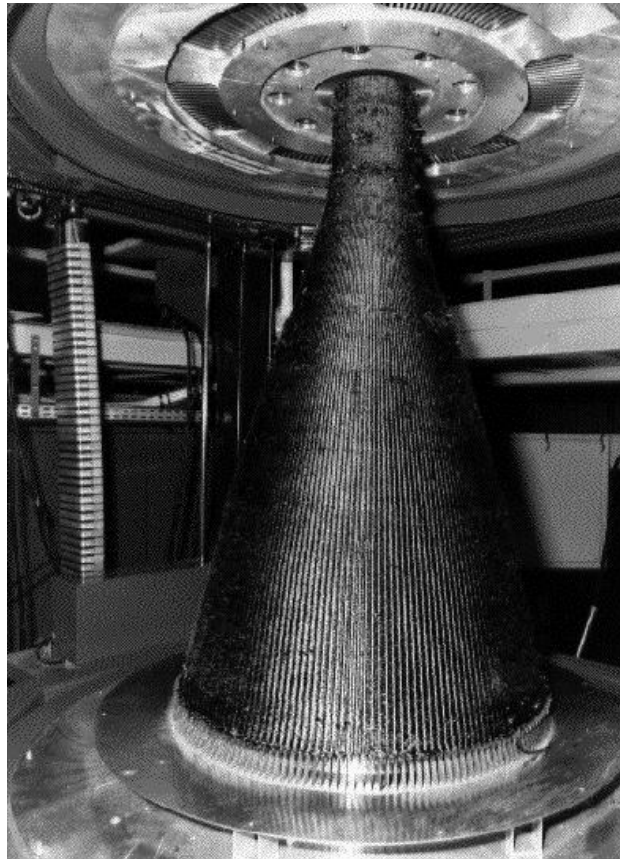


Fig. 3.20 Carbon fibre woven preform (3D weave) for the space program. (Courtesy of Hexcel.)

Further Reading

- Bunsell, A.R., (Ed), (1988), *Fibre Reinforcement for Composite Materials*, (Elsevier, Amsterdam.)
- Kaslikov, V.I., (Ed), (1995) *Fibre Science and Technology*, (Chapman & Hall London.)
- Wallenberger, F.T., (Ed), (2000) *Advanced Inorganic Fibers: Processes, Structures, Properties, Applications*, (Kluwer Academic, Dordrecht.)

Chapter 3: Problems

You are strongly recommended to solve these problems in the order given. Data needed will be found in tables in this and other chapters of the book.

- 3.1 The largest crack in the surface of a sample of tungsten wire is $2.7\mu\text{m}$ deep. What is the strength of the piece of wire?
- 3.2 Compare the maximum loads that can be supported by a Kevlar fibre, a boron fibre, and a 0.10mm diameter nylon fibre.
- 3.3 A boron fibre has a surface step which is $13\mu\text{m}$ high. The radius at the inner corner of the step is $0.30\mu\text{m}$. Will the stress at the corner reach the theoretical strength ($E/15$) at a lower applied stress than the usual breaking strength of boron fibres?
- 3.4 Calculate the strength of a $1.3\mu\text{m}$ diameter iron whisker which has a Frank-Read source extending across half the fibre diameter, and able to generate an infinite amount of slip on a plane with a normal at 5° to the fibre axis. For iron $b = 0.248\text{nm}$ and $E = 212\text{GPa}$.
- 3.5 The compressive strength of a Kevlar fibre is about one-sixth of its tensile strength. What is the smallest diameter of rod on which the fibre can be wound without damage due to excessive compression?
- 3.6 Compare the minimum radii that can be used in the weaving of stiff carbon, boron, and E-glass fibres. If the glass fibres are spun, what is the minimum number of fibres that should be used in the yarn if it is to be used for weaving with the maximum possible flexure? Assume that the compressive and tensile strengths of these fibres are the same.

- 3.7 The distribution of surface cracks in a production run of glass fibres is such that each 10cm length has, on average, 1 crack which is $1\mu\text{m}$ long, 10 cracks which are $0.1\mu\text{m}$ long, etc., so that the number of cracks of length $a\mu\text{m}$ is $1/a$. Derive a relationship representing the strength of the fibres as a function of fibre length, and hence calculate the strength for a 3.0mm length of glass.
- 3.8 An E-glass fibre $10.2\mu\text{m}$ diameter and 3.0cm long falls upon another fibre at a speed of 46mms^{-1} . Assume that it is stopped by the fibre it hits, and as a result the stationary fibre is cracked. Calculate the surface area of crack produced if all the kinetic energy goes into producing the crack. If the crack has a constant depth around the whole of the fibre circumference, what would the strength of the fibre be reduced to as a result of the crack.
- 3.9 Calculate the maximum load that can be supported by a roving which consists of 1224 E-glass fibres and 15 boron fibres. (Hint: check the fibre strain; and assume that the glass fibres have the same strength and all the boron fibres have the same strength.)
- 3.10 Some stiff carbon fibres, $7.8\mu\text{m}$ in diameter, were added to S-glass fibres to increase the modulus of the yarn prior to weaving. The yarn contained 204 fibres each with $10.4\mu\text{m}$ diameter. How many carbon fibres need to be added in order to marginally increase the yarn load carrying capacity.

Chapter 3. Selected Answers

Answers are rounded off to the appropriate numbers of significant figures.

3.1 1.03GPa

3.3 Yes (2.0GPa)

3.5 2.6mm

3.7 2.0GPa

3.9 48kg

4. COMPOSITE MECHANICS: LONG FIBRES

In this chapter we will deal principally with composites which have fibres that are continuous and straight throughout the material. We are therefore able to derive simple approximate relations based on the assumption of equality between the fibre and matrix stresses or strains, at least until one or other component is about to fail.

One of the most useful forms of composite for the construction of high-performance structural elements for aerospace is the laminate, made from aligned fibre tapes containing also partly polymerized matrix (or metal powder). These "Prepregs" are also made with woven fibres; they have inferior stiffness, and cannot have such high fibre volume fractions, but are generally tougher and somewhat easier to handle than aligned fibre tapes. The structure is made by bonding the laminae together with the fibres aligned in directions best suited to the stresses to be encountered. This is a laminate. This chapter will briefly describe the properties of laminae and laminates. Since these usually have fibre volume fractions of 40% or more, this treatment assumes such levels of fibre content.

Random fibre structures are also treated herein, using laminate theory. A complete list of the symbols used in this and other chapters is given in the Appendix.

4.1 Axial Modulus and Strength

When the fibres are aligned and continuous, a stress in the same direction as the fibres extends the fibres and the matrix more or less equally. (This is not the case with stresses in any other direction, or when the fibres are short. These cases will be discussed later.) This assumption of isostrain, which is actually an approximation, but a rather good one, leads to a very simple expression for the Young's modulus. However, it may break down at the moment of fracture of the composite.

In this section we will consider first the modulus for a perfectly elastic system, then the apparent modulus for a system with one component extended beyond its elastic limit. Finally we will derive a simple expression for strength.

4.1.1 Young's Modulus For a Perfectly Elastic System

Fig. 4.1 shows part of a unidirectional fibre composite, such as a pultrusion, with a stress in the fibre direction, σ_1 . It is usual to use 1, 2, and 3 to indicate directions in unidirectional composites and laminae. 1 is normally the fibre direction. The bar, length L , extends an amount u . Thus the strain is

$$\varepsilon_1 = u / L \quad (4.1)$$

We assume that both fibres and matrix have the same strain. The stress in the fibres will therefore be $\sigma_f = E_f \varepsilon_1$ and the load carried by the fibres will be the product of

this and the total fibre area across the bar section, AV_f . Here A is the cross section of the bar and V_f is the fibre volume fraction. Similarly, the load carried by the matrix is $AV_m\sigma_m$, the subscript m referring to the matrix.

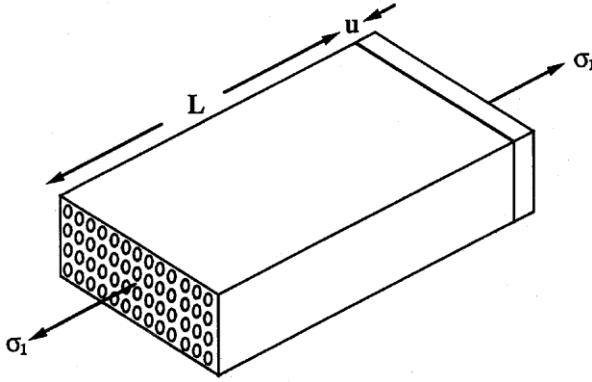


Fig. 4.1 Unidirectional fibre composite. The fibres are in the 1 direction.

The total load carried by the composite is $A\sigma_1$. So adding the fibre and matrix contributions and dividing throughout by A we have

$$\sigma_1 = (V_f E_f + V_m E_m) \varepsilon_1 \quad (4.2)$$

This immediately gives the Young's modulus, $E_1 = \sigma_1/\varepsilon_1$:

$$E_1 = V_f E_f + V_m E_m \quad (4.3)$$

Thus this composite obeys the **Rule of Mixtures** for modulus.

4.1.2 Stress-Strain Relations When One or Both Components Yield

Most fibres used as reinforcements display no inelastic behaviour, at least at moderate temperatures. So we will first consider the case of the matrix yielding. We only need an expression for composite strains greater than the matrix yield strain, ε_{my} , since we use equation (4.2) for $\varepsilon_1 < \varepsilon_{my}$.

After yielding, most metals or polymers used as matrices show little increase in stress as strain is increased further. (Figs. 1.1 and 1.3 show typical metal and polymer behaviour.) So this part of their stress strain curves can, with little loss in accuracy (for the composite at least) be represented by a straight line parallel to the strain axis: See Fig. 4.2; line labelled *matrix*.

Also shown in Fig. 4.2 is a line representing the fibre behaviour. The composite stress-strain line lies between these, and since for $\varepsilon_1 > \varepsilon_{my}$ its slope is $V_f E_f$ while for $\varepsilon_1 < \varepsilon_{my}$ it is $V_f E_f + V_m E_m$, the equation for $\varepsilon_1 > \varepsilon_{my}$ must be

$$\sigma_1 = V_f E_f \varepsilon_1 + V_m E_m \varepsilon_{my} \quad (4.2a)$$

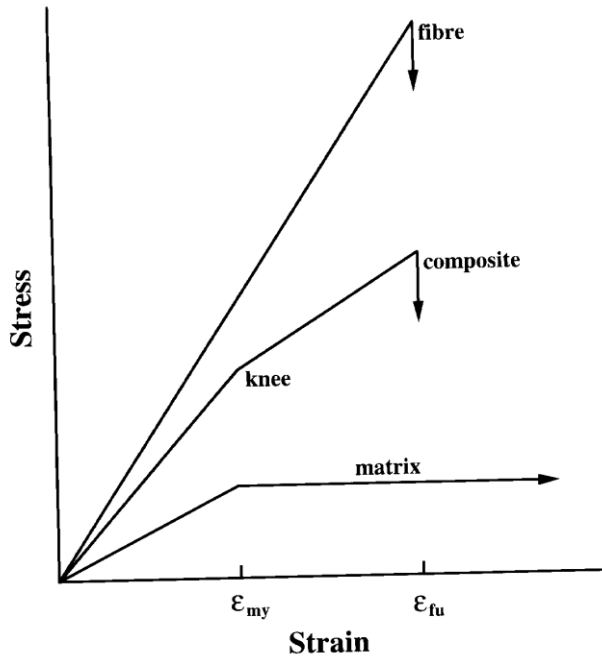


Fig. 4.2 Stress-strain plot for an elastic fibre, a yielding matrix and these combined into a composite.

The point where the change in slope is located is usually referred to as the "knee". The knee is not normally observed in unidirectional high performance reinforced polymers because $E_m \ll E_f$.

For high temperature applications where both fibres and matrix may yield we cannot make the above approximations but instead have to use an equation involving mixture rule behaviour:

$$\sigma_1 = V_f \sigma_f(\epsilon_1) + V_m \sigma_m(\epsilon_1) \quad (4.2b)$$

where $\sigma_f(\epsilon_1)$ and $\sigma_m(\epsilon_1)$ are the stresses in fibres and matrix expressed as functions of strain. Two knees can then exist, one when the matrix yields and one when the fibre yields.

4.1.3 Tensile Strength

To estimate the strength with any accuracy we need to understand the failure process in detail. Due to the completely different failure processes occurring in polymers, metals, and ceramics, even in the absence of fibres, one expression is unlikely to cover all cases very adequately. However, an approximation is possible.

First, consider the fibres. As long as the fibres constitute a moderate fraction of the total cross section, (say 10% or more), there will usually be a sudden failure involving all the fibres fracturing. Thus the contribution of the fibres to the strength will be $V_f \sigma_{fu}$, σ_{fu} being the fibre strength.

Now the matrix is generally very weak compared with the fibres. Its contribution, $V_m \sigma_m^*$ (where σ_m^* is stress endured by the matrix during the failure process) will be much less than that of the fibres. Thus we don't go far wrong when we write

$$\sigma_{1u} \cong V_f \sigma_{fu} + V_m \sigma_{mu} \quad (4.4)$$

where σ_{mu} is the ultimate strength of the matrix.

At this stage further refinement is not useful because σ_{fu} itself is not known with any accuracy. Fibre strengths are often flaw controlled, and consequently are very variable. Furthermore even if we knew all about the fibre strength before making a composite, the manufacturing process will often change it, normally not beneficially. In practice, σ_{fu} measured on lengths in the range 20-50 mm is usually good enough to estimate σ_{1u} , and equation (4.4) is accurate enough.

4.1.4 Weight Fractions

Note that for some composites, weight fractions V_{fw} are given instead of volume fractions. To convert, use the density ratio

$$\rho^* = \rho_f / \rho_m \quad (4.5)$$

Then

$$V_f = V_{fw} / [\rho^*(1 - V_{fw}) + V_{fw}] \quad (4.6)$$

4.2 Off-axis Properties

The calculation of elastic moduli, apart from the Young's modulus in the fibre direction, is presently surrounded by controversy, because of disagreements over the approximations needed. This matter is discussed at some length by Jones, and the interested student should refer to the reading list at the end of this chapter.

In this description we will present the most simple theory. For elastic properties the fibres are lumped together in a rectangular prism, with matrix material attached to two opposite sides of it and either the stresses or the strains in both components are the same.

4.2.1 Transverse Young's Moduli

Figure 4.3a represents a view of an aligned fibre composite, stressed transversely to the fibres. For the analysis we lump all the fibres together, in a band normal to the stress, Fig. 4.3b. Consequently, the stress in fibres and matrix is the same, so that the strains are $\varepsilon_f = \sigma_2 / E_f$ and $\varepsilon_m = \sigma_2 / E_m$. The total displacement, $\varepsilon_2 t$, is the sum of fibre and matrix displacement $V_f \varepsilon_f t$ and $V_m \varepsilon_m t$, so that

$$\varepsilon_2 = V_f \varepsilon_f + V_m \varepsilon_m \tag{4.7}$$

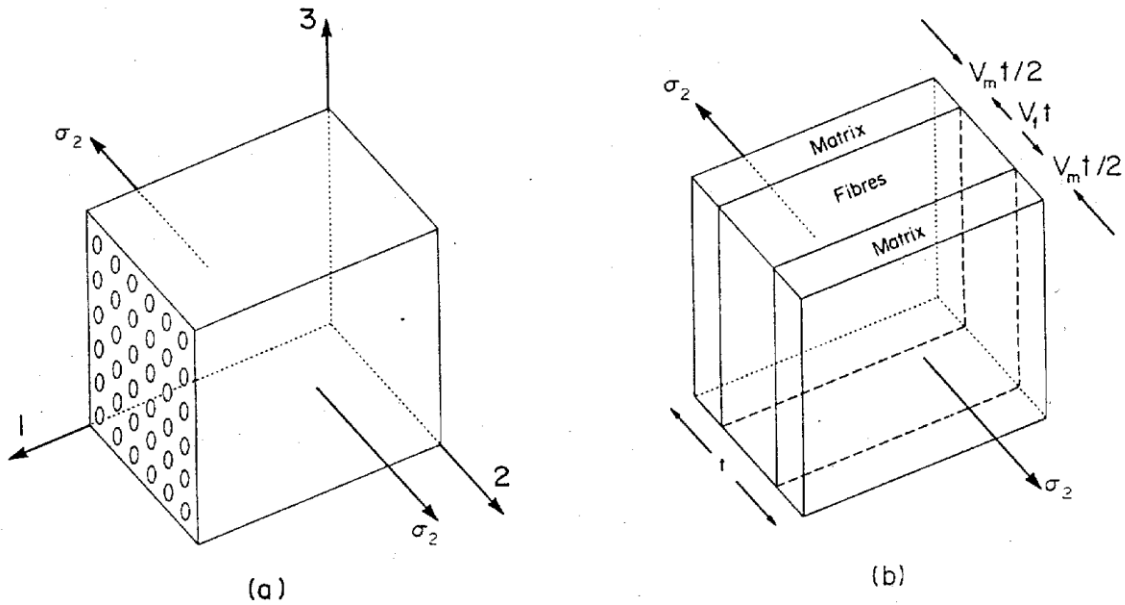


Fig. 4.3 (a) Axes used for composites. The fibres are in the 1 direction, and the applied stress is in the 2 direction. (b) Lumped fibres and matrix.

and since $E_2 = \sigma_2 / \varepsilon_2$ we can substitute for ε_2 , ε_f and ε_m in the above equation and obtain

$$\frac{1}{E_2} = \frac{V_f}{E_f} + \frac{V_m}{E_m} \tag{4.8}$$

The same equation is obtained for E_3 .

We can easily extend this treatment to the case of planar random fibres. Such composites will have moduli normal to the plane which are also given by equation (4.8). In the case of most reinforced polymers $E_f \gg E_m$ and so $E_2 = E_3 \sim E_m / V_m$.

Some fibres have transverse moduli which are substantially different from their longitudinal moduli. In these cases the transverse fibre modulus should be used for E_f in equation (4.8). In Chapter 6 we will show that this model is good enough in many cases, but that a more refined, but still simple model, gives better results in some cases.

4.2.2 Shear Moduli

As in the previous case we assume that the fibres and matrix experience the same stress, this time the shear stress τ_{12} (Fig. 4.4). The total matrix displacement, u_m , is equal

to $V_m t \gamma_m$ and the total fibre displacement, u_f , is $V_f t \gamma_f$ where γ 's are the appropriate shear strains. Thus

$$\gamma_{12} = \frac{u_m + u_f}{t} = V_f \gamma_f + V_m \gamma_m \quad (4.9)$$

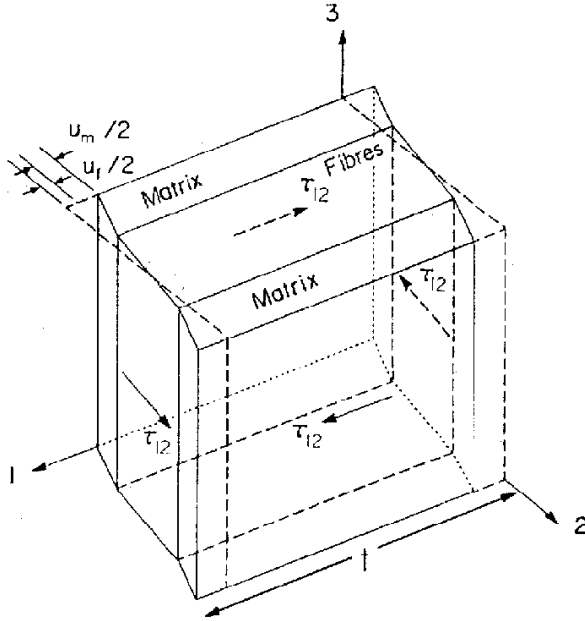


Fig. 4.4 Free shear of a composite under shear stress τ_{12} .

But $\gamma_f = \tau_{12}/G_f$, $\gamma_m = \tau_{12}/G_m$ and $\gamma_{12} = \tau_{12}/G_{12}$, so that

$$\frac{1}{G_{12}} = \frac{V_f}{G_f} + \frac{V_m}{G_m} \quad (4.10)$$

The same equation is obtained for G_{13} , and for in-plane shears with planar-random fibre reinforced materials. This analysis cannot be used to estimate G_{23} . In addition, there may be cases where the shear is constrained. This could well be the case in laminates, where effective shear moduli can be higher.

Fig. 4.5 shows the shear constrained in such a way that deformation is restricted to planes at right angles to the fibre axes. In this case both fibres and matrix suffer the same shear strain γ_{12} . Thus the fibre shear stress will be $\tau_f = G_f \gamma_{12}$ and the load borne by the fibres for a total cross section A will be $AV_f G_f \gamma_{12}$. Similarly, for the polymer, the load will be $AV_m G_m \gamma_{12}$. This is analogous to the development used for E_1 , see section 4.1.1 and leads, as before, to a Rule of Mixtures result, this time for the constrained shear modulus G_c :

$$G_c = V_f G_f + V_m G_m \quad (4.11)$$

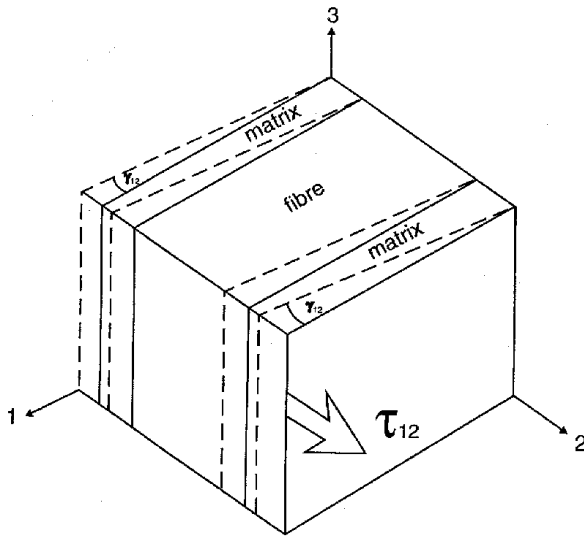


Fig. 4.5 Constrained shear: deformation restricted to planes normal to the fibre axes.

In problems #4.17 and 4.19 we examine whether the shear restraints which occur in laminates can be interpreted in terms of a simple increase in effective shear modulus, such as the above.

4.2.3 Poisson's Ratios

When the composite is subject only to a stress σ_1 (Fig. 4.6), the matrix will contract, normal to the stress, with a total displacement $u_m = -\nu_m \epsilon_1 V_m t$ and the fibres with a total displacement amount $u_f = -\nu_f \epsilon_1 V_f t$.

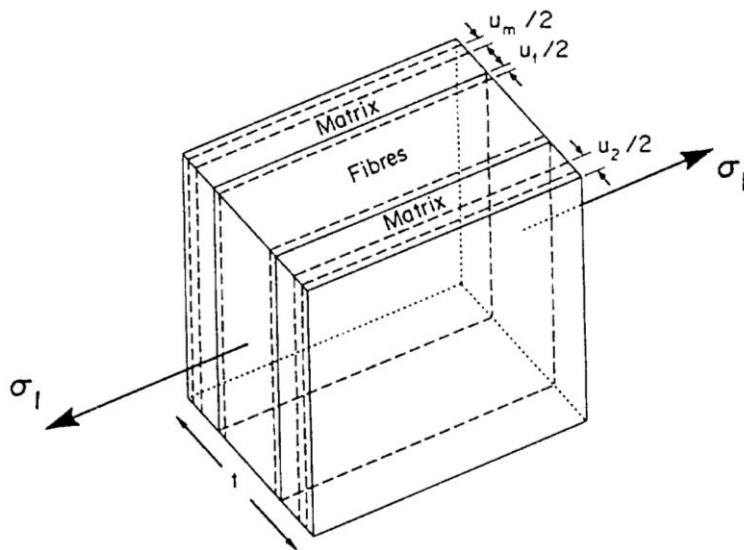


Fig. 4.6 Composite showing Poisson's shrinkage in the 2 direction due to stress in the 1 direction.

The total contraction, u_2 , is the sum of u_f and u_m , and the corresponding composite strain, $\epsilon_2 = u_2/t$. Thus

$$\varepsilon_2 = -(V_f \nu_f + V_m \nu_m) \varepsilon_1 \quad (4.12)$$

and since $\nu_{12} = -\varepsilon_2/\varepsilon_1$

$$\nu_{12} = V_f \nu_f + V_m \nu_m \quad (4.13)$$

By symmetry $\nu_{12} = \nu_{13}$ and ν_{21} and ν_{31} can be obtained using equation (1.55).

Poisson's ratios of matrices and fibres are listed in Table 4.1. This simple analysis cannot be used to obtain ν_{23} , nor can it be used for planar random fibres.

Table 4.1 Poisson's Ratios for Various Fibre and Matrix Materials

Metal	ν	Polymer	ν	Ceramic	ν
Aluminium	0.345	-		Alumina	0.20
Copper	0.343	Epoxy	0.34	Boron	0.21
Iron (steel)	0.287-0.295	Kevlar ⁺	0.35	Carbon	0.35 ⁺
Mg	0.291	Nylon	0.33	Cement	0.26
Molybdenum	0.293	Polycarbonate	0.37	Glass	0.22
Nickel	0.293	Polyester	0.34	Silica	0.171
Titanium	0.361	Polyimide	0.33	Silicon	0.27
Tungsten	0.280	Polystyrene	0.33	Silicon carbide	0.19

⁺ Transverse shrinkage of fibres

4.2.4 Transverse and Shear Strengths

For the transverse and apparent shear strengths we assume a geometrically perfect composite, with the fibres equispaced, Fig. 4.7, and perfectly adhering to the matrix. Then, when we pull it in the transverse direction, Fig. 4.7a it will fail across the polymer. Hence $\sigma_{2u} = \sigma_{mu}$.

This appears to be an upper bound because we are ignoring the stress concentrations created by the fibres as well as possible adhesive failure between fibres and matrix.

Furthermore, some fibres are weak in transverse tension, so that the failure plane can include fractured fibres (e.g. B-Al). However, when the fibres are not well aligned, as with some pultrusions, some fibres cross the crack plane, thus increasing σ_{2u} . So as a first approximation we will assume that the transverse strength is equal to the matrix strength. σ_{2u} will be considered in more detail in section 6.3.1.

For the apparent shear strength, Fig. 4.7b, we can envisage failure entirely in the polymer, again assuming perfect adhesion and also assuming that the polymer does in fact have a shear failure mode.

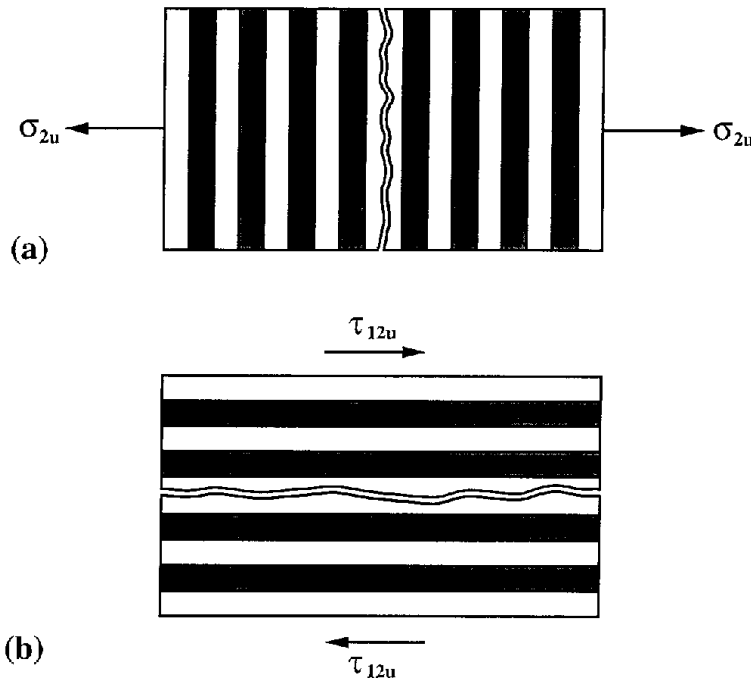


Fig. 4.7 Failure of a perfect unidirectional composite (a) transversely to the fibres; (b) in shear.

Hence $\tau_{12u} \cong \tau_{mu}$. This is not an upper bound. If the fibres are not straight the failure either causes fibre fractures, or alternatively the failure surface diverts to follow the fibres. In either case τ_{12u} is increased. (We will examine the evidence for and against shear failure of polymer and composite in Chapter 6.)

4.3 Laminae

Figure 4.8 shows an aligned fibre lamina. Such laminae are the building blocks used to make high-performance structural elements. An understanding of their properties is essential if we are to analyse structures made from them.

4.3.1 Stress-Strain Relations in the Principal Directions

For laminae we can assume that plane stress conditions are approximately met. Thus half the terms in our equations relating stresses to strains (equations (1.48) to (1.56)) are very close to zero. Further simplification results because the laminae are orthotropic. In Fig. 4.8 the fibres are in the 1 direction. The plane stress state is defined by

$$\sigma_3 = \tau_{23} = \tau_{31} = 0 \quad (4.14)$$

Strains are still present normal to the plane of the lamina:

$$\varepsilon_3 = S_{13}\sigma_1 + S_{23}\sigma_2 \quad (4.15)$$

The in-plane strain-stress relations become

$$\begin{Bmatrix} \varepsilon_1 \\ \varepsilon_2 \\ \gamma_{12} \end{Bmatrix} = \begin{bmatrix} S_{11} & S_{12} & 0 \\ S_{12} & S_{22} & 0 \\ 0 & 0 & S_{66} \end{bmatrix} \cdot \begin{Bmatrix} \sigma_1 \\ \sigma_2 \\ \tau_{12} \end{Bmatrix} \quad (4.16)$$

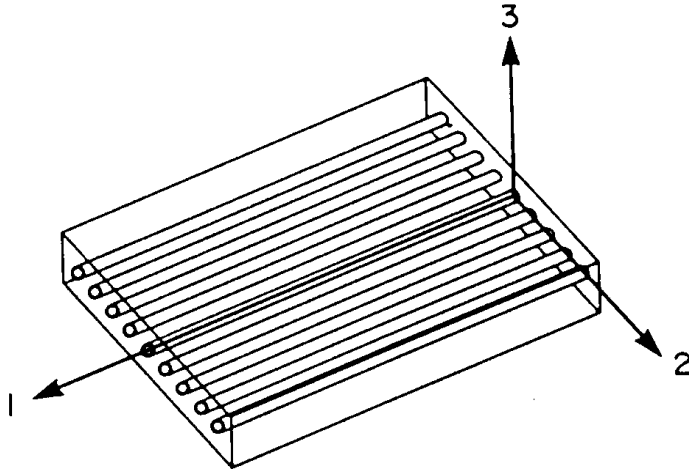


Fig. 4.8 Axes used for aligned fibre lamina.

Engineering constants can be used in place of the compliances S_{11} , S_{12} , S_{22} and S_{66} . They are given in equation (1.64).

The strain-stress relations can be inverted using reduced stiffnesses, Q_{ij} :

$$\begin{Bmatrix} \sigma_1 \\ \sigma_2 \\ \tau_{12} \end{Bmatrix} = \begin{bmatrix} Q_{11} & Q_{12} & 0 \\ Q_{12} & Q_{22} & 0 \\ 0 & 0 & Q_{66} \end{bmatrix} \cdot \begin{Bmatrix} \varepsilon_1 \\ \varepsilon_2 \\ \gamma_{12} \end{Bmatrix} \quad (4.17)$$

where

$$Q_{11} = \frac{S_{22}}{S_{11}S_{22} - S_{12}^2} = \frac{E_1}{1 - \nu_{12}\nu_{21}} \quad (4.18)$$

$$Q_{12} = \frac{-S_{12}}{S_{11}S_{22} - S_{12}^2} = \frac{\nu_{12}E_2}{1 - \nu_{12}\nu_{21}} \quad (4.19)$$

$$Q_{22} = \frac{S_{11}}{S_{11}S_{22} - S_{12}^2} = \frac{E_2}{1 - \nu_{12}\nu_{21}} \quad (4.20)$$

and

$$Q_{66} = 1/S_{66} = G_{12} \quad (4.21)$$

In practice $\nu_{12}\nu_{21}$ is usually very small and can be neglected ($\nu_{12}\nu_{21} = \nu_{12}^2 E_2/E_1$).

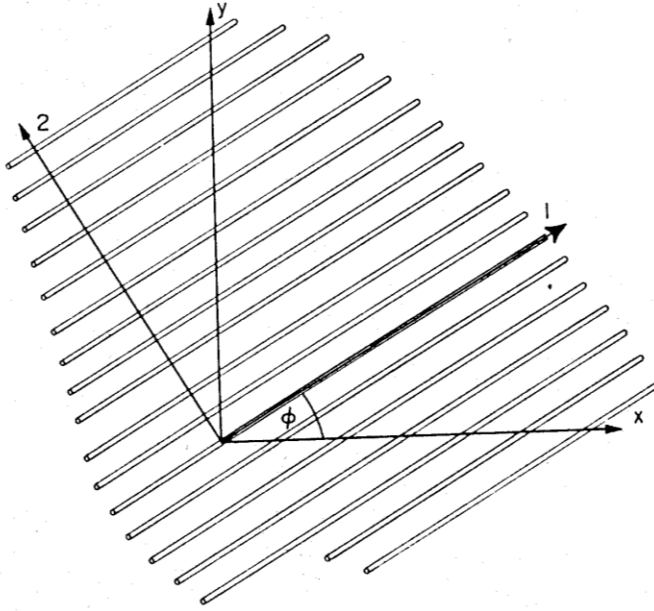


Fig. 4.9 Laminate axes (x, y) and lamina axes (1, 2).

4.3.2 Oblique Compliances

To determine the compliances in directions other than the 1 and 2 directions (and hence the moduli in the other directions) we use equations (1.13) and (1.15), together with the analogue of equation (1.13) for the stress parallel to the plane shown in Fig. 1.13. We will use our original x and y axes in Fig. 1.13 for the 1 and 2 axes, and use the direction of σ as our new x axis, as shown in Fig. 4.9. Thus instead of equation (1.13) we have

$$\sigma_x = \sigma_1 \cos^2 \phi + \sigma_2 \sin^2 \phi - 2\tau_{12} \sin \phi \cos \phi \tag{4.22}$$

and instead of equation (1.15) we have

$$\tau_{xy} = (\sigma_1 - \sigma_2) \sin \phi \cos \phi + \tau_{12} (\cos^2 \phi - \sin^2 \phi) \tag{4.23}$$

We obtain σ_y by considering a plane at right angles to the diagonal plane in Fig. 1.13. Thus

$$\sigma_y = \sigma_1 \sin^2 \phi + \sigma_2 \cos^2 \phi + 2\tau_{12} \sin \phi \cos \phi \tag{4.24}$$

These three equations can be written in matrix form:

$$\begin{pmatrix} \sigma_x \\ \sigma_y \\ \tau_{xy} \end{pmatrix} = \begin{pmatrix} \cos^2 \phi & \sin^2 \phi & -2 \sin \phi \cos \phi \\ \sin^2 \phi & \cos^2 \phi & 2 \sin \phi \cos \phi \\ \sin \phi \cos \phi & -\sin \phi \cos \phi & \cos^2 \phi - \sin^2 \phi \end{pmatrix} \cdot \begin{pmatrix} \sigma_1 \\ \sigma_2 \\ \tau_{12} \end{pmatrix} \tag{4.25}$$

If we write our transformation matrix as $[T]$, we find that the same transformation applies to the strains $\varepsilon_x, \varepsilon_y$, and $\gamma_{xy}/2$ with respect to the strains $\varepsilon_1, \varepsilon_2$, and $\gamma_{12}/2$, see equations (1.33) and (1.34):

$$\begin{vmatrix} \varepsilon_x \\ \varepsilon_y \\ \gamma_{xy}/2 \end{vmatrix} = [T] \cdot \begin{vmatrix} \varepsilon_1 \\ \varepsilon_2 \\ \gamma_{12}/2 \end{vmatrix} \quad (4.26)$$

The stress-strain relationships for these axes are

$$\begin{vmatrix} \varepsilon_x \\ \varepsilon_y \\ \gamma_{xy} \end{vmatrix} = \begin{vmatrix} \bar{S}_{11} & \bar{S}_{12} & \bar{S}_{16} \\ \bar{S}_{12} & \bar{S}_{22} & \bar{S}_{26} \\ \bar{S}_{16} & \bar{S}_{26} & \bar{S}_{66} \end{vmatrix} \cdot \begin{vmatrix} \sigma_x \\ \sigma_y \\ \tau_{xy} \end{vmatrix} \quad (4.27)$$

where $[\bar{S}]$ is the transformed compliance matrix, which can be evaluated by suitable matrix manipulation to give

$$\bar{S}_{11} = S_{11} \cos^4 \phi + (2S_{12} + S_{66}) \cos^2 \phi \sin^2 \phi + S_{22} \sin^4 \phi \quad (4.28)$$

$$\bar{S}_{12} = S_{12} (\cos^4 \phi + \sin^4 \phi) + (S_{11} + S_{22} - S_{66}) \cos^2 \phi \sin^2 \phi \quad (4.29)$$

$$\bar{S}_{22} = S_{11} \sin^4 \phi + (2S_{12} + S_{66}) \cos^2 \phi \sin^2 \phi + S_{22} \cos^4 \phi \quad (4.30)$$

$$\bar{S}_{16} = (2S_{11} - 2S_{12} - S_{66}) \cos^3 \phi \sin \phi - (2S_{22} - 2S_{12} - S_{66}) \cos \phi \sin^3 \phi \quad (4.31)$$

$$\bar{S}_{26} = (2S_{11} - 2S_{12} - S_{66}) \cos \phi \sin^3 \phi - (2S_{22} - 2S_{12} - S_{66}) \cos^3 \phi \sin \phi \quad (4.32)$$

$$\bar{S}_{66} = (2[S_{11} + S_{22}] - 4S_{12} - S_{66}) \cos^2 \phi \sin^2 \phi + S_{66} (\cos^4 \phi + \sin^4 \phi) \quad (4.33)$$

Notice that we now have shear stress-tensile stress interactions, although these were not present when the axes were normal to the planes of symmetry in the structure. We can write these expressions in terms of the engineering constants, using equation (1.64). For example

$$\frac{1}{E_x} = \frac{\cos^4 \phi}{E_1} + \left(\frac{1}{G_{12}} - \frac{2\nu_{12}}{E_1} \right) \cos^2 \phi \sin^2 \phi + \frac{\sin^4 \phi}{E_2} \quad (4.34)$$

This result can also be derived directly, without the matrix manipulations, as follows. Consider the lamina shown in Fig. 4.9, stressed by σ_x only (i.e. σ_y and τ_{xy} are zero). We can reverse the sign of ϕ in equation (4.25) to give

$$\begin{vmatrix} \sigma_1 \\ \sigma_2 \\ \tau_{12} \end{vmatrix} = [T(-\phi)] \cdot \begin{vmatrix} \sigma_x \\ \sigma_y \\ \tau_{xy} \end{vmatrix} \quad (4.35)$$

where we now have a counterclockwise rotation. This reverses the sign of the $\sin\phi$ terms only. Thus $\sigma_1 = \sigma_x \cos^2\phi$, $\sigma_2 = \sigma_x \sin^2\phi$ and $\tau_{12} = -\sigma_x \sin\phi \cos\phi$ and using equation (4.16), this gives

$$\varepsilon_1 = S_{11}\sigma_1 + S_{12}\sigma_2 = S_{11}\sigma_x \cos^2\phi + S_{12}\sigma_x \sin^2\phi \quad (4.36)$$

$$\varepsilon_2 = S_{12}\sigma_1 + S_{22}\sigma_2 = S_{12}\sigma_x \cos^2\phi + S_{22}\sigma_x \sin^2\phi \quad (4.37)$$

$$\gamma_{12} = S_{66}\tau_{12} = -S_{66}\sin\phi \cos\phi \quad (4.38)$$

Since, from equation (4.26)

$$\varepsilon_x = \varepsilon_1 \cos^2\phi + \varepsilon_2 \sin^2\phi - \gamma_{12} \sin\phi \cos\phi \quad (4.39)$$

we can use equations (4.36-4.38) for ε_1 , ε_2 , and γ_{12} to obtain

$$\varepsilon_x = \sigma_x \left\{ S_{11} \cos^4\phi + (2S_{12} + S_{66} \cos^2\phi \sin^2\phi + S_{22} \sin^4\phi) \right\}$$

Finally writing $1/E_x = \varepsilon_x/\sigma_x$ and substituting for the compliances gives

$$\frac{1}{E_x} = \frac{\cos^4\phi}{E_1} + \left(\frac{1}{G_{12}} - \frac{2\nu_{12}}{E_1} \right) \cos^2\phi \sin^2\phi + \frac{\sin^4\phi}{E_2} \quad (4.34a)$$

which is the same as the earlier equation (4.34)

We have two extra engineering constants, $\eta_{xyx} = E_x \bar{S}_{16}$ which can be evaluated using equations (4.31) and (1.64), and η_{xyy} . Notice that if we express the engineering constants as functions of ϕ , $E_x(\phi) = E_y(\pi/2 - \phi)$ and $\eta_{xyx}(\phi) = \eta_{xyy}(\pi/2 - \phi)$.

The engineering strain-stress relations are

$$\begin{vmatrix} \varepsilon_x \\ \varepsilon_y \\ \gamma_{xy} \end{vmatrix} = \begin{vmatrix} 1/E_x & -\nu_{xy}/E_x & \eta_{xyx}/E_x \\ -\nu_{xy}/E_x & 1/E_y & \eta_{xyy}/E_x \\ \eta_{xyx}/E_x & \eta_{xyy}/E_x & 1/G_{xy} \end{vmatrix} \cdot \begin{vmatrix} \sigma_x \\ \sigma_y \\ \tau_{xy} \end{vmatrix} \quad (4.41)$$

Also present are out-of-plane strains ε_3 (this is present when $\phi = 0$) and γ_{13} and γ_{23} (only present when $\phi \neq 0$).

Figure 4.10 shows the elastic constants, E_x and G_{xy} as a function of ϕ for E -glass-epoxy with $V_f = 0.5$. It is assumed that E_1 is given by the Rule of Mixtures, equation (4.3), and E_2 , G_{12} and ν_{12} are given by equations (4.8), (4.10), and (4.13). (Because E_y is complementary to E_x we do not need to plot it separately.)

Figure 4.11 shows the interaction terms ν_{xy} and η_{xyx} for the same composite. (η_{xyy} can be obtained from η_{xyx} .)

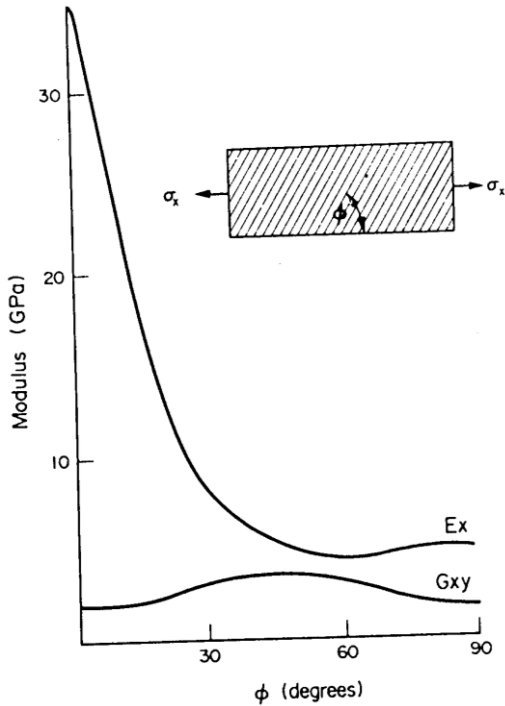
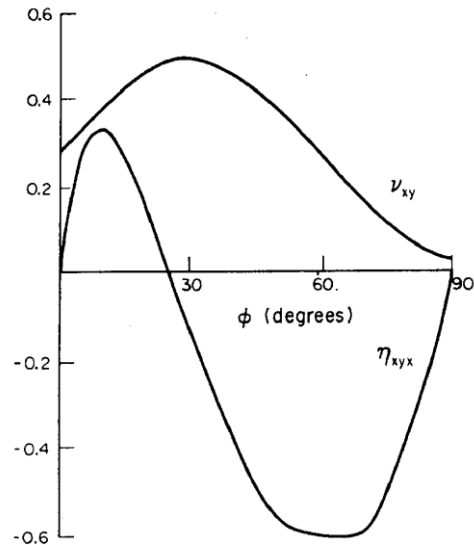


Fig. 4.10 Young's modulus and shear modulus oblique to the fibre direction in a glass-epoxy lamina with $V_f = 0.5$. ($E_1 = 35$ GPa, $E_2 = 5$ GPa, $G_{12} = 1.9$ GPa and $\nu_{12} = 0.3$).

Fig. 4.11 Poisson's ratio, and interaction term η_{xyx} oblique to the fibre direction for the glass-epoxy lamina shown in Fig. 4.10 (insert).



The shapes of the curves for the elastic constants depend a great deal on the degree of anisotropy of the lamina, the relative heights and sharpness of the peaks increasing with increasing anisotropy. For certain values of the constants, E_x can exceed E_1 for a range of values of ϕ , while with other values E_x can be less than E_2 . These situations are usually mutually exclusive; the former does not occur with glass-, carbon-, Kevlar-, or silicon carbide - polymers.

The existence of the shear stress-tensile stress interaction makes it difficult to perform off-axis tests on unidirectional laminates. For example, the grips normally used

for tensile tests will not permit shear at the ends of the specimen. Consequently, during such tensile tests the specimens distort and buckle.

4.3.3 Oblique Reduced Stiffnesses

The reduced stiffnesses, Q_{ij} were introduced in equation (4.17). When the axes are transformed from 1, 2 to the oblique set x, y , we use transformed stiffnesses \bar{Q}_{ij} :

$$\begin{vmatrix} \sigma_x \\ \sigma_y \\ \tau_{xy} \end{vmatrix} = \begin{vmatrix} \bar{Q}_{11} & \bar{Q}_{12} & \bar{Q}_{16} \\ \bar{Q}_{12} & \bar{Q}_{22} & \bar{Q}_{26} \\ \bar{Q}_{16} & \bar{Q}_{26} & \bar{Q}_{66} \end{vmatrix} \cdot \begin{vmatrix} \varepsilon_x \\ \varepsilon_y \\ \gamma_{xy} \end{vmatrix} \quad (4.42)$$

The \bar{Q}_{ij} are determined by similar transformations to those used for the \bar{S}_{ij} . The results also are very similar to those for the \bar{S}_{ij} (equations (4.28-4.33)).

$$\bar{Q}_{11} = Q_{11} \cos^4 \phi + 2(Q_{12} + 2Q_{66}) \cos^2 \phi \sin^2 \phi + Q_{22} \sin^4 \phi \quad (4.43)$$

$$\bar{Q}_{12} = Q_{12} (\cos^4 \phi + \sin^4 \phi) + (Q_{11} + Q_{22} - 4Q_{66}) \cos^2 \phi \sin^2 \phi \quad (4.44)$$

$$\bar{Q}_{22} = Q_{11} \sin^4 \phi + 2(Q_{12} + 2Q_{66}) \cos^2 \phi \sin^2 \phi + Q_{22} \cos^4 \phi \quad (4.45)$$

$$\bar{Q}_{16} = (Q_{11} - Q_{12} - 2Q_{66}) \cos^3 \phi \sin \phi + (Q_{12} - Q_{22} + 2Q_{66}) \cos \phi \sin^3 \phi \quad (4.46)$$

$$\bar{Q}_{26} = (Q_{11} - Q_{12} - 2Q_{66}) \cos \phi \sin^3 \phi + (Q_{12} - Q_{22} + 2Q_{66}) \cos^3 \phi \sin \phi \quad (4.47)$$

$$\bar{Q}_{66} = (Q_{11} + Q_{22} - 2[Q_{12} + Q_{66}]) \cos^2 \phi \sin^2 \phi + Q_{66} (\cos^4 \phi + \sin^4 \phi) \quad (4.48)$$

As with the compliances we find there are shear-tensile interactions terms \bar{Q}_{16} and \bar{Q}_{26} which did not exist in the transformed matrix (i.e. $\bar{Q}_{16} = \bar{Q}_{26}$ in equation (4.17)).

4.3.4 Oblique Strength Properties

Figure 4.12 shows the results of early experiments to determine the effect of testing aligned silica-aluminum obliquely to the fibre direction. The strength falls off rapidly with angle.

These results can be explained quite well by a maximum stress theory. Let the laminate strengths in the principal directions be σ_{1u} , σ_{2u} and τ_{12u} . For a uniaxial applied stress, σ_x , the stresses in the principal material directions can be obtained using the transformation matrix $[T]$ given in equation (4.25):

$$\begin{vmatrix} \sigma_1 \\ \sigma_2 \\ \tau_{12} \end{vmatrix} = [T] \cdot \begin{vmatrix} \sigma_x \\ \sigma_y \\ \tau_{xy} \end{vmatrix} \quad (4.49)$$

with $\sigma_y = \tau_{xy} = 0$. When σ_1 reaches σ_{1u} , and σ_2 reaches σ_{2u} and τ_{12} reaches the apparent shear strength, τ_{12u} , equation (4.49) gives the following three limiting conditions:

$$\sigma_x = \sigma_{1u} / \cos^2 \phi \tag{4.50}$$

$$\sigma_x = \sigma_{2u} / \sin^2 \phi \tag{4.51}$$

$$\sigma_x = \tau_{12u} / \sin \phi \cos \phi \tag{4.52}$$

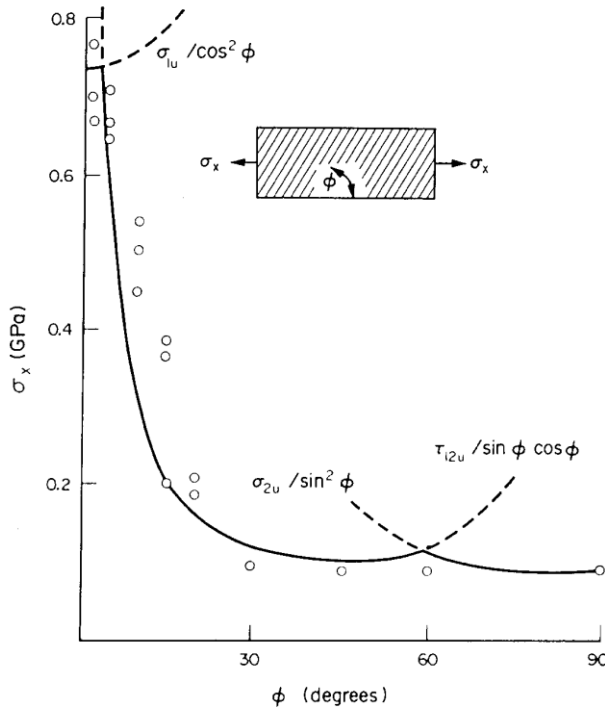


Fig. 4.12 Effect of fibre orientation on strength for silica-aluminium. Lines are drawn for maximum stress criterion for failure. (After Jackson, P.W., and Cratchley, D.,1966, J. Mech Phys. Solids, 14, 49.)

The ultimate strength in any direction ϕ to the fibres is the least of these values of σ_x for that value of ϕ . The curves shown in Fig. 4.12 were drawn using these equations. We observe three regions as ϕ increases.

1. For small ϕ , $\sigma_x = \sigma_{1u} / \cos^2 \phi$. This region ends when $\tan \phi = \tau_{12u} / \sigma_{1u}$ i.e. when σ_x given by equation (4.50) is equal to σ_x from equation (4.52).

2. For $\phi > \tan^{-1} (\tau_{12u} / \sigma_{1u})$ the strength is given by equation (4.52). This region ends when $\tan \phi = \sigma_{2u} / \tau_{12u}$.

3. For $\phi > \tan^{-1} (\sigma_{2u} / \tau_{12u})$ up to $\phi = \pi/2$, the strength is given by equation (4.51).

The maximum stress theory does not accurately predict the off-axis strength of reinforced polymer laminae. Figure 4.13 shows some results obtained with E-glass-epoxy. The curves with the cusps were drawn using equations (4.50) to (4.52). The experimental results fit a much smoother curve.

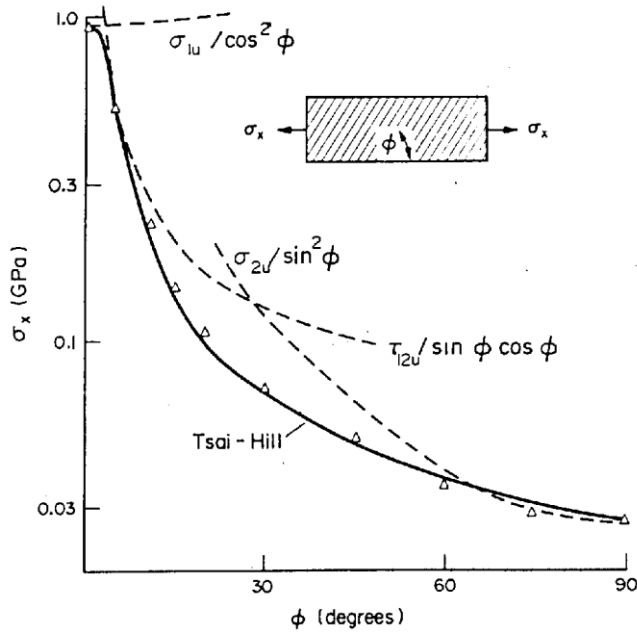


Fig. 4.13 Comparison of maximum stress criterion, and Tsai-Hill criterion for E-glass-epoxy, with experimental results. (After Tsai, S., 1968. Fund. Aspects of Fib. Reinf. Plas. Comp. (Ed. Schwartz, R.T. and Schwartz, H.S. Interscience, 3.)

An alternative theory, which uses a yield criterion for anisotropic materials introduced by Hill, and involves six independent constants, provides the appropriate smooth curve. (It is often incorrectly referred to as a distortional energy failure theory.) When a lamina is under a general state of stress the Hill criterion reduces to

$$\frac{\sigma_1^2}{\sigma_{1u}^2} - \frac{\sigma_1 \sigma_2}{\sigma_{1u}^2} + \frac{\sigma_2^2}{\sigma_{2u}^2} + \frac{\tau_{12}^2}{\tau_{12u}^2} = 1 \tag{4.53}$$

For σ_{1u} , σ_2 and τ_{12u} we use failure rather than yield stresses, as suggested by Hill. Using equation (4.49), again with $\sigma_y = \tau_{xy} = 0$, and substituting into equation (4.53) values of σ_1 , σ_{2u} , and τ_{12} so obtained, we find

$$\frac{\cos^4 \phi}{\sigma_{1u}^2} + \left(\frac{1}{\tau_{12u}^2} - \frac{1}{\sigma_{1u}^2} \right) \cos^2 \phi \sin^2 \phi + \frac{\sin^4 \phi}{\sigma_{2u}^2} = \frac{1}{\sigma_x^2} \tag{4.54}$$

The smooth curve shown in Fig. 4.12 was drawn using this equation.

(This approach has been developed further, by the introduction of more terms into the failure criterion. Although this might sometimes improve the prediction of the experimental results slightly, it is at the expense of much complication: see the reading list at the end of this chapter.)

A weakness of both the maximum stress and Tsai-Hill criteria is that they appear not to apply to real composite structures. Structures are designed to make as much use of the fibre strength as possible. Thus they are designed so that the fibres take the load, rather than the matrix. However, in the experiments which form the basis for these failure criteria, the fibres were not relieving the matrix of any significant fraction of the

load. Tsai's samples, for example, had widths, w , of about 11 mm and gauge lengths, l , of about 203 mm. So, for any fibre angle greater than about 3° , the matrix had to support nearly all the load, and so failed. No fibres were broken. To avoid this situation, the test specimen gauge length should be given by

$$l = w \cot \phi \quad (4.55)$$

Furthermore, his experimental results for balanced angle ply laminates were almost the same as for single laminae for stiffness as well as strength. As we shall show later (see Fig. 4.16) unidirectional laminae and angle ply laminates should have quite different stiffnesses. Whether these tests (Figs. 4.12 and 4.13) were measuring material properties is therefore debatable.

4.4 Laminates

Advanced composites are laminates of continuous aligned fibre composite laminae, or sometimes woven fibre composite laminae. The matrix is normally epoxy resin, but can be polyester for less exacting requirements, or polyimides, when good properties at temperatures above about 150°C are required, or thermoplastics such as PEEK when the matrix needs to be tough. Metal matrices are rarely used; ceramics even less.

The laminates should be designed to make the most efficient use of the directional nature of the laminae. Structural elements made from isotropic materials generally have redundant strength. The ideal design objective for laminates is to arrange for the strength and stiffness in any direction to be no greater than that required by the expected loads, with the appropriate safety factors. Such a procedure should result in the minimum structural weight. In this section a brief description of the main characteristics of laminates will be presented.

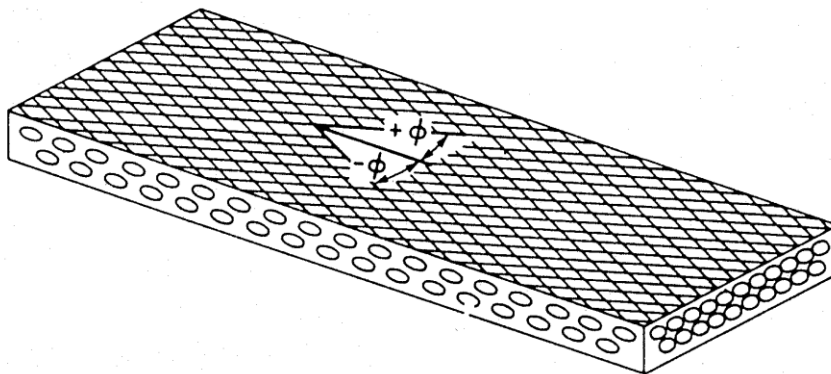


Fig. 4.14 Fibre directions in a two-layer laminate.

4.4.1 General Description of Laminates

The simplest types of fibre laminates are made by bonding together identical laminae, with particular fibre orientations with respect to each other. In cross-ply

laminates the orientations are parallel to and at right angles to a particular direction. Usually fibres in adjacent layers are at right angles to each other. In angle-ply laminates each layer has the fibres oriented at either $+\phi$ or $-\phi$ to some particular direction (see Fig. 4.14).

For special effects laminae may contain different types of fibre (hybrid composites) or have different matrices.

Laminates are often made so that they are symmetric about their central plane. A three-layer angle-ply laminate is symmetric if the two outer laminae are identical with respect to fibre direction and construction. If all three laminae have the same construction (including thickness, fibre volume fraction, etc.) then it is a regular symmetric angle-ply laminate. (Normally, though, symmetric laminates have an even number of layers.)

An antisymmetric cross-ply or angle-ply laminate consists of an even number of layers, where adjacent layers have fibres at 90° to each other (cross-ply) or at some other fixed angle (angle-ply).

The most widely accepted nomenclature for the orientation of successive layers involves a list of the angles with subscripts indicating the number of layers, together with s for "symmetrical". Thus

$$[90_2/0_3]_{2s}$$

means that there are two 90° layers at the surface, three 0° layers next, then two more 90° and three more 0° layers. We have now reached the centre plane of the composite, and the sequence is repeated in reverse, so that the other surface also has two 90° layers.

For angles between 0° and 90° a $+$ and $-$ sign is included, the $+$ indicating an anticlockwise rotation relative to the 0° direction (see Fig. 4.14). Thus

$$[\pm 30/\mp 45/0_2]_{3s}$$

means that the outside layer is oriented at $+30^\circ$, the next layer at -30° , followed by a layer at $+45^\circ$, then one at -45° and two at 0° . This is all repeated three times, and then the whole sequence is repeated in reverse. Commas are often used instead of slashes.

If fabric is used, e.g. with orientation at 45° to the principal direction, then this is designated with subscript f as follows.

$$[45_f/0/90/0]_s$$

This has such fabric on the outside surfaces.

If a symmetrical laminate has an odd number of layers then the central layer is indicated with a bar over; e.g.

$$[0/\overline{90}]_s$$

is a three ply composite with the 90° ply in the middle.

4.4.2 Introduction to Laminate Theory

The mechanical properties of fibre laminates are quite different from isotropic homogeneous materials. This is because of the strongly directional nature of the mechanical properties of the layers, and because of the complex interactions between the layers.

Classical laminate theory dates from the later 1950's and can be expressed with apparent simplicity by matrix notation.

However, this conceals a great deal of complexity. The layers interact to produce extra effects, sometimes undesirable. A striking example of this is observed with a two-layer angle-ply laminate. When this laminate is stressed along an axis of symmetry (or any other axis) it twists (see Fig. 4.15) due to coupling between bending and extension. Symmetric laminates with even numbers of layers are usually used to avoid this problem.

The twisting effect due to coupling between bending and extension falls off with the number of layers, when the $+\phi$ and $-\phi$ laminae are alternated. It becomes unimportant when there are more than 10 such layers. It has its maximum effect when $\phi = 45^\circ$ i.e. a cross-ply laminate stressed along a bisector of the interply angle.

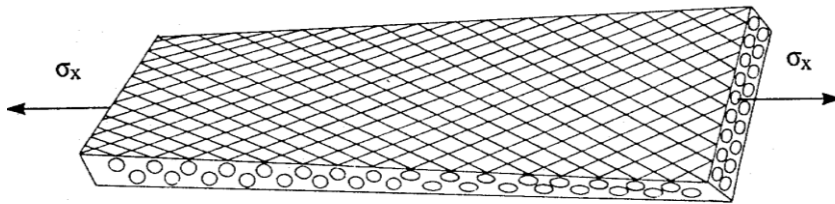


Fig. 4.15 Twisting of an unbalanced laminate due to a stress along an axis of symmetry.

Sometimes coupling is required to produce special effects. For example, some twist in turbine blades can be produced by the appropriate laminate design, together with control of the residual stresses that arise during curing. Also a two layer $0/90$ laminate can be used to estimate the resin shrinkage directly from its curvature if it is molded as a flat plate and then released. The reader who wants to take this up in more detail is referred to the reading list at the end of this chapter. Here we will only consider some relatively simple examples.

In high performance composites designs, where symmetric laminates are usually used, the analysis is relatively straightforward. This is because tensile-twisting interaction effects can be ignored and the 16 and 26 terms are zero. Thus, the forces per unit lengths, N , applied to the laminate can be expressed in terms of the strains using the laminate extensional stiffnesses A_{ij} , i.e.

$$\begin{vmatrix} N_x \\ N_y \\ N_{xy} \end{vmatrix} = \begin{vmatrix} A_{11} & A_{12} & A_{16} \\ A_{12} & A_{22} & A_{26} \\ A_{16} & A_{26} & A_{66} \end{vmatrix} \cdot \begin{vmatrix} \varepsilon_x^0 \\ \varepsilon_y^0 \\ \gamma_{xy}^0 \end{vmatrix} \quad (4.56)$$

where the ε_x^0 etc. indicate the strains in the mid plane, and

$$A_{ij} = \sum_{k=1}^n \bar{Q}_{ij} (z_k - z_{k-1}) \quad (4.57)$$

The z 's are the distances from the mid plane. Here $A_{16} = A_{26} = 0$, since z is positive above the mid plane and negative below it.

Flexure can be treated equally simply for applied moments M resulting from curvature κ

$$\begin{vmatrix} M_x \\ M_y \\ M_{xy} \end{vmatrix} = \begin{vmatrix} D_{11} & D_{12} & D_{16} \\ D_{12} & D_{22} & D_{26} \\ D_{16} & D_{26} & D_{66} \end{vmatrix} \cdot \begin{vmatrix} \kappa_x \\ \kappa_y \\ \kappa_{xy} \end{vmatrix} \quad (4.58)$$

$$D_{ij} = \frac{1}{3} \sum_{k=1}^n \bar{Q}_{ij} (z_k^3 - z_{k-1}^3) \quad (4.59)$$

and again due to the symmetry $D_{16} = D_{26} = 0$.

The treatment can be simplified still further for a symmetric angle ply laminate if the laminae (plies) are all made from the same prepreg tape, thickness t after cure. Thus $z_k - z_{k-1} = t$ and $\sigma_x = N_x / [n t]$ so that equation (4.56) becomes

$$\begin{vmatrix} \sigma_x \\ \sigma_y \\ \tau_{xy} \end{vmatrix} = \begin{vmatrix} \bar{Q}_{11} & \bar{Q}_{12} & 0 \\ \bar{Q}_{12} & \bar{Q}_{22} & 0 \\ 0 & 0 & \bar{Q}_{66} \end{vmatrix} \cdot \begin{vmatrix} \varepsilon_x \\ \varepsilon_y \\ \gamma_{xy} \end{vmatrix} \quad (4.60)$$

This matrix can be inverted to give the strains in terms of the stresses. Thus

$$\begin{vmatrix} \varepsilon_x \\ \varepsilon_y \\ \gamma_{xy} \end{vmatrix} = \begin{vmatrix} \hat{S}_{11} & \hat{S}_{12} & 0 \\ \hat{S}_{12} & \hat{S}_{22} & 0 \\ 0 & 0 & \hat{S}_{66} \end{vmatrix} \cdot \begin{vmatrix} \sigma_x \\ \sigma_y \\ \tau_{xy} \end{vmatrix} \quad (4.61)$$

where

$$\hat{S}_{11} = \bar{Q}_{22} / (\bar{Q}_{11}\bar{Q}_{22} - \bar{Q}_{12}^2) = 1 / E_x \quad (4.62)$$

$$\hat{S}_{12} = \bar{Q}_{12} / (\bar{Q}_{11}\bar{Q}_{22} - \bar{Q}_{12}^2) = -\nu_{12} / E_x \quad (4.63)$$

$$\hat{S}_{22} = \bar{Q}_{11} / (\bar{Q}_{11}\bar{Q}_{22} - \bar{Q}_{12}^2) = 1 / E_y \tag{4.64}$$

$$\hat{S}_{66} = 1 / \bar{Q}_{66} = 1 / G_{xy} \tag{4.65}$$

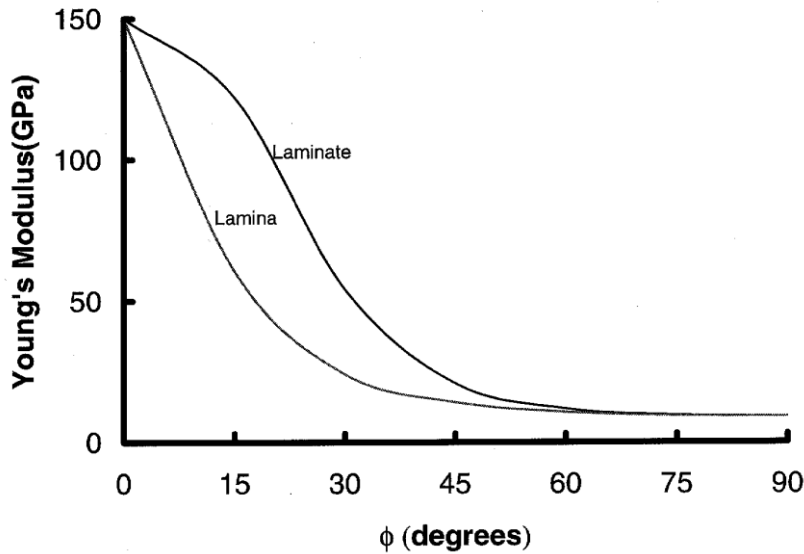


Fig. 4.16 E_x for angle ply laminate compared with unidirectional lamina: carbon epoxy with $E_1 = 150\text{GPa}$, $E_2 = 9\text{GPa}$, $G_{12} = 6\text{GPa}$ and $\nu_{12} = 0.27$.

Hence the engineering constants can be calculated:

$$\nu_{xy} = \bar{Q}_{12} / \bar{Q}_{22} \tag{4.66}$$

and

$$E_x = \bar{Q}_{11} - \nu_{xy}\bar{Q}_{12} \tag{4.67}$$

using equations (4.43), (4.44) and (4.45) for the \bar{Q}_{ij} .

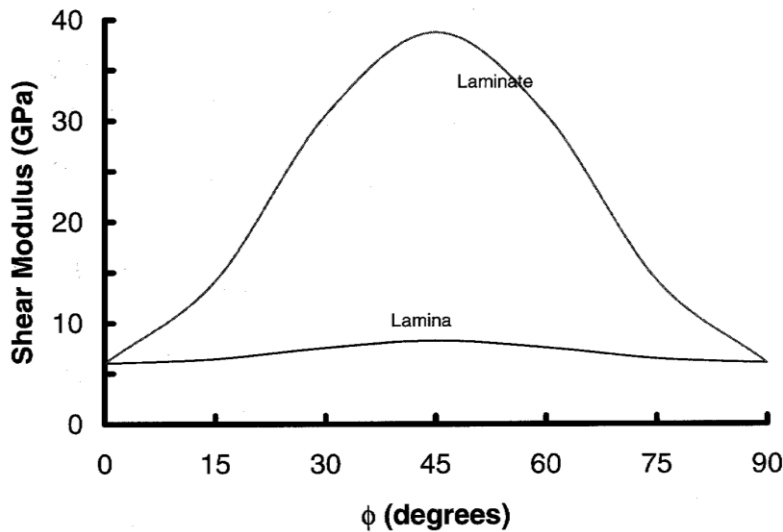


Fig. 4.17 Angle ply laminate shear modulus, G_{xy} , compared with unidirectional lamina. Carbon epoxy: see Fig. 4.16 for data.

G_{xy} can be determined directly from equation (4.65) using equation (4.48) for \bar{Q}_{66} and E_y can be determined using equation (4.67) since $E_y(\phi) = E_x(90 - \phi)$.

These equations should be compared with equations (4.28) for $1/E_x$, (4.29) for $-v_{xy}/E_x$, (4.30) for $1/E_2$ and (4.33) for $1/G_{xy}$ for the off-axis uniaxial laminate (or single lamina). Fig. 4.16 compares E_x for the two cases, for carbon-epoxy. It may be seen that the deformation is constrained in the angle ply laminate. This increases the modulus by about a factor of two at 15° .

G_{xy} is compared in Fig. 4.17. Once more the interlaminar constraining effects are quite large. The Poisson's ratio is also much increased; see Fig. 4.18.

The values for E_2 and G_{12} used for these figures, i.e. 9GPa and 6GPa respectively, are within the range of values measured on practical laminae. These are somewhat higher than the inverse Rule of Mixtures values. The Poisson's ratio, i.e. 0.27, while close to the Rule of Mixtures value, is also within the range observed in practice.

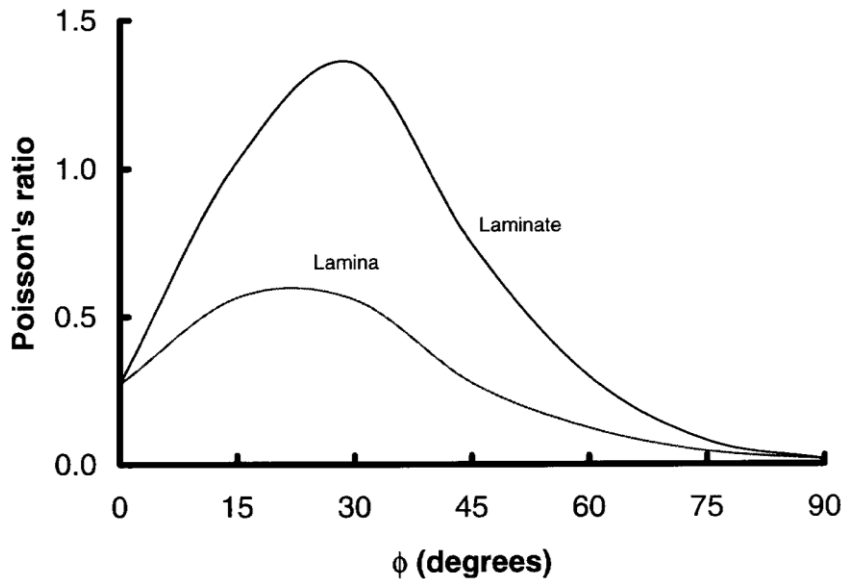


Fig. 4.18 Angle ply laminate Poisson's ratio, v_{xy} , compared with unidirectional lamina. Carbon epoxy: see Fig. 4.16 for data.

The engineering constants for $[0/90]_s$ laminates also can be treated very simply, as long as the laminae are made using the same prepreg tapes, so that t is constant. Here we use mean values; thus

$$A_{ij} = 2t(Q_{ij}(0) + Q_{ij}(90)) \quad (4.68)$$

and instead of equation (4.60) we have

$$\begin{vmatrix} \sigma_x \\ \sigma_y \\ \tau_{xy} \end{vmatrix} = \begin{vmatrix} (Q_{11} + Q_{22})/2 & Q_{12} & 0 \\ Q_{12} & (Q_{11} + Q_{22})/2 & 0 \\ 0 & 0 & Q_{66} \end{vmatrix} \cdot \begin{vmatrix} \varepsilon_x \\ \varepsilon_y \\ \gamma_{xy} \end{vmatrix} \quad (4.69)$$

and our compliances are

$$\hat{S}_{11} = \frac{2(Q_{11} + Q_{22})}{(Q_{11} + Q_{22})^2 - 4Q_{12}^2} \quad (4.70)$$

$$\hat{S}_{12} = \frac{Q_{12}}{(Q_{11} + Q_{22})^2 - 4Q_{12}^2} \quad (4.71)$$

$$\hat{S}_{22} = \hat{S}_{11} \quad (4.72)$$

$$\hat{S}_{66} = 1/Q_{66} \quad (4.73)$$

Thus, substituting values etc. we find

$$E_x = \frac{(E_1 + E_2)^2 - 4\nu_{12}E_2^2}{2(E_1 + E_2)(1 - \nu_{12}\nu_{21})} \quad (4.74)$$

$$\nu_{xy} = 2\nu_{12}E_2 / (E_1 + E_2) \quad (4.75)$$

and

$$G_{xy} = G_{12} \quad (4.76)$$

4.4.3 Strength Results With Wide Pieces

Practical considerations have led to tests that involved relatively long and slender specimens. It has already been mentioned that Tsai used 11mm wide and 203mm long samples. The results shown in Fig. 4.11 came from reinforced metal specimens designed to ensure that, even at the lowest angle, no fibre went from one end to the other of the specimens. (The width used was 4.5mm and the length 25.4mm. The experiments were designed to test the 1961 theory due to Stowell & Liu: equations (4.50) – (4.52). Interested readers can follow this up through the reference given in the caption to Fig. 4.12.)

Moderately long and narrow specimens are normally used for tensile tests on metals and polymers. This ensures that end effects, especially the local stresses induced by the grips, do not influence the results. However, with laminates we are obliged to use short and wide test specimens to minimize the edge softening effect.

Simply testing a wider and shorter specimen, and so loading the fibre at least partially, changes the picture completely. Fig. 4.19 shows such a specimen which has been tested to failure. It can be seen that all the fibres between the notches have been broken. The strength of this sample was much higher than estimated from the failure criteria, equations (4.50) – (4.52) and (4.54).

The specimen shown in the figure is a four layer balanced angle ply laminate $[\pm 15]_s$. Such laminates are easier to test than unidirectional materials tested obliquely, since as indicated in section 4.4.2 they do not twist when loaded. Tsai tested such

laminates also and got very similar results to those shown for unidirectional laminates, Fig. 4.12, probably because these specimens had the same 11mm width and 203mm length so that the fibres were not significantly stressed.

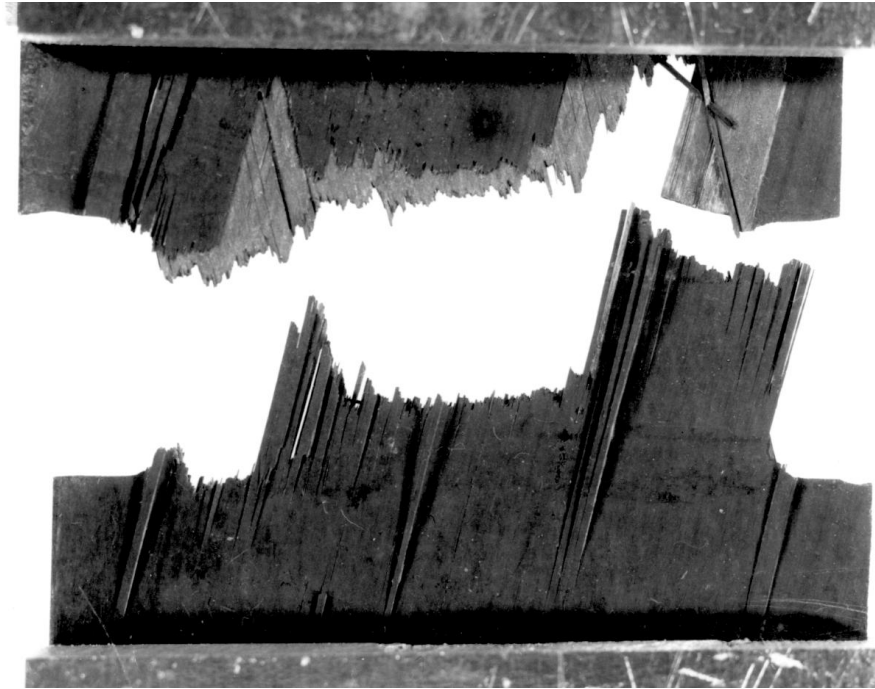


Fig. 4.19 Failed carbon-epoxy 15° angle ply laminate. Gauge length 20mm and width between the notches 34 mm.

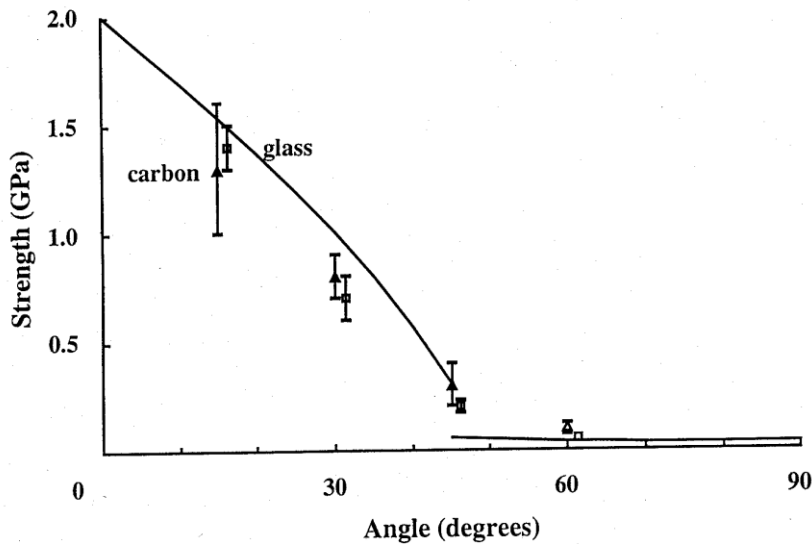


Fig. 4.20 Results of tests on angle ply laminates with 2 cm gauge length and 34 mm width between the notches. (After Khatibzadeh, M. and Piggott, M.R., 1996, *Comp. Sci. Tech.* 56, 1443-51.)

The wider specimens give a much less precipitous decline of strength with angle: see Fig. 4.20. This is a linear plot for strength, while Fig. 4.13 was a logarithmic one, so the difference is much larger than suggested by a casual glance. The decline of strength with ϕ appears to be approximately linear up to 45°.

An approximate fit can be obtained if we assume that the centrally located fibres break, while those near the edges slide off. The fraction that slides off is $\tan \phi / \tan \phi_0$ where ϕ_0 depends on the geometry of the gauge length (ideally $\tan \phi_0 =$ the width of the specimen between the notches divided by the gauge length). The fraction that involves fibre failure is equal to $1 - \tan \phi / \tan \phi_0$. Thus

$$\sigma_x \cong \sigma_{1u} (1 - \tan \phi / \tan \phi_0) + \tau_{12u} / [\cos^2 \phi \tan \phi_0] \tag{4.77}$$

Here we have assumed that there is no loss of fibre strength when the fibres are stressed obliquely, and that the apparent shear failure contribution is given by equation (4.52) multiplied by $\tan \phi / \tan \phi_0$. The curve fit was done for $\phi_0 = 48^\circ$ and $\tau_{12u} = 60\text{MPa}$.

For $\phi > \phi_0$, we assume that no fibres are broken, and since equation (4.51) gives a lower result than equation (4.52), we use equation (4.51), as for the maximum stress theory, with $\sigma_{2u} = 30\text{MPa}$, as for Fig. 4.13.

This type of test is still not good enough for design purposes, because of the variable edge effect represented by $\tan \phi_0$. Edge effects are further reduced when tubes are tested by applying internal pressure. (Although these tubes may leak before breaking, they can be tested to destruction using a rubber bladder inside.) In some early tests in 1978, in which tubes with different winding angles were pressurized until they broke, the decrease in strength was approximately linear with ϕ , between 30° and 60° . At $\phi = 30^\circ$ the strength was about four times higher than the Tsai-Hill prediction, equation (4.54).

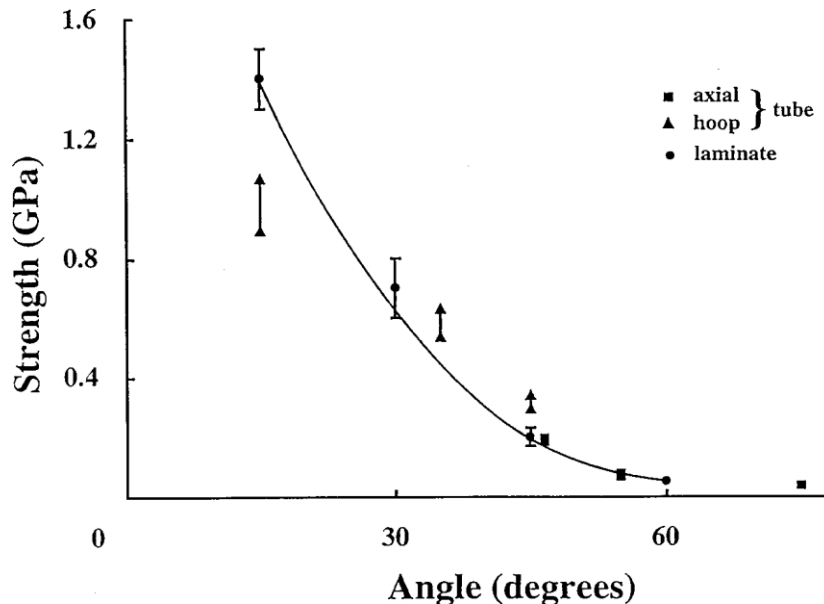


Fig. 4.21 Comparison of test results from short notched specimens for glass-epoxy laminates, shown in Fig. 4.20, with results from tests on glass-polyester filament wound tubes. (Tube results after Soden, P.D., Kitching, R., Tse, P.C., Tsavalas, Y. and Hinton, M.J., 1993, *Comp. Sci. Tech.* 46, 363-78.)

More recent work with better glass fibres and improved polymers gives much higher strengths, and provides strong support for the tests on the short, wide laminates. Fig. 4.21 shows the results from filament wound glass-polyester tubes subjected to hoop stress only ($\phi = 15\text{-}45^\circ$) and axial stress only ($\phi = 45\text{-}75^\circ$). Also shown (the line joining the solid circles) are the glass-epoxy angle ply laminate results for short, wide specimens.

The agreement is moderately good, except for the 15° results, where the flat laminate strength is greater. It should be noted that the axial tests on the tubes are not directly comparable with the flat laminate results. This is because axially tested tubes can collapse inward. As can be seen from the 45° results, this reduces the strength by at least 50%.

The filament wound tubes giving the results shown in Fig. 4.21 were very resistant to cracking, and performed better under biaxial tensile stresses than under uniaxial.

There are good reasons for expecting Kevlar laminates to be more tolerant than glass or carbon when $\phi > 40^\circ$. This is because single fibre tests give higher results for Kevlar than for glass at high angles; see Fig. 4.22. In these tests, single fibres were deeply embedded in epoxy resin, with their ends exposed. They were then pulled obliquely at a range of angles, ϕ , and their strength, $\sigma_{fu\phi}$, measured. The embedded depth was such that they broke rather than pulling out. In Fig. 4.22 the lines drawn on the curves are given by

$$\sigma_{fu\phi} = \sigma_{fu0} \left\{ 1 + (1 - \phi / \phi_h)^{1/3} \right\} \quad (4.78)$$

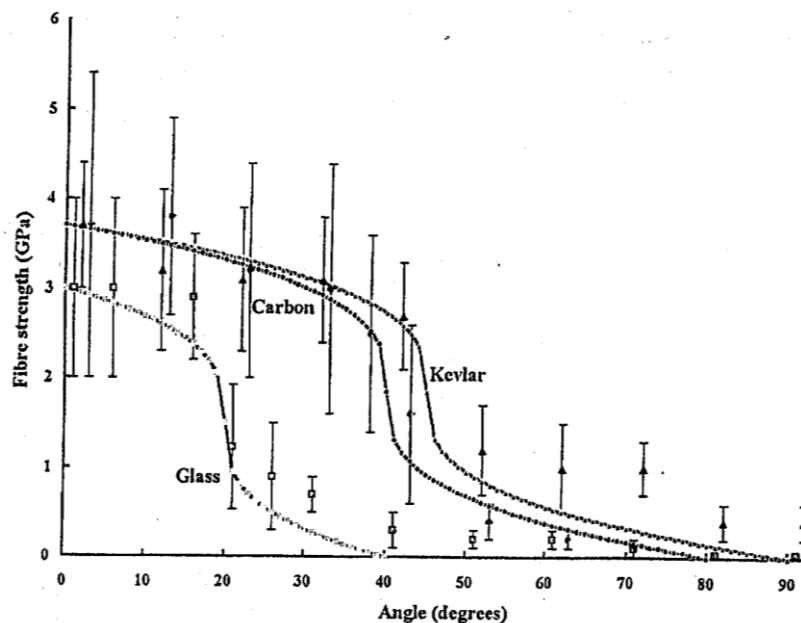


Fig. 4.22 Single fibres pulled obliquely: breaking strength vs angle of pull. (After Khatibzadeh, M. and Piggott, M.R., 1996, *Comp. Sci. Tech.* 56, 1435-42.)

Here $\sigma_{f_{i0}}$ is the strength for $\phi = 0$ and ϕ_h is the angle for which $\sigma_{f_{i\phi}} = \sigma_{f_{i0}}/2$, i.e. the half strength angle. Half strength angles ranged from about 20° for glass to 45° for Kevlar. Carbon had $\phi_h = 40^\circ$, but this was reduced to 30° when the resin was cured at high temperature. Thus ϕ_h depends on the hardness of the resin as well as on the fibre properties. (The error bars in Fig. 4.22 indicate one standard deviation on either side of the mean values.) These results probably represent upper limits for the fibre contribution to the strength of angle ply laminates.

More recent results with carbon-epoxy angle ply laminates highlight the test coupon aspect ratio problem. Fig. 4.23 shows some results from 20mm long samples, 25mm and 43mm wide. Also shown are strengths obtained with ASTM D3039 standard samples which have a gauge length of 150mm and a width of 25mm. The standard samples (marked ASTM) gave the lowest results at all angles tested (15° to 60°) and were about half of the 43mm wide, 20mm long sample results at 15° and 30° . The 25mm wide coupons were about 25% weaker at 15° and 30° but were about the same at 45° - 90° . Although these samples were not notched, the 43mm wide samples gave about the same results as the notched samples shown in Fig. 4.20.

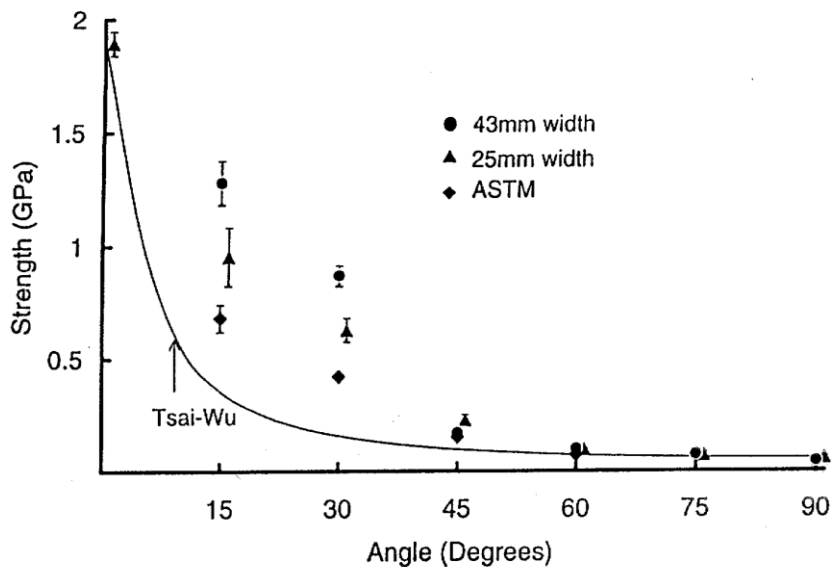


Fig. 4.23 Strength results from carbon-epoxy angle ply laminates. ASTM D 3039 standard samples used, as well as 20mm long samples, 25mm wide and 43mm wide, as marked. Samples unnotched. (After Wang J., and Piggott, M.R., 2000, *Polymer Comp.* 21, 506-13.)

(The solid line marked Tsai-Wu in Fig. 4.23 is from a theory similar to Tsai-Hill, equation (4.54), but including compressive strength as well. It is treated in some texts as an industry standard and is widely used in computer design software. Designs based on it will surely be ponderous.)

4.4.4 Elastic Constants for Wide Samples

The recent work with tubes also suggests that the elastic constants are probably underestimated if results from narrow specimens are used. Again they lend strong support to the tests on the wide angle ply laminates. Fig. 4.24 compares the nominal

stiffness of the angle ply laminates with the Young's modulus estimated from equation (4.67) for S-glass epoxy.

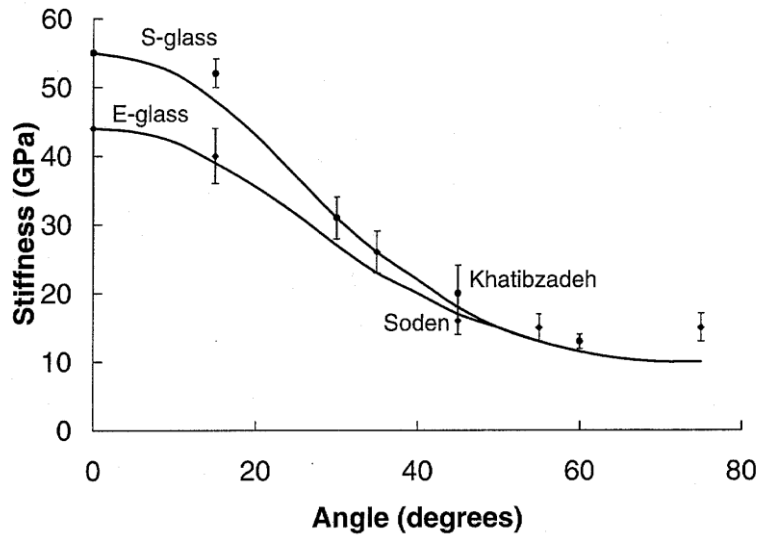


Fig. 4.24 Stiffness versus ϕ for wide glass-epoxy $\pm \phi$ balanced angle ply laminates and equivalent tube structures. The solid circles are nominal stiffnesses for the S-glass epoxy laminates. The diamond shapes are Young's moduli for the E-glass epoxy tubes. (After Khatibzadeh, M. and Piggott, M.R., 1997, *Comp. Sci. Tech.*, **56**, 1443-51 For Soden references, see Fig. 4.21.) Solid lines are given by equation (4.67) with $E_1 = 56\text{GPa}$ (S-glass); $E_1 = 44\text{GPa}$ (E-glass).

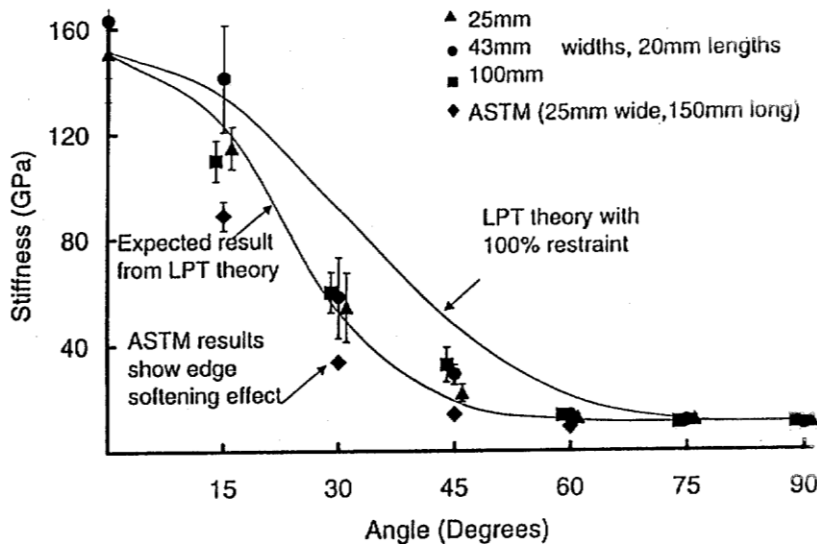


Fig. 4.25 Tensile moduli of unnotched carbon-epoxy angle ply laminates. Upper line is \bar{Q}_{11} and lower line is E_x (equation (4.67)). Specimen dimensions as indicated.

These stiffnesses were obtained from the cross head movement in the tests on wide laminates used for Fig. 4.21. They are normalized to give the Rule of Mixtures modulus (equation (4.3)) for $\phi = 0^\circ$. The laminate result is somewhat high for $\phi = 15^\circ$; otherwise the laminate theory (equation (4.67)) and wide laminate results are in good agreement. Also shown in the Figure are Soden et al's measurements on tubes using

strain gauges. These are compared with the theoretical curve for E-glass-epoxy. Again, agreement with equation (4.67) is moderately good.

Elastic constants were also measured in the tests shown in Fig. 4.23. Fig. 4.25 shows that the apparent stiffness depends on test coupon aspect ratio, the ASTM result being the lowest, and except for the $[\pm 15]_s$ samples, the 100mm wide, 20mm long samples being the highest. (The anomalous 15° result is probably due to the difficulty of ensuring stress uniformity in the widest specimens). The upper line is \bar{Q}_{11} , equation (4.43) and the lower line is E_x , equation (4.67). ASTM D 3039 underestimates the modulus, and the standard has recently been modified to take account of this.

Fig. 4.26 shows the apparent Poisson's ratios of these composites. In this case we conclude that the ASTM coupon is working well. The solid line is for ν_{xy} from equation (4.66) and agreement is good at all angles tested. The low results for the lower aspect ratio specimens are due to the grip constraint.

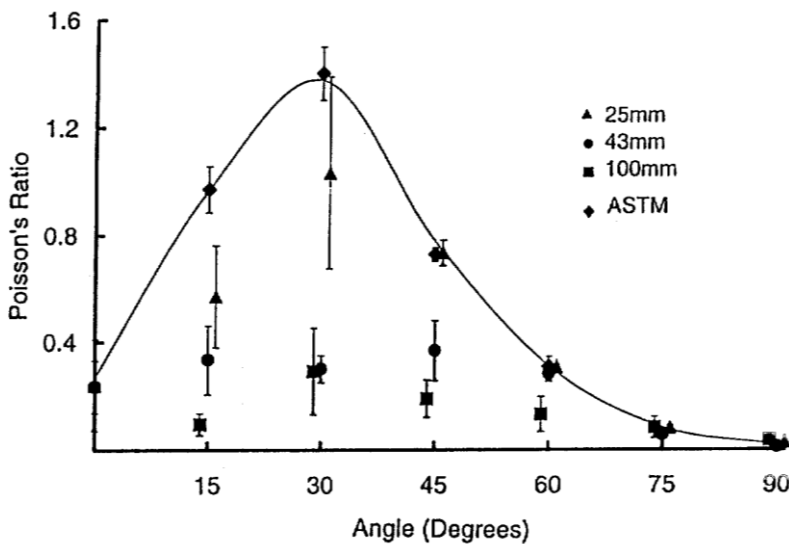


Fig. 4.26 Poisson's ratios of unnotched carbon-epoxy angle ply laminates. Line is ν_{xy} (equation 4.66). Specimen widths as indicated.

Soden et al also obtained results for Poisson's ratio which agreed moderately well with laminate theory with a maximum at $[\pm 35]_s$, of 0.55 ± 0.09 , as compared with a theoretical value of 0.52. High Poisson's ratios have been reported by Hine et al; see Fig. 4.27. They used ultrasound at 2.5MHz. The high value of 1.9 at $[\pm 20]_s$ is accompanied by an out of plane expansion, giving $\nu_{xz} = -0.6$. The curves were drawn using measured lamina elastic constants.

(When a solid is stressed in tension, the atoms move further apart so one might expect the volume to increase. (The only known exception to this is rubber, which has ν very close to 0.5 at low stress. Here the molecules are perceived as having hinges, so that they can re-align, and hence elongate without volume change.) So the sum $\nu_{xy} + \nu_{xz}$ would be less than 1.0. In Fig. 4.27, this is not the case. This is because the only firm

requirements are that all moduli, including the bulk modulus should be positive. This is another example of the counter - intuitive nature of laminates.)

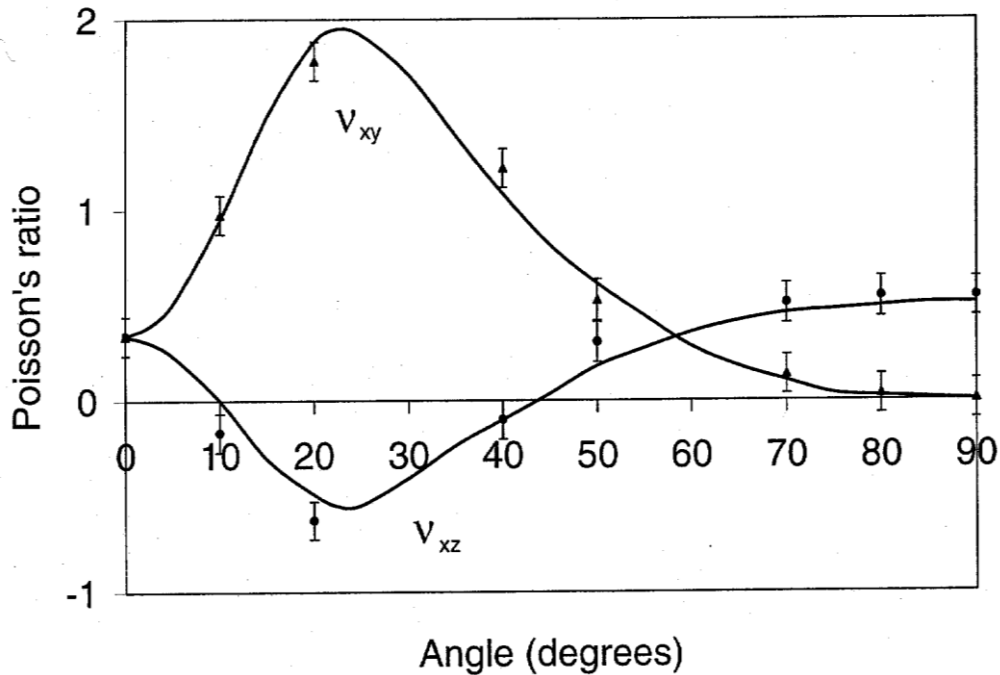


Fig. 4.27 Poisson's ratios for carbon-epoxy laminates made from laminae with $E_1 = 174\text{GPa}$, $E_2 = 15.5\text{GPa}$. (After Hine, P.J., Duckett, R.A. and Ward, I.M., 1997, *J. Mat. Sci. Lett.* **16**, 541-4.)

4.4.5 Design Problems With Laminates

Designers of aircraft usually use combinations of 0° , 90° and $\pm 45^\circ$. A very simple process is used for the initial design. They assume weighting factors, 1.0 for unidirectional fibres in the stress direction and 0.1 when normal to the stress direction (i.e. only 10% of the unidirectional strength is allowed for these layers). They combine proportions of these, according to design requirements, with a number of pairs of $\pm 45^\circ$, also weighted at 0.1. Final design is based on the allowable strain. Other values of ϕ are seldom used.

Unfortunately, transverse plies (i.e. 90°) are prone to cracking and this is a major thrust of current laminate research. Cracking also occurs with smaller off axis angles, but there has been relatively little research on this.

We know that, with filament wound tubes, leaking occurs before final burst. For example, with a 75° winding angle, similar to a $[\pm 15]_s$ laminate, leakage is very slight, but started at about 40% of the burst stress, in Soden and his group's work. With 55° ($[\pm 35]_s$ equivalent) this increased to 60% and was about 90% for $\pm 45^\circ$, with much more copious leakage in both these cases.

TABLE 4.2 - Results of Tensile Tests on S Glass-epoxy Laminates: Wide Samples

Laminate	First crack		Breaking Point		Stress Ratio	Stiffness (GPa)
	Stress (MPa)	Strain (%)	Stress (MPa)	Strain (%)		
$[\pm 30]_{2s}$	380±50	1.52	390±50	1.56	0.97	25
$[\pm 40]_{2s}$	250±30	1.56	270±30	1.69	0.93	16
$[0\pm 60]_s$	380±40	1.65	390±40	1.70	0.97	23
$[90/\pm 45/0]_s$	320±90	1.39	450±30	1.96	0.71	23

Careful observation of flat sheets during tensile testing confirms that 90° plies should be avoided. Other, less crack prone structures could well provide the stiffness and strength needed, as indicated in Table 4.2. In this table the stiffnesses are Young's moduli estimated using equation (4.57) etc., and the same data as used for the upper curve in Fig. 4.24. The strains were evaluated on the assumption of elastic behaviour up to failure. It is notable that the $[0/\pm 60]_s$ structure gives the highest first crack strain and the $[90/\pm 45/0]_s$ gives the lowest.

However, angle ply laminates have the problem of high Poisson's ratios: see Figs 4.26 and 4.27. Thus, if constrained at the ends, a sheet of angle ply laminate will develop transverse stresses near the ends, and will assume a slight hour glass shape near the centre. The effect is dependent on the E_1/E_2 ratio for the material used to make the laminate.

Fig. 4.28 shows $\nu_{xy\max}$ plotted vs E_1/E_2 , (log scales) using equation (4.66). For very flexible matrices, ν_{xy} can be very high. For example rubbers can have Young's moduli of 2MPa or less, see Table 1.1, giving $E_2 \sim 8$ MPa. So when reinforced with stiff carbon, $E_1/E_2 \sim 19,000$ and $\nu_{xy\max} \sim 50$.

The effect is independent of G_{12} , so long as this is not greater than E_2 (G_{12} is usually about $0.6 E_2$). The line in Fig. 4.28 is given approximately by

$$\nu_{xy\max} = \nu_{12} + 0.45 \sqrt{E_1 / E_2} \quad (4.79)$$

for $0.3 < \nu_{12} < 0.4$ where $\nu_{xy\max}$ is the maximum value of ν_{xy} . The value of ϕ giving $\nu_{xy\max}$ decreases as E_1/E_2 increases. These values of ϕ are shown at the top of the figure.

This result seems rather remarkable; especially when the same plot is obtained when the shear modulus is zero. If it were due to a scissoring effect, one would expect this to be resisted by a shearing action and hence shear modulus should be important. In many texts it is pointed out that laminate theory is contrary to intuition. This result is a case in point.

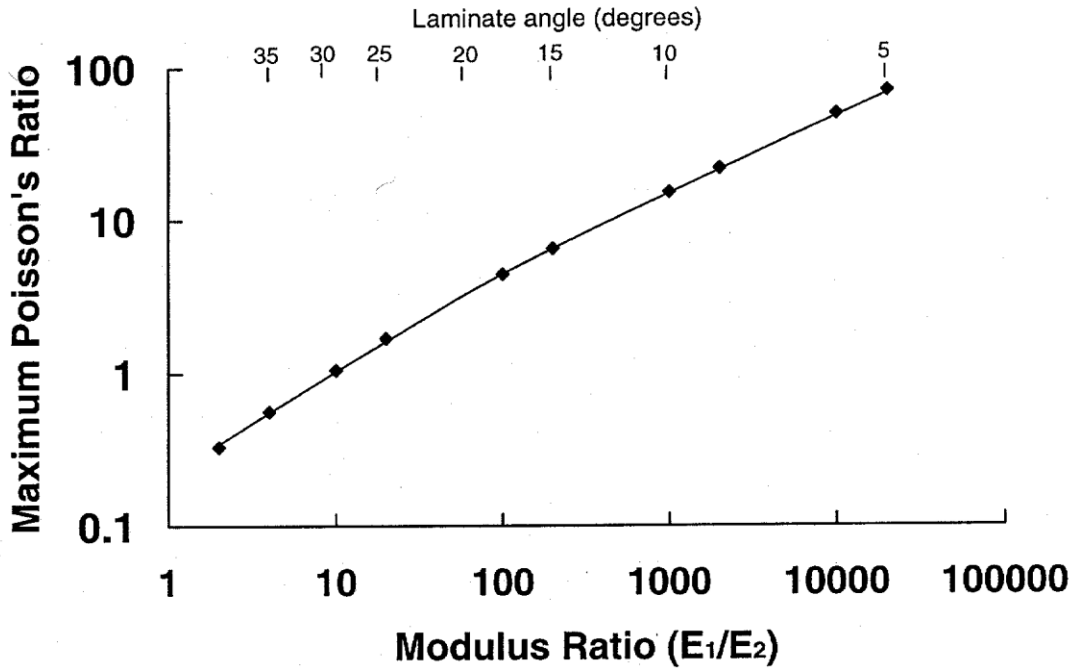


Fig. 4.28 Maximum angle ply laminate Poisson's ratios plotted vs. modulus ratio E_1/E_2 . Laminate angle for maximum shown at top.

There are additional failure modes that do not occur at all with isotropic materials. For example, the laminate can split apart due to interlaminar stresses. These stresses are very high at the edge of the laminate, but at about one laminate thickness distant from the edge they become negligible. They are present near any free edge, such as a round hole. However, the stresses are affected by the stacking sequence of the laminae, and splitting can be minimized or even prevented by using the appropriate sequence. A structure which is particularly sensitive to delamination is $[+35_2/-35_2/0_2/90_2]_s$. Even with an extremely tough matrix, such as polyetherether ketone (PEEK), it delaminates at a strain of about 0.9%. Delamination is catastrophic and complete. The specimen breaks into two pieces at the $0^\circ/90^\circ$ ply interfaces.

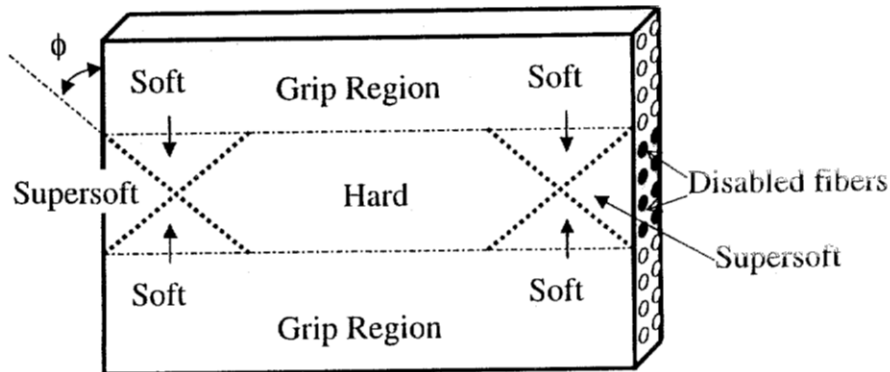


Fig. 4.29 Short wide sample showing the three softness regions.

It should be appreciated that, with composites, the material itself is usually designed for a particular application. To make the best use of these versatile materials, it is important to construct a laminate that just meets the requirements, including appropriate safety factors. This means that anisotropy must be a part of the design. If, through the use of inappropriate criteria (eg. Tsai-Hill, or maximum stress) the material is overdesigned, it may be more economical to use a metal.

4.4.6 Edge Softening Effect

The modulus results shown in Fig. 4.25 can be explained, at least qualitatively, if we suppose that fibres which terminate at the specimen edges instead of going fully into both grips are partially unloaded as they approach the specimen edges. Thus the load near the edges is borne mainly by the polymer, leading to an edge softening effect.

To attempt a quantitative analysis of this we use Fig. 4.29. The region labelled "supersoft" only has fibres which terminate at the edges. Let this have a modulus of E_{x1} which is assumed to be constant throughout this region. Similarly, we will assume E_{x2} for the soft region and E_{x3} for the hard region. The apparent modulus of the whole gauge length can be evaluated by summing the various contributions. This is accomplished by integration.

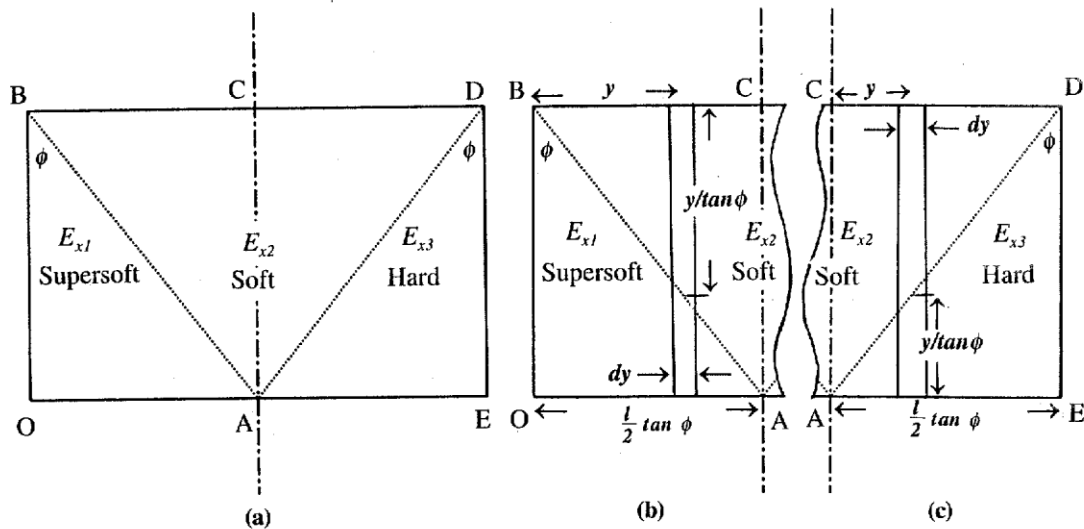


Fig. 4.30 Upper half of left hand edge region shown in Fig. 4.29, (a) region considered, (b) left half of this, (c) right half of this.

Fig. 4.30a shows the top half of the left hand edge region, with OE being along the centre line of the gauge length, and BD being where the composite enters the upper grip. First consider $OACB$, Fig. 4.30b. The x axis is here vertical, in keeping with the notation that gave us E_x . So the y axis is to the right. The element, distant y from O , having width dy extends distance $y/\tan\phi$ into the soft region, the remainder, i.e. $l - y/\tan\phi$, being in the supersoft region. (l is the gauge length). These regions are in series as far as

the loading is concerned, so we add the compliances. So the effective modulus E for the strip is given by:

$$\frac{1}{2E} = \frac{l/2 - y \cot \phi}{E_{x1}} + \frac{y \cot \phi}{E_{x2}} \quad (4.80)$$

The modulus contribution of OACB is therefore the reciprocal sum of these, obtained by integration:

$$E_{OAC} = \cot \phi \int_0^{l \tan \phi / 2} \frac{E_{x1} E_{x2} dy}{l E_{x2} / 2 + y \cot \phi (E_{x1} - E_{x2})} \quad (4.81)$$

Doing the integration and re-arranging gives

$$E_{OAC} = \frac{E_{x1} E_{x2}}{E_{x1} - E_{x2}} \ln \left\{ \frac{E_{x1}}{E_{x2}} \right\} \quad (4.82)$$

The modulus contribution of AEDC can be treated similarly. Starting our y axis at A instead of O , Fig. 4.30c, we have

$$E_{AED} = \cot \phi \int_0^{l \tan \phi / 2} \frac{E_{x2} E_{x3} dy}{l E_{x3} / 2 + y \cot \phi (E_{x2} - E_{x3})} \quad (4.83)$$

In this E_{x2} replaces E_{x1} , and E_{x3} replaces E_{x2} in equation (4.80). Thus, without further ado, we can write

$$E_{AED} = \frac{E_{x2} E_{x3}}{E_{x2} - E_{x3}} \ln \left\{ \frac{E_{x2}}{E_{x3}} \right\} \quad (4.84)$$

We can now obtain the modulus of the whole test specimen by adding the various contributions in the appropriate proportions:

$$E_x = \frac{1}{w} \{ (w - 2l \tan \phi) E_{x3} + l \tan \phi (E_{OAC} + E_{AED}) \} \quad (4.85)$$

So our final result is

$$E_x = E_{x3} - \frac{l \tan \phi}{w} \left[2E_{x3} - \frac{E_{x1} E_{x2}}{E_{x1} - E_{x2}} \ln \left\{ \frac{E_{x1}}{E_{x2}} \right\} - \frac{E_{x2} E_{x3}}{E_{x2} - E_{x3}} \ln \left\{ \frac{E_{x2}}{E_{x3}} \right\} \right] \quad (4.86)$$

For some test coupon aspect ratios, and for some angles (ϕ) the hard region may be small or absent. Examples are shown in Fig. 4.31. As an exercise, the student should develop the appropriate integrals to use instead of equations (4.80) and (4.82). See the problems at the end of this chapter.

When the ASTM sample has a strain gauge near the centre, it will measure the stiffness of the supersoft region. Thus

$$E_{x1} = E_{ASTM} \quad (4.87)$$

where E_{ASTM} is the modulus so measured. For the hard region we expect the upper bound of the modulus to be \bar{Q}_{11} and Fig. 4.25 indicates that \bar{Q}_{11} is indeed the mean modulus of the 43mm wide, 20mm long $[\pm 15]_s$ specimen. Thus

$$E_{x3} \leq \bar{Q}_{11} \tag{4.88}$$

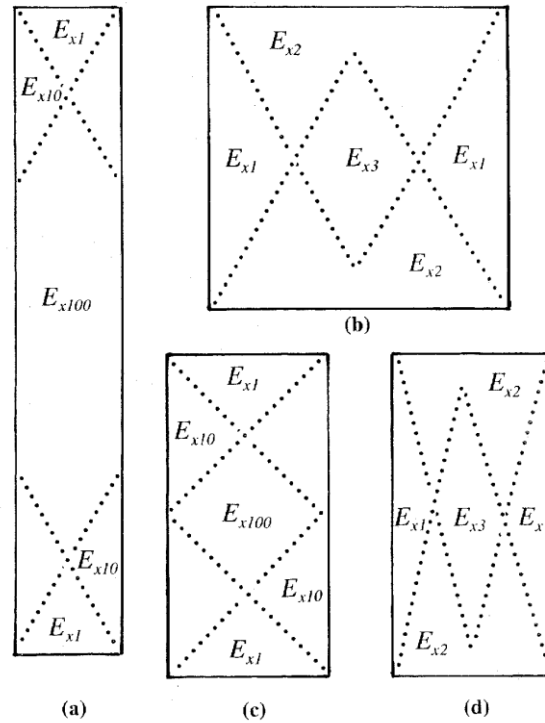


Fig. 4.31 Specimens for tensile testing with applied stress going up and down the page. (a) ASTM coupon has aspect ratio of 6, and the supersoft region is subdivided into regions E_{x1} , E_{x10} and E_{x100} for $[\pm 30]_{ns}$ laminate, (b) $[\pm 30]_{ns}$ laminate with test aspect ratio of 1, (c) and (d) $[\pm 45]_{ns}$ and $[\pm 15]_{ns}$ with test aspect ratio of 2.

For E_{x2} we have

$$E_{ASTM} < E_{x2} < E_{x3} \tag{4.89}$$

If we let

$$E_{x2} = (E_{ASTM} + \bar{Q}_{11})/2 \tag{4.90}$$

and use the upper bound for E_{x3} , we get only moderate agreement with the experimental results: see Fig. 4.32. In this figure the uppermost line is for the 100mm wide specimen, and the lower is for the 25mm wide specimen. This subject would evidently benefit from further experimental tests and theoretical analysis.

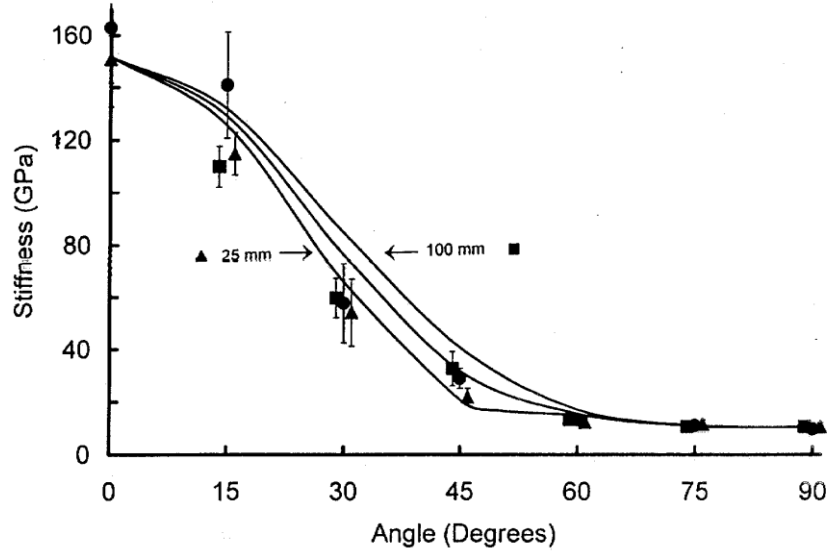


Fig. 4.32 Experimental results for Young's modulus of angle ply laminates with curves given by equation (4.86) with $E_{x1} = E_{ASTM}$, $E_{x3} = \bar{Q}_{11}$ and $E_{x2} = \frac{1}{2} (E_{x1} + E_{x3})$.

4.5 Random Fibre Structures

SMC's are sheet molding compounds. These have the fibres all approximately in one plane, but randomly oriented in that plane. The structure is similar to the chopped strand mat shown in Fig. 3.13, although the fibres bundles in SMC's are normally about 25mm long.

We treat these laminates as made up of an infinite number of microlaminae with fibres in different directions. Each microlamina is strained by an amount ϵ_x . The in-plane modulus E_r is given by the total stress, divided by ϵ_x , i.e.

$$E_r = \frac{1}{\pi \epsilon_x} \int_{-\pi/2}^{\pi/2} \sigma_x d\phi = \frac{1}{\pi} \int_{-\pi/2}^{\pi/2} \bar{Q}_{11} d\phi$$

Performing the integration, remembering that $\cos^4\phi = (\cos 4\phi + 4\cos 2\phi + 3)/8$, etc. we find that

$$E_r = \frac{1}{8}(3Q_{11} + 2[Q_{12} + 2Q_{66}] + 3Q_{22}) \quad (4.92)$$

Substituting the engineering constants using equations (4.18) to (4.21), we obtain

$$E_r = \frac{3E_1}{8(1 - \nu_{12}\nu_{21})} + \frac{\nu_{12}E_2}{4(1 - \nu_{12}\nu_{21})} + \frac{3E_2}{8(1 - \nu_{12}\nu_{21})} + \frac{G_{12}}{2} \quad (4.93)$$

This simplifies, since $\nu_{12}\nu_{21} = \nu_{12}^2 E_2/E_1$, $\nu_{12} \cong 0.3$ (equation (4.13)), and $E_2 \ll E_1$ for most aligned fibre laminates. Thus $1 - \nu_{12}\nu_{21} \cong 1.00$. Also $G_{12} \cong E_2 / 2.6$ (from equations (4.8) and (4.10)) with $E_f \gg E_m$ and $\nu_m \cong 0.3$, or with $\nu_f \cong \nu_m \cong 0.3$. Thus

$$E_r = \frac{3}{8} E_1 + \frac{5}{8} E_2 \quad (4.94)$$

The strength is usually given by an analogous equation

$$\sigma_{ru} = \frac{3}{8} V_f \sigma_{fu} + \frac{5}{8} V_m \sigma_{mu} \quad (4.95)$$

We can also calculate the shear modulus. We carry out the same procedure as for tension, except that we apply a shear strain γ_{xy} . Thus we integrate Q_{66} with the result

$$G_r = \frac{3E_1 + E_2 (1 - 2\nu_{12})}{8(1 - \nu_{12}\nu_{21})} + \frac{G_{12}}{2} \quad (4.96)$$

Making the same approximations as before, this reduces to

$$G_r = \frac{1}{8} E_1 + \frac{1}{4} E_2 \quad (4.97)$$

Thus G_r is approximately equal to $E_r/3$.

For composites having fibres which are random in three dimensions (these are not strictly laminae) the expressions usually used for modulus and strength are

$$E_R = V_f E_f / 5 + V_m E_m \quad (4.98)$$

and

$$\sigma_{Ru} = V_f \sigma_{fu} / 5 + V_m \sigma_{mu} \quad (4.99)$$

Equation (4.99) should be regarded as an upper bound, since the matrix may not be strained sufficiently, before the composite fractures, for it to be able to contribute its full strength.

In random fibre composites the fibres cannot be packed so closely as in aligned fibre laminae. Thus V_f cannot be so great. Because of this it is difficult to make the composite stronger and stiffer than the matrix when the fibres are random in three dimensions, where the packing problem is particularly severe. The maximum V_f achievable depends on fibre aspect ratio, being smaller for larger aspect ratios. However, if the fibres are more efficiently packed together by making them shorter, an aspect ratio penalty has to be taken into account.

Further Reading

These books propound the traditional approach to strength:

Jones, R.M., (1975) *Mechanics of Composite Materials*, (McGraw-Hill, New York).

Whitney, J.M., Daniel, I.M., and Pipes, R.B., (1982). *Experimental Mechanics of Fiber Reinforced Composite Materials*, (Society for Experimental Stress Analysis, Brookfield Centre, CT).

Gibson, R.F., (1994), *Principles of Composite Material Mechanics*, (McGraw Hill, New York).

These articles propound and compare failure theories:

Composites Science and Technology 58, (1998), 999-1254.

Chapter 4: Problems

Note: for all problems the fibres are aligned and continuous, except where stated otherwise; use ROM or IROM for E_1 , E_2 , etc unless suggested otherwise.

- 4.1. Estimate the Young's modulus in the fibre direction for S glass-epoxy with $V_f = 0.64$.
- 4.2. Estimate the stress in the fibre direction supported by Kevlar 149-epoxy at a strain of 1.35%. $V_f = 0.71$.
- 4.3. Estimate the axial strength of SiC (SCS6) reinforced pure annealed aluminium with $V_m = 0.41$.
- 4.4. Calculate the stress at the knee in Nicalon reinforced titanium if the titanium has a yield stress of 410MPa and $V_f = 0.57$.
- 4.5. Estimate the axial Young's modulus of stiff carbon-epoxy with $V_{fw} = 0.50$. The density of the epoxy is 1230kgm^{-3} .
- 4.6. Calculate the maximum possible weight fraction for the above stiff carbon epoxy, assuming that the fibres are hexagonally packed and the composite is void free.
- 4.7. Calculate the axial strength of Nextel 610 Al_2O_3 reinforced magnesium if the metal has a yield strength of 108MPa and a weight fraction of 0.63.
- 4.8. A carbon-epoxy is to be designed to have a Young's modulus of 55GPa. Estimate the volume fraction of the cheapest carbon fibres that would be needed.
- 4.9. Calculate E_1 , E_2 , G_{12} , and ν_{12} for aligned continuous E-glass-epoxy for $V_f = 0.71$, and hence determine the compliance matrix.
- 4.10. Determine the stiffness matrix for an aligned continuous lamina of B-Al with $V_f = 0.67$.
- 4.11. Calculate the three strains ε_1 , ε_2 and γ_{12} for a $V_f = 0.45$ aligned S-glass-polyester lamina stressed at right angles to the fibre direction, in the plane of the lamina. The modulus of the polyester is 2.47GPa. The applied stress is 45MPa.
- 4.12. Evaluate E_x , E_y , G_{xy} and ν_{xy} for aligned continuous tungsten-nickel for $\phi = 30$, and $V_f = 0.62$. E_m for nickel is 200GPa and $\nu_m = 0.31$.

- 4.13. How much would the elastic constants change if the above laminate was $[\pm 30]_{ns}$ instead of $[+30]_n$?
- 4.14. Calculate approximate the Young's and shear moduli for planar random Kevlar-epoxy when the fibres are very long and $V_f = 0.38$. Compare these with more accurate estimates
- 4.15. A carbon-epoxy has $Q_{11} = 151$, $Q_{12} = 1.95$, $Q_{22} = 6.47$ and $Q_{66} = 3.24$. Estimate E_x , E_y , G_{xy} and ν_{xy} for a $[0, 90 \pm 45]_s$ assuming that they are the mean values for $[0/90]_s$ and $[\pm 45]_s$ acting separately.
- 4.16 Show that three of the above results are in error by more than 15% when lamination theory is used and the appropriate \bar{Q}_{ij} are developed and evaluated.
(Hint, term these \hat{Q}_{ij} , then estimate the appropriate \hat{S}_{ij} from these.)
- 4.17 Estimate E_x , E_y , G_{xy} and ν_{xy} for a $[0/\pm 60]_s$ laminate made from the same material as question 4.15. How much better are these properties than the $[0/90/\pm 45]_s$ above?
- 4.18 Calculate G_{12} needed in equation (4.34) to give the correct result for E_x for a $[\pm 45]_{ns}$ ply laminate made from the same material as in question 4.15. Compare with G_c , estimated assuming $\nu_f = \nu_m = \nu_{12}$. (Hint: use angle ply laminate equations for $[0]_s$, and $[90]_s$ to derive E_1 , E_2 , etc. Is G_c or the actual G_{12} closer to the value needed?
- 4.19 Using $G_c = 5.70$, how well does equation (4.34) estimate E_x for $[\pm 30]_s$ and $[\pm 60]_s$ laminates, as compared with the laminated plate theory. Assume, again, that the material is as described in equation (4.15).
- 4.20 Determine the apparent modulus of a $[\pm 20]_s$ composite coupon which has a width of 50mm and a length of 20mm given that $E_{x3} = 120\text{GPa}$, $E_{x2} = 100\text{GPa}$ and $E_{x1} = 80\text{GPa}$.
- 4.21 Develop an expression analogous to equation (4.86) for the case shown in Fig. 4.31b. Then apply it for $\bar{Q}_{11} = E_{x3} = 1.2 E_{x2} = 1.44 E_{x1}$ to determine the apparent coupon modulus is terms of \bar{Q}_{11} .
- 4.22 Estimate E_x (apparent) for the ASTM D3039 for $E_{x1} = \bar{Q}_{11}/2$, $E_{x2} = (E_{x1} + E_{x3})/2$ and $E_{x3} = \bar{Q}_{11}$ for the carbon-epoxy shown in Fig. 4.16. Assume that the sample is tested with the strain gauge at the centre. The material is a $[\pm 30]_s$ angle ply laminate made with the carbon-epoxy described in Fig. 4.16.
- 4.23 Compare the mean value of E_x given by equation (4.34) with E_R from equation (4.57) for the glass-epoxy described in Fig. 4.9.

- 4.24 Develop an expression analogous to equation (4.34) for G_{xy} from first principles and show that it is in agreement with equation (4.33).

Chapter 4. Selected Answers

- 4.1. 55.3GPa
- 4.3. 2.38GPa
- 4.5. 150GPa
- 4.7. 0.208; 481MPa
- 4.9. $S_{11} = 0.0193$, $S_{12} = -0.0049$, $S_{22} = 0.126$, $S_{66} = 0.334$
- 4.11. $\varepsilon_1 = 0.033\%$, $\varepsilon_2 = 1.03\%$, $\gamma_{12} = 0.0$
- 4.13. $E_x = 349$ or 12% greater, $E_y = 324\text{GPa}$ or 10% greater, $\nu_{xy} = 0.211$ or 29% greater, $G_{xy} = 186\text{GPa}$ or 54% greater.
- 4.15. $E_x = E_y = 45.2\text{GPa}$, $\nu_{xy} = 0.504$, $G_{xy} = 20.8\text{GPa}$.
- 4.17. They are all the same, with $E_x = E_y = 54.9\text{GPa}$, $\nu_{xy} = 0.319$ and $G_{xy} = 20.8\text{GPa}$.
- 4.19. Not very well; $[\pm 30]_s$, 21.9 instead of 39.1GPa. $[\pm 60]_s$, 8.3 instead of 7.2GPa.
- 4.21. $0.71 \bar{Q}_{11}$.
- 4.23. Mean $E_x = 6.8\text{GPa}$; $E_R = 24\text{GPa}$.

5. COMPOSITE MECHANICS: SHORT FIBRES

When the fibres are short, we can no longer assume that the strains in the fibres and the matrix are the same. We need therefore to look in more detail at the interactions between the fibres and the matrix. Normally, when the composite is pulled the fibres are extended less than the matrix. This causes shears to develop at the fibre surfaces. These shears bring about the transfer of stresses between the fibres and the matrix.

The interactions between fibres and matrix are extremely complex, and imperfectly understood. The first attempt to explain the reinforcing effect of the fibres was based entirely on elastic interactions. This was initially developed by Cox in 1952, and is now referred to as the shear lag theory. These ideas have been refined by others, but have stood the test of time, and the refinements have added a great deal to the complexity without improving the predictions very greatly.

However, the Cox analysis, as will be shown, suggests that the stresses near the fibre ends rise very quickly to values which can exceed the matrix strength. Thus shear failure at the interface was predicted near the fibre ends long before the fibres have been stressed enough to break. Because of this, the Cox analysis and its successors have only been used to estimate the Young's modulus of a composite.

For the strength, a completely different approach has been used. This assumed yielding and/or frictional slip at the interface. Such inelastic processes *require* that the stress-strain plot of a unidirectional short fibre composite should be curved. While some early evidence is claimed to support this, recent extensive and careful tests with composites made with short glass and carbon fibres have failed to reveal any detectable curvature, even with fibres only 1 mm long or shorter. (The only exceptions were a few cases in which the fibres had silicone coatings on their surfaces.) Thus the yielding/slip theory is not supported by recent research.

In this chapter we describe the Cox theory: it is simple and adequate for most estimations of Young's modulus. For strength, a crack failure process is described which leads to a result for strength which bears a strong resemblance to the yielding/slip theory, but does not require a curved stress-strain plot.

Recent papers which present the evidence for this new approach, together with a full discussion of earlier work (with references) appear in the reading list at the end of this chapter.

A complete list of the nomenclature used appears in Appendix A.

5.1 Elastic Stress Transfer

We assume that both fibres and matrix behave elastically, and that the interface transfers the stress from fibres to matrix without yielding or slip. Each fibre is surrounded by other fibres which are packed in an orderly fashion, for example, hexagonally, as shown in Fig. 5.1. The matrix tensile strain is assumed to be constant at the ring of nearest neighbours, at distance R from the fibre we are considering, and we assume that we can equate this matrix tensile strain, ϵ_m , with the composite tensile strain, ϵ_1 .

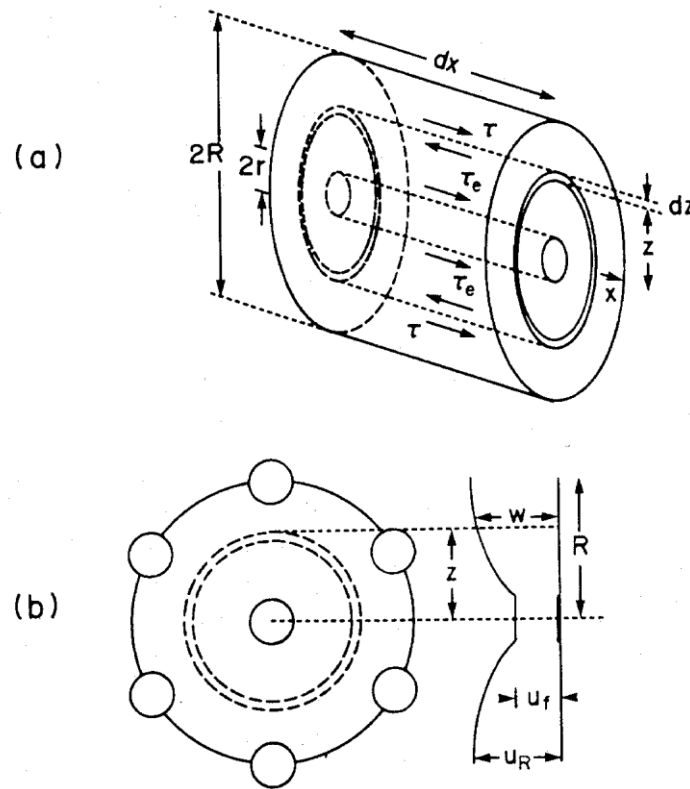


Fig. 5.1 (a) Short length of fibre and surrounding matrix, (b) fibre with nearest neighbours, hexagonally packed and associated displacements along the fibre axis.

We thus have a stress distribution with circular symmetry, i.e. the matrix displacement w (Fig. 5.1), and the shear stress, τ , does not vary with orientation about the fibre axis. They are both, however, a function of the radial distance z from the fibre axis.

Equate the shear forces at distance z with those at the fibre surface ($z = r$) in the composite element shown in Fig. 5.1b:

$$2\pi z\tau dx = 2\pi r\tau_e dx \tag{5.1}$$

or

$$\tau = r\tau_e/z \tag{5.2}$$

Now the ratio of τ , to the shear strain, dw/dz , is equal to the matrix shear modulus G_m , so that

$$\frac{dw}{dz} = \frac{\tau}{G_m} = \frac{\tau_e r}{G_m z} \quad (5.3)$$

This equation is integrated:

$$\int_{u_f}^{u_R} dw = \frac{\tau_e r}{G_m} \int_r^R \frac{dz}{z} \quad (5.4)$$

to give

$$u_R - u_f = \frac{\tau_e r}{G_m} \ln(R/r) \quad (5.5)$$

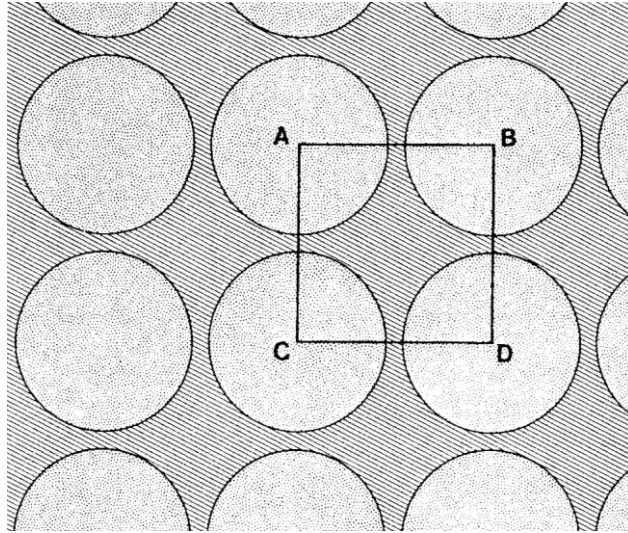


Fig. 5.2 Fibres in a square-packed arrangement.

The value of R/r depends on the fibre packing. Consider square packing, Fig. 5.2. The box $ABCD$ has area R^2 , and includes one complete fibre cross-section (the sum of the quarter sections at each of the four corners). Thus the volume fraction of the fibres, V_f , which is equal to the area fraction, is $V_f = \pi r^2/R^2$, so that

$$\ln(R/r) = \frac{1}{2} \ln(\pi/V_f) \quad (5.6)$$

Similarly, for hexagonal packing

$$\ln(R/r) = \frac{1}{2} \ln(2\pi/\sqrt{3} V_f) \quad (5.7)$$

(The reader should derive this as an exercise). The difference between the two results is quite small. For $V_f = 0.50$, for example, square packing gives 0.919 for $\ln(R/r)$ while hexagonal packing gives 0.991. We will write

$$\ln(R/r) = \frac{1}{2} \ln(P_f/V_f) \quad (5.8)$$

where P_f is the packing factor.

Substituting equation (5.8) into equation (5.5) and rearranging gives

$$\tau_e = \frac{E_m(u_R - u_f)}{(1 + \nu_m)r \ln(P_f/V_f)} \quad (5.9)$$

(remember that $G = \frac{1}{2}E/[1 + \nu]$).

The fibre stress will change from σ_f to $\sigma_f + d\sigma_f$ along an element of length dx ; see Fig. 5.3. For the surface shear forces to be in equilibrium with the tensile forces in the fibre

$$\pi r^2 d\sigma_f = -2\pi r dx \tau_i \quad (5.10)$$

Hence, for elastic stress transfer, $\tau_i = \tau_e$ and so

$$\frac{d\sigma_f}{dx} = -\frac{2\tau_e}{r} \quad (5.11)$$

Substituting for τ_e from equation (5.9):

$$\frac{d\sigma_f}{dx} = -\frac{2E_m(u_r - u_f)}{(1 + \nu_m)r^2 \ln(P_f/V_f)} \quad (5.12)$$

The fibre displacement, u_f , can be calculated from the fibre stress, since the fibre strain is $\varepsilon_f = du_f/dx$. Thus

$$\frac{du_f}{dx} = \frac{\sigma_f}{E_f} \quad (5.13)$$

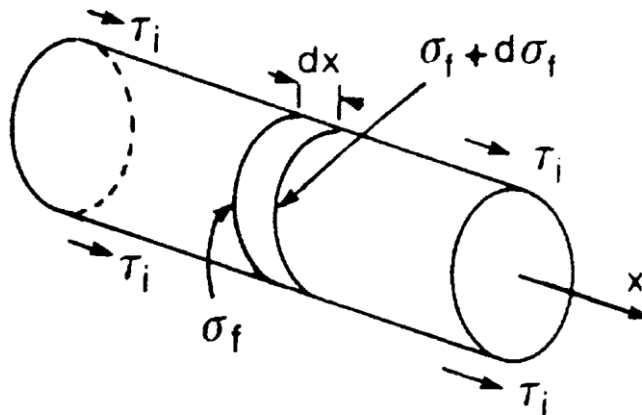


Fig. 5.3 Short length of fibre.

At $z = R$, $du_R/dx = \epsilon_m$ which we assume $= \epsilon_1$. We can, therefore, differentiate equation (5.12) and substitute for du_R/dx and du_f/dx :

$$\frac{d^2 \sigma_f}{dx^2} = \frac{2E_m(\epsilon_1 - \sigma_f / E_f)}{(1 + \nu_m)r^2 \ln(P_f / V_f)} \tag{5.14}$$

We now introduce the dimensionless parameter, n , where

$$n^2 = 2E_m / [E_f(1 + \nu_m)\ln(P_f/V_f)] \tag{5.15}$$

and the differential equation may be written

$$\frac{d^2 \sigma_f}{dx^2} = \frac{n^2}{r^2} (\sigma_f - E_f \epsilon_1) \tag{5.16}$$

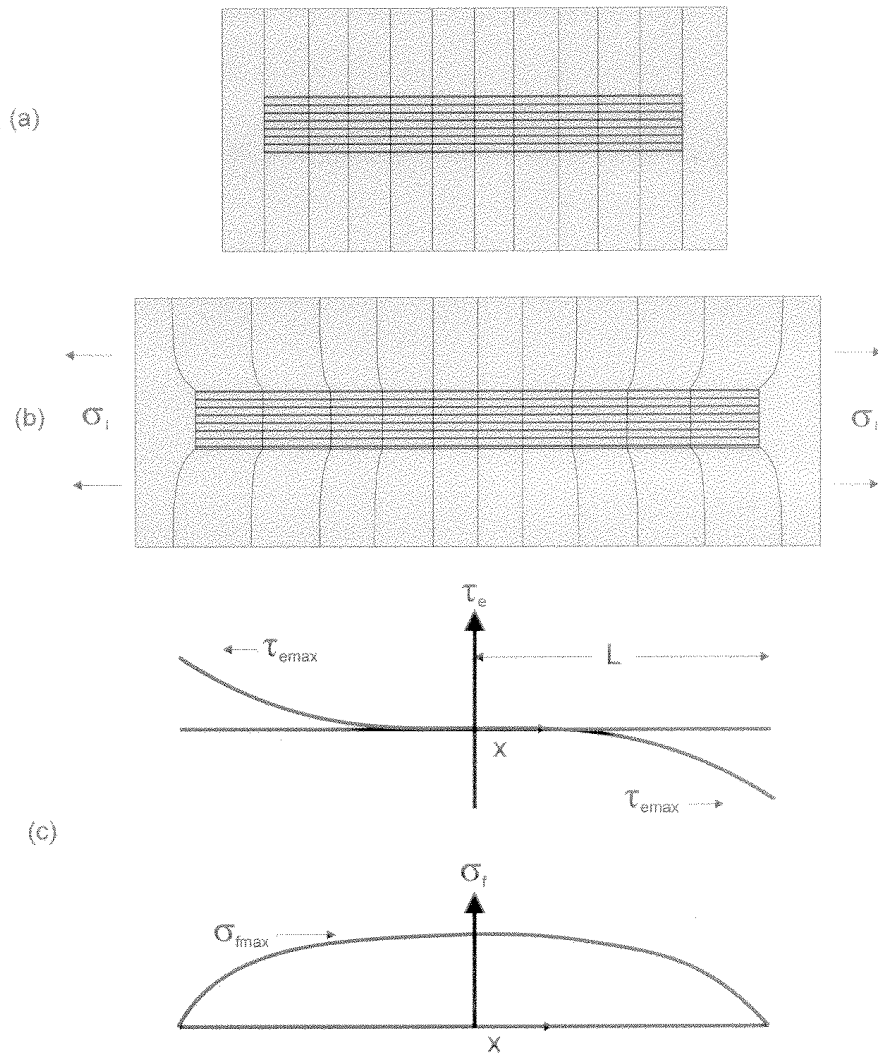


Fig. 5.4 Single fibre composite element: (a) unstressed and (b) stressed. (c) shows the fibre-matrix interfacial stress and the fibre internal stress for elastic stress transfer.

This has the solution

$$\sigma_f = E_f \varepsilon_1 + B \sinh(nx/r) + D \cosh(nx/r) \quad (5.17)$$

where B and D are constants determined by the boundary conditions. Assume that no stress is transferred across the fibre ends, i.e. $\sigma_f = 0$ at $x = L$ and $x = -L$ (see Fig. 5.4).

Thus $B = 0$ and $D = -E_f \varepsilon_1 / \cosh(ns)$, where $s = L/r$, the fibre aspect ratio. Equation (5.17) becomes

$$\sigma_f = E_f \varepsilon_1 \sinh(nx/r) / \cosh(nx/r) \quad (5.18)$$

Differentiating this, and multiplying of the result by $-r/2$ (see equation (5.11)) gives us τ_e :

$$\tau_e = \frac{1}{2} n E_f \varepsilon_1 \sinh(nx/r) / \cosh(nx/r) \quad (5.19)$$

The fibre stress and surface shears are shown schematically in Fig. 5.4.

In the composite there are many fibres. Consider a composite containing fibres which all have the same length and diameter, and are all parallel, but are otherwise randomly positioned, as shown in Fig. 5.5. Then any section normal to the bar axis, MN for example, will intersect fibres at all possible positions along their lengths, so long as there are a very large number of them in the cross-section.

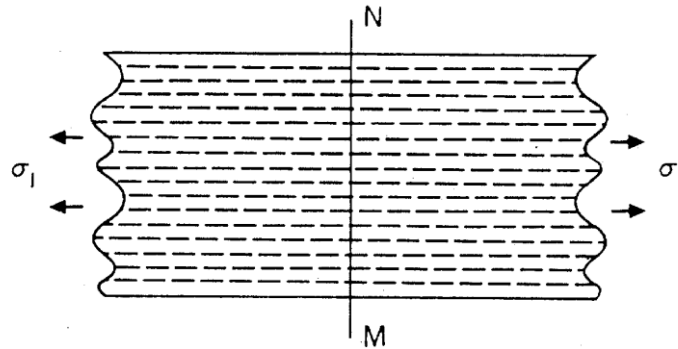


Fig. 5.5 MN represents a random cross-section in an aligned fibre composite.

The load carried by the fibres will be the total fibre area across the bar section, multiplied by the average fibre stress. The area fraction is equal to the volume fraction in any random cross section; consequently the load carried by the fibres is $AV_f \bar{\sigma}_f$ where A is the area of the cross section, V_f is the volume fraction and $\bar{\sigma}_f$ the average stress of the fibres. Similarly, the load carried by the matrix is $AV_m \bar{\sigma}_m$, the subscript m referring to the matrix.

The total load carried by the composite is $A\sigma_1$, the fibres being aligned in the 1 direction. Consequently the composite obeys the RULE OF AVERAGES:

$$\sigma_1 = V_f \bar{\sigma}_f + V_m \bar{\sigma}_m \tag{5.20}$$

To determine the composite stress we use the Rule of Averages, so we must first calculate the average fibre stress, $\bar{\sigma}_f$. We integrate equation (5.18) for this;

$$\bar{\sigma}_f = \frac{E_f \varepsilon_1}{L} \int_0^L \left\{ 1 - \frac{\cosh(nx/r)}{\cosh(ns)} \right\} dx \tag{5.21}$$

$$= E_f \varepsilon_1 \left\{ 1 - \frac{\tanh[ns]}{[ns]} \right\} \tag{5.22}$$

and for the matrix assume that $\bar{\sigma}_m = E_m \varepsilon_1$. Substituting $\bar{\sigma}_f$ and $\bar{\sigma}_m$ into equation (5.20) gives

$$\sigma_1 = \left\{ V_f E_f \left(1 - \frac{\tanh[ns]}{[ns]} \right) + V_m E_m \right\} \tag{5.23}$$

This is the stress-strain relationship for the composite.

The maximum fibre stress, σ_{fmax} is at the centre, and is given by equation (5.18) with $x = 0$:

$$\sigma_{fmax} = E_f \varepsilon_1 \left\{ 1 - \operatorname{sech}[ns] \right\} \tag{5.24}$$

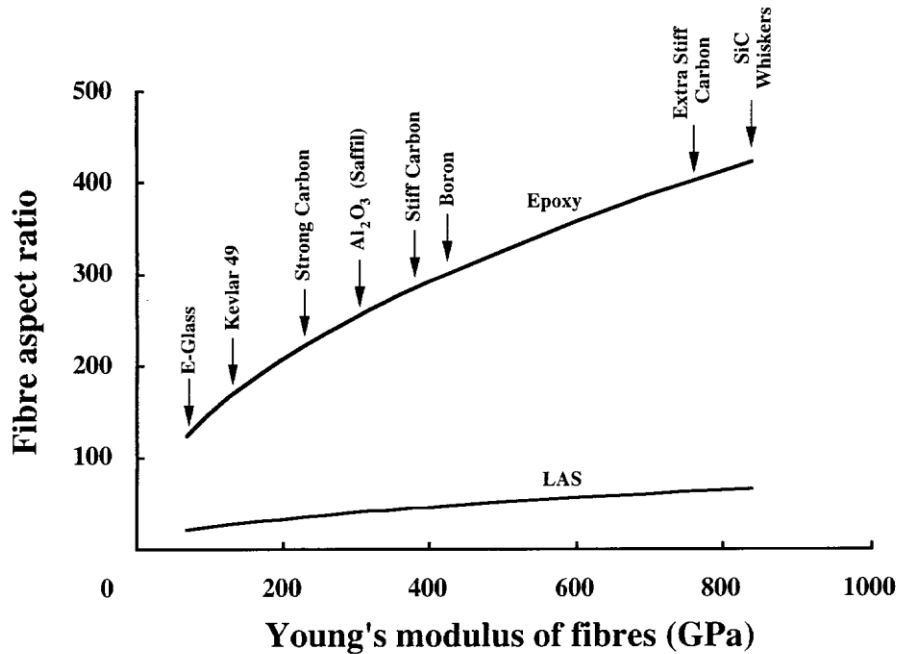


Fig. 5.6 Fibre aspect ratio required for Young's modulus to be within 5% of the Rule of Mixtures value: epoxy and lithium aluminosilicate matrices. ($V_f = 0.5$.)

This theory is approximate. We have neglected the stress transfer across the fibre ends, and the stress concentration there, which greatly increases τ_e at the ends. We have

also neglected the extra load thrown on the ring of fibres surrounding the end region of each fibre, and the extra load on the matrix in this region. These effects will all be unimportant for $s > 10$, except for the underestimation of τ_e . The increased τ_e at the fibre ends will affect the onset of fibre debonding discussed later.

Table 5.1 Fibre Lengths (mm) Required to Achieve 95% Reinforcement Efficiency for Young's Modulus. (Unidirectional Composites with $V_f = 0.5$ and Hexagonal Packing.)

Fibres and Whiskers			Fibre Lengths in Matrices with Moduli (GPa) indicated		
Reinforcement	E_f (GPa)	d (μm)	Epoxy (2.5)	Aluminium (71)	LAS ² (100)
E-glass	72	10	1.2	0.23	0.19
S-glass	85	10	1.3	0.25	0.20
Kevlar 49	130	12	1.7	-	-
Polyethylene ¹	170	27	5.1	-	-
SiC (Nicalon)	185	10	2.0	0.37	0.30
Steel	212	100	21.	4.0	3.2
Carbon (AS4)	233	8	1.8	0.33	0.27
Al ₂ O ₃ (Saffil)	300	3	0.76	0.14	0.11
Al ₂ O ₃ (Nextel 610)	373	11	3.1	0.58	0.47
SiC (SCS6)	410	140	41	7.8	6.2
Carbon (Stiff)	377	5	1.4	0.27	0.21
Tungsten	411	100	30	5.5	4.4
Boron	420	140	42	7.9	6.3
Carbon (Stiffest)	827	10	4.2	0.79	0.63
SiC whiskers	840 ³	1	0.42	0.079	0.063
Al ₂ O ₃ whiskers	2250 ³	1	0.69	0.13	0.10

Notes:

1. Spectra 1000, 2. Lithium alumino silicate, 3. Whisker with maximum Young's modulus

5.2 Elastic Stress-Strain Relationships

Equation (5.23) states that stress is directly proportional to strain. Thus all stress-strain curves are straight lines in the region governed by this equation. For ns values greater than 3.0, $\tanh(ns) = 1.00$ with an error of less than 0.5%. So for moderately long fibres equation (5.23) becomes

$$E_1 = V_f E_f \left(1 - \frac{1}{ns} \right) + V_m E_m \tag{5.28}$$

Furthermore, for $ns \geq 20$ the composite modulus will be within 5% of the Rule of Mixtures value. This requires that s be in the range 120 to 400 for reinforced epoxies with moderate $V_f s$; see Fig. 5.6.

Fibre lengths ($2L$) required for no more than 5% deviation range from about 0.11 mm for the very fine ($3\mu\text{m}$) Al_2O_3 (Saffil) in a ceramic matrix (lithium alumino silicate) to 42mm for the rather coarse ($140\mu\text{m}$) boron in an epoxy matrix; see Table 5.1. The results for the aluminium matrix are very close to those for the ceramic. Shorter lengths would be required for higher modulus matrices ($2L \propto 1/\sqrt{E_m}$) and SiC whiskers give the shortest lengths of all.

Typical stress-strain plots are shown in Fig. 5.7. These have been terminated at the highest stress that can be applied before the interfacial shear stress at the fibre ends reaches the apparent matrix shear strength (assumed to be ~ 60 MPa). The maximum value of τ_e is at the fibre end, $x = L$, so from equation (5.19) we find

$$\tau_{e_{max}} = \frac{1}{2} n E_f \varepsilon_1 \tanh (ns) \tag{5.29}$$

Let the strain corresponding to $\tau_{e_{max}} = \tau_{mu}$ be ε_{1mu} , where τ_{mu} is the apparent shear strength of the matrix. We can now rewrite equation (5.26) for the evaluation for this strain

$$\varepsilon_{1mu} = 2 \tau_{mu} \coth (ns) / n E_f \tag{5.30}$$

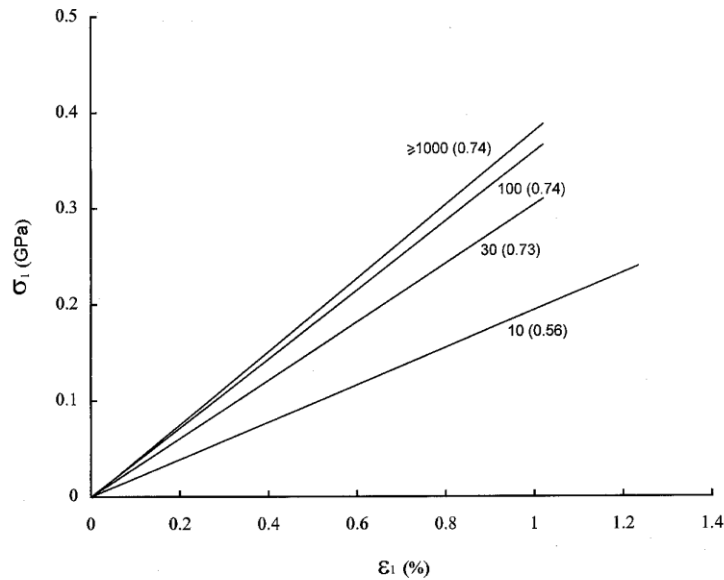


Fig. 5.7 Theoretical stress-strain curves for E-glass-epoxy up to the loosening point for aspect ratios 10, 30, 100 and > 1000 , as marked. The maximum fibre stresses (GPa) at the loosening point are also indicated.

Some change in behaviour is expected at this point, which we will call the loosening point. With reinforced polymers separation across the fibre ends occurs. Fig. 5.8 shows this for a glass fibre in an epoxy resin matrix. The debonding is progressive and extends around the end and then along the circumferential surface.



Fig. 5.8 Progressive debonding at a fibre end. The applied strain increases from left to right in the picture.

The exact value of the loosening strain depends on the quality of the adhesion at the fibre end. With good adhesion it is possible for σ_{mu} to be exceeded. Poor adhesion leads to early failure. Thus it is more appropriate to identify τ_{emax} with an apparent interfacial debonding stress, τ_d . So instead of equation (5.27) we have

$$\varepsilon_{1s} = 2\tau_d \coth(ns)/nE_f \quad (5.28)$$

where we have written ε_{1s} for the loosening strain.

The corresponding composite stress σ_{1s} is obtained by substituting ε_{1s} into equation (5.23):

$$\sigma_{1s} = \frac{2\tau_d}{nE_f} \left\{ (V_f E_f + V_m E_m) \coth(ns) - \frac{V_f E_f}{ns} \right\} \quad (5.29)$$

Equations (5.28) and (5.29) define the loosening point. The maximum fibre stress for loosening, σ_{fmax} is

$$\sigma_{fmax} = 2\tau_d \tanh(ns/2)/n \quad (5.30)$$

In Fig. 5.7 we have assumed $\tau_d = \sigma_{mu}$ (= 60MPa) and have indicated σ_{fmax} (in brackets) for each aspect ratio. It is clear that loosening occurs in this case when $\sigma_{fmax} \leq 0.8\text{GPa}$ which is very much less than the fibre strength (see Table 3.2). Moreover, in the

next chapter we will show that shear failure normally does not take place in polymers (instead, most polymers, fail in tension when sheared). In Chapter 8 we will provide evidence that indicates the interface fails in a fuzzy tensile mode.

5.3 Composite Strength

5.3.1 Reinforced Polymers

The experimental evidence (see further reading at the end of the chapter) indicates that stress-strain plots are straight lines up to the failure stress, with a slope (i.e. a Young's modulus) governed by equation (5.25). Thus, as mentioned earlier, a fracture analysis rather than a yielding and slip treatment is required. We therefore consider the stress required to break a composite containing a multitude of small cracks at the fibre ends. These probably develop at the loosening point which, as shown earlier (equation 5.30), is when the fibre is stressed to about one quarter of its strength, i.e. long before the composite is expected to fail.

A unidirectional composite will be considered initially with all the fibres having the same aspect ratio and with the ends randomly disposed as shown in Fig. 5.5. An element of a developing crack is shown in Fig. 5.9. All the fibres are assumed to have debonded at their ends, and the crack passes through and incorporates the debond at the end of the fibre labelled number 5. The crack goes around the end of fibre number 6, and in opening it pulls out numbers 2, 3, 8 and 9, and breaks numbers 1, 4, and 7.

Fibres extending only a short distance from the crack, such as number 6, will contribute to the breaking force only through the fracture cone shown in section in Figure 5.9. This contributes a force which, very roughly, is equal to the matrix strength operating over an area equivalent to the fibre cross section. (The end is assumed already to have failed; what has to be broken for the crack to grow is the sloping sides of the cone). The force F_{fm} is thus

$$F_{fm} = \pi r^2 \sigma_{mu} \quad (5.31)$$

The fraction of fibres involved is $5r/L$.

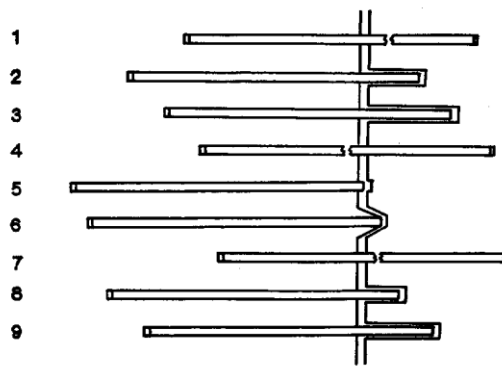


Fig. 5.9 A developing crack in a unidirectional short fibre composite.

Fibres extending a moderate length, i.e numbers 2, 3, 8 and 9, debond completely and pull out. (In the case of metals the debonding may possibly accompany the pull out; with polymers and ceramics debonding appears to occur first.) We assume that pull out is resisted by a constant shear stress τ_i . So, for a fibre extending a distance L_e from the crack plane, the fibre stress needed is

$$\sigma_f = 2\tau_i L_e / r \quad (5.32)$$

(The force exerted by the fibre, $\pi r^2 \sigma_f$ is resisted by the shear force $2\pi r L_e \tau_i$)

If L_e is too great, the fibres cannot be pulled out because σ_f would be too large, and the fibres would break instead. Writing L_{ce} for the length just great enough to break the fibres, and replacing σ_f by σ_{fu} in equation (5.32) we have

$$\sigma_{fu} = 2\tau_i L_{ce} / r \quad (5.33)$$

$2L_{ce}$ is called the *critical fibre length*. Thus a fibre of length $2L_{ce}$, with L_{ce} on either side of the crack, will break, while a fibre slightly less long than $2L_{ce}$, similarly disposed, will not. For any given matrix and associated interface therefore, there exists a *critical fibre aspect ratio* $s_c = 2L_{ce}/r$: where

$$s_c = \sigma_{fu} / 2\tau_i \quad (5.34)$$

It is important to appreciate that the critical length should be measured by carrying out a *pull out test*. Table 5.2 gives some typical values for $2L_{ce}$ and s_c from our own work. (Note L_c is commonly used for the fibre critical length, which is equal to $2L_{ce}$ in our terminology.)

Table 5.2 indicates that only very short lengths can normally be pulled out. This is particularly the case with carbon in the high performance thermoplastics, such as PEEK where little more than 0.1mm can be pulled out.

For the fibres that can be pulled out the average length protruding is $(L_{ce} + 5r)/2$ so the average force to pull one of these fibres out is F_{fp} where

$$F_{fp} = \pi r \tau_i (L_{ce} + 5r) \quad (5.35)$$

The fraction of fibres involved is $(L_{ce} - 5r)/L$.

Fibres numbers 1, 4 and 7 fracture instead of pulling out. The force required is

$$F_{fu} = \pi r^2 \sigma_{fu} \quad (5.36)$$

and the fraction of these fibres is $1 - L_{ce}/L$.

Table 5.2 Maximum Pull Out Lengths L_{ce} and Critical Aspect Ratios s_c .

Fibre	Matrix	L_{ce} (mm)	s_c
	Polyester, 20°C cure	3.0	275
	Polyester 80°C cure	1.5	135
E Glass	Epoxy RT cure	1.3	120
	Epoxy 130°C cure	0.6	55
	Polyethylene (low density)	1.5	135
	PEEK	0.3	27
Kevlar	Epoxy 80°C cure	0.6	100
	Polyethylene (low density)	1.2	200
C(AS4)	Epoxy 135° cure	0.12	30
	Polyethylene (low density)	0.7+	175
	PEEK	0.10+	25

+ end of linear region of debonding force vs embedded length plot; longer pulled out lengths assumed to be due to unduly weak interfaces.

To break the matrix we need a force σ_{mu} per unit cross section of matrix, or $V_m \sigma_{mu}$ per unit cross section of composite. If there are N fibres per unit cross section of composite, then the total force required to break it is the sum of each force F_{fu} , F_{fp} and F_{fm} multiplied by N and the respective fractions, $5r/L$, $(L + 5r) / L$ and $(1 - L_{ce} / L)$, plus the matrix contribution. So long as $L > L_{ce}$ this gives

$$\sigma_{1u} = N (\pi r \tau_i [L_{ce}^2 + 25r^2] / L + \pi r^2 \sigma_{fu} [1 - L_{ce} / L] + 5\pi r^3 \sigma_{mu} / L) + V_m \sigma_{mu} \quad (5.37)$$

Writing $V_f = N\pi r^2$ and replacing L/r by s , L_{ce}/r by s_c and $\sigma_{fu}/2\tau_i$ by s_c , this reduces to:

$$\sigma_{1u} = V_f \sigma_{fu} [1 - s_c / s - 12.5 / (s s_c)] + [V_m + 5V_f] \sigma_{mu} \quad (5.38)$$

For shorter fibres, i.e. with $5 < s \leq s_c$ we have no fibres that break, but some pull out. These fibres protrude, on average, $\frac{1}{2}(L + 5r)$. Thus F_{fp} becomes

$$F_{fp} = \pi r \tau_i (L + 5r) \quad (5.39)$$

and these fibres constitute a fraction $1 - 5r/L$ of the total. F_{fu} is zero and F_{fm} remains the same. Proceeding as before, we obtain

$$\sigma_{1u} = V_f \sigma_{fu} [s_c / \{2s\}][1 - 25 / s^2] + [V_m + 5V_f/s] \sigma_{mu} \quad (5.38a)$$

Finally for $s \leq 5$ we have

$$\sigma_{1u} \leq \sigma_{mu} \quad (5.39)$$

and we assume that the crack simply joins together the debonds at the fibre ends. No significant pull out force is exerted, and no fibres are broken.

The fibre contribution to composite strength is shown vs fibre aspect ratio in Fig. 5.10. What is plotted here is the multiplier for $V_f \sigma_{fu}$ in equations (5.38) and (5.38a). This is asymptotic to 1.0, and how quickly it approaches unity depends on s_c ; a smaller s_c gives a faster approach. s_c was chosen to be 30, the value for carbon in epoxy (Table 5.2), and for $s < 30$ equation (5.38a) was used. This curve is labelled strength.

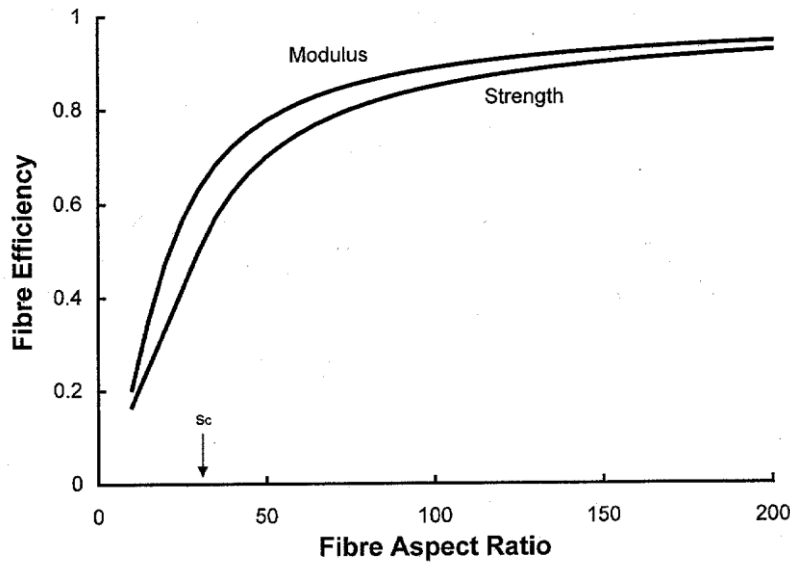


Fig. 5.10 Fibre contributions to strength and modulus. Carbon-epoxy with $E_f = 233\text{GPa}$ and $s_c = 30$.

For comparison the equivalent Young's modulus factor, $1 - \tanh(ns)/[ns]$ has been plotted (curve labelled modulus) for the same carbon-epoxy; see equation (5.23). The curves are very similar, and can be almost coincident. (They are just about coincident for a carbon fibre reinforced polymer with $s_c = 18$.)

5.3.2 Reinforced Metals

The idea of the fibre critical length, which actually originated in the pulp and paper industry, was applied to reinforced metals using a very simple approach. The metals first considered as matrices were very ductile (silver, copper and aluminum) and could be assumed to be elastic-perfectly plastic as a first approximation. (Elastic-

perfectly plastic materials are elastic up to the yield stress, and then strain indefinitely at the yield stress σ_{my} .) Thus the stress strain curve obeys Hooke's Law up to σ_{my} and then has a sharp corner and runs parallel to the strain axis: see Fig. 4.2. The ultimate strength, σ_{mu} is equal to σ_{my} . The shears at the fibre-metal interface were assumed to be equal to the shear strength near the ends, and zero in the centre regions of the fibres: see Fig. 5.11. This should be compared with Fig. 5.4.

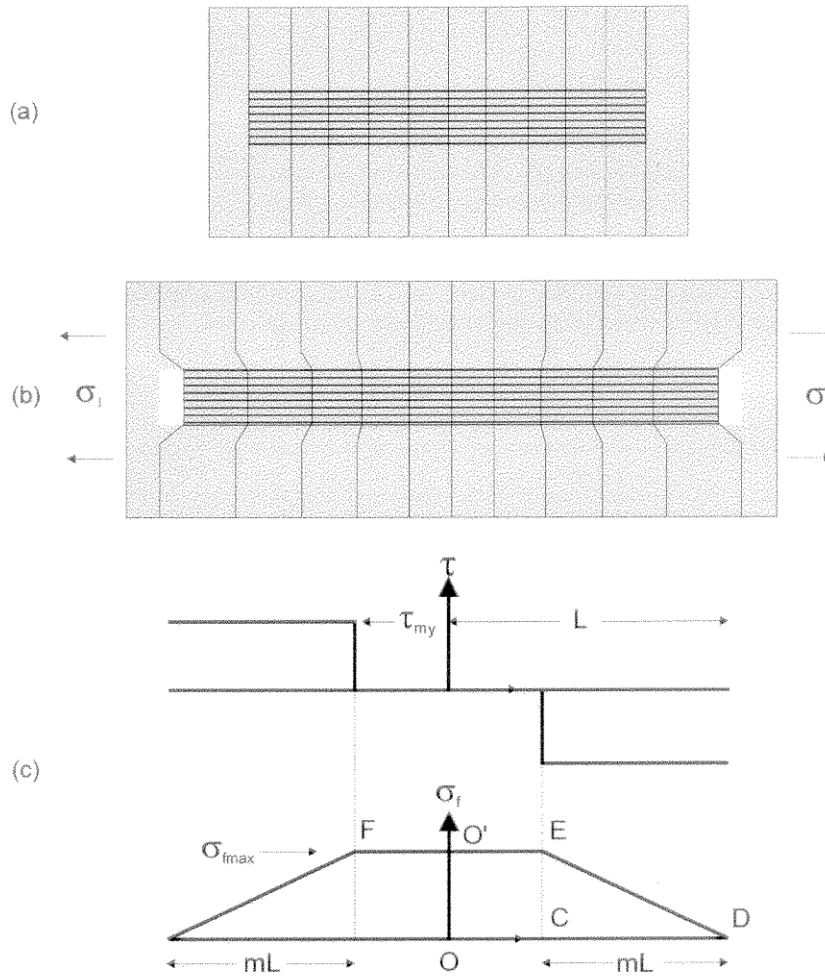


Fig. 5.11 Single fibre composite element (a) unstressed and (b) stressed. (c) shows the fibre-matrix interfacial stress and fibre internal stress for a fibre in an elastic-perfectly plastic matrix.

In the end region ED $\tau_i = \tau_{my}$ ($= \tau_{mu} = \frac{1}{2} \sigma_{mu}$ [Tresca yield criterion] or $\sigma_{mu} / \sqrt{3}$ [von Mises criterion]). Thus, using equation (5.11) with $\tau_e (= \tau_i) = \tau_{my}$

$$\frac{d\sigma_f}{dx} = -\frac{2\tau_{my}}{r} \tag{5.40}$$

which on integration gives a linear variation of fibre stress with distance x . Assuming $\sigma_f = 0$ at the fibre ends, $x = L$ we thus obtain

$$\sigma_f = (2 \tau_i / r)(L - x) \tag{5.41}$$

In the centre regions, O'E, where $x \leq L(1-m)$ the stress is constant, i.e. $\sigma_f = \sigma_{f\max}$ where

$$\sigma_{f\max} = 2m s \tau_{my} \quad (5.42)$$

and $s = L/r$, as before (equation (5.17)).

The average stress is the area under the line O'ED (Fig. 5.11) divided by half the length of the fibre, i.e.

$$\bar{\sigma}_f = \sigma_{f\max} (1 - m/2) \quad (5.43)$$

so that the composite stress comes to

$$\sigma_1 = V_f \sigma_{f\max} (1 - m/2) + V_m \bar{\sigma}_m \quad (5.44)$$

where the fraction of the fibre, m , having yielding metal at the interface is a function of the applied strain.

When the fibres are long, we must break them to break the composite; thus $\sigma_{f\max} = \sigma_{fu}$. Since from equation (5.42)

$$m = \sigma_{f\max} / [2s \tau_{my}] \quad (5.45)$$

substituting this in equation (5.43), and writing σ_{fu} in place of $\sigma_{f\max}$ we have the composite breaking strength

$$\sigma_{1u} = V_f \sigma_{fu} (1 - \sigma_{fu} / [4s \tau_{my}]) + V_m \bar{\sigma}_m \quad (5.46)$$

Short fibres cannot be broken. This is because m cannot be greater than 1.0. So from equation (5.44), for fibre breakage s cannot be less than $\sigma_{f\max} / [2 \tau_i]$. Thus there is a critical aspect ratio, given by s_c

$$s_c = \sigma_{fu} / [2\tau_{my}] \quad (5.45)$$

which is clearly analogous to the earlier critical aspect ratio, given in equation (5.34). The only difference is the use of τ_i instead of τ_{my} .

For reinforced metals with $s < s_c$ we use

$$\sigma_{1u} = V_f s \tau_i + V_m \sigma_{my} \quad (5.46)$$

When the fibres have $s > s_c$, failure is expected to take place when the composite strain is ε_{fu} ($= \sigma_{fu} / E_f$). In this case we can allow for work hardening of the matrix. To do this we evaluate $\bar{\sigma}_m$ at ε_{fu} , using the actual stress-strain curve of the metal matrix.

This treatment has not been entirely substantiated experimentally. s_c is very much less for metals than for polymers, and adequate alignment of the very short fibres needed for critical experiments may well not have been achieved. Fig. 5.12 compares results at

250°C with 0.50mm diameter tungsten in copper (Kelly and Tyson), at left, with results at room temperature with 0.13 mm diameter stainless steel in aluminum (Cratchley, at right). There does seem to be a marked aspect ratio effect in both cases. However, Cratchley found that he only broke the fibres: none pulled out. He concluded that his effects were entirely due to imperfect alignment. Kelly and Tyson, with much smaller aspect ratio fibres, and hence much more difficult to align accurately, claimed that misalignment was not important. However, Cratchley did an additional series of experiments where much trouble was taken with the alignment. The aspect ratio effect then all but disappeared.

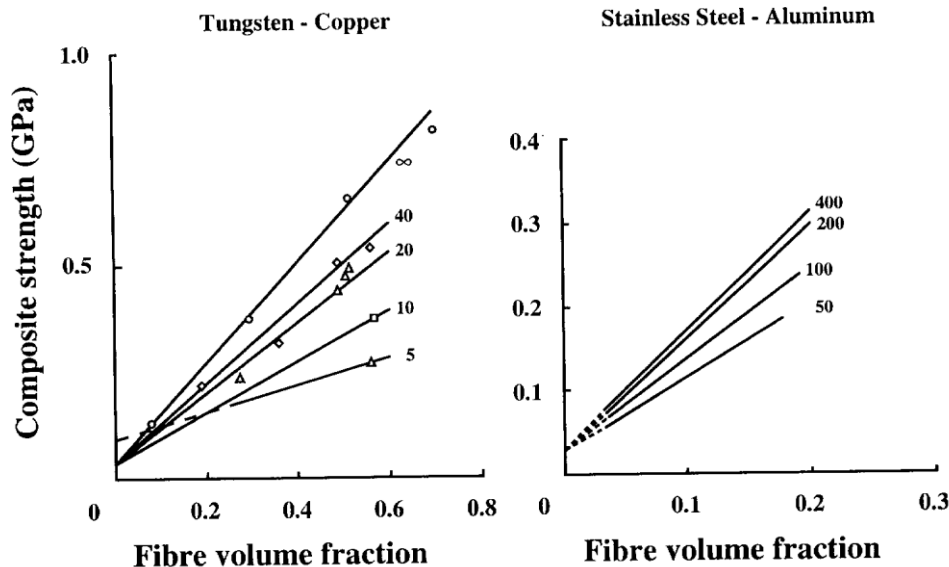


Fig. 5.12 Effect of fibre aspect ratio on composite strength. The numbers adjacent to the lines are the aspect ratios. (After Kelly, A., and Tyson, W.R., 1965, *High Strength Materials*, (Ed. V.F. Zackay, Wiley, New York), Chpt. 13, and Cratchley, D, 1963, *Powder Met.* 6, 59-72.)

Another weakness in the Kelly claim for progressive metal matrix yielding in the interface region is that the stress-strain plots should have been curved. Such curved plots appear not to have been published by his research group. Furthermore, as mentioned in the Preface, Kelly went so far as to misrepresent some work with Al_2O_3 whiskers in epoxy to bolster his claim that such curves may be observed.

Although Kelly and Tyson found no voids at the ends of their fibres, cavitation at the fibre ends has subsequently been observed: see Fig. 5.13. Such failure could initiate the same type of process as described in section 5.3.1 for polymers. However, such cavitation is very rare.

In addition, there is a body of opinion that fibre strengthening in reinforced metals is due to changes in the metal matrix resulting from thermal stresses. These arise from the difference in thermal contraction between the metal and the fibre as the composite is cooled from the manufacturing temperature. The stresses cause extensive dislocation

arrays which harden the matrix, and so make it stronger. This has been clearly demonstrated with whiskers, at least; see Fig. 5.14.

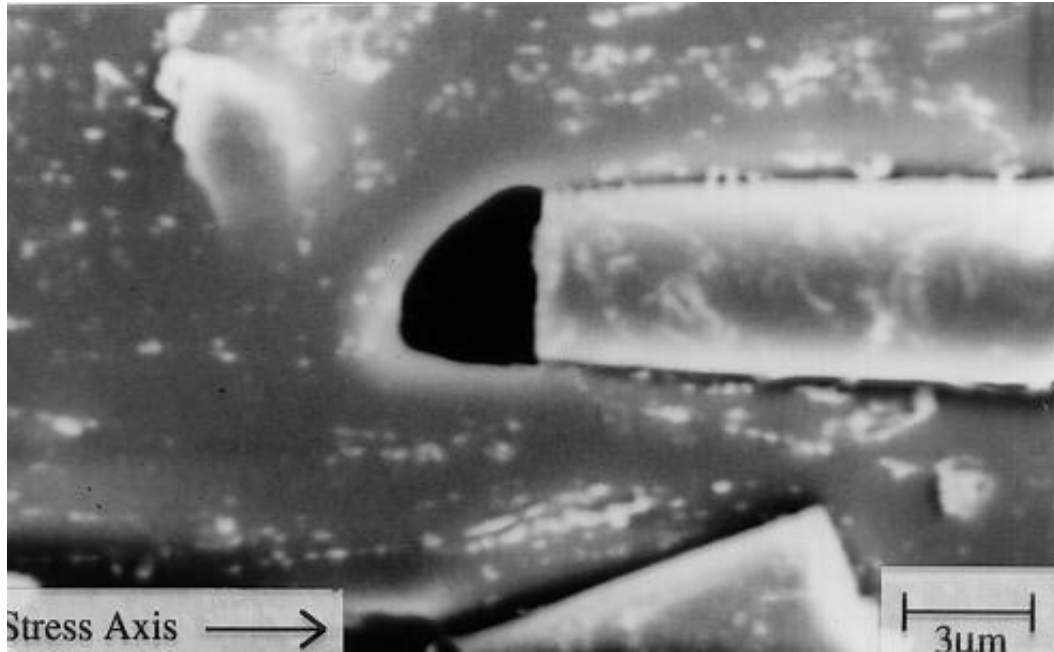


Fig. 5.13 Cavity at the end of a silicon carbide whisker in aluminium (Courtesy T.W. Clyne; see Clyne, T.W., and Watson, M.C., 1991, *Comp. Sci. Tech.* **42**, 25-56.)

Thus, yielding and progressive shear flow of a metal matrix, close to the interface, as envisaged by the early researchers in this field, appears to be too simplistic, and could well be invalid. This will be discussed in more detail in Chapter 8, where recent developments in our understanding of the fibre-matrix interface are described.

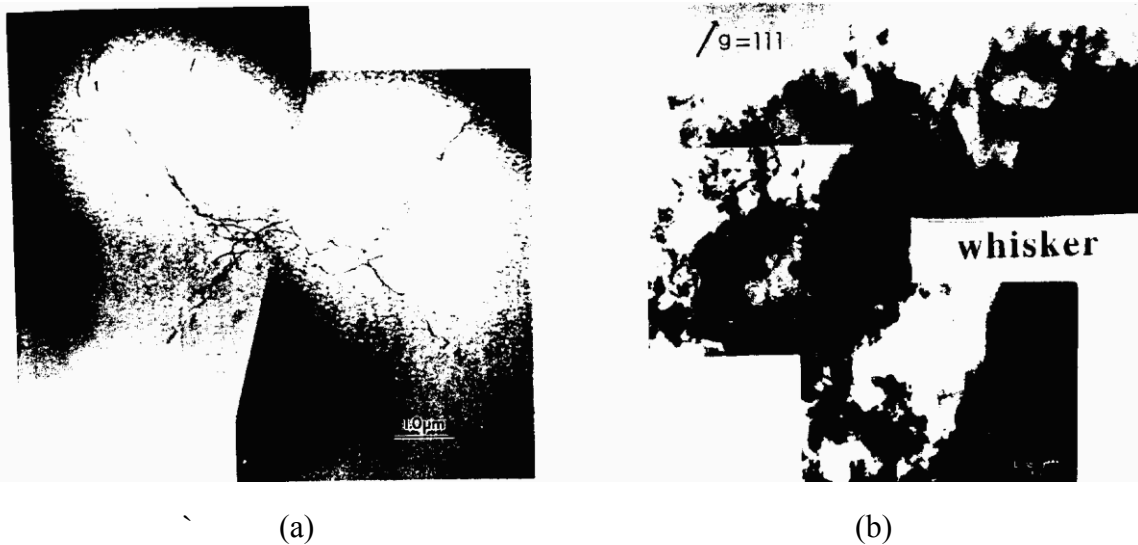


Fig. 5.14 Dislocation arrays around a silicon carbide whisker in aluminium: (a), Al matrix; (b), end of whisker (After Shi, N. and Arsenault, R.J., 1994, *Ann Rev. Mater Sci.* **24**, 321-57.)

5.3.3 Reinforced Ceramics and Cements

Reinforced ceramics and cements have minimal bonding between the fibres and the matrix. So stress transfer is normally assumed to take place through friction across the interface near the fibre ends. Thus, in theory, we can use the equations of section 5.3.1 as a first approximation. Instead of τ_i we use μP where μ is the coefficient of friction and P is the pressure across the interface. More advanced treatments are available, which allow for Poisson's shrinkages of fibres and matrix. However, in view of the paucity of experiments on well characterized systems (well aligned fibres, known values for s_c , etc.) the simple equations developed in section 5.3.1 are adequate for present purposes.

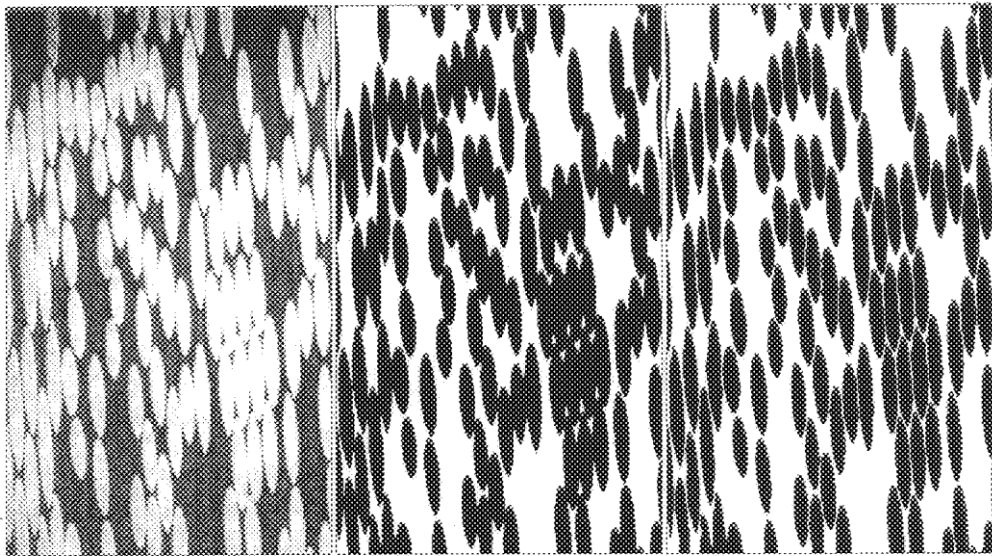


Fig. 5.15 Section of an aligned fibre composite cut at about 10° to the main fibre direction. At left is original digitized picture, centre is reduced to black and white. At right, individual fibres have been separated. (A full description of this technique is given by Yurgartis, S.W., 1987, *Comp. Sci. Tech.* 30, 279-94.)

5.4 Misorientation Effects

We cannot make short fibre composites (or any other type of composite for that matter) with the fibres perfectly aligned. So we must allow for misaligned fibres. To do this we measure the fibre orientations. One good way of doing this is to cut and polish a section at 5° or 10° to the main fibre direction. The fibres intersect the plane to give ellipses; see Fig. 5.15. The ratio of major to minor axes gives the angle with respect to the plane of the cut. From this the misorientation can be determined.

An alternative way to do this is to cut and polish a section normal to the main fibre direction, and digitize the image obtained in a microscope. Then the section can be repolished and rescanned. With modern computer pattern recognition software plus some specialized programming, the original fibres can be identified in their new positions: see

Fig. 5.16. By doing this two or three times more, both angular information and fibre waviness information can be obtained. This technique is also suitable for randomly oriented fibres.

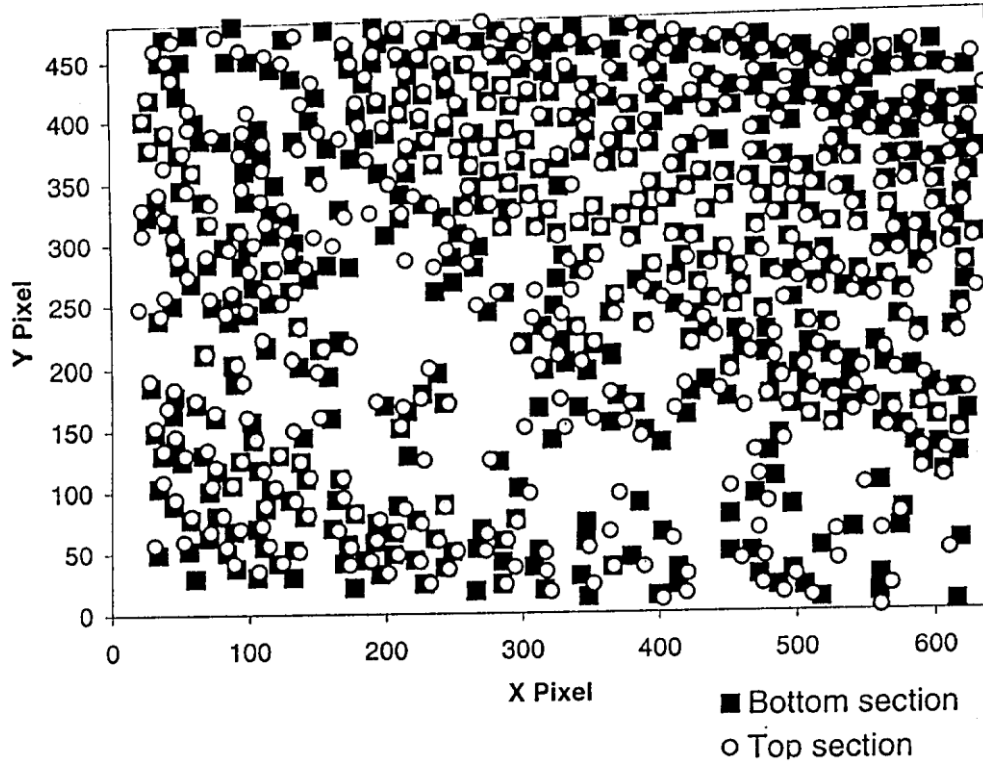


Fig. 5.16 Fibre images superposed. Original fibre positions indicated by circles and new positions after repolishing indicated by squares.

An experimental angular distribution obtained with short fibres is shown in Fig. 5.17. Note that we have only included in-plane misorientations; out of plane orientation errors tend to be much smaller in these composites.

From our misalignment data, we calculate misalignment modulus and strength factors, χ_1 and χ_3 . We divide our composite into hypothetical laminates containing fibres with different misorientations ϕ , e.g. $\pm 2.5^\circ$, $\pm 10^\circ$, $\pm 30^\circ$ and $\pm 67.5^\circ$. Taking χ_1 first, we estimate an equivalent A_i [equation (4.57)]. The relative thickness of each laminate, t , is given by the relative number of fibres in the range of angles corresponding to each ϕ value, as indicated in Fig. 5.16. The value of χ_1 is given by

$$\chi_1 = \frac{\sum_{k=1}^n \bar{Q}_{11} t_k}{E_{LOM} \sum_{k=1}^n t_k} \quad (5.49)$$

with $n = 4$ (four layers) in this case. Subscript *LOM* refers to Law of Mixtures. (In the original work referenced under Fig. 5.17, $1 / \bar{S}_{11}$ was used instead of \bar{Q}_{11} , so χ_1 was underestimated.)

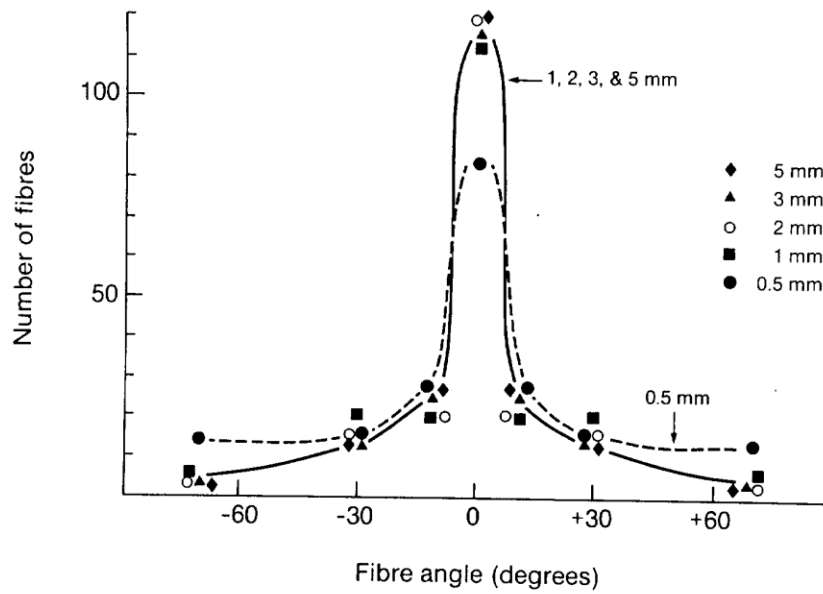


Fig. 5.17 Fibre angle distributions in short fibre composites. Fibre lengths indicated on the curves. (After Sanadi, A.R. and Piggott, M.R., 1985, J. Mater. Sci. 20, 421-430.)

For strength we do the same. Thus

$$\chi_3 = \frac{\sum_{k=1}^n \sigma_{fu\phi k} t_k}{\sigma_{LOM} \sum_{k=1}^n t_k} \tag{5.50}$$

but we do not use equation (4.40) to estimate the required values of $\sigma_{u\phi}$. Instead we use data from experiments in which the strengths of fibres crossing cracks obliquely are measured. These were introduced in Chapter 4, and Fig. 4.22 shows the results. It can be seen that the decrease in strength with increasing angle depends on the fibre, being greatest for glass and least for Kevlar.

Table 5.3 Half Strength Angles, Normalized Mean Strengths, and Normalized Mean Strengths Estimated from Equation 5.53.

Fibre	Resin	Cure	ϕ_h	Expt*	eq.(5.53)*
Glass	Epoxy	20°C 24h	20°	0.31	0.22
Kevlar	Epoxy	20°C 24h	45°	0.53	0.50
Carbon	Epoxy	20°C 24h	40°	0.44	0.44
Carbon	Epoxy	80°C 3h	30°	0.35	0.33

* Experimental and curve fit values for $\bar{\sigma}_{fu} / \sigma_{fu0}$.

As indicated in Chapter 4, the results can be represented quite well for carbon, and not quite so well for Kevlar and glass by a one third power equation (equation (4.78)). This equation is empirical, fits the experimental results moderately well for ϕ up to ϕ_h , and predicts quite well the mean fibre strength for fibres at all angles in a plane. Table 5.3 summarizes the results of the experiments shown in Fig. 4.22.

We obtain the mean fibre strength by integration of equation (4.78)

$$\bar{\sigma}_{fu} = \frac{1}{90} \int_0^{2\phi_h} \sigma_{fu\phi} d\phi \quad (5.51)$$

which gives

$$\bar{\sigma}_{fu} = \sigma_{fu0} \phi_h / 90 \quad (5.52)$$

for ϕ_h in degrees, and on condition that $2\phi_h \leq 90^\circ$. (The less good agreement in the case of glass and Kevlar is due to the strength being underestimated for $\phi > \phi_h$. This has very little effect on $\bar{\sigma}_{fu}$ for Kevlar, but a significant effect for glass as can be seen from Table 5.3.)

To estimate $\sigma_{u\phi}$ we use

$$\sigma_{u\phi} = V_f \sigma_{fu\phi} + V_m \sigma_{mu} \quad (5.53)$$

It will be noted that we can estimate σ_{ru} more accurately than in equation (4.54) if we know ϕ_h , and if we assume that the fibres are long enough to be fully loaded. Thus

$$\sigma_{ru} = V_f \sigma_{fu0} \phi_h / 90 + V_m \sigma_{mu} \quad (5.54)$$

for ϕ_h in degrees.

Our full expression for Young's modulus is

$$E_1 = \chi_1 \chi_2 V_f E_f + V_m E_m \quad (5.55)$$

with

$$\chi_2 = 1 - \tanh[ns]/[ns] \quad (5.56)$$

and for strength it is

$$\sigma_{1u} = \chi_3 \chi_4 V_f \sigma_{fu} + V_m \sigma_{mu} \quad (5.57)$$

with

$$\chi_4 = 1 - s_c/[2s] - 12.5/[ss_c] \quad (5.58)$$

for $s > s_c$ and, for $s < s_c$

$$\chi_4 = (s_c/[2s])(1 - 25/s^2) \quad (5.59a)$$

For strength, this method only works when misorientations are quite small. When they are moderately large, as in partly aligned short glass or carbon fibre reinforced

injection moldings, cracks grow by a fibre avoidance process; see Fig. 5.18. Strengths tend to be rather low and the concept of critical aspect ratio has not been found to be useful.

5.5 Variable Fibre Length

We handle variable fibre length in an analogous way to fibre misorientations, i.e. we classify the fibres into groups with lengths in certain ranges, then we prepare a weighted sum to determine the fibre contribution. Thus if P_{sk} is the fraction of fibres having aspect ratios $s_k \pm \Delta s$ where $\Delta s = \frac{1}{2}(s_{k+1} - s_k) = \frac{1}{2}(s_k - s_{k-1})$, etc., then

$$\chi_4 = \sum_{k=1}^v P_{slk} \left\{ 1 - \frac{s_c}{2s_k} - \frac{12.5}{s_k s_c} \right\} + \sum_{k=1}^w P_{ssk} \left\{ \left(\frac{s_c}{2s_k} \right) \cdot \left(1 - \frac{25}{s_k s_c} \right) \right\} \quad (5.59b)$$

where P_{slk} and P_{ssk} are the fractions as above for longer ($s > s_c$) and shorter ($s \leq s_c$) fibres.

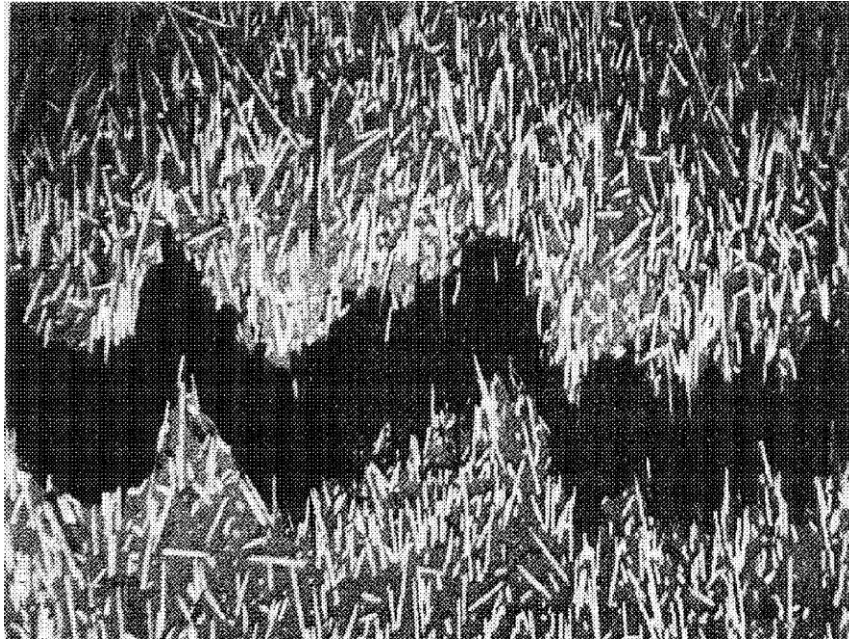


Fig. 5.18 Crack avoidance in carbon-polycarbonate. Photo courtesy of J.F. Mandell. (After Mandell, J.F., Huang, D.D., and McGarry, F.J., 1982, ASTM STP, 772, 3-32.)

Further Reading

- Cox, H.L, (1952), *Brit. J. Appl. Phys.* 3, 72-9.
 Kane, M.W., (1959), *Pulp & Paper Magazine of Canada*, 60, (#12), 259-65.
 Piggott, M.R., Ko, M. and Chuang, H.Y., (1993), *Comp. Sci. Tech.* 48, 291-9.
 Piggott, M.R., (1994), *J. Comp. Mater*, 28, 588-606.
 Outwater, J.O., (1956), *Modern Plastics*, 33, 156.

Chapter 5: Problems

You are strongly recommended to solve these problems in the order given. Data needed will be found in tables in this and other chapters of the book.

- 5.1. Show that $P_f = 2\pi/\sqrt{3}$ when the fibres are hexagonally packed.
- 5.2. Estimate the interfacial shear stress at the fibre ends for epoxy with aligned short silica fibres having lengths (a) 1.00mm and (b) 100 μ m and a volume fraction of 0.40. The strain is 0.50% and $P_f = 3.20$.
- 5.3. What is the ratio of the maximum to the mean fibre stress for silicon nitride reinforced aluminum below the knee. $V_f = 0.37$ and (a) $s = 10$ and (b) $s = 100$. Assume the fibres are square packed.
- 5.4. Calculate the stress and strain at the loosening point for long ($ns > 1000$) Kevlar fibre reinforced epoxy having an apparent interfacial shear strength of 26MPa and a volume fraction of 0.5 with $P_f = 3.30$.
- 5.5. Calculate the diameters of glass, Kevlar and carbon fibres used for the experiments which gave the data given in Table 5.2.
- 5.6. Which fibre-polymer system in Table 5.2 had the greatest interfacial shear stress. Estimate the shear stress. (Assume AS4 has a strength of 3.8GPa; the Kevlar was Kevlar 49)
- 5.7. Which fibre-polymer system in Table 5.2 had the least interfacial shear stress. Estimate the shear stress. (Assume AS4 has a strength of 3.8GPa; the Kevlar was Kevlar 49)
- 5.8. Estimate the strength of short aligned E glass-polyester (80°C) with fibre lengths of (a) 12mm and (b) 1.0mm: $V_f = 0.44$. The strength of the polyester is 93MPa, and the diameter of the glass was 12 μ m.
- 5.9. How long would strong carbon fibres have to be if, when embedded in PEEK, the composite achieves 95% efficiency for strength. Assume that $V_f = 0.5$ and that the tensile strength of PEEK is $\sqrt{3}$ times the apparent interfacial shear strength.
- 5.10. Do the same estimation for C-PEEK except for modulus rather than strength. Assume a packing factor of 3.40 and that the matrix has a modulus of 7GPa and a Poisson's ratio of 0.34.

- 5.11. What strength efficiency would be achieved by Kevlar fibres, if they had a length such that they had, with epoxy, a Young's modulus efficiency of 95%. Assume $V_f = 0.5$.
- 5.12. Using Figs. 3.9, 5.10 and Table 5.1, estimate the strength efficiency of the extra stiff carbon reinforced epoxy. Assume that the apparent interfacial shear strength is half the tensile strength of the epoxy.
- 5.13. If an apparent interfacial shear strength equal to half the matrix tensile strength can be achieved with unidirectional SiC whisker reinforced pure Al, estimate the strength of the composite when the whisker length is (a) 0.020mm and (b) 0.50mm. $V_f = 0.27$.

Chapter 5. Selected Answers

- 5.3 (a) 1.26 and (b) 1.02
- 5.5 22, 12 and $8\mu\text{m}$
- 5.7 Glass-polyester (20° cure), 6.2MPa.
- 5.9 2.0 mm.
- 5.11. 64%
- 5.13 (a) 0.16GPa and (b) 2.68GPa.

6. MATRIX DOMINATED PROPERTIES

The feeble resistance of the unidirectional composite to stresses transverse to the fibres is due mainly to the relatively low strength of the matrix. This is especially so with polymer matrices, where low moduli can also contribute to low properties. Furthermore, when the fibre-matrix interface is weak, the interface can dominate the transverse properties. Other properties are similarly sensitive to the matrix and the interface. In this chapter we introduce the basic principles which underlie some of these properties. We do not include fracture toughness here, although it is also very dependent on the matrix and interface; this is discussed in Chapter 7. The interface itself is discussed in Chapter 8. Our understanding of the processes governing these properties, and incidentally fracture toughness and the interface, is incomplete at the time of writing. This is because the shear failure processes in the matrices used for fibre composites are not fully understood. This is particularly the case with polymers, and so the failure processes in the polymers will be discussed first.

We also need to consider the real structure of the composite, taking into account the fact that fibres are not normally perfectly straight or perfectly uniformly packed. These and other structural anomalies are discussed in the second section, labelled Mesostructures. We then go on to discuss particular properties, i.e. off-axis strength, shear strength compressive strength and fatigue resistance. The relevant moduli are also discussed.

Because many more experimental results are available for reinforced polymers than for reinforced metals and ceramics, this treatment concentrates on reinforced polymers. Results for metals and for ceramics and cements will be found in Chapter 11.

6.1 Shear Failure Processes in the Matrix

The first sign of incipient failure in a ductile material is yielding. This appears to be better understood than the termination of the process, when the sample breaks into two or more pieces. Part of the reason for this is that fracture is more complex, there being at least two modes, i.e ductile and brittle. Furthermore, simple compression is unlikely to lead to breakage, except with a very brittle material. Under compression, yielding and shear flow only, are normally observed; even glass can be permanently indented as a result of shearing processes involved when a harder material, such as a diamond indenter, is pressed into the surface.

6.1.1 Yielding

Simple tensile and shear stresses can cause yielding of metals and polymers. However, the processes involved are quite different. Figs. 1.1 and 1.3 show tensile stress-strain curves for two metals and two polymers. It was already noted (on pp. 5-6) that the elastic limit is at much higher strains for polymers than for metals. This has led to the use of a different definition of yield point. For metals, the standard (North American)

definition of yielding is the 0.2% offset value. This is the stress at the point where the strain is 0.2% higher than the elastic value. At higher strains ($> 0.5\%$ for the steel shown in Fig. 1.1), permanent deformation occurs: see Fig.1.2.

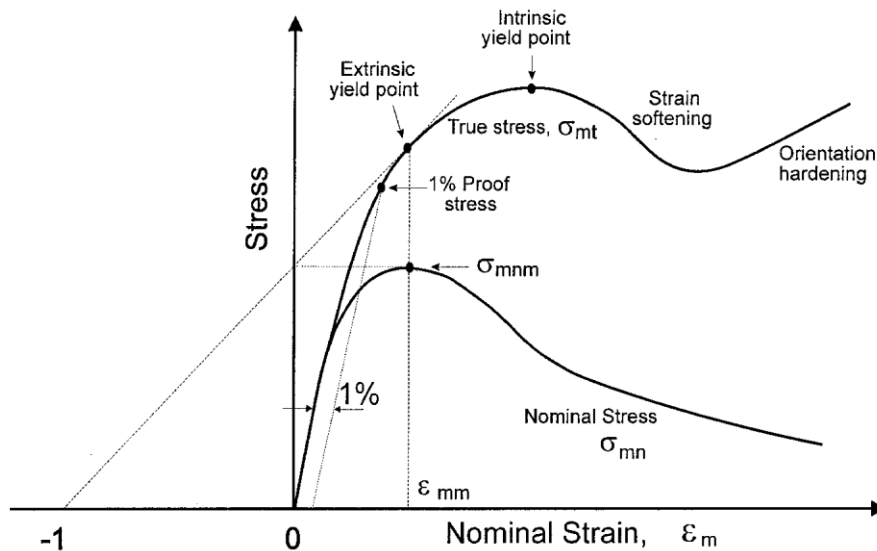


Fig. 6.1 Schematic drawing of true tensile stress and nominal tensile stress vs nominal strain for a typical amorphous glassy polymer. (After Bowden, P.B., 1973, *The Physics of Glassy Polymers*, Ed. R.N. Haward; Applied Science Publishers, London, Chapter 5.)

With polymers, permanent deformation does not occur until the deviation from linearity is much greater than 0.2%. To clarify this issue we need to replot our stress-strain curves so that non-uniform deformation and necking are taken into account. For this we use the true stress, σ_{mt} , i.e. the load divided by the cross section in the necked region, instead of the nominal stress, σ_{mn} (load/initial cross section). When we plot σ_{mt} versus nominal strain (change in length/original length), ϵ_m , a peak is not usually observed with metals, as mentioned on p. 5, but a peak is often seen with polymers.

Fig. 6.1 shows a schematic true tensile stress-nominal strain curve for a typical amorphous glassy polymer such as polycarbonate, with, below, the nominal stress. Two yield points are indicated, the extrinsic and intrinsic yield points. The extrinsic yield point corresponds to the maximum nominal stress, σ_{mnm} , with the strain being ϵ_{mm} . At this stage, strains are recoverable, and no permanent deformation is observed after the stress is removed. The intrinsic yield point is the point beyond which permanent deformation normally occurs. At still higher strains, the true stress often decreases, i.e. strain softening takes place. Beyond this, at still higher strains, the polymer chains tend to become oriented and the material becomes stiffer, so increasing the stress again.

Also shown in Fig. 6.1 is the 1% proof (or offset) stress, where the strain is 1% higher than the elastic value. This stress, unlike the 0.2% offset stress for metals, is of

little interest since there is no transition in behaviour: on removal of the stress the strain disappears also.

In addition, a line is drawn on Figure 6.1 which touches the true stress curve and intersects the strain axis at -1 . It is the tangent at the extrinsic yield point, and it intersects the stress axis at σ_{mmm} . This is Considère's construction, which was originally proposed for metals. During plastic deformation the volume of a metal does not change significantly. Because of this

$$\sigma_{mt} = (1 + \varepsilon_m) \sigma_{mn} \quad (6.1)$$

The slope of the true stress-nominal strain curve, therefore, is

$$\frac{d\sigma_{mt}}{d\varepsilon_m} = \sigma_{mn} + (1 + \varepsilon_m) \frac{d\sigma_{mn}}{d\varepsilon_m} \quad (6.2)$$

which at $\sigma_{mn} = \sigma_{mmm}$ reduces to

$$\frac{d\sigma_{mt}}{d\varepsilon_m} = \sigma_{mmm} \quad (6.3)$$

since $d\sigma_{mn} / d\varepsilon_m = 0$ when $\sigma_{mn} = \sigma_{mmm}$.

The equation of the tangent to the true stress curve at the extrinsic yield point (the dashed line) may thus be obtained using equation (6.2) for the slope, and the co-ordinates of the yield point. i.e., $\sigma_{mty} = (1 + \varepsilon_{mm})\sigma_{mmm}$ and $\varepsilon_m = \varepsilon_{mm}$. Thus

$$\sigma_{mty} = (1 + \varepsilon_m) \sigma_{mmm} \quad (6.4)$$

It can be seen that this line must intersect the strain axis at -1 ($\sigma_{mty} = 0$) and the stress axis at σ_{mmm} ($\varepsilon_m = 0$)

Thus, when the true stress-nominal strain curve has been obtained, the maximum nominal stress can be determined, and also the extrinsic yield point, using Considère's construction. Although polymers do not deform plastically at constant volume, the construction is widely used for polymers as well as metals.

Unlike metals, the yielding of polymers is pressure dependent at relatively low pressures. The shear yield stress of most polymers decreases approximately linearly with pressure. Thus

$$\tau_y = \tau_0 - \mu P_h \quad (6.5)$$

where μ is a constant, equal to about 0.2 in the case of polymethyl methacrylate and P_h is the hydrostatic component of the stress tensor which is positive when the stresses are tensile. P_h is given by

$$P_h = \frac{1}{3} (\sigma_x + \sigma_y + \sigma_z) \quad (6.6)$$

The shear yield stress in the absence of pressure, τ_0 , can be estimated by finding the yield stress in uniaxial tension, σ_{yt} and that in uniaxial compression σ_{yc} . Using the Tresca yield criterion, the shear yield stress is half either σ_{yt} or σ_{yc} according to whether the test is tensile or compressive (see page 27). Thus, in tension

$$\sigma_{yt} = 2\tau = 2\tau_0 - 2\mu \sigma_{yt} / 3 \quad (6.7)$$

since $P_h = \sigma_{yt} / 3$, and for compression, with $P_h = -\sigma_{yc} / 3$ we have

$$\sigma_{yc} = 2\tau = 2\tau_0 + 2\mu \sigma_{yc} / 3 \quad (6.8)$$

Eliminating μ between equations (6.7) and (6.8) gives

$$\tau_y = \left(\frac{1}{\sigma_{yt}} + \frac{1}{\sigma_{yc}} \right)^{-1} \quad (6.9)$$

i.e. an inverse Rule of Mixtures expression. For metals the tension and compression true stress-strain curves are the same within a percent or so. For polymers, they can be quite different. For example, a 20°C cured epoxy had $\sigma_{yt} = 55$ and $\sigma_{yc} = 99$, giving $\tau_y = 35$ MPa. Corresponding figures for PEEK were 91 and 138 giving 55MPa. The intrinsic yielding strains were 5% or more.

Ceramics normally yield only when stressed at very high temperatures (> one half of the absolute melting temperature) or when indented with a very hard and sharp indenter, such as in a hardness tester: see Fig. 2.14; their yielding will therefore not be discussed here.

6.1.2 Breaking Apart

Separation into two or more pieces may be regarded as the termination of the failure process. This is usually, but not always, preceded by yielding in polymers and metals. With polymers, crazing may also occur before total separation. Crazes are multiple cracks. They are usually quite small and narrow, and perpendicular to the stress. They are bridged by polymer chains oriented in the stress direction. This restricts their size, i.e. they do not normally grow out of control. This permits the development of the crack arrays that constitute crazing. Organic liquids can be very active in promoting crazing.

We expect breaking apart to be possible in both shear and tension. However, in shear this is rare. A widely used shear test for composites was invented by N. Iosipescu. This involves the notched specimen shown in Fig. 6.2. When used for neat polymers, shear failure does not occur. With brittle polymers, especially thermosets, the failure is tensile at 45° to the shear; Fig. 6.2 left. With ductile thermoplastics the sample deforms up to the limit of movement possible in the fixture; Fig. 6.2 right. (As shown in section 1.3, pure shear arises from the simultaneous action of tension at +45° and compression at -45°).

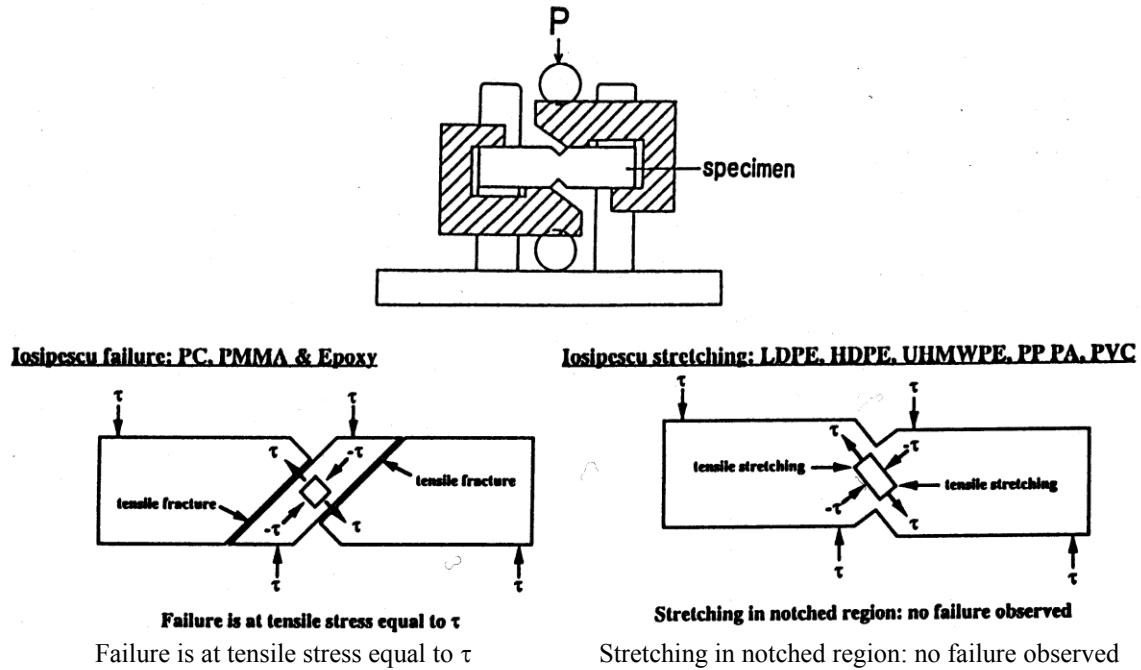


Fig. 6.2 Iosipescu test on neat polymers: ductile polymers stretch while more brittle polymers break at 45°. (After Liu, K., and Piggott, M.R., 1998, Polym. Eng. Sci. 38, 60-68.)

In an attempt to force a shear failure, and hence get a better measure of shear strength, the standard Punch Test has been used. This however, gave an apparent strength which was quite close to the tensile strength for the more ductile polymers; see Fig. 6.3.

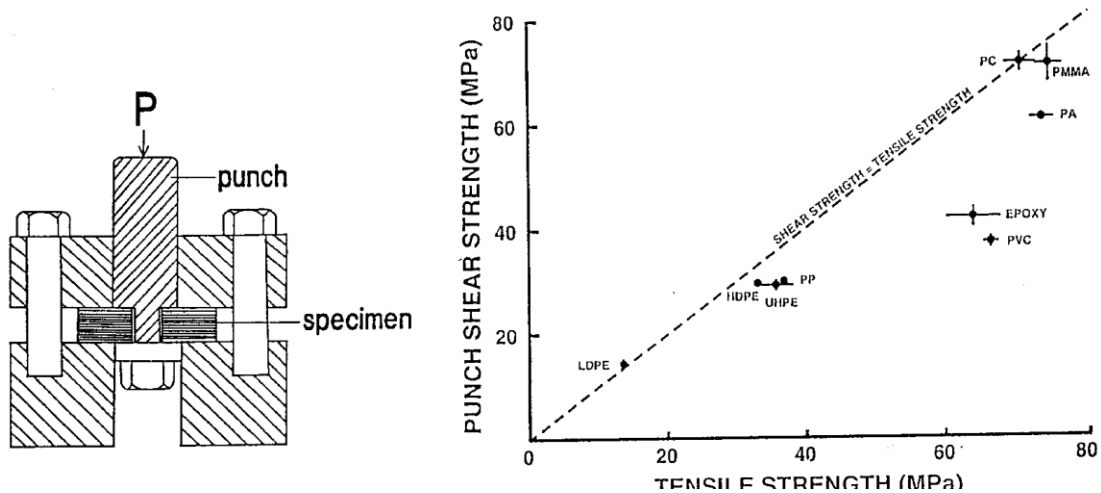


Fig. 6.3 Punch shear strength vs nominal tensile strength for polymers.

The punch test was capable of delivering very high shear strains. The spacing between punch and die is about 12.5 μm (ASTM D732). With a 3mm thick sheet of polymer the force was still rising in many cases (see Fig. 6.4) when the punch displacement was 1mm, i.e. a nominal shear strain of 1000/12.5 or 8000%. This accounts for the lack of success with the ductile polymers in the Iosipescu test.

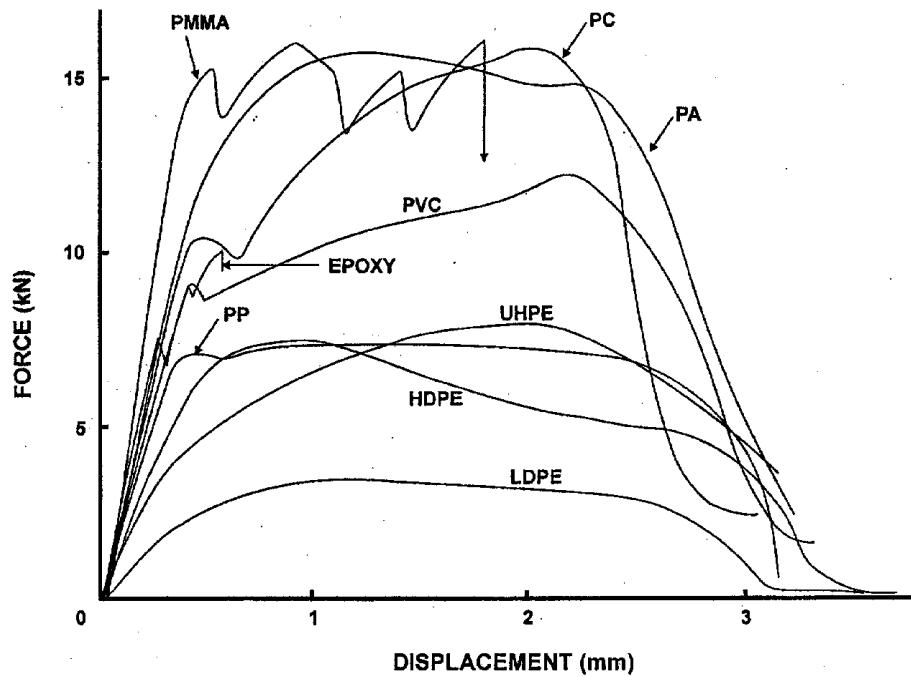


Fig. 6.4 Force-displacement curves during testing in the Punch test.

Furthermore, the actual failures in the punch test were tensile, in all cases except low and high density polyethylene and polypropylene. Examination of the fracture surfaces showed tensile cracks in all the other cases examined. Fig. 6.5 shows a typical tensile crack in the punch fracture surface of nylon. It can be seen that it has matching striations on either side confirming the tensile nature of the crack opening.

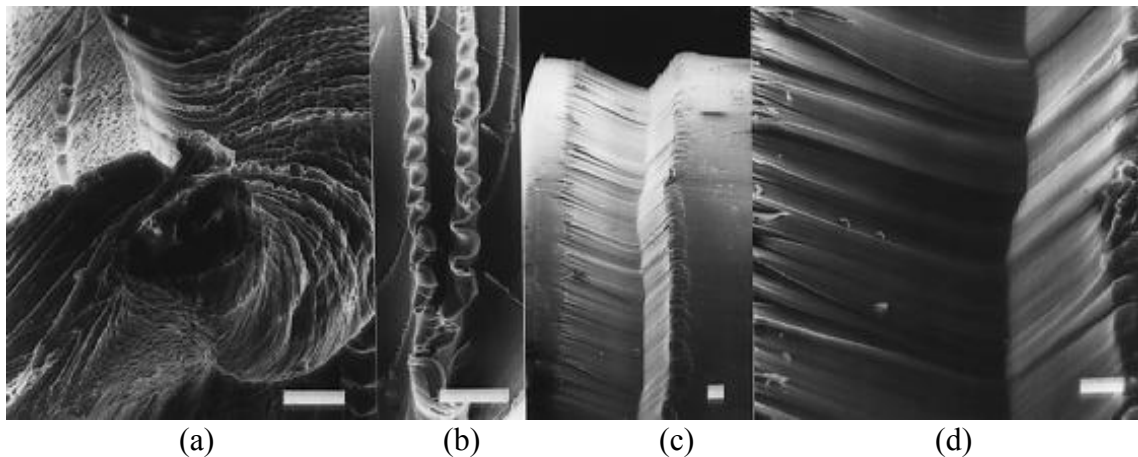


Fig. 6.5 Fractographs of nylon (a) and (b) tensile failure showing spiral and leafy structures and (c) and (d) punch fracture showing crack with matching striations. Bars represent $100\mu\text{m}$.

Polymers, being long chain molecules, with cross links in the case of the thermosets, can be modelled with string, or wire if backbone stiffness is to be simulated.

(Cross links could also be simulated with extra elements of string or wire.) Fig. 6.6 shows the expected response of such a structure to shear and tension. The end result is the same: the molecules align themselves in the direction of the tensile displacement. Failure of such a structure is thus dominated by the tensile component.

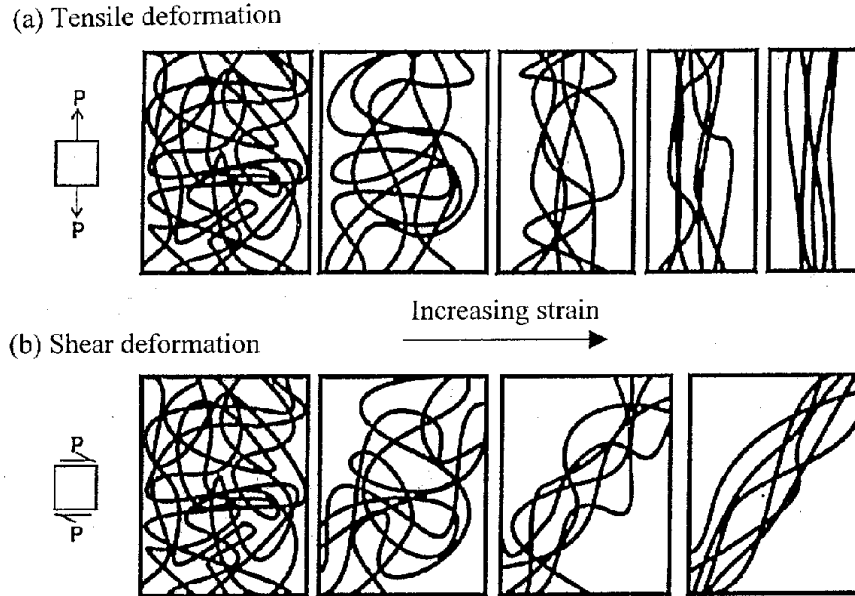


Fig. 6.6 At top, large tensile deformations of polymers modelled with string. At bottom large shear deformations similarly modelled.

The exceptions to this are the simplest and shortest chain polymers. We can model these as fine "fibres", as shown in Fig. 6.7, and determine the conditions for them to pull out, rather than break. This should give the maximum chain length for liquid-like behaviour, if we assume that true polymer liquids can shear to an infinite extent without chain scission (i.e. no "fibres" breaking.) In Fig. 6.7 an idealized polyethylene chain is crossing a shear failure zone at a small angle. The intense shear ensures that this section of the polymer chain is effectively straight. Each CH_2 group on the chain is attracted to neighbouring CH_2 groups on other chains by Van der Waals forces.

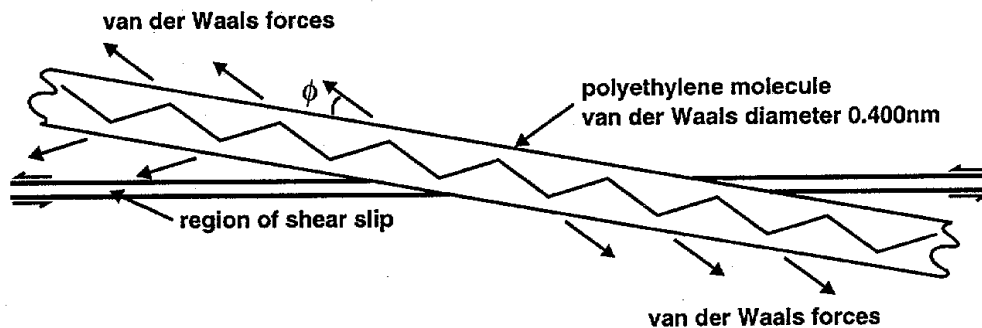


Fig. 6.7 Schematic drawing of a single polyethylene molecule crossing a region of intense shear.

Assume these forces are equivalent to stresses σ_v which act at an angle ϕ . Let the length, L , of the molecule on the upper side of the failure zone be greater than that on the lower side. Then the pull out force F is given by

$$F = \pi dl \sigma_v \cos \phi \quad (6.10)$$

where d is the diameter of the molecular chain [compare equation (6.10) with equation (5.32)].

If the strength of the chain is σ_{th} then F cannot exceed $\frac{1}{4}\pi d^2 \sigma_{th}$. Using equation (2.19) for σ_{th} this means that

$$\pi dL \sigma_v \cos \phi > \frac{E}{m} \left\{ \frac{n}{m} \right\}^{\frac{n}{m-n}} \quad (6.11)$$

Thus the maximum value for L , L_{\max} , is given by

$$L_{\max} = \frac{dE}{4m\sigma_v \cos \phi} \left\{ \frac{n}{m} \right\}^{\frac{n}{m-n}} \quad (6.12)$$

so that the maximum polymer length for no fibre fracture (or chain scission) is $2L_{\max}$.

The polymer chain has a C-C bond angle of 109.5° or $2\arctan\sqrt{2}$, so the maximum number of carbon atoms in the polymers is N_{\max} where

$$N_{\max} = 2\sqrt{3} L_{\max} / a_0 \quad (6.13)$$

Here a_0 is the length of the C-C single bond. Eliminating L_{\max} between equations (6.12) and (6.13) gives

$$N_{\max} = \frac{\sqrt{3}dE}{2a_0m\sigma_v \cos \phi} \left\{ \frac{n}{m} \right\}^{\frac{n}{m-n}} \quad (6.14)$$

For d we use the size of a CH_3 group, i.e. 0.40nm and for σ_v we use the tensile strength of low density polyethylene (LDPE), i.e. 13.6MPa. The stiffness of the carbon-carbon bond, E , comes to about 1020GPa and $a_0 = 0.154$ nm. We assume $\phi = 45^\circ$, and we use the known values of n and m for silicon, i.e. 12 and 8 since values for carbon are not readily available. This gives $N_{\max} \sim 8800$, which corresponds to a molecular weight (MW) of 124,000. Since the MW of LDPE is less than 124,000 no chain scission takes place.

For high density polyethylene (HDPE), with a strength of 33.2 MPa, $N_{\max} \sim 3600$ with a corresponding MW of 50,000. This is less than the MW of HDPE, so some small amount of chain scission may occur in this case.

These models should be contrasted with those used for metals. The ideal metal atoms are almost spherically symmetric and can be modelled with ball bearings. Shear

deformation takes place by sliding of the most closely packed planes, as shown in Fig. 6.8. (This is of course a very idealized process. Dislocation movement governs the plastic deformation process of real metals, as briefly described in section 2.2.)

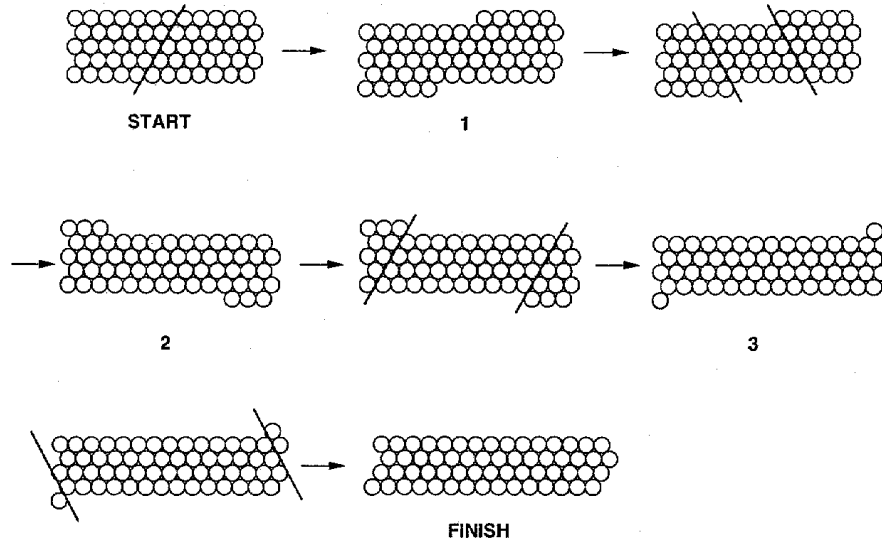


Fig. 6.8 Large plastic tensile deformation of metals modelled with spheres.

Since normal samples of metal are polycrystalline, the process shown in Fig. 6.8 only occurs to a very limited extent. The ductility rapidly becomes exhausted, and actual failure of metals is normally tensile, involving the cavitation process shown schematically in Fig. 6.9.

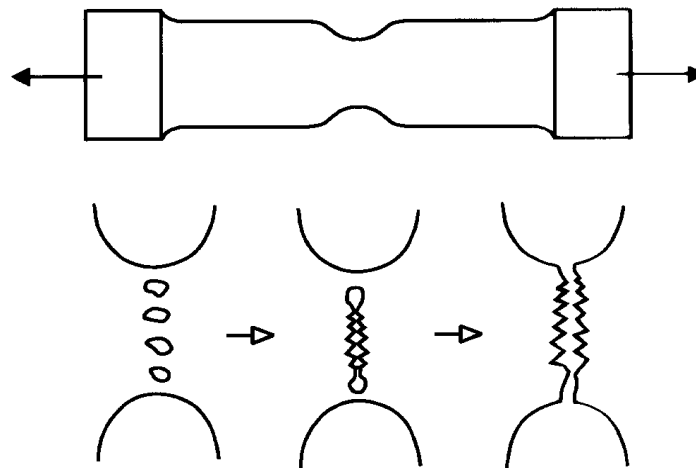


Fig. 6.9 Cavitation failure of a ductile metal (After Cottrell, A.H. ,1967, *An Introduction to Metallurgy*, Edward Arnold, London, p. 388.)

With ceramics at room temperature, and with very hard metals such as the steels used for razor blades, tensile failure is brittle, and initiated by tiny cracks. The energy release can be violent enough for the test piece to break into many fragments.

6.2 Internal Structures in Composites: the Mesostructure

It is convenient and useful to have a term which encompasses no more and no less than structures associated with fibre arrangements and straightness. We have microstructures and macrostructures for large and small textures. Mesos is the Greek word for middle, and is appropriate for this concept in fibre composites. We will define our structural levels as follows:

1. Microstructures: These exist on the scale of the fibre diameter or less, and include the fibre geometry (surface and end), interface or interphase, and extend to nearest neighbour fibres, so that interactions which take place between adjacent fibres can be included in the associated micromechanics. Dimensions are from nanometres to a few micrometres. These are usually a carefully controlled part of the structure.

2. Mesostructures or middle rank structures: These are on the scale from a few micrometres to millimetres, and are usually not controlled to any significant degree. Mesomechanics is used to describe interactions at this level.

3. Macrostructures: These include the type of lay up used, skin-core structures, etc. The scale is from about 0.1mm to tens of mm in thickness and could include much larger expanses in the plane of the composite. These are features of the overall design of the composite, and this level is the concern of macromechanics.

Some overlap between these levels is generally involved, but what is unique about mesostructures, apart from size, is that up till now they have usually been unintentional.

Mesostructures of many types can be identified. So some form of classification is required. Two sets of criteria or parameters will be considered here.

1. Disorder/Order
2. Orientation and packing effects.

These give four classes of mesostructure.



Fig. 6.10 Woven carbon fibre tows containing thousands of fibres have built-in waviness in this compression moulding. Two tows go across the picture from left to right. Other tows are seen end-on.

6.2.1 Disorder Mesostructures

Orientation. These features include fibre waviness, such as shown in Fig. 6.10. This can be synchronized, as shown here. (Synchronization is inevitable when woven materials are used.) Waviness may be characterized by amplitude and wavelength, and in the general case, Fourier analysis may be used to quantify the waviness in terms of amplitude and frequency. More random forms of waviness are present in aligned fibre laminates and in multidirectional laminated structures, in which woven materials are not used.

Packing. Fibre packing arrangements are often disordered. Fig. 6.11 shows a cross section of a composite in which we can identify, on the left, voids, matrix rich areas and fibre rich areas, and on the right, at higher magnification, possible fibre contacts.

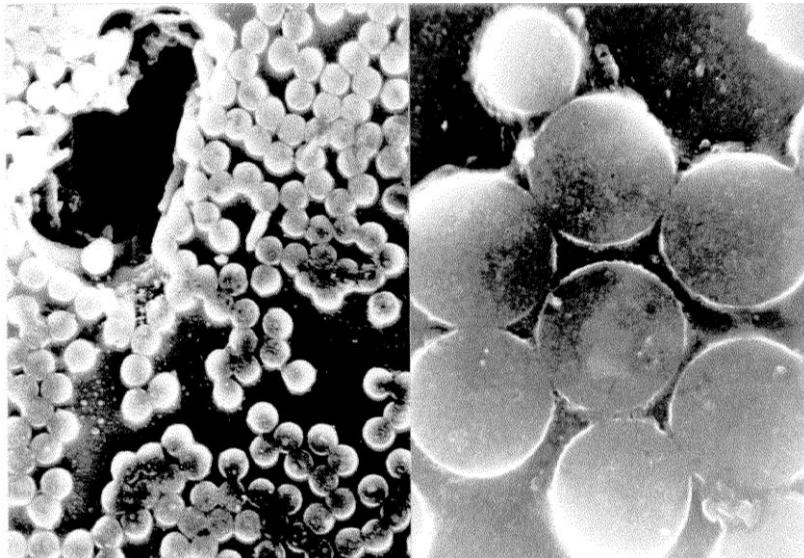


Fig. 6.11 Cross section of a carbon-epoxy pultrusion showing a void, resin rich areas and fibre rich areas. Fibre contacts may be seen at higher magnification at right.

6.2.2 Order Mesostructures

Orientation. In short fibre composite mouldings, flow in the moulding process generates preferred fibre orientations, Fig. 6.12. Near the surface of the mould the fibres are parallel to the surface (Fig. 6.12 left) while in the centre of a thick moulding they tend to be normal to the surface. Truly random fibre orientations are quite difficult to achieve. Fig. 6.12 (right) shows the centre of a thin (3 mm thick) moulding. Here, some residual orientation parallel to the mould surface is noticeable.

Packing. Two structures can be recognized here:

1. Fibre bundling, with the bundles retaining their integrity over considerable distances. This is inevitable with woven fibre composites as shown in Fig. 6.10. It

occurs to a lesser extent in other composite forms, but can be quite noticeable in filament windings, especially if the fibres retain some twist.

2. End synchronization. Incomplete dispersion of chopped fibres can leave fibre ends approximately coplanar, see Fig. 6.13.

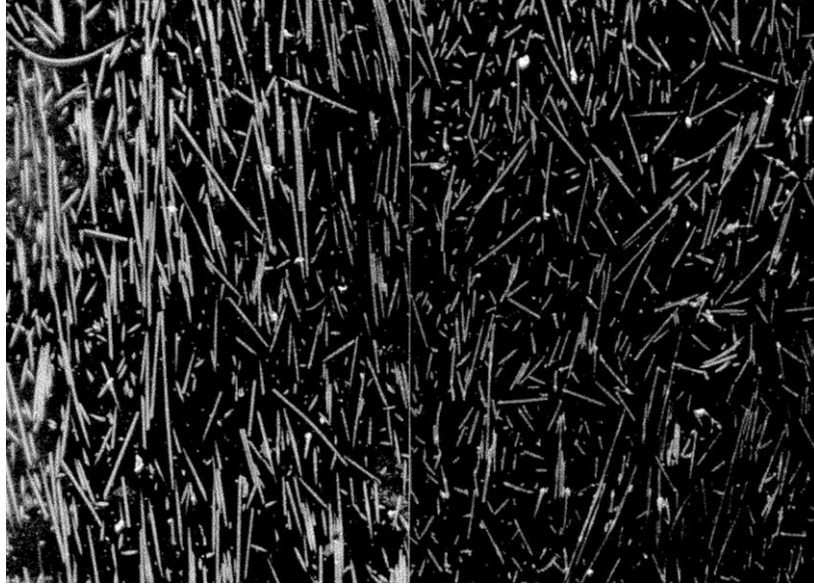


Fig. 6.12 A 3 mm thick glass-nylon 66 injection moulding showing at left, fibres parallel to the mould surface and at right, fibres more random near the centre but still showing some tendency for alignment in the flow direction.

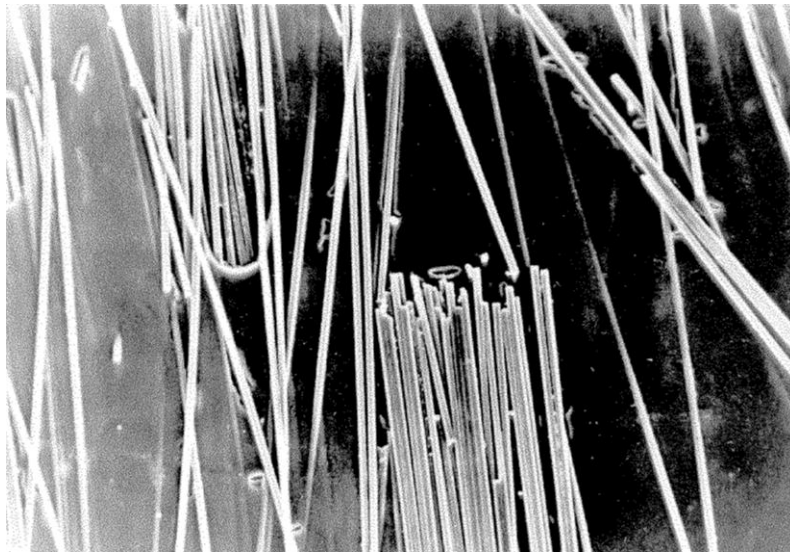


Fig. 6.13 Fibre end synchronization in an aligned short carbon fibre-epoxy compression moulding.

Since this is a relatively new subject, there may be other mesostructures not yet identified; even additional classes of mesostructures. So far there is very little information on the effects of mesostructures on properties, except in the case of the

compressive strength. In our description of properties in what follows we will discuss possible mesostructure effects. However, we must emphasise that this discussion is tentative. Hopefully you, the reader, will take up some of the ideas here and test them yourself.

6.3 Transverse Properties

These are properties at right angles to the fibres in unidirectional composites. In Chapter 4 we introduced very simple models for the transverse tensile strength, σ_{2u} , Fig. 4.7a, and modulus, E_2 , Fig. 4.3, of unidirectional composites. Here we will discuss some experimental results with reinforced polymers in the light of more sophisticated models, as well as the simple ones. Transverse compressive strengths will be briefly discussed in section 6.5.

6.3.1 Tensile Strengths

Two tensile strengths perpendicular to the fibres can be identified, σ_{2u} and σ_{3u} . There seems to be little reason to expect much difference between them, since they are controlled by the same two factors, i.e., the matrix strength and the interface strength. Moreover, the stress concentrations introduced by the fibres should be more or less the same in the two directions. So we will discuss models for σ_{2u} , usually referred to as the transverse strength, and assume they apply also to σ_{3u} , the through-thickness strength.

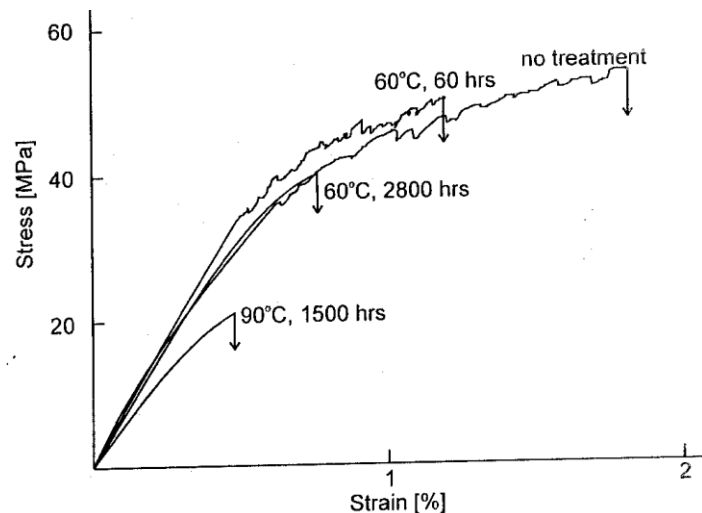


Fig. 6.14 Typical stress-strain curves for commercial composites as received, and after immersion in water for the times and temperatures indicated. (After Chan, M. and Piggott, M.R., (1999), *Composites Interfaces* 6, 543-56.)

The simple model for well adhering fibres, which gives $\sigma_{2u} = \sigma_{mu}$ is commonly observed with reinforced polymers when the matrix is not very brittle. Testing requires care: the edges of the specimen must be polished until mirror smooth to remove any notches or other stress raisers. Under these conditions $[0]_{18}$ AS4 - PEEK with $V_f = 0.61$

gave $\sigma_{2u} = 92 \pm 3\text{MPa}$ with $\sigma_{mu} = 91\pm 1\text{MPa}$, and a commercial carbon-epoxy moulding gave $\sigma_{2u} = 53 \pm 2\text{MPa}$, which is equal that to the strength of a good epoxy resin. Moreover, this reinforced epoxy was ductile: see Fig. 6.14. (Also shown in the figure is the effect of water immersion.)

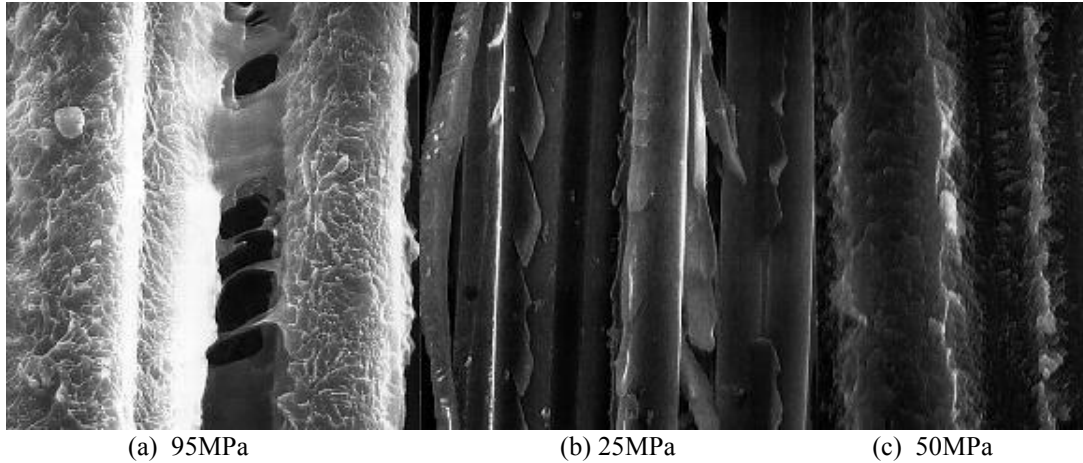


Fig. 6.15 Transverse fracture surfaces and approximate strengths for carbon reinforced plastics with transverse strengths as indicated. (a) PEEK compression moulding, (b) epoxy pultrusion, and (c) commercial epoxy moulding.

Fractographs of these failures, shown in Fig. 6.15a and c, confirm the excellent adhesion. No bare fibre was exposed.

In the event of a weak adhesive bond between the fibres and the matrix, as is normally the case for reinforced ceramics, we can expect σ_{2u} to be less than σ_{mu} with, in addition, progressive weakening as more fibres are added. Both our simple square packed and hexagonal models (Fig. 6.16) have a fibre separation of $R - 2r$, over which the matrix strength operates, and a length πr where adhesive forces operate.

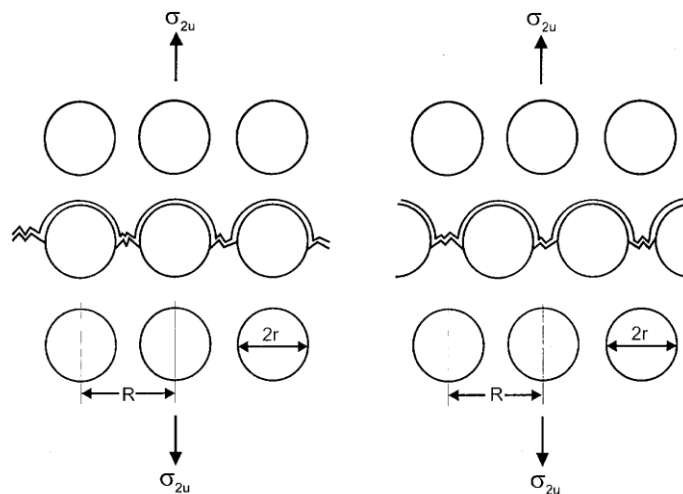


Fig. 6.16 Transverse failure path with square packed fibres and hexagonally packed fibres when adhesion is weak.

Assume that there is an interphase of strength σ_a , which contributes a force $\pi r \sigma_a$ per unit fibre length. Then

$$R\sigma_{2u} = \pi r \sigma_a + (R - 2r)\sigma_{mu} \quad (6.15)$$

and since $r/R = \sqrt{V_f / P_f}$ for both square and hexagonal packing, see equation (5.8), we can eliminate R and r to obtain

$$\sigma_{2u} = \pi \sqrt{V_f / P_f} \sigma_a + \left\{1 - 2\sqrt{V_f / P_f}\right\} \sigma_{mu} \quad (6.16)$$

Fig. 6.17 shows that for square packing, i.e. $P_f = \pi$, when adhesion is effectively nil, σ_{2u} is very low for $V_f > 0.4$. However even moderate adhesion can have a substantial effect: $\sigma_a / \sigma_{mu} = 0.2$ gives a threefold improvement at $V_f = 0.6$, while $\sigma_a / \sigma_{mu} = 0.5$ brings the strength to $0.83 \sigma_{mu}$.

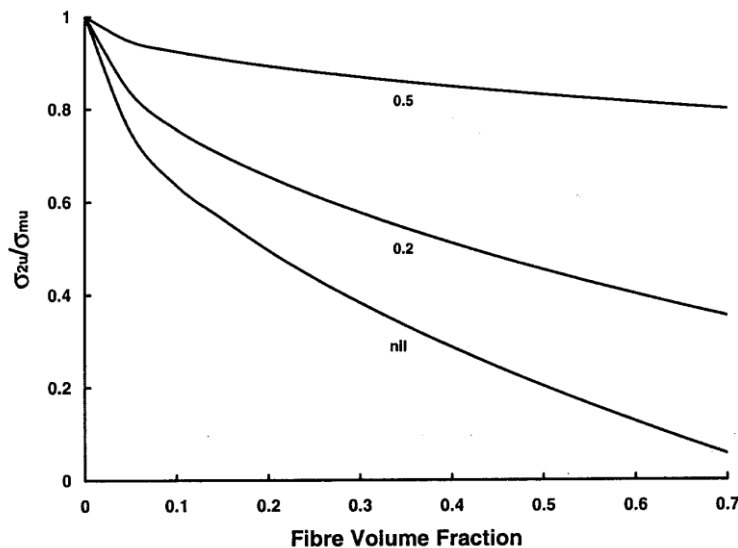


Fig. 6.17 Normalized transverse strength vs. V_f for different levels of adhesion between fibres and matrix.

(The alert reader will notice that the $\pi r \sigma_a$ term in equation (6.15) is approximate. The displacement in the interphasial layer is not purely tensile; it varies from pure shear, τ_a , to pure tension, σ_a , and back to shear as the failure propagates around the fibre. In addition, we neglect the stress concentrations introduced by the relatively stiff fibres.)

With polymer matrices the effect of poor adhesion is clearly demonstrated with the HMU fibres: see Table 6.1. These fibres do not adhere at all well to epoxy resin and lie approximately on the nil adhesion line in Fig. 6.17. (i.e. within one standard deviation). The AS4 adheres somewhat better, with results close to the line $\sigma_a / \sigma_{mu} = 0.4$. This moderately weak adhesion is confirmed by the bare fibre visible in Fig. 6.15b.

When adhesion is poor, fibre wetting is also a problem, Imperfect wetting can cause voids which can further decrease the transverse strength.

Table 6.1 Transverse Strengths (MPa) of Carbon Fibre Pultrusions with an Epoxy Matrix

Fibre	$V_f = 0.2$	$V_f = 0.3$	$V_f = 0.4$	$V_f = 0.6$
AS4	32 ± 6	29 ± 7	29 ± 7	27 ± 3
HMU	13 ± 2	–	12 ± 2	–

Notes: Carbon fibres were from Hercules (now Hexcel): AS4, surface treated to improve adhesion; HMU is a higher Young's modulus fibre without surface treatment. Resin was Shell EPON 815 epoxy resin with 4.8% Pacific Anchor 1171 curing agent cured at 50° for 2 hr and 150° for 2 hr. $\sigma_{mu} = 49 \pm 3$ MPa and $E_m = 3.0 \pm 0.1$.

Reinforced ceramics and brittle metals and polymers can have lower strengths than this simple theory [equation (6.16)] suggests. This is because of the notch effect of the fibres. A threefold stress concentration is present with a cylindrical void. Fibres themselves do not give such big stress concentrations, but local stresses are increased, and the effect is greater at higher fibre volume fractions. Thus a fibre volume fraction effect is expected. This is particularly the case with brittle matrices, since they do not yield to relieve the stresses. Due to the great difference in modulus from the matrix, this effect should be particularly noticeable with reinforced brittle polymers such as polyimides

With reinforced polymers, the through thickness strength is sometimes measured. Originally this was done by making a very thick laminate, bonding solid pieces to each face, and reducing the centre section by grinding it. Then it was pulled apart. Unfortunately, the thick laminates were not always representative of the same laminate in thinner sections.

A better method is the curved beam strength (CBS) test, ASTM 6415. For this an L-shaped piece is moulded and flexed in a special holder; see Fig. 6.18. The specimens can be 2-12mm thick, but the inner radius of the curve is fixed at 6.4mm. A typical force-distance plot for a 2.5mm thick unidirectional carbon-epoxy laminate is also shown in Fig. 6.18. The CBS is defined as the moment required to cause failure of unit width of sample. In practice, the L can bend significantly during the test, and this must be taken into account.

The through thickness strength, σ_{3u} , can be estimated directly from the CBS. The somewhat unwieldy expression in the Standard can be approximated to

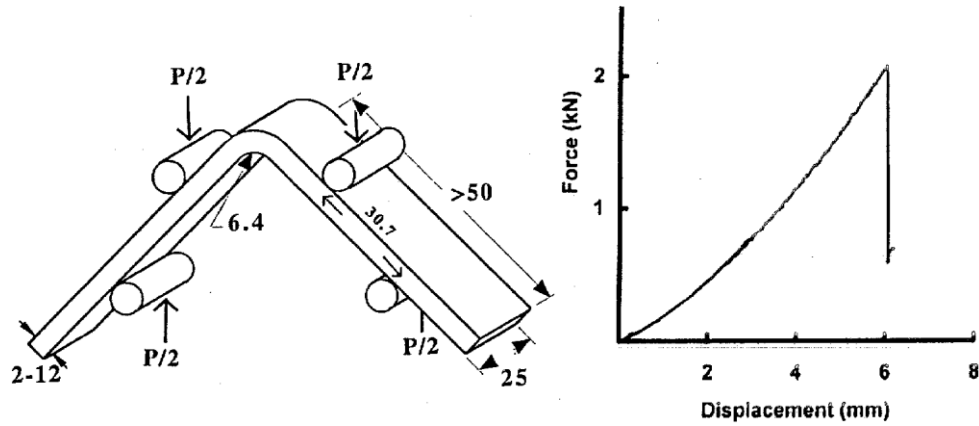


Fig. 6.18 L shaped beam used for CBS test, ASTM D6415. At right is a typical force-displacement plot.

$$\sigma_{3u} = 5.8(t - 1.66)^{1/5} CBS / (6.4 + t)^2 \quad (6.17)$$

Here the thickness t is in mm, and CBS is in N, giving σ_{3u} in MPa. This is accurate to within 6% for the whole range of thicknesses allowed. Moreover, it is good for E_x / E_3 from 4 to 25. (This range covers all laminates from cross-ply glass-polymer to unidirectional carbon-polymer.) See Fig. 6.19; the dashed line is equation (6.17).

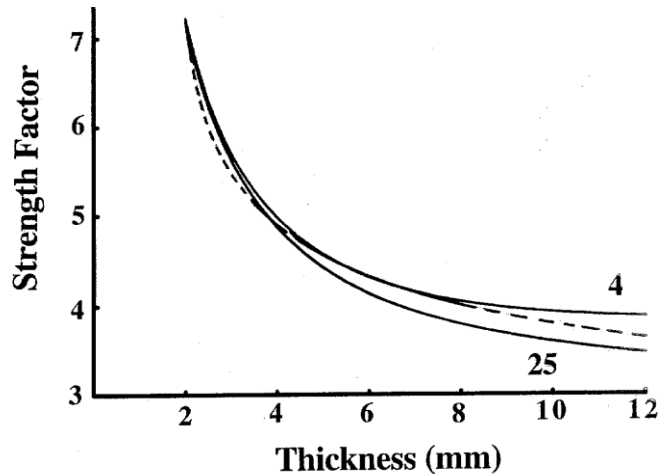


Fig. 6.19 Equation (6.17) compared with exact expressions for $E_x/E_3 = 4$ and 25.

The method is not suitable for angle ply laminates, nor for investigating the effect of hot water, or other agents that soften the polymer. This is because the flexure becomes excessive. Table 6.2 gives some results obtained with the test. It will be noted that the coefficients of variation for σ_{3u} were 10% or more. Thus the approximate formula [equation (6.17)] is quite good enough for these samples.

These results suggest that σ_{2u} and σ_{3u} can be equal in favourable circumstances. However, the curved beam results may not be representative of a flat laminate because

the relatively sharp curvature in the tested area promotes more resin flow there. Acknowledging this, D6415 requires the measurement of V_f in this region.

Table 6.2 Curved Beam Strengths (CBS) and Corresponding Through Thickness (σ_{3u}) and Transverse Strengths (σ_{2u}) for Unidirectional Laminates

Laminates	CBS (kN)	σ_{3u} (MPa)	σ_{2u} (MPa)
Carbon-epoxy	0.63 ± 0.06	50 ± 5	62 ± 4
Carbon-polyimide	0.57 ± 0.11	45 ± 9	46 ± 2

Mesostructures. These are likely to affect the coefficient of variation (CV) for the transverse strength, rather than the strength itself. This is because such mesostructures as fibre waviness and uneven packing are likely to vary from place, and so from specimen to specimen cut from the same moulding. Compression mouldings made from prepregs can have low CV's. For example the CV of the moulding giving the results shown in Fig. 6.14, at 4%, were less than for epoxy itself which can have a CV of 6%. The more tough PEEK had a CV of 1-2%, whilst for carbon-PEEK (APC2) it was 3%. These mouldings do have slight fibre waviness (see Fig. 6.39), but lab-made pultrusions can have much more, and this is accompanied by much higher CV's. Table 6.1 give results having CV's in the range 12-24%.

6.3.2 Young's Moduli

Here we consider two moduli, E_2 and E_3 . We showed in the previous section that there appears to be no good reason to expect σ_{2u} and σ_{3u} to differ very much, and indeed, experiments show that they can be equal. Similarly, we expect $E_2 \cong E_3$. Moreover ultrasonic measurements of E_2 and E_3 on a carbon-epoxy laminate (by the same group referenced under Fig. 4.27) showed that they were the same with a measurement accuracy of $\pm 2\%$.

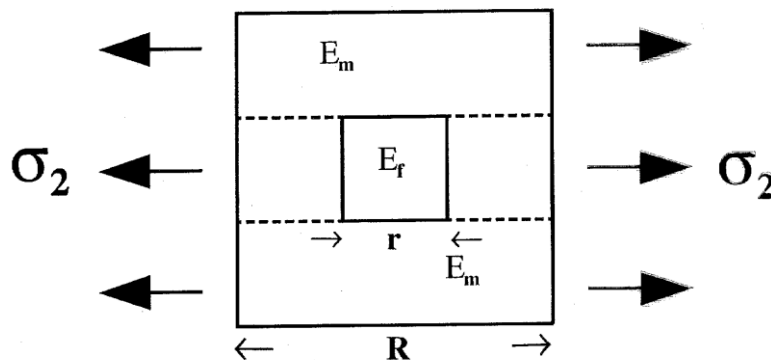


Fig. 6.20 Square fibre model.

Rough estimates for E_2 and E_3 use the inverse Rule of Mixtures (IROM), equation (4.8), with E_f given by the transverse fibre modulus. We can refine the model for E_2 , Fig. 4.3, by considering square packing of square section fibres; see Fig. 6.20.

Here we have a series/parallel arrangement with

$$V_f = 4r^2 / R^2 \quad (6.18)$$

In the series region the modulus, E_s is, from equation (4.8),

$$E_s = \frac{1}{V_{fs} / E_{ft} + (1 - V_{fs}) / E_m} \quad (6.19)$$

where E_{ft} is the transverse fibre modulus, and

$$V_{fs} = 2r / R \quad (6.20)$$

This region is in parallel with the fibre free region having modulus E_m and volume fraction $1 - V_{fs}$. Thus, applying the Rule of Mixtures.

$$E_2 = V_{fs} + (1 - V_{fs}) E_m \quad (6.21)$$

Substituting equations (6.18) to (6.20) into equation (6.21) gives

$$E_2 = E_m \left\{ 1 - \sqrt{V_f} + \frac{\sqrt{V_f}}{1 - \sqrt{V_f} (1 - E_m / E_{ft})} \right\} \quad (6.22)$$

We also note that the model implies a stress concentration in the series region, since both regions are assumed to have the same strain ε_2 . Thus the stress in the series region, σ_{2s} , is given

$$\sigma_{2s} = E_s \varepsilon_2 = E_s \sigma_{2u} / E_2 \quad (6.23)$$

which using equations (6.19) and (6.22) gives

$$\sigma_{2s} = \sigma_2 \left\{ 1 - \left(\sqrt{V_f} - V_f \right) \left(1 - E_m / E_{ft} \right) \right\} \quad (6.24)$$

For $E_{ft} \gg E_m$ this gives a maximum overstress of about 33%. Although modest, it supports the notion that the interface has to be stronger than the matrix to leave polymer adhering to the fibres as shown in Fig. 6.15.

Table 6.3 gives some modulus results for pultrusions made with various fibres in the same polymer and compares them with the simple models. Here IROM does not take into account any difference between the fibre transverse and longitudinal moduli, while TIROM does.

Table 6.3 Transverse Young's Moduli (GPa) for Glass, Carbon and Kevlar Pultrusions Compared with Results from Simple Models

		$V_f = 0.2$	$V_f = 0.4$	$V_f = 0.6$	
Glass	Experiment	6.0 ± 0.2	7.0 ± 0.2	9.6 ± 1.1	
	IROM ¹	3.7	4.9	7.1	
	Square ²	4.0	5.9	9.7	
Carbon	Experiment	4.4 ± 0.2	5.6 ± 0.3	7.8 ± 0.2	
	IROM ¹	3.7	5.0	7.4	
	TIROM ²	3.3	3.8	4.3	$E_{ft} = 6.0$
	Square ³	3.4	3.9	4.5	$E_{ft} = 6.0$
Kevlar	Experiment	4.2 ± 0.2	4.1 ± 0.2	4.0 ± 0.2^4	
	IROM ¹	3.7	4.9	5.9^4	
	TIROM ²	2.9	2.8	2.7^4	$E_{ft} = 2.5$
	Square ³	2.9	2.8	2.7^4	$E_{ft} = 2.5$

Notes:

1) Equation (4.5), 2) Equation (4.8) with E_{ft} replacing E_f , 3) Equation (6.21), 4) these results were for $V_f = 0.5$. Matrix was Shell EPON 815 epoxy resin cured with 4.8% Pacific Anchor 1171 at 50°C for 1 h and 150°C for 2 h. $\sigma_{mu} = 49 \pm 3$ MPa and $E_m = 3.0 \pm 0.1$ GPa .

For glass, the square model fits the results better than IROM, but still gives unduly low results at low V_f . For carbon TIROM and the square model, using $E_{ft} = 6.0$ GPa, differ very little, and give low results. In this case IROM appears to be best. With Kevlar, having $E_{ft} = 2.5$ GPa, i.e. less than E_m , the IROM result is not useful, while the other two models give about the same low results.

Results with carbon fibre prepreps appear to fit the IROM predictions moderately well, (i.e. ignoring the reduced transverse fibre modulus). For example the laminates having the fracture surfaces shown in Fig. 6.15 had $V_f = 0.60$ and $E_2 = 7.5 \pm 0.4$ GPa and the carbon-PEEK (APC2) had $V_f = 0.61$ and $E_2 = 9.7 \pm 0.4$ GPa with $E_m = 3.9$ GPa. In view of their closeness to IROM, more sophisticated models for transverse modulus do not seem to be worthwhile.

The results for all the fibres suggest that their presence might increase E_m , perhaps by inducing some crystalline order.

With reinforced metals and ceramics the theoretical results are not so dependent on the model used, since E_m is closer to E_f and fibre volume fractions and are usually lower. In Chapter 11 we will find that, for boron-aluminium, the IROM modulus is

exceeded by about 20% (Fig. 11.8) while SiC-Al only achieves about 90% of the IROM value. With reinforced ceramics, transverse tests are normally precluded by their extreme weakness in this direction; see Fig. 11.22

The Halpin-Tsai criterion may be used for fitting known results, since it involves an adjustable parameter.

It should finally be noted that transverse breaking strains, ε_{2u} , are often low: they are little more than σ_2 / E_2 unless the polymer is very tough. Even with carbon-PEEK (APC2) ε_{2u} is only about 1.3%. (σ_{2u} / E_2 gives 0.95%). Since carbon fibre breaking strains are typically 2% this means that any laminate having 90° plies is susceptible to transverse cracking (see Table 4.2).

6.4 Shear Strengths

In an aligned fibre composite we cannot assume that the subscripts used for shear strain are reversible: e.g. γ_{12} is not necessarily the same as γ_{21} . Using the same definition as in Fig. 1.10 for stresses, i.e. that the first subscript denotes the plane and the second the direction, we have six possible shearing strains; all apparently different; see Fig. 6.21.

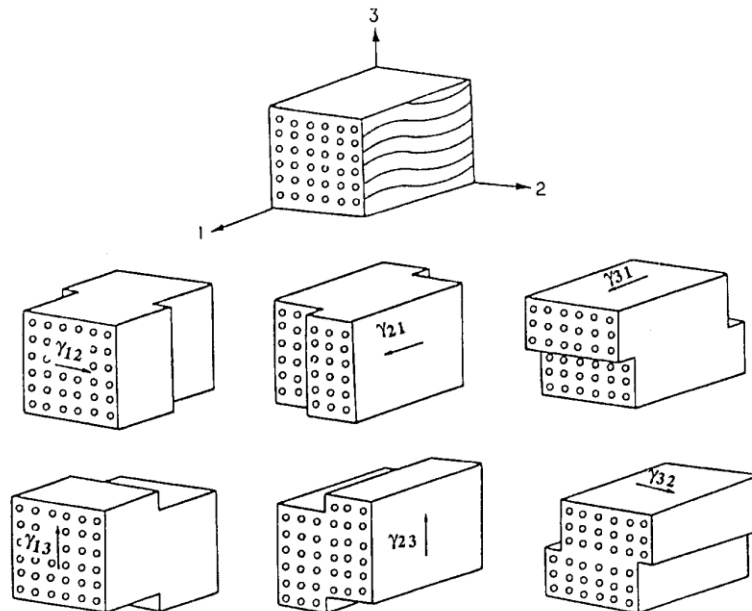


Fig. 6.21 Shear failure modes for unidirectional composites.

Two shear strains, i.e. γ_{12} and γ_{13} , involve shearing of the fibres. Since τ_{12} can also activate γ_{21} and τ_{13} can activate γ_{31} , and since the fibres are very shear resistant we do not observe much γ_{12} or γ_{13} with polymer and soft metal matrices. Instead γ_{21} and γ_{31} are activated. With τ_{23} , however, two strains are possible. With wavy fibres as shown, γ_{23} would probably be preferred over γ_{32} , unless the fibre waves were synchronized. (In

addition, there is the possibility here of mixed γ_{23} and γ_{32} , deformation.) These composites therefore have four possible yielding directions in shear: γ_{12} , γ_{13} , γ_{23} and γ_{32} .

With cross ply and angle ply fibre laminates and woven fibre composites, γ_{21} and γ_{23} , are strongly inhibited, since they involve shearing the fibres, and we are left with two shear deformations only, γ_{31} and γ_{32} , which are in-plane shears. With transversely isotropic composites, such as some pultrusions, generating γ_{21} and γ_{31} would be equally easy or difficult, since they are parallel to the fibres. On the same basis γ_{23} and γ_{32} would require the same shear stress, since they go across the fibres.

Although shear strains can be generated, true shear failure does not occur. Fig. 6.22 shows a typical shear fracture surface obtained with a carbon-epoxy pultrusion tested in the Iosipescu test. Notable is the fine leaf-like structure in the polymer, called shear hackle. The development of this is explained by the joining up of cavities produced by the tensile component of the shear stress, as shown in Fig. 6.23. This process requires some opening up of the failure crack, so the process is not pure shear. We therefore have shear induced failure, but no true shear strength for a composite, as for the polymers themselves. (See section 6.1.2).

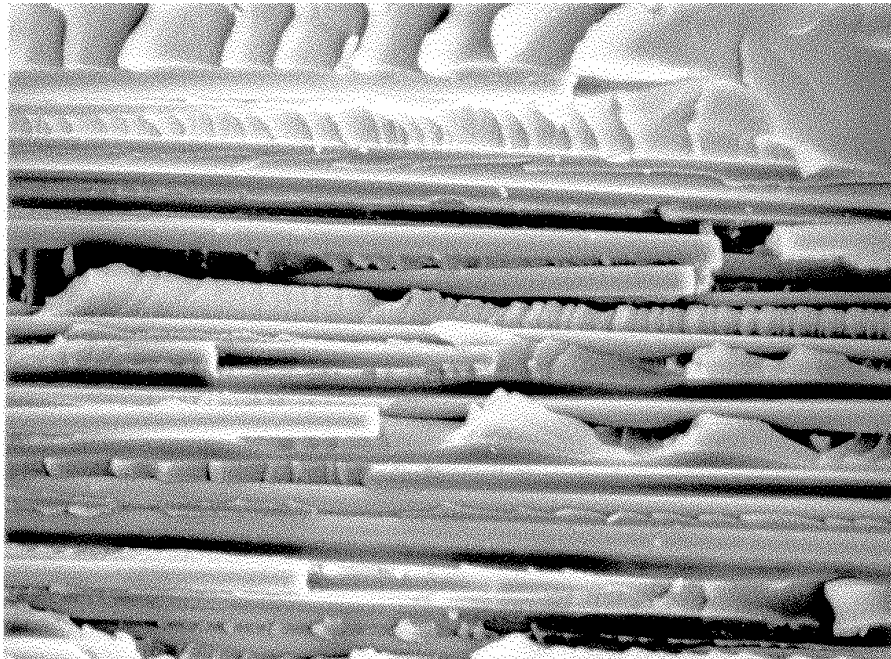


Fig. 6.22 Shear fracture of a carbon-epoxy pultrusion showing five broken fibres. Shear hackle is prominent in the matrix rich region at the top of the picture.

Shear induced failure can occur at higher stresses than σ_{2u} . The reason for this is that the fibres inhibit the failure process, instead of making it more easy, as is the case in the transverse tensile test. This can readily be seen in the case of the short beam test. This test is widely used, but mistrusted by composites researchers. In this test, a short specimen is subject to three point bending: see Fig. 6.24. The distance between the supports should be four times the specimen thickness (or five times for glass-epoxies;

ASTM D2344). It can be shown, using equations (1.6) and (1.8), that the maximum tensile and compressive stresses, σ_x and $-\sigma_x$ are no greater than 8 times the maximum in-plane shear stress, τ_{xy} (10 times for glass). Thus, if shear-induced failure takes place at about σ_{mu} , i.e. $\sim 60\text{MPa}$, neither axial compressive failure nor tensile failure is initiated in a good composite.

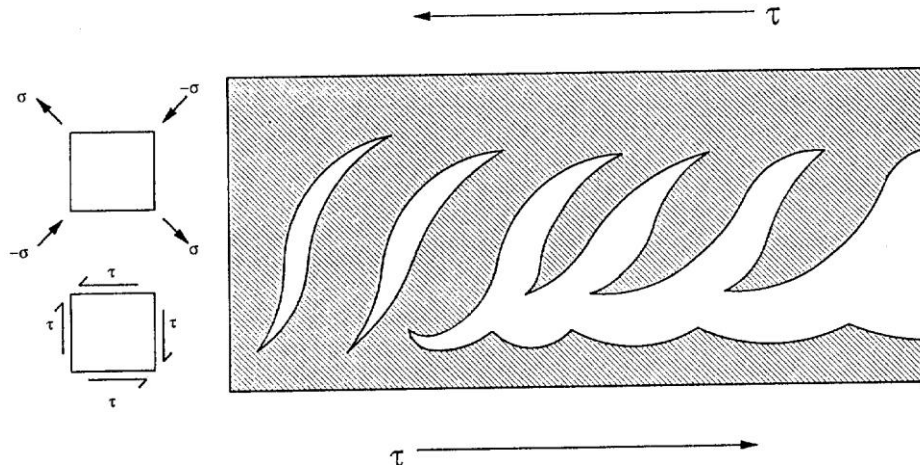


Fig. 6.23 Origin of shear hackle in a fibre composite. Cracks form normal to the tensile component of the stress, open up, and join up to complete the fracture. (After Faliba, S.S. and Snider, J.A., *Int. Encyclopedia of Composites*, (Ed. S.M. Lee, VCH Publishers, New York, 1990, 2, 268-89.)

The short beam method is only one of many methods used to test the apparent shear strength of composites. Each method gives a different result, since each method is really measuring the resistance to some sort of tensile failure, with more or less hindrance caused by the presence of the fibres. This is a form of "steric hindrance".

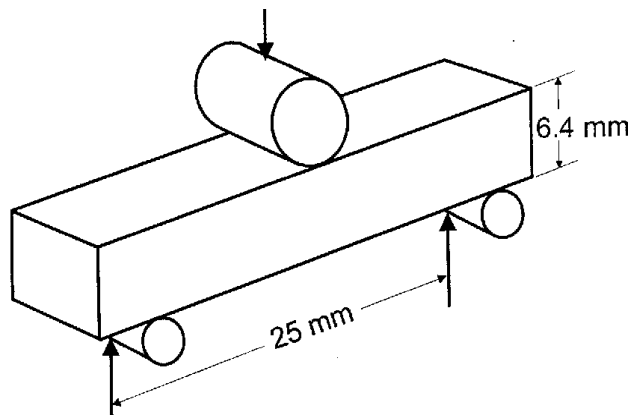


Fig. 6.24 Short beam test (ASTM D2344).

Shear induced failure is very strongly influenced by the matrix, as shown in Fig. 6.25. Carbon-epoxy pultrusions were tested using the Iosipescu test (or V notched beam test ASTM D5379; see Fig. 6.2). The line labelled 0° had the fibres aligned along the long sides of the sample and 90° refers to the case where the fibres were parallel to the shorter side. Some of the difference between the apparent matrix shear strength and that of the

composite may be due to fibres crossing the fracture plane. These fibres may be broken in the test, and examples of such broken fibres are evident in Fig. 6.22.

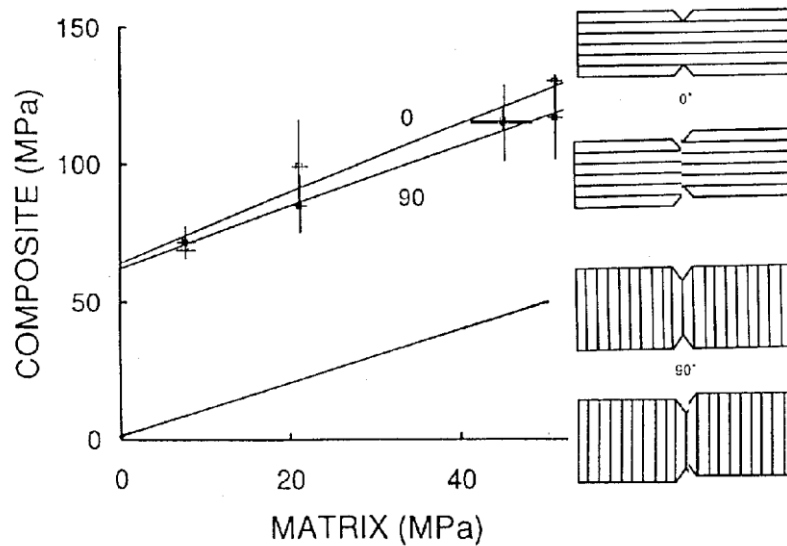


Fig. 6.25 Composite Iosipescu apparent shear failure stress vs. polymer matrix punch apparent shear failure stress for carbon-epoxy tested at 120, 100, 60 and 20°C. (After Liu, K., and Piggott, M.R., 1993, Proc. CANCOM, 23-32.)

We conclude that shear induced failure is matrix dominated, with some possible contribution from fibre failures, when these cross the crack plane. There is, however, no such thing as a composite shear strength. The failure stress depends very strongly on the influence of the fibres, and the geometric details of the test in relation to the fibre geometry.

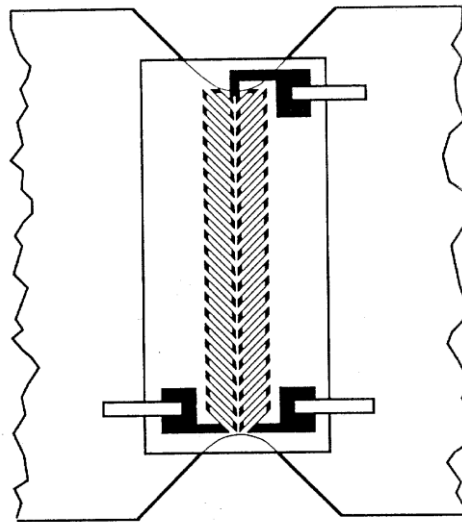


Fig. 6.26 A shear gauge mounted on a V notched beam. (After Ifju, P.G., 1994, Expt. Mech. 34, 369-78.)

Shear moduli for unidirectional mouldings (G_{12}) made from carbon and glass fibre preregs are generally in the range 4.7 to 6.4GPa. The V notched beam test is most convenient for measuring shear moduli. Since the shear is not quite uniform across the notch, a special strain gauge is used. Fig. 6.26 shows it in place on a V notched beam.

6.5 Compressive Strengths

There are three principal compressive strengths in a fibre composite; σ_{1cu} , σ_{2cu} and σ_{3cu} . Both σ_{2cu} and σ_{3cu} are considered to be shear type failures, which occur at about 45° to the stress axis, in a fibre avoidance mode. Values for these strengths are somewhat higher than the matrix compressive strength, being typically 200-300MPa for unidirectional carbon-epoxy laminates. These high values reflect the difficulty of inducing a tensile failure in a compressive test.

There is still much to be learned about σ_{1cu} . It is classified herein as matrix dominated, and widely considered so to be. However, there are cases where, in fact, the compressive strength of the fibres themselves directly determine this compressive strength of the composite.

One reason for our lack of understanding is the difficulty of measuring the compressive strength, especially along the fibre axis of unidirectional fibre composites. In this section, methods used for this will be discussed first. Then will follow a description of the compressive properties of fibres and unidirectional composites. Finally the ideas used to explain the compressive strength will be critically reviewed.

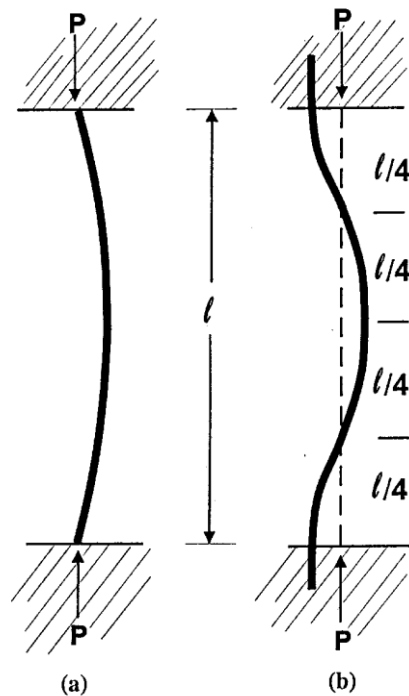


Fig. 6.27 Column buckling: (a) unsupported; (b) ends supported.

6.5.1 Testing Methods

The main problem with compression testing is the tendency of the specimen to buckle elastically, i.e. before it has reached a stress high enough to cause any damage. This is an unstable state, and if the test is continued the buckling worsens, and the specimen suffers flexural failure.

It is called *Euler* buckling after the person who first solved this elasticity problem. For a beam with ends that are free to rotate, see Fig. 6.27a, with thickness d , width b and length l , buckling occurs when the stress reaches σ_b given by

$$\sigma_b = \frac{\pi^2 E}{12} \cdot \left(\frac{d}{l}\right)^2 \quad (6.25)$$

When composites are compression tested, they are normally tightly held at the ends, so not free to rotate; see Fig. 6.27b. This increases the stress fourfold.

In these expressions, the material is isotropic, with E = Young's modulus. For orthotropic composites, Bogetti et al (see reading list at the end of this chapter) suggested that a correction factor be used. Thus

$$\sigma_b (\text{composite}) \cong \sigma_b (\text{isotropic}) / \left[\frac{\pi^2 E}{12} \cdot \left(\frac{d}{l}\right)^2 \right] \quad (6.26)$$

Since G_{xz} can be very much less than E_x the correction factor is significant, even for the relatively low l/d values normally used for compression tests with unidirectional composites. For example, in the Celanese test described later, it is 3.2.

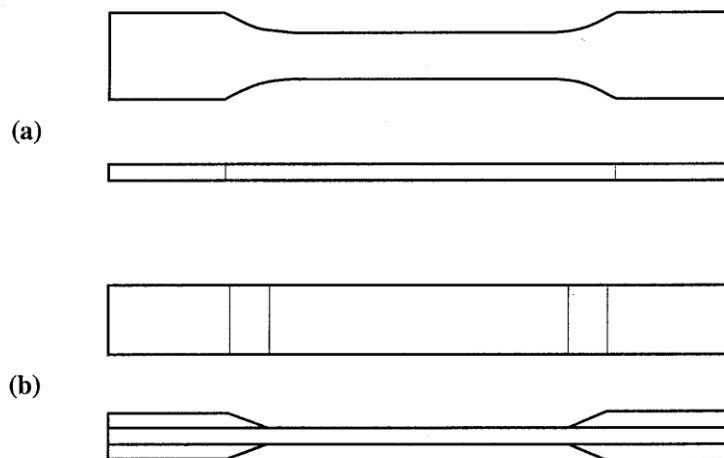


Fig. 6.28 Specimens used for tensile and compression testing: (a) typical "dogbone" shape used for isotropic metals and polymers, and (b) thickened sample needed for composites.

In addition to their low shear stiffnesses, composites easily delaminate and spring apart. In a compression test they will do this at a relatively low stress, unless the ends are rigidly clamped. Another problem with composites, and especially unidirectional ones, is that the "dogbone" shape used for metals does not work. The shape, shown in Fig. 6.28a distributes the gripping forces, but allows the centre section to slide out. Instead, samples must be thickened in the grip region; see Fig. 6.28b. This is normally accomplished by gluing end tabs on the specimen, and such tabbed specimens are used for tensile testing as well. (ASTM D3039: this test is only suitable for laminates with a small proportion of oblique plies, see section 4.4.3.) The tabs are usually aluminium but woven fibre composites are also often used.

One of the simplest tests is the ASTM D695 method; Fig. 6.29a. In its original form this was used without end tabs, and was intended for rigid polymers. It is now widely used for composites by the aerospace industry, but with tabbed specimens. This prevents "brooming" or splitting at the unsupported ends. The specimen is prevented from buckling by being lightly clamped between thick steel plates. Loading is through the ends, which extend about 3 mm beyond the plates.

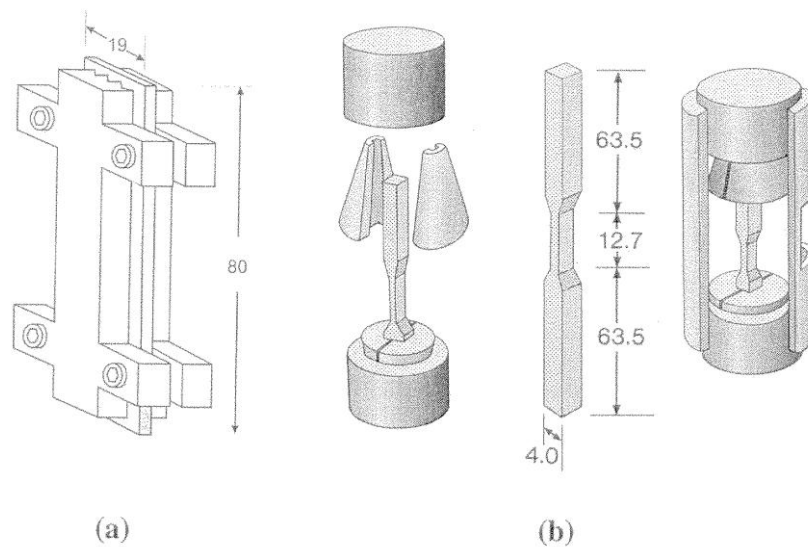


Fig. 6.29 (a) ASTM D695 compression test and (b) Celanese compression test. Dimensions are mm.

The Celanese method, Fig. 6.29b, and the IITRI method, 6.30a, are both endorsed by the ASTM (D3410). In both cases the specimen is tabbed, and loading is by shear through the wedging action of the grips. The IITRI method permits the use of the wider specimens (up to 38mm) compared with 6.35mm for the Celanese.

The Celanese method has been criticized for having excessive stress concentrations at the grips. However, as Fig. 6.31 shows, it produces results for a unidirectional carbon-epoxy which are indistinguishable from those obtained using the IITRI fixture. Fig. 6.31 also shows that the tabbed D695 method produces higher results

for this material. Nevertheless, a new end loading fixture developed at Imperial College, see Fig. 6.30b, produces still higher results, especially if the end tabs are only partly bonded: see Fig. 6.31.

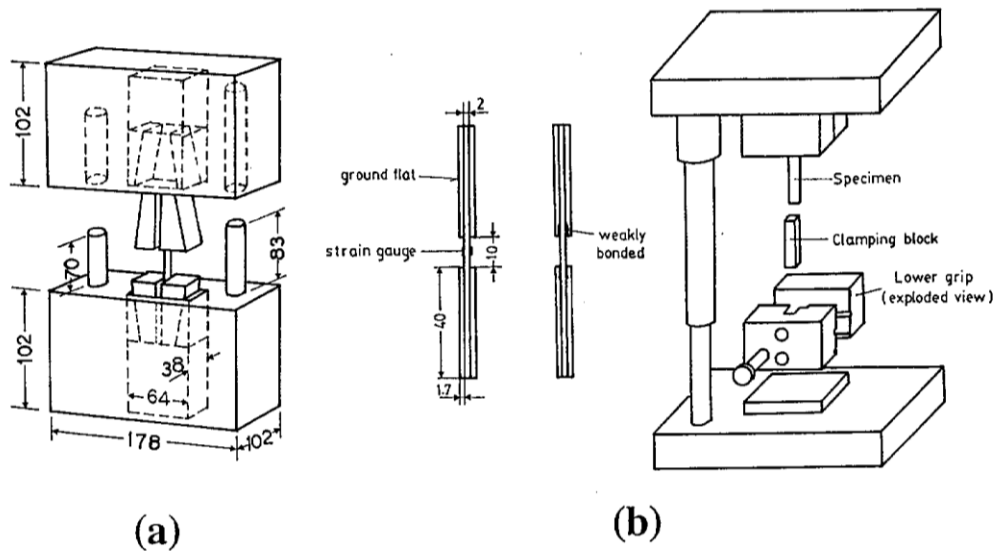


Fig. 6.30 (a) IITRI compression test, (b) Imperial College Compression test. Dimensions are mm.

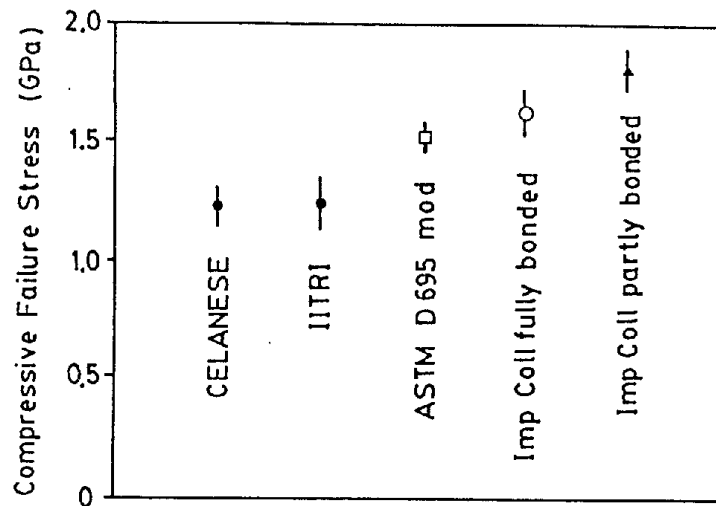


Fig. 6.31 Results for the compressive strength of unidirectional XAS carbon-914C epoxy using different methods. ASTM D695 samples had end tabs. (After Haerberle, J.G., and Mathews, F.L., 1989, Proc. ECCM 4, 517-23.)

Still higher results can be obtained with sandwich beams in four point bending. The ASTM beam, see Fig. 6.32, uses a honeycomb filling and is rather large, cumbersome and expensive to make and test. Smaller beams; see e.g. Fig. 6.33, have been used with good results. AS4-PEEK withstood 1.8GPa without breaking in this test (the acrylic core failed prematurely instead). Meanwhile direct compression of a small carbon-epoxy beam with an epoxy core gave a strength of 2.02GPa.

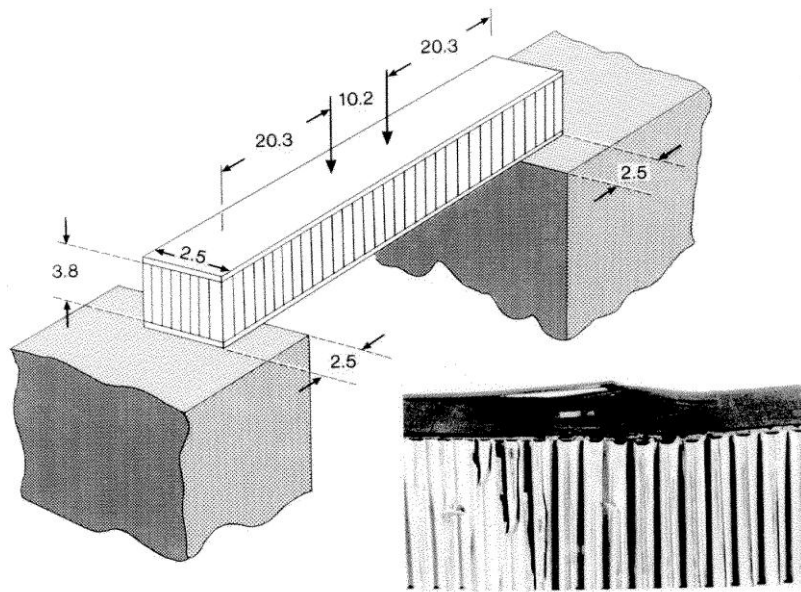


Fig. 6.32 ASTM D3410 Sandwich beam specimen with failed specimen at bottom right. Dimensions are cm.

The results of conventional compression tests on unidirectional composites tend to be rather scattered, with coefficients of variation of 10-20%; see Fig.6.31. This can be reduced by testing cross ply specimens. When the contribution of the cross plies is discounted the strength of the axial plies appears to be greater than for the unidirectional case in the same test. However, there is some uncertainty in using this approach. The compact sandwich beam test, on the other hand, had small scatter, i.e. about $\pm 3\%$.

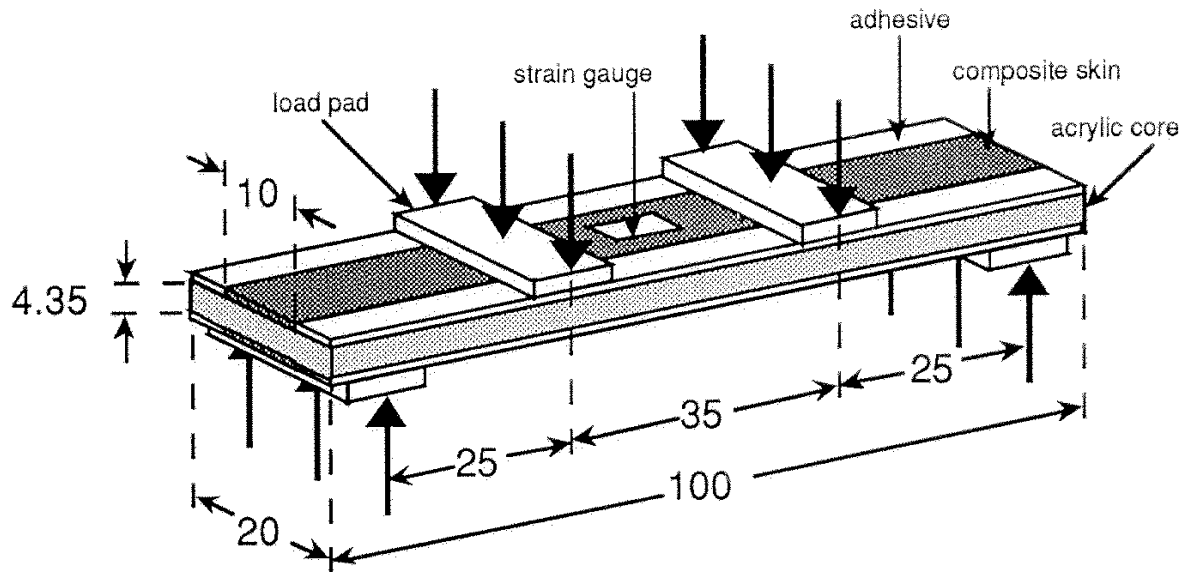


Fig. 6.33 Compact sandwich beam test. (After Mrse, A. and Piggott, M.R., 1993, J. Comp. Sci. Tech. 46, 213-17.)

ASTM is currently developing a new standard test method using a combined loading compression (CLC) test fixture for untabbed specimens. These should not contain more than 50% of 0° plies.

6.5.2 Testing Single Fibres and Fibre Bundles

There is some evidence that fibres are more resistant to compression when tested singly than when part of a composite laminate. However, there is also evidence that the modulus of some fibres could be less in compression than in tension. It is generally accepted that, for polymer fibres such as Kevlar (polyaramid) and Spectra (polyethylene), the modulus in compression may be less than half the tensile modulus.

Glass appears to be unaffected, since when unidirectional laminates were tested, the modulus was independent of strain, whether tensile or compressive: see Fig. 6.34. Carbon, also shown in Fig. 6.34, had a continuously decreasing modulus with decreasing strain, being reduced at -1% strain to about 60% of its value at $+1\%$ strain. The decrease in modulus for carbon is unlikely to be entirely due to fibre waviness in the composite, since the fibres in the glass reinforced composite are also likely to be wavy. Thus, in discussing single fibre results, we must take the reduced modulus into account.

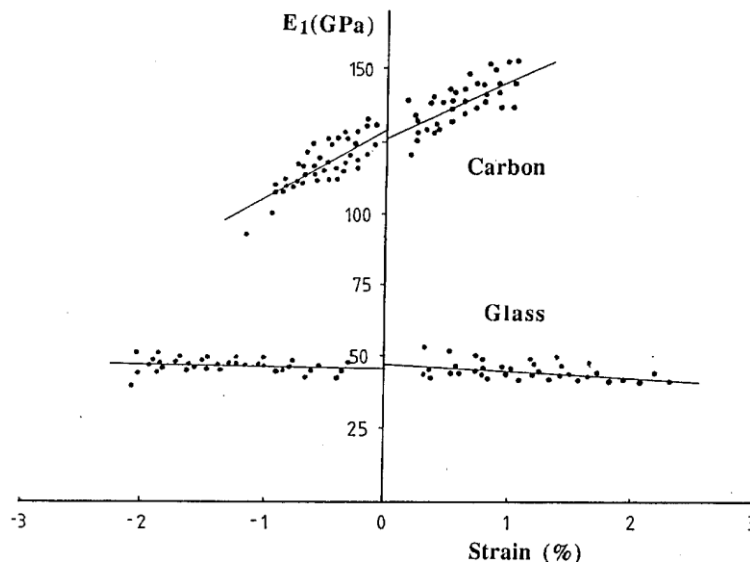


Fig. 6.34 Modulus vs strains for glass and carbon fibres. (Data obtained from tests on composites. (After Harper, J.F., and Heumann, T.O., *Composites Evaluation*, Ed. J. Herriot, Butterworths, Oxford, 1987, 189-193.)

Neither a single fibre nor a fibre bundle can be tested in compression without some support. This can take the form of a relatively massive block of matrix. Since most of the load is taken by the polymer block, the result of the test is an estimate of the fibre breaking strain. Stresses are not obtained, and cannot be derived unless the modulus is known with certainty. Thus the single fibre results will be presented as breaking strains rather than stresses. Fig. 6.35 shows some results obtained using electrical resistance

measurements on single carbon fibres by De Teresa (the triangles) and microscopic observation of fibre bundles by Hahn and Sohi. The fibre bundles were in epoxies with different tensile failure strains: EPON 828, with $\epsilon_{mu} = 9\%$ (the squares) and EPON 815 with $\epsilon_{mu} = 14\%$. The results are plotted as compressive failure strains vs. tensile breaking strains.

Hahn and Sohi's glass fibres, with a tensile breaking strain of about 4.8%, were strongly affected by the yielding of the polymer when the bundle reinforced specimens were compressed. With the carbons, differences can, however, still be seen even before the polymer yielded. De Teresa's results are remarkable for the high compressive strains that his fibres could withstand. Grafil 33-500 gave 3.8%, and AS4 3.6%. The result for AS4 is nearly twice that achieved with AS4 reinforced PEEK where the strongest specimen that failed in the compact flexure test had a failure strain of 1.73%.

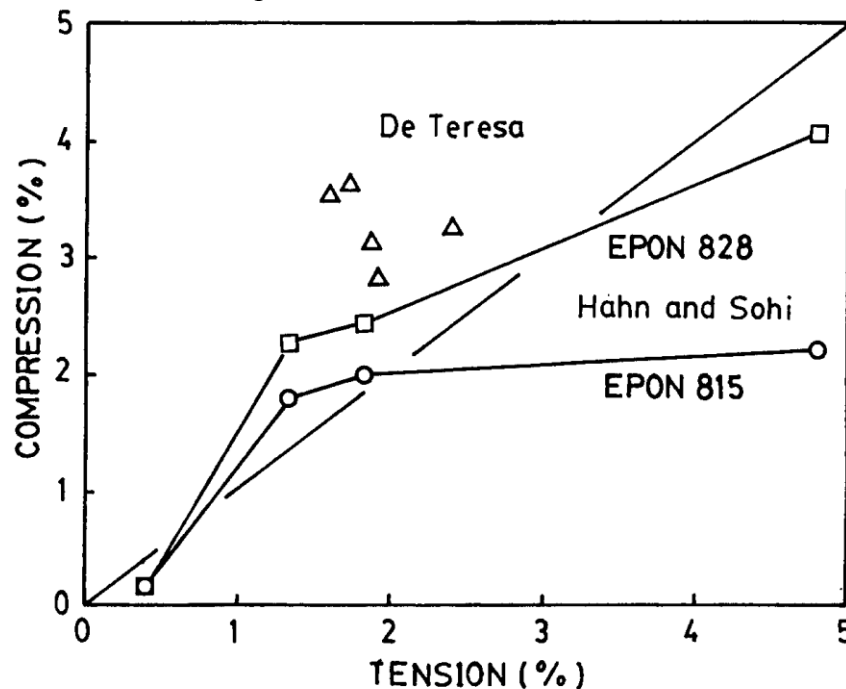


Fig. 6.35 Compressive vs tensile failure strains for fibre bundles in epoxy (After Hahn, H.T., and Sohi, M.M., 1986, *Comp. Sci. Tech.* 27, 25-41 and De Teresa, S.J. *Proc. 14th Mech. of Composites Rev.*, Dayton OH, 1989, 45-52.)

We now turn to the ideas advanced to explain compressive strengths.

6.5.3 Failure Processes in Perfect Unidirectional Composites

The simplest failure process is found with the polymer fibres. These are relatively weak in compression and appear to obey a rule of mixtures expression

$$\sigma_{1cu} = V_f \sigma_{fcu} + V_m \sigma_{mu} \quad (6.27)$$

Here σ_{fcu} is the compressive strength of the fibres. Experiments have been carried out with steel wire reinforcement where the yield strength of the steel could be varied by heat

treatment. The linear relationship indicated by equation (6.27) was obeyed quite well when σ_{1cu} was plotted vs. the flexural strength of the steel: see Fig. 6.36.

With stronger fibres elastic buckling is a possible failure mechanism. This is difficult to treat for small circular fibres, but Rosen examined flat lamellar reinforcements on an elastic and a yielding foundation. The elastic foundation gave the result

$$\sigma_{1cu} \cong G_m/V_m \tag{6.38}$$

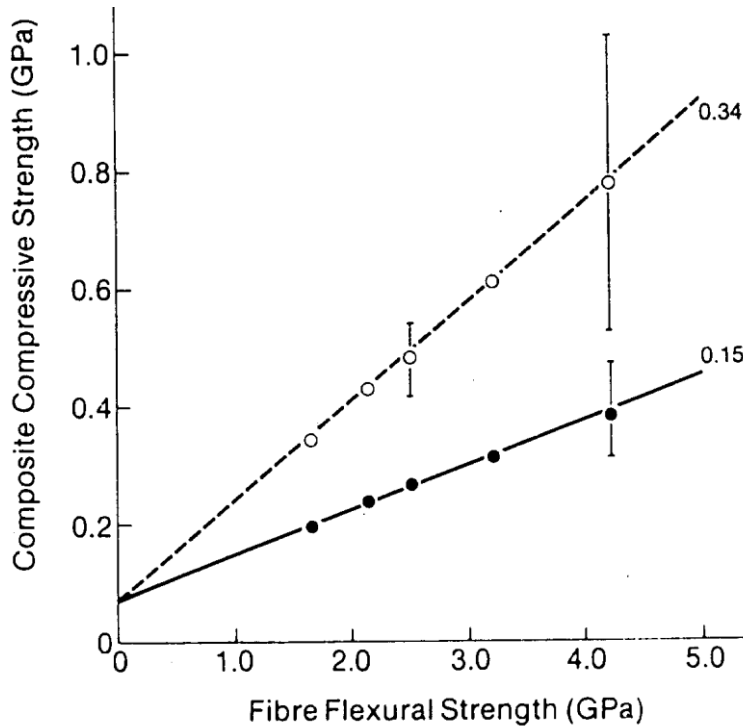


Fig. 6.36 The compressive strength of epoxy reinforced with steel vs flexural strength of the steel at $V_f=0.34$ and 0.15 . (After Piggott, M.R., and Wilde, P., 1980, J. Mat. Sci. 15, 2811-15.)

and the yielding foundation gave

$$\sigma_{1cu} = \sqrt{V_f E_f \sigma_{my} / 3V_m} \tag{6.29}$$

This was for in-phase buckling. Out of phase buckling was also considered but gave extremely high results except for $V_f < 0.2$.

While there seemed to be some possibility of agreement with some results with glass-epoxies, using a judicious combination of equations (6.28) and (6.29) the predictions appear to be too high for carbon, especially at low V_f . Fig. 6.37 compares equation (6.28) with some results due to Hancox. (For carbon, equation (6.29) predicts higher values than equation (6.28) for $V_f > 0.2$) Both equations are concave upwards when plotted vs. V_f whereas experimental results are either linear or concave down as shown in Fig. 6.37. The same concave down V_f variation has been obtained with glass.

Moreover, equation (6.29) predicts higher values for high modulus carbon, whereas the experimental results are lower in this case.

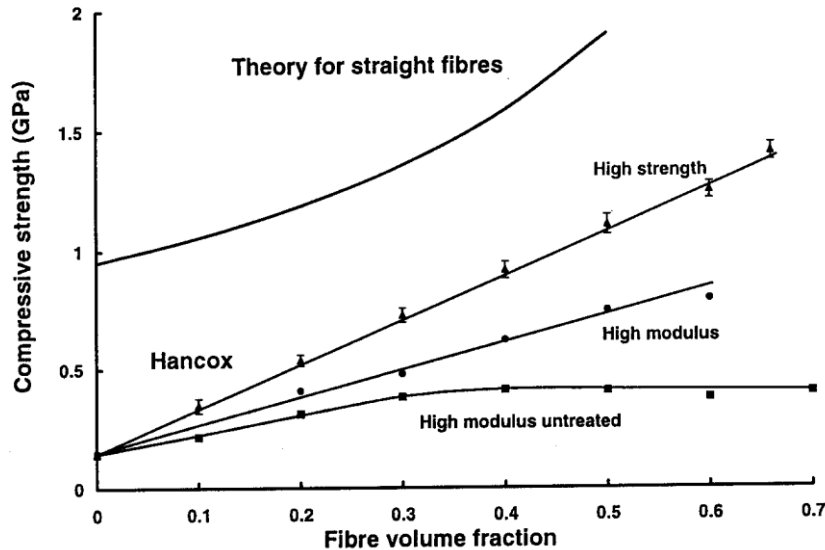


Fig. 6.37 Equation (6.28) compared with experimental results for carbon epoxies (After Rosen, B.W., 1964, *Fibre Composite Materials*, ASM, OH, p. 58., and Hancox, N.L., 1975, *J. Mater. Sci.* 10, 234-42.)

Considering the above shortcomings, the predictive value of any buckling theory of initially flat plates, or straight fibres for that matter, appears to be open to serious doubt. For fibres which are strong in compression it seems to be much more profitable to take the actual structural details, i.e. the mesostructures into account.

6.5.4 Failure Processes in Imperfect Unidirectional Composites

The most elementary treatment assumes that the fibres have some average deviation ϕ . This deviation was modelled by Argon as a kink generated by two dislocations. An energy analysis gave the result

$$\sigma_{1cu} = \tau_u / \phi \quad (6.30)$$

In a composite it is not clear whether τ_u should be the composite shear strength or that of the matrix. Argon used them interchangeably in the text, but cited evidence which originally came from Fried's work, to the effect that the compressive strength of a composite was proportional to the composite shear strength.

Fried's results relate to composites with large void contents. As can be seen from Fig. 6.38, he found that his short beam flexure results, τ_{sbs} , and the compressive strength, σ_{cu} , of filament wound plates, both decreased roughly linearly with void content. The two correlations, when combined, gave

$$\sigma_{cu} = 13.2 \tau_{sbs} + C \quad (6.31)$$

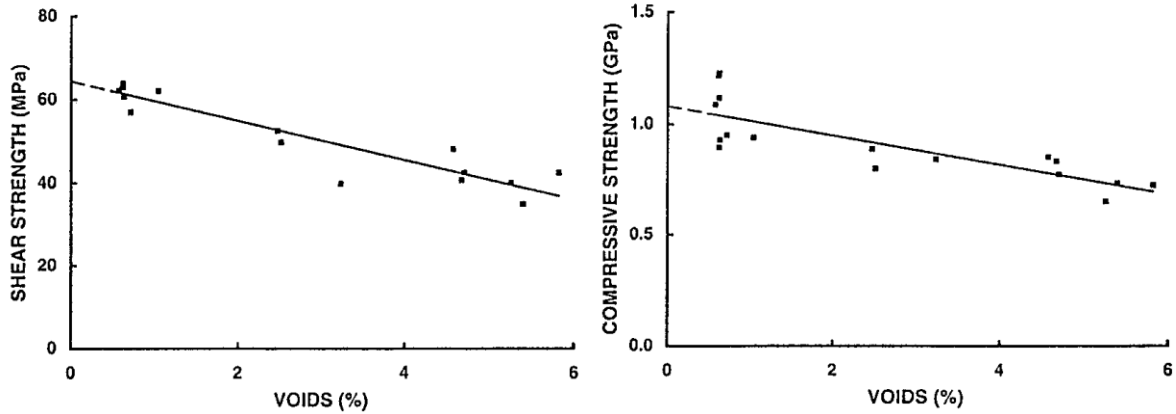


Fig. 6.38 Apparent shear strength in short beam test, τ_{sbs} vs. void content and compressive strength vs. void constant (After Fried N., 1965, Proc. 20th, Ann. Conf. SPI Reinforced Plastics Div., Section 1c.)

We use σ_{cu} rather than σ_{1cu} because the plates had two thirds of the fibres aligned parallel to the stress axis and one third perpendicular to it (i.e. they were not unidirectional). C is a constant equal to about 220MPa. Thus, Argon's assumption is not justified by the evidence*. Furthermore, the void contents were high (see Fig. 6.38) so the composites were weak, and it is not surprising that this weakness affected both τ_{sbs} and σ_{cu} . Fried's work in no way provides evidence supporting equation (6.30).

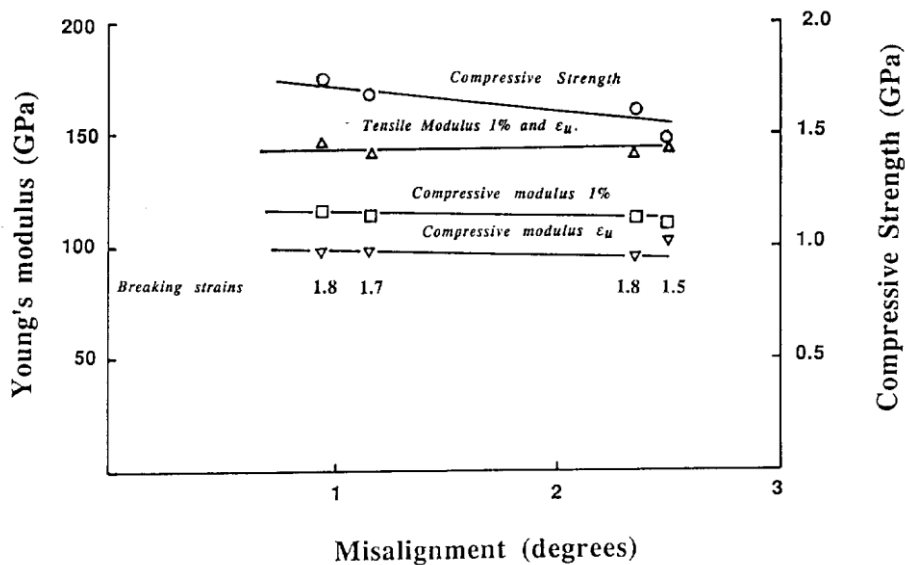


Fig. 6.39 Compressive strength, breaking strains and tensile and compressive modulus vs fibre misalignment (After Mrse, A. and Piggott, M.R., 1993, J. Comp. Sci. Tech, 46, 219-27.)

* The evidence came by way of an article by Broutman - see Further Reading at the end of this Chapter. Moral: always go to the original work.

Recently Argon's idea has been revived, but making the assumption that τ_u is the matrix yield strength. Since equation (6.30) does not involve V_f , the experimental results shown in Fig. 6.37, and much subsequent experimental work, does not seem to have been taken into account.

There does, nevertheless, appear to be a fibre misalignment effect: see Fig. 6.39. It can be more convincingly accounted for by including additional aspects of the structure apart from the mean angle of deviation. As a first step, we let the fibre divagations be represented as sine waves, or combinations thereof. The simple sine wave, Fig. 6.40, is fully described by two parameters, i.e. amplitude and wavelength. The curve can be conveniently expressed using the dimensionless parameters, x , y , a and λ :

$$y = a \sin(2\pi x/\lambda) \tag{6.32}$$

where xd and yd are distances, as indicated in Fig. 6.40, d being the fibre diameter (or fibre bundle diameter, if many fibres act in concert). ad and λd are the amplitude and wavelength of the sine wave.

The fibre radius of curvature has a minimum value R_f , given by $-d/(d^2y/dx^2)$:

$$R_f = d\lambda^2/4\pi^2 a \tag{6.33}$$

at $x = \frac{1}{4}\lambda, \frac{3}{4}\lambda$, etc., and the fibre here presses strongly against the matrix, with pressure P , Fig. 6.40.

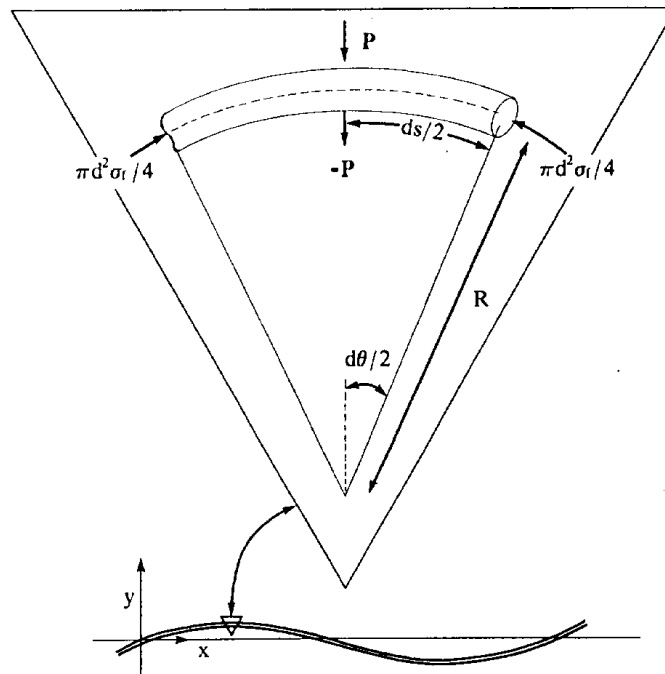


Fig. 6.40 Curved fibre, with stresses acting on the fibre antinode.

When P reaches the matrix yield stress, σ_{my} the matrix will be pushed aside by the fibre, and the radius R_f , will decrease, causing the pressure to increase, further reducing R_f and increasing P , since

$$P = \pi d \sigma_{fc} / 8 R_f \quad (6.34)$$

Here σ_{fc} is the compressive stress in the fibre. So we estimate the maximum fibre stress σ_{fcmax} for this unstable state by replacing P by σ_{my} and re-arranging the equation:

$$\sigma_{fcmax} = 8 R_f \sigma_{fc} / \pi d \quad (6.35)$$

A local matrix yielding at the antinodes triggers composite failure and as the bulk of the polymer is still elastic we expect the matrix stress to be $\sigma_{fcmax} E_m/E_f$. So the failure stress is

$$\sigma_{1cu} (yielding) = \{8 R_f \sigma_{my} / \pi d\} \{V_f + V_m E_m/E_f\} \quad (6.36)$$

An alternative failure mechanism is splitting, with the matrix failing at a tensile stress σ_{mtu} . In this case we have P operating over the fibre diameter. This is resisted by the adhesive strength at the fibre surface, σ_a , and by σ_{mtu} over the webs of polymer between the fibres: see Fig. 6.41.

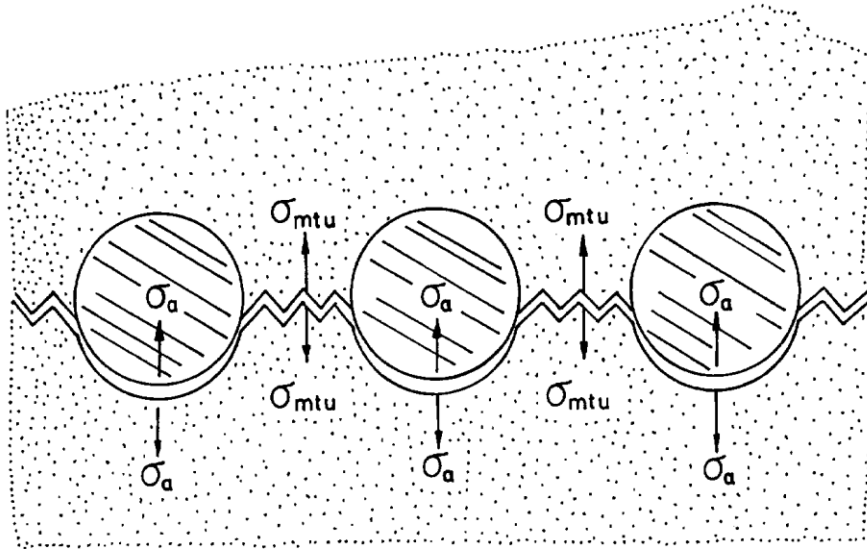


Fig. 6.41 Interface and matrix failure due to transverse forces exerted by fibre flexure.

Instead of equation (6.15) we have

$$2rP = \sigma_a \pi r + \sigma_{mtu} (R - 2r) \quad (6.37)$$

and proceeding as before this gives

$$\sigma_{1cu} (splitting) = (4R_f / \pi d) (\pi \sigma_a + \{ \sqrt{P_f / V_f} - 2 \} \sigma_{mtu}) \{ V_f + V_m E_m/E_f \} \quad (6.38)$$

with R_f given by equation (6.33) for both equations (6.36) and (6.38).

Fig. 6.42 illustrates two composites which give results that fit equation (6.36), up to a limiting or critical stress, where a change in failure mode occurs. In the case of Kevlar the mode changes from matrix yielding, equation (6.36), to fibre failure, equation (6.27). In the case of glass, equation (6.36) governs behaviour up to a higher stress, then splitting failure, equation (6.38), takes place. At lower stresses, both the glass and Kevlar composites fit the equation

$$\sigma_{1cu} = 9\sigma_{my} \quad (6.39)$$

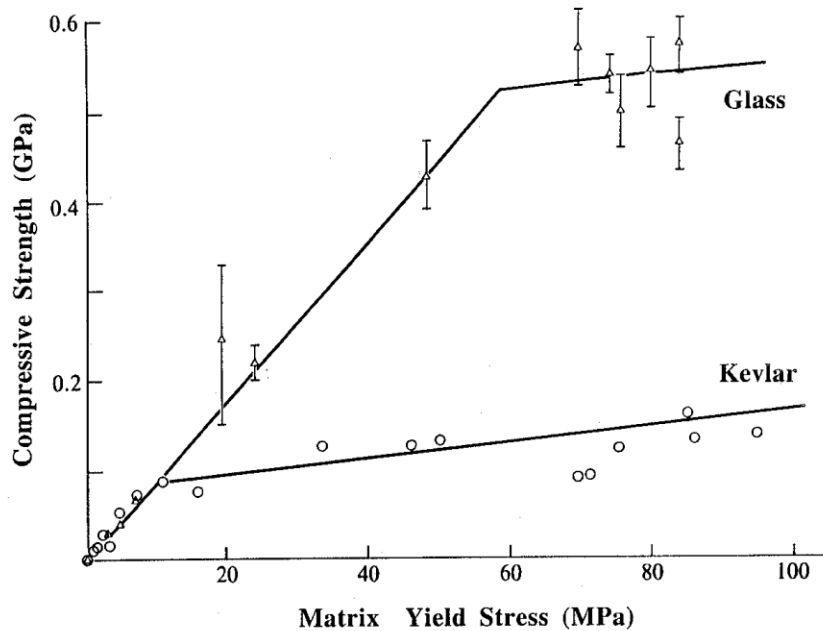


Fig. 6.42 Compressive strength vs matrix yield strength for Kevlar and glass-polyester pultrusions. (After Piggott, M.R., 1981, J. Mat. Sci. 16, 2867-45.)

(Note that in this work, the metallurgist's definition of σ_{my} was used. It was, however, observed that σ_{yc} , see equation (6.8), was roughly equal to $1.7\sigma_{my}$ for a wide range of polyesters and an epoxy. Thus $\sigma_{1cu} \cong 5\sigma_{yc}$.)

Fig. 6.43 shows the results of some experiments in which the adhesion between the fibres and polymer was altered. These are fitted to equations (6.36) and (6.38) with the values of σ_{my} and σ_a given.

The fibre curvature will also affect the modulus, since P will cause elastic deformation of the matrix when $P > \sigma_{my}$. When this happens, the composite has two compliances:

1. $1/E_f$ due to the elastic shortening of the fibres, and
2. $1/E_{fl}$ resulting from the increase in a and decrease in λ due to the action P .

Thus the effective modulus of the fibre is reduced from E_f to E_{cf} where

$$E_{cf} = (1/E_f + 1/E_{fl})^{-1} \quad (6.40)$$

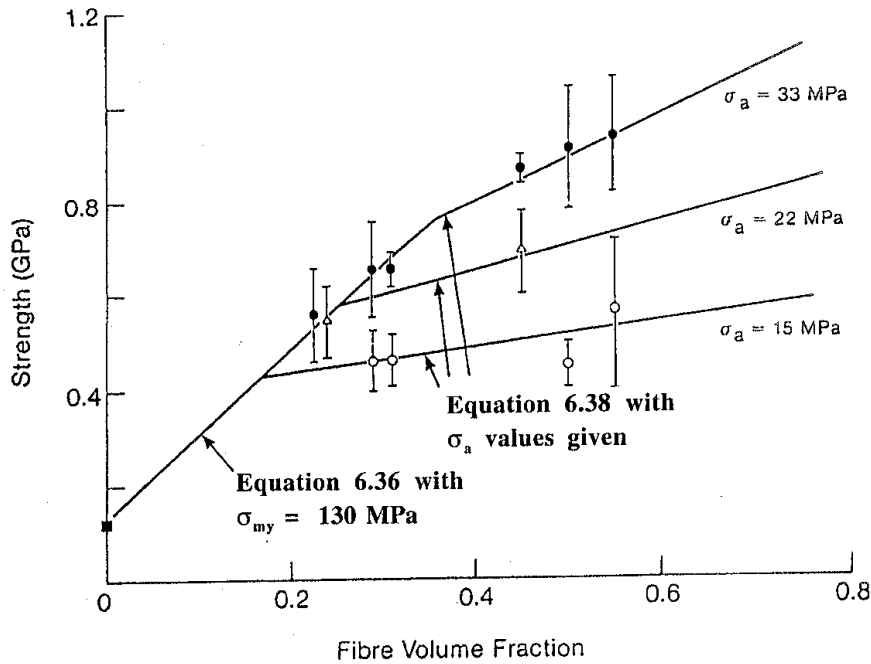


Fig. 6.43 Fitting results for fibres with various levels of adhesion. The solid circles are for fibres with the sizing intact, the triangles are for solvent treated fibres and the solid circles were for fibres with sizing removed by pyrolysis (After Piggott, M.R., *Developments in Reinforced Plastics*, Ed., G. Pritchard, Elsevier, London 1985, 4, Chpt. 4.)

The following simplified model demonstrates the principles involved in the estimation of E_{fl} .

We assume that, due to the sideways pressure, P , the matrix deforms elastically ($P < \sigma_{my}$) so that a increase and λ decreases. Meanwhile the fibre length remains constant. (We deal with the decrease in fibre length separately, later.) From $x = 0$ to $x = \lambda/4$, Fig. 6.40, we can approximate the fibre length, s , as

$$s \cong \frac{1}{4} \sqrt{\lambda^2 + 2\pi^2 a^2} \tag{6.41}$$

(This is a very good approximation; better than 0.2% for $\lambda > 10a$).

Differentiating this equation with $s = \text{constant}$ gives

$$da/d\lambda = -\lambda / [2\pi^2 a] \tag{6.42}$$

and if we assume that da/a is the transverse strain in the polymer, then

$$da/a = -P/ E_m \tag{6.43}$$

Since modulus is stress/strain

$$E_{fl} = \sigma_{fc} / [d\lambda / \lambda] \tag{6.44}$$

and substituting equations (6.42) and (6.43) into equation (6.44) gives, for the wavy modulus component

$$E_{fl} = \sigma_{fc} E_m \lambda^2 / [2\pi^2 a^2 P] \quad (6.45)$$

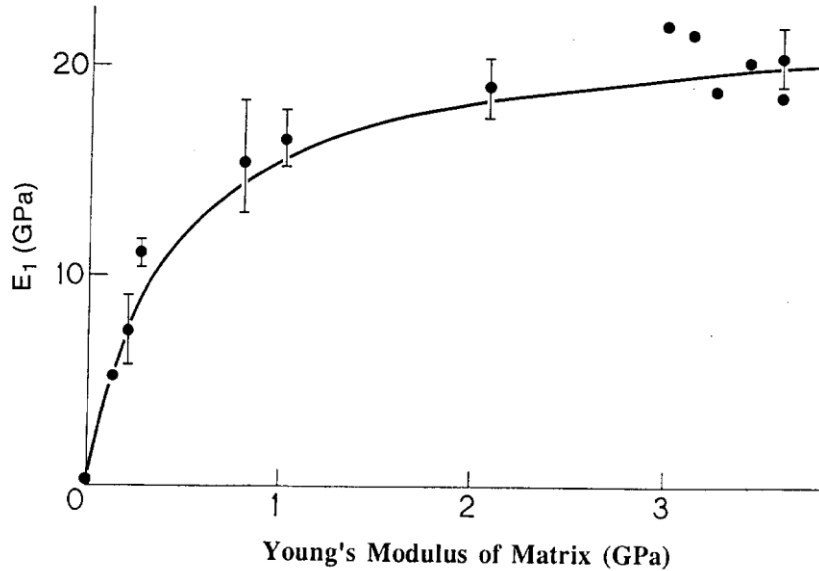


Fig. 6.44 Young's modulus of composites vs Young's modulus of resin. Glass-polyester pultrusions. The curve is drawn using equation (6.42) with $E_{fl} = 160E_m$. (After Piggott, M.R., 1981, *J. Mater. Sci.* 16, 2837-45.)

Lastly, from equations (6.33) and (6.34)

$$\sigma_{fc} / P = 2\lambda^2 / [\pi^3 a] \quad (6.46)$$

so substituting this into equation (6.45) gives

$$E_{fl} = \lambda^4 E_m / [\pi^5 a^3] \quad (6.47)$$

and since we use the Rule of Mixtures with E_{cf} (equation (6.40)) replacing E_f , we obtain the modulus in compression, E_{1c}

$$E_{1c} = \frac{V_f}{1/V_f + 1/V_m} + V_m E_m \quad (6.48)$$

Young's moduli have been measured in a series of experiments where σ_{my} , and hence E_m ($E_m \cong 43\sigma_{my}$) was varied over wide limits; see Fig. 6.44. Using equation (6.48), we can estimate E_{fl} , with the results shown in Fig. 6.45. Most of the results fit the line shown with

$$E_{fl} \cong 160E_m \quad (6.49)$$

The results below the line were for $E_{fl} \cong 80E_m$, suggesting adhesion failure, (i.e. the fibres were pushing on the convex side but not pulling on the concave side; see Fig.

6.40). These results were above the transition in behavior shown in Fig. 6.42, and it seems highly probable therefore, at these higher stresses, that the fibres have debonded from the polymer.

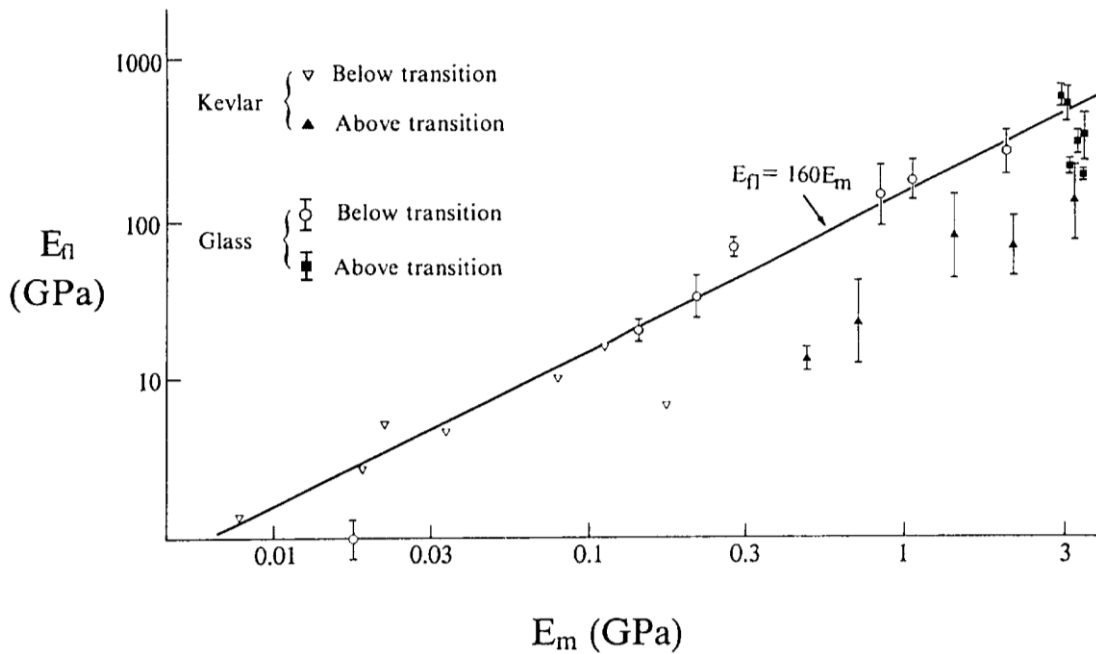


Fig. 6.45 E_f for Kevlar and glass-polyester vs E_m . For transitions see Fig. 6.38.

To maximize the compressive strength, this analysis shows that attention should be paid to the mesostructure. In particular the fibres should be as straight as possible (R_f as large as possible) and as well dispersed as possible to avoid bundling, (i.e. unduly large values of d).

Other factors of importance are good fibre-matrix adhesion, high matrix yield and tensile strength and high matrix compressive strength. Tough matrices are better than brittle ones since they inhibit splitting failure. Finally, the fibres should have a high compressive strength.

There are a wide diversity of theoretical treatments in the literature; the sine wave theory appears to have the widest experimental support at the moment.

6.6 Fatigue Endurance

In fatigue studies with laminates, cracks are observed to develop in the off-axis plies, sometimes quite early on in the fatigue life. However, final failure appears to be largely determined by the plies with fibres oriented in the stress direction. Hence, a key step in the treatment of fatigue failure is to deal with the failure of unidirectional composites taking the mesostructure into account.

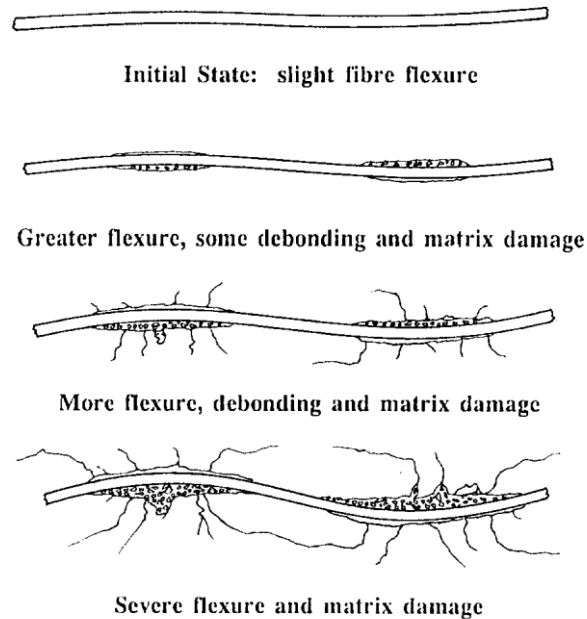


Fig. 6.46 Development of damage during fatigue. (After Piggott, M.R. and Lam, P.W.K., 1991, ASTM STP 1110, 686-695.)

In unidirectional composites the fibres normally take most of the load. So the first determinant of fatigue life is the endurance of the fibres themselves. Glass, for example, is known to have limited endurance under a static load ("static fatigue"). This is an environmental effect: the life is much prolonged in the absence of moisture. Glass fibres, which are normally protected from moisture by a silane coating, also suffer from this form of fatigue.

There is at present no clear evidence that other ceramic fibres are weakened directly by fatigue stresses, so for these we must consider the detailed structure of the composite; in particular fibre straightness. Fig. 6.46 shows wavy fibres which under varying stress can damage the matrix due to the transverse stresses. A process of matrix attrition takes place at the antinodes as shown.

This process causes an increase in the waviness so that eventually the fibres can fail at a stress less than the tensile strength due to the additional flexural stresses. The evidence for this type of failure process comes from experiments in which six properties were monitored during tension-tension fatigue of carbon-epoxy pultrusions. These were 1) Young's modulus, 2) flexural modulus, 3) Poisson's ratio, 4) hysteresis loop energy, 5) increase in size of a circular hole in the centre of the specimen, and finally 6) some specimens were taken out and tested to failure to determine the residual strength.

The Young's modulus showed a slight decline and the flexural modulus had a more noticeable decline, Fig. 6.47. This was particularly striking for composites made

with poorly adhering fibres. The loss in flexural modulus indicates that the composite was debonding and cracking parallel to the fibres.

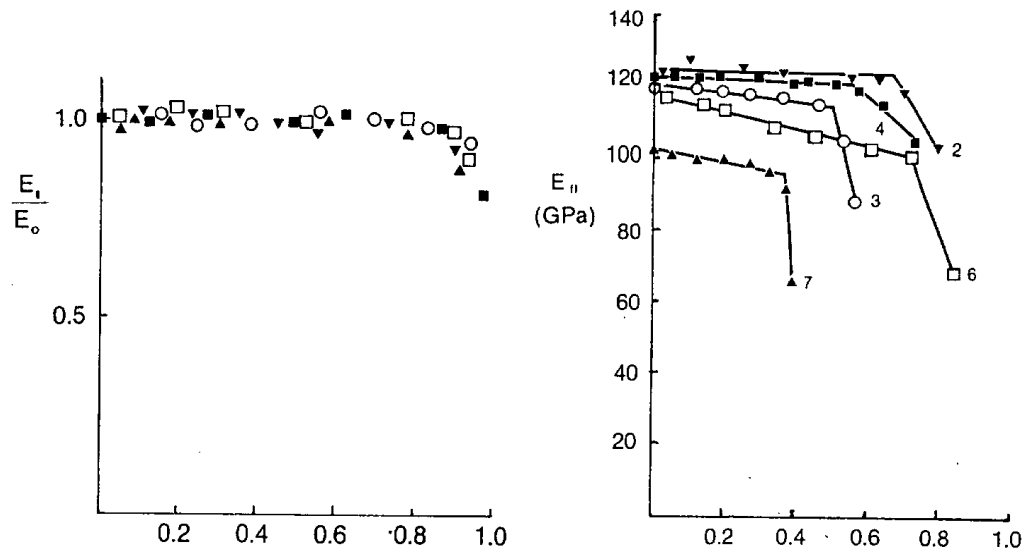


Fig. 6.47 Relative change in Young's modulus (left) and actual flexural modulus (right) during tensile-tensile fatigue ($R = 0.1$). Carbon-epoxies containing expanding monomers (TMSOC and DNSOC) and plasticizer (DMF). Some fibres coated with silicone oil. (After Lam, P.W.K., and Piggott, M.R., 1989, *J. Mater. Sci.* 24, 4427-4431.)

Poisson's ratio increased, providing additional evidence of splitting, and the holes drilled in the samples grew transversely to a much greater extent than the longitudinal growth, again indicating splitting and debonding.

The hysteresis loss indicated that work was being done on the specimen. This was causing the attrition of the polymer, and the failed specimens contained much powdered polymer on the failure surfaces. Finally, there was a gradual loss in strength of the specimen.

An additional weakening mechanism that can come into play is fibre fretting. This involves fibres damaging each other by rubbing together. This will predominate in resin poor regions, where the fibres are close together, and can come into contact after adhesion failure and some polymer attrition. Again, the mesostructure plays a major role, and endurance can be improved by having the fibres as straight as possible, and as evenly dispersed as possible.

The reduced fatigue endurance under tension-compression fatigue and compression-compression fatigue as compared with tension-tension fatigue suggests that the matrix attrition process is predominant.

More detailed information on the fatigue process will be given in sections 10.2 (polymers), 11.4.3 (metals) and 11.7.3 (ceramics).

Further Reading

Hull, D. (1981) *An Introduction to Composite Materials* (Cambridge University Press), Section 7.4.

Swift, D.G., (1975) *J. Phys. D.* **8**, 223-40.

Argon, A.S., (1972), *Treatise on Materials Science and Technology* (Ed. H. Herman, Academic Press, New York.), 79-114.

Bogetti, T.A., Gillespie, J.W., and Pipes, R.B., (1988) *Comp. Sci. Tech.* **32**, 57-76.

Summerscales, J., (Ed.), (1998) *Microstructural Characterization of Fibre Reinforced Composites*, (Woodhead Publishing Co., Cambridge & Warsaw.)

Chapter 6: Problems

- 6.1. Estimate the maximum shear stress and associated nominal shear strain for low density polyethylene from Fig. 6.4. The diameter of the punch was 24mm.
- 6.2. Calculate the shear yield stress for the polyester giving the highest results shown in Fig. 6.42. Assume that the intrinsic compressive yield stress is equal to $1.7\sigma_{my}$, and the intrinsic tensile yield stress was 70% of the compressive.
- 6.3. Use Fig. 1.3 to estimate the intrinsic yield stresses for polycarbonate and polyethylene assuming no volume change and no significant difference between the intrinsic and extrinsic strains.
- 6.4. If polypropylene has a tensile strength of 37MPa and when straightened out a chain diameter of about 0.80nm, estimate the maximum number of backbone chain carbon atoms the polymer can have to avoid chain scission when tensile tested. Also estimate the molecular weight.
- 6.5. Assume that a carbon fibre is debonded along the whole of its length and is equivalent to a Griffith-Irwin crack having a length equal to the fibre diameter. What would be the transverse strength of the composite?
- 6.6. Estimate the transverse strength of a glass-epoxy composite with $V_f = 0.31$ where the tensile strength of the fibre-matrix interfacial bond is 23MPa.
- 6.7. A 4.4mm thick sheet of cross-ply glass-epoxy has a curved beam strength of 1.1 ± 0.1 kN. Determine its through thickness strength, and using Fig. 6.19, determine whether the error in using the approximate equation is greater than the coefficient of variation of the result.

- 6.8. A carbon-epoxy unidirectional laminate has a curved beam strength of 680N. If the epoxy had a strength of 47MPa, what was the strength of the fibre-matrix bond? The laminate was 5.6mm thick and had $V_f = 0.71$, hexagonally packed.
- 6.9. A better approximation to a circular section fibre than the square section fibre of side $2r$ shown in Fig. 6.20 is a square fibre of the same size with oblongs added to each face width r and thicknesses $r/2$. Estimate E_2 / E_m in this case for $V_f = 0.6$ with a fibre with a modulus so large that E_m / E_{ft} can be neglected, and compare it with E_2 / E_m using the square model and IROM.
- 6.10. What would be the matrix Young's modulus for the IROM model to fit the experimental results in table 6.3?
- 6.11. Show that the maximum tensile stress in the matrix, σ_{mm} , in the short beam test, can be reduced to the approximate form $\sigma_{mm} = \tau_{max} (1 + az - 4z^2)$ with $z = -y/d$ (Fig. 1.12) and $a = \text{constant}$. Hence show that for a $[0]_{32}$ carbon-epoxy beam, tested with $2l/d = 5$, the apparent shear strength, τ_{13u} , should be approximately equal to the polymer tensile strength. Estimate the maximum error δ for $\tau_{13u} = \sigma_{mu} (1 + \delta)$ and the maximum distance below the centreline for the failure. Assume the fibres are perfectly straight, with none on the neutral plane.
- 6.12. Assuming that the strength of the carbon fibres used to make the pultrusions giving the results shown in Fig. 6.25 was 3.0GPa, what fraction of the fracture surface area do you expect to contain broken fibre ends?
- 6.13. The compressive strength of a Kevlar-epoxy pultrusion was found to be 173MPa. Estimate the compressive strength of the fibres. Assume the polymer is elastic up to the failure strain of the composite and $V_f = 0.30$.
- 6.14. If a unidirectional composite could be made with perfectly straight carbon fibres having the highest compressive strain shown in Fig. 6.35, what would its strength be for $V_f = 0.68$. (Assume the epoxy resin matrix is elastic at this strain, and that the fibres were stiff carbon.)
- 6.15. A unidirectional laminate, made having 0.10mm thick laminae, is found to have misaligned fibres. Further examination shows that the maximum deviation is 3° , which is restricted to one region of one of the laminae where a region of $+3^\circ$ deviation is separated by a region of -3° deviation by a distance of 2.4 mm. What would be its compressive strength, if the fibres were well bonded and the matrix was tough but yielded at a stress of 45MPa. Assume the effective fibre bundle diameter is equal to the laminate thickness.
- 6.16. Estimate the compressive strength and modulus of a composite made with the plain weave fibres shown in Fig. 3.17. Assume, for simplicity, that the fibre

bundles are round and that the polymer can fail by yielding at 63MPa, has a modulus of 3.9GPa, and that the transverse fibres contribute 250 MPa. $V_f = 0.47$.

- 6.17 In a cross ply laminate the HMS carbon fibres were slightly wavy at the beginning of a fatigue experiment, with a wavelength of 1.6 mm and an amplitude of 10nm. It was subject to tensile-tensile fatigue at a maximum stress of 200MPa and a minimum of 10MPa. If the fibre waviness amplitude increases by 0.1% per cycle and the tensile strength of the matrix was 55MPa, what would be the number of cycles to failure assuming the fibres were very well bonded in the matrix.

Chapter 6 Selected Answers

- 6.1 49MPa; 98.
- 6.3 69MPa; 9.6MPa.
- 6.5 150MPa.
- 6.7 70MPa; CV is 9% while the maximum error < 2%.
- 6.9 7.07, compared with IROM, 3.33 and square, 5.29.
- 6.11 0.16% and 2% of the thickness below the centre line.
- 6.13 0.55GPa.
- 6.15 5.4GPa.
- 6.17 3900 cycles

7. BRITTLE FRACTURE PROCESSES

In this chapter we will discuss the general principles involved in the fracture failure of composites. Fibre reinforced materials are not as tough as standard structural metals such as steels and aluminium alloys. This is an impediment to their widespread use in load bearing situations.

The problem is only partly due to the brittleness of the main fibres used, i.e. glass and carbon. With polymers, the matrix itself is often brittle and, even when tough polymers such as PEEK are used, the fibres inhibit the energy absorbing processes. This is true with metal matrices as well; carbon fibres make very brittle aluminium matrix composites, even when the aluminium is pure. With ceramics, on the other hand, some limited toughening is possible, due to energy absorbing processes at the fibre-matrix interface.

The anisotropy encountered in strength and stiffness extends also to toughness. The unidirectional fibre composite can be moderately resistant to failure normal to the fibres, while very brittle transverse to them. Furthermore, laminates designed to have good in-plane properties (e.g. “quasi-isotropic” forms such as $[0/+45/90/-45]_{ns}$) can easily delaminate under flexure. This is particularly serious with such structures as aircraft wings, where impact from an accidentally dropped tool can cause internal delamination. Such damage is invisible when carbon or Kevlar is used, thus posing a hidden danger.

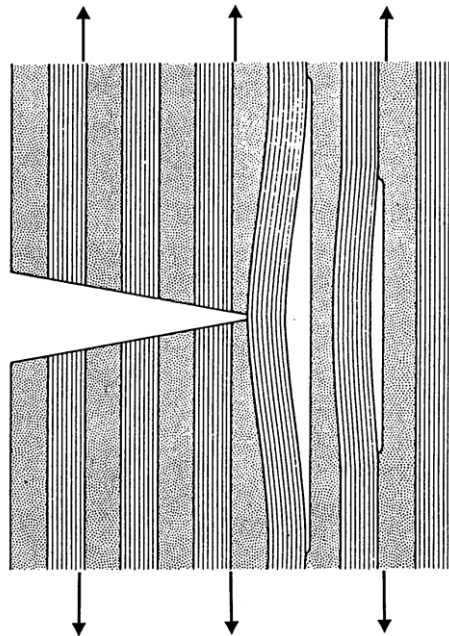


Fig. 7.1 Splitting at the crack tip in a unidirectional fibre composite.

An additional problem is that through thickness fracture resistance is difficult to measure. This is because cracks are easily diverted: see Fig. 7.1. Here the applied stress is normal to the crack plane, but splitting occurs parallel to the fibres, due to the

transverse stress. (This stress is illustrated in Figs. 2.11 and 2.12.) Such crack diversion occurs in the Izod and Charpy tests, as well as in tensile tests, when unidirectional composites are used.

7.1 Fracture Mechanics

7.1.1 Fracture modes

Notches and cracks were introduced in Chapter 2, and it was shown in section 2.3.2 that, for crack propagation, energy considerations are paramount. This involves the concept of surface energy, and its analogue, \mathcal{G} , the work of fracture (section 2.3.4). Fracture toughness, \mathcal{K} , was shown to be useful for measuring fracture resistance in isotropic materials, and \mathcal{G} could be obtained from it using equation (2.20).

Only one mode of fracture was considered in Chapter 2, i.e. the crack opening mode. Two other modes are thought to be important for metals, a shearing mode (Mode II) and a shear scissoring mode (Mode III). These are illustrated in Fig. 7.2, and the \mathcal{G} 's and \mathcal{K} 's are accordingly subscripted \mathcal{G}_I , \mathcal{G}_{II} , \mathcal{K}_I , etc.

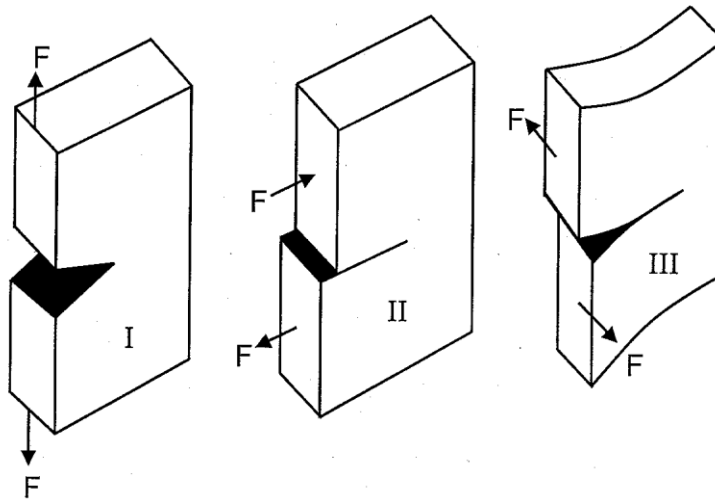


Fig. 7.2 The three basic modes of fracture.

Since most polymers do not fail in shear, modes II and III are less important than mode I. With metal and ceramic matrices, the processes contributing to modes II and III have received little attention.

Delamination is the mode of failure for which \mathcal{G}_{II} and \mathcal{G}_{III} have been studied the most. In this type of failure, it is the initiation of the process which is considered to be most important. Then it is found experimentally that

$$\mathcal{G}_{II} > \mathcal{G}_{III} > \mathcal{G}_I \quad (7.1)$$

See Fig. 7.3 for a comparison of \mathcal{G}_{II} and \mathcal{G}_I

Being the smallest, \mathcal{G}_I is the most critical parameter. Furthermore, it is now considered that \mathcal{G}_{II} is related to \mathcal{G}_I :

$$\mathcal{G}_{II} = \mathcal{G}_I + f(E_m, \sigma_{my}, t) \tag{7.2}$$

where f is some function of the thickness, t , of the resin rich layers between the plies. The matrix modulus, E_m , and the matrix tensile yield stress, σ_{my} , are also thought to be involved.

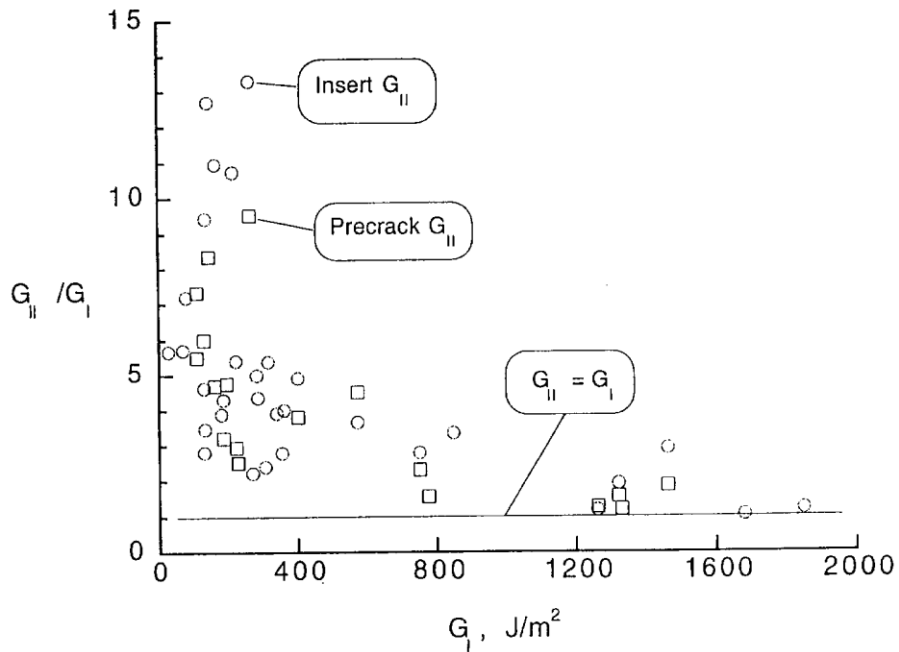


Fig. 7.3 Ratio of mode II to mode I toughness for reinforced plastic laminates. (After O'Brien, T.K., 1997, NASA TM 110280.)

In view of the prime importance of \mathcal{G}_I we will concentrate our attention on that, and so drop the I subscript so that, instead, we may use subscripts indicating directions relative to the composite axes. Thus, in the rest of this chapter, \mathcal{G} indicates opening mode fracture, and \mathcal{K} the opening mode fracture toughness.

\mathcal{K} is less important than \mathcal{G} for fibre composites, and can be estimated therefrom. While, for metals, the plane strain fracture toughness is important, for composites, plane stress toughness is used. Thus the $1 - \nu^2$ in equation (2.20) is dropped and instead we have

$$\mathcal{K}_j^2 = E_{\mathcal{K}j} \mathcal{G}_j \tag{7.3}$$

Here the subscript \mathcal{K} connotes conversion to \mathcal{K} and j indicates the stress direction in the test. $E_{\mathcal{K}j}$ is the appropriate stiffness. For example, a unidirectional composite stressed in the 1 direction has $\mathcal{K}_1^2 = E_{\mathcal{K}1} \mathcal{G}_1$ and

$$E_{\kappa_1} = \sqrt{2} / \sqrt{S_{22} (\sqrt{S_{11} S_{22}} + S_{12} + S_{66} / 2)} \quad (7.4)$$

Similarly, a laminate stressed in the x direction has κ_x , which is related to \mathcal{G}_x using equation (7.3), with E_{κ_x} for E_{κ_j} . E_{κ_x} is calculated using equation (7.4), with \hat{S}_{ij} replacing the S_{ij} therein.

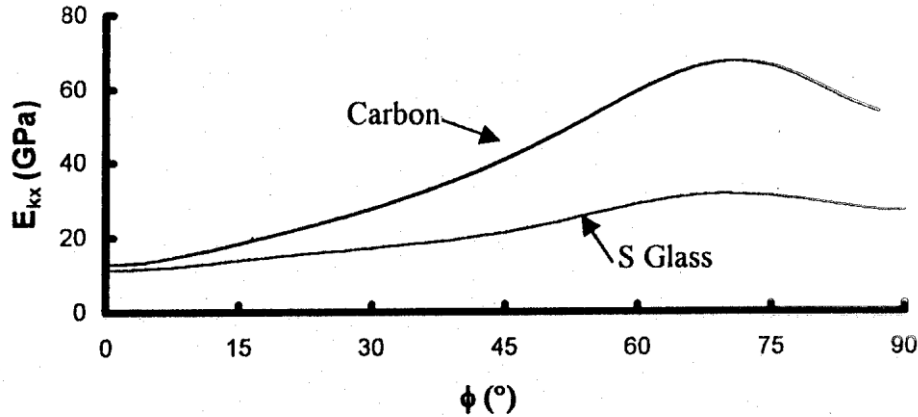


Fig. 7.4 The conversion stiffness E_{κ_x} for $[\pm \phi]_{ns}$ carbon-epoxy and glass-epoxy angle ply laminates plotted vs the ply angle ϕ .

For angle ply laminates, substitution using equations (4.62) to (4.65) gives

$$E_{\kappa_x} = \frac{\sqrt{2} (\hat{Q}_{11} \hat{Q}_{22} - \hat{Q}_{12}^2)}{\sqrt{\hat{Q}_{11} \left\{ \sqrt{\hat{Q}_{11} \hat{Q}_{22} - \hat{Q}_{12}^2} + (\hat{Q}_{11} \hat{Q}_{22} - \hat{Q}_{12}^2) / 2 \hat{Q}_{66} \right\}}} \quad (7.5)$$

Fig. 7.4 shows E_{κ_x} plotted vs ϕ for carbon-epoxy with $E_1 = 150$ GPa, $E_2 = 9.0$ GPa, $G_{12} = 6.0$ GPa and $\nu_{12} = 0.27$, and S glass-epoxy with $E_1 = 57$ GPa, $E_2 = 10.0$ GPa, $G_{12} = 4.0$ GPa and $\nu_{12} = 0.25$. The more anisotropic carbon gives a much greater variation with angle ply angle.

7.1.2 Fracture Toughness Testing

Conventional tests with (isotropic) metals are done with the single edge notched specimen shown in Fig. 7.5a. The notch must be extended and made more sharp at the tip by fatiguing the specimen. This test is not suitable for measuring κ_1 for unidirectional fibre composites because they split too easily. This is because the crack is blunted rather than sharpened by fatigue. Furthermore, the wedging action of the loading pins allow them to pull out under very small applied forces due to the weakness and brittleness of the composite transverse to the fibres.

Nevertheless, other laminates can be tested with a modified single edge notch sample, and a new ASTM standard E1922-97 uses the sample shown in Fig. 7.5b. κ_x

was measured with a narrow notch cut with a jeweller's saw. The crack opening displacement (COD) was monitored while the specimen was pulled. \mathcal{K}_I was calculated from the maximum force, F_{max} . For a $[90/-45/0/+45]_{4s}$ AS4 carbon-epoxy laminate \mathcal{K}_x was found to be $57 \pm 3 \text{ MPa m}^{1/2}$. (The corresponding \mathcal{G}_x was $85 \pm 9 \text{ kJm}^{-2}$.)

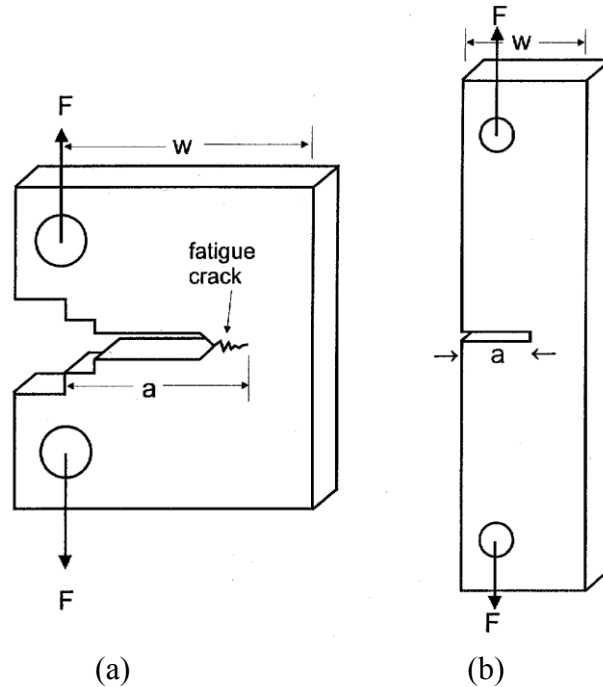


Fig. 7.5 Single edge notch fracture toughness specimens. (a) standard specimen for metals, ASTM E1290; (b) standard for through the thickness fracture resistance for fibre reinforced laminates, ASTM E1922.

Data reduction involved a complicated algebraic expression for the ratio crack length a to total sample width w . Since the nature of the process gives variable results, as can be seen (the coefficient of variation of \mathcal{K} was 5%), a simple expression will suffice. For the allowed range of crack lengths, i.e. $0.5 < a/w < 0.6$ the following expression is accurate to better than 2%:

$$\mathcal{K}_{Ic} = F_{max}(33.3a/W - 9.8)/[t\sqrt{W}] \quad (7.6)$$

where t is the thickness of the sample.

This test is not suitable for angle ply laminates since few of the fibres break. (This is the same narrow coupon problem as encountered with unnotched tests, such as ASTM D3039.) Testing wider samples gives more convincing results. For example, for $[\pm 15]_s$ all the fibres can be broken with double edge notched samples 43 mm wide having a 20 mm gauge length. Such tests show that, over a wide range of notch depths, \mathcal{K}_x is approximately constant: see Fig. 7.6. For $[\pm 30]_s$ about 86% of fibres were broken, so the

actual toughness may be a little higher than the value of about $59 \pm 6 \text{ MPa m}^{1/2}$ indicated in the figure for carbon-epoxy. For $[\pm 45]_s$ and higher angles few fibres were broken, so the method is unreliable. It should be noted here that angle ply laminates can apparently be very tough. The \mathcal{K}_x results of $86 \pm 8 \text{ MPa m}^{1/2}$ for $[\pm 15]_s$ corresponds to $\mathcal{G}_x = 0.7 \pm 0.1 \text{ MJm}^{-2}$.

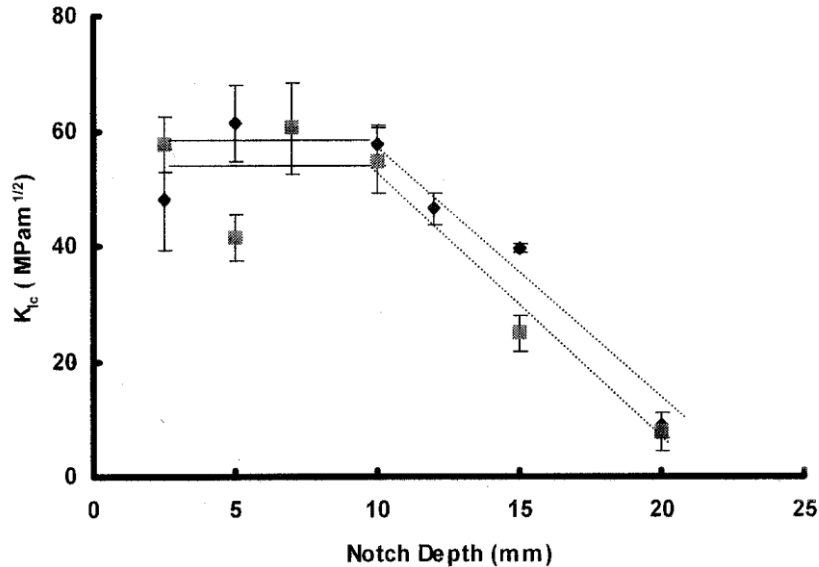


Fig. 7.6 Fracture toughness vs notch depth for carbon-epoxy and S glass-epoxy $[\pm 30]_s$ laminates. After Piggott, M.R., and Zhang, W., 2001 Proc. SAMPE Symp. 2321-7)

Photoelastic tests indicate that the crack tip stress distributions for angle plies are different from the isotropic case. The method gives fringes for constant $\sigma_a - \sigma_b$ where σ_a is the upper and σ_b the lower principal stress. The fringes should very roughly follow the lines shown in Fig. 2.10, since σ_b is relatively small. For a quasi-isotropic $[0/+45/90/-45]_s$ laminate they do; see Fig. 7.7a (this gave $\mathcal{K}_x = 23 \pm 4 \text{ MPa m}^{1/2}$). For $[\pm 30]_s$ however, Fig. 7.7b, the fringes tend to be redirected towards the fibre directions at low applied stresses, and they become complex as stresses approach the fracture stress, Fig. 7.7c.

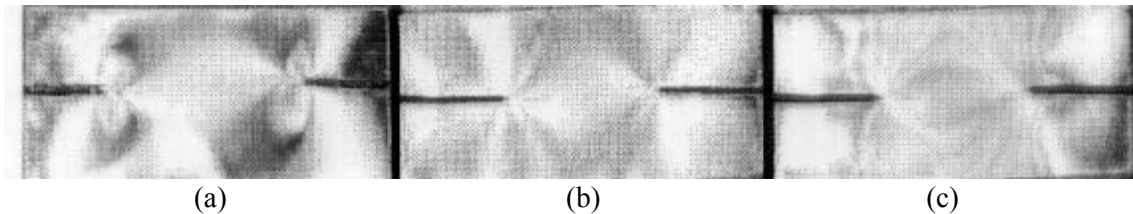


Fig. 7.7 Photoelastic fringe patterns for notched carbon-epoxy laminates (a) $[0/+45/90/-45]_s$ at 80% of the breaking stress, σ_{xu} (b) $[\pm 30]_s$ at 0.25 σ_{xu} and (c) $[\pm 30]_s$ at 0.8 σ_{xu} .

For unidirectional composites, such as pultrusions with square or close to square sections, the notched slow bending test devised by Tattersall and Tappin can give good results. The notches leave an inverted V of material under the loading force; see Fig.

7.8a. Thus, as the crack proceeds, the crack front becomes longer. This favours slow and controlled crack growth. The test is successful only when the load falls relatively slowly from the peak value, as shown in Fig. 7.8b. Fig. 7.8c shows a broken sample.

\mathcal{G} is obtained from this test as the area under the force-distance plot divided by the cross sectional area remaining after the sample was notched. For a sample of width w and thickness t , this is $wt/2$, (or less if the triangle has a smaller base or height than the width or thickness).

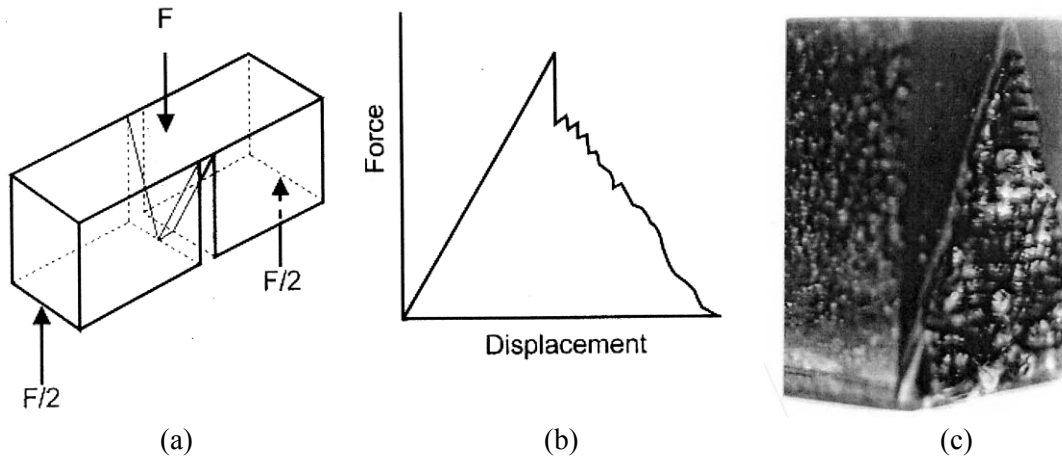


Fig. 7.8 Tattersall-Tappin test. (a) notched sample, (b) typical force-displacement plot for a successful test and (c) fracture surface of a carbon fibre bundle reinforced polyester resin, with \mathcal{G}_1 about 4 kJm^{-2} , (After Tattersall, H. and Tappin, G., *J. Mater Sci.* 1, 1966, 296-301 and Fila, M., Bredin, C., and Piggott, M.R., *J. Mater. Sci.* 7, 1972, 983-8.)

Since the work of delamination is generally very much less than the through thickness work, this has been studied in much more detail. It is normally tested, for the opening mode, using the double cantilever beam shown schematically in Fig. 7.9. The sample is moulded with a release film in the centre, which provides a notch, with equivalent length a_0 from the centre of the loading blocks. PTFE is recommended for this film when low temperatures ($<177^\circ\text{C}$) are used for moulding, and polyimide for higher temperature resins. The specimen thickness, h , is $4 \pm 1 \text{ mm}$, the width, b , should be 20-25mm, the length $L \geq 125 \text{ mm}$ and $a_0/h > 10$.

\mathcal{G}_3 is calculated from the force F and displacement, δ , at which the force vs. displacement plot first deviates from linearity. Thus

$$\mathcal{G}_3 \cong 3F\delta/2b a_0 \quad (7.7)$$

This gives the work of fracture for initiation of failure. This equation is approximate and can be refined by taking into account possible rotation. The ASTM "round robins" yielded $85 \pm 15 \text{ Jm}^{-2}$ for carbon epoxy (AS4-3501-6) and mean values of 0.98 to 1.3 kJm^{-2} for AS4-PEEK with $13\mu\text{m}$ thick Kapton used for the release film.

Since energy absorption is the essence of fracture resistance, the next three sections of this Chapter will be devoted to processes which enhance or inhibit the absorption of energy. This treatment will be kept as simple as possible, with more complex interactions reserved for Chapter 8 where the interface is discussed.

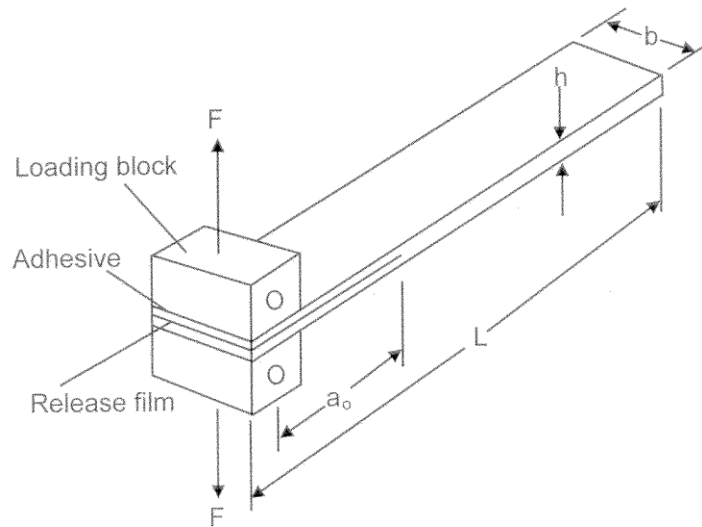


Fig. 7.9 Double cantilever beam method used for measuring Mode I interlaminar fracture toughness. (ASTM D5528: piano hinges may be used in place of loading blocks.)

7.2 Through Thickness Fracture

For \mathcal{G}_1 we are not able to use mixture rules. Instead we must take account of matrix effects on the fibres, fibre effects on the matrix, and energy absorption at the interface. Thus we write

$$\mathcal{G}_1 = V_f \mathcal{G}_f^* + V_m \mathcal{G}_m^* + V_i \mathcal{G}_i \quad (7.8)$$

where $\mathcal{G}_f^* > \mathcal{G}_f$, the work of fracture of unsupported fibres. For Kevlar reinforced composites, this term may be significant, but for carbon and glass, with \mathcal{G}_f only a few Jm^{-2} , it is not. This is because the toughness enhancement, $\mathcal{G}_f^* / \mathcal{G}_f$ is probably not very great.

No results are available for $\mathcal{G}_f^* / \mathcal{G}_f$ for glass, carbon or Kevlar, but \mathcal{G}_f^* has been found to be about 1.4MJm^{-2} for stainless steel in an aluminium alloy. This is about the value for 18-8 stainless steel in the undrawn state, which had a strength of about 620MPa. Since these wires had a strength of 3.1GPa, we can be sure that, unsupported, they were not as tough as the undrawn material. It seems probable that $\mathcal{G}_f^* / \mathcal{G}_f$ may be about 3-5 in this case. Fig. 7.10 shows some results from this work.

\mathcal{G}_m^* can be very much less than \mathcal{G}_m because the small diameter of the fibres, and their proximity to each other, markedly reduces the thickness of the plastic zone at the crack faces. This zone can be more than 1mm for a tough metal. The presence of well bonded fibres with $V_f \sim 0.5$ can reduce it to a few fibre diameters ($\sim 50\mu\text{m}$) i.e. a twenty fold reduction.

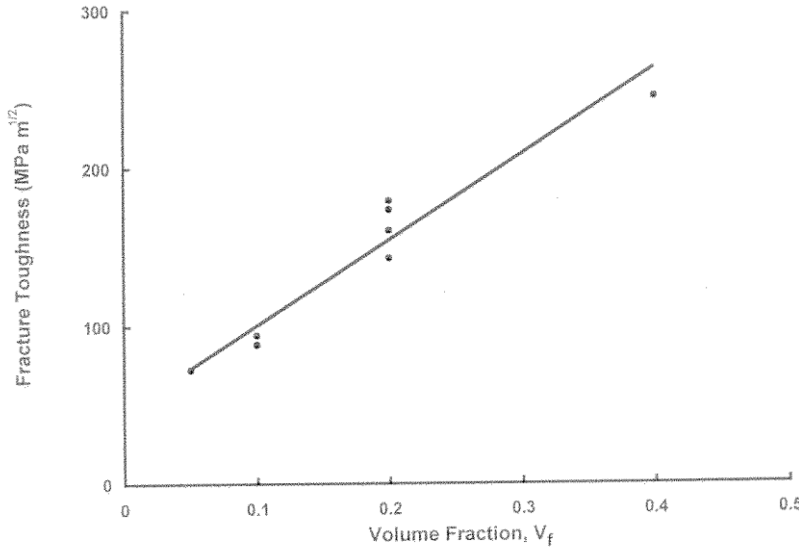


Fig. 7.10 Fracture toughness for unidirectional stainless steel-aluminium alloy (After Gerberich, W.W., 1971, J. Mech. Phys. Solids, 19, 71-87.)

7.2.1 Fibres Unidirectional, Continuous and Flawed

\mathcal{G}_{ii} refers to interactions at the interface. When a unidirectional continuous fibre composite breaks, the fibres do not normally break in the fracture plane: see Fig. 7.11. This is because they contain flaws. A well bonded fibre breaks at a flaw near the fracture plane, so the fibre ends are pulled out and work is done.

If we assume a constant shear stress, τ_i , at the interface, the work per fibre is simply the mean force times the distance moved during pull out, i.e. $(2\pi rL)(\tau_i)(L/2)$ where L is the length of fibre fragment pulled out. For N fibres per unit cross section, the total work is N times this, and since $V_f = \pi r^2 N$, we can write

$$\mathcal{G}_{ii} = \tau_i L^2 / r \tag{7.9}$$

for unit V_f , or using s , as previously,

$$\mathcal{G}_{ii} = \tau_i r s^2 \tag{7.10}$$

For \mathcal{G}_{ii} given by equation (7.9) we can estimate τ_i since the work of fracture was about 6.4kJm^{-2} and $r = 4\mu\text{m}$. For L^2 we use the histogram shown in Fig. 7.11 which indicates a mean value of L^2 of $9300\mu\text{m}^2$. This gives $\tau_i \cong 3\text{MPa}$ which is reasonable for a non-adhering system such as this.

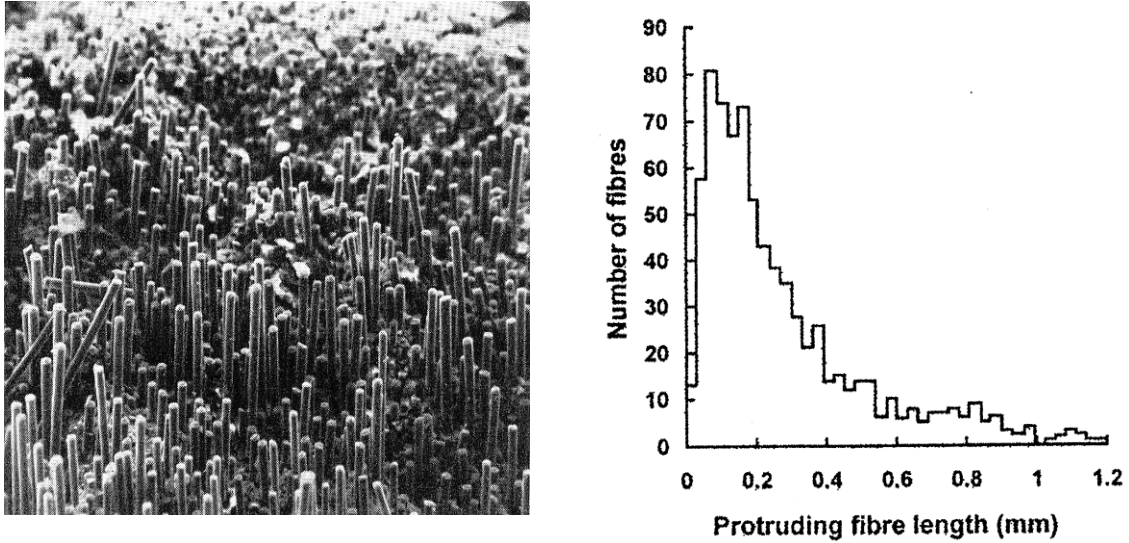


Fig. 7.11 Fracture surface showing carbon fibres pulled out of a borosilicate glass and, at right, typical distribution of fibre lengths observed. (After Phillips, D.C., 1972, *J. Mater. Sci.* 7, 1175-97 and 9, 1974, 1847-54.)

The pulled out value of s depends on how well the fibres are bonded. Poorly bonded fibres give long pulled out lengths and high work of fracture together with low resistance to shear: see Fig. 7.12. Although τ_i is reduced by poor bonding, the effect is overwhelmed by the increase in s , since this appears as the square in equation (7.10). These results have been explained, qualitatively at least, by assuming a fibre flaw distribution which gives, for the fibre strength

$$\sigma_{fu} = \sigma_{fu0} (s / s_0)^{-q} \quad (7.11)$$

where σ_{fu0} , s and q are constants. The fibre is supposed to debond up to a critical flaw, then break and pull out. The work of pull out is dependent on the matrix shrinkage pressure: see Fig. 7.13. (A detailed description of this process is given in Chapter 8.)

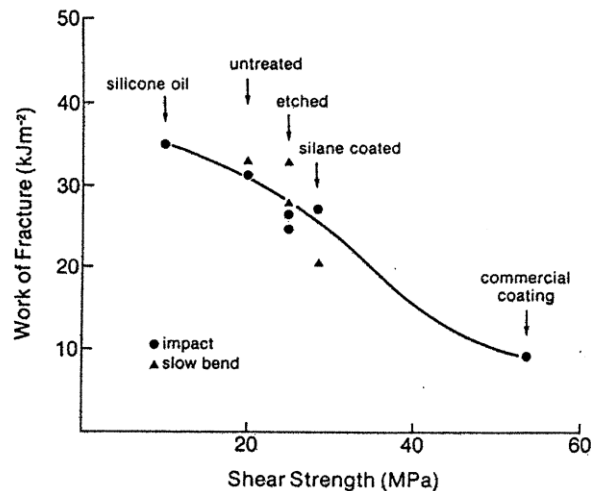


Fig. 7.12 Work of Fracture vs apparent shear strength for unidirectional carbon-polyester. (After Harris, B., Beaumont, P.W.R., and de Ferran, E.M., 1971, *J. Mater. Sci.* 6, 238-51.)

7.2.2 Fibres Unidirectional, Continuous and Unflawed

With fibres of uniform strength, such as Kevlar, fibre failure is expected to occur in the crack plane, since that is where the fibre stress is greatest. The fibre is stretched during crack opening, sliding against the matrix and thus doing work. After it breaks it retracts into the matrix, losing its stored elastic energy, equal to $\pi r^2 l \sigma_f / [2E_f]$ for a length l of fibre at constant stress, σ_f .

Consider the elastic energy of the part of the fibre, length l_c , near the crack face, where slip has taken place (Fig. 7.14). Since the fibre eventually breaks, $l_c = r s_c$. We include only elastic energy arising from crack-induced stresses.

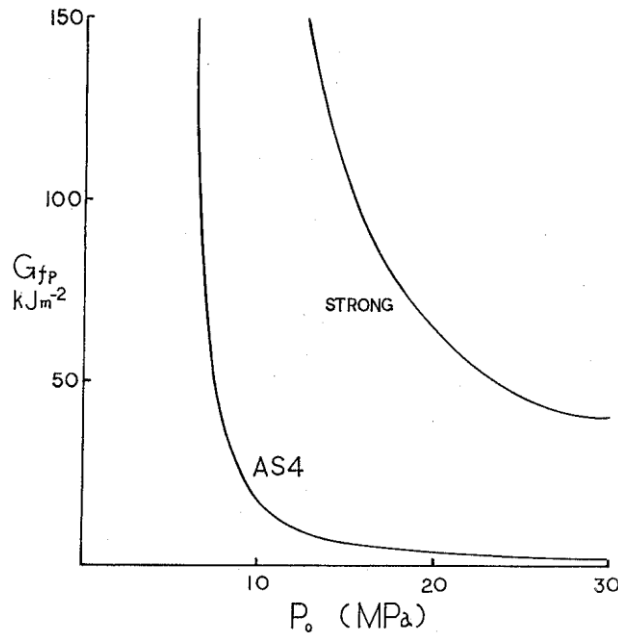


Fig. 7.13 Work of fibre pull out, G_{fp} vs. shrinkage pressure for unidirectional AS4 carbon and more highly flawed “strong” carbon reinforced polymers (After Piggott, M.R., 1995, *Polymers and Polymer Composites*, 3, 267-76.)

If x is the distance of the fibre element from the crack plane, then σ_f is given by a simple force balance. Shear stress τ_i (again assumed to be constant) is exerted over the length $l_c - x$ to give the fibre force, i.e.

$$\pi r^2 \sigma_f = 2\pi r \tau_i (l_c - x) \quad (7.12)$$

and this simplifies to

$$\sigma_f = 2(l_c - x) \tau_i / r \quad (7.13)$$

The elastic energy dU_{fb} of the element is

$$dU_{fb} = 2\pi (l_c - x)^2 \tau_i^2 dx / E_f \quad (7.14)$$

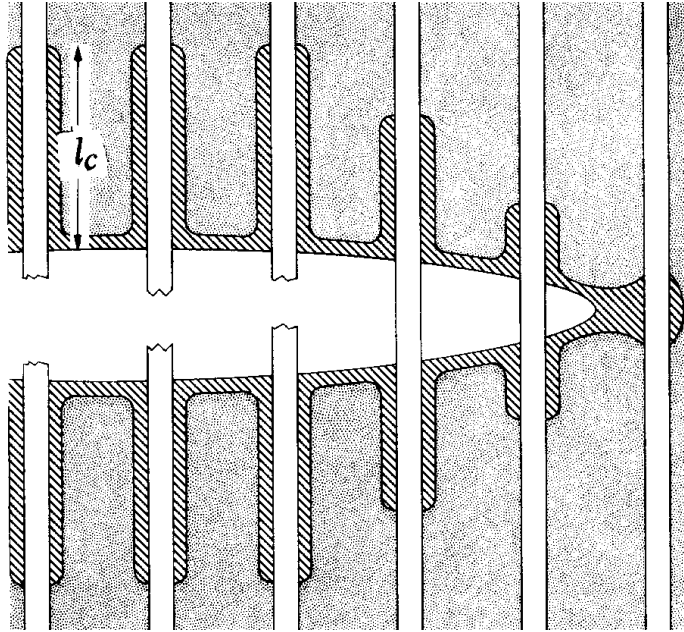


Fig. 7.14 Continuous fibres which fail in the crack plane as the crack opens. Length l_c is involved in the stretching, sliding and retraction processes. Hatched regions indicate these fibre slip zones.

The work done by the element in sliding against the matrix is

$$dU_{mf} = 2\pi\tau_i u dx \quad (7.15)$$

where u is the displacement of the fibre element relative to the matrix, given by

$$u = \int_x^{l_c} \varepsilon_f dx \quad (7.16)$$

(At $x = l_c$ the fibre strain, and displacement arising from the crack-induced stress, are assumed to be zero.) ε_f , the fibre strain, can be determined from the fibre stress given in equation (7.13). Substituting for ε_f and integrating the equation thus obtained gives

$$u = \tau_i (l_c - x)^2 / [rE_f] \quad (7.17)$$

Substituting the expression for u into equation (7.15) shows that $dU_{mf} = dU_{fb}$. The total work is the sum of dU_{fb} and dU_{mf} integrated between l_c and 0. Thus

$$U_{fb} + U_{mf} = \frac{2}{E_f} \int_{l_c}^0 2\pi\tau_i^2 (l_c - x)^2 dx \quad (7.18)$$

The corresponding work of fracture, $V_f \mathcal{G}_{fb}$, is equal to $2N (U_{fb} + U_{mf})$ where N is the number of fibres per unit area. Doing the above integration, and replacing l_c by $\sigma_{fu} d / [4 \tau_i]$ where d is the fibre diameter ($= 2r$) and $N\pi r^2$ by V_f , we obtain

$$\mathcal{G}_{fb} = \frac{d\sigma_{fu}^3}{6E_f\tau_i} \tag{7.19}$$

For Kevlar, with $E_f = 130\text{GPa}$, $d = 12\mu\text{m}$ and $\sigma_{fu} = 3.5\text{GPa}$, $V_f\mathcal{G}_{fb}$ comes to about 13kJm^{-2} when $V_f = 0.5$ and $\tau_i = 25\text{MPa}$.

Despite their small diameters, individual fibres contribute a moderate amount of work through this process as is evident from this result. With the fibres bundled, as in the original roving or tow, with, for example, 1600 fibres, the work can be increased forty fold, since the bundle diameter is about $40d$. Fig. 7.8c shows a fracture surface for a bundled fibre composite. These gave works of fracture of more than 100kJm^{-2} with low volume fractions ($\sim 10\%$) of glass fibres, and somewhat less for a carbon with E_f about six times higher. The dependence on E_f and τ_i as indicated in equation (7.19) was verified in these experiments, but the actual work of fracture was about twice as high, indicating that other energy absorbing processes were also at work.

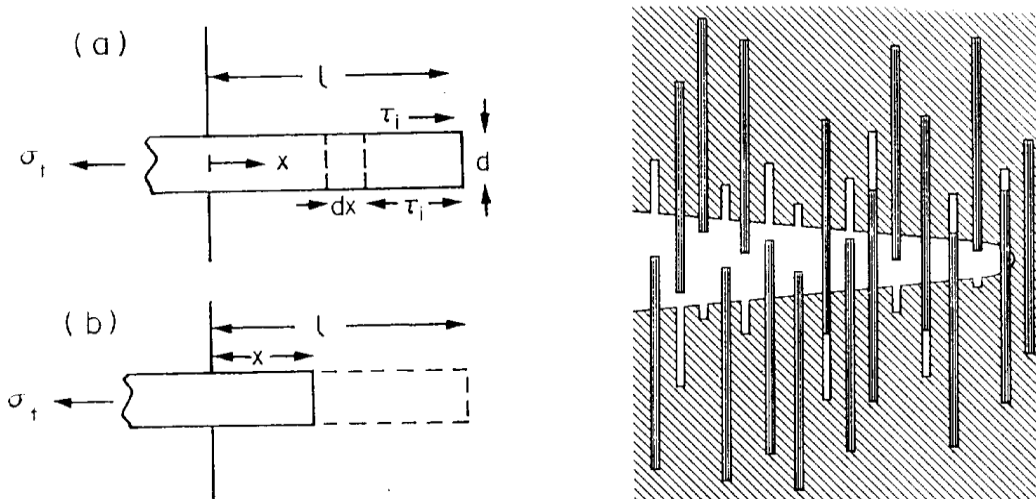


Fig. 7.15 (a) and (b) define the terminology used for one single short fibre being pulled out from one side of the crack shown at the right.

7.2.3 Short Unidirectional Fibres

We consider aligned fibres all having the same aspect ratio. Fig. 7.15. shows, at the right, the situation around the crack tip. The opening of the crack under the applied stress has caused fibres to pull out from both faces. To calculate the contribution of this process to \mathcal{G} , consider one fibre, Fig.7.15a.

We assume that the interfacial shear stress, τ_i , is constant during fibre pull-out. When the fibre has an embedded length l , the force required to pull it out is $2\pi r l \tau_i$. The force exerted by the fibre is $\pi r^2 \sigma_f$, so that

$$\sigma_f = 2l \tau_i / r \quad (7.20)$$

If $l/r > s_c (= \sigma_{fu} / 2\tau_i)$, $\sigma_f > \sigma_{fu}$ and the fibre will break rather than pulling out. For the moment, consider a fibre with an aspect ratio less than s_c . It will pull out, and while doing so σ_f will decrease linearly with the embedded length. The work of pull-out is

$$U_{fp} = \int_0^l 2\pi r x \tau_i dx \quad (7.21)$$

therefore

$$U_{fp} = \pi r l^2 \tau_i \quad (7.22)$$

If there are N fibres crossing unit area of crack, the number with an embedded length between l and $l + dl$ on one side of the crack is $Ndl/[2L]$, where $2L$ is the fibre length. (We are assuming the fibres are randomly disposed, but parallel to each other.) The work done by these fibres in pulling out is $V_f \mathcal{G}_{fp} / 2$, since we are considering one side only of the crack. The work can be determined by summing the relevant values of U_{fp} for all the fibres. Thus

$$V_f \mathcal{G}_{fp} = 2 \int_0^L \frac{NU_{fp}}{2L} dl \quad (7.23)$$

so that the work of fracture for pull-out is

$$\mathcal{G}_{fp} = d \tau_i s^2 / 6 \quad (7.24)$$

since $V_f = N\pi r^2$ and $s = L/r$.

This has its maximum value when $s = s_c$, which is

$$\mathcal{G}_{fpmax} = d \sigma_{fu}^2 / [24\tau_i] \quad (7.25)$$

For a carbon-epoxy with $\tau_i = 60\text{MPa}$, $\sigma_{fu} = 4.0\text{GPa}$, and $d = 8\mu\text{m}$, $V_f \mathcal{G}_{fpmax}$ comes to about 50kJm^{-2} for a composite containing 60% of fibres. So, under ideal conditions, fibre pull-out can contribute significantly to the work of fracture.

7.2.4 Long Unidirectional Fibres

Consider fibres with $s \geq s_c$. As for pull-out, the number of fibres with embedded lengths between $l + dl$, on one side of the crack, is $Ndl/2L$. However, this time some fibres will break and others will not, according to the embedded length. To calculate the work of fracture in this case we must sum the appropriate amounts of U_{fp} and U_{fb} :

$$V_f \mathcal{G}_{Li} = 2 \int_0^{l_c} U_{fp} dl + 2 \int_{l_c}^{2L-l_c} U_{fb} dl \quad (7.26)$$

Making the appropriate substitutions (equations (7.20) and (7.17)) remembering that $V_f \mathcal{G}_{fb} = 4U_{fb}$ and $V_f = N\pi r^2$ we obtain

$$\mathcal{G}_{Li} = \frac{d\sigma_{fu}^3}{6\tau_i} \left\{ \frac{1}{8\tau_i s} + \frac{1}{E_f} \left(1 - \frac{\sigma_{fu}}{2\tau_i s} \right) \right\} \quad (7.27)$$

A plot of \mathcal{G}_{Li} as a function of aspect ratio is shown in Fig. 7.16. The plot, presented in dimensionless form, shows that \mathcal{G}_{Li} has its maximum value at $s = s_c$ or $s \leq s_c$, \mathcal{G}_{fp} has been plotted. The importance of fibre-breaking strain, for fibres with high aspect ratios, is clearly demonstrated.

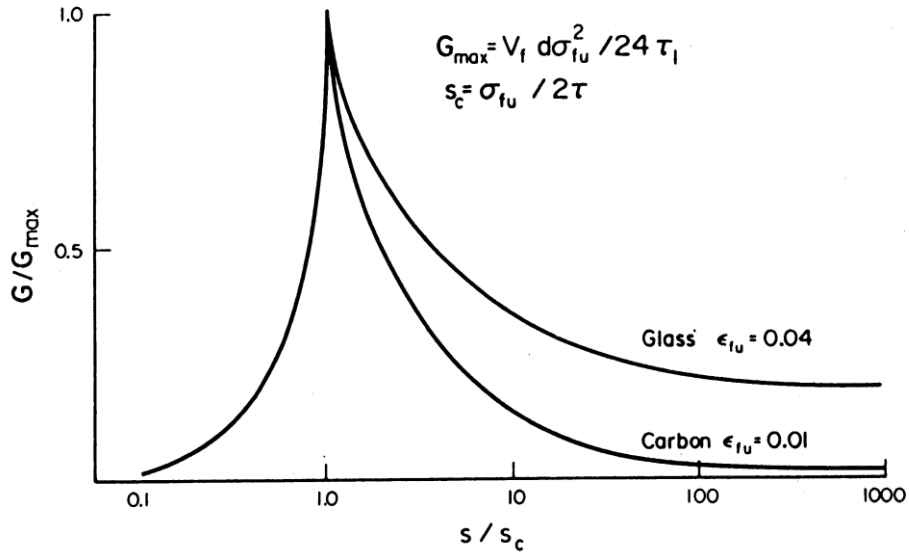


Fig. 7.16 Effect of fibre aspect ratio on toughness.

7.2.5 Fibres Crossing Cracks Obliquely

If we assume that the fibres can operate individually, it is appropriate to use the approximate expressions governing the strength of fibres pulled obliquely, i.e. equation (4.78). Thus, for the continuous uniform strength fibre case, we simply replace σ_{fu} in equation (7.19) by $\sigma_{fu\phi}$. However, such a failure process is extremely improbable in a unidirectional composite, because splitting failure normally requires much less work, so should take place instead. Nevertheless, a $[\pm\phi]_{ns}$ angle ply laminate does not have this problem, so we make the substitution in this case, to give

$$\mathcal{G}_{x1} = \frac{d\sigma_{fu0}^3}{12E_f\tau_i} \left\{ 1 + \left(1 - \frac{\phi}{\phi_h} \right)^{1/3} \right\} \quad (7.28)$$

for $\phi \leq \phi_h$. Here $V_f \mathcal{G}_{x1}$ is the work of fracture for an angle ply laminate made with fibres having uniform strength. (ϕ_h is the fibre half strength angle equal to 45° for Kevlar in 20°C cured epoxy: see e.g. Fig. 4.22). This produces a low result compared with those given in section 7.1.2; see problem 7.14.

When the fibres are short, the critical length is reduced to $s_{c\phi}$ where

$$s_{c\phi} = \frac{s_c}{2} \left\{ 1 + \left(1 - \frac{\phi}{\phi_h} \right)^{1/3} \right\} \quad (7.29)$$

so that equation (7.24) could be used for $s < s_{c\phi}$ and, for $s_{c\phi} < s < s_c$, equation (7.27) could be used with σ_{fu} replaced by $\sigma_{fu\phi}$. The long fibre case could be treated similarly. However, in both these cases splitting failure is more probable than failure involving fibre breaks if the fibres are unidirectional.

A case which restricts splitting is the random fibre case. Such a composite, made with fibres having $s > s_c$ will fracture by breaking the more oblique fibres (i.e. these with $s > s_{c\phi}$) and pulling out the rest. So we use the analysis in the previous paragraph, plus integration with respect to ϕ . Since the purely random case is uncommon, the actual fibre orientation distribution should be taken into account in the integration.

7.3. Delamination Fracture

\mathcal{G}_3 is analogous to σ_{2u} in a unidirectional composite because the failure initiation involves only the polymer and the interface. Two extreme cases are shown schematically in Fig. 7.17.

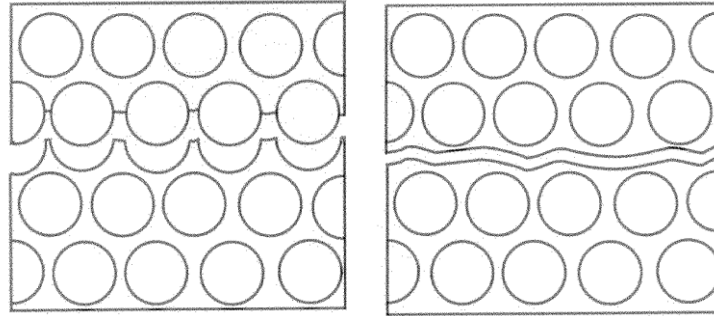


Fig. 7.17 Schematic drawings showing delamination failure (a) for $\mathcal{G}_i \ll \mathcal{G}_m$ and (b) $\mathcal{G}_i \gg \mathcal{G}_m$.

For $\mathcal{G}_i \ll \mathcal{G}_m$ we expect the fracture to propagate preferentially at the interface, with matrix fracture only in the webs between the fibres. In this case, we use equation (6.16) with σ_a replaced by \mathcal{G}_i and σ_{mu} replaced by \mathcal{G}_m , i.e.

$$\mathcal{G}_3 = \pi \sqrt{V_f / P_f} \mathcal{G}_i + \{1 - 2 \sqrt{V_f / P_f}\} \mathcal{G}_m \quad (7.30)$$

for a composite in which the fibres are packed uniformly.

For $\mathcal{G}_i \gg \mathcal{G}_m$, only matrix failure is expected, so,

$$\mathcal{G}_3 = \mathcal{G}_m \quad (7.31)$$

When $\mathcal{G}_i \sim \mathcal{G}_m$, \mathcal{G}_3 is difficult to predict, although examination of the fracture surfaces after the event could yield relative areas A_f of fibre and A_m of matrix, so that we might expect

$$\mathcal{G}_3 = A_f \mathcal{G}_i + A_m \mathcal{G}_m \tag{7.32}$$

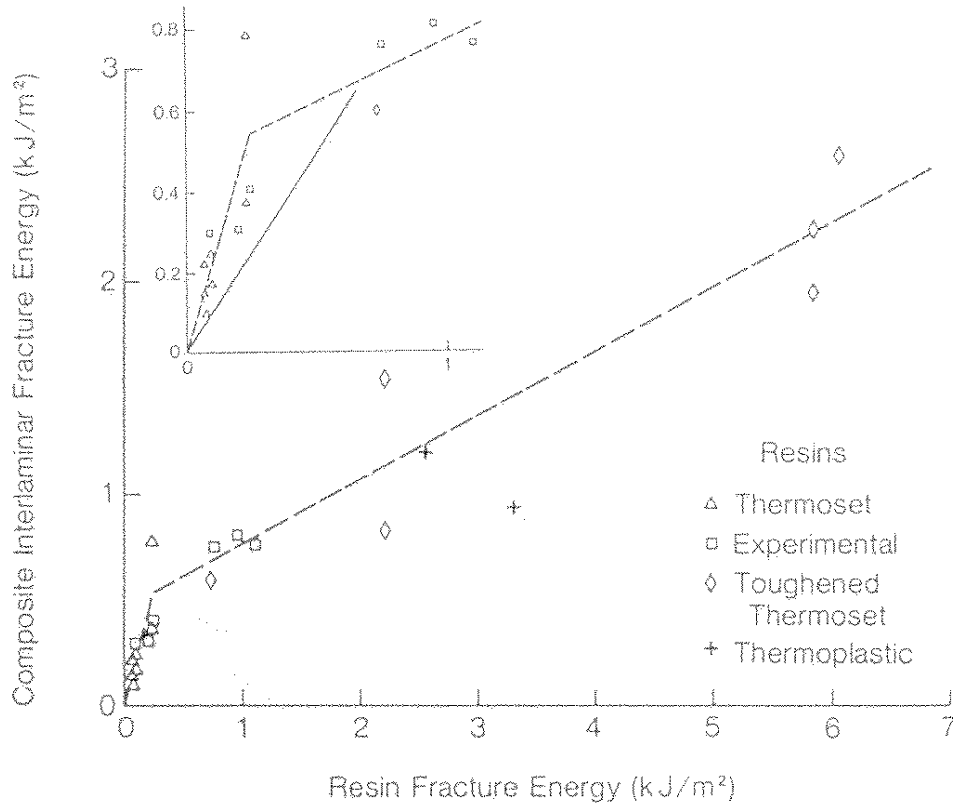


Fig. 7.18 \mathcal{G}_3 plotted vs \mathcal{G}_m , with, inset, region near origin enlarged. (After Hunston, D.L., 1984, Comp. Tech Rev 6, 176-80.)

Equation (7.32) will of course apply in the non uniformly packed case whenever bare fibres can be seen (Remember that $A_f + A_m > 1$ since the fracture surfaces are rough, so the total surface area of each half of the fractured sample can be greater than the initial cross sectional area.)

These observations do not agree with the well known result shown in Fig. 7.18 This indicated that, near the origin, \mathcal{G}_3 was about $2.3\mathcal{G}_m$, while for $\mathcal{G}_m > 0.2\text{kJm}^{-2}$, the slope of the line was reduced to 0.31. The reason for the high slope near the origin is that the \mathcal{G}_3 values used were not initiation values. Fibre bridging took place and this increased \mathcal{G}_3 .

For the tougher matrices it is considered that we should use \mathcal{G}_m^* rather than \mathcal{G}_m , again, as in equation (7.8) with $\mathcal{G}_m^* \ll \mathcal{G}_m$ for very tough matrices such as PEEK. Hence the lower slope starting at about $\mathcal{G}_3 = 0.5\text{kJm}^{-2}$.

7.4. Inhibition By Fibres of Matrix Plastic Work

The plastic work at fracture surfaces of metals can be estimated using X-rays. A worked zone with a strain ε_r of about 100% has been observed. The thickness, t_r , of this zone can be estimated by successive etching and re-X-raying. A similar worked zone is thought to be formed during the brittle fracture of polymers: see Fig. 7.19. If the yield stress of the material is σ_{my} , then the work of fracture (per unit area) is

$$\mathcal{G}_m = 2 \sigma_{my} \quad (7.33)$$

since the work done is stress x strain x volume. (Remember, there are two surfaces after fracture: see question 2.11.) Thus for pure aluminium with a yield stress of 60MPa (Table 1.1) and having a work of fracture of 140kJm^{-2} (Table 1.2), $t_r = 2\text{mm}$ for $\varepsilon_r = 1.0$.

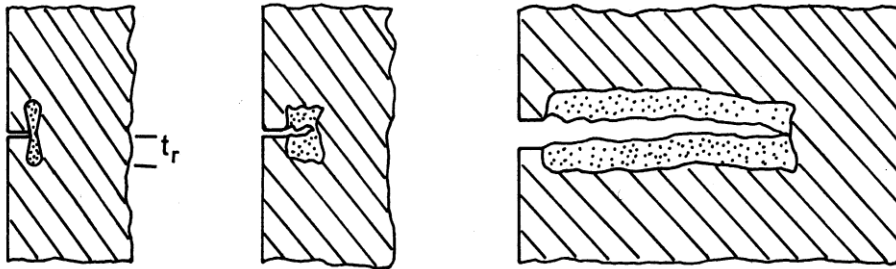


Fig. 7.19 Worked zone at fracture surfaces, as observed in steel, and thought to occur in other metals and polymers. (After Hall, E.O., 1953, *J. Mech Phys. Solids*, 1, 227-37.)

For through thickness fracture it may be assumed that the worked zone is restricted by the fibres to the critical transfer length, when they are closely packed. Thus

$$\mathcal{G}_{mt}^* = 2 \sigma_{my} \varepsilon_r L_{ce} \quad (7.34)$$

and using equation (5.33) for L_{ce} for metals with $2 \tau_i \sim \sigma_{my}$ equation (7.34) becomes

$$\mathcal{G}_{mt}^* = \sigma_{fu} \varepsilon_r d \quad (7.35)$$

where d is the fibre diameter and we are assuming perfect bonding of the fibres and Tresca yielding at the fibre surface. For $7.2 \mu\text{m}$ diameter carbon fibres with a strength of 3.8GPa (Table 3.2) in aluminium this gives $\mathcal{G}_{mt}^* \cong 27\text{kJm}^{-2}$, a more than three fold reduction with $\varepsilon_r = 1.0$. If the fibres also reduce ε_r the reduction will be even greater.

For delamination fracture the effect is much more severe, since t_r cannot be much greater than R (see Figs. 5.1 and 7.20). Thus, using equation (5.8) and writing \mathcal{G}_{md}^* for the appropriate work of fracture

$$\mathcal{G}_{md}^* \leq \frac{1}{2} \sigma_{my} \varepsilon_r d \sqrt{P_f / V_f} \tag{7.36}$$

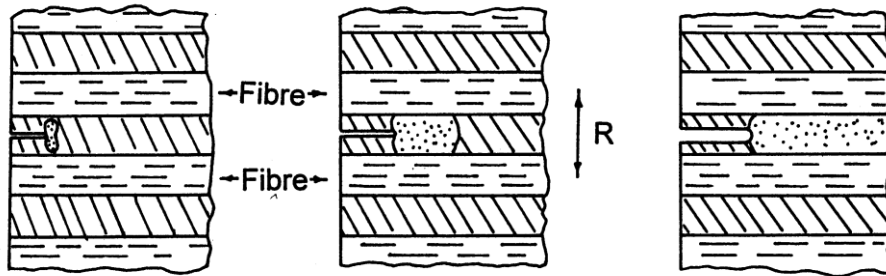


Fig. 7.20 Inhibition of matrix plastic work. The worked region is not expected to extend beyond the first fibres . (After Piggott, M.R., 1988, J. Mater Sci. 23, 3778-81.)

For a polymer with a yield stress of 50MPa, containing 60% carbon fibres packed hexagonally, $\mathcal{G}_{md}^* \leq 0.49\text{kJm}^{-2}$. This constitutes a very severe limitation, again assuming $\varepsilon_r = 1.0$. It provides a simple explanation for the behaviour change at 500Jm^{-2} shown in Fig. 7.18. However, the result shown in Fig. 7.18 should be treated with extreme caution. Initiation values were not used. Fibre bridging effects could result in overestimation of \mathcal{G}_3 for all \mathcal{G}_m values.

7.5. Impact Damage Evaluation

In aircraft structures, a major concern is that a heavy impact can cause internal damage in laminates which cannot be seen, as mentioned at the beginning of this Chapter. This causes delamination, and for sufficiently heavy impacts, fibre breakage and misorientation as well. These three damage processes reduce the compressive strength. (Their effects on the tensile strength are less serious, and delamination in particular will have a very small effect.) However, in compression, delamination reduces the effective thickness of the laminate, and so reduces the buckling resistance. For example, if we compare the critical stress, equation (6.25), for one sheet of thickness d , with two sheets, thickness $d/2$ each, the load capacity is halved.

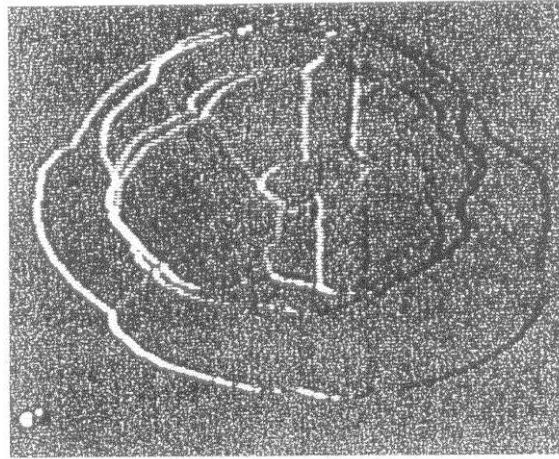


Fig. 7.21 Three dimensional reconstruction of impact damage within a laminate. (After Girshovich, S., Gollesman, T., Rosenthal, H., Drucker, T. and Steinberg, Y., 1992, ASTM STP 1128, 183-99.)

Compression resistance is important in many aircraft parts, for example the upper surfaces of the wings. So the industry (led by Boeing) developed a special test to evaluate this particular weakening effect of impact damage. Called “compression after impact”, this test was first codified in about 1982, and revised in 1988. In the test an oblong plate about 152mm x 102mm is supported centrally over a hole 127 x 76 sq mm, and impacted at the centre with known energy, using a dropping weight having a rounded steel tip with a radius of about 7.9mm. The sample sustains damage at various levels, which can be detected using ultrasonics; see Fig. 7.21.

The sample is then mounted in a simple fixture which restrains all four edges so that it can be loaded in compression without general buckling, see Fig. 7.22. In this way the compressive load is induced to initiate failure in the impacted region. The result is reported as the apparent strength, i.e. load/(sample width x sample thickness), together with the impact energy used and the class of impact. (There are two classes, according to whether aluminium on top of wood was used for the specimen support, or 25mm or greater thickness of steel was used.)

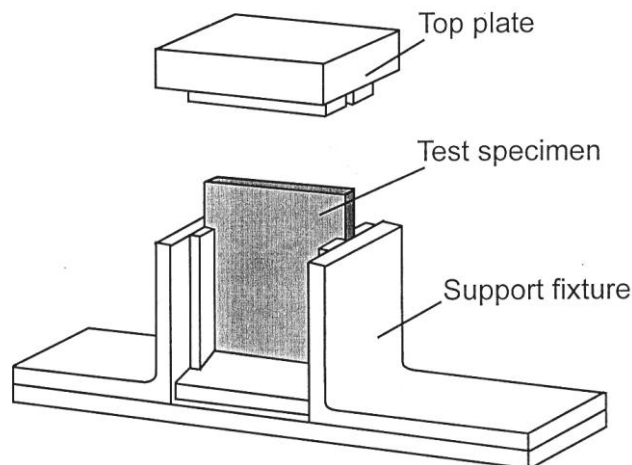


Fig. 7.22 Fixture for compression testing of impacted specimen. (After Boeing Specification Support Standard BSS 7260.)

A new ASTM test has been developed to replace this, which should introduce this type of damage in a more controlled manner. This is a quasi static indentation test (D6264). It uses a standard universal testing machine, so does not require specialized equipment. The sample is a 152mm square which is supported either centrally over a 127mm circular hole in a 200mm square plate of aluminium or steel, 40mm thick, or by a flat steel plate at least 12.7mm thick with no hole. An indenter with a 12.7mm diameter hemispherical tip is pressed into the sample at a constant speed, typically of 1mm per minute when the support has a hole in it and about one tenth the speed for the rigidly backed case. Force-displacement curves are reported (cross head movement often being adequate for this) together with maximum force, and other special features, such as F_1 , shown in Fig. 7.23. Further evaluation, such as compression testing, is chosen by the user.

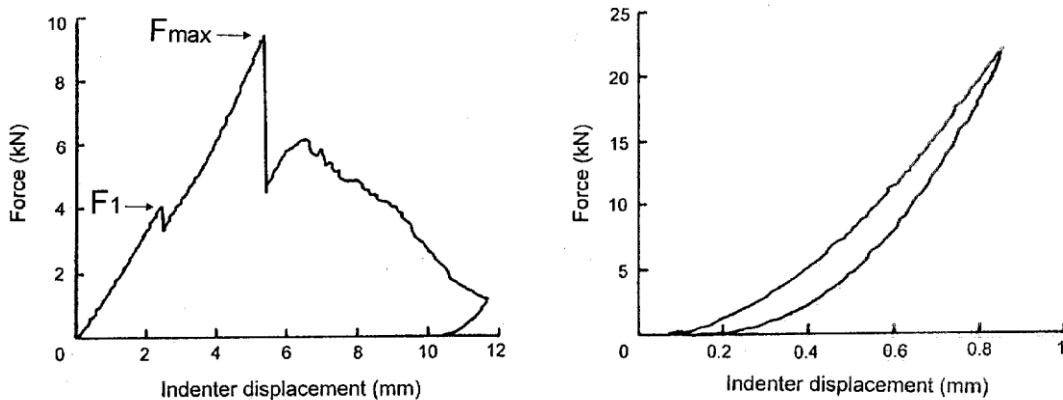


Fig. 7.23 Typical force-displacement curves for (a) simply supported test (i.e. over hole) and (b) rigidly backed test. (After ASTM D6264.)

This test should be useful as a measure of damage tolerance generally. Flexure testing could be carried out after quasi static indentation. Flexural rigidity, EI (see equations (1.1) and (1.2)) is determined by the cube of the specimen thickness of $d/2$ for each half. A flexural test is easier to carry out than a compression test, requires very little in special equipment (usually a flexure test set-up is readily available) and does not have the uncertainties associated with the compression test (see section 6.5.1).

Further Reading

General Fracture Mechanics

Barsom, S.T., and Rolf, J.M., (1977), *Fracture & Fatigue Control in Structures*, (Prentice Hall, Englewood Cliffs, N.J.)

Brown, W.E., (Symp. Chair), (1995), *Fracture Toughness Testing and Its Applications*, ASTM STP 381.

Fracture of Composites:

Sendeckyj, (Symp. Chair), (1975), *Fracture Mechanics of Composites*, ASTM STP 593.

O'Brien, T.K., (Ed.), (1991), *Composite Materials: Fatigue and Fracture* 3, ASTM STP 1110.

Stinchcomb, W.W., and Ashbaugh, N.E., (Eds.), (1993), *Composite Materials: Fatigue and Fracture* 4, ASTM STP 1156.

Martin, R.H., (Ed.), (1995), *Composite Materials: Fatigue and Fracture* 5, ASTM STP 1230.

Armanios, E.A., (Ed.), (1997), *Composite Materials: Fatigue and Fracture* 6, ASTM STP 1285.

Bucinell, R.E., (Ed), (1998), *Composite Materials: Fatigue and Fracture* 7, ASTM STP 1330

Williams, J.G., (1990), *Proc. Inst. Mech. Eng.* 204, 209-18.

Chapter 7: Problems

- 7.1 A sample for a through thickness toughness test had a width of 26mm, a length of 120 mm and a thickness of 4mm. With a notch length of 13mm, the specimen failed when the force was 2.8kN. Estimate the fracture toughness of the sample.
- 7.2 The sample in question 7.1 was cross-ply glass-epoxy made from laminae having $Q_{11} = 50\text{GPa}$, $Q_{22} = 10\text{GPa}$, $Q_{12} = 3.0\text{GPa}$, and $Q_{66} = 5.0\text{GPa}$. Calculate the work of fracture.
- 7.3 Estimate E_{xx} for an S-glass epoxy $[\pm 30]_s$ laminate assuming the Rule of Mixtures for E_1 and ν_{12} and IROM for E_2 and G_{12} with $V_f = 0.65$. Hence estimate \mathcal{G}_x for $\mathcal{K}_x = 57\text{MPa}\sqrt{m}$.
- 7.4 Do the same calculations as per question 7.3 for carbon-epoxy $[0/+45/190/-45]_s$ and hence calculate \mathcal{G}_x for $\mathcal{K}_x = 18\text{MPa}\sqrt{m}$. Assume the laminae had the properties given in Fig. 4.16. (Hint: estimate $\hat{Q}_{ij} = A_{ij}/[nt]$ and hence estimate \hat{S}_{ij} as in equation 7.4, etc.)
- 7.5 In a delamination test on carbon-epoxy a 25mm wide beam was used which was 4.1mm thick with a release film in it which was 45mm long. When the applied force reached 170N the displacement deviated from linearity and was 1.3mm at this point. Estimate the work of fracture.
- 7.6 The same test as in question 7.5 was carried out with carbon fibres in an unknown polymer matrix. This time the force was 390N and the displacement was 4.3mm when it deviated from linearity. Use this data and Fig. 7.18 to determine what type of polymer it was.
- 7.7 A unidirectional fibre reinforced ceramic had a work of fracture of 780Jm^{-2} . When the fracture surface was examined it had fibres protruding from it, with lengths all close to 88 microns. The fibre diameter was $10\mu\text{m}$ and the volume fraction was 0.35. Estimate the interfacial shear stress.
- 7.8 Estimate the root mean square pull out length for silicone coated glass fibres in a composite with an apparent shear strength of about 10MPa. Assume the fibre diameter was 11 microns, the interfacial shear stress was 2.3MPa and the fibre volume fraction was 0.57. (Hint: check Fig. 7.12)
- 7.9 In Fig. 7.8c the fibre bundle rods were made from tows having 1440 fibres. They were encased in resin so that the fraction of fibres in the rods was 0.70. The fibres had a diameter of 6 microns, an average strength of 2.3GPa and modulus of 440GPa. Estimate the work of fracture for a bundle volume fraction of 8% and an

interface shear yield stress of 17MPa. The polyester matrix failed with a work of fracture too small to be measured.

- 7.10 Show that, if the wires used to reinforce the aluminium in Fig. 7.10 were 0.50mm diameter and the aluminium neither yielded at the interface nor work hardened, the work of fracture of individual wires, as supported by the matrix, was 1.12MJm^{-2} .
- 7.11 Estimate the work of fracture for unidirectional steel wire reinforced brass. Assume that the brass yields and work hardens at the interface. The work of fracture of the brass was 11.2kJm^{-2} , and for the steel was 0.91kJm^{-2} . The wires had a diameter of 1.27 mm and constituted 47% of the volume.
- 7.12 A chopped carbon fibre reinforced aluminium was designed to give the maximum work of fracture with the fibres fully dispersed and parallel. What fibre length would be needed if the cheapest carbon were used and constituted 47% of the total volume, and what would be the work of fracture. Assume the aluminium was pure, with $\mathcal{G}_m = 300\text{Jm}^{-2}$ and did not work harden.
- 7.13 If the aluminium matrix in question 7.12 did work harden during the reinforcement process so that its tensile yield stress increased to 120MPa and toughness decreased to 20Jm^{-2} , how would this affect the work of fracture if the same length of fibre were used.
- 7.14 Estimate the work of fracture for a $[\pm 15]_s$ carbon-epoxy laminate assuming $\phi_n = 30^\circ$, and the cheapest fibres were used. The fibres debonded, so that interfacial shear stresses were frictional with a coefficient of friction of 0.3. The polymer was cured at 180°C and $V_f = 0.65$. The matrix was brittle.
- 7.15 What would the interfacial shear stress have to be to give the result for the S glass $[\pm 30]_s$ laminates shown in Fig. 7.6. Assume all the fibres fractured and that ϕ_0 is the same as for E glass, and use E_{xx} already calculated in question 7.3. $d = 10\mu\text{m}$, $V_f = 0.68$ and the matrix was brittle.
- 7.16 If the fibres restrict the polymer strain to 10% as well as restricting the plastic work zone, estimate the upper limit for the work of delamination for a carbon-epoxy laminate where the fibres are hexagonally packed and failure is as in Fig. 7.17b. The fibre diameter was 8 microns and $V_f = 0.64$. Assume the matrix yields at 80% of the ultimate tensile strength.
- 7.17 Compare the buckling stress for a unidirectional carbon-PEEK laminate with a thickness of 6.0mm which has been split down the middle in an impact test with that for the unsplit material. It was tested with its ends free to rotate on a span of 30mm. $V_f = 0.61$, the most economical fibres were used and $\nu_m = 0.35$. (Hint see sections 6.3 and 6.5; use Rule of Mixtures and IROM)

Chapter 7: Selected Answers

7.1 $30\text{MPa}\sqrt{m}$

7.3 $E_{xx} = 13.1\text{GPa}, \mathcal{G} = 0.25\text{MJm}^{-2}$

7.5 0.29kJm^{-2}

7.7 2.9MPa

7.9 2.9kJm^{-2}

7.11 1.67MJm^{-2}

7.13 18kJm^{-2} ; reduced by 73%.

7.15 1.5MPa

7.17 Unsplit 1.84GPa , split 0.86GPa .

8. INTERFACE MECHANICS AND TESTING

The simplest fibre composite has three components: the fibres, the matrix, and what lies between them. The third component, often called the interphase, is as important in determining composite properties as either of the others. This is because the forces must be transferred from the matrix to the fibres and back again. This is the role of the interphase, so it should ideally be designed to perform this function as efficiently as possible.

For brevity, this region will be referred to herein as the interface, although it usually has a significant thickness.

Interface structures, chemical compositions etc. are highly specific to the fibre-matrix system, and highly varied, and will not be discussed here. For reinforced polymers see section 9.2, metals, sections 11.3 and 11.4, and ceramics section 11.6.2.

In this chapter we will describe how the apparent interface shear strength has been measured, the problems with these measurements, their possible invalidation as a result of stress concentrations and brittle fracture, and how purely tensile processes can account for apparent shear failure. Next we use the equations developed here to explain the work of fibre pull out as it relates to through thickness fracture, and lastly we describe some relatively recent attempts to develop non axisymmetric tests for interface strength. First, however, we will review the composite properties which are affected by having a strong or weak interface.

8.1 Properties Sensitive to Interface Strength

These are dealt with in more detail in the appropriate sections. However, it is useful to bring them together here to appreciate more fully which properties are affected by the interface strength, and to what extent.

The transverse strength of a unidirectional composite (section 6.3) is directly affected by the interface. For a carbon-epoxy pultrusion, for example, when the interface strength is vanishingly small this strength can be as low as 6MPa, compared with 30MPa for a pultrusion with the normal adhesive strength at the interface. Also directly affected are the delamination resistance of high performance laminates (section 7.3) and the strength and stiffness of composites made with short fibres (section 5.3).

Less strongly affected are the apparent shear strength of a unidirectional composite (which is really a transverse strength with steric hindrance, section 6.4.) and also the compressive strength (section 6.5) and the fatigue resistance (section 6.6). These are all positive effects: good adhesion improves the properties.

Resistance to crack propagation across the fibers is improved by having adhesion which is only moderately good, and Fig. 7.12 shows the effect on the work of fracture and on the short beam flexure resistance for carbon fibres treated in various ways. The work of fracture benefit is particularly important in reinforced ceramics (see Fig. 7.11).

Finally, well adhering fibres usually give composites with the best environment resistance. This is particularly important with glass reinforced plastics which, unless the glass has a well adhering silane coating on it, are severely degraded by water immersion.

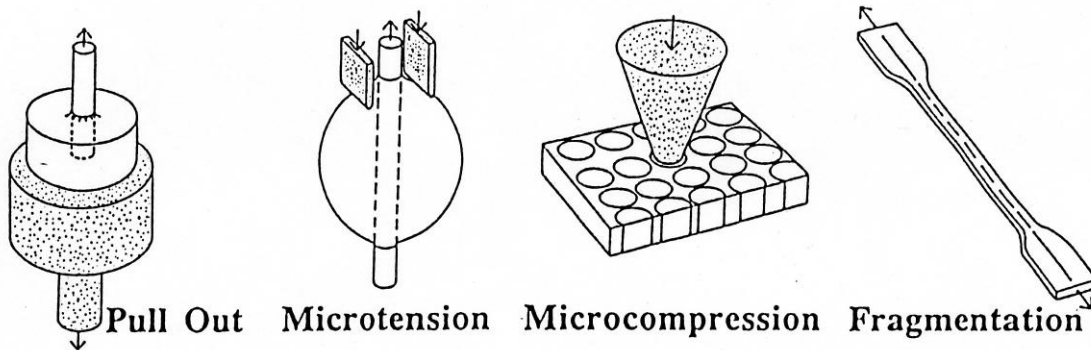


Fig. 8.1 Four shear methods for estimating the apparent interface strength.

8.2 Direct Measurement of Interface Strength

Four methods are currently used for interface testing; see Fig. 8.1. The pull out and microtension methods are roughly equivalent, differing only in details of the geometry. Microcompression is the inverse of pull out: the fibre is pushed instead of being pulled. The fragmentation method has a single fibre and the polymer is pulled, causing the fibre to break into small lengths.

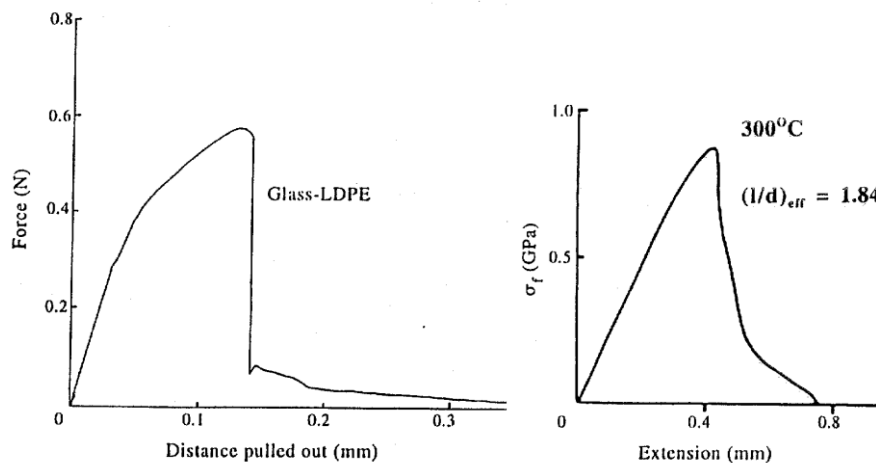


Fig. 8.2 Force-distance plots for glass-polyethylene and tungsten copper. (After Piggott, M.R., and Dai, S.R., 1991, *Polymer Eng. Sci.* **31**, 1246-9 and Tyson, W.R., 1964, Ph.D. thesis, Cambridge.)

The pull out method is perhaps the earliest, being used for tungsten-copper in 1964. Fig. 8.2 compares the pull out curve obtained with this system at 300°C with tests on glass-polyethylene. In experienced hands in a properly equipped laboratory the method can be carried out on a routine basis with high modulus carbon fibres with diameters as small as 8 μ m.

The microtension test was developed more recently (~ 1985) and was called the "microbond test" by its inventors. Very small drops are cured directly on the fibres in the case of thermosets. With thermoplastics, a small length of filament or thin ribbon is attached to or hung on the fibre, then heated to melt it and form the drop.

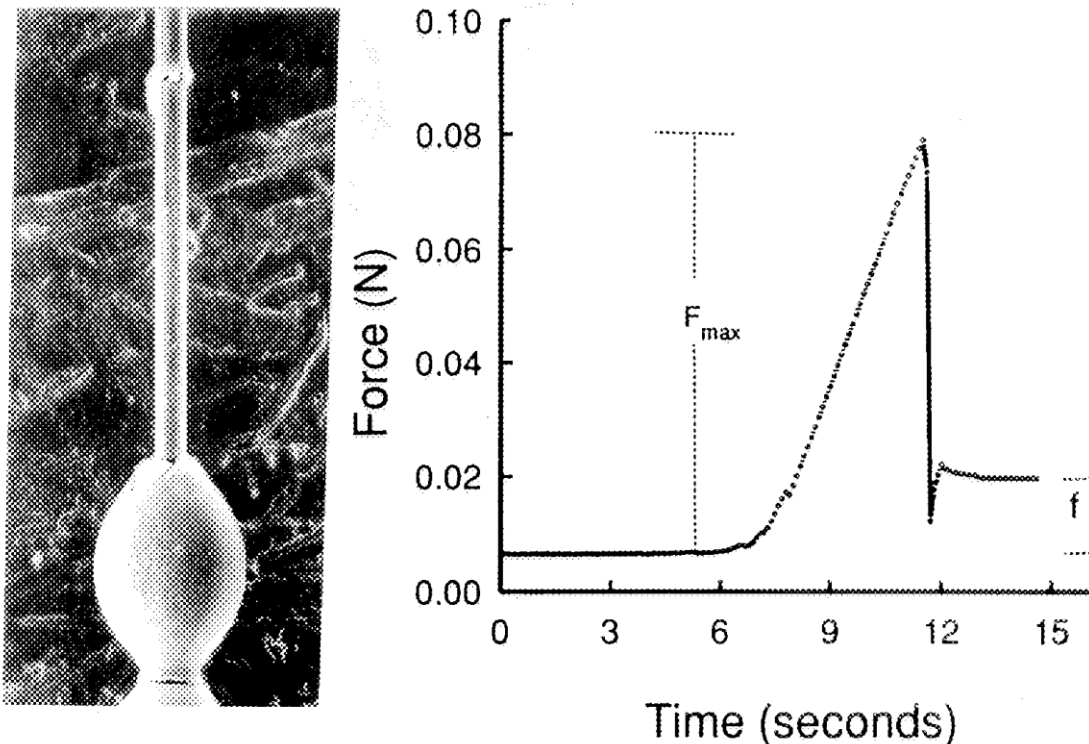


Fig. 8.3 At left, Microtension test droplet after debonding and displaced till in contact with another droplet. At right, force variation during a typical test. (After Miller, B., Muri, P. and Rebenfeld, L., 1987, *Comp. Sci. Tech.* 28, 17-32, and Biro, D.A., Pleizier, G. and Deslandes, Y., 1993, *Comp. Sci. Tech.* 46, 293-302.)

Fig. 8.3 shows an epoxy drop on a carbon fibre which has been pulled down until it contacted a second drop. Since the fibre passes right through the droplet, the force does not fall to zero. After debonding there is a very roughly constant frictional force as shown in the force-time curve at the right.

Both these methods permit the estimation of the apparent bond shear strength as a function of embedded length, L . The system used to pull on the fibre should preferably have maximum stiffness. In practice this means keeping the free length of fibre as short as possible (< 0.5 mm: the free length is the distance between the gripping point and the polymer surface). This permits the observation of transitions in the debonding process.

With the pull out test, it is important to allow the polymer to shrink freely on to the fibre. Thus, if a metal or ceramic capsule is used to hold the polymer during a high temperature cure, or for melting a high temperature thermoplastic such as polyetheretherketone (PEEK), it must be coated with a suitable release agent. If this is not done, the polymer may stick to the container and because of its high thermal contraction, develop a tensile stress across the interface with the fibre.

A mean interfacial shear strength, τ_{im} , is usually estimated from these tests. If the maximum force developed during pull out is F_{max} then a simple force balance gives

$$\tau_{im} = F_{max} / [2\pi rL] \quad (8.1)$$

The microcompression (or microindentation) method first appeared in 1980, and was christened the microdebond test. This is the only method which tests a fibre in situ in a composite. A thin slice of composite is prepared; see Fig. 8.1. When the slice is mounted, a fibre is selected and pushed down with an indenter. The force is monitored: see Fig. 8.4 *load profile*. The appropriate drop in force is not always easy to identify, so the noise emitted by debonding is sometimes used as well: see Fig. 8.4 *acoustic emission signals*. To obtain the bond strength from the force peak requires numerical methods; either finite element or boundary element methods are used. This method is much used for reinforced metals.

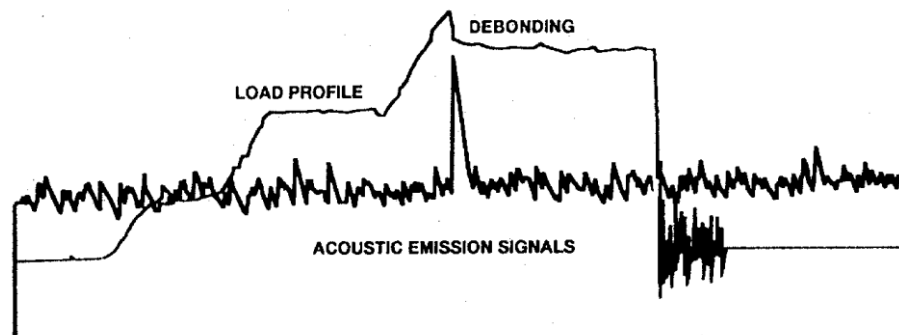


Fig. 8.4 Force vs displacement in microcompression test, together with the accompanying acoustic signal. (After Chen, E.J.H., and Young, J.C., 1991, *Comp. Sci. Tech.* 42, 189-206.)

The fragmentation method was first used with reinforced metals in the early 1960's and was applied to polymers shortly thereafter (1968). Usually a single fibre is used, but two or more have also been tested in the same polymer test bar. The bar is pulled and fibre breaks are monitored in the microscope, or by the noise they make when they fracture. (each fracture produces a click, which can be counted). The pulling continues until no further fibre breakage occurs ("saturation"). Only ductile polymers can be used as matrix. The polymer must be tough and also have a breaking strain greater than three times that of the fibre. Otherwise the polymer may fail prematurely.

At saturation the fibres are broken into pieces ranging from half the critical length to about the critical length. The average length, $2L_m$, therefore, is about three quarters of

the critical length. (Better estimates of this can be made with the help of statistical analysis.) From L_m we can estimate the critical aspect ratio; thus

$$s_c = 4L_m / [3r] \quad (8.2)$$

(see section 5.3 and remember that $2L$ is used for the fibre length in Chapter 5.) Using equation (5.34), therefore, with $\tau_i = \tau_{im}$:

$$s_c = \sigma_{fu} / [2\tau_{im}] \quad (8.3)$$

we can estimate the mean apparent shear strength:

$$\tau_{im} = 3 \sigma_{fu} r / [4 L_m] \quad (8.4)$$

The strengths of many fibres used as reinforcements are flaw controlled, so that σ_{fu} is greater for short lengths than long lengths. Typical values for the critical length can be as small as 0.3mm, so σ_{fu} used in equation (8.4) must be the correct value for this order of length. This is done by testing a longer length, e.g. 25mm and using a statistical analysis, usually one originally developed by Weibull, to estimate the strength at the shorter length.

(The use of the fragmentation method led to our understanding of the weak bonding obtained with carbon fibres which were not oxidatively surface treated. Fig. 8.5 (left) shows results obtained which gave birth to the suggestion that the fibres had a soft carbon layer on them that was removed by the oxidation. That it was carbon was recently confirmed using the laser Raman technique. When untreated carbon fibres were pulled out of a polymer, carbon could still be detected inside the holes they left; see Fig. 8.5 at right.)

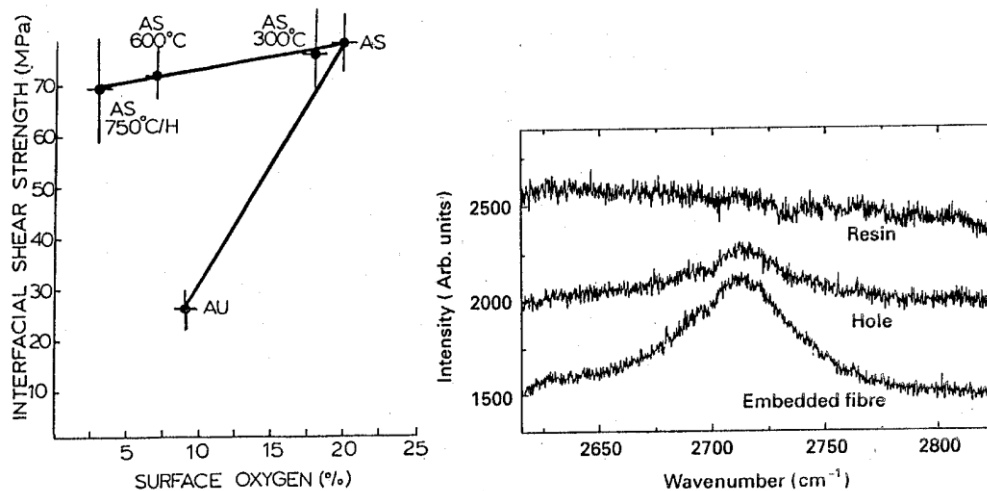


Fig. 8.5 At left, apparent interface strength from fragmentation tests and at right, confirmation that carbon remains behind in the hole left when a non-surface treated carbon fibre is pulled out. (After Drzal, L.T., 1983, SAMPE J., 19, # 5, 7-13 and Gu, X.H., Young, R.J. and Day, R.J., 1995, J. Mater Sci. 30, 1409-19.)

8.3 Problems with Direct Interface Measurements

Unfortunately, there are problems on at least three levels with these methods. These include a) stress concentrations b) failure processes and c) whether such a property as an interface shear strength has any physical meaning. Because of these difficulties, the subject has become highly mathematical, but fortunately the problems can be understood without going into higher mathematics.

8.3.1 Stress Concentrations in the Pull Out Experiment

We use the analysis presented in section 5.1, but with different boundary conditions. Before any debonding has occurred, we let the stress on the fibre at the point it enters the polymer be σ_{femax} , and within the polymer we let it be σ_{fe} . Thus $\sigma_{fe} = \sigma_{femax}$ at $x = 0$. We assume no stress transfer across the fibre end; hence $\sigma_{fe} = 0$ at $x = L$; see Fig. 8.6.

With these boundary conditions and with $\epsilon_1 = 0$ (i.e. we neglect any tensile stresses in the polymer), equation (5.17) gives

$$\sigma_{fe} = \sigma_{femax} \sinh[n(l-x)/r]/[\sinh(ns)] \tag{8.5}$$

Here

$$n = \sqrt{E_m/[E_f(1 + \nu_m)\ln(R/r)]} \tag{8.6}$$

$2R$ being the diameter of the matrix, which is assumed to be a cylinder; see equations (5.5) and (5.15). Using equation (5.11) we can estimate the shear stress, τ_e , causing this elastic stress transfer:

$$\tau_e = \frac{1}{2} n \sigma_{femax} \cosh[n(l-x)/r]/[\sinh(ns)] \tag{8.7}$$

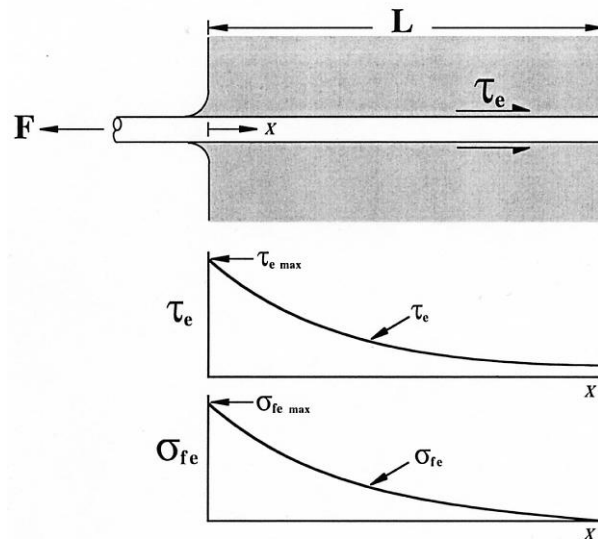


Fig. 8.6 Schematic drawing of pull out specimen before debonding showing interfacial shear stress τ_e and fibre stress σ_{fe} as envisaged in simple models.

which is a maximum for $x = 0$. This gives

$$\tau_e = \frac{1}{2} n \sigma_{f_{max}} \coth(ns) \quad (8.8)$$

If we suppose that $\tau_{e_{max}}$ cannot exceed some maximum apparent interface shear strength, τ_{iu} , we can determine the fibre stress when debonding starts. Thus, in equation (8.5), let $\sigma_{f_{max}} = \sigma_{fA}$ when $\tau_{e_{max}} = \tau_{iu}$, so that

$$\sigma_{fA} = 2 \tau_{iu} \tanh(ns)/n \quad (8.9)$$

In pull out experiments with ductile matrices we might expect interface yielding at a lower stress, τ_{iy} , with a corresponding maximum fibre stress $\sigma_{f_{max}} = \sigma_{fy}$ where

$$\sigma_{fy} = 2 \tau_{iy} \tanh(ns)/n \quad (8.10)$$

With either debonding initiation or matrix yielding we expect the plot of pulling force vs distance moved by the force to show a transition. Before yielding and debonding the behaviour should be elastic and reversible. Thus the plot should be linear up to the transition. After the transition the compliance should increase and so the plot starts to curve away. Such behaviour is apparent in both plots in Fig. 8.2.

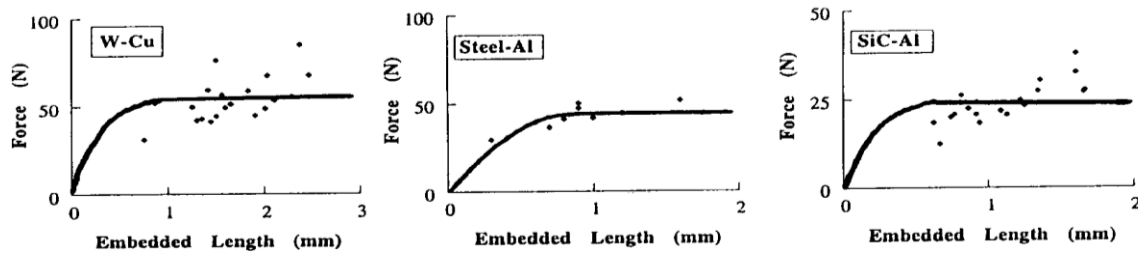


Fig. 8.7 Force at first transition in pull out curve for metal matrix systems fitted to equation (8.10) by choice of τ_{iy} . (After Ravichandran, M.V., Piggott, M.R., Coyle, T.W., and Thorpe, S.J., 1996, *Composites Interfaces* 3, 343-69.)

In the case of reinforced metals, this behaviour has recently been examined in detail. Fig. 8.7 shows the force at the transition plotted vs. embedded length for three different systems. The curves were plotted using equation (8.10) with τ_{iy} chosen for the best fit. The fits are not very good, but more serious, the τ_{iy} values needed were high: for steel-Al τ_{iy} exceeded the tensile yield stress.

Metals are normally found to yield approximately according to the von Mises criterion, i.e. $\tau_{my} = \sigma_{my} / \sqrt{3}$ (This is a little higher than the Tresca criterion of $\frac{1}{2} \sigma_{my}$ see equation (1.12) and the line beneath it.) When the τ_{iy} values are compared with $\sigma_{my} / \sqrt{3}$, the only agreement seen was for steel pulled out of aluminium alloy. Thus metal yielding was not convincingly demonstrated. (Note that, if the metal had already yielded before the pull out test was performed, because of differential thermal shrinkage, the transition could correspond to the initiation of further yielding, or debonding.)

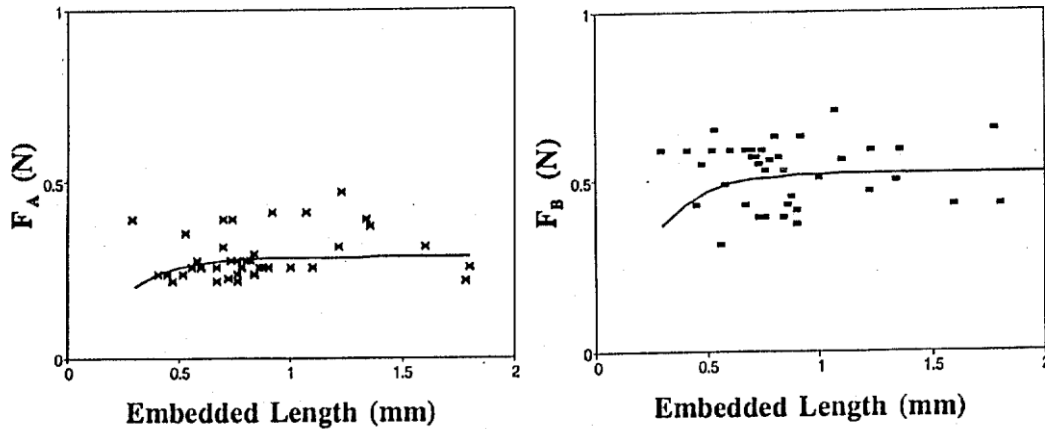


Fig. 8.8 Forces at first and second transitions in pull out curves for glass-epoxy. (After Piggott, M.R., and Xiong, Y., 1996, ASTM STP 1290, 84-99; see also Chen, P. and Piggott, M.R., 1998, J. Thermoplastic Comp. Mater, 17, 33-45.)

In the case of reinforced plastics, two transitions are often observed as can be seen in Fig. 8.2 for glass - LDPE. These have been examined for the glass-epoxy system and the carbon-PEEK system. Fig. 8.8 shows the glass-epoxy results for the first and second transitions. The results can be seen to be even more scattered than with metal systems. The curves shown were fitted to equations (8.9) and (8.10) with $\tau_{iy} = 25 \pm 6$ MPa and $\tau_{iu} = 44 \pm 8$ MPa. If we compare the τ_{iy} value with the yield stress for the polymer as defined in equation (6.9), it appears to be a little low, but taking into account uncertainties in the curve fit, the value is not unreasonable so. The value obtained for carbon-PEEK, i.e. 65 ± 25 MPa covers a wide enough range to be consistent with the shear yield strength.

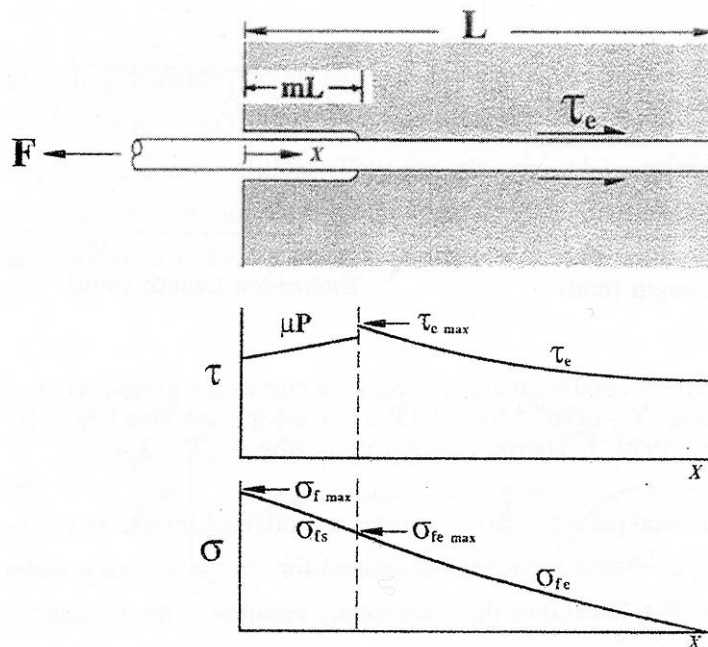


Fig. 8.9 Schematic drawing of pull out specimen which has partly debonded and with frictional stress constant.

We could use the second transition to estimate τ_{iu} . However, two transitions are not always observed, and in any case, most researchers use the maximum force.

Unfortunately the maximum force can be affected by friction during debonding. For simplicity, we will neglect the Poisson's shrinkage of the fibre for the moment, and assume that the debonded zone, length mL , is subject to a constant interfacial shear μP_0 , see Fig. 8.9, where μ is the coefficient of friction and P_0 is the polymer shrinkage pressure. We proceed as for equation (8.4), except our boundary conditions are $\sigma_{fe} = \sigma_{femax}$ at $x = mL$. This changes equation (8.5) to

$$\sigma_{fe} = \sigma_{femax} \sinh[n(l - x)/r]/\sinh(n\bar{s}) \tag{8.11}$$

for $x \geq L(1 - m)$, with

$$\bar{s} = s(1 - m) \tag{8.12}$$

For $x < mL$ we use equation (5.11) with τ_i replaced by μP_0 and integrate i.e.

$$\int_{\sigma_{fe\ max}}^{\sigma_{fs}} d\sigma_f = -2\mu P_0 \int_{mL}^x \frac{dx}{r} \tag{8.13}$$

which gives

$$\sigma_{fe} = \sigma_{femax} + 2\mu P_0 (mL - x) \tag{8.14}$$

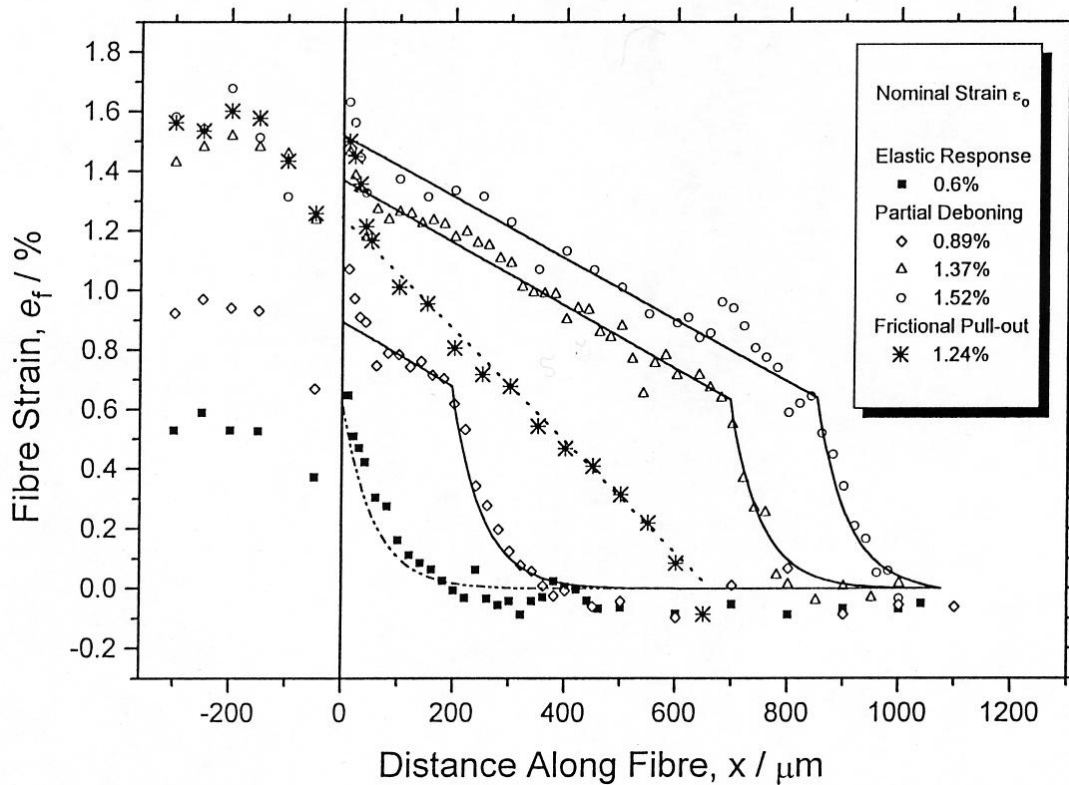


Fig. 8. 10 Laser Raman results for Kevlar epoxy fibre pull out experiment (After Andrews, J.C., Bannister, D.J., and Young, R.J., 1996, J. Mater. Sci. 31, 3893-913.)

As before, we let $\sigma_{f_{max}} = \sigma_{fA}$ when $\tau_{e_{max}} = \tau_{iu}$ [see equation (8.9)]. The maximum fibre stress $\sigma_{f_{max}}$ is at the fibre entry point, i.e. $x = 0$. Thus

$$\sigma_{f_{max}} = 2\mu P_0 ms + 2\tau_{iu} \tanh(ns)/n \quad (8.15)$$

Laser Raman results with polymer fibres which do not bond very strongly show that the treatment, although much simplified, can fit the results very well. Fig. 8.10 shows the stresses in the fibres. First they decrease linearly from the entry point, as expected from equation (8.14). Then they decrease according to equation (8.11). Different levels of fibre stress give different amounts of the linear and hyperbolic regions. $\sigma_{f_{max}}$ appears to be constant, with $\epsilon_f \cong 0.7\%$, and with τ_{iu} about 40MPa.

The maximum shear stress is thought to be underestimated using these equations. Finite element analyses (FEA) give higher stresses near the entry point than predicted by equation (8.7); see Fig. 8.11. They also give high stresses close to the fibre embedded end, where according to equation (8.8), they should be approaching zero. For short embedded lengths these stresses can be higher than those at the entry point. Furthermore, using FEA we have $\tau_i = 0$ at the fibre entry point. The smaller the elements, the more sharp the fall. The laser Raman method is not sensitive enough to detect this nil shear stress, nor to detect the sharp peaks shown in Fig. 8.11.

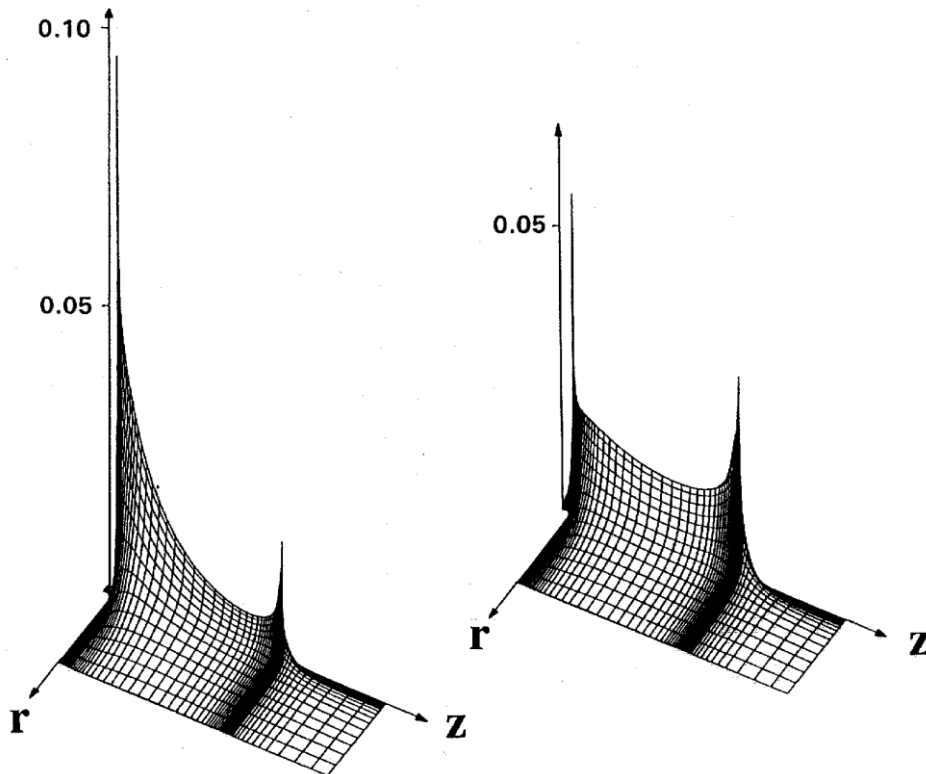


Fig. 8.11 Finite element results for interfacial shear stresses in pull out experiment for glass at left, and carbon at right, in polycarbonate matrix. (After Marotzke, C, 1994, Comp. Sci. Tech.

The very high stresses close to the entry point are reduced by the meniscus there. Unless steps are taken to prevent it, the surface tension causes a capillary rise effect. However, if the system is allowed to equilibrate, the meniscus is small.

This is because the meniscus has two curvatures R_1 and R_2 , see Fig. 8.12. R_1 is the curvature as the meniscus is traced in the radial direction, and R_2 is the circumferential radius of the meniscus. The reduction in pressure of the liquid beneath the meniscus, P , is given by

$$P = \psi (1/R_1 - 1/R_2) \quad (8.16)$$

and R_1 represents concavity (reduced pressure) and R_2 represents convexity (increased pressure). Thus the pressure under the meniscus is very much less than for a meniscus inside a capillary of internal diameter equal to the external diameter of the fibre. (ψ is the surface tension and surface energy of the liquid.)

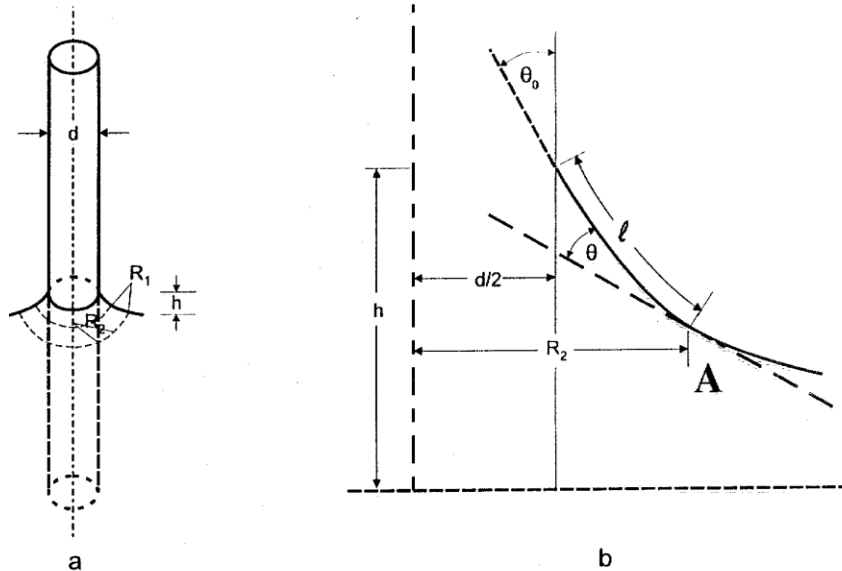


Fig. 8.12 Meniscus at the point of entry into a polymer (a) schematic drawing, (b) details of meniscus.

The capillary rise, h (see Fig. 8.12b) can be treated as a bounding value problem. Equation (8.16) requires that R_1 is everywhere less than R_2 . Consider any point A on the meniscus, Fig. 8.12b. Since R_2 is the distance between the fibre axis and A, it must be less than the distance l along the meniscus, plus half the fibre diameter. Hence, the upper bounding value for R_1 is

$$R_1 = l + d/2 \quad (8.17)$$

Using intrinsic co-ordinates, l for arc length and θ for angle, equation (8.17) may be rewritten

$$d\theta/dl = l + d/2 \quad (8.18)$$

This integrates with $\theta = \theta_0$ at $l = 0$ (Fig. 8.12b) to give

$$l = d(e^{\theta-\theta_0} - 1)/2 \quad (8.19)$$

For zero contact angle, $\theta_0 = 0$, l is a maximum, so the upper bound of the distance along the arc to the point where the surface of the liquid is horizontal ($l = \pi/2$) is given by

$$l = \frac{d}{2}(e^{\pi/2} - 1) \quad (8.20)$$

and since R_1 increases monotonically with l , the upper bound of h is $2l/\pi$, i.e.

$$h < \frac{d}{\pi}(e^{\pi/2} - 1) \quad (8.21)$$

which comes to

$$h < 1.22d \quad (8.22)$$

Thus the capillary rise, at equilibrium, has an upper bound which is little more than the fibre diameter.

8.3.2 Stress Concentrations in the Fragmentation Experiment

The fragmentation test, which involves a fully embedded fibre, is analysed following the treatment in section 5.3. In section 5.3.1 we estimated the critical aspect ratio, s_c , assuming that τ_i is constant. Fig. 8.13 (left) shows the situation envisaged for fibres with $s < s_c$, $s = s_c$ and $s > s_c$.

We start by reviewing the simplest treatment, which was suggested for metals in Section 5.3.2. Fig. 5.11 shows the interface shear assumed, and the corresponding fibre stresses. With $\tau_i = 0$ in the middle section of the fibre, the fibre and matrix strains are the same there. Thus

$$\sigma_{f\max} = E_f \varepsilon_1 \quad (8.23)$$

Equation (5.44) with the matrix stress equal to $E_m \varepsilon_1$, and with equation (5.45) for m , and equation (8.23) for σ_{\max} gives

$$\sigma_1 = V_f E_f \varepsilon_1 (1 - E_f \varepsilon_1 / [4s \tau_{my}]) + V_m E_m \varepsilon_1 \quad (8.24)$$

This, with $E_{1s} = \sigma_1 / \varepsilon_1$, can be rearranged to give

$$E_{1s} = E_1 - V_f E_f^2 \varepsilon_1 / [4s \tau_{my}] \quad (8.25)$$

where E_1 is the Rule of Mixtures modulus, equation (4.3).

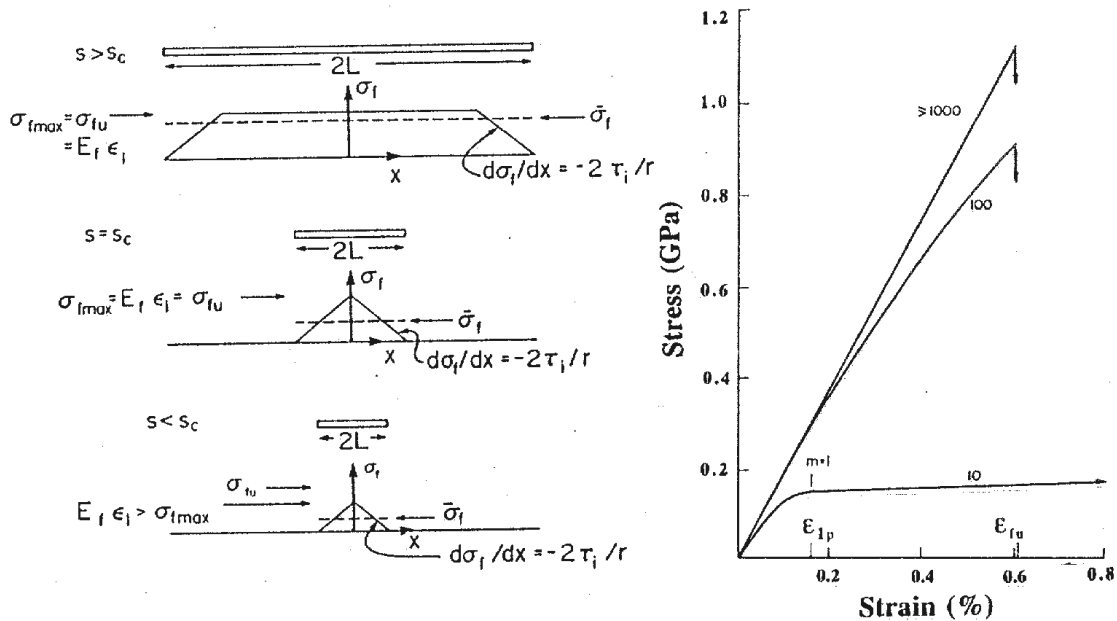


Fig. 8.13 Fibres with lengths greater than, equal to and less than the critical value, with stresses σ_f , σ_{fmax} , etc. as envisaged in simple model, at left. At right is composite stress-strains plots given by equation (8.25) for $\tau_{my} = 25\text{MPa}$ and $V_f = 0.55$. Aspect ratios marked on the curves.

The stress-strain plots should be curved, with E_{1s} continuously decreasing as strain is increased. Examples of such theoretical plots, for fibres with different aspect ratios, are shown in Fig. 8.13, at the right. These are not observed in practice⁺.

The assumption of $\tau_i = 0$ in the central length of the fibre is, unfortunately, rather too simplistic. Early analyses showed that, in this region, elastic stress transfer should be taking place. Fig. 8.14 shows the interface stress and resulting fibre stresses envisaged.

The fibre end regions experience approximately constant shear stresses which are frictional in the fibre fragments in the fragmentation test. Thus we replace τ_{my} with μP_0 where, as for equation (8.13), μ is the friction coefficient and P_0 is the interfacial pressure which, again, we will assume to be constant. Using the treatment in section 5.3.2 with σ_{fmax} replaced by σ_{fi} , we obtain

$$\sigma_{fi} = 2\mu P_0 ms \tag{8.26}$$

For the central region we use equation (5.17) with n given by equation (8.6) and boundary conditions $\sigma_{fe} = \sigma_{fi}$ at $x = \pm L(1-m)$. This gives

$$\sigma_{fe} = E_f \epsilon_1 - (E_f \epsilon_1 - \sigma_{fi}) \cosh[nx/r] / \cosh(n\bar{s}) \tag{8.27}$$

with \bar{s} defined in equation (8.12).

⁺ The claim in Kelly's book, "Strong Solids" (2nd Edition), see Fig. 5.12 therein, does not withstand careful scrutiny of the original paper.

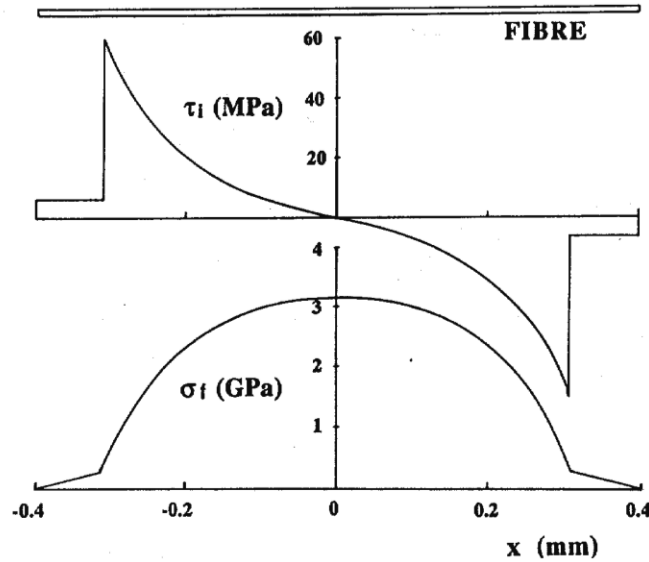


Fig. 8.14 Modification of simple single fibre model to include elastic stress transfer.

The highest shear stresses are now at the boundaries of the elastic stress transfer region. We will again suppose that these cannot exceed some apparent interfacial shear strength τ_{iu} . Thus differentiating equation (8.21) and multiplying by $r/2$ as before (see equations (5.18) and (5.19)), then evaluating τ_e at $x = \pm L(1-m)$. gives

$$\tau_{iu} = \frac{n}{2}(E_f \varepsilon_1 - \sigma_f) \tanh(n \bar{s}) \tag{8.28}$$

This, and the earlier treatment in section 5.1 appears to work very well in some cases. Fig. 8.15a shows the strains in a single fully bonded P55 carbon fibre in epoxy, as estimated using the laser Raman technique. The fibre was 1mm long with a diameter of $2r = 10.7\mu m$, and had a Young's modulus of 379GPa. The resin bar was 3mm thick, had $E_m = 2.9$ and $\nu_m = 0.4$. Thus n came to about 0.031.

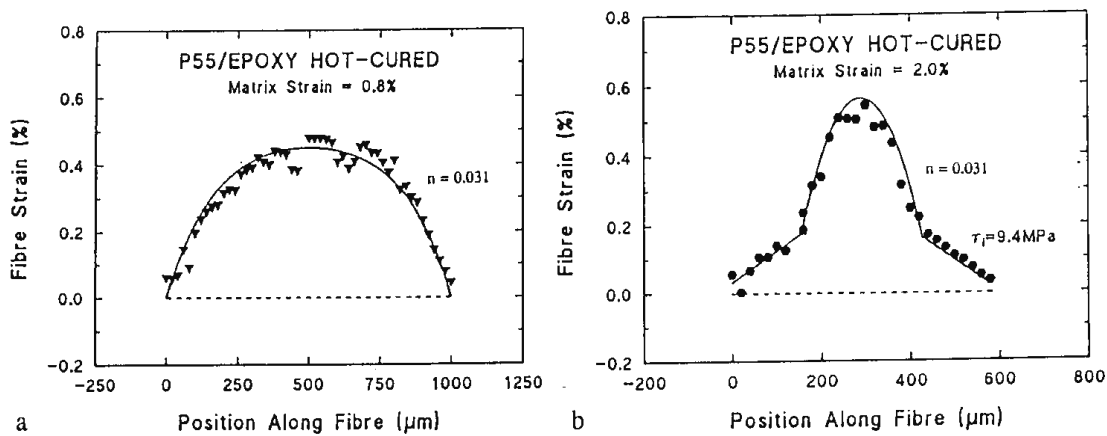


Fig. 8.15 Laser Raman results for a single P55 carbon embedded in epoxy (a) before fragmentation and (b) one fragment after fragmentation (After Huang, Y. and Young, R.J., 1995, Composites 26, 541-50.)

The curve fit was made using equation (5.18) with these data, except that 0.48% was used for ε_1 , since there was a residual strain of about -0.32% in the fibre prior to stressing. (This came about because of the relative polymer shrinkage after the 80°C cure. $\Delta\alpha\Delta T$ came to about 64.5×60 microstrain = 0.39% and stress relaxation probably accounts for the remaining 0.07% strain. Here $\Delta\alpha$ is the difference between the thermal expansion coefficients of polymer and fibre and ΔT is the change in temperature from the T_g or thereabouts, to the test temperature.) This figure should be compared with Fig. 5.4.

Fig. 8.15b shows a P55 fibre which has been fragmented. The fragment shown has a length of about 0.6mm. This figure is very similar to the fibre stress plot shown in the lower half of Fig. 8.14. For $x > L(1-m)$ the frictional shears, μP_0 , come to about 9.4MPa. From the slope at $x = \pm L(1-m)$ we find that $\tau_{iu} \cong 64$ MPa. Using equation (8.28) with $\sigma_{fi} / E_f = 0.17\%$ and $\varepsilon_1 = 1.68\%$ (i.e. $2.00 - 0.32$) gives $\tau_{iu} = 80$ MPa. Thus the curve fit seems to be underestimating τ_{iu} somewhat. This is not surprising when the statistical errors in evaluating the fibre strains are taken into account. The slope is changing rapidly at $x = L(1-m)$ so it is easy to underestimate the true value.

The difference between τ_{im} and τ_{iu} is large. In the case shown in Fig. 8.15b, τ_{im} , using equation (8.4) with σ_{fu} estimated directly from fragment breaking strains comes to 22MPa. This is barely one third of τ_{iu} .

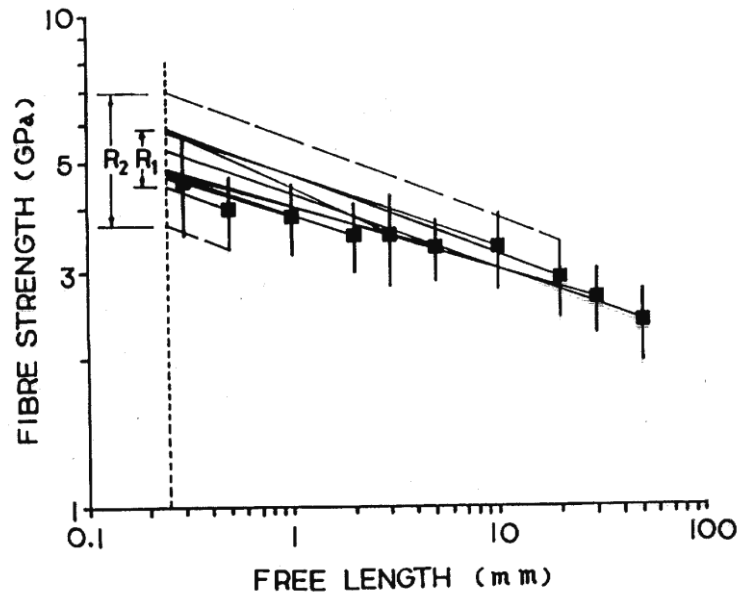


Fig. 8.16 AS4 carbon fibre strengths measured at different lengths, (After Dai, S.R., and Piggott, M.R., 1993, *Comp. Sci. Tech.* **49**, 81-7.)

One further note on inaccuracies in the fragmentation test concerns the evaluation of σ_{fu} . Most researches have used some extrapolation from tests at lengths longer than L_c . This is bad science. Extrapolations should only be used when unavoidable. To illustrate the errors associated with such extrapolations, Fig. 8.16 shows tests on short lengths of

carbon fibres. The lines going back to 0.25 mm free length are Weibull extrapolations. Their intersections range from about 4.5 to 6.0GPa. (Most researchers use the Weibull analysis.) The \pm one standard deviation limits have also been extrapolated. These give the range R_2 shown.

It is thus not surprising that fragmentation and pull out experiments give different values for τ_{im} . As Fig. 8.17 shows, they do not even correlate very well. Note especially the region marked A.

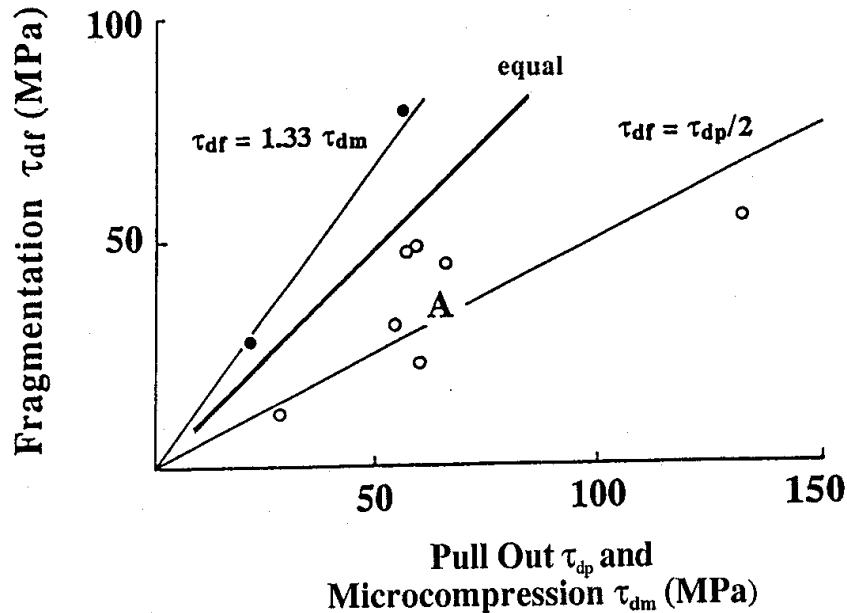


Fig. 8.17 Apparent interfacial shear strengths as measured by fragmentation test vs that measured by single fibre pull out. Also shown are microcompression results. (After Jacques, D. and Favre, J.P., 1987, Proc. ICCM VI, 5.471-80, and Mandell, J.F., Grande, D.F., Tsiang, T.H. and McGarry, F.J., 1986, ASTM STP 893, 87-108.)

8.3.3 The Value of n

Some advocates of the Raman technique consider that they have shown experimentally that the fragmentation test is invalid. The reader will by now appreciate that there are good physical reasons why this should be so.

There is also a fairly strong feeling that the Cox approach may be invalid. This is because curve fitting can give anomalous values for n . Table 8.1 shows some values of n , n_{exp} say, obtained by determining "half heights", $h_1/2$ from laser Raman plots for pull out and fragmentation. To determine $h_1/2$, we first determine the asymptotic values i.e. when $\sinh[nx/r]/\sinh(n\bar{s})$ for pull out, or $\cosh[nx/r]/\cosh(n\bar{s})$ for fragmentation, are very close to 1.0. Then we take any other point on the elastic part of the curve, determine its height, h_1 , and its abscissa, x_1 , say. Then we find the value of x for $h_1/2$. Let this be x_2 ; see Fig. 8.18a for the pull out case and Fig. 8.18b for the fragmentation case.

As an exercise (problem 8.6), the reader should show, using equations (8.11) and (8.27) and others, that for all but the shortest fibres,

$$n \cong r \ln 2 / |x_2 - x_1| \quad (8.29)$$

Using the absolute value makes it possible to apply equation (8.29) to the right hand end of the single short fibre composite or the fragmentation plot. If this is done it is found that the left end and right end values can differ somewhat.

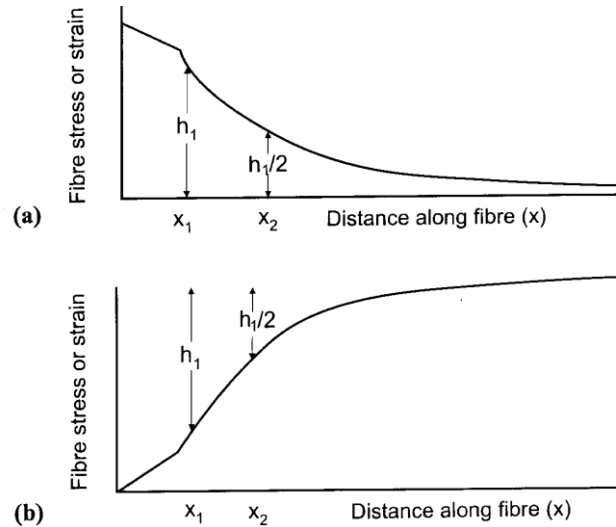


Fig. 8.18 Illustrating a simple method for estimating n from Raman results (a) for fibre pull out and (b) for fragmentation configurations.

This observation has led some to propose that R/r should be adjusted to fit the results, using an effective R , and supposing that the stresses die away from the axis in some different fashion from that given in equation (5.2). Since this equation involves a force equilibrium, this approach is questionable.

In any case, R/r appears as a logarithm, and for n , we go further and take the square root of this, equation (8.6). Thus R can vary from $5r$ to more than $10^{15}r$ to satisfy the experimental n values given in Table 8.1.

A more cogent approach is to suppose that the development in section 5.1 is faulty in some way so that a radically new approach is needed. The problems are as follows:

- a) shear in the fibre is neglected
- b) tensile strains in the matrix are assumed to be constant
- c) stress transfer across the fibre ends is ignored
- d) stress concentrations due to sharp corners near the fibre ends are not taken into account
- e) shear stresses should be zero at the fibre end in the single fibre composite, and at the fibre entry point in the pull out experiment.

With the appropriate boundary conditions, most of these problems may be resolved.

Table 8.1 Comparison of Experimental (n_{exp}) and Theoretical (n_{theory}) values of n .

1000n Test Type		$n_{\text{exp}} / n_{\text{theory}}$		System
32	Frag	0.90 (left end)	1.06 (right end)	P55 C-epoxy ¹
35	Frag	1.03 ^a (left)	-	Al ₂ O ₃ -epoxy ²
35	Frag	1.41 ^a (left)	-	Al ₂ O ₃ -epoxy ²
53	Pull Out	1.47 ($\epsilon_f = 0.4\% \& 0.5\%$)	0.82 ($\epsilon_f = 0.9\%$)	Twaron ^b -PP ³
57	Frag	1.39 (left)	1.79 (right)	Kevlar-epoxy ⁴
221	Frag	0.35 ^c (left)	0.5 ^c (right)	Al ₂ O ₃ -ZrO ₂ -glass ⁵
221	Frag	0.27 ^d (left)	0.45 ^d (right)	Al ₂ O ₃ -ZrO ₂ -glass ⁵

Notes:

a) Excellent fit to Cox theory; authors' values, b) polyaramid fibre in polypropylene, c) No strain, d) 0.05% applied strain

References

- 1 Y. Huang and R.J. Young, *Composites* **26**, (1995), 541-50
- 2 R.B. Yaltee and R.J. Young, *Composites* **29A** (1998), 1353-62
- 3 M. Heppenstall-Butler, D.J. Bannister and R.J. Young, *Composite*, **27A**, (1996), 833-8.
- 4 C. Galiotis, *Comp. Sci. Tech.* **42**, (1991), 125-50.
- 5 R.J. Young and X. Yang, *Composites* **27A**, (1996), 737-41.

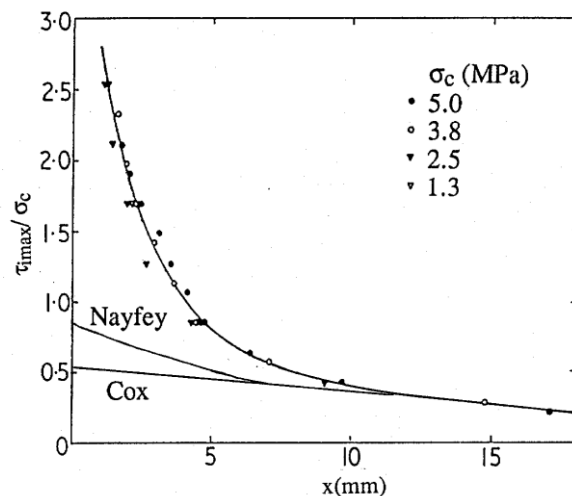


Fig. 8.19 Results from photoelastic analysis of a model system containing an approximately square (4mm x 4.7mm) aluminum alloy rod embedded in epoxy (solid line) compared with two theories (dashed lines). (After Tyson, W.R., and Davis, G.J., 1965, *Brit. J. Appl. Phys.* **16**, 199-205, Cox, H.L., 1952, *ibid.*, **3**, 72-9 and Nayfeh, A.H., 1977, *Fib. Sci. Tech.* **10**, 195-209.)

There have been many attempts to do this. Fig. 8.19 shows a comparison of early experimental results with a theory that appeared many years later. The experiments were not axisymmetric, so the Cox equations (which are described here in section 5.1) and the Nayfeh equations had to be modified slightly to allow for this. As can be seen, the Nayfeh equation is only marginally better. A more recent approach uses Bessel functions, and an adjustable parameter, D , to fit the curves. Fig. 8.20 shows this fitted to some Raman results for a single short fibre composite. Clearly a precise fit cannot be achieved due to experimental variability.

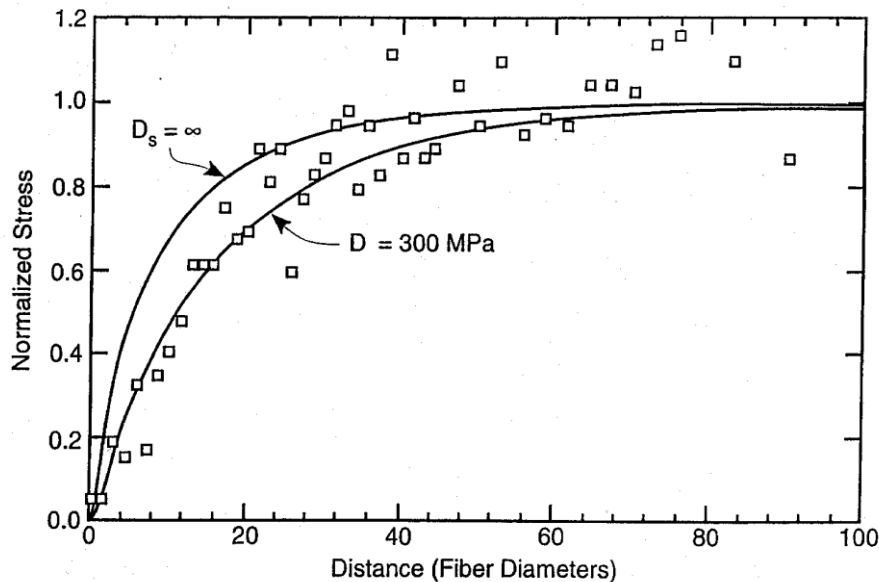


Fig. 8.20 Nairn's " D " fitted to Raman results for a single 390 GPa modulus carbon fibre fully embedded in epoxy. (After Nairn, J.A., and Liu, Y.C., 1997, *Int. J. Solids Structures*, 34, 1255-81.)

Cox may be being unjustly criticized. The failure to have correct boundary conditions may not always be very serious. For example, at the fibre end in the single fibre composite, or at the fibre entry point, the shear stress must be zero. This is interpreted as meaning that the shear stress in the polymer must be zero. An interesting point then arises. As can be seen from the finite element results in Fig. 8.11, the shear stress peak is roughly 0.64 diameters from the fibre end. Is this the correct position for the peak? Apparently not. The finer the finite element mesh, the closer the peak is to the entry point. Thus, if we make the mesh so fine that each node corresponds to an atom or less, it should be possible to have the peak right at the entry point.

That the peak actually is at the entry point can be justified, if we take into account the atomic nature of materials. Imagine the fibre and polymer being made up of cubes or balls joined by springs, as for the dislocation in Fig. 2.4a. In the present case, we have two types of spring: stiff ones, represented by rods for the fibre, and flexible ones as in Fig. 2.4a for the polymer; see Fig. 8.21. Clearly the top fibre atom in column #4 experiences a shear stress (and a tensile stress) while the fibre atom in column #3 does not. Meanwhile, all the atoms in the polymer experience shear stresses.

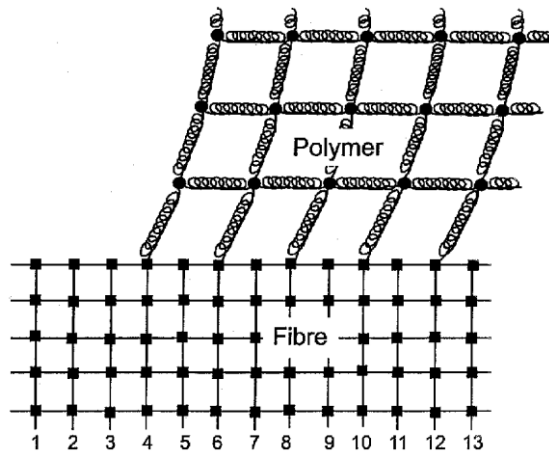


Fig. 8. 21 Atomistic model showing that the shear stress starts at the first atom inside the polymer in the pull out experiment. (The shear stress has a step function there.)

The same applies to the single fibre composite. Thus to devise a complex mathematical formalism to show shear stresses falling to zero at a small distance from the end may not be necessary.

The Cox approach is essentially very simple and works particularly well when $E_f \gg E_m$ as can be seen for the polymer matrix results in Table 8.1. This is obvious when it is expressed in dimensionless form, i.e.

$$\frac{d^2 \varepsilon_f}{dx_d^2} = n^2 (\varepsilon_f - \varepsilon_1) \tag{8.30}$$

with $x_d = x/r$ and ε_1 approximately constant. In this equation n appears in the role of a strain equalization coefficient.

Furthermore, the Cox theory can be fitted very well to the elastic parts of both pull out and fragmentation results from Raman studies. This suggests that equation (8.30) truly represents the physical processes involved. The only problem is the value of n .

There is a precedent for this. Equation (2.15) has been extraordinarily successful in predicting results from fracture tests, and is the basis for what might be termed a "fracture industry". However, the value of ψ is several orders of magnitude too low: we use \mathcal{G} instead. n (Table 8.1) is much less than one order of magnitude in error and can be very close to the theoretical value. We could, therefore, take the ratio $n_{\text{exp}}/n_{\text{theory}}$ to be the strain transfer efficiency factor.

We have already seen that it may not be reasonable to adjust R . Nevertheless, it may be reasonable to look for reasons to adjust the elastic constants, E_m and E_f . (We have already noted in section 6 that E_m may need adjustment to explain experimental results for E_2). Too high a value of n_{exp} in a polymer matrix composite, suggests that E_m needs

adjusting upwards or E_f downwards (e.g. a fibre skin effect - both Kevlar and carbon are good candidates for this). Too low a value suggests reducing E_m . In the case of the reinforced glass in Table 8.1, it may be worth looking for an interphase with the appropriately reduced properties.

With fragmentation it is important to allow for any damage to the fibre embedded end. Polymer fibres can fibrillate when cut, providing a sort of anchor at the end. This can invalidate estimates of n_{exp} derived from measurements at the initial fibre ends.

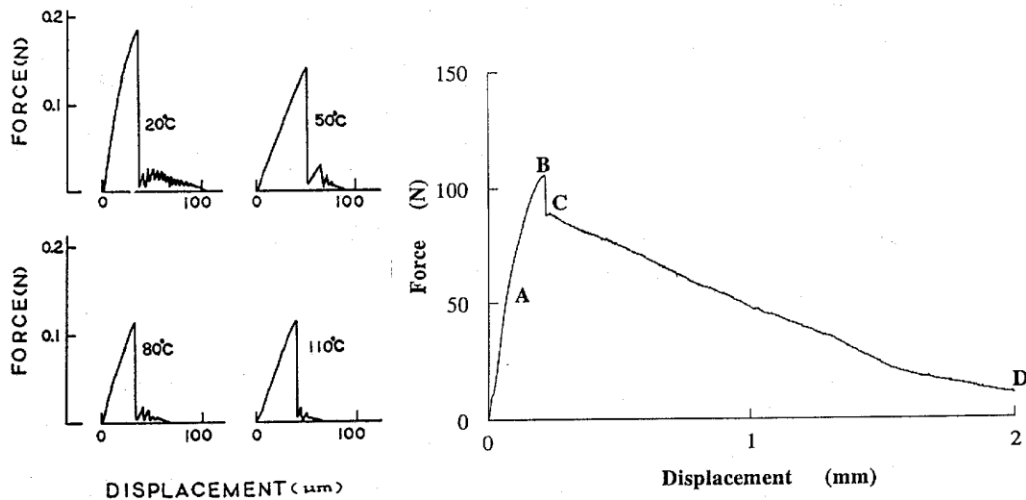


Fig. 8.22 Force-distance plots, at left, for carbon pulled out of epoxy at different temperatures. and at right, for tungsten-copper at 20°C (After Piggott, M.R., and Wang, Z.N., 1991, Proc. Amer. Soc. Comp. 723-31, and Ravichandran, M.V., Piggott, M.R., Coyle, T.W., and Thorpe, S.J., 1996, Comp. Interfaces 3, 343-69.)

8.3.4 Brittle Failure

In the pull out test the final failure is normally sudden. This is found, even for ductile metal matrices such as copper or aluminium when tested at room temperature; see Fig. 8.22 at right and also for ductile polymer matrices such as polyethylene; see Fig. 8.2a. (The apparent ductility for tungsten-copper at 300°C also shown in Fig. 8.2b seems to be unusual. Fig. 8.22, at left, shows that failure is still sudden with carbon-epoxy at 100°C.)

Further evidence that it is a brittle process comes from the large scatter in the maximum pull out forces. Fig. 8.23 shows results from both metals and polymers, again ductile ones. These show the same variability as is observed when testing the strength of brittle materials such as glass.

The same observations are made in the microtension test. The fragmentation experiment does not lend itself to analysis of the failure process, but it is widely accepted that here too, the process is probably brittle.

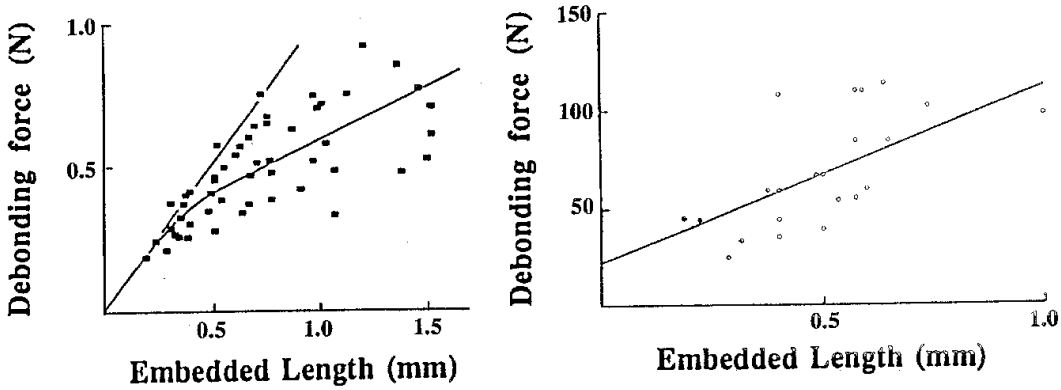


Fig. 8.23 Debonding force vs embedded length for pull out from ductile matrix systems. At left is glass-polyethylene and at right is steel-Al alloy.

For pull out, a simple analysis can give insight into brittle failure. When the fibre is pulled, both fibre and matrix store strain energy. For the fibre, this is U_f , given by

$$U_f = \frac{1}{2} \int \sigma_{fe} \varepsilon_f dV \tag{8.31}$$

where V is the volume of fibre involved, i.e. πr^2 per unit length. With the x axis as shown in Fig. 8.6, and replacing ε_f by σ_{fe} / E_f ,

$$U_f = \frac{\pi r^2}{2E_f} \int_0^L \sigma_f^2 dx \tag{8.32}$$

for an embedded length L , and using equation (8.5) for σ_{fe} gives

$$U_f = \frac{\pi r^2 \sigma_{fe \max}}{2E_f \sinh^2(ns)} \int_0^L \sinh^2(n[L-x]/r) dx \tag{8.33}$$

Remembering that $2\sinh^2 y = \cosh 2y - 1$ this integrates to give

$$U_f = \pi r^3 \sigma_{f0}^2 (\coth(ns) - n \bar{s} / \sinh(ns)) / [4n E_f] \tag{8.34}$$

after inserting the limits, and doing some re-arrangement.

For the matrix, the strain energy U_m is the displacement u_m , multiplied by the force, i.e. τ_e , times the area over which it operates. Thus

$$U_m = \int_0^L u_m \tau_e \pi r dx \tag{8.35}$$

u_m is the complement of u_f in equation (5.5) with u_R assumed to be zero. Therefore, using this equation with $u_m = u_f$ and $u_R = 0$, gives

$$U_m = \frac{\pi r^2 \ln(r/R)}{G_m} \int_0^L \tau_e^2 dx \quad (8.36)$$

Using equation (8.7) for τ_e and equation (8.6) for n (remember $G_m = E_m / [2\{1 + \gamma_m\}]$) this comes to

$$U_m = \frac{\pi r^2 \sigma_{fe}^2}{2E_f \sinh^2(ns)} \int_0^L \cosh^2[n(l-x)/r] dx \quad (8.37)$$

which on integration and re-arrangement gives

$$U_m = \frac{\pi r^3 \sigma_{fe}^2}{4nE_f} \left(\coth(ns) + \frac{ns}{\sinh^2(ns)} \right) \quad (8.38)$$

The total energy is U_e where

$$U_e = U_f + U_m \quad (8.39)$$

so substituting from equations (8.24) and (8.29) we get

$$U_m = \frac{\pi r^3 \sigma_{fe}^2}{2nE_f} \coth(ns) \quad (8.40)$$

We now follow the treatment used in section 2.3.2. Suppose the fibre debonds over a length dL at the point where it enters the polymer. Surface energy dU_s is required, given by

$$dU_s = 2\pi r \mathcal{G}_i dL \quad (8.41)$$

Also, the fibre, over a length dL , has elastic energy dU_{fe} , given by

$$dU_{fe} = \pi r^2 \sigma_{fe}^2 dL / [2 E_f] \quad (8.42)$$

and the fibre remaining adhered to the polymer, and the polymer itself, suffers a change in energy dU_e given by the differential of equation (8.40):

$$\frac{dU_e}{dL} = \frac{\pi r^2 \sigma_{fe}^2}{2E_f} \operatorname{cosech}(ns) \quad (8.43)$$

As for equation (2.31), we need dU (total)/ dL . Summing equations (8.41), (8.42) and (8.43) for dU (total)/ dL , putting this equal to zero gives

$$\frac{dU_{total}}{dL} = 0 = 2\pi r \mathcal{G}_i + \frac{\pi r^2 \sigma_{fe}^2}{2E_f} - \frac{\pi r^2 \sigma_{fe}^2}{2E_f} \operatorname{cosech}(ns) \quad (8.44)$$

and since $1 - \operatorname{cosech}^2(ns) = -\coth^2(ns)$, this gives

$$\sigma_{fe} = 2 \sqrt{E_f \mathcal{G}_i / r} \tanh(ns) \quad (8.45)$$

If we write

$$\tau_d = n \sqrt{E_f \mathcal{E}_i / r} \quad (8.46)$$

then equation (8.45) is the same as equation (8.9) with τ_d replacing τ_{iu} . Thus τ_d is an apparent shear strength for the initiation of the debonding process. No prior crack appears to be necessary; the stress concentration is provided by the modulus discontinuity at the interface.

If the elastic energy associated with a single fragment is estimated in the same way as above, again using the equations developed in Section 5.1, it is found that the apparent shear stress at debonding, τ_d , given by equation (8.46), can replace τ_{iu} in equation (8.28). It can, of course, also replace τ_{iu} in equation (8.15)

Since interfaces appear to be brittle, and since we know from pull out experiments that results can be fitted to equations such as equation (8.15) as shown for example in Fig. 8.10, it seems reasonable to use τ_d instead of τ_{iu} .

8.3.5 Interface Failure When Sheared

The interfacial debonding process is not a simple shear process, as taken for granted hitherto. If it were, the apparent interfacial shear strength should never exceed the polymer strength, since the adjacent polymer should fail if the interface were too strong. However, with both fragmentation and pull out, this rule has been observed to fail; see Fig. 8.24.

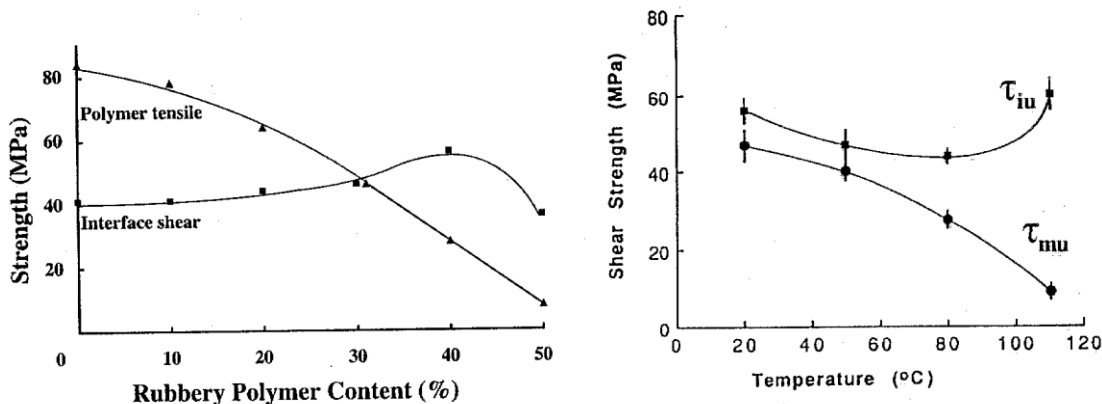


Fig. 8.24 Comparison of apparent interfacial strength with polymer strength. At left, τ_{im} measured using the fragmentation method and at right, using the pull out method. (Fragmentation results after Netravali, A.N., Schwartz, P. and Phoenix, S.L., 1989, Polymer Composites. 10, 385-8.)

We will discuss the pull out test, since this clearly shows what is happening during failure. The failure usually involves at least three steps. First the interface near the fibre entry point starts to debond. This is clear from Fig. 8.10 which shows frictional stress transfer near the fibre entry point and elastic transfer near the embedded end. Next

the debonding arrests while the embedded end itself debonds. Finally, fast debonding takes place. The shear stress required for this fast debonding can be very high.

Fig. 8.25 illustrates these stages with glass in room temperature cured epoxy. These specimens were prepared in such a way that there was virtually no meniscus at the fibre entry point. Furthermore, the fibre free length was only 0.2-0.3mm in these experiments. The resin was room temperature cured, so was highly transparent. The corresponding force-distance plot is also shown. Debonding starts at point A where a change in slope occurs. A second change in slope occurs at point B, when the end debonds. At point C, just before fibre failure, the stress in the polymer still bonded to the fibre can be very high.

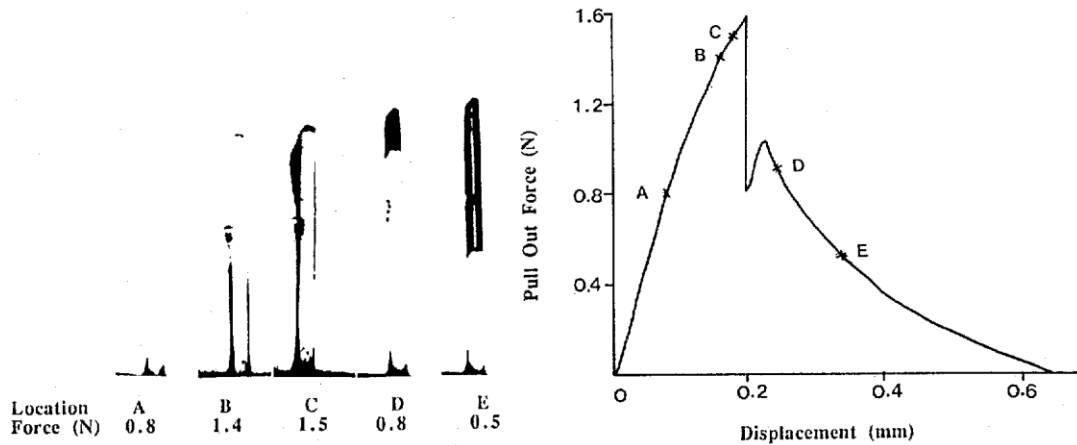


Fig. 8.25 Progressive debonding made visible in a glass-epoxy pull out specimen together with the associated force-distance plot. Correspondences indicated by A, B, C, etc. (After Piggott, M.R., and Xiong, J., 1994, *Comp. Sci. Tech.* 52, 535-40.)

To show that this is so, we use the frictional analysis (equation (8.13)) but relax the condition that the pressure is approximately constant. The pressure, P , has 3 components:

1. The shrinkage pressure due to the curing process, P_0 .
2. The matrix Poisson's shrinkage pressure, given approximately by $\gamma_f E_m / [(1 + \gamma_m) E_f]$.
3. The fibre Poisson's shrinkage tensile stress, given approximately by $\gamma_s \sigma_{fs}$, where σ_{fs} is the fiber stress in the debonded region, and

$$\gamma_s = \gamma_f E_m / [(1 + \gamma_m) E_f] \quad (8.47)$$

Poisson's ratios γ_f and γ_m for fibres and matrix are given in Table 4.1. (For friction to be significant, P must be greater than zero. If $P < 0$, some limited friction can still operate if the fibres are not straight; however, friction will be small unless the fibres have relatively very large asperities.)

To determine the fibre stress in the debonded region, we use equation (5.11) with τ_e replaced by μP and with $\epsilon_m \sim 0$, i.e no significant matrix Poisson shrinkage. This gives

$$\frac{d\sigma_{fs}}{dx} = \frac{-2\mu(P_0 - \nu_s \sigma_{fs})}{r} \tag{8.48}$$

Equation (8.13) becomes

$$\int_{\sigma_{fe\max}}^{\sigma_{fs}} \frac{\sigma_{fs}}{\sigma_{fs} - P_0/\nu_s} = \frac{2\nu_s \mu}{r} \int_r^x dx \tag{8.49}$$

which on integration gives

$$\sigma_{fs} = P_0/\nu_s + (\sigma_{fe\max} - P_0/\nu_s) \exp\{2\nu_s \mu(x/r - ms)\} \tag{8.50}$$

and with $\sigma_{fs} = \sigma_{f\max}$ at $x = 0$ gives

$$\sigma_{f\max} = P_0/\nu_s + (\sigma_{fe\max} - P_0/\nu_s) \exp\{2\nu_s \mu ms\} \tag{8.51}$$

If $\sigma_{f\max} > P_0/\nu_s$ then $\sigma_{f\max} = \sigma_{fe\max}$ and no frictional stress transfer takes place. Hence, for frictional stress transfer $\sigma_{f\max} < P_0/\nu_s$. The fibre in Fig. 8.25 has $\sigma_{f\max} = 3.94$ MPa. so P_0 needs to be greater than 20.4 MPa. This is too high for a room temperature cured epoxy. So the fibre separates from the polymer, with a visible gap, as shown in Fig. 8.25, and frictional stress transfer is probably negligible.

Thus, at stage C a bonded length of about 0.06 mm is probably supporting the full load of 1.5N. So $\tau_{im} \sim 540$ MPa. (equation (8.1) with $L = 0.06$ mm). This is about an order of magnitude higher than the tensile strength of the polymer. Such an excessively high stress can only be present when there is a severe constraint preventing polymer failure.

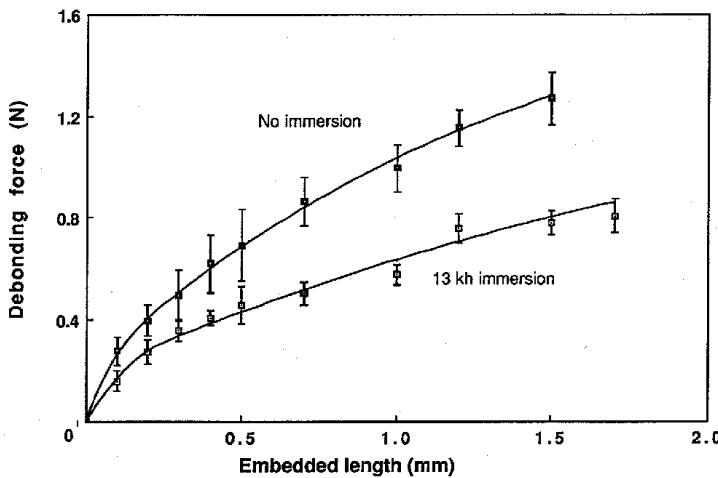
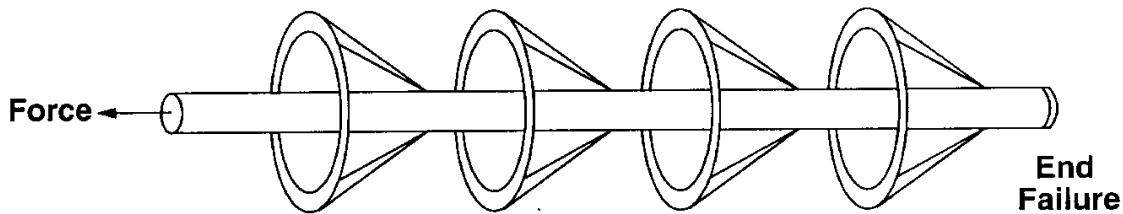


Fig. 8.26 Debonding force vs embedded length for glass pulled out of polyester. Lower curve is after 13kh immersion in 60°C water. (After Chua, P.S., Dai, S.R., and Piggott, M.R., 1992, J. Mater. Sci. 27, 919-24.)

Not all pull out experiments have $\sigma_{f\max} > P_0/\nu_s$. Fig. 8.26 shows some results with glass-polyester where F_{\max} increases with increasing embedded length. The increase

above the asymptotic value, $2\pi r^2 \tau_{iu} \tanh(ns)$, is due to friction with P not constant; compare equations (8.10), (8.15) and (8.51).

Once it is appreciated that most polymers do not separate by a shearing process, the problem of unduly large apparent shear stresses can be resolved. All the current interface tests are virtually axisymmetric. Tensile failure would therefore have to take place on conical surfaces which cannot easily join up; see Fig. 8.27. (This should be contrasted with the plane shear case; see Fig. 6.20.) Taking into account also the decrease in shear stress with distance from the fibre surface (equation (5.21) and the area of the conical surface, which is proportional to the cube of the distance from the axis, we have a fourth order inhibition.



Tensile Cracks

Fig. 8.27 Schematic drawing of conical failures required in an axisymmetric test when the interface is stronger than the polymer. (After Piggott, M.R., 1996, *Comp. Sci. Tech*, 55, 269-76.)

Near the fibre entry point, at the polymer surface, such inhibition is relaxed, and a 45° conical surface is produced. Fig. 8.28 shows one on a carbon fibre which had been pulled out of epoxy. As can be seen, the cone angle is very close to 45° . We have seen similar cones on metal wires embedded in epoxy to a depth of one or two diameters, and then pulled out. (In these cases the tip of the cone coincided with the embedded end of the fibre.)

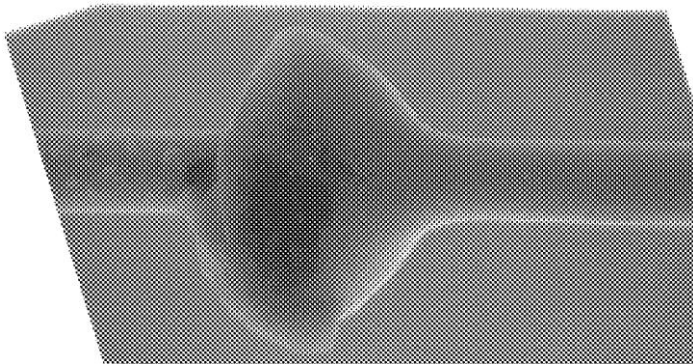


Fig. 8.28 Failure cone from polymer surface material when a carbon fibre is pulled out of epoxy. The part of the fibre that was embedded is at the right.

Since shear failure cannot take place, the process is tensile, and friction plays a major role. No surface is perfectly smooth on a nanometer scale. Fig. 8.29 illustrates this on a carbon fibre, as seen in the scanning force microscope.

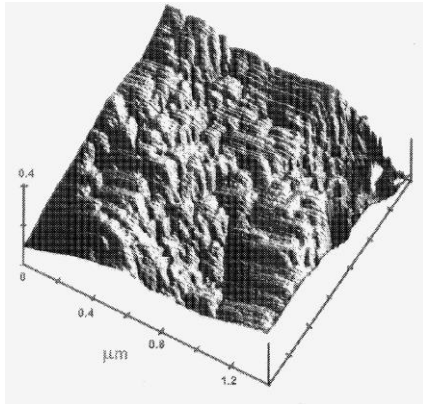


Fig. 8.29 Scanning force micrograph of a PAN precursor HTA carbon fibre after electrochemical activation. (After Zhdan, P.A., Bors, M. and Castle, J.E., 1998, *Comp. Sci. Tech.*, 58, 559-70.)

The process envisaged for a rough fibre being pulled out of a polymer is shown schematically in Fig. 8.30, with the roughness represented as a zig-zag pattern. Debonding is a gradual process with no clearly identifiable debonding point. Bonds, whether covalent, hydrogen or van der Waals, are assumed to break, and re-form to a limited extent. Any such reformation will take place at asperities as part of the normal friction process.

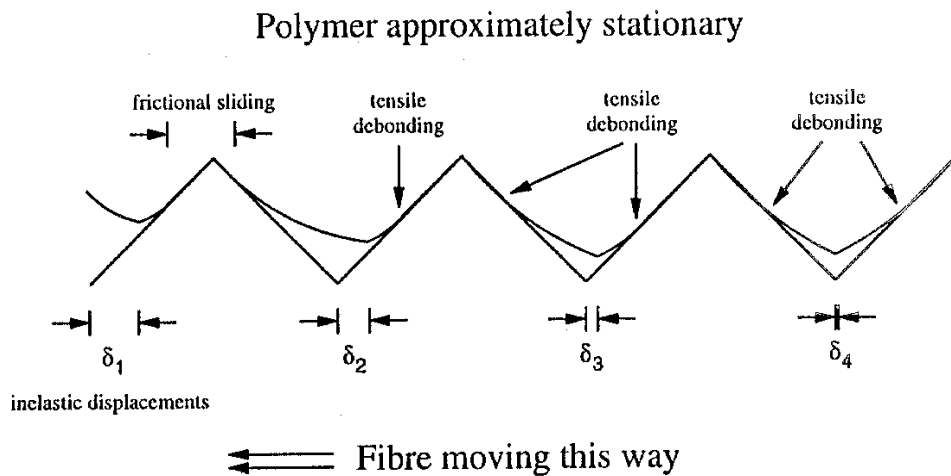


Fig. 8.30 Schematic drawing of the failure process envisaged for an axisymmetric test. (e.g. fibre pull out, fragmentation and microcompression) in a polymer matrix. Fibre roughness is represented by the zigzag line. (After Piggott, M.R., 1996, *Comp. Sci. Tech.*, 55, 269-76.)

The fibre, in the lower part of Fig. 8.30, moves to the left and has a displacement at the first notch of δ_1 . The relative motion between the first asperity and the polymer is envisaged as entirely frictional, since it has moved completely away from the part of the polymer to which it was originally bonded. (This can involve some degree of new bond formation and subsequent breaking.) It also involves ploughing. The second notch and asperity have not moved so far ($\delta_2 > \delta_1$), so debonding is not complete. To effect its movement the asperity has a resolved component of force pushing upwards on the polymer, and causing the tensile failure near its leading edge.

The third notch has a still smaller displacement, δ_3 and is even less debonded. Debonding here is proceeding nearer the notch root, and also near the trailing edge of

asperity number 2. Finally, the displacement of the fourth notch, δ_4 , is even less and debonding has barely started. Thus, on a nanoscale we have a fuzzy debonding front. The movement of the fibre pushes the polymer aside, and this causes tensile debonding. The debonding is accompanied by friction.

When the debonding process gets within about 10-20 diameters of the fibre embedded end, end debonding takes place. This makes the fibre-polymer system more compliant so that the debonding front is temporarily arrested. Debonding of the final short section of polymer then restarts and continues as before. Two-way debonding is precluded by this process because of the fibre displacement required for the process envisaged. This displacement decreases monotonically from the fibre entry point.

This process does not preclude pure sliding failure with atomically smooth surfaces, such as single-crystal whiskers are supposed to have. However, even here tensile stresses may well be developed across the interface when bonding is very good, due to Poisson shrinkage of the whiskers.

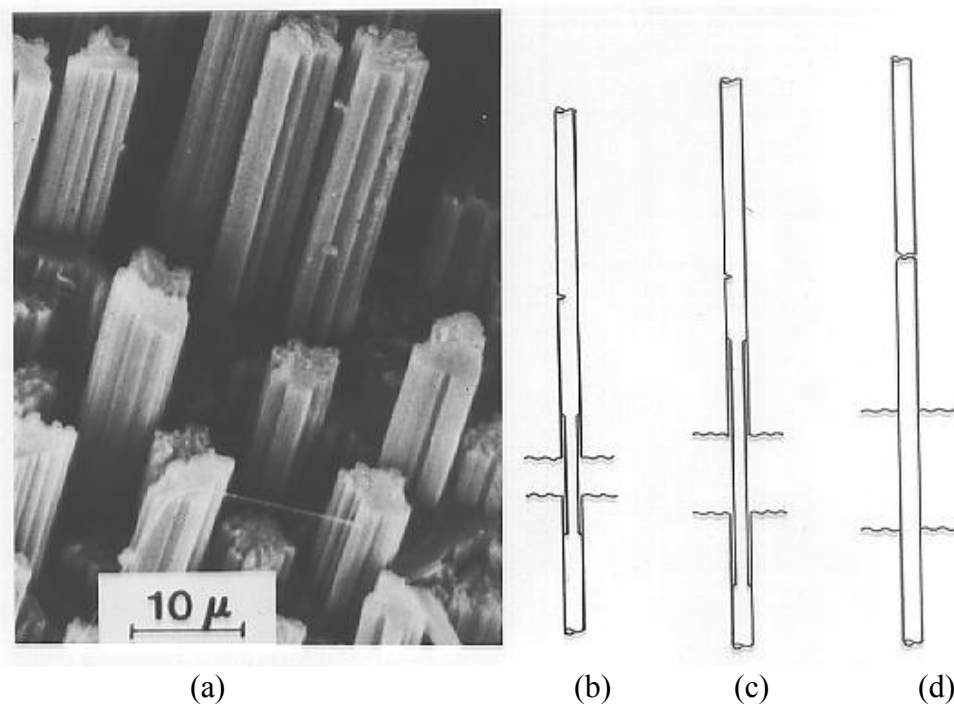


Fig. 8.31 Micrograph of a fracture surface showing pulled out fibres, together with a schematic drawing of fibres bridging a crack. Crack opens progressively from b to d, while fibre debonded length increases. It eventually reaches the crack, which causes $\sigma_{f_{\max}}$ (equation (8.51)) to fall to zero. (Photo courtesy of R.T. Woodhams.)

8.4 Work of Fibre Pull Out in Composite Fracture

Fig. 8.31, at the left, shows fibres pulled out during fracture across a unidirectional continuous fibre composite. At the right is shown the situation envisaged

for a single, partly debonded brittle fibre bridging a crack. The fibre contains flaws, one of which is exaggerated in the drawing to make it easily visible. Although the fibre stress is highest in the crack plane, fibre fracture does not necessarily occur there. This is because brittle fibres, such as glass and carbon, have strengths which are controlled by such surface flaws (or internal ones) distributed randomly. So, instead, the fibre breaks at a nearby flaw.

When a small stress is applied, so that the crack opening is small, only a small length of the fibre debonds as shown schematically in Fig. 8.31b. As the stress is increased, the crack opens more and more, the fibre is more highly stressed, and debonding proceeds along the fibre till it reaches the flaw. The fibre then breaks, relaxes, and starts to pull out (Figs. 8.31c and d). The pull out stage of the process is governed by equations (8.48) to (8.51) with $\sigma_{f_{max}} = 0$.

To understand this process we need to know the fibre strength (σ_{fu}) - length (L_t) relationship. There is a limited amount of data on this; see Fig. 8.32 for glass and Kevlar, and Fig. 8.17 for carbon.

For most ceramic fibres, the strength can be represented by one or more straight lines on a log-log plot; i.e.

$$\sigma_{fu} = \sigma_{fu0} (L_t / 2r)^{-q} \tag{8.52}$$

with constants σ_{fu0} and q having different values for different length ranges. (This equation is equivalent to equation (7.11).) In the case of Kevlar, Fig. 8.32 shows that there is no significant variation of strength with length.

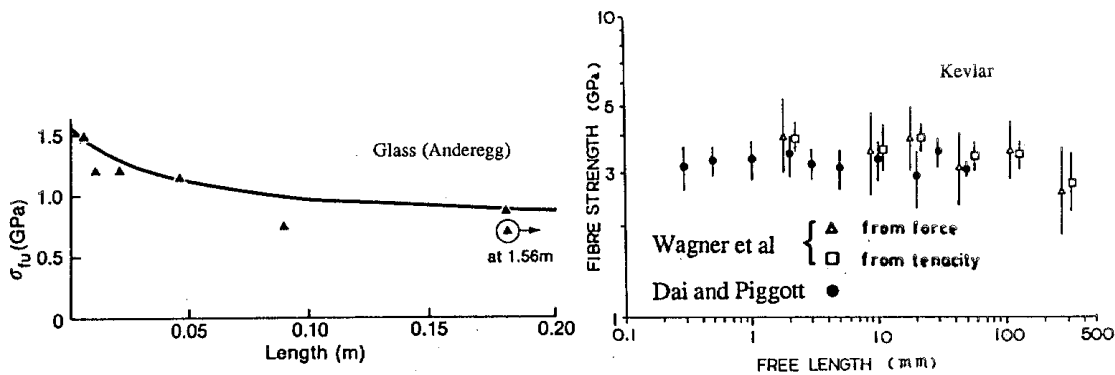


Fig. 8.32 Fibre length-strength relationships for glass and Kevlar. (After Anderegg, F 1939, Ind. Eng. Chem. 31, 290-8, Dai, S.R. and Piggott, M.R., 1993, Comp. Sci. Tech 49, 81-7, and Wagner, H.D., Phoenix, S., and Schwartz, P., 1984, J. Comp. Mater 18, 312-28. See also Metcalf, A.S. and Schmitz, K.G. (1964) ASTM Proc. 64, 1075-93.)

For simplicity we will use equation (8.52) with only one set of values, since this most clearly illustrates the principles of the process envisaged. (In any case any extra precision obtained by involving multiple sets of constants is not likely to be useful, since all the above data refer to carefully treated fibres. Fibres in real composites may well be

more damaged.) Note that the treatment only applies to glass and carbon or other fibres with demonstrated length-strength dependencies. It does not apply to Kevlar.

For fibres to debond and then break during the composite fracture process, a necessary condition is that the curves given by equations (8.50) with $m = 0$ and equation (8.52) must touch, as shown in Fig. 8.33. We can effect this by increasing σ_{fs} (equation (8.50) with $m = 0$). Let the curves touch at a distance x_b from the crack plane (Fig. 8.33). There is only a single value for x_b , since σ_{fs} vs x is convex upward ($d^2\sigma_{fs}/dx^2 < 0$) for all x) and σ_{fu} vs L_t is concave upward ($d^2\sigma_{fu}/dL^2 > 0$) for all L_t). To find x_b , we put the first derivatives equal:

$$D_L(\sigma_{fu})_{L_t=2x_b} = D_x(\sigma_{fs})_{x=x_b} \tag{8.53}$$

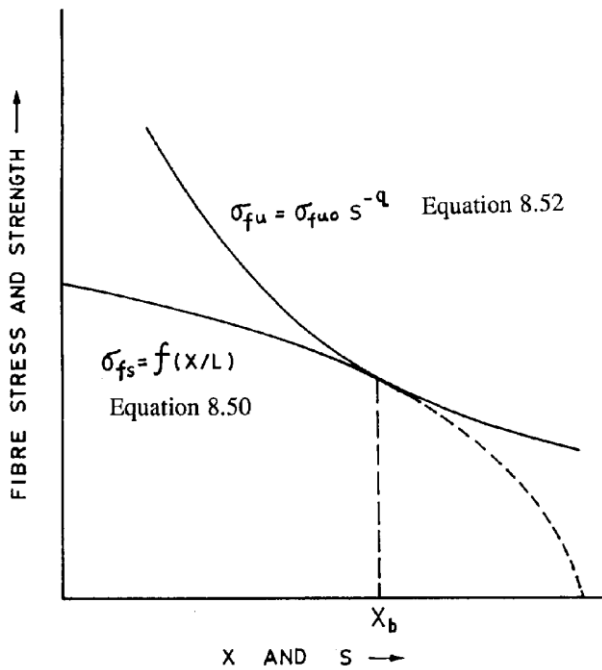


Fig. 8.33 Schematic drawing of stresses near the crack, equation (8.51), and the fibre length-strength relationship, equation (8.52) with $s = L_t/r$

with $\sigma_{fs} = \sigma_{fu}$ (Note that by using $L_t = 2x_b$ we are assuming an average distance between flaws of $2x_b$) Using equations (8.49) and (8.52) this gives

$$s_b = \frac{q\sigma_{fu0}}{4\mu\{P_0s_b^q - v_s\sigma_{fu0}\}} \tag{8.54}$$

where we have written s_b for x_b/r

Fig. 8.34 shows s_b , estimated from equation (8.54) by iteration, vs P_0 , for AS4 carbon-epoxy with $E_f = 233$ GPa, $v_f = 0.30$, and $\mu = 0.30$. σ_{fu0} and q were estimated from Fig. 8.17 using a single set of values for the best fit over the whole range of lengths, i.e. 5.15 GPa and 0.070 respectively. Also shown in Fig. 8.34 (labelled STRONG) is the effect of higher values of σ_{fu0} and q . These values, i.e. $q = 0.18$ and $\sigma_{fu0} = 11.3$ GPa correspond to more flawed fibres, and give much higher values of s_b .

(Note that for low values of q , i.e. less than 0.01, equation (8.54) reduces to

$$s_b = \frac{q\sigma_{fu0}}{4\mu\{P_0 - \nu_s\sigma_{fu0}\}} \quad (8.54a)$$

(The use of this approximate equation eliminates the need for numerical (iterative) methods.)

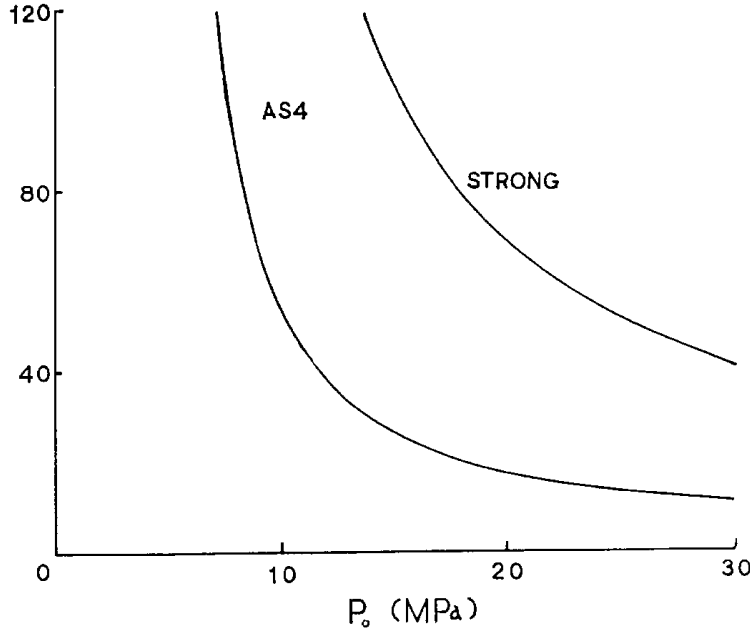


Fig. 8.34 Mean pulled out length (expressed as aspect ratio, s_b) for flawed fibres crossing cracks in polymers with shrinkage pressure P_0 .)

To estimate the work of pull out we can estimate σ_{f0} from our expression for σ_{fs} , since, after fibre fracture, for $\sigma_{fs} = 0$ at $x = x_b$. Thus, integrating equation (8.49) using these boundary condition gives:

$$\sigma_{fs} = [P_0/\nu_s][1 - \exp\{a(x/x_b - 1)\}] \quad (8.55)$$

where

$$a = 2\mu\nu_s s_b \quad (8.56)$$

At $x = 0$, $\sigma_{fs} = \sigma_{f0}$ where

$$\sigma_{f0} = \{P_0/\nu_s\}[1 - e^{-a}] \quad (8.57)$$

As the fibre pulls out σ_{f0} decreases. For a pulled out distance y , σ_{f0} is given by

$$\sigma_{f0} = [P_0/\nu_s][1 - \exp\{a(y/x_b - 1)\}] \quad (8.58)$$

and the work of pull out is

$$U_{fp} = \pi r^2 \int_0^{x_b} \sigma_{f0} dy \quad (8.59)$$

which, using equation (8.58) for σ_{f0} gives, on integration

$$U_{fp} = 2\pi r x_b^2 \mu P_0 [a - 1 + e^{-a}]/a^2 \quad (8.60)$$

This process contributes a work of fracture, per unit V_f of

$$\mathcal{G}_{fp} = 2\pi r s_b^2 \mu P_0 [a - 1 + e^{-a}]/a^2 \quad (8.61)$$

This has already been plotted; see Fig. 7.13. This work is potentially much greater than the work of debonding. If we assume debonding up to x_b , this gives a contribution per fibre of

$$U_{db} = 2\pi r x_b \mathcal{G}_i \quad (8.62)$$

where \mathcal{G}_i is the work of fracture of the interface. The composite work of fracture generated for unit V_f is

$$\mathcal{G}_{db} = 2 s_b \mathcal{G}_i \quad (8.63)$$

The upper bound for \mathcal{G}_i is probably about 0.3 kJm^{-2} which gives $\mathcal{G}_{db} < 0.3s_b \text{ kJm}^{-2}$. This upper bound for \mathcal{G}_{db} can therefore be estimated as a function of P_0 using Fig. 8.34 simply by multiplying s_b by 0.3. For low cure shrinkage pressures ($\sim 10 \text{ MPa}$) quite respectable values of \mathcal{G}_{db} , i.e. up to at least 36 kJm^{-2} appear to be possible. However, Fig. 7.13, which is also plotted vs P_0 , indicates works of fracture nearly five times higher than this. In Fig. 7.13 the curves become asymptotic at a critical pressure of about 6 MPa for AS4 and 10 MPa for the more highly flawed "strong" fibres. The highly flawed fibres give much higher values of toughness for a given pressure than the more uniform AS4.

8.5 Non Axisymmetric Tests

The problem with the tests currently used to estimate interface strength is that they are approximately axisymmetric, and the main stress introduced in the test is shear. Hence the normal, tensile, failure process for polymers, and probably metals too, is not available. Thus, if we wish to investigate the interface strength, we need to promote tensile failure instead. Two ways have been recently examined.

8.5.1 Transverse Strength

As shown in Chapter 6, the transverse strength is strongly influenced by the interface tensile strength σ_a . Fig. 8.35 shows some fracture surfaces obtained when unidirectional samples were broken in the transverse test. It can be seen that, with carbon-PEEK (APC2) and a commercial molding of carbon-epoxy, no bare fibre is exposed.

Measurements on the PEEK alone showed that

$$\sigma_{2u} = \sigma_{mu} \tag{8.65}$$

so σ_a must be greater than σ_{mu} , since we expect stress concentrations at the interface. This is probably also true for the commercial moulding. The laboratory prepared pultrusions were weaker, and there was much bare fibre exposed, Fig. 8.35 at the left. σ_a was less than σ_{mu} in this case.

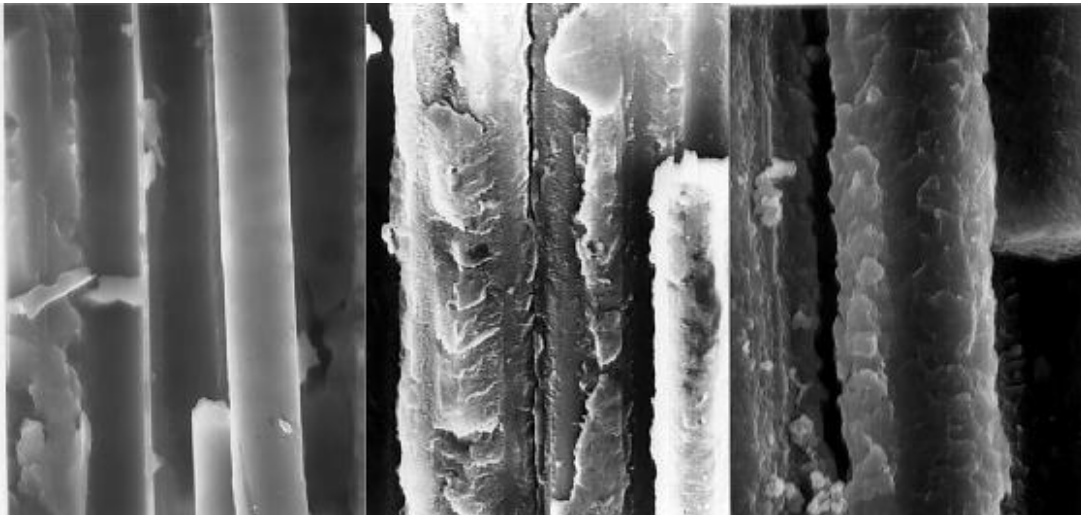


Fig. 8.35 Transverse fracture surfaces of carbon fibre composites. Left; lab made epoxy pultrusion: centre; commercial epoxy based molding: right; PEEK.

We can make a very rough estimate of σ_a if we examine the fracture profile, and measure the length of bare fibre exposed, L_f , and the length of matrix, L_m . Table 8.2 shows the results of these measurements, expressed as L_m / L_t where

$$L_t = L_f + L_m \tag{8.66}$$

Included are tests with systems where no adhesion is expected, i.e. HMU carbon and DC 20 release agent coated AS4.

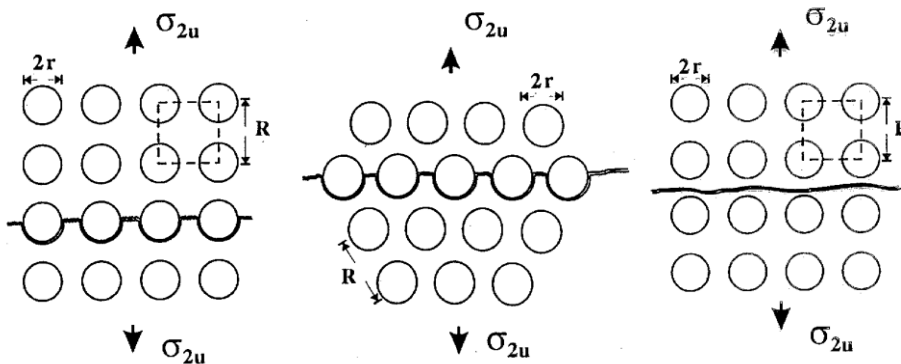


Fig. 8.36 Ideal transverse fractures in uniformly packed composites (a) $\sigma_a > \sigma_{mu}$, square packing, (b) $\sigma_a > \sigma_{mu}$, hexagonal packing and (c) $\sigma_a < \sigma_{mu}$.

We can also estimate the length of the "minimum matrix route" L_{mm} ; see Fig. 8.36 (cf. Fig. 6.16.). Here $L_f = \pi r$ and $L_m = R - 2r$. Writing $P_f = \pi$ for square packing and $2\pi/\sqrt{3}$ for hexagonal packing (see section 5.1), in both cases we have

$$L_{mm}/L_t = \left\{1 - 2\sqrt{V_f/P_f}\right\} / \left\{\sqrt{V_f/P_f}(\pi-2)+1\right\} \quad (8.67)$$

Table 8.2 compares L_{mm}/L_t for hexagonal packing with the experimental values. The carbon fibre systems with very poor or no adhesion have $L_m/L_t < L_{mm}/L_t$. The better adhering systems, on the other hand, have $L_m/L_t > L_{mm}/L_t$. These observations provide a very rough method for estimating σ_a .

Table 8.2. Observed Relative Fracture Profile Lengths L_m/L_t vs Minimum Values for Hexagonal Packing, as shown in Figure 8.36

Fibre	V_f	L_m/L_t	L_{mm}/L_t
AS4	0.2	0.49	0.42
AS4	0.3	0.37	0.32
AS4	0.4	0.32	0.24
DC* AS4	0.3	0.30	0.32
HMU	0.2	0.31	0.42
HMU	0.4	0.19	0.24

* Fibres coated with silicone release agent

Fig. 8.37 shows L_m/L_t plotted vs σ_{2u}/σ_{mu} . The results divide into two groups. The poor adhesion group is close to the line

$$L_m/L_t = \sigma_{2u}/\sigma_{mu} \quad (8.68)$$

which is consistent with $\sigma_a = 0$. The other results are close to the line

$$L_m/L_t = \sigma_{2u}/\sigma_{mu} - 0.2 \quad (8.69)$$

which suggests that we can write

$$L_m \sigma_{mu} + 0.2 L_t \sigma_{mu} = L_t \sigma_{2u} \quad (8.70)$$

so that we identify $0.2 L_t \sigma_{mu}$ as the interface contribution to $L_t \sigma_{2u}$. Hence

$$(L_t - L_m) \sigma_a = 0.2 L_t \sigma_{mu} \quad (8.71)$$

which gives

$$\sigma_a = 0.2 \sigma_{mu} / (1 - L_m / L_t) \tag{8.72}$$

For $\sigma_{mu} \sim 50$ MPa, the results in Table 8.2 suggest that $\sigma_a \sim 20$ MPa for AS1, 25-30 MPa for AS4, and about 30 MPa for glass.

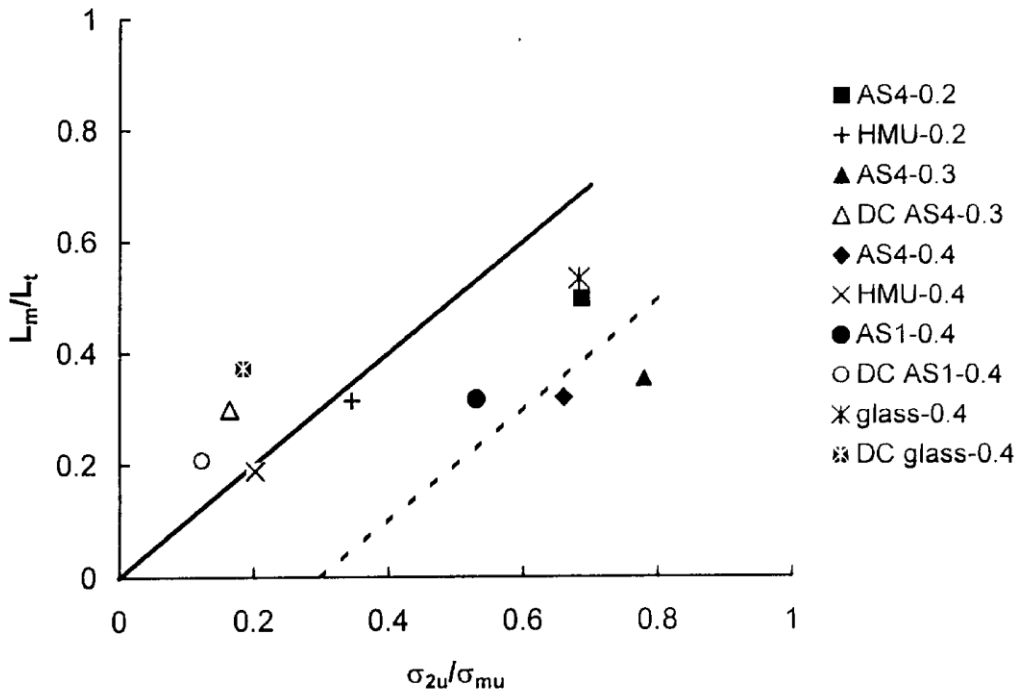


Fig. 8.37 Normalized matrix fracture profile length/(L_m / L_t) vs normalized transverse strength ($\sigma_{2u} / \sigma_{mu}$) After Chan, M. and Piggott, M.R., 1999, Composite Interfaces, 6, 543-56.)

8.5.2 Peel Tests

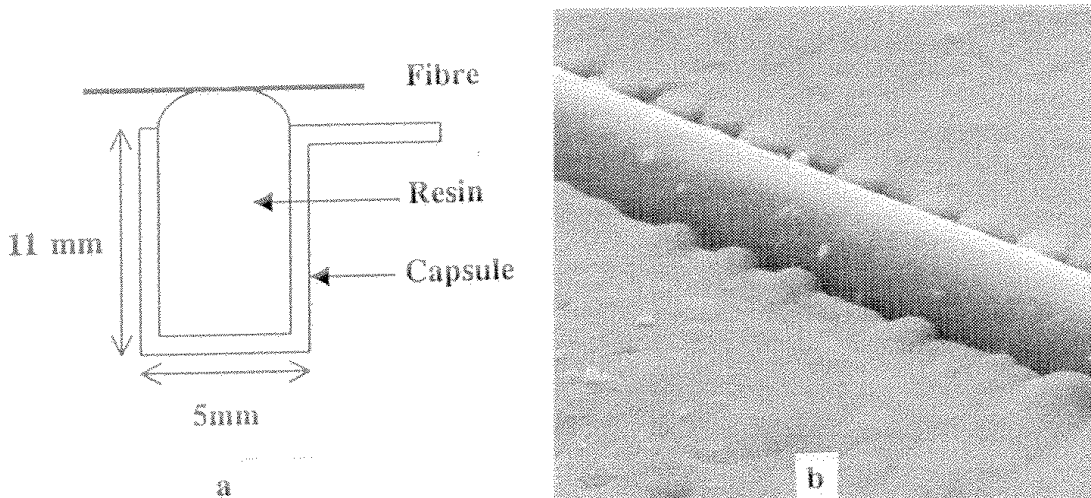


Fig. 8.38 (a) set up for fibre partial embedment, (b) fibre embedded to half its diameter. (After Alimuddin, M.A., and Piggott, M.R., 1999, Polymer Composites, 20, 655-63.)

A single fibre of glass, carbon, or Kevlar can be placed on a polymer surface, allowed to sink in to half its diameter, and then the polymer cured around the lower half: see Fig. 8.38.

When peeled off normal to the surface the force-distance plot resembles those obtained from macro peel tests; see Fig. 8.39b. If the fibre is too deeply embedded it breaks without peeling giving the force-distance plot shown in Fig. 8.39a. If part of it is too deeply embedded, it breaks after a few peel starts and stops, as in Fig. 8.39c. We use the peak values to estimate the upper bound for the work of fracture.

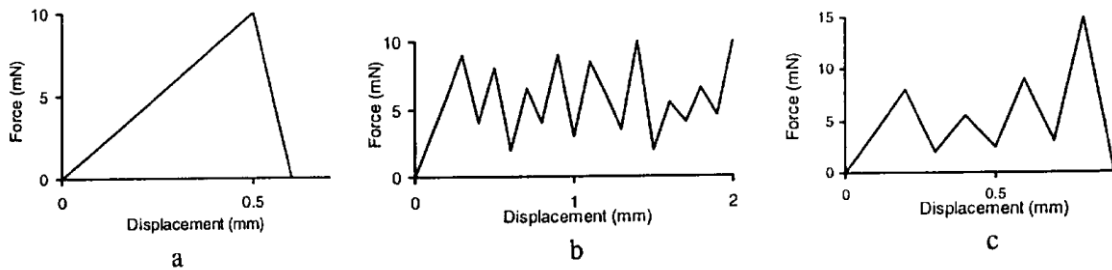


Fig. 8.39 Force-displacement plots (a) embedment too deep; fibre broke, (b) successful embedment and peel and (c) partially successful peel with final fibre break.

Let these peak values be F_1 , F_2 and F_3 , etc. as shown in Fig. 8.40b. The normal peel shown in Fig. 8.40a and the oblique peel shown in Fig. 8.40c can both be analysed by evaluating the work done. Let this be U where

$$U = \int F dy \tag{8.73}$$

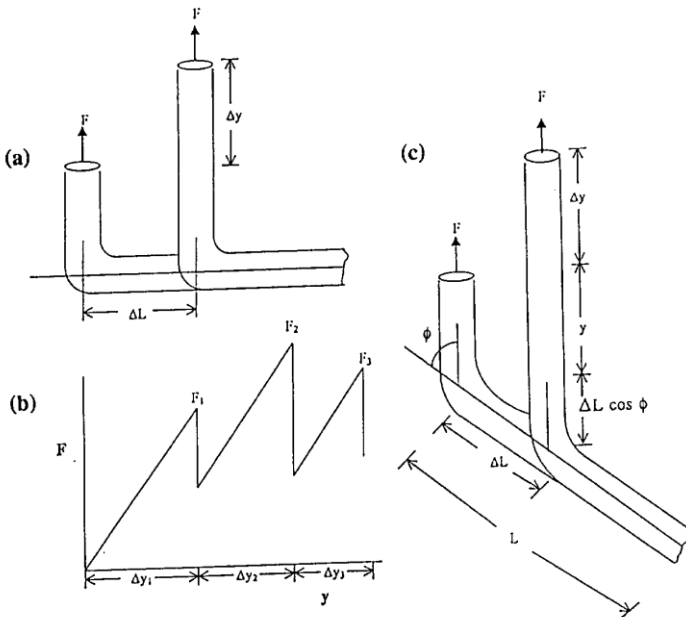


Fig. 8.40 (a) 90° peel over length ΔL , (b) stylized force-distance plot and (c) peel at angle ϕ over length ΔL .

and we assume that the fibre is totally elastic during the peel process. We evaluate U , step by step. Thus,

$$U_1 = F_1 \Delta y_1 / 2 \quad (8.74)$$

(see Fig. 8.40b) and, assuming that on debonding, the force drops to zero, although the load cell does not respond fast enough to record this, and no energy is dissipated in the loading system;

$$U_2 = F_2 \Delta y_2 / 2 \quad (8.75)$$

so that, in general

$$U_k = F_k \Delta y_k / 2 \quad (8.76)$$

For the normal peel $\Delta y = \Delta L$, see fig. 8.40a. The work of fracture, \mathcal{G}_i is therefore

$$\mathcal{G}_i = \frac{F \Delta L}{2d \Delta L} = \frac{F}{2d} \quad (8.77)$$

So for a total of n debonds, we can estimate the mean work of fracture

$$\bar{\mathcal{G}}_i = \frac{1}{2nd} \sum_{k=1}^n F_k \quad (8.78)$$

or

$$\bar{\mathcal{G}}_i = \bar{F} / (2d) \quad (8.79)$$

For the oblique case with peel angle ϕ , Fig. 8.40c, consider a total bonded length of L , and a debond of ΔL . By inspection,

$$L + y = L - \Delta L + \Delta L \cos \phi + y + \Delta y \quad (8.80)$$

so that

$$\Delta y = \Delta L (1 - \cos \phi) \quad (8.81)$$

Using the same development as in equations (8.73) to (8.79)

$$\bar{\mathcal{G}}_i = \bar{F} (1 - \cos \phi) / (2d) \quad (8.82)$$

so that \bar{F} vs $1/(1 - \cos \phi)$ should be constant if \mathcal{G}_i is independent of ϕ .

The dashed curves in Fig. 8.41 are drawn based on the values of \mathcal{G}_i estimated at 90° . As can be seen, the fit is moderately good down to about 20° , but then equation (8.82) predicts values which are too great. This is probably because we have ignored the fibre tensile strain, which at $\phi = 10^\circ$ is quite significant (i.e. 0.37% for glass and 0.26% for carbon). This extra strain could well assist the debonding process. It is therefore recommended that the peel tests be carried out at angles of 30° or more.

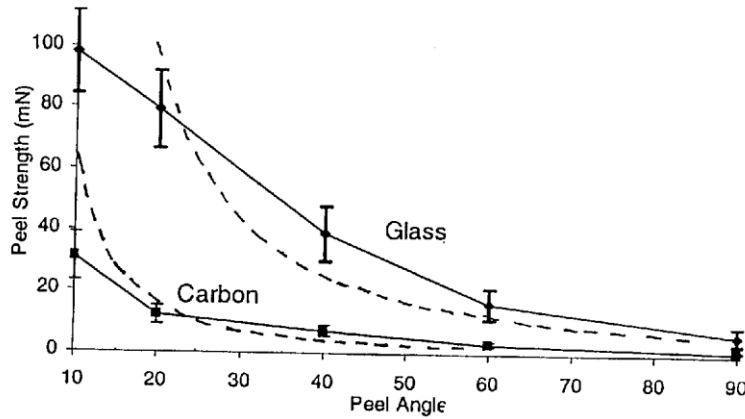


Fig. 8.41 Peel force vs peel angle for single glass and carbon fibres. Dashed curve is given by equation (8.82)

Kevlar cannot be peeled at 90° to yield a work of fracture. Table 8.3 gives works of fracture estimated from the 90° peel. The values for Kevlar are anomalously large due to defibrillation: see Fig. 8.42 which compares Kevlar and glass.

Table 8.3. Peel Strengths and Interface Fracture Toughnesses (Upper Bounds)

Polymer Type	σ_{mu}^1 (MPa)	Fibre Type	Diameter (μm)	Peel Strength (mN) ²	Interface Work (Jm^{-2}) ³
Epoxy	50	Glass	22	6 ± 2	140
		Carbon	8	1 ± 0.3	60
		Kevlar	12	6 ± 1	250
Epoxy	121	Glass	22	6 ± 2	140
		Carbon	8	2 ± 1	130
		Kevlar	12	5 ± 2	210
PEEK	92	Glass ⁴	10	2 ± 1	100
		Carbon	8	2 ± 1	130
LDPE	14	Glass	22	9 ± 2	200
		Carbon	8	2 ± 1	130
		Kevlar	12	6 ± 2	250

Notes:

1. Tensile strength of polymer, 2) \pm indicate \pm one standard deviation, 3) coefficients of variation are about two times those for the peel strengths, 4) Glass had elastomer surface coating.

Table 8.3 also gives results for other systems. Some of the failures are illustrated in Fig. 8.43. With polyethylene, Fig. 8.43a, the polymer is stretched considerably before failure. The high strength epoxy fails in a more brittle manner, Fig. 8.43b. With

PEEK, which gave as strong a bond with carbon as did the strong epoxy, little damage can be seen, Fig. 8.43c. What is remarkable in Figs. 8.43a and b, is the obvious resistance to shear failure on the part of the interface and the polymer. Remember that a polymer, which is a relatively low modulus material, can readily move aside to let the fibre out.

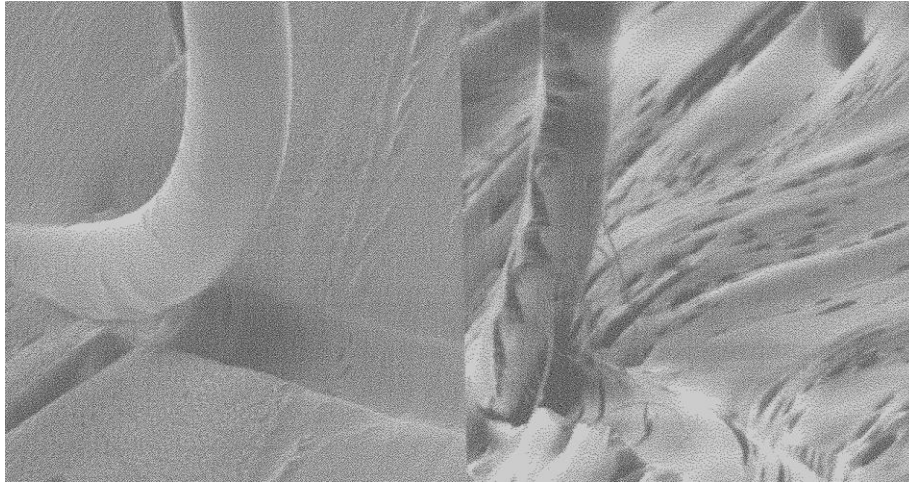


Fig. 8.42 Partially peeled fibres, glass at left, Kevlar at right.

8.6 Conclusions

The traditional shear tests can give very misleading results. If the paper referenced under Fig. 8.37 is examined, it will be noted that pull out gives mean values of up to 70 MPa for the apparent shear strength when the tensile strength may be 30 MPa or less. Furthermore, commercial composites can be made nowadays so that interface failure is totally suppressed (see Fig. 8.35). (These interfaces also very successfully resisted water attack - up to 1500 h at 90°C.)

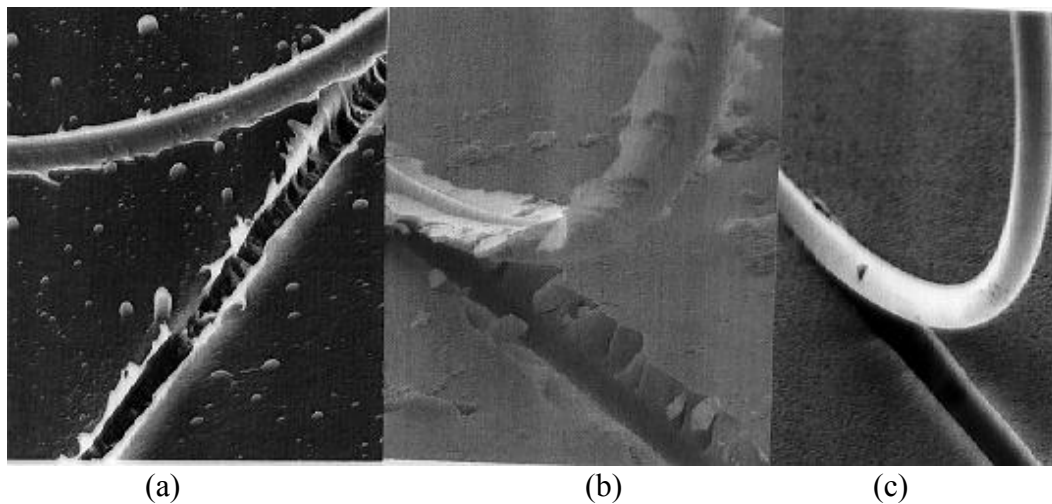


Fig. 8.43 8µm diameter carbon fibres being peeled from (a) low density polyethylene, (b) high strength epoxy and (c) PEEK.

In view of this, the traditional tests are likely to be abandoned in favour of transverse testing. Transverse tests relate directly to essential composite properties, and examination of the fracture surfaces readily reveals whether there is problem with a weak interface.

The peel test seems likely to be selected as a research technique. It still involves a great deal of shear and there is plenty of scope for theoretical analysis here.

Further Reading

Ishida, H. And Maurer, F.H.J., (Eds) *Composite Interfaces*: 6 issues p.a. starting 1993 (VSP Utrecht, The Netherlands)

Ishida, H. And Koenig, J.C., (Eds), (1986), *Composite Interfaces*. (Proc. 1st Int. Conf. On Composite Interfaces - ICCI-I, (Elsevier, North Holland, New York). (Subsequent ICCI's held in even numbered years.)

Jones, F.R., (Ed.), (1989), *Interfacial Phenomena in Composite Materials*, (Proc. 1st Int. Conf. - IPCM-I, (Butterworths London).

(Subsequent IPCM's held in odd numbered years.)

Chapter 8: Problems

- 8.1 An E glass fibre, $19.0\mu\text{m}$ diameter, was embedded in a 6.00mm diameter cylinder of epoxy to a depth of 2.70mm . A force of 0.87N was required to pull it out. Estimate the mean and maximum shear stresses at the interface at the instant of pull out.
- 8.2 The carbon fibres giving the pull out curves shown in Fig. 8.22 were $8.0\mu\text{m}$ in diameter had a Young's modulus of 233GPa , and were embedded to a depth of 0.1mm . The diameter of the polymer in the capsule used was 6.0mm . Compare the maximum shear stresses with the mean shear stresses at the interface at failure.
- 8.3 Fig. 8.3 shows a T300 carbon fibre, $7.0\mu\text{m}$ diameter, with a modulus of 231GPa with a droplet of epoxy on it. If the force required to debond it was 103mN , and the droplet can be assumed to behave as a cylinder with half the maximum diameter of the droplet, what were the mean and the approximate maximum interfacial shear stresses at debonding.
- 8.4 Assume the force-time plot shown in Fig. 8.3 was for a 120°C cured epoxy drop on a T300 fibre. If the drop was $42\mu\text{m}$ long and was equivalent to a cylinder having a diameter of $14\mu\text{m}$, estimate the mean debonding shear stress, the frictional stress, and the approximate coefficient of friction. (Hint: coefficients of

thermal expansion are given in Tables 3.3 and 10.7; neglect any chemical shrinkage.)

- 8.5 A fragmentation test was carried out using the carbon fibres shown in Fig. 8.16. At saturation the mean fragment length was 0.25mm. Estimate the mean interfacial shear stress (a) using extrapolation from 0.30mm and (b) from 2.0mm. The fibre diameter was 8.0 μ m.
- 8.6 Show that equation (8.29) can be derived from earlier equations and explain the assumptions involved.
- 8.7 Estimate the value of n needed to fit the results shown in Fig. 8.20 and comment on the goodness of fit compared with D .
- 8.8 Calculate the work of debonding for the microtension test described in question 8.3.
- 8.9 Estimate τ_d and the work of debonding for the fibre shown in Fig. 8.15a assuming that it was at this point in the experiment that the fibre fragmented.
- 8.10 Compare the average shear stress for W-Cu at 1300°C (Fig. 8.2) with the maximum shear stress at 20°C (Fig. 8.7). Compare your results with τ_{mu} using the von Mises criterion. Also estimate \mathcal{G}_i assuming that n was the same in both cases. The fibre diameter was 0.25mm and the capsule diameter was 6.4mm. The Young's modulus of copper is 130GPa.
- 8.11 Calculate the fibre pull out force at which the fibre Poisson's shrinkage just balances the residual pressure in a pull out test for E glass-epoxy, for a cure temperature of 120°C. Assume that the pressure across in the interface arises solely from relative shrinkage from the cure temperature.
- 8.12 Make the same calculation as in question 8.11 for the stiffest carbon embedded in a 350°C cured polyimide which has a coefficient of expansion of 46MK⁻¹.
- 8.13 Estimate the mean pull out length during fracture for 8.0 μ m diameter AS4 carbon fibres embedded in an 180°C cured epoxy. Take into account the 0.41% volume change due to chemical shrinkage, in addition to thermal effects. Use the same data as used for Fig. 8.34.
- 8.14 What would be the value for s_b in the above question for a fibre Poisson's ratio of 0.35 and Young's modulus of 233GPa instead of the values used above.
- 8.15 What is the maximum cure temperature for indefinite pull out for a unidirectional glass-epoxy with a coefficient of interface friction of 0.47. The fibres had $d = 9.9\mu$ m, $\sigma_{f,0} = 3.86$ GPa and $q = 0.027$. Include the chemical shrinkage. (Hint: assume 15,000 is close enough to infinity)
- 8.16 Show that, if interface failure occurs over an average arc length of $2r\theta$ along the fibre surface during a transverse test, and the rest of the failure is in the matrix,

then $\cos\theta = \sigma_a / \sigma_{mu}$ assuming that σ_a acts over the whole arc length. Hence estimate L_t/r for $\sigma_a = \sigma_{mu} / 2$ and $V_f = 0.60$. Assume square packing. (Hint: first find the minimum value of σ_{2u})

Chapter 8: Selected Answers

- 8.1. 5.4MPa, 103MPa.
- 8.3. 72MPa, 172MPa
- 8.5. (a) 0.11GPa, (b) 0.14GPa.
- 8.7 $n = 0.035$: points so widely scattered at 20 diameters that the fit for n is acceptable within experimental error.
- 8.9 8.6Jm^{-2} .
- 8.11 1.95GPa.
- 8.13 $48\mu\text{m}$ ($P_0 = 27.4\text{MPa}$)
- 8.15. 142°C .

9 REINFORCEMENT OF POLYMERS

Reinforced polymers have a history dating back to the early years of this century. The first United States patent for a structural composite was taken out in 1916; this was a tube made by hot pressing layers of fibrous material with a suitable binder.

Natural fibres, obtained from wood or flax, were used in early composites; they were prepared in the form of papers and fabrics, and embedded in phenolic resins by hot pressing. Strengths of 200MPa were readily obtainable, with moduli of 20GPa and a density of about 1.50Mgm^{-3} . These composites were a considerable improvement on unreinforced plastics; the matrix on its own has a tensile strength of 40MPa, and a modulus of 3.5GPa. The cellulose fibres, however, were affected by moisture, and in high humidity environments the composite swelled and became weaker. Despite this, there is still interest in natural fibre composites, as a use for waste wood fibres and other cheap natural fibres. (Papier maché is a variation on this theme, and in 1867 the US Naval Academy purchased four 4m long boats made with manilla paper and glue.)

The material which is popularly called "fibreglass" (a misnomer, since the word describes only one part of the composite) and which is used widely these days in boats, specialty cars, and a host of other structures, was developed originally by the military for radar domes on aircraft in 1941. It consists of glass-polyester and has greatly superior properties to cellulose-polymers.

Glass-polymers of a great variety of types are now widely used. Glass comprises 99% of all fibres used, though at least two other types of fibres (carbon and Kevlar) are being increasingly used to reinforce polymers. This chapter will be concerned with the polymers, how good adhesion is assured with reinforcing fibres, and how composites are manufactured. The main emphasis will be on high performance composites.

9.1 The Polymers

When low performance composites, such as very short glass fibre reinforced nylons are taken into account, a very wide range of polymers are used as matrices, so a general description of polymers will be given.

Polymers are extremely high molecular weight materials with carbon normally being in a high proportion. The carbon atoms, which may number in the millions in a single molecule, are connected together to form long chains and extensive networks. Other elements (most notably silicon together with oxygen – the silicones) can also form long chains and networks, and other elements (e.g. oxygen, nitrogen, and sulphur) can be present in the carbon chains. Attached to the chains, which form a backbone for the structure, are hydrogen atoms, organic groups, inorganic groups and radicals.

The diversity of possible compounds is immeasurable, so there will always be exceptions to any general observations. However, we will attempt to describe their properties in a general way.

Polymers are usually characterized by low moduli and strengths. This is due to the deformability of the complex networks, and the sliding that can take place between the long chains. Compared with the ductile metals, they are not very tough, and indeed some are very brittle, especially at temperatures below 0°C. Polymers are not resistant to heat. Some nylons, for example, soften at less than 100°C. Few polymers can be taken above 200°C without serious loss of properties, due to softening, melting, and permanent changes such as chain scission. Polymers that can survive at all at 300°C are rare. Furthermore, polymers absorb water, leading to swelling, softening and some loss of properties. However, the versatility and ease of handling of polymers often more than makes up for these disadvantages, and during the last 50 years polymers have taken over from metals in a wide range of applications where load-bearing properties are not an overriding consideration. In any case, low modulus is sometimes an advantage. Polyethylene garden hoses and rubber tyres are successful because of their low moduli.

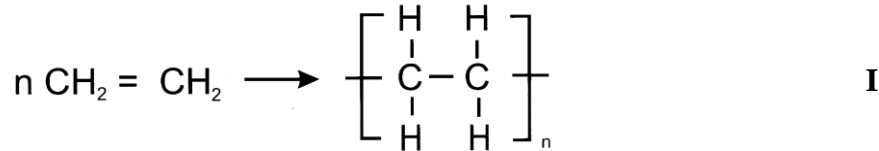
There are two distinct classes of polymers: thermoplastics and thermosets. The thermoplastics (of which nylon is a good example) can be melted, and thus can easily be shaped after the chemical reactions have taken place which produce the backbone - the polymerization reaction. In the molten state they are viscous liquids which can easily be moulded in most cases. Thermosets on the other hand, start off as viscous liquids at room temperature and usually require heat to promote the polymerization reaction. The product formed is a three-dimensional network which cannot be melted. Epoxy resin is a good example of a thermoset. The fusibility of the thermoplastics is due to their having a long chain or branch chain structure, in contrast to the network structure of the thermosets. Thermosets cannot be shaped after polymerization, and so are polymerized in moulds having the final shape required. Special, partly cured thermosets, have been developed for use as matrices in composites. These are soft and easily mouldable, and are hardened to their infusible state by heating, usually while in the mould.

Thermosets are the main type of polymer used for high performance load-bearing composites (often referred to as advanced composites) because of the relative ease of producing the composite without damaging the fibres significantly, and without the need to chop the fibres into short lengths. However, special high temperature resistant thermoplastics have been developed recently to make high performance composites which are more resistant to splitting or delamination than the epoxies normally used for high performance composites.

When thermosets or thermoplastics are used, shrinkage of the matrix occurs during the manufacture of the composite. With thermoplastics the shrinkage is due to the thermal contraction in cooling from the melting point and so can, in principle, be calculated directly. With thermosets, the shrinkage due directly to the chemical reaction must also be taken into account. The shrinkage may be important for the composite, since it can provide a compressive radial stress at the fibre surface which assists in transferring the stress from the matrix to the fibre. Shrinkage has been the subject of much research and is discussed in the next chapter.

9.1.1 Thermoplastics

Polyethylene (PE), chemically the simplest polymer, is made by the polymerization of ethylene:



(Ethylene is called the monomer, sometimes shortened to mer.) A large range of polyethylenes is available, according to the value of n , and according to whether the chain is linear or branched. Further complexity is added when it is appreciated that a sample of PE contains many molecules with different values of n . n can have a wide range or a narrow range. Thus, many grades of PE are available according to the mean value of n , its range, and the degree of chain branching.

The properties vary according to the above. The most crystallizable PE's have the least chain branching; the least crystalline have the lowest density, ρ . Thus at 50% crystallinity, $\rho = 0.90 \text{Mgm}^{-3}$; at 95% (about the maximum possible) $\rho = 0.96 \text{Mgm}^{-3}$. Mechanical properties, on the other hand, increase with increasing n : PE's with molecular weights (MW) lower than 10,000 (i.e. $n < 700$) are waxes while those with MW $> 100,000$ can be tough solids with Young's moduli (E_m) up to 1.1GPa.

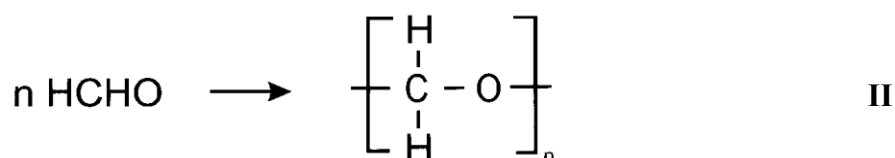
Polyethylenes are classified by acronyms such as LDPE, i.e. low density which can have a wide range of molecular weights (with E_m increasing slightly with increasing MW), HDPE (high density) which have MW's - in the range 40,000 to 300,000, and UHMWPE with MW $> 3\text{M}$ (ASTM definition; weight average). UHMWPE with MW $\sim 6\text{M}$ is reported to have an abrasion resistance ten times better than carbon steel.

One step up in chemical complexity is polyvinylchloride (PVC). In this case, one of the hydrogens in the structure indicated in I, is replaced by chlorine. This is the most important example of the vinyl polymers, in which one hydrogen is replaced by another element. More than one hydrogen can be replaced. For example, when two, attached to the same carbon atom, are replaced by chlorine, we have polyvinylidene chloride, PVDC, $[\text{CH}_2.\text{CCl}_2]_n$, used for food wrapping ("Saran"). All four hydrogens can be replaced. Thus polytetrafluoroethylene $[\text{CF}_2.\text{CF}_2]_n$, PTFE, is a low friction polymer with good chemical resistance.

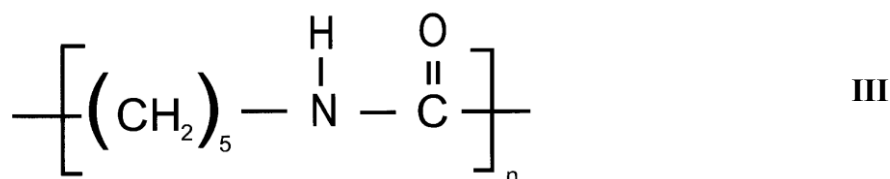
The next step up in chemical complexity is to replace a hydrogen with a chemical group. Perhaps the simplest is polypropylene (PP) where a CH_3 group substitutes for a hydrogen. This is useful for fibre making, packaging, containers, etc. Acrylonitrile has the nitrile (CN) group replacing a hydrogen, polystyrene a benzene group (C_6H_5), and polymethyl methacrylate (PMMA) has a CH_3 group and a COO CH_3 group attached to the same carbon, as in polyvinylidene chloride. This is very clear plastic, used for windows ("plexiglass" or "lucite").

In these polymers the backbone chain is carbon so that the CH_3 , CN , COOCH_3 , C_6H_5 , etc. comprise side groups. With increasing size and complexity of the side groups the structure becomes more stiff and has a lower thermal expansion coefficient.

An alternative method of stiffening the structure is to include other atoms in the main chain. One of the simplest examples of this is the addition of oxygen to form the acetals or polyoxymethylenes:



Another example is nylon, which has nitrogen in the chain. There are several different nylons, usually referred to as polyamides (PA), with different degrees of complexity. One of the simplest used commercially is nylon 6:

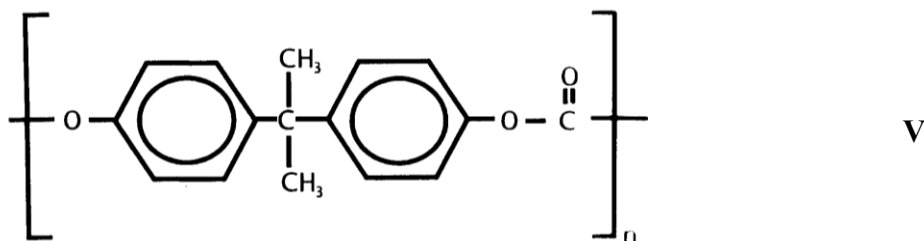


Polyurethanes (PU) have an extra O in the chain

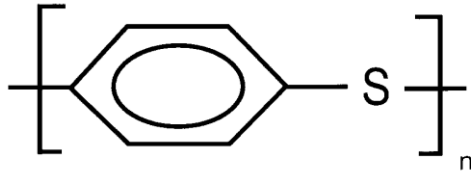


These are usually used as elastomers and thermosetting forms, but have special uses as thermoplastic matrices for pultrusions.

Polycarbonates (PC) have CO_3 together with benzene hexagonal "rings":

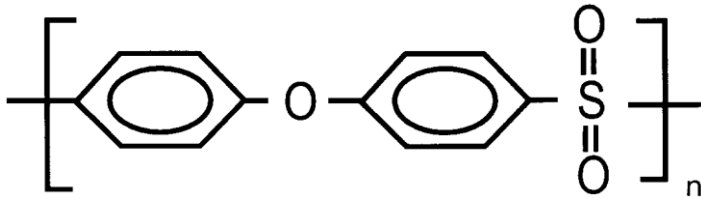


The benzene rings in the backbone structure can be used to stiffen it and increase its resistance to heat. The simplest example which uses this approach is probably polyphenylene sulphide (PPS):



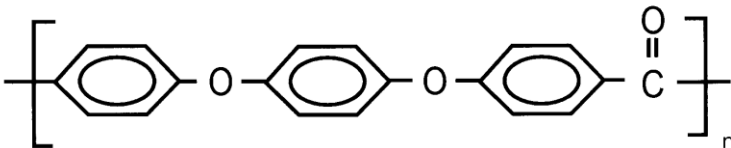
VI

This has a high melting temperature (288°C) but a relatively low glass transition temperature, T_g (85°C). Replacing sulphur with SO_2 produces a sulphone, for example polyether sulphone (PES), which also has two benzene rings linked with an oxygen atom:



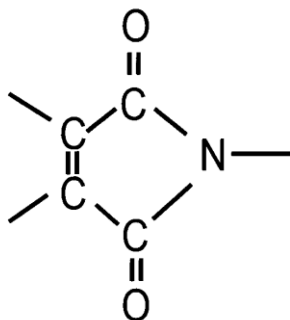
VII

This oxygen comprises an ether linkage. The polymer melts at 315°C and has a T_g of 260°C. The terminology is not fully descriptive as can be seen by this example. For example, assuming that polyphenylene oxide (PPO) is the same as PPS with the S replaced by O would be a mistake. In addition to replacing the O, PPO has CH_3 groups on each side adjacent carbon atom to the one attached to the O. Polyetheretherketone (PEEK):



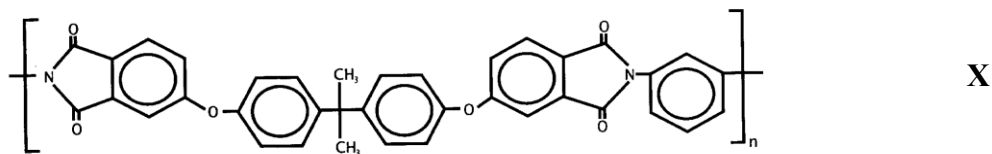
VIII

has a still higher melting temperature (420°C) but a T_g of only 144°C. The highest T_g 's are obtained with polyimides which involve the imide group:



IX

which, in the earlier imides, was attached to a benzene ring as in polyetherimide (PEI):



This can be important for thermal stability.

A variety of polyimides are available, some of which have $T_g > 370^\circ\text{C}$. Such high temperature resistant thermoplastics are particularly important for high performance composites. These polyimides are often referred to as pseudo thermoplastics because they are very difficult to process, are sometimes not reprocessible and are frequently processed before complete polymerization. They are very resistant to solvents and chemicals, and are flame resistant.

Increasing complexity in the structure is achieved by copolymerization. In copolymers the backbone chain can include more than one monomer. For example, styrene and acrylonitrile are copolymerized to make SAN (StyreneAcryloNitrile). A wide range of these are manufactured, accompanied by an alphabet soup of acronyms (see Appendix B). Also, polymers can be mixed in blends or alloys. Particularly important in reinforced plastics are mixtures containing rubber particles, which impart toughness to the matrix.

Moreover, a wide range of additives are used; these include pigments, stabilizers (to resist oxygen), plasticizers (to soften), flame retardants (e.g. Sb_2O_3), fillers (e.g. CaCO_3) and stiffening agents such as glass beads. These are seldom used in high performance composites, but quite commonly used otherwise.

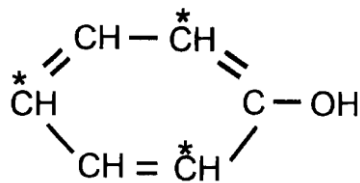
The most widely used polymers, PE, PVC, PP and PS are termed general purpose polymers. Tonnages manufactured are in the order given, PE being the highest. All are available in fibre reinforced form: normally chopped glass fibres, but chopped carbon is often used to impart electrical conductivity for electromagnetic shielding. These polymers, when unreinforced, are generally quite weak ($< 40\text{MPa}$, although polyethylene can be moderately tough) and have relatively high thermal expansion coefficients ($\alpha \cong 100 - 325\text{MK}^{-1}$).

"Engineering polymers", although not well defined, generally refer to stronger ($> 40\text{MPa}$) and lower thermal expansion ($\alpha < 100\text{MK}^{-1}$) polymers. All the polymers described here, except the general purpose polymers and PVDC, have been classified as engineering polymers. However, PTFE is weak ($< 35\text{MPa}$) and is only included by those who consider its use in low friction engineering applications justifies its eligibility. High performance fibre reinforced thermoplastics are made with the more intractable high melting temperature engineering polymers, such as PES (VII), PPS (VI), PEEK (VIII) and PEI (X). Thus special methods are needed to combine them with fibres, as will be described in Section 9.3. Resistance to organic fluids, such as aircraft fuel, oils and solvents is often an important factor in the choice of polymer for this purpose. Thus the polymers preferred are ones that are most difficult to dissolve. Although these polymers

are based on stiff molecules, Young's moduli greater than 5GPa require a high degree of ordering of the molecules (i.e. crystallinity).

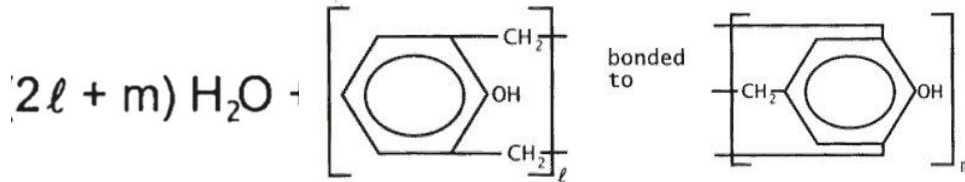
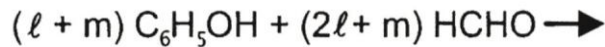
9.1.2 Thermosets

These are three dimensional structures, rather than chains or branched chains. The chemical requirement for the formation of a thermoset is that the monomer must have a functionality of more than 2. Ethylene (I) has a functionality of two, i.e. both carbon atoms are reactive and can link up with other carbon atoms to produce chains. Phenol (C_6H_5OH) has three reactive carbon atoms. These are adjacent and opposite to the carbon in the benzene ring which is bonded to the OH group. They are marked with asterisks:



XI

One of the first synthetic polymers to be manufactured was phenol-formaldehyde resin, or bakelite:



XII

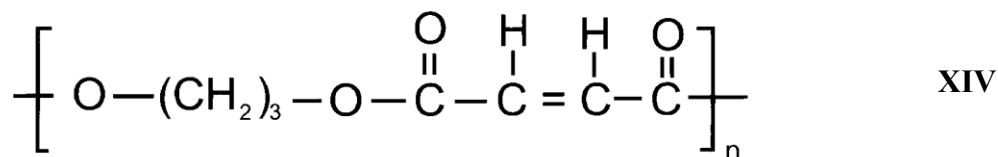
with $m > 0$ for a three dimensional network. This reaction produces water and is called a "condensation reaction", in common with many other polymerization reactions which produce water. A wide range of phenol based polymers, "phenolics", are available and are important as matrices for fibre composites. However, the water produced in the reaction must be able to escape, otherwise the polymer contains excessive voids.

Unsaturated polyesters, usually referred to just simply as polyesters, are another important family of polymer matrices. An ester is the result of a condensation reaction between an alcohol and an organic acid:



R_1 and R_2 are organic groups, such as CH_3 , C_2H_5 , C_6H_5 , or could be much more complex. To obtain the required functionality of three or more, the alcohol must contain two OH groups (this is a diol) or more, and the acid must contain two COOH groups (diacid) or more. In addition, the acid must be unsaturated, i.e. a double bond must exist

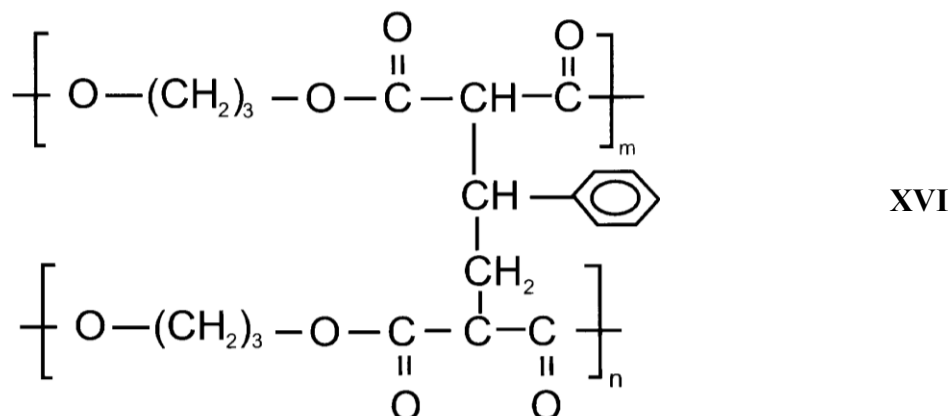
between two of the carbon atoms in the acid. For example, ethylene glycol $\text{HOH}_2\text{C}\cdot\text{CH}_2\text{OH}$ and maleic acid $\text{HOCHC}:\text{CHCOOH}$ produce a linear unsaturated polyester. (In the glycol the stop indicates a single bond between the carbon atoms; in the acid the colon represents the double bond.) The ester:



can then be cross linked using styrene



to give



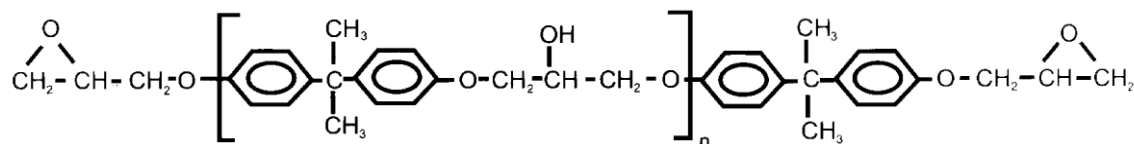
A wide range of diols and diacids may be used, to produce a multitude of different polyesters.

Vinyl esters are a variation on this theme, using a monofunctional unsaturated acid (i.e. only one COOH group) which is reacted with a diepoxide (described below) to produce a polymer with unsaturated sites only at the ends. This is then cross linked with styrene as for normal esters, except that the epoxide groups are the sites for the cross links. Vinyl esters have superior chemical resistance and mechanical properties compared with regular polyesters.

Epoxides are three membered oxirane (or ethoxylene) rings containing an oxygen atom:



As with the polyesters, they are short chain polymers in the uncured state. The most common one, DGEBA, has the structure:

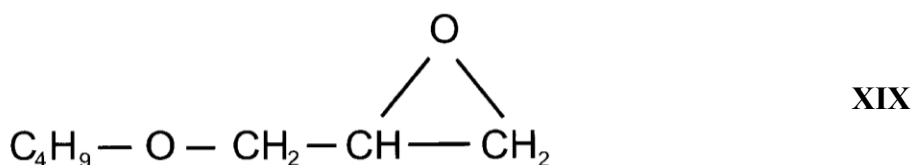


XVIII

and the acronym stands for Di Glycidyl Ether of Bis phenol A. n is usually small. For n equal to zero or one, the uncured epoxy is liquid. For $n = 2$ or more, it is solid and is usually used as a solution in a solvent such as methyl ethyl ketone (MEK). The resin is usually a mixture of epoxies with different values of n , and therefore, the epoxide equivalent is given. This is the weight per epoxide (WPE). Thus for $n = 1$, WPE = 303. A typical resin, Shell's EPON 828, has WPE = 185-192, so that $n = 0$ for most of the molecules present.

(Note that vinyl esters commonly have structures which are almost the same as XVIII except that the terminal epoxy groups are replaced by unsaturated acids.)

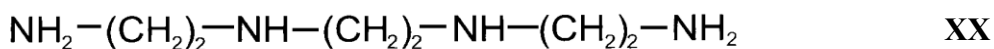
The resins with $n < 1$ are often quite viscous, e.g. 10-16Pa.s (100-160 poises) for EPON 828. For ease of processing, reactive diluents are sometimes used. Thus EPON 815 has a viscosity, η , of 0.5 to 0.7Pa.s due to the addition of butyl glycidyl ether:



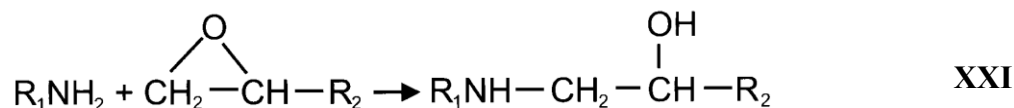
XIX

(the glycidyl group is the oxirane group plus the extra CH_2). This reactive diluent takes part in the hardening reaction, and so reduces the properties to a lesser degree than non-reactive diluents. Losses in mechanical properties, and temperature and chemical resistance result. For example EPON 815 should not be used above 120°C , while EPON 828 can be used up to 200°C with the appropriate hardener. Many different reactive diluents are used with more or less efficiency in reducing η . They often have one or more oxirane group.

Curing takes place by opening the oxirane ring, normally reducing the oxygen to OH in the process. Amines are the most commonly used for this and a popular one is triethylene tetramine (TETA):



which has two primary amine (NH_2) groups. The amine groups react as follows



where R_1 represents all to the left of the final NH_2 group in XX and R_2 represents all to the right of the first oxirane group in XX. Each amine group can react with two oxirane groups and each secondary amine (NH) can react with one. Thus TETA has a functionality of six. This reaction, with EPON 815 or 828, takes place at room temperature and produces heat. A wide range of amines is available.

Next most important are anhydrides of dibasic acids:



where R_1 and R_2 are organic groups. (These are absent in maleic anhydride; instead the CH groups at the left are joined by a double bond.) The anhydrides require accelerators such as tertiary amines



(here R_1 , R_2 and R_3 are organic groups). The anhydride reacts through a complex series of reactions to open the oxirane ring and produce cross links which include the acid. The advantage of this is that the reaction rate can be controlled by the amount of accelerator used. In addition, heat is usually required to initiate the reaction. This affects the properties, and, of course, the rate of heat produced (called the "exotherm").

A third class of curing agent is the "Lewis" acids based on G.N. Lewis's definition of an acid as an electron pair acceptor, as in

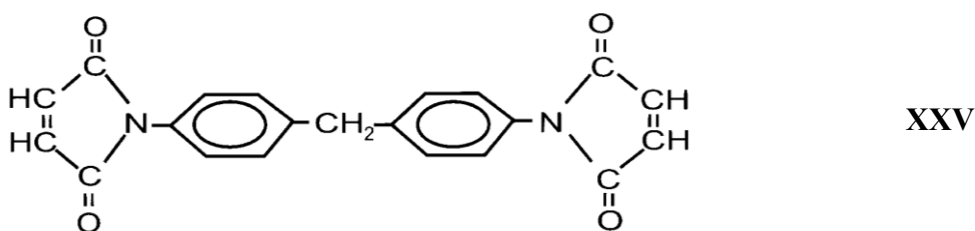


where $2e^-$ represents the electron pair. BF_3 is a moderately strong Lewis acid, which is usually used in a "complex". This is an association with an organic group that dissociates when heated. The BF_3 catalyses the homopolymerization of epoxy. Thus, it opens up oxirane rings by attaching itself temporarily to the oxygen, freeing it from one of the carbons, and then facilitating its bonding to another reactive carbon elsewhere. This releases the BF_3 for further action of this type. The epoxy shown in XX has one such oxygen (in the OH group) for $n = 1$, together with two oxirane groups, so has a functionality of three. For $n = 0$ (functionality 2), the complexing agent (usually an amine) must take part in the reaction, so the polymer involves the complexing agent, and is not a true homopolymer. For an EPON 828 with WPE = 190, functionality = 2.13 so a

significant amount of cross linking can occur. This approach has the advantage that the reaction can be controlled. BF_3 -amine complexes are available with a wide range of different dissociation temperatures, and hence cure temperatures. When mixed with the epoxy resin, the mixture is very stable at temperatures well below the dissociation temperature of the complex. This makes them very useful for prepregs.

Finally, epoxy systems have been developed which can be cured using an electron beam, instead of heat. This method of curing shows great promise for use in filament winding and fibre placement.

Thermosetting polyimides contain the group shown in XI. Bismaleimides are typical examples, which contain two (bis = twice) maleimide groups. A precursor, for example is methylene dianiline bismaleimide:



Early polyimides were produced by a condensation reaction, and so generated water vapour which created problems with consolidation. However, bismaleimides can be produced without volatile by-products. There are a wide range of thermosetting polyimides available with Tg's up to 350°C which can be used at temperatures up to 315°C . They are also very resistant to solvents, can be flame resistant and can have low thermal expansion coefficients ($\sim 30 \text{ MK}^{-1}$).

Additives, such as those described in section 9.1.1, are also used with thermosets.

9.2 The Interface

It is important to ensure that the polymer wets the fibre quickly and efficiently, and that a good bond is produced. Thus most fibres are coated with a thin surface film of polymer. However, other surface treatments are used, which are specific to the individual fibres, and have at least three roles.

1. **Surface protection.** Ceramic fibres such as glass and carbon are brittle and very easily damaged, as mentioned in Chapter 3. These fibres are therefore coated with a relatively soft polymeric material in order to prevent them touching each other or anything else, since even light contact can damage them enough to cause a significant loss in strength. Starch is used for glass (it can be deposited from water) when the fibres are sold to processors who want to do their own surface treating. Carbon is usually treated with epoxy resin: often not fully cured and usually containing very little curing agent. Kevlar, not being brittle, is usually not surface treated.

2. **Lubrication.** In the processing of fibres to produce premixes, prepregs, preforms, filament windings, pultrusions etc, they have to be unspooled and taken to the site of the operation through loops and eyes. These are often made of hard metals or ceramics. So to ease the passage of the fibres, the surface treatment used for glass contains a lubricant.

3. **Adhesion Promotion.** Glass is coated with a material that bonds strongly to the fibres and has an organic "tail" that interacts beneficially with the polymer. The end that bonds to the glass is usually a siloxane, i.e. containing the $-\text{SiO}_3$ group. The organic tail is a moderately long chain hydrocarbon which can penetrate a thermoplastic matrix during processing and form an "interpenetration bond" or alternatively, in the case of thermoset matrices, a reactive group appropriate for epoxy, polyester or polyimide, etc. is contained in the tail. Carbon fibres have soft friable surface layers which must be removed (see section 8.2). Oxidation is used for this; either with strong acids or oxidising agents or by heating in the presence of oxygen. The resulting surface has good adhesion due to the presence of active groups such as $=\text{CO}$. This activity can be enhanced by plasma treatment, using a high voltage high frequency field in a partial vacuum to produce the plasma. Kevlar, usually untreated, does not adhere well to polymers. However, adhesion can be improved by plasma treatment. These fibres should be dried before use.

Sizings for glass comprise 0.3 to 6% of the fibre weight; with carbon 2% is typical.

9.3 Premixes

The materials used to make fibre reinforced polymers are supplied in a number of different forms. The fibres are available as cloths, tapes, mats, etc. as described in section 3.5, but it is often advantageous to combine the fibres with the resin prior to the production of an article.

If a thermoset is used, it is combined with the fibres in a partly polymerized state, so that it can flow, when moulded, to take the desired shape. Once shaped, it is heated to complete the polymerization and make the shape permanent. Thermoplastics may also be combined with fibres prior to production. These are heated during moulding to melt the polymer. Composites can also be moulded directly from mixtures of chopped fibres and powdered matrix.

The premixed materials have a number of important advantages. The quality of the product is reproducible, and the manufacture of components is simple, and can often be automated. The fibre content can be very high, yet they can be uniformly distributed. A wide range of these premixes is available, and their use takes the chemistry out of construction.

A widely used premixture is the sheet moulding compound. To make this, the fibres are cut into short lengths (e.g. 5 cm) and sandwiched between layers of partly cured thermosets supported by polyethylene films as shown in Fig. 9.1. The paste can contain other fillers, and pigments, etc. The mixture is then compacted by rolling, and wound up

on a spool. It is then stored, so that the resin cures to the limited extent required, or the partial polymerization can be effected by heating. The polyethylene surface films are removed just prior to use.

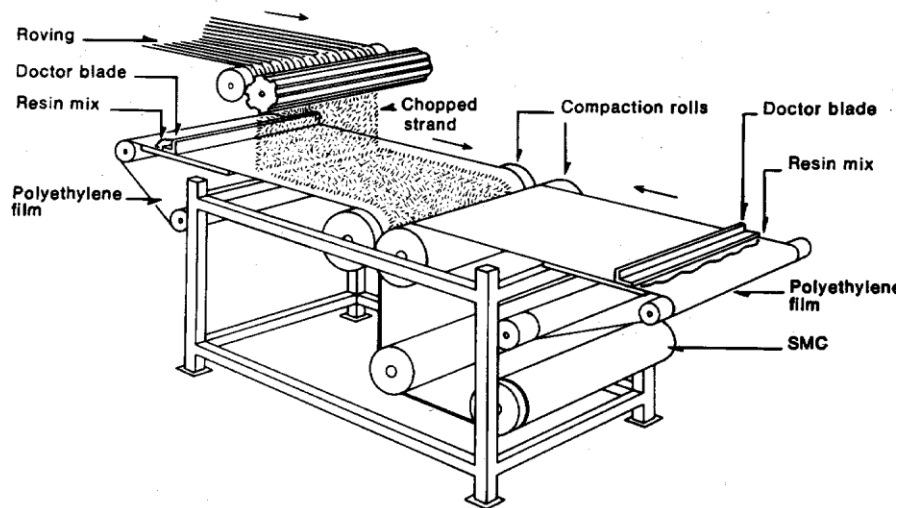


Fig. 9.1 Typical arrangement used for making sheet moulding compounds. (Courtesy PPG Industries.)

The fibres are usually randomly oriented in the plane of the sheet, but may, for special applications, be aligned to a moderate degree by passing through closely spaced parallel bars between the fibre chopper and the polymer film.

Another widely used premixture is the bulk moulding compound (BMC). This also contains short fibres (typically 3 to 30mm) and also has a thermoset resin in a partly cured state, so that the mixture has a doughy consistency. It also contains additives of various types (e.g. pigments, etc.) and is supplied in bulk form as its name implies, or can be extended into rope-like form. In either case, molding can cause quite large volume changes. "TMC", short for thick sheet molding compound is another variant on this type of material. Glass is the usual reinforcement for SMC's, BMC's and TMC's; BMC's require special care because of their shrinkage during cure.

Continuous fibre-resin mixtures are usually called "prepregs", and can be in the form of tape or sheets, with woven or straight fibres. The resin used is either a thermoplastic or a partly cured thermoset. Prepreg tapes are also made with aligned short fibres, and aligned whiskers. In the thermoplastic case the prepreg can be made with comingled polymer and reinforcing fibres, or with powdered polymer. They are partly consolidated by heat and pressure. With thermosets the fibres pass through a bath of resin, and are partly cured in an oven, before being wound, with release film between layers, on spools. Glass, carbon, and Kevlar prepregs are widely available.

Thermoplastic premixes are also produced in the form of pellets. These contain short fibres (typically 3 mm), which also have been embedded in the resin, usually by extrusion. Additives such as pigments may be included, and the pellets may contain the

fibres at the concentration to be used for the product, or at higher concentration for subsequent dilution in the forming process. Glass is the usual reinforcement in this case.

9.4 Manufacturing Methods

A large number of different methods are used for the manufacture of the reinforced polymer product. The method chosen in any particular instance depends on the type of size of article being produced, the number of identical articles to be made, and the strength, stiffness, and other properties required of the material. The methods may be divided into two categories, those that require pressure and those that do not. In the next few sections some of the many moulding methods used for the manufacture of reinforced plastic articles will be described. This description is far from exhaustive; many specialized companies use many different approaches with these highly amenable materials.

9.4.1 Hand Lay-Up

The simplest method of making a composite is to lay the fibres onto a mould by hand, paint the resin on, and allow it to cure. This requires very little capital investment, and though labour-intensive, is still much used because of its great versatility.

The fibres can be in the form of random mat or cloth, and very large structures can easily be built if room temperature curing resins (e.g. epoxy or polyester) are used. The resin can be sprayed rather than brushed on. The moulds do not need to be particularly strong, and can be made, for example, with balsa wood, and covered with plaster. More permanent moulds can be made with reinforced plastics.

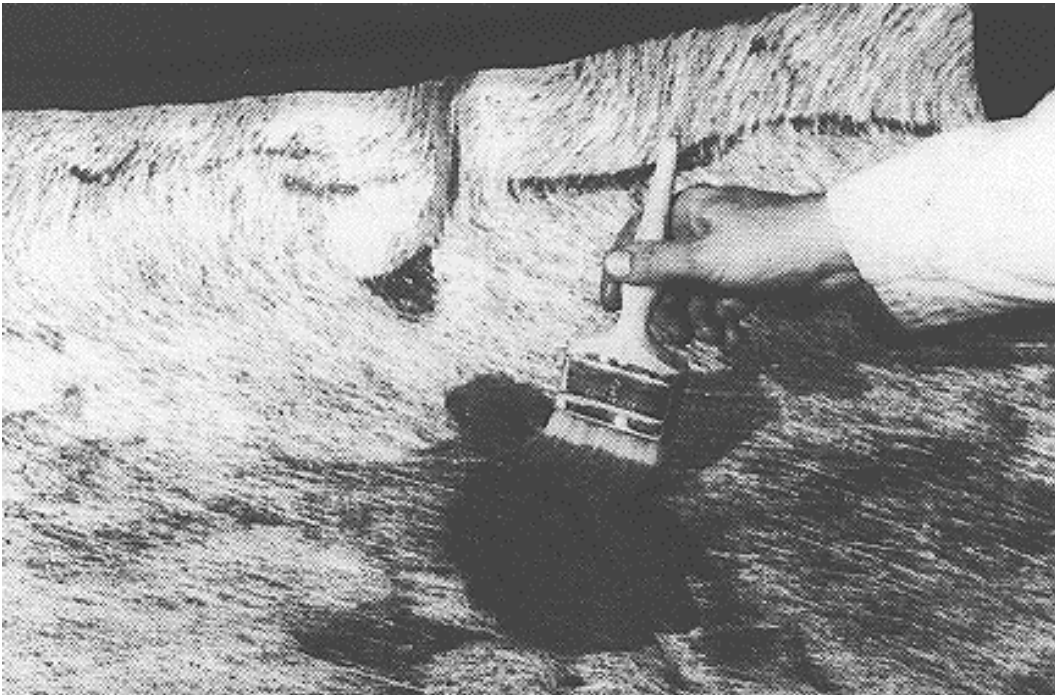


Fig. 9.2 Resin is applied by brush in the hand lay-up process. (Courtesy Fibreglass, UK.)

Fig. 9.2 illustrates this process. First the mould is coated with a release agent to ensure that the part can be removed. Next the gel coat is applied. This is usually a pigmented resin layer to give good appearance, and may be sprayed on. When this is tacky the fibre mat or cloth is laid on manually, and more resin is applied by pouring, brushing, or spraying. Next the layer is rolled or a squeegee is used to ensure thorough impregnation and wetting of the fibres. (The removal of trapped air is particularly important.) Further layers are then added in the same way until the required thickness is obtained. The curing of the moulded part may be accelerated by heating.

9.4.2 Spray-up

In this method the fibres and resin are sprayed together onto the mould as shown in Fig. 9.3. The layers deposited are densified with rollers or squeegees as for hand lay-up. Gel coats are often used for good surface finish. Spray-up can be used to mould more complex shapes than hand lay-up. However, since the fibres have to be chopped in the spray gun, the composite produced cannot be as strong as hand laid-up composites with cloth or other continuous fibre forms.

Polyester or other thermosetting resins are usually used. Very large parts are cured at room temperature, but with smaller parts the curing may be accelerated by bag moulding (section 9.4.8). The moulds used do not need to be strong, and can be made with wood and plaster, or fibreglass.

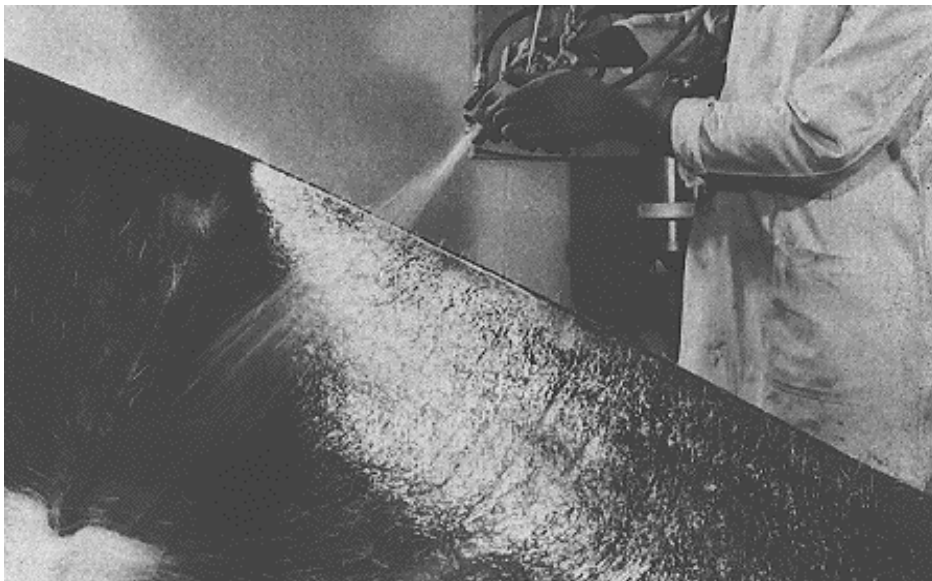


Fig. 9.3 Spray-up process for small boat making. (Courtesy Fibreglass, UK.)

9.4.3 Filament Winding

This process consists of winding continuous filament over a suitably shaped mandrel. The filaments are in bundles which usually consist of thousands of individual fibres, and are referred to as rovings (fibreglass) or tow (carbon). The fibres are

impregnated with resin just before they go onto the mandrel for the wet winding process (Fig. 9.4). There is also dry winding process; in this, prepreg tapes are used. Epoxy resins are often used for the matrix, though polyester and vinyl ester and other resins may also be used. Methods for filament winding reinforced thermoplastics have been developed recently. These involve heating at the line of contact between the material (prepreg, or reinforcing fibres plus polymer fibres or polymer film) and whatever is already present on the mandrel. A similar approach for thermosets uses electron beam curing.

It is usual to rotate the mandrel, though a stationary mandrel is sometimes used. Two winding methods are available; polar (or planar) winding, in which each layer of fibres is wound without spaces or cross-overs, and helical winding, in which both spaces and cross-overs occur. In both winding processes the fibres are laid onto the mandrel in a helical pattern, and the helix angle is chosen to suit the application. The arrangements of the fibres at the ends are most important for pressure vessels, and poorly designed fibre patterns can lead to early failure at the ends.

The construction of the mandrel requires considerable skill. It must not collapse under the large pressure resulting from the fibre-winding tension, and must be easily removed when the process is complete. Segmented metal forms (usually steel) are most commonly used, and they may be faced with plaster.

This method produces very strong composites, and very large cylindrical and spherical vessels can be built.

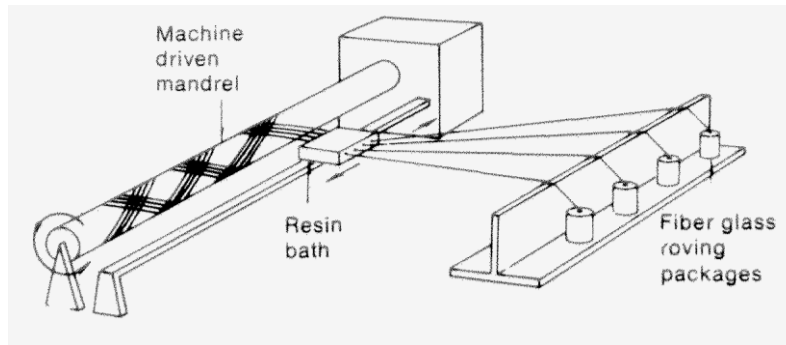


Fig. 9.4 Filament Winding. (Courtesy PPG Industries.)

9.4.4 Fibre Placement

Filament winding can only be used to place fibres on convex surfaces. On flat surfaces the fibres and resin are not properly consolidated, and concave surfaces are bridged by the fibres. The fibre placement method eliminates these problems.

This method uses a robotic head which can move in three dimensions. For large structures the robotic assembly can be moved on rails along the length of the specimen; see Fig. 9.5. The former on which the material is laid down may rotate or be stationary. The head can be heated to partly cure the resin as it places the material, or melt the resin,

as required for a thermoset or thermoplastic. Also, the electron beam curing method may be used.

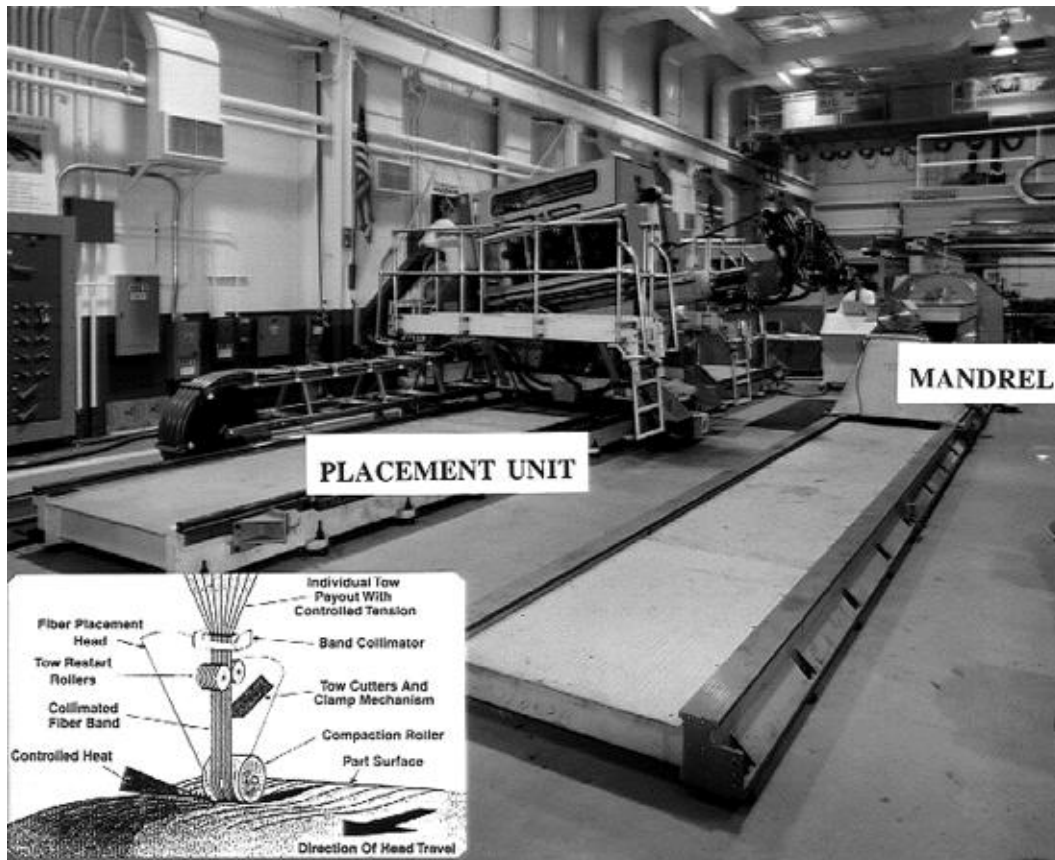


Fig. 9.5 Fibre placement machine with inset, details of process. (Courtesy of Cincinnati Machine.)

9.4.5 Pultrusion

This is a method which is used to make very strong aligned fibre composites. The fibres are impregnated with resin and pulled through a die shaped to produce the desired cross-section in the product. The method is suitable for use with thermosets. The die is heated to promote setting of the resin after it has impregnated the fibres; see Fig. 9.6. Further heat may be applied either before the composite enters or after it leaves the mould. When the material has hardened it is cut into suitable lengths.

Many types of sections are available from the pultrusion process: see Fig. 9.7. Furthermore, woven materials can also be pultruded, so that the strength normal to the axis can be increased. This is particularly useful for structures such as I beams. Finally, very large pultrusions for such structures as bridge decks can now be manufactured.

Recently thermoplastics have been developed for pultrusion. One, involving a special polyurethane (see IV) and catalyst, decomposes to some degree (i.e. the polymer chain gets shorter) during processing. This greatly reduces the viscosity. The chains then

lengthen again during cool down. The other involves a prepolymer mixed with catalyst, which melts during processing, then cures extremely rapidly. A special polycarbonate (see V) or a thermoplastic polyester such as polybutylene terephthalate (PBT) are used. (See XIII for ester: phthalic acid is a benzene ring with two COOH acid groups on it.)

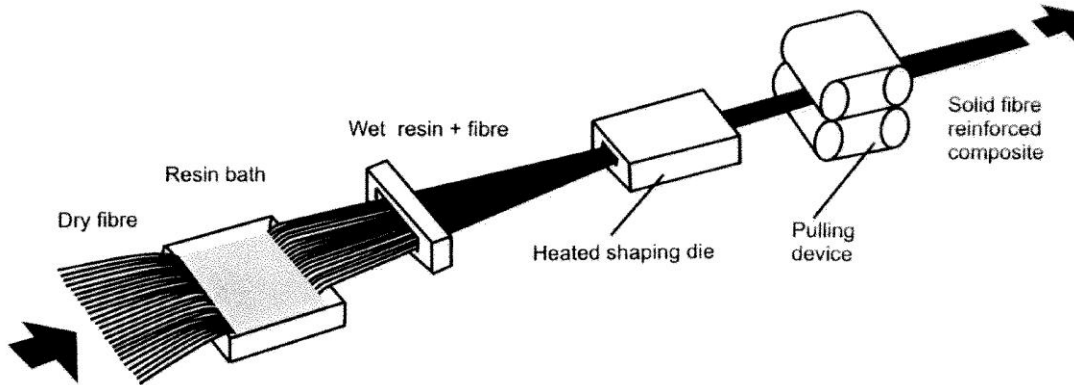


Fig. 9.6 Continuous pultrusion.

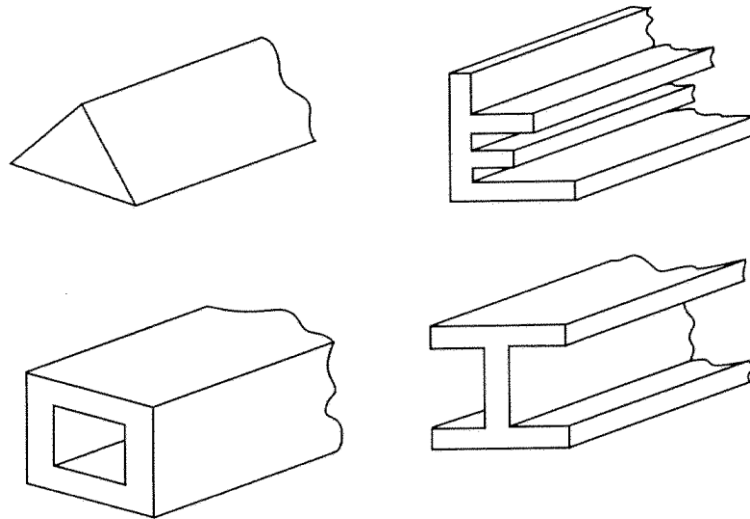


Fig. 9.7 Examples of small sections which may be pultruded.

9.4.6 Tube Rolling

We now move on to methods requiring external pressure. The principle of the tube rolling method is illustrated in Fig. 9.8. The method is used to produce finite lengths of tube, usually of small diameter, for such uses as golf club handles, billiard cues, fishing rods, etc. Diameters range from a few mm up to about 100mm. Prepregs are most suitable for rolling, and woven fibre prepregs are most common.

It is usual to cut the material out into the shape required to make the complete roll, and it is important to have the fibres appropriately oriented. This is called convolute rolling. Alternatively, prepregs can be spirally rolled, a process that can be mechanized.

Both methods can be used to produce tapered tubes. Special rolling tables are available, together with automatic prepreg cutting machines to cut the prepreg into the special shapes required.

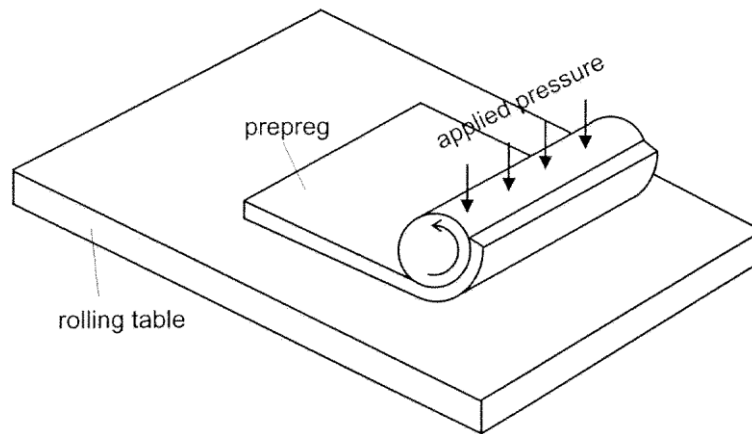


Fig. 9.8 Principle of tube rolling.

9.4.7 Cavity Moulding Methods

Injection moulding requires very large pressures and a mould which has the appropriately shaped cavity for the piece to be molded. The method is widely used for thermoplastic polymers without reinforcement, but low performance fibre composites are also made this way. These typically contain chopped glass fibres which have been further degraded by extrusion, so that their lengths are 1mm or less.

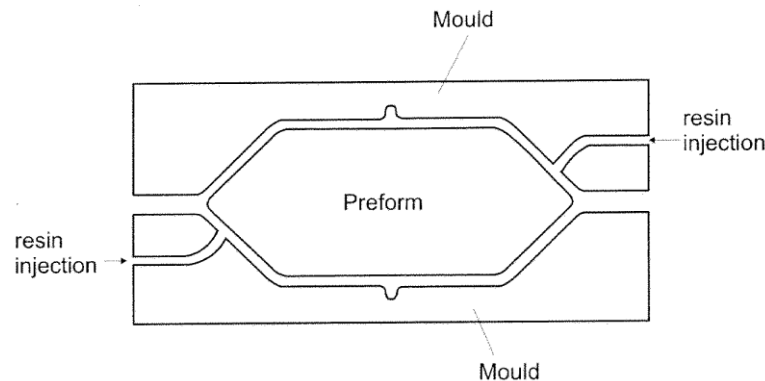


Fig. 9.9 Principle of resin transfer moulding.

A similar method can be used for resin transfer moulding (RTM), which normally uses a thermoset, and hence can be carried out at low pressures. In this case a "preform" is made in a separate operation. This preform consists of fibres with a small trace of resin, which has been shaped, as required for the final structure. The spray-up method is often used for this, but preforms can also consist of three dimensionally woven structures made with continuous fibres. The preform is inserted into the mould cavity, and the resin-hardener mixture is injected therein; see Fig. 9.9. Heating hardens the resin

to complete the process. To ensure good impregnation, the air may be evacuated from the mould before resin transfer. This process is also referred to as structural RRIM (i.e. reinforced reaction injection moulding). Simple RRIM involves the injection of milled glass fibres together with the resin and hardener. The resin-hardener interaction is the reaction referred to in this rather unwieldy name. The structural RRIM is also sometimes referred to as SRMM. (We regret the alphabet stew which develops when fibres are added.)

9.4.8 Bag Moulding

This method may also be used for making large parts. There are three different ways in which the moulding may be done, as shown in Fig. 9.10. The pressure bag system is relatively expensive since the combined mould-pressure vessel can only be used for one shape. The vacuum bag and the autoclave are very versatile, and relatively cheap.

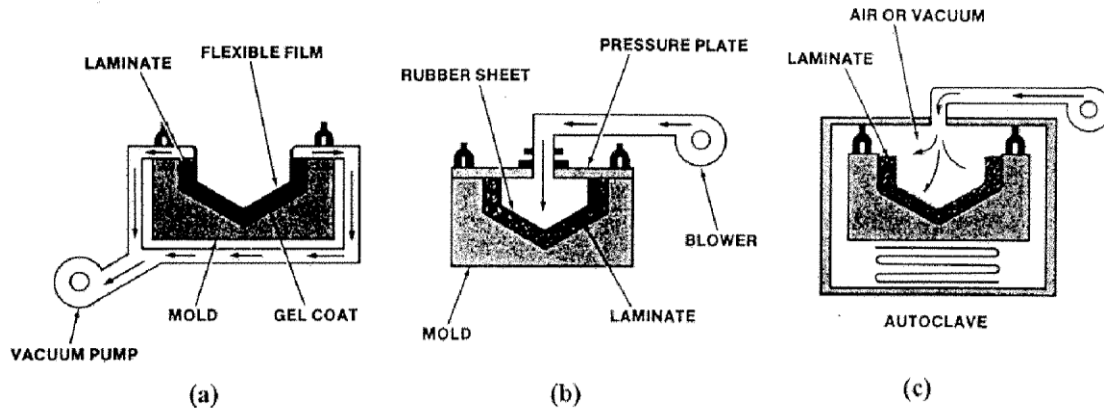


Fig. 9.10 Bag moulding methods. (a) vacuum, (b) pressure, (c) autoclave. (Courtesy of Fiberglas Canada, now Owens Corning.)

The aircraft industry is a major user of the autoclave method, and employs very large autoclaves to manufacture wing parts, etc. Prepregs which are precut on automatic cutting tables are normally used. Moulds are made from steel, nickel, aluminium, graphite, reinforced plastics, or plaster. Laying up the part is a major operation, since it involves first, cutting the prepreg into the appropriately shaped pieces, then laying them up on the mould, with layers in the required orientations.

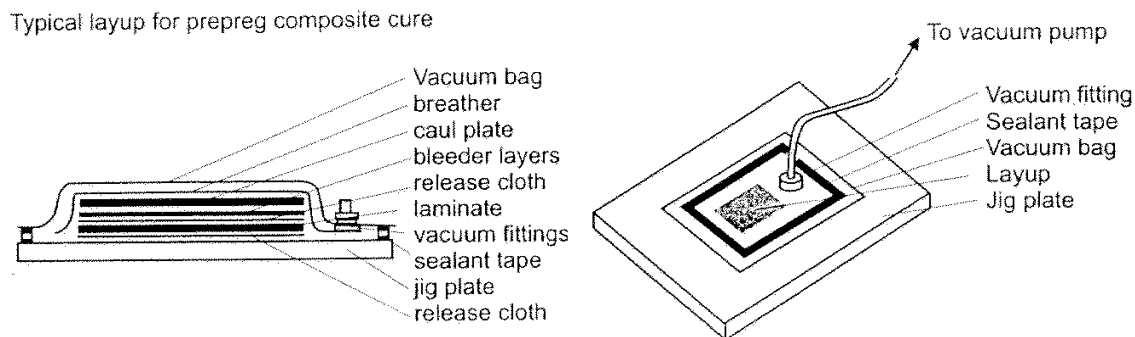


Fig. 9.11 Schematic drawing of arrangement used for autoclave moulding of aircraft parts.

Parts, such as honeycomb layers are added, together possibly with fasteners or any other components which are required to be moulded in. Beneath the laminate structure there is a release cloth to ensure that the laminate can easily be removed from the mould (usually called the "tool"). More release cloth goes on top, then bleeder layers (often random fibre mat) then a "breather" layer to facilitate air removal, typically made from a polyester fibre mat for mouldings at 120°C or less. Finally, there is the vacuum bag, and also around the edge, a sealant tape or plasticene-like material, together with vacuum fittings: see Fig. 9.11.

The whole assembly is evacuated, then rolled on a carriage into the autoclave which has vacuum lead-throughs, so that the vacuum can be maintained during cure. Once all the parts are in the autoclave, pressure is applied, and the whole assembly inside is then cured. This may involve several heating steps with controlled rates of heating and cooling, usually with microprocessor control.

9.4.9 Matched Die Moulding

This method is used for the production of large numbers of identical parts. The moulds are expensive but fast production rates can be obtained.

The reinforced plastic is cured between two heated mould surfaces, usually under high pressure, in a space of carefully controlled size and shape (Fig. 9.12). The fibres and matrix can be combined in a number of different ways prior to moulding. Four such premixes have been described in section 9.1.3: i.e. sheet moulding compounds, bulk moulding compounds, prepregs and pellets. In addition, the wet fabric method may be used. In this the reinforcement, in fabric form, is impregnated with uncured resin immediately prior to moulding.

Since considerable heat and pressure are used in this process, the moulds are usually made of metal. However, when moderate temperatures are used, cheaper flexible plunger moulds may be employed.

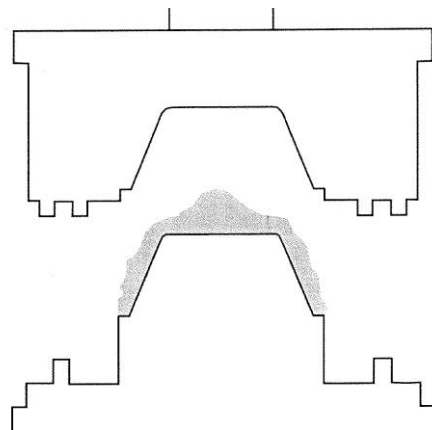


Fig. 9.12 Matched die moulding. (Courtesy of Fibreglas Canada, now Owens Corning.)

Cold-press moulding can be used with thermosets, the curing taking place inside the mould, or with reinforced thermoplastic sheets which are heated just prior to insertion in the mould.

9.4.10 Laminates and Sandwich Construction

High performance composites are usually made by lamination, i.e., the fixing together of sheets of aligned fibre reinforced polymers (or materials). The polar method of filament winding is an example of this form of structure, but other methods of manufacture already described in this chapter can be used to produce the same structural form. A typical method of continuous laminate construction is shown in Fig. 9.13.

Normally each successive layer of the laminate has a different fibre direction from the previous one, except for the two layers at the centre. Usually the layers are "balanced", i.e. they consist of an even number of sheets, arranged so that the interface between the two sheets at the centre is a mirror plane of symmetry. This is to avoid unwanted twisting and other distortions which occur with unbalanced laminates after cure and when the laminate is stressed. The fibre directions used are chosen to suit the magnitude and directions of the stresses that are expected to be encountered. Very high volume fractions of reinforcement can be obtained in laminates, and this is much the most efficient way of providing bi-directional or approximately transversely isotropic reinforcement. (Random fibres provide transversely isotropic reinforcement, but at the cost of low volume fraction and poor reinforcement efficiency.)

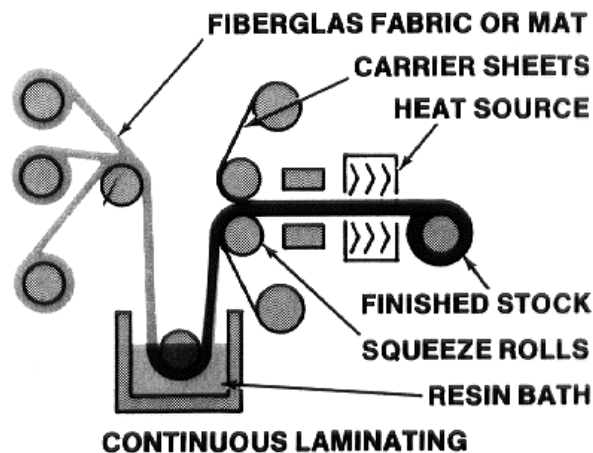


Fig. 9.13 Continuous laminating. (Courtesy of Fiberglas Canada, now Owens Corning.)

Sandwich construction is a method of obtaining the maximum stiffness in a structure when light weight is needed. This type of construction is widely used in aerospace applications, and examples are shown in Fig. 9.14. The outer skins may consist of high modulus, high strength composites, or aluminium, while the centre is a material of very low density, usually either a honeycomb type of structure, or a foam. For aerospace, the parts are normally cured in the autoclave as described in section 9.4.8.

The sandwich is designed to be used in flexure. Thus the skin on one side must withstand tensile stresses, and the other skin must withstand compressive stresses. The filling of the sandwich needs only to resist shear stresses. Honeycomb fillings of reinforced plastic and aluminium provide the most efficient cores, having relatively large values of the ratio of apparent shear strength to density.

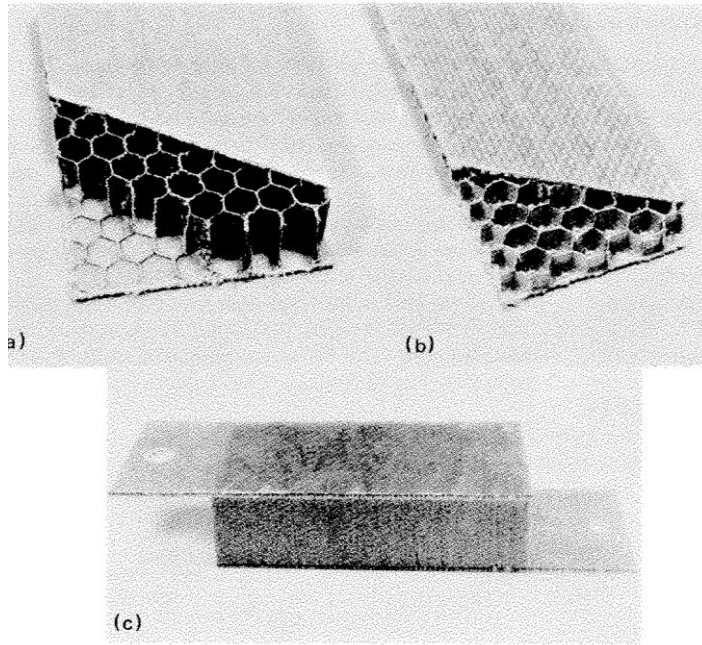


Fig. 9.14 Fibre-polymer sandwich constructions. (a) Kevlar-epoxy aluminium honeycomb, (b) Kevlar-epoxy polymer honeycomb, (c) glass-polyester polymer foam.

A critical feature of both laminates and honeycomb structures is the adhesion between the layers. Neither structures can operate efficiently without a very strong adhesive bond between layers of components.

Further Reading

Rodriguez, F., (1982), *Principles of Polymer Systems*, (2nd edition), (McGraw Hill, New York.)

Astrom, B.T., (1997), *Manufacture of Polymer Composites*, (Chapman & Hall, London.)

Chapter 9: Problems

You are recommended to use rounded numbers for atomic weights (e.g. 16 for oxygen) in these problems.

- 9.1 Estimate the average number of carbon atoms per molecule in HDPE and abrasion resistant UHMWPE.
- 9.2 If a sample of polystyrene had the same number of backbone carbon atoms as the HDPE in question 9.1 above, what would be its molecular weight?
- 9.3 Estimate the proportion of molecules having $n = 1$ for a DGEBA epoxy with a WPE of 190. Assume there are none with $n > 1$
- 9.4. For a DGEBA epoxy with a WPE of 255, what would be the proportion of molecules with $n = 2$, if there were none with $n = 1$ or $n > 2$.
- 9.5 A honeycomb material was made from a 5052 aluminium alloy with a strength of 355MPa. If the wall thickness was 25 microns throughout the structure and the structure was hexagonal, with a side of 3.18mm, calculate the nominal density. Also estimate the apparent shear strength, assuming that all the shear load is borne by the set of cell walls (on third of the total) parallel to the shear force.
- 9.6 To make a hexagonal honeycomb, sheets of aluminium were bonded together so that, when expanded, the cell walls parallel to the original sheet direction were of double thickness, i.e. 50 microns, while leaving the $\pm 60^\circ$ walls with 25 microns thickness. What difference does this make to the strength and density as compared with a material where all the walls were 25 μm thick.

Chapter 9: Selected Answers

- 9.1 12,000; 430,000
- 9.3 6.0%
- 9.5 0.025Mgm⁻³, 0.54MPa.

10 REINFORCED POLYMER PROPERTIES

Fibre reinforced polymers comprise a wide range of materials - all the way from short randomly oriented glass fibre reinforced nylons with low fibre contents to unidirectional fibre and laminate constructions with 60-70% of continuous high performance fibres. At the lower end of the scale, the polymer may be weakened and embrittled by the fibres, but the fibres impart extra stiffness and lower thermal expansion. At the high end, the material can rival steel for strength and stiffness, with the added benefit of much lighter weights and better corrosion and fatigue resistance.

These benefits come with some costs, however. High performance composites tend to be brittle, with delamination occurring very easily, in the same way that wood splits. They are sensitive to moisture, though to a much smaller extent than wood. They cannot be used at high temperatures; the employment of special polymer matrices can permit use for short times at 300°C, but many composites should not be used above 100°C. Creep can be a problem with short fibre composites. Finally, reinforced plastics are difficult to join and the massive joints required can greatly reduce the weight advantage of the composite.

This chapter discusses these properties, briefly describes hybrid composites and the making of, and properties of joints.

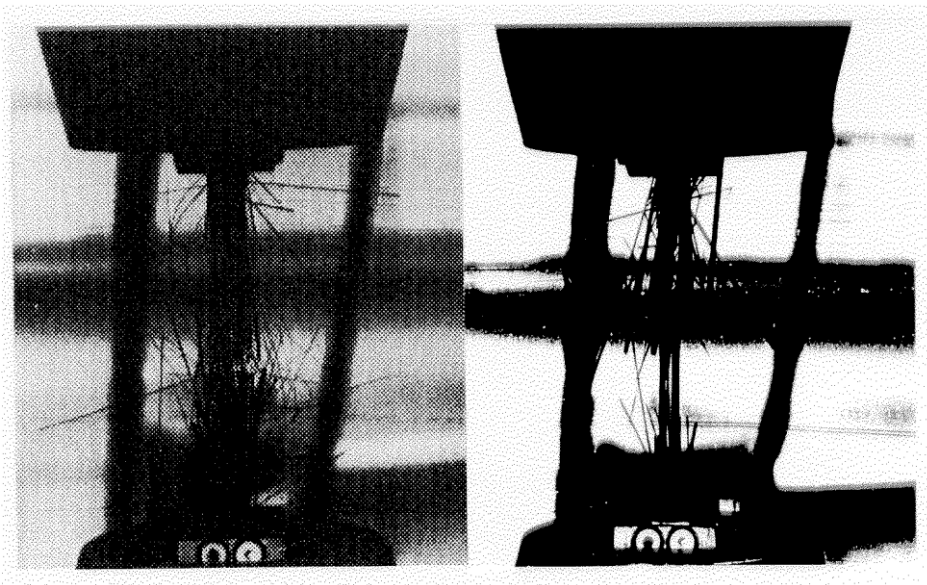


Fig. 10.1 At left, fibrous failure and at right chunky failure of unidirectional carbon-epoxy in tensile tests.

10.1 Mechanical Properties

A very wide range of properties is possible, since there is a wide choice of possible matrices and reinforcing materials. In addition, fibres may be chopped into various lengths, and randomly oriented or organized in a wide variety of ways. Also, the matrix may contain fillers and pigments, etc., which usually degrade its properties.

(Fillers are often used to reduce the price of the material, and it is interesting that chopped glass fibres have been used for this purpose, rather than as a reinforcement.)

In view of the wide range of possible properties this section will not contain an exhaustive description of them, but rather will give a few significant values, and discuss trends.

10.1.1 Strengths and Stiffnesses

Well made unidirectional composites obey the Rule of Mixtures for modulus (equation 4.3) and may reach the Rule of Mixtures for strength (equation 4.4). However unidirectional composites often fail prematurely by splitting. This gives a brush-like or chunky failure, such as shown in Fig. 10.1. Furthermore, however carefully such tests are carried out, stress concentrations are inevitably present in the grips, the 10° tapered end tabs probably giving the lowest at about 11%: see Fig. 10.2.

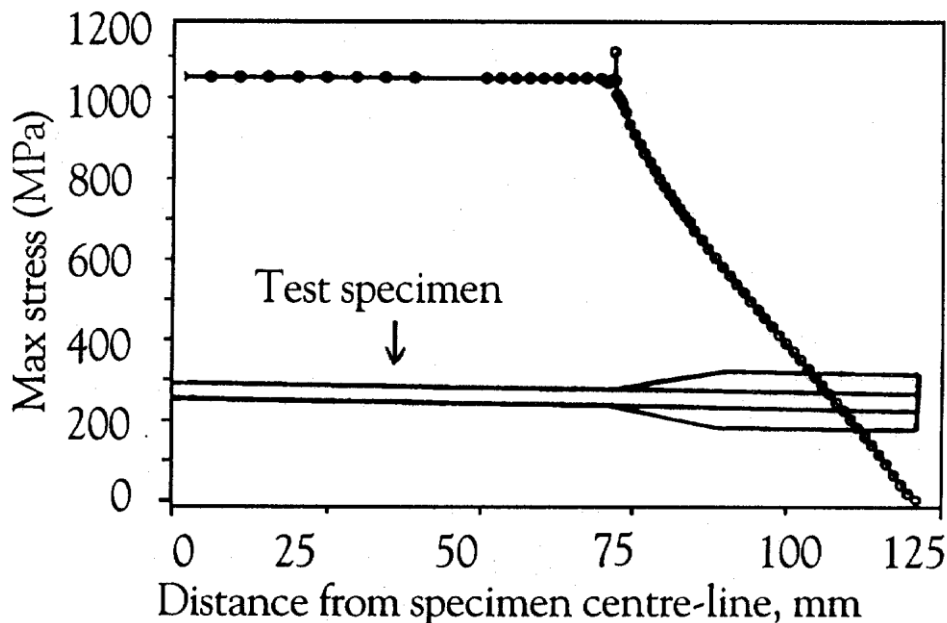


Fig. 10.2 Maximum stresses in end tabbed test coupon estimated by finite element analysis. (After Piggott, M.R. and Loken, D., *Polymers and Polymer Composites*, 1, (1993), 253-60.)

Since the strength and modulus of most polymers are so low, compared with the fibres usually used for reinforcement, we can often ignore the matrix contribution and not be far wrong in assuming that a well-made aligned fibre reinforced polymer can have a strength of $V_f \sigma_{fu}$ and a modulus of $V_f E_f$.

Commercial production does not meet these high standards, and we find that unidirectional glass fibre composites usually reach only about 65% of the mixture rule for strength, although they do often reach the mixture rule for modulus.

With glass cloths, reinforcement is in two directions, with correspondingly less in each, so that only about 25% of the rule of mixtures value is obtained for strength,

although the modulus reaches 65% of the mixture rule value. (Note that relative strengths in other than the fibre directions will be a little less than this.) With random mat the values are correspondingly less.

Table 10.1 Approximate Fraction of Rule of Mixtures Values Obtained for Strength and Modulus for Various Fibre Configurations, and Maximum Volume Fractions for Glass Reinforced Plastics

Fibre Configuration	Modulus ⁺ Fraction	Strength ⁺⁺ Fraction	Maximum V_f
Random mat	0.20	0.15	0.4
Cloth	0.65	0.25	0.5
Unidirectional	1.00	0.65	0.8

⁺Fraction of $V_f E_f$ and ⁺⁺ fraction of $V_f \sigma_{fu}$, both achieved in commercial production. (In both cases the matrix contributions are small enough to be neglected)

In addition, the highest volume fraction that can be obtained with random mat is only about 0.4 due to inefficiency of fibre packing. For woven cloths V_f can be 0.5, and with unidirectional fibres, good composites can be made with $V_f = 0.7$. Table 10.1 summarizes these results.

Similar results are obtained with boron, carbon, and Kevlar, but often greater care is taken with the production of these more expensive composites, so that the unidirectional strength fraction is usually close to 1.0 instead of 0.65. (Carefully made aligned glass reinforced plastics also have strength fractions of 1.0.)

Table 10.2 Effect of Fibre Waviness on the Mechanical Properties of glass-epoxy laminates. All values except Poisson's ratios and apparent shear strength adjusted to $V_f = 0.5$

Fibre	σ_{tens}^1 (GPa)	E_{tens}^2 (GPa)	ν_{exp}^3	ν_{xy}^4	σ_{ucomp}^5 (GPa)	E_{comp}^6 (GPa)	τ_u^7 (MPa)
Straight ⁸	0.40 ± 0.03	21 ± 1	0.24 ± 0.01	0.277	0.58 ± 0.04	26 ± 1	49 ± 4
Noncrimp	0.39 ± 0.03	19 ± 1	0.30 ± 0.03	0.285	0.40 ± 0.05	21 ± 4	37 ± 3
Satin weave	0.31 ± 0.03	19 ± 1	0.26 ± 0.03	0.280	0.38 ± 0.05	19 ± 1	49 ± 3

Notes: 1) tensile strength; 2) Young's modulus; 3) Experimental Poisson's ratio; 4) ν_{xy} from Equation 4.13; 5 and 6) Compressive strength and modulus; 7) Apparent shear strength.

8) 18 layer laminate, not quite balanced, 6 layers each 0° and 90°, 3 layers +45° and 3 layers -45°. The other two laminates had the same fibre orientations with a similar lay up order.

Data from G.A Bibo, P.J. Hogg and M. Kemp, Comp. Sci. Tech. 57, 1997, 1221-41.

In the case of laminates the behaviour is far more complex. A set of glass-epoxy laminates made (a) with straight fibres, (b) with a weave with minimal fibre waviness

("noncrimp") and (c) with a weave which involved a great deal of waviness, were compared for tensile, compressive and flexural properties. Some of the results are shown in Table 10.2.

The waviness reduced the strength and modulus in compression quite noticeably, had a small effect on tensile strength, but had little consistent effect on the other properties.

The compressive strengths of glass fibre and carbon fibre reinforced polymers are usually close to, or somewhat less than, their tensile strengths. Boron reinforced polymers are generally about 20% stronger in compression than in tension. This is probably due to the larger diameter of the boron. Kevlar fibre reinforced materials have poor compressive properties, owing to the weakness of the Kevlar fibres when compressed. For example, the compressive strength of $V_f = 0.6$ aligned Kevlar reinforced epoxy was only 0.28GPa, while its tensile strength was 1.66GPa. Kevlar reinforced polymers should thus not be used in situations where considerable compressive stresses have to be supported (for instance, in flexure, the $V_f = 0.6$ Kevlar reinforced epoxy only has a strength 0.58GPa).

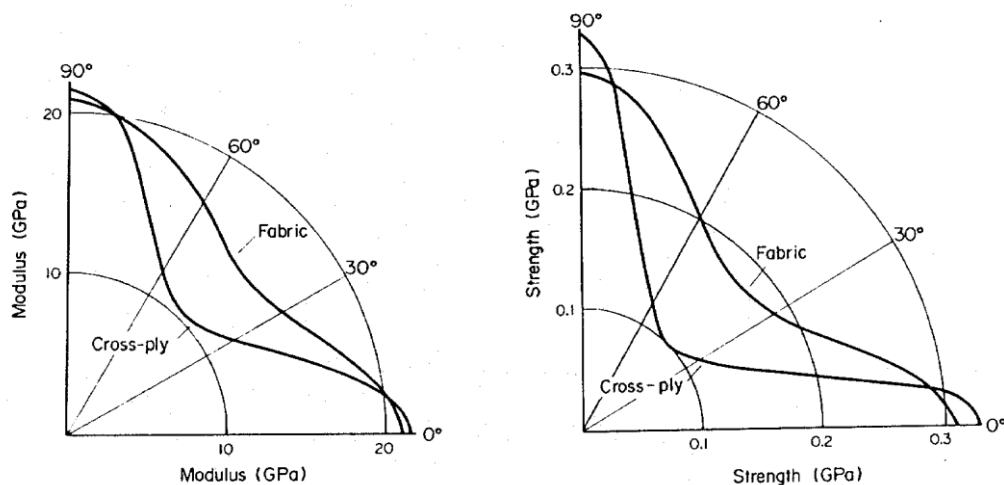


Fig. 10.3 Polar plots of modulus (left) and strength (right) of glass-epoxy laminates.

The strength and moduli of aligned fibre composites and laminates in directions other than the fibre directions are best represented graphically in the polar plots shown in Fig. 10.3. However, the stiffness and strength matrices may also be used. Table 10.3 gives some data on aligned carbon-epoxy.

Large quantities of reinforced thermoplastics are manufactured with fibres chopped to very short lengths. These composites have very much poorer mechanical properties than those described above. However, they can be moulded with relative ease using injection and extrusion machines, so long as the fibre length is kept below 10 mm and volume fractions of fibers are below 0.2. The composites produced have greater strength, higher modulus, and usually greater impact strength than the unreinforced matrix. In addition, the thermal expansion is reduced, and properties are less dependent on temperature.

Table 10.3 Elastic Constants and Strength Data for Transversely Isotropic Aligned Carbon-Epoxy

Compliances (GPa ⁻¹):	$S_{11} = 0.0049$ $S_{22} = S_{33} = 0.21$ $S_{23} = -0.0060$ $S_{12} = S_{13} = -0.0016$ $S_{44} = S_{55} = 0.16$ $S_{66} = 0.44$
Strengths (GPa):	$\sigma_{1u} = 0.97$ $\sigma_{2u} = \sigma_{3u} = 0.018$ $\tau_{12u} = \tau_{23u} = \tau_{31u} = \text{spurious}^*$

* see section 6.1.2

If cheap fibres are used the short fibre composite is often cheaper than the unreinforced matrix. There is usually little advantage in using the more expensive fibres (boron, carbon, and Kevlar) in these composites. Usually about a two fold increase in strength and modulus can be obtained with glass while little more improvement can be obtained with the more expensive fibres. Both thermoplastics and thermosets are used in these moulding compounds.

Table 10.4 Work of Fracture (Jm⁻²) for the Resin Matrices (\mathcal{G}_m) and for Delamination of Composites in the Opening Mode (\mathcal{G}_3).

Fibre	Resin	\mathcal{G}_m	\mathcal{G}_3
AS1 Carbon	Brittle Epoxy	69	155
AS4 Carbon	Brittle Epoxy	69	255
T300 Carbon	Brittle Epoxy	80	100
T6000 Carbon	Toughened Epoxy	2200	830
T300 Carbon	Polysulphone	2500	1200
T300 Carbon	Polyetherimide	3300	935
AS4 Carbon	DuPont J2 polyamide	1600	1200 ¹
E glass	Brittle Epoxy	-	264 ²

Notes: All results from D.L. Hunston, Comp. Tech. Rev. 6, (1984) 176-80, except 1) A.R. Wedgewood, K.B. Su and J.A. Nairn, SAMPE J. 24, (#1) 41-5 and 2) X.J. Prel., P. Davies, M. Benzeggag, and F.X. de Charentenay, ASTM STP, 1012, (1989), 251-69.

10.1.2 Toughness

High performance composites are often made with high Tg epoxies and polyimides which tend to be brittle. Thus they tend to delaminate easily, and as can be seen in Fig. 7.16, works of fracture can be less than 200 kJm^{-2} . This has led to the development of toughened epoxies and composites made with high performance thermoplastics such as PEEK. Some opening mode delamination data is given in Table 10.4. (When using this table, it should be remembered that many literature results overestimate the initial resistance to crack propagation: see section 7.3.)

In the early days, much effort went into trying to evaluate the work of fracture of unidirectional laminates broken at right angles to the fibres. Special techniques were required; see Fig. 7.6. This is because such "across the grain" fracture required two or three orders of magnitude more work than splitting. The ASTM standard fracture toughness test shown in Fig. 7.5 is only suitable for some multi-directional laminates for this reason.

With non-fibre reinforced materials it is essential that toughness is measured using a sample with a notch which is very sharp (a sufficiently sharp notch is usually obtained with metals by machining a notch and then fatiguing the specimen). With composites this is not effective for notches which are expected to grow normal to the fibres, owing to the notch-blunting effect of the fibres. In the ASTM standard tests shown in Fig. 7.6, the notch is neither rounded nor sharp. Instead it has a width of 0.015 or less of the specimen width.

Table 10.5 Fracture Toughness Values for Carbon-Epoxy and Carbon-Polyimide Laminates

Structure	Matrix	K_{Ic} ($\text{MPa}\sqrt{m}$)
$[(0/90)_3/\bar{0}]_s$	Epoxy	19 ± 3^1
$[(90/0)_3/\bar{90}]_s$	Epoxy	17 ± 2^1
$[0/\pm 60/0/\pm 60/\bar{0}]_s$	Epoxy	23 ± 4^1
$[90/-45/0/+45]_{4s}$	Epoxy	57 ± 3^2
$[(0/90)_3/\bar{0}]_s$	Polyimide	84 ± 1^1
$[(90/0)_3/\bar{90}]_s$	Polyimide	45 ± 2^1

Data from 1). J.H. Underwood, I.A. Burch and S. Bandyopadhyay, ASTM STP 1110, 1991, 667-83, and 2) ASTM Standard E 1922, 1997.

This standard was only developed very recently and few results are available. However, results of comparative tests on the fracture toughness calculated from notched strength tests on laminates are given in Table 10.5.

To convert to the corresponding works of fracture requires a knowledge of the elastic constants: see equations (7.3–7.5). For example, the laminate with a fracture toughness of $57 \text{ MPa}\sqrt{\text{m}}$ had an E_{kx} of 38GPa, giving a work of fracture of 85kJm^{-2} . This is much greater than the works of delamination, Table 10.4, and comparable with values for structural steels and aluminiums (see Table 1.2). Still greater works of fracture have been observed in our work with angle ply laminates. For example $[\pm 15]_s$ carbon-epoxy had $\mathcal{G}_x = 0.7 \pm 0.1\text{MJm}^{-2}$ and glass-epoxy $0.5 \pm 0.1\text{MJm}^{-2}$.

Moreover, it has been shown that the notched strength does obey the Griffith criterion (equation (2.18)) moderately well. For very small notches, the strength is about the same as the unnotched strength. But beyond a notch or hole size of about 2 mm, a very wide range of laminates has the strength inversely proportional to the square root of the notch (or hole) size. Fig. 10.4 shows plots from a literature survey of results from carbon and glass fibre laminates.

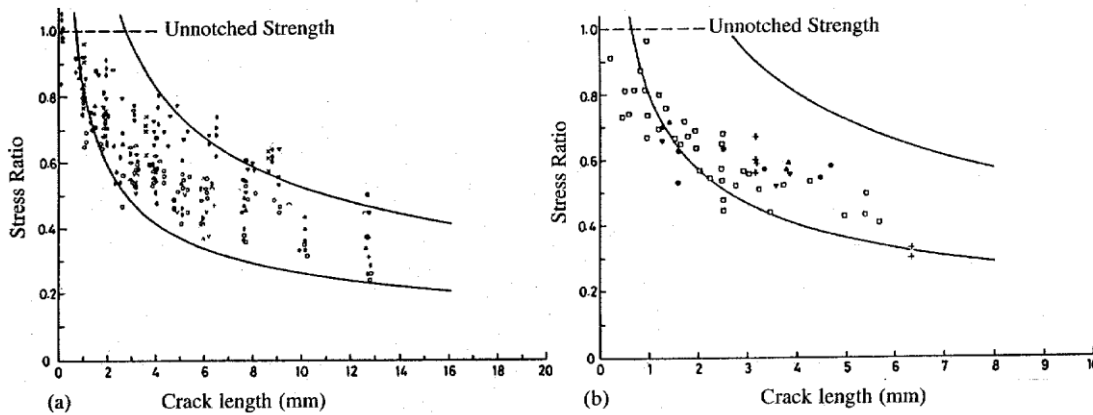


Fig. 10.4 Ratios of unnotched to notched strengths for carbon (at left) and glass (at right) fibre laminates. The curves are given by equation (2.37), the upper curves being $K_{Ic} / \sigma_u = 0.09\text{m}^{1/2}$ and the lower $0.045\text{m}^{1/2}$. (After Wells, J.K. and Beaumont, P.W.R., Scripta Metallurgica 16, 1982, 99-103.)

Table 10.6. Results from Work of Fracture and Impact Tests on Unidirectional Fibre Reinforced Epoxy ($V_f \sim 0.6$)

Reinforcing Fibre	Work of Fracture (kJm^{-2})
Boron	18*
Carbon	40*+
S-Glass	130*
Kevlar	140+

* Work of Fracture Tests, and + Impact Test.

Fracture mechanics tests have not been successful with unidirectional fibre composites due to difficulties in getting the crack to propagate in the desired direction.

Instead, representative toughness data, taken from impact and other tests for aligned fibre composites are given in Table 10.6. It may be seen that the least tough fibre composites are the boron fibre reinforced ones, carbon being next, then glass, and the most tough being Kevlar. The relative brittleness of the carbon materials is probably due to the small diameter and high modulus of the fibres. The Kevlar composites are tough because the fibres have some toughness.

10.2 Fatigue

The fatigue properties of fibre reinforced polymers are good compared with aluminium. After 10^6 cycles, a typical aluminium alloy retains less than 20% of its strength (see Fig. 1.4). Under the same conditions (equal tensile and compressive stresses during each stress cycle) unidirectional carbon fibre reinforced epoxy, for example, retains at least 30% of its strength. Under purely tensile fatigue conditions it can retain more than 90% of its strength. Boron reinforced polymers perform almost as well as this, while glass fibre reinforced polymers perform rather less well.

Fig. 10.5a summarizes some results from high performance and low performance composites. (Note that internal heat is produced when reinforced polymers undergo cyclic stressing. True fatigue effects, as distinct from effects due to heat, are thus only found at frequencies of less than 10 Hz at low stress levels and 1 Hz at high stress levels.)

The poorer fatigue resistance of glass reinforced polymers is associated with the lower modulus of glass, and hence the greater strain suffered by the composite. Moreover, there may be some weakening of the glass due to traces of moisture.

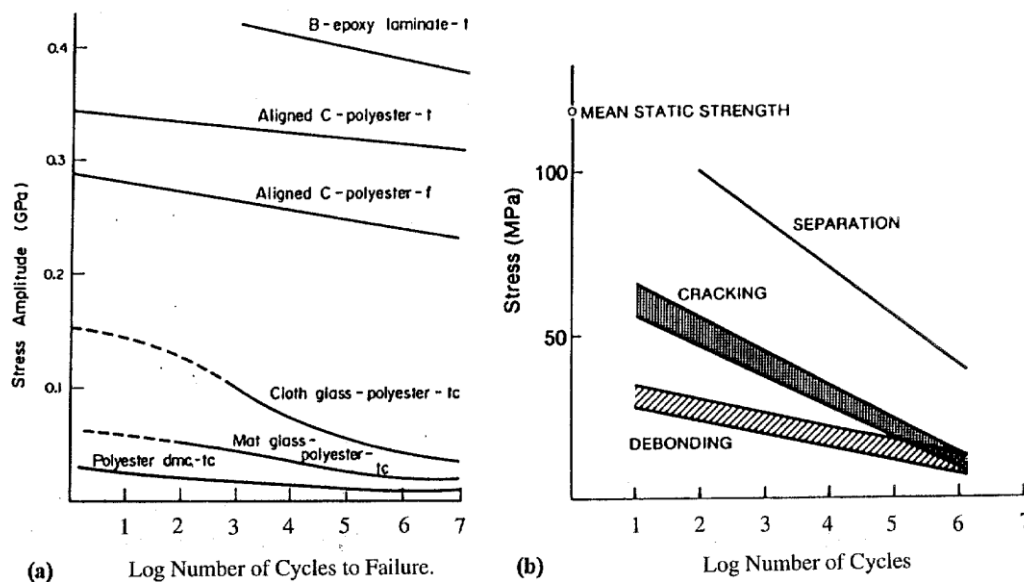


Fig. 10.5 An approximate comparison of fatigue behaviour. (a) Modes of Testing: t = tension, tc = tension-compression and f = flexure. Also dmc = dough moulding compound. (After Harris, B, 1977, *Composites* 8, 214-20). (b) Stages in the failure of chopped glass-polyester. (After Owen, M.J., Smith, T.R., and Dukes, R., 1969, *Plastics and Polymers*, 37, 227-33.)

10.2.1 Multidirectional Composites

With multidirectional composites, fibre-matrix bond failure may be the first indication of fatigue; next the matrix starts to fail, and finally complete separation takes place. These processes are well illustrated by chopped strand mat glass fibre laminates, which have relatively poor fatigue properties (Fig.10.5b). Debonding has also been observed during shear fatigue.

In addition, compressive stresses during the fatigue cycle have a large effect on the fatigue life. Thus is illustrated in Fig. 10.6. A material which is unaffected by compressive stress would have the 10^6 cycles results in the form of two straight lines at angles of $\pm 45^\circ$ to the abscissa, meeting at the ordinate at 520MPa. The experimental results fall below the line by an amount depending on how symmetrical the stress cycle is.

The greater the proportion of fibres there are in the direction of the applied stress, the greater the fatigue life. This is because the process is related to the maximum strain; the strain will be kept to a minimum if the number of fibres directed along the stress axis is a maximum. The effect of the fibre volume fraction on the fatigue life also depends on the matrix strain. Thus for the same matrix strain, the fatigue life is independent of fibre volume fraction. (The corresponding stress, of course is related to the volume fraction by the Rule of Mixtures.)

Different lamination arrangements result in different matrix strains. So the results for one lamination arrangement cannot be used to predict the fatigue life of a different arrangement.

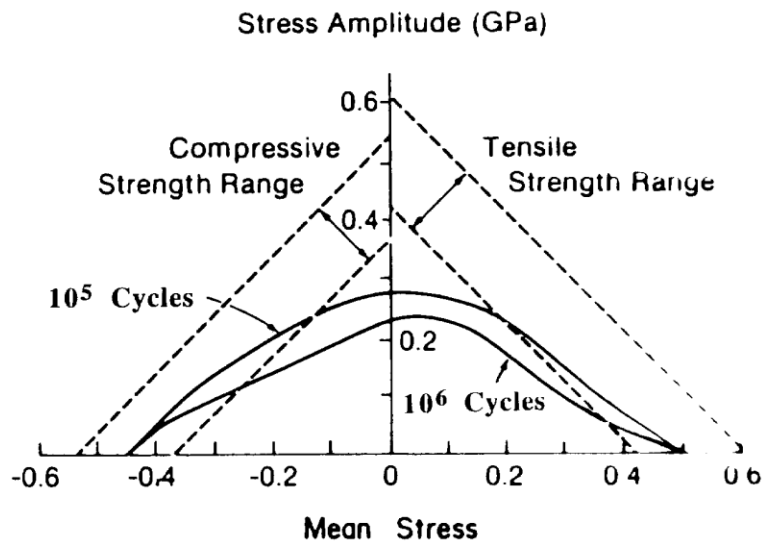


Fig. 10.6 Fatigue failure envelopes for carbon-epoxy laminates $0 \pm 45^\circ$ orientation. (After Bevan, L.G., 1977, *Composites* 8, 227-32.)

The fatigue properties are affected by notches. The presence of a hole reduces the fatigue life, and a slot reduces it even further, as shown in Fig. 10.7. This, again probably reflects the increased strains in the region of the notch.

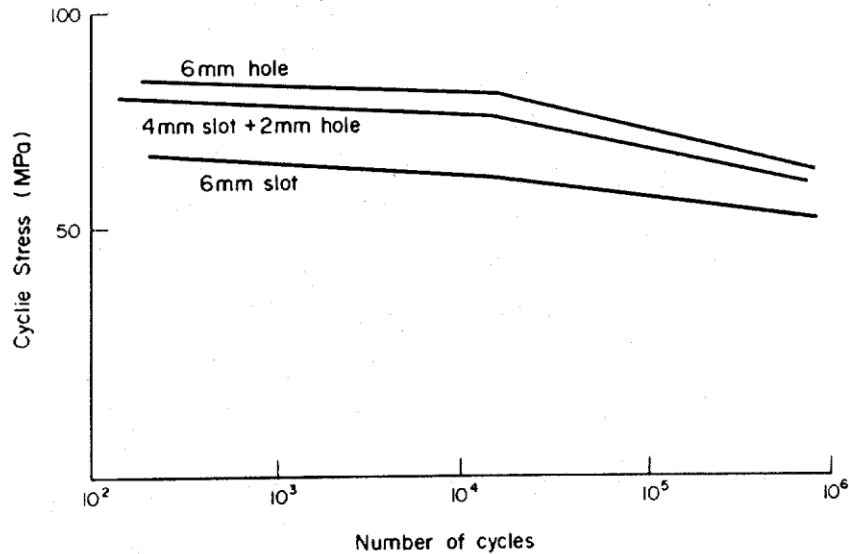
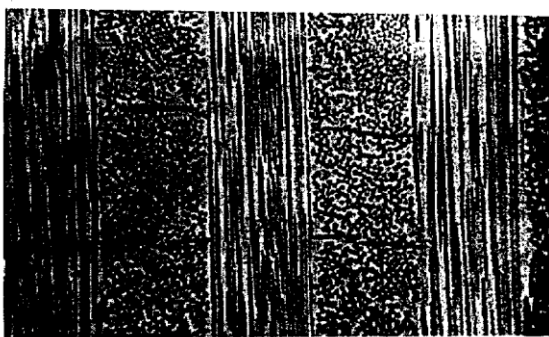
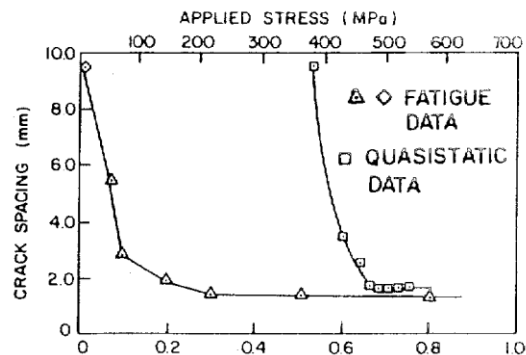


Fig. 10.7 Effect of different types of notch on the fatigue of glass-epoxy laminates. (After Carswell, W.S., *Composites* 8, 1977, 251-4.)

The details of the failure process in laminates have been thoroughly investigated. The off-axis plies split in the early stages of the process. Fig. 10.8a shows cracks which have developed in an S-glass-epoxy cross ply laminate. When fibres are in other directions, these plies also split and Fig. 10.8b shows the development of cracks in the $\pm 45^\circ$ layers (left hand curve) during fatigue. If, instead, the composite is simply subject to monotonically increasing stress, a similar crack density results, as shown in the right hand curve. This is an illustration of the so called characteristic damage state, which appears to be a material property.



(a)



(b)

Fig. 10.8 At left, cracks developed in S-glass-epoxy cross ply laminates during fatigue, and at right crack development in 45° plies of a $[0, 90, \pm 45]_s$ carbon-epoxy laminate; triangles during fatigue and squares during simple loading. (After Broutman, L.J., and Sahu, S., 24th Ann. Tech. Conf., SPI, 1969, Section 11D, and Reifsnider, K.L., Schulte, K., and Duke, J.C., ASTM STP 813, 1983, 136-59.)

Although loss of strength occurs because of the failures in the off-axis plies together with progressive delamination, final failure is governed by the 0° plies in a

normal laminate. Work on this was briefly mentioned in section 6.6. Here we will provide more detail of the experimental results and conclusions. The work was carried out using special low shrinkage polymer matrices to make unidirectional carbon fibre reinforced pultrusions and revealed the following:

1) The stiffness decreased continuously, see Fig. 10.9. This was also the case for tensile-tensile fatigue ; see 6.43. Moreover, flexural stiffness was more greatly affected than tensile stiffness; this is also shown in Fig. 6.43. In both cases, the rate of stiffness decrease was greatest near the end of the fatigue life.

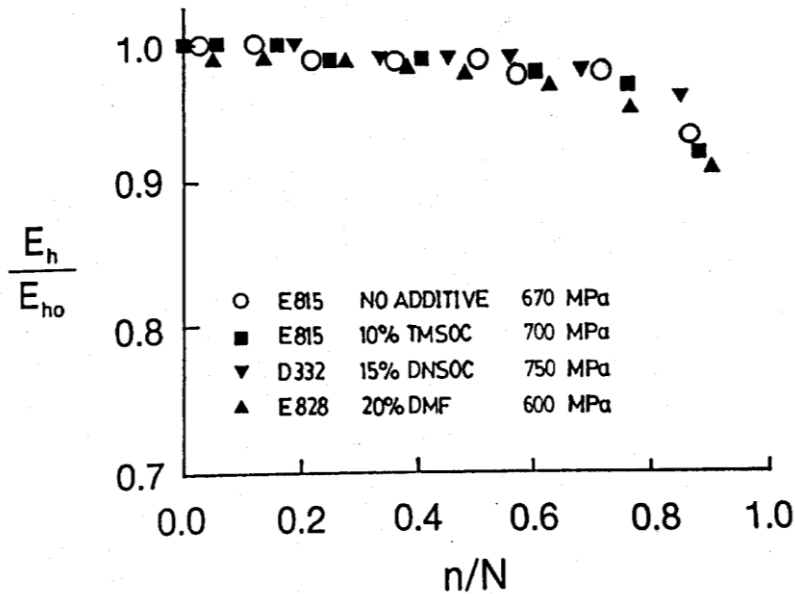


Fig. 10.9 Stiffness reduction during the fatiguing process. Tension-compression fatigue ($R = -0.3$); spiro orthocarbonates (TMSOC and DNSOC) added as indicated; also non reactive solvent, dimethylformamide (DMF). Resins were DGEBA epoxies (E815 etc.). Maximum stresses as indicated. (After Lam, P.W.K., and Piggott, M.R., *J. Mater. Sci.* 24, 1989, 4427-31.)

2) The energy absorbed during fatiguing increased continuously; see Fig. 10.10.

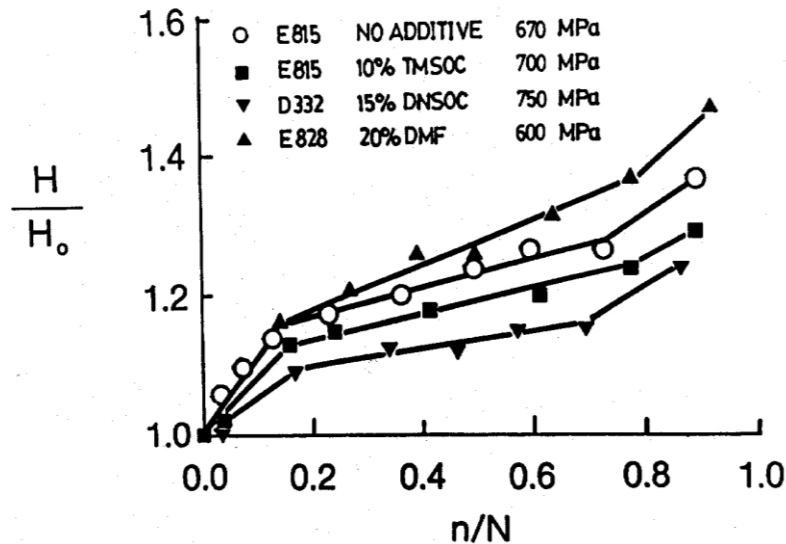


Fig. 10.10 Energy absorbed during fatigue; systems and conditions were the same as for Fig. 10.9.

3) Poisson's ratio increased; see Fig. 10.11

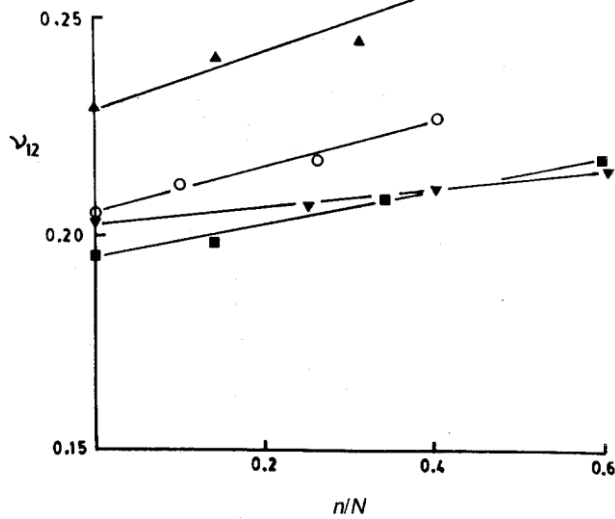


Fig. 10.11 Increase in Poisson's ratio during fatigue; systems and conditions were the same as for Fig. 10.9, but $R = 0.1$ tension-tension fatigue.

4) A hole at the centre of the specimen increased in width at a greater rate than its increase in length; see Fig. 10.12.

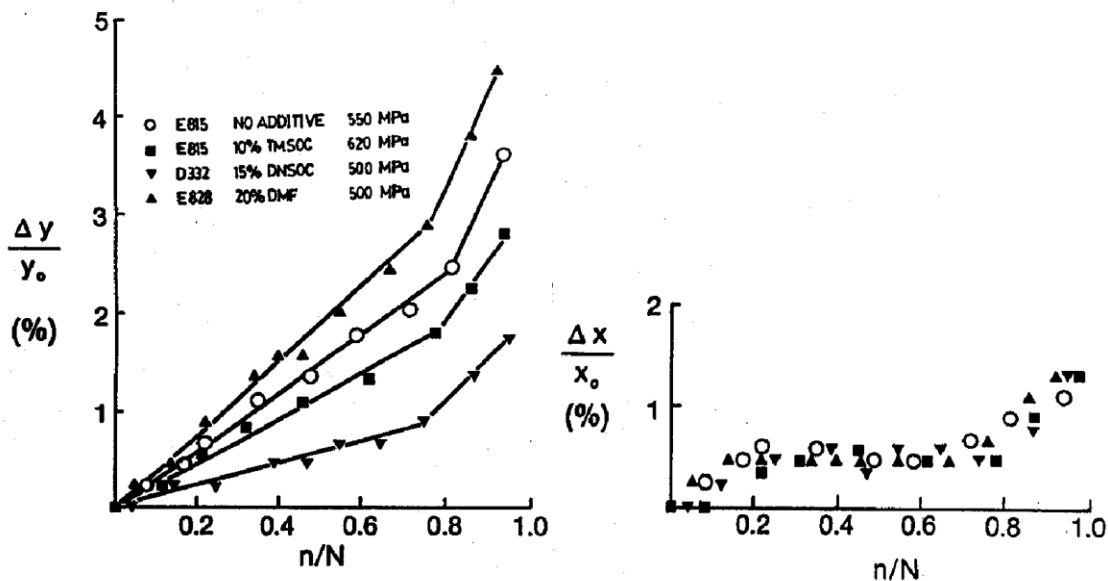


Fig. 10.12 Effect of fatigue on width and length of an originally circular hole; systems were the same as for Fig. 10.11; maximum stresses were as indicated.

5) The slope of the S-N curve was less for laminates with lower polymer shrinkage stresses, but greater when fibres were poorly adhering, Fig. 10.13.

Although splitting plays a role (see Fig. 10.14), and there has been some evidence that the failure strain is approximately constant, it is likely that more subtle processes are also involved. Once a laminate has been reduced (by splitting, etc.) to the state where the load is entirely supported by the 0° fibres, the initial fibre waviness could play a major role in the process. When this happens, a fixed strain criterion is no longer valid,

according to our modulus loss and strength loss evidence in Fig. 10.9, etc. Instead the waviness increases due to the fatigue process as illustrated in Fig. 6.42. The mechanism envisaged for this was the cominution of the matrix by the work induced by the transverse stresses arising from the straightening and relaxing of the fibres under the oscillatory stresses. The matrix powder thus produced could have moved to the fibre nodes, again under the influence of the oscillatory transverse (and longitudinal) stresses.

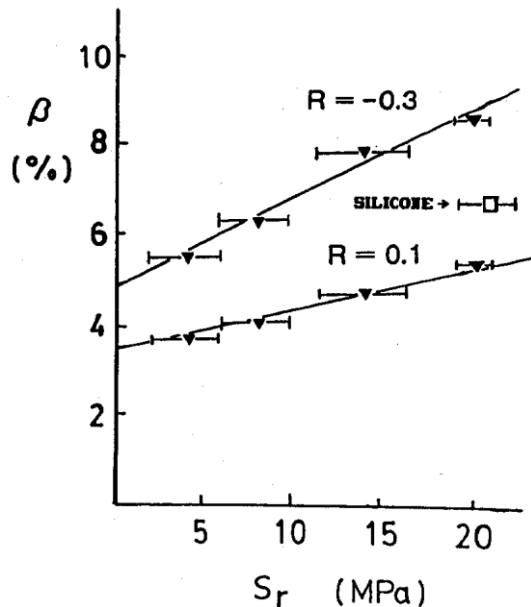


Fig. 10.13 Effect of polymer shrinkage stress, S_r , on slope of S-N curve, β . Stress ratios, R , as indicated. Composites made with fibres coated with silicone resin were tested at $R = 0.1$.

Eventually the fibres could have been subject to significant flexural stresses due to the ever increasing waviness, which thus gradually increased the maximum tensile stresses experienced by the fibres. This could have caused the relatively low stress failure; see Fig. 10.6. It should be noted that this process does not require the relative modulus and strength decreases to be the same.

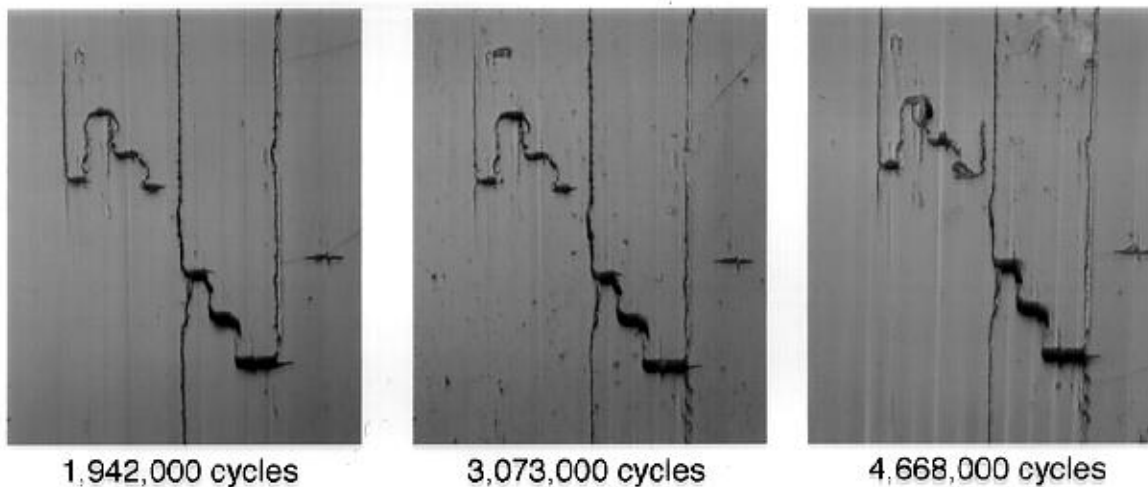


Fig. 10.14 Development of Splitting During Fatigue of Carbon-Epoxy (After Gamstadt, E.K., PhD. Thesis, Lulea University of Technology, Sweden).

In addition, increased waviness could increase fibre-fibre contacts, leading to fibre fretting (i.e. rubbing) failure. Moreover, with glass fibres, traces of moisture significantly reduce the fibre strength after a long period of time; see Fig. 10.15. (This shows the fraction of fibres which broke after a given length of time at a fixed stress.) This could contribute to the more rapid fatiguing of glass fibre composites.

An alternative mechanism has the fibres breaking at their weakest points, throwing extra loads on to neighbouring fibres, which subsequently break. Meanwhile the matrix splits, making stress transfer more difficult and thus exacerbating the problem. Although this seems to be supported by the surface cracks shown in Fig. 10.14, our evidence of modulus loss (Fig. 10.9) does not support this because of the extent of fibre breakage required: see problem 10.21)

However, it should be noted that fatigue has not been a problem when high performance laminates have been used in aircraft and other load bearing applications. As can be seen from Figs. 10.9 and 10.13, the effects are quite small. Little is known about the resistance of angle ply laminates to fatiguing; it must be borne in mind that wide specimens must be tested for any useful results to be obtained (see section 4.4.3). Thus the result shown in Fig. 10.6, where the laminates contained off-axis plies, should be treated with caution. Fatigue tests on pressurized tubes are needed if we are to accurately quantify fatigue effects on laminates containing angle plies.

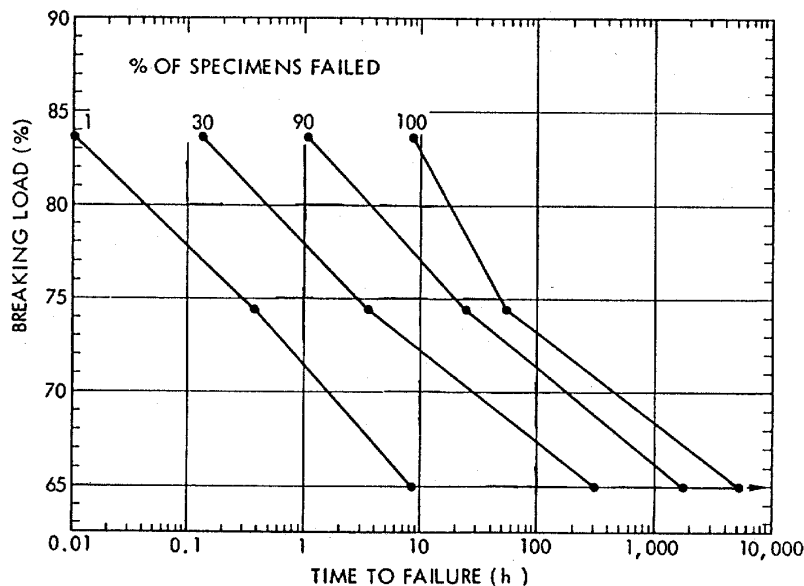


Fig. 10.15 Static fatigue of glass as indicated by the proportions of fibres that failed after a certain time, while kept at a fixed fraction of the breaking load. (After Chiao, T.T and Moore, R.L., 1971, *J. Comp. Mater.* 5, 2-11.)

10.3 Creep

Polymers creep at room temperature at stresses far below their ultimate strengths. Figure 10.16 (a) shows that at room temperature an epoxy resin creeps markedly at 34MPa (and it still creeps significantly at 3.4MPa). The addition of fibres with sufficiently great aspect ratios to give good stress transfer (i.e. s greater than $10s_c$) greatly

reduces the creep of the polymer. If continuous ceramic fibres (boron, carbon, or glass) are used, and they are aligned in the stress direction (for uniaxial stressing) creep is almost eliminated altogether. However, creep can still occur when the stress is not in the fibre direction, and can be quite substantial for relatively small angles between the stress axis and the fibre alignment axis.

When biaxial stresses are present, laminates with fibres in appropriate directions can be used to keep creep rates down to a very low level. There is some residual creep, however, because the polymer layers between the laminae can creep to a small extent.

In the case of glass fibre reinforced polymers, creep rupture occurs at stresses somewhat below the short term ultimate tensile strength, even though no creep strain is observed. In the region near the breaking stress, a 0.3% increase in stress decreased the life by a factor of ten. This is probably due to the "static fatigue" of the glass fibres, and is probably due to the presence of traces of moisture, Fig. 10.15 shows some results obtained with S glass-epoxy strands.

In contrast with ceramic fibres, Kevlar fibres do creep significantly, even at room temperature; Fig. 10.16a shows the creep of Kevlar fibres at two stresses at room temperature. Because of this, polymers reinforced with continuous Kevlar fibres creep at room temperature when stressed in the fibre direction. The creep curves for an epoxy resin containing 50% Kevlar have regions of primary creep and secondary creep (in this latter region the creep strain rate is approximately constant). Results obtained, plotted as creep strain vs log time, are shown in Fig. 10.16b. These curves can be accounted for in terms of the creep of the matrix and the fibres. The matrix controls the early stages of the creep process, while the fibres control the later stages. In addition, low stress creep depends on matrix creep, while creep at high stresses is governed by the fibre creep properties.

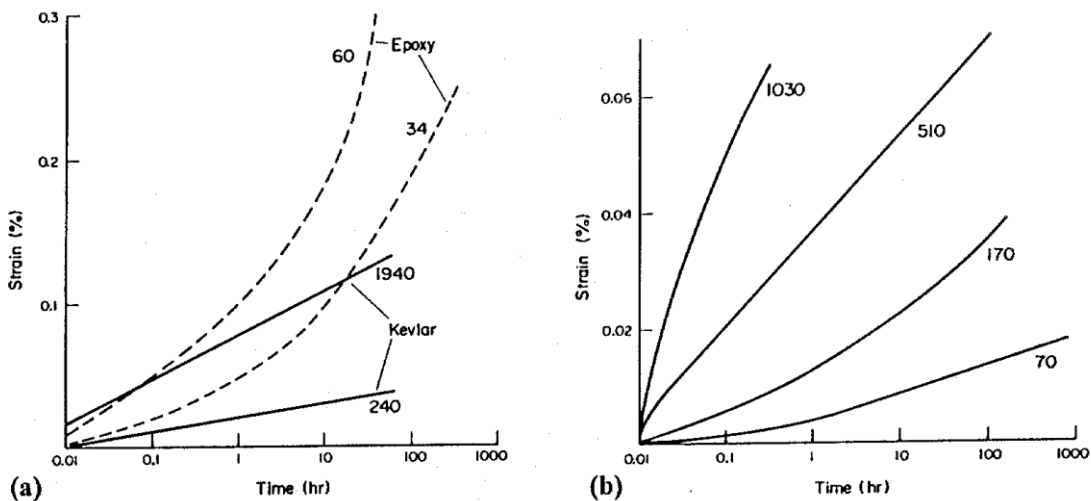


Fig. 10.16 Room temperature creep curves for (a) Kevlar fibres and a cycloaliphatic epoxy resin and (b) Kevlar-epoxy. The applied stresses (MPa) are marked on the curves. (After Erikson, R.H., 1976, Composites 7, 189-94.)

Finally, a knowledge of the creep properties of laminates containing angle plies requires appropriate tests on tubes to avoid effects due to edge softening and gripping constraints.

10.4 Environment Effects

Agents in the normal ambient environment which can degrade the properties of reinforced polymers include ultraviolet radiation, heat, organic fluids and water.

10.4.1 Radiation, Heat and Residual Stress

Ultraviolet radiation and heat both degrade the polymer. Where a large intensity of ultraviolet radiation is expected to be present polymers are normally treated with materials which will absorb the radiation, which would otherwise cause chain scission. This solves the problem, but adds significantly to the cost of the polymer. The fibres in reinforced polymers usually absorb this radiation, so the problem is very much reduced, and the radiation only affects the very thin layer of polymers between the free surface and the fibres nearest the surface.

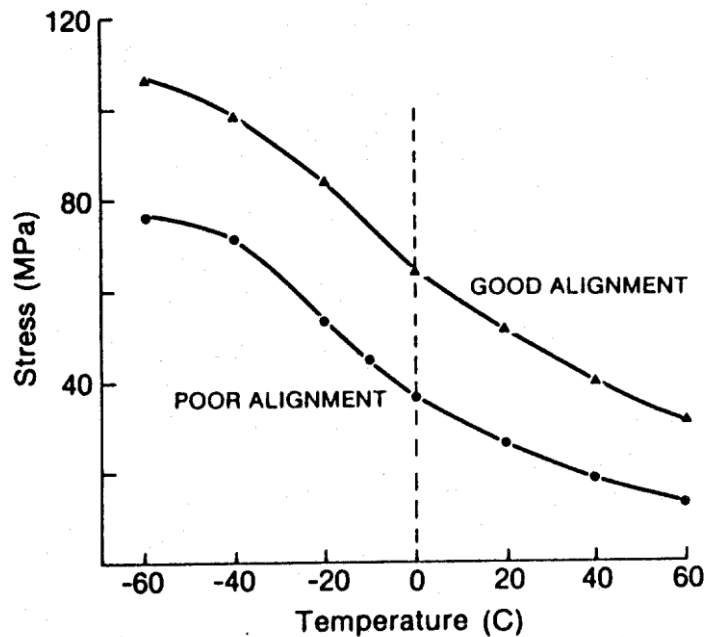


Fig. 10.17 Creep of chopped glass-polypropylene. Stress is that required to cause 0.1% strain after 100s. (After Darlington, M.W., McGinley, P.L. and Smith, G.R., May 1977, *Plastics and Rubber: Materials and Applications*, 51-8.)

Heat also causes decomposition of polymers, and severely limits the usefulness of reinforced polymers above about 200°C. The maximum temperature depends on the polymer. The creep rate of short fibre reinforced polymers is greatly increased by heat. Fig. 10.17 shows the temperature variation of the stress which, after being applied for 100s gives rise to a strain of 0.1% for short glass fibre reinforced polypropylene. It is clear that the material loses a great deal of its stiffness when heated. Continuous fibre reinforced polymers are not so badly affected, but loss of properties occurs at the softening point of the polymer. Special polymers, most notably polyimides, have been developed to combat this problem. They extend the useful temperature range of reinforced polymers to about 300°C.

At low temperatures polymers become brittle, but reinforced polymers continue to be able to support loads without loss of properties, except under conditions where multiple cracking of the polymer can occur. This has been observed in the case of steel wire reinforced polymers, under stress at liquid nitrogen temperatures, but glass reinforced polymers have performed well at low temperatures.

The cure process involves polymer shrinkage which leaves the composite with internal stresses which can be quite high. The shrinkage arises from two processes.

1. With thermosets, the chemical reactions involved bring some of the atoms closer together in the molecule. This is usually referred to as chemical shrinkage. Volume decreases of as much as 5% can be observed with polyesters, giving tensile strains of up to 2% if fully restrained by the fibres. Epoxies typically change in volume by only about 1-2%.

Table 10.7. Approximate Thermal Expansion Coefficients, MK^{-1} , for Glass Reinforced Polymers (α_c) and the Unreinforced polymers (α_m)

Reinforced Thermosets	α_m	α_c	V_f
Polyester moulding compounds	50-100	14	0.15
Phenolic moulding compounds	25-60	8	0.12
Filament wound glass-epoxy	55-65	4	0.63
Pultruded glass-polyester	50-100	5	0.63
Reinforced thermoplastics*	α_m	α_c	V_f
PVC and PPO	55-70	20	0.22
PP, ABS, SAN	70-100	29	0.22
PE (medium density)	140-160	31	0.22
Acetal	81	34	0.22

* for acronyms see section 9.1.1. and Appendix B

2. With high temperature cured thermosets, the stresses due to chemical shrinkage are mostly relieved at the cure temperature. However, on cooling to the use temperature, differential thermal shrinkage occurs, giving a strain ε_T :

$$\varepsilon_T \cong \int_{T_s}^{T_u} \Delta\alpha dT \quad (10.1)$$

Here $\Delta\alpha$ is the difference between the thermal expansion coefficients of the polymer, α_m and the fibres, α_f , T_s is the softening temperature of the polymer, and T_u is the use temperature of the composite. The stresses in thermoplastic composites also arise from differential thermal shrinkage and so are also governed approximately by this equation. (The equation is approximate because the fibres are not infinitely stiff; a more detailed treatment is given in Chapter 11.) For a unidirectional carbon-epoxy laminate with $\alpha_f = -$

0.5MK^{-1} and $\alpha_m = 30\text{MK}^{-1}$ cured at 200°C , ε_T comes to about 0.54% leaving a tensile stress in the polymer of 14MPa. (see Tables 3.3 and 10.7)

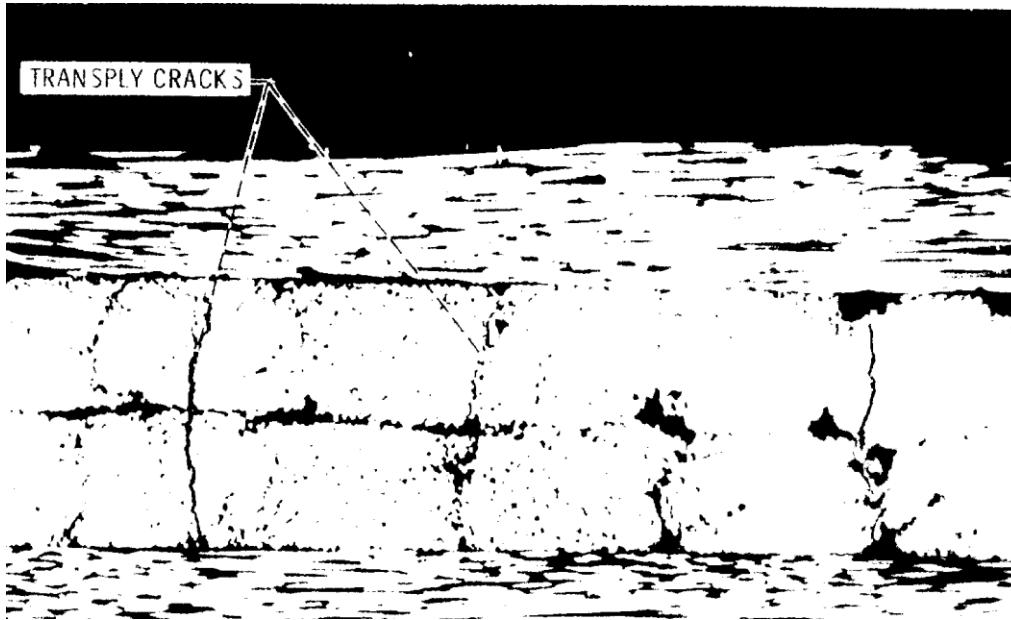


Fig. 10.18 Cracking due to residual thermal stresses in carbon-epoxy laminate produced during manufacture. (After Chamis, C.C., 1978, Proc. ICCM2, 221-239., Courtesy of the Metallurgical Soc., AIME.)

The high strains induced in the polyester can lead to cracking; see Fig. 10.18. The residual stresses can be estimated from the bending and twisting they cause in unbalanced laminates. This is demonstrated most starkly in the $[0,90]$ two layer laminate. Here the stresses, σ_T , can be estimated from the radius of curvature, R_T ,

$$\sigma_T = \frac{h}{24R_T} (E_1 + E_2) \quad (10.2)$$

for a total laminate thickness of h . For a strain difference, $\Delta\varepsilon$, due to cure, or differential thermal shrinkage,

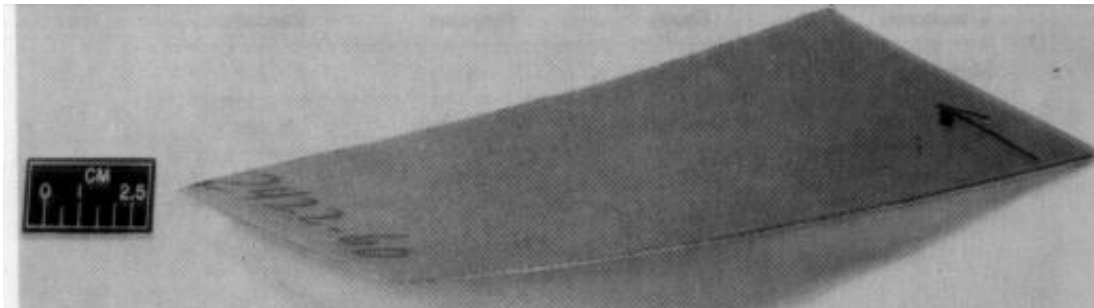


Fig. 10.19 Unsymmetric laminate warped due to thermal expansion differences. Kevlar fabric-epoxy (After Chamis, C.C. 1978, Proc. ICCM2, 221-39, Courtesy of the Metallurgical Soc., AIME.)

$$R_T = \frac{h}{2\Delta\varepsilon} \left[1 + \frac{1}{12} (E_1 + E_2) \left(\frac{1}{E_1} + \frac{1}{E_2} \right) \right] \quad (10.3)$$

(You are invited to develop this equation as an exercise: see problem # 10.15 at the end of the chapter.) Fig. 10.19 shows an example of thermally induced twisting.

10.4.2 Water and Other Fluids

Water affects both the polymer and the polymer-fibre interface. In the case of Kevlar fibres it affects the fibres as well. Fig. 10.20 shows the absorption of water at 100°C by carbon, glass, and Kevlar fibre reinforced epoxy. In the case of the glass and carbon, the absorption is about the same as that for the equivalent amount of resin, while Kevlar absorbs much more.

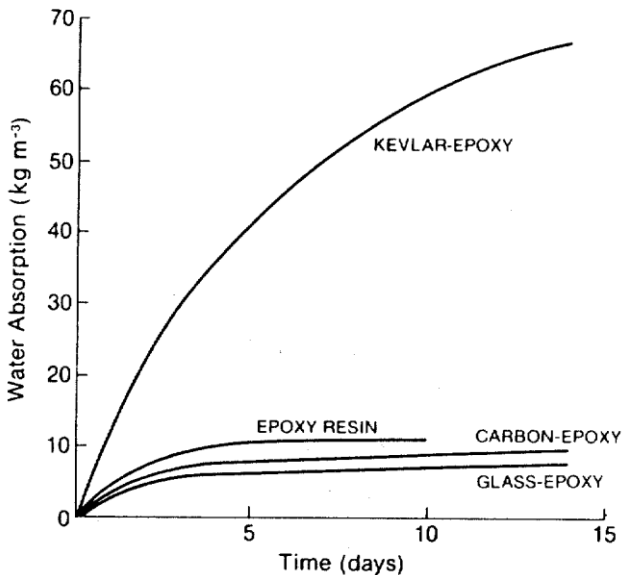


Fig. 10.20 Moisture absorption of epoxy resin and composites at 100°C. (After Phillips, D.C., Scott, J.M., and Buckley, N., 1978, Proc. ICCM2, 1544-9.)

The absorbed water has a large effect on the apparent shear strength of the Kevlar-epoxy, reducing it by 50%, but does not affect the shear failure strain. With carbon- and glass-epoxy, the apparent shear strengths are not much affected, but the shear failure strains are reduced by about 40%. Drying out the materials does not restore the properties. In addition, the moisture affects the shear fatigue properties of the glass- and carbon-epoxies, but not the Kevlar-epoxy. Fig. 10.21 shows its effect on the fatigue curves for glass and carbon. The loss in fatigue strength is not recovered when the materials are dried out.

Absorption of fluids softens the polymer matrix, expands it, and can also weaken it. The seriousness of these effects depends on the amount of fluid absorbed and, to a lesser extent, on the rate at which the fluid is absorbed and diffuses within the polymers. Effects due to fluids can be quite serious, so the diffusion process in fibre composites will be treated in some detail.

10.4.3 The Absorption and Diffusion Process

For a good understanding of the effect of water on a polymer composite, a knowledge of the absorption of water by the resin and the fibre-resin interface is required. The resin behaviour is normally relatively simple: it obeys Fick's Law and in humid air the moisture absorbed at equilibrium, M_s , obeys the power law relationship $M_s = M_1(RH)^b$. Here M_1 and b are constants, and M_s is the saturated weight gain as a fraction of the original weight of the polymer and RH is the relative humidity. Both M_1 and RH depend on the resin and M_s depends only slightly on temperature. For Henry's Law to be obeyed, $b = 1$, but it is found that b can be greater with polymers.

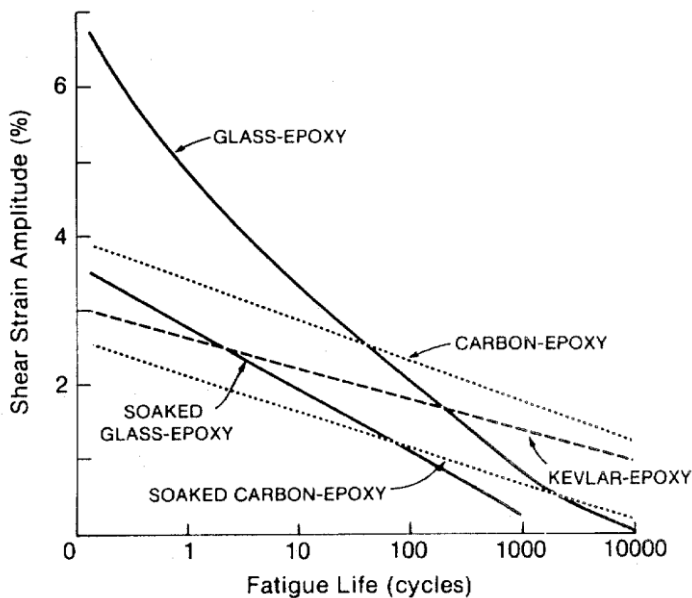


Fig. 10.21 Effect of water soaking for seven days at 100°C on shear fatigue lives. The Kevlar-epoxy was not significantly affected. (After Phillips, D.C., Scott, J.M., and Buckley, N. 1978, Proc. ICCM2, 1544-9.)

Fig. 10.22 compares the water absorption of two DGEBA type epoxy resins at 23°C and 100°C. Also shown is a resin containing a monomer designed to reduce the shrinkage stresses. (This is dinorbornene spiro ortho carbonate - here abbreviated to DNSOC). The weight gain is plotted vs $\sqrt{\text{time}}$ because Fickian behaviour requires that, when plotted this way, a linear region is observed near the origin. If this has a slope β , then the diffusion coefficient, D , is given by

$$D = \pi h^2 \beta^2 / [16 M_s^2] \quad (10.4)$$

for a sheet of thickness, h . (The other dimensions of the sheet must be $\gg h$.)

Fig. 10.22 shows that Fick's Law is obeyed by all three resins. However, the DER 332 starts to lose weight after about 16h at 100°C. This is due to the water attacking the resin and leaching out (i.e. dissolving) small fragments of the molecule. Adding the DNSOC reduces this effect. These resins were cured with a BF_3 complex. The EPON 815, which contains butyl glycidyl ether, was cured with TETA. (See section 9.1 for more information on the chemistry involved.)

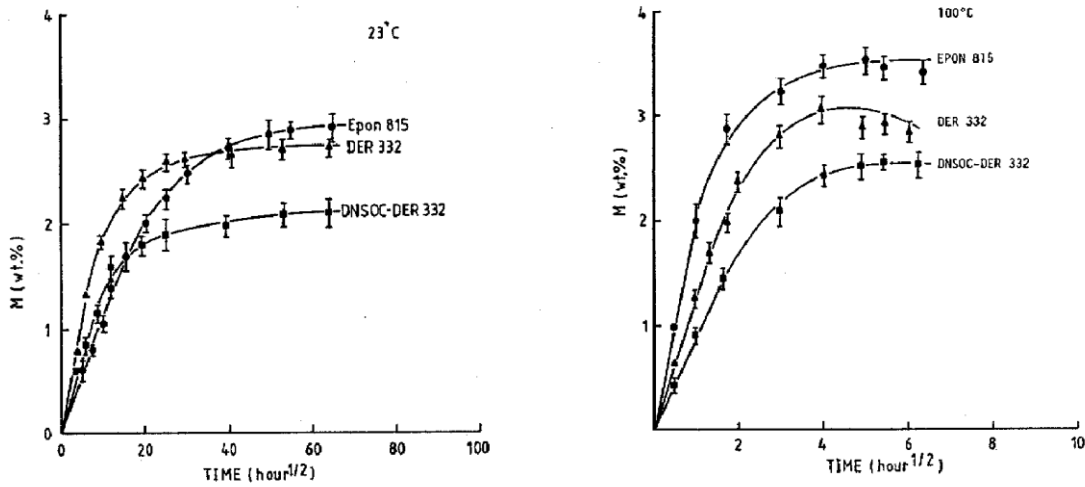


Fig. 10.22 Water absorption of epoxy resins at 23° (at left) and 100°C (at right). (After Woo, M. and Piggott, M.R., 1987, J. Comp. Tech. Res. 9, 101-7.)

Resins can be used which have much smaller water absorption. For example PEEK only absorbs about 0.4% of water at 23°; see Fig. 10.23. This resin also obeys Fick's Law. The effects observed in humid air are very similar, with M_1 somewhat less than M_s for immersion at the same temperature.

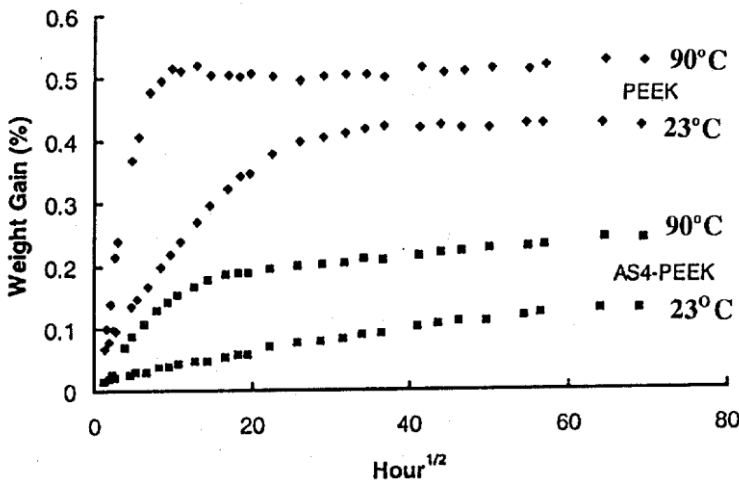


Fig. 10.23 Water absorption of PEEK at 23°C and 90° (upper curves) and absorption by unidirectional carbon-PEEK composite (lower curves). (After Zhang, A. and Piggott, M.R., J. Thermoplastic Comp. 2000, 13, 162-72.)

M_s generally increases slightly with temperature, both for immersion, Fig. 10.24 (top plot) and humidity exposure, (other curves). The diffusion constant for the EPON 815 is a linear function of relative humidity at 23°C; see Fig. 10.25. Here the immersion value was used for the point at 100% RH.

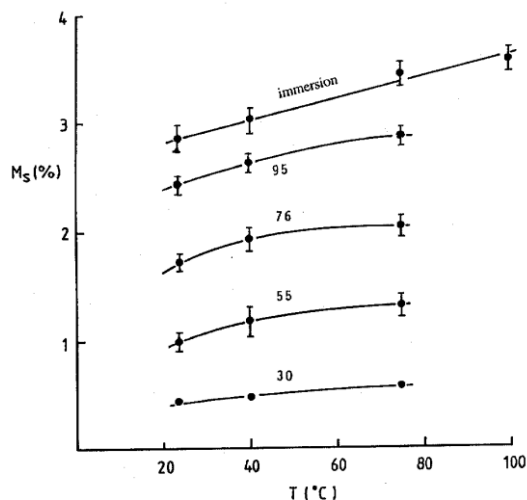


Fig. 10.24 Variation with temperature of water equilibrium content of EPON 815-TETA cured resin, for immersion and exposure at relative humidities indicated on curves.

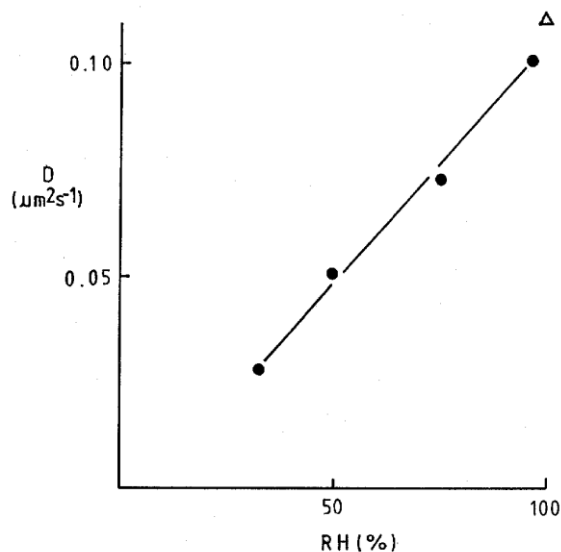


Fig. 10.25 Diffusion constant at 23°C as a function of relative humidity with 100% RH value from water immersion.

D is given as a function of temperature by the Arrhenius equation

$$D = D_0 \exp(-E_a/RT) \quad (10.5)$$

where D_0 is a constant, E_a is the activation energy and R is the gas constant, so that straight lines are obtained when $\ln D$ is plotted vs $1/T$; see Fig. 10.26. Some typical M_s and D values are given in Table 10.8.

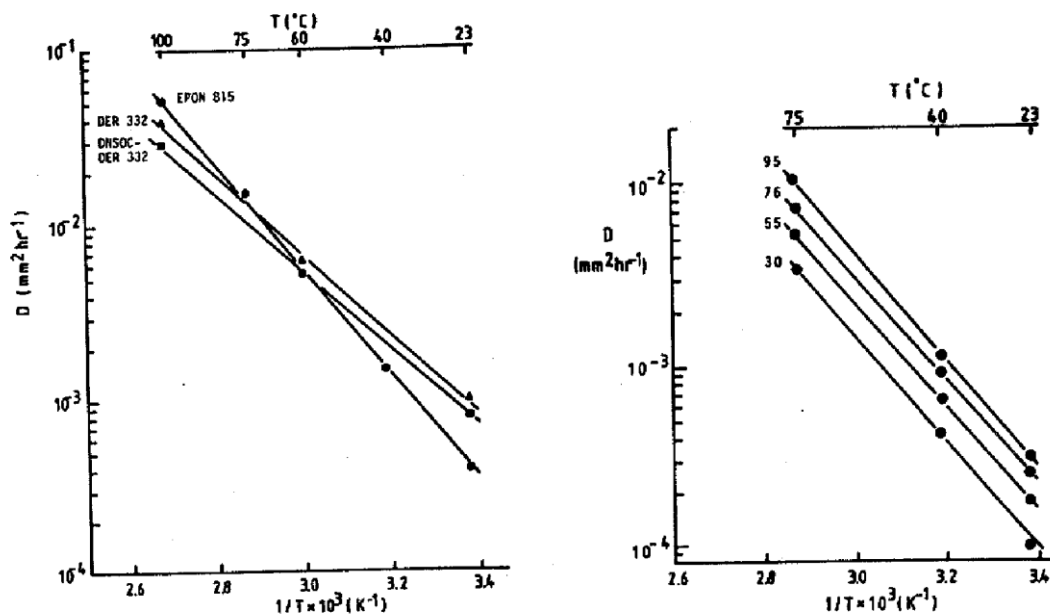


Fig. 10.26 Arrhenius plots for water diffusion constant. At left, immersion of three epoxy resins, at right, humidity exposure of EPON 815, with humidities as indicated.

Carbon and glass fibres absorb some water, Fig. 10.27, with carbon absorbing much less than glass. Fibre bundles were used in this experiment, and as they were sized (surface coated), the effect is strongly influenced by the sizing. Unidirectional composites absorbed less water than the polymer, with the effect depending on the amount of fibres present as shown in Fig. 10.28.

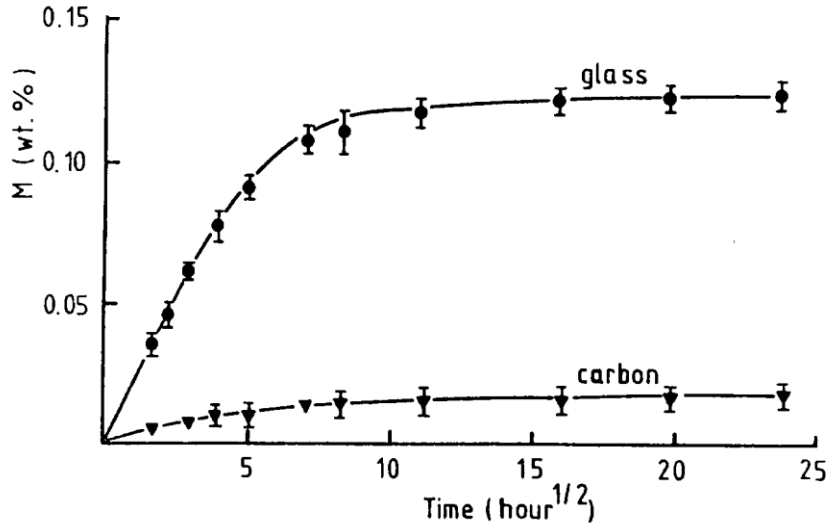


Fig. 10.27 Water absorption of glass fibre rovings and carbon fibre tows at 98% RH at 23°C. (After Woo, M. and Piggott, M.R., 1987, J. Comp. Tech. Res. 9, 162-6.)

Table 10.8 Typical Values for Water Absorption, M_s , and Diffusion Constant, D , for Water Immersion at Room Temperature (except where noted)

Resin Type	Resin	M_s (%)	D ($\mu\text{m}^2\text{s}^{-1}$)
TP ¹	Nylon 66	4.8	3.6
TP	PEEK	0.42	0.98
TS ²	Polyester	2.1 ³	4.3 ³
TS	Epoxy	3.0	0.12
TS	Polyimide	1.2 ⁴	8 ⁴

Note:

1) Thermoplastic, 2) Thermoset. In the case of the thermosets there is a wide range of polymers of each type. Thus the values for a particular polymer can be quite different from those given here. 3) 60°C values; nylon was tested at 90% RH. 4) 60°C values, estimated from composite results assuming $V_f = 0.6$ and $D_c/D_p = 0.58$ (see Fig. 10.34.)

The composites obeyed Fick's Law, but this is not always observed with unidirectional composites. Moreover, cross ply laminates normally do not obey Fick's Law, see Fig. 10.29; this may be because of the residual stresses in the composite. These stresses, which normally put the polymer in tension, increase the diffusivity. Water swells the polymer and plasticizes it, reducing the Young's modulus and increasing D . Thus, the residual stresses are slowly relieved as the water diffuses into the material. Hence the diffusivity slowly decreases.

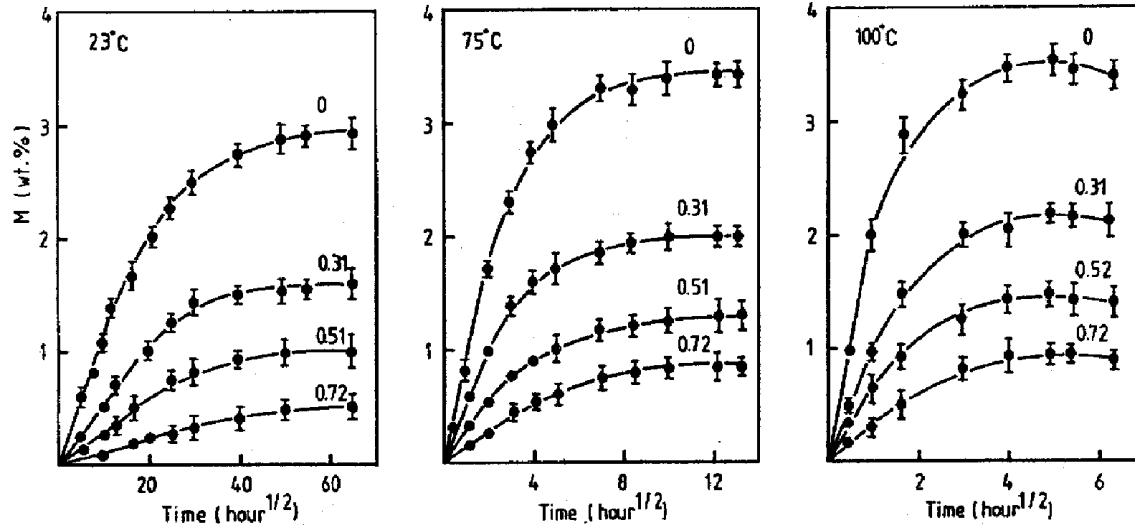


Fig. 10.28 Water absorption of glass-EPON 815 epoxy with fibre volume fractions as indicated, at 23°C, 75°C and 100°C.

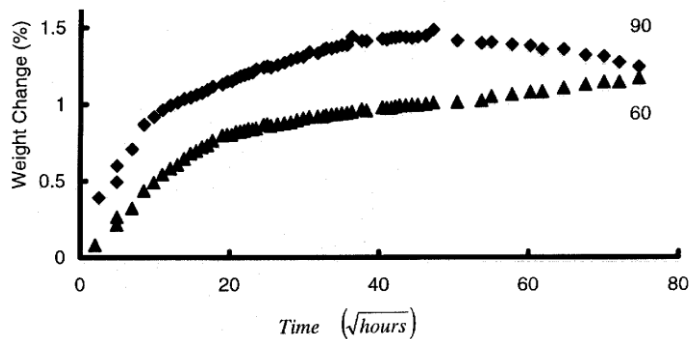


Fig. 10.29 Water absorption of carbon-epoxy cross ply laminates at 90°C and 60°C. (After Qian, M., M.A.Sc. thesis, U of Toronto, 2000.)

The relative amount of water absorbed in a composite is often given by a simple mixture rule

$$V_{wc} = V_{wf}V_f + V_mV_{wm} \quad (10.6)$$

Here the V 's represent volume fractions, and subscripts c , f and m indicate composite fibres and matrix, together with w for water. However, there can be preferential absorption at the fibre-matrix interface. Fig. 10.30 shows that for glass fibres in EPON 815 equation (10.6) is obeyed quite well both for immersion and humidity exposure.

However, the DER 332 and the DNSOC (= "spiro") have high interface absorption, which can be seen as a slight separation at the interface under the microscope.

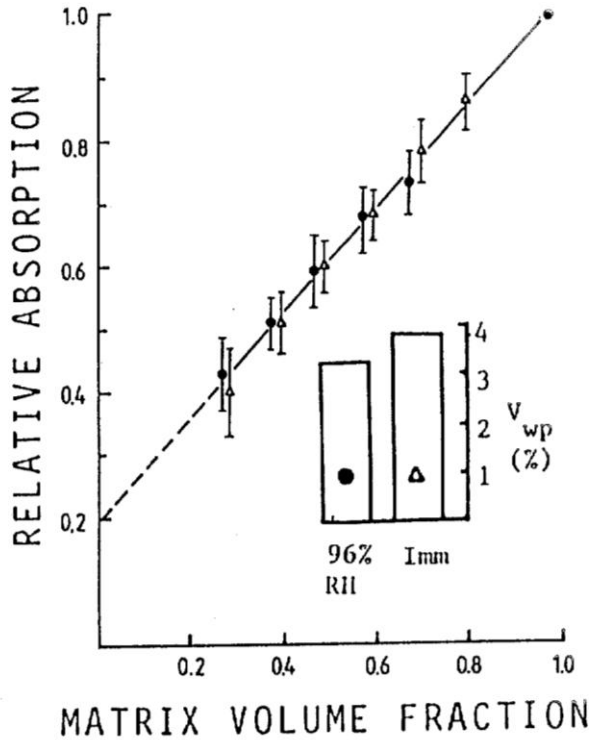


Fig. 10.30 Relative water absorption at saturation at 60°C for glass-epoxy at 96%. Inset shows the water absorption by the resin alone. Here $V_{wp} \equiv V_{wm}$.

The inset in Fig. 10.30 shows the total amounts absorbed in each case. From these and similar results at other temperatures, the amount of water preferentially absorbed at the glass fibre surface when embedded in EPON 815 can be estimated; see Fig. 10.31. With carbon, since much less water was absorbed on the sized fibres, Fig. 10.27, and the results did not fit equation (10.6) very well, it was not possible to draw similar conclusions.

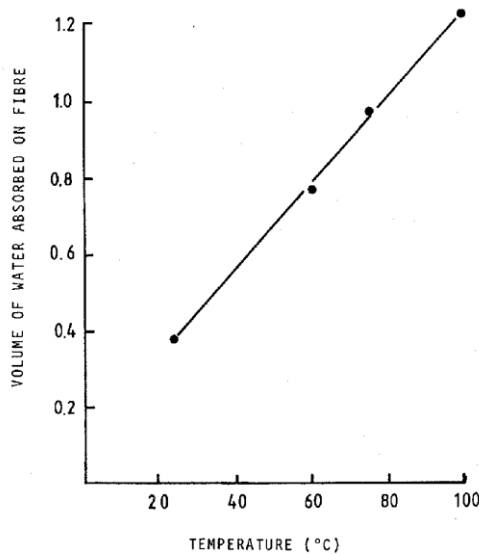


Fig. 10.31 Estimated amounts (%) of water absorbed at interface for glass in EPON 815.

The diffusion constants for water can be calculated moderately easily if we assume that the interface does not allow preferential diffusion. There is some evidence that it does in the case of glass, however. When tritiated water is allowed to diffuse along the interface in a thin section of a polymer containing two short fibres, the tritium can be detected at the surface where it emerges. These experiments were carried out with glass fibres having various surface treatments, giving the results shown in Table 10.9. Fig. 10.32 shows the set up used and pictures obtained.

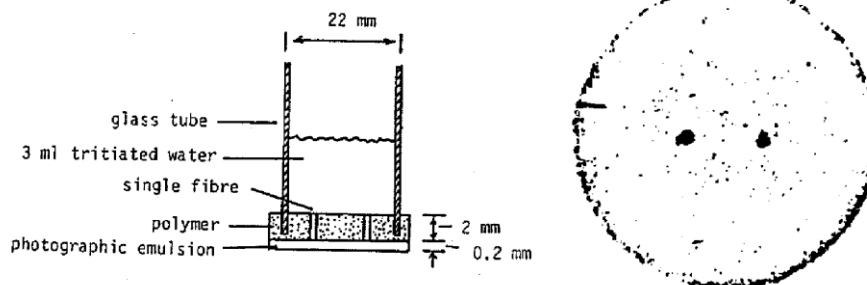


Fig. 10.32 At left, is set up used for water transmission experiment, and at right, is a typical tritium exposure. (After Chua, P.S, Dai, S.R., and Piggott, 1992, *J. Mater Sci.* 27, 919-24.)

Table 10.9 Transit Times for Water Along Glass Interphase with Polyester, Over Distance of 2 mm. Fibres Surface Treated as Indicated.

Fibre Treatment	Transit Time (h)
None	210
Sizing extracted with THF ¹	310
Pyrolysed ²	140
MPS coated ³	170
MPS coating extracted with THF ⁴	280

Notes:

1) Fibres immersed 1 h in tetrahydrofuran; 2) Fibres heated to 400°C for 10 min to remove sizing; 3) γ -methacryloxypropyltrimethyl siloxane coated from aqueous solution onto pyrolysed fibres, 4) fibres as in 3 immersed 1 h in tetrahydrofuran

10.4.4 Diffusion Model

We will first consider a model including an interphasial region with preferential diffusion and then show how this reduces to a simple closed form solution when its

thickness is zero. Here D_i and D_m are diffusion constants for the interface and matrix, with the fibres having D_f . An electrical resistance analogy is used. The treatment is the same for electrical and heat conductivity.

We will consider diffusion at right angles to fibres which are positioned in a regular square array. (Diffusion along the fibres, a trivial case, will not be considered.) One unit of the structure, involving a quarter of a fibre cross section is shown in Fig. 10.33. The fibre volume fraction, V_f , relates the size of the unit, a , to the fibre diameter, $2r$. Thus

$$r/a = 2\sqrt{V_f/\pi} \tag{10.7}$$

We will consider a current passing from bottom to top of the unit. The resistance of the unit to the passage of the current will be the sum of the resistances of the elements Δy as y goes from 0 to a .

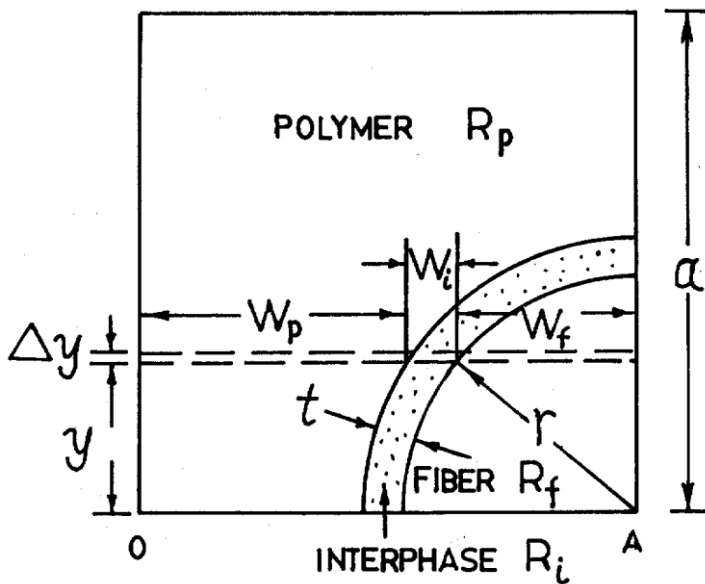


Fig. 10.33 Model used for diffusion analysis of square packed fibre composite with interphase. Unit cell of structure is shown.

Each element, from $y = 0$ to $y = r$, has three resistances in parallel. Thus the resistance of the element ΔR is a reciprocal sum of the resistances of polymer, interphase, and fibre, that is, ΔR_p , ΔR_i and ΔR_f , respectively

$$\Delta R = \left[\frac{1}{\Delta R_p} + \frac{1}{\Delta R_i} + \frac{1}{\Delta R_f} \right]^{-1} \tag{10.8}$$

If the w 's represent the appropriate widths, see Fig. 10.33, we can evaluate the ΔR s

$$\Delta R = \Delta y \left[\frac{w_p}{R_p} + \frac{w_i}{R_i} + \frac{w_f}{R_f} \right]^{-1} \tag{10.9}$$

for unit thickness of the element, where the R 's are the appropriate resistivities. Now, for $y \leq r$

$$w_p = a - \sqrt{(r+t)^2 - y^2} \quad (10.10)$$

$$w_i = \sqrt{(r+t)^2 - y^2} - \sqrt{r^2 - y^2} \quad (10.11)$$

and
$$w_f = \sqrt{r^2 - y^2} \quad (10.12)$$

Substituting these into equation (10.9), we obtain, for $y < r$

$$\Delta R = \frac{R_p R_i R_f}{R_i R_f (a - \sqrt{(r+t)^2 - y^2}) + R_p R_f (\sqrt{(r+t)^2 - y^2} - \sqrt{r^2 - y^2}) + R_p R_i (\sqrt{r^2 - y^2})} \Delta y \quad (10.13)$$

The total resistance R of the unit is obtained by letting Δy tend to zero, so that ΔR becomes dR and Equation (10.13) is thus converted to the integral, IR , where

$$IR = \int_0^r dR \quad (10.14)$$

We also add the resistance of the region $y = r$ to $y = r + t$, where we have no fibre, and the resistance of the region $y = r + t$ to $y = a$ where there is the polymer only. This gives

$$R = IR_1 + \int_r^{r+t} \frac{R_p R_i}{R_i a + (R_p - R_i) \sqrt{(r+t)^2 - y^2}} dy + R_p (a - r - t) / a \quad (10.15)$$

The first integral IR_1 must be solved by numerical methods, while the second integral in Equation (10.15) gives an inverse tangent. We will write IR_2 for the second integral.

We can now evaluate the diffusivities, since these are the reciprocal of the resistances. Thus $D_p = 1/R_p$, and similarly for the interface D_i , D_i , the fibre D_f , and the composite D_c . It is convenient to express the result in dimensionless form

$$D_c/D_p = [D_p \{ID_1 + ID_2\} + 1 - (r+t)/a]^{-1} \quad (10.16)$$

where ID_1 is equivalent to IR_1

$$ID_1 = \int_0^r \left[\frac{dy}{(D_i - D_p) \sqrt{(r+t)^2 - y^2} + (D_f - D_i) \sqrt{r^2 - y^2} + D_p a} \right] \quad (10.17)$$

and ID_2 is equivalent to IR_2 and can be integrated

$$ID_2 = \frac{\frac{\pi}{2} - \sin^{-1} \left\{ \frac{r}{(r+t)} \right\} - \left\{ \frac{2}{\sqrt{1-c^2}} \right\} \left\{ \tan^{-1} \sqrt{\frac{1-c}{1+c}} - \tan^{-1} \sqrt{\frac{1-c}{1+c}} t' \right\}}{D_i - D_p} \quad (10.18)$$

where

$$c = (r + t)(D_i - D_p) / [a D_p] \tag{10.19}$$

and

$$t' = \tan \left[\frac{1}{2} \sin^{-1} \left\{ \frac{r}{r+t} \right\} \right] \tag{10.20}$$

We can now, in principle, estimate the diffusivity of the composite, if we know the diffusivities of fibres, resin and interphase and the thickness of the interphase. These latter two are not normally known however. Nevertheless, the diffusivity results from the works referenced in Figs. 10.24 and 10.27 can be plotted on a master curve as shown in Fig. 10.34, and fitted to equations (10.16) to (10.20). To do this we take a compound dimensionless variable that includes both t and D_i , i.e. tD_i / rD_p and by trial and error, involving repeated numerical evaluations of ID_1 , we obtain a moderately good fit with

$$tD_i / rD_p = 0.15 \tag{10.21}$$

and $D_f = 0$.

Note that if $t = 0$ equation (10.14) integrates to give the closed form solution

$$\frac{D_c}{D_p} = \left[\frac{D_p}{D_p - D_f} \left\{ \frac{2}{\sqrt{1-c^2}} \tan^{-1} \frac{\sqrt{1+c}}{\sqrt{1-c}} - \frac{\pi}{2} \right\} + 1 - 2\sqrt{\frac{V_f}{\pi}} \right]^{-1} \tag{10.22}$$

with

$$c = 2 \left\{ 1 - \frac{D_f}{D_p} \right\} \sqrt{\frac{V_f}{\pi}} \tag{10.23}$$

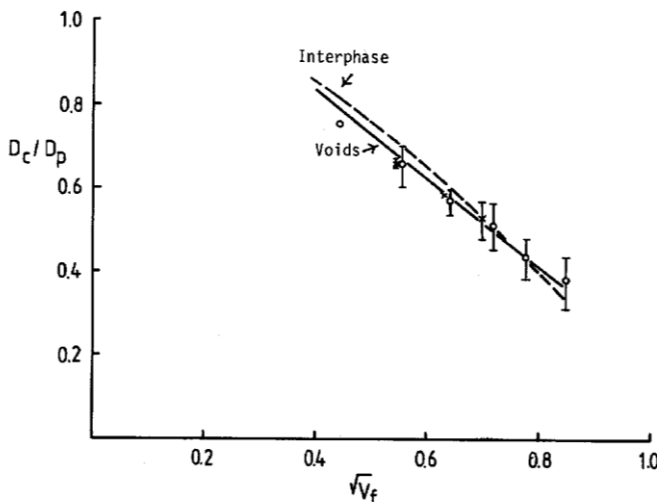


Fig. 10.34 Results fitted for glass-epoxy and carbon-epoxy diffusion. Dashed line using interphase model with $t D_i / rD_p = 0.15$. Solid line is for no interphase with voids having $D_v = 15D_p$. (After Woo, M., and Piggott, M.R., 1968, J. Comp. Tech. Res. 10, 10-24.)

It should be noted that a slightly better fit can be obtained if the voids which were present in these composites (with $V_v \sim V_f/60$) provided a faster diffusion path so that $D_v = 15D_p$. The analysis of this case gives almost a straight line in the region of interest; see line labelled "voids" in Fig. 10.34. Note, further, that an increase in D_p due to stress

cannot be used to explain these results. This, instead, raises and steepens the "interphase" line.

10.5 Hybrid Composites

The great advantage of composite materials for the designer is the versatility of the material. Its properties can be controlled by variation of the type, amount, orientation and length of fibre and type of matrix used, and to a limited extent by control of the interface. Thus, to a degree, the material can be designed to suit the application.

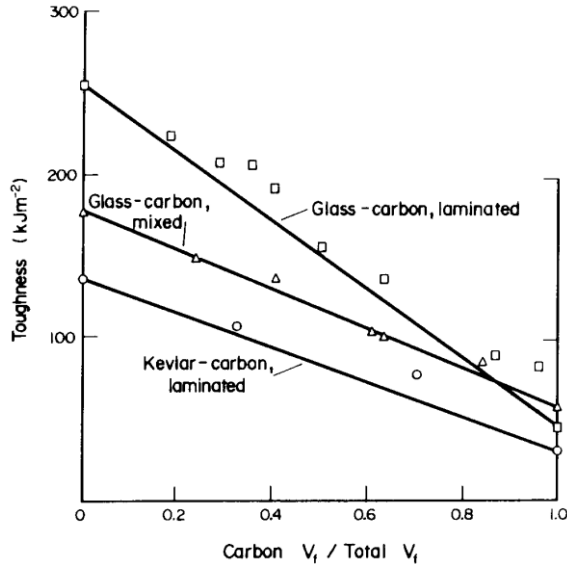


Fig. 10.35 Toughness of hybrids containing carbon. (After Dorey, G., Sidey, G.R. and Hutchings, J., 1978, *Composites* 9, 25-32, Hancox, N.L. and Wells, H., 1973, *ibid.* 4, 26-30, and Harris, B. and Bunsell, A.R., 1975, *ibid.* 6, 197-201.)

However, it was soon noticed that much finer control of material properties could be obtained by making composites which included different types of fibre. Thus, for optimum stiffness and toughness, a mixture of carbon and Kevlar is better than glass, or Kevlar alone. Figure 10.35 shows this effect. Laminates can be made in which each lamina contains a different fibre type. Alternatively, the composite can be made by intimately mixing fibres of different types. These are both hybrid composites. There have been suggestions that with mixed fibre composites, synergistic effects might be obtained. The toughness results in Fig. 10.35 seem to indicate this, since all the experimental points are above the lines joining the works of fracture of the respective non-hybrids. The evidence is not conclusive, however. Little error will result from assuming that the toughness of hybrids is given by the expression

$$\mathcal{G}_1 = (V_{fa} \mathcal{G}_{1a} + V_{fb} \mathcal{G}_{1b})(V_{fa} + V_{fb}) \quad (10.24)$$

where \mathcal{G}_{1a}^* and \mathcal{G}_{1b}^* are the works of fracture of the non-hybrid composites and V_{fa} and V_{fb} are the volume fractions of the two fibre types. In this expression $V_{fa} + V_{fb} = \text{constant}$.

The expression simplifies if \mathcal{G}_{1a} and \mathcal{G}_{1b} are proportional to the respective fibre volume fractions, given by $\mathcal{G}_{1a} = V_{fa} \mathcal{G}_{1a}^*$, etc.

$$G_1 = V_{fa} G_{1a}^* + V_{fb} G_{1b}^* \tag{10.25}$$

(Here we are disregarding small contributions from the matrix work of fracture.)

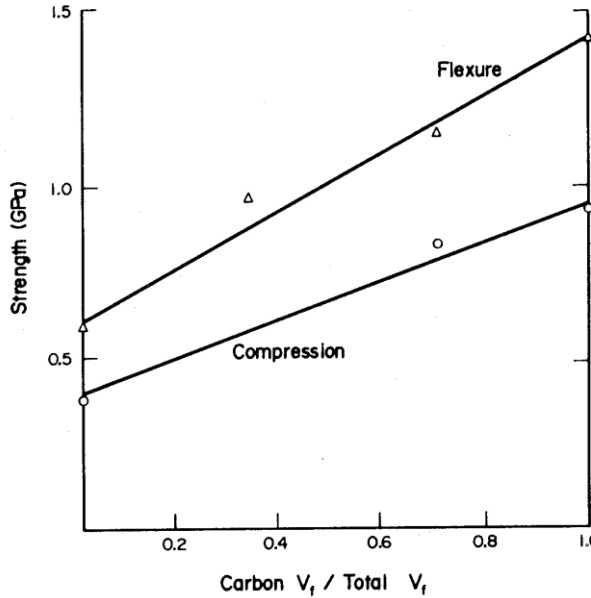


Fig. 10.36 Compressive and flexural strengths of carbon-Kevlar-epoxy laminated hybrids. (After Dorey, G., Sidey, G.R., and Hutchings, J., 1978, Composites 9, 15-32.)

The Young's modulus of the hybrid is also given by an expression like equation (10.25).

Thus

$$E_1 = V_{fa} E_{fa} + V_{fb} E_{fb} \tag{10.26}$$

Hybrid composites obey this expression well. If the total volume fraction of fibres, $V_{fa} + V_{fb}$ is small, we should add $V_m E_m$ to the right-hand side of equation (10.26).

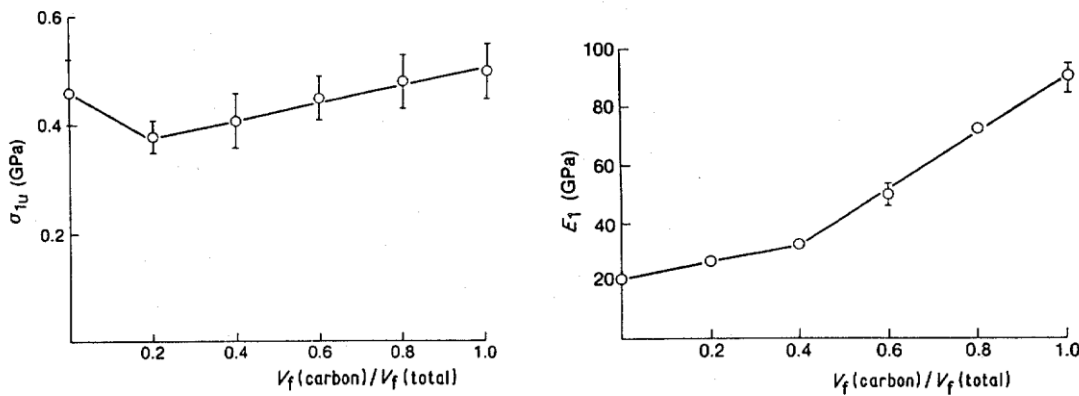


Fig. 10.37 Compressive strength (left) and modulus (right) for high modulus carbon-glass-polyester hybrid-polyester pultrusions. (After Piggott, M.R., and Harris, B., J., 1981 Mater Sci. 16, 687-93.)

The compressive strength and modulus of unidirectional hybrids has been investigated in some detail. Carbon-Kevlar-epoxy laminated hybrids do appear to obey a

Rule of Mixtures expression for strength (Fig. 10.36). However, cohibitive effects have been observed for both strength and modulus in unidirectional comingled pultrusions. Four examples were investigated. Fig. 10.37 shows the compressive strengths and moduli for high modulus carbon-glass-polyester hybrids. Both properties show cohibitive effects.

Fig. 10.38 illustrates the Kevlar-high modulus carbon-polyester case. Only the modulus shows the cohibitive effect. Also tested in this series of experiments were high modulus carbon-polyester-high strength carbon-polyester hybrids, which showed no clear trends, and Kevlar-glass-polyester hybrids which behaved linearly for strength but showed no clear trends for modulus.

The flexural properties depend on how the composite is made. Rule of Mixtures expressions give a reasonable representation for some intermixed hybrids, and even some laminated hybrids (Fig. 10.36). Other laminates do not obey the Rule of Mixtures for strength or modulus in flexure. One reason for this is that the stressing system is complex in a hybrid laminate.

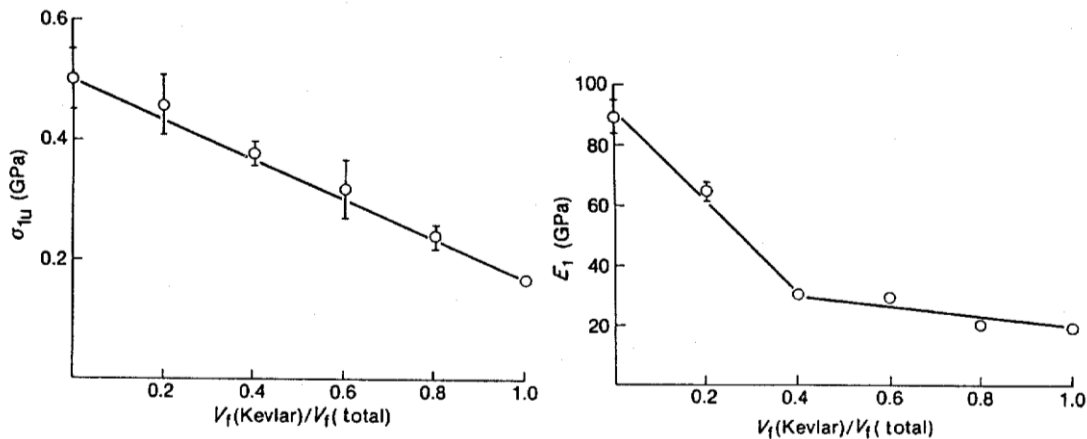


Fig. 10.38 Compressive strength (left) and modulus (right) for Kevlar-high modulus carbon-polyester hybrid-pultrusions.

If the laminate is to be flexed, it is advantageous to put the stiffer fibre at the surfaces to promote maximum stiffness. However, this fibre is then subject to a higher stress, and early failure can be expected. The design of laminates for use in flexure must be governed by the failure strains of the component fibres.

The tensile strength of a laminate is also controlled by the failure strains of the fibres. Figure 10.39a shows that tensile strengths generally lie below the Rule of Mixtures. We expect the lower breaking-strain fibres to break first. This does not necessarily precipitate composite failure. These fibres can, in some circumstances, break up into their critical lengths, when they can still contribute reinforcement to the extent of $0.5V_{fa}\sigma_{fua}$. The composite strength is thus

$$\sigma_{1u} = 0.5V_{fa}\sigma_{fua} + V_{fb}\sigma_{fub} \quad (10.27)$$

when V_{fb} is relatively large; see Fig. 10.39(b). When $V_{fb} = 0$, the composite strength is $V_{fa} \sigma_{fua}$. The composite fails when $\epsilon_1 = \epsilon_{fua}$. Thus when there are small amounts of the higher breaking strain fibre we have an expression of the type

$$\sigma_{1u} = V_{fa} \sigma_{fua} + V_{fb} \sigma_{fub} \tag{10.28}$$

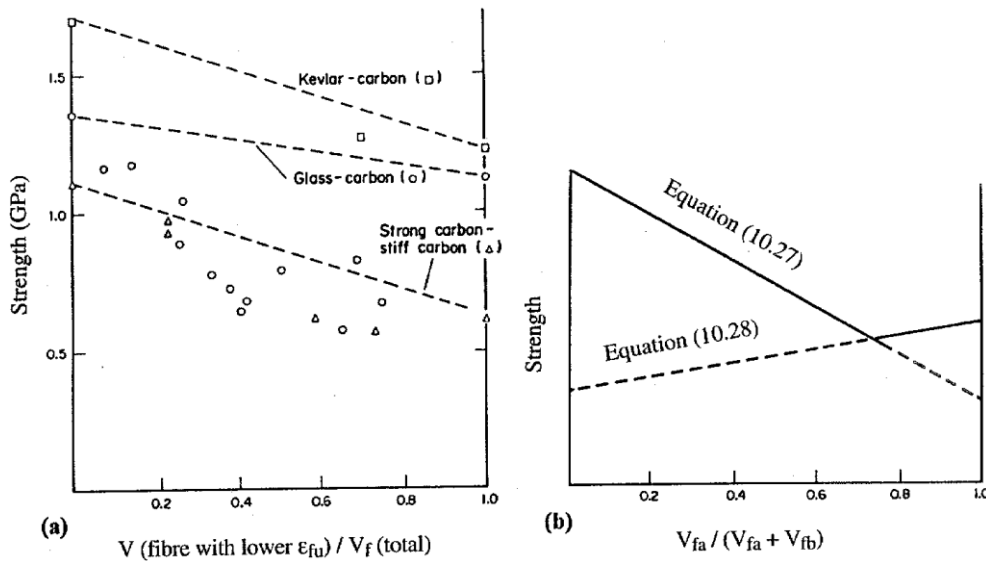


Fig. 10.39 (a) Tensile strength of hybrids. (Data from Aveston, J. and Kelly, A. 1980, Phil. Trans. Roy. Soc., A294, 519-39, Dorey, G., Sidey, G.R., and Hutchings, J., 1978, Composites 9, 25-32, Edwards, H.E., Parratt, N.J. and Potter, K.D., 1978, Proc ICCM2, 975-93.) and (b) Expected variation for hybrid with fibres of different breaking strains.

This is also shown in Fig. 10.39b. (This graph was plotted for the combination of stiff and strong carbon fibres.) Ideally the strength will be given by equation (10.27) or (10.28), whichever is the greater. However, in practice there is no guarantee that the composite can withstand the breaking up of the lower breaking strain fibre. Thus equation (10.27) is an upper bound and equation (10.28) is a lower bound for the tensile strength of hybrids.

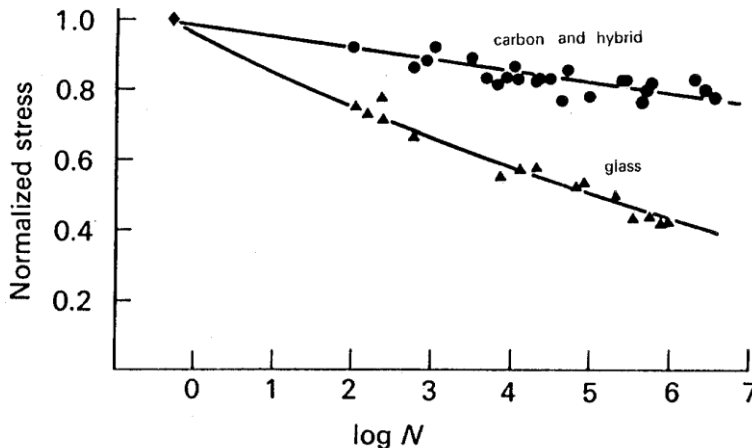


Fig. 10.40 Fatigue of glass-epoxy $[\pm 45/0/2]_{2s}$ laminates (lower curve) and carbon-epoxy and carbon-glass-epoxy hybrids (upper curve), $R = 0.1$. (After Dickson, R.F., Fernando, G., Adam, T., Reiter H., and Harris, B., 1989, J. Mater. Sci. 24, 227-33.)

Unfortunately, we seldom know the values of σ_{fua} and σ_{fub} in the composite with any accuracy. There are two reasons for this. One is the damage that the fibres suffer during composite manufacture. The other is that the strength of the fibres having the critical length is seldom known. This is generally greater than the strength as normally measured (see Fig. 8.16).

Finally, there is some evidence of a hybrid effect in fatigue with glass-carbon-epoxy laminates. Fig. 10.40 shows the S-N plot for glass-epoxy (lower line) and for carbon-epoxy and glass-carbon epoxy (upper line). Using the normalized stress, i.e. stress at failure divided by tensile strength, the 50-50 carbon-glass hybrid gave results which were indistinguishable from those for carbon alone. Moreover, the slope for the glass is 2.8 times greater than the slope for the other composites. These were $[\pm 45/0_2]_{2s}$ laminates tested at $R = 0.1$ tension-tension fatigue. The layers were interleaved with ± 45 glass as the outside layers, then 0 carbon, 0 glass, ± 45 carbon, 0 glass, 0 carbon then the same reversed.

10.6 Joints

In a complicated structure it is usually necessary to divide the structure into more elementary parts, construct these, then join them together.

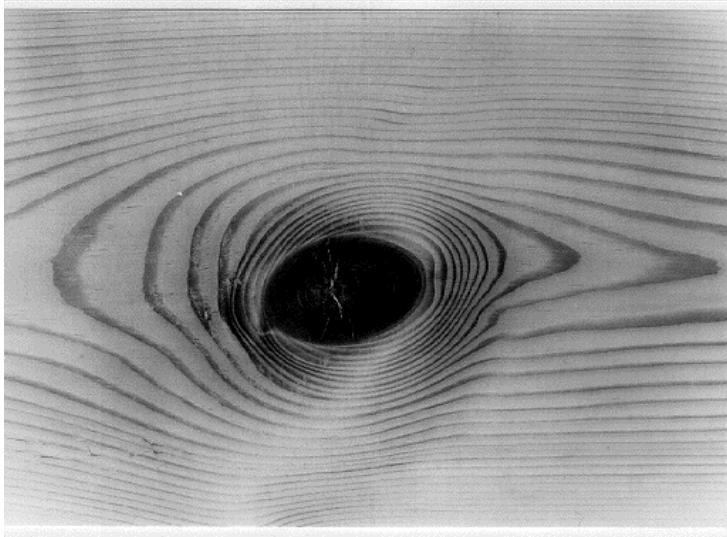


Fig. 10.41 Nature's joint. Note how the grain changes around the joint, indicating a change in fibre orientation.

Composites present special problems for joining because of their extreme anisotropy. Even cross-ply laminates have problems because of their low out-of-plane properties. Nature has solved the problem (Fig. 10.41) by so arranging fibre growth around the joint that it has optimum properties. This approach is not usually available to designers of composites.

The most cost-effective methods of joining isotropic materials are usually either bolts or rivets. Rivets are seldom suitable for composites, but bolts are often cost effective in joining laminates to each other, or to sheets of other materials. Due to the low apparent shear strength of the composite the bolt clamping load should be spread

over a large area by the use of washers, as shown in Fig. 10.42. The washers should be as large as possible, consistent with weight requirements.

Figure 10.43 shows that the strength of the joint is a linear function of washer diameter. It is usually an advantage to have the clamping load high, but the maximum is limited by the material. Figure 10.43 also shows that with glass-epoxy the joint strength is greatly increased by good clamping, though there is little to be gained by having the load greater than about 15 MN.

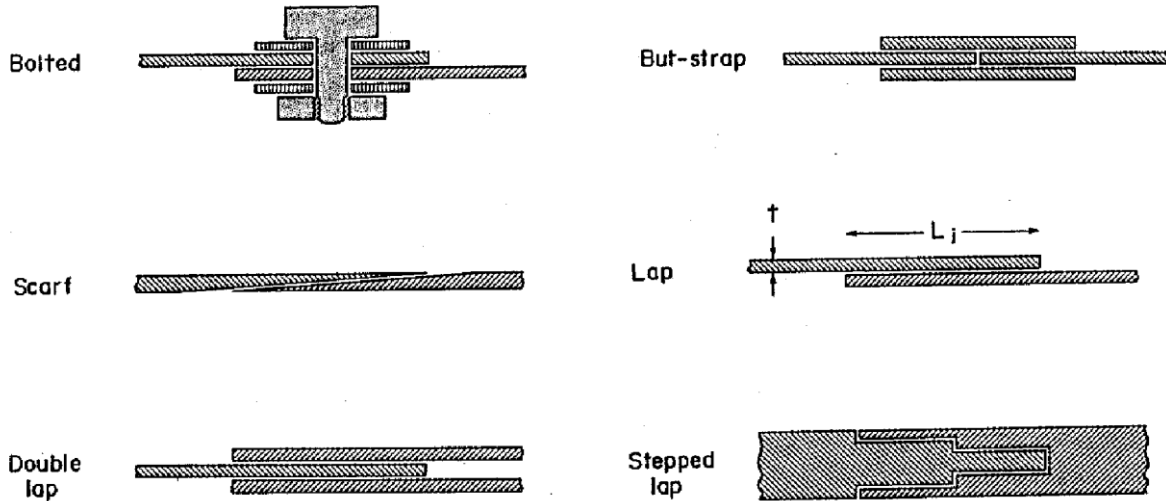


Fig. 10.42 Types of joint suitable for joining laminates and sheets.

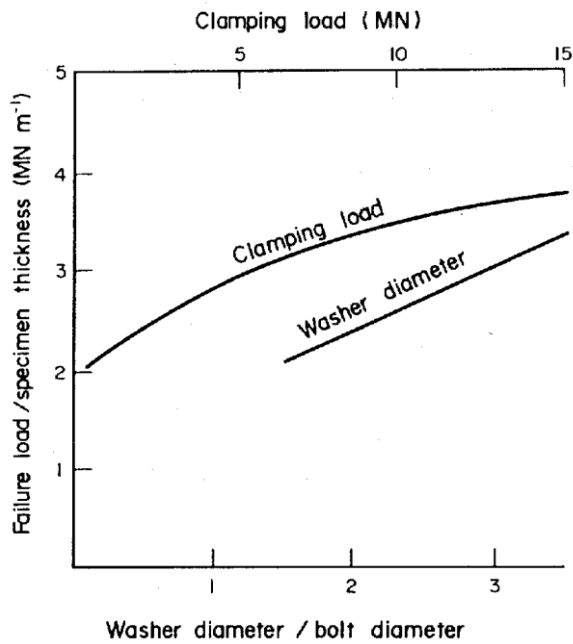


Fig. 10.43 Effect of clamping load and washer diameter on the load-carrying capacity of a bolt in a glass fibre laminate. (After Stockdale, J.H. and Matthews, F.L., 1976, Composites 7, 34-38.)

Bolted joints should be well fitting for maximum effectiveness. They should not be too close to the edge of the sheet, but about five bolt diameters (Fig.10.44) is usually

sufficient. They should only be used with extreme caution for unidirectional fibre composites, though, since they can very easily shear out under load.

Glued joints are normally used for unidirectional fibre composites. Butt-strap, scarf, and lap joints of various types are the main forms used for unidirectional composites and laminates. Examples are shown in Fig.10.42.

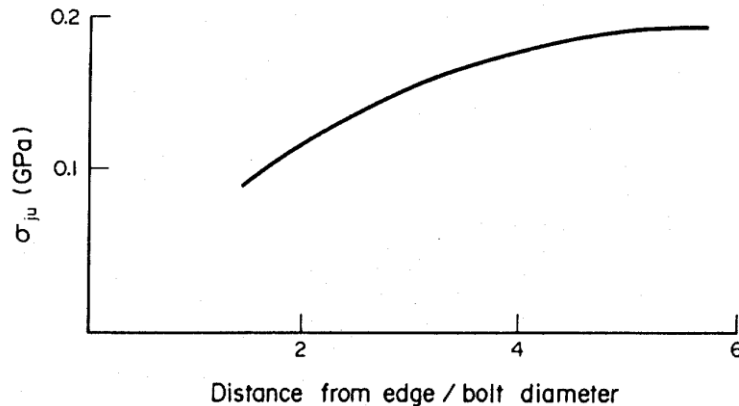


Fig. 10.44 Composite stress at joint failure (σ_{ju}) vs distance of bolt from edge for boron-epoxy laminate/aluminium joint. (After Grimes, G. C., and Greimann, L.F., 1974, *Composite Materials* 8, 1-35, Ed. Chamis, C.C., Academic Press.)

In all these joints the length of the joint is calculated assuming that the adhesive has an apparent shear strength τ_{au} . Thus, for sheets of thickness t , and a joint of L_j , the single lap joint can transmit a stress σ_{ju} where

$$\sigma_{ju} = L_j \tau_{au}/t$$

Equation (10.29) only works, however, for thin laminates, as shown in Fig. 10.45. Stress concentrations occur in this type of joint, which can be reduced by chamfering the edges. Moreover, as we showed in section 6.1.2, shear failure is not normally observed with polymers.

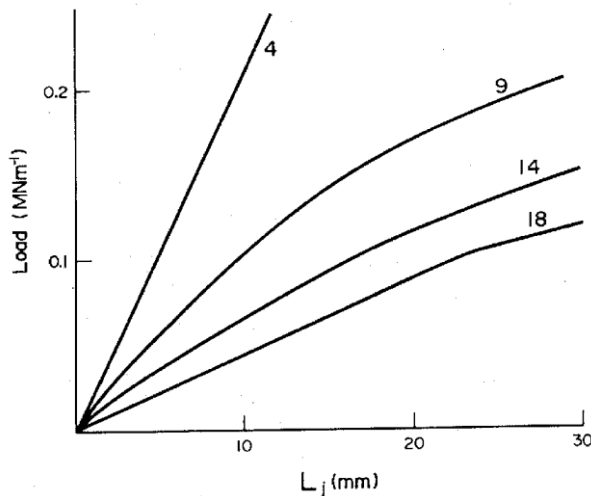


Fig. 10.45 Load on each ply per unit width of joint as a function of lap length, L , for glued double-lapped glass-polymer/aluminium joints. The figures on the curves indicate the numbers of layers in the laminates. (After Grimes, G.C., and Greimann, L.F., 1974, *Composite Materials* 8, 1-35., Ed. Chamis, C.C., Academic Press.)

The stress concentrations become serious when laminates with more than four layers are joined in this way. Thus, the effective value of τ_{au} is reduced to a small fraction

of its value for thin laminates. In this case the butt-strap, scarf, and single or double lapped joints should not be used. Instead the stepped lap should be employed.

Glued joints are affected by cyclic stresses, and show the type of fatigue behaviour usually observed with composites. Figure 10.46 shows that a joint strength decreases monotonically with number of stress cycles, without any indication of a fatigue limit. This was a scarf joint between unidirectional carbon-epoxy and aluminium.

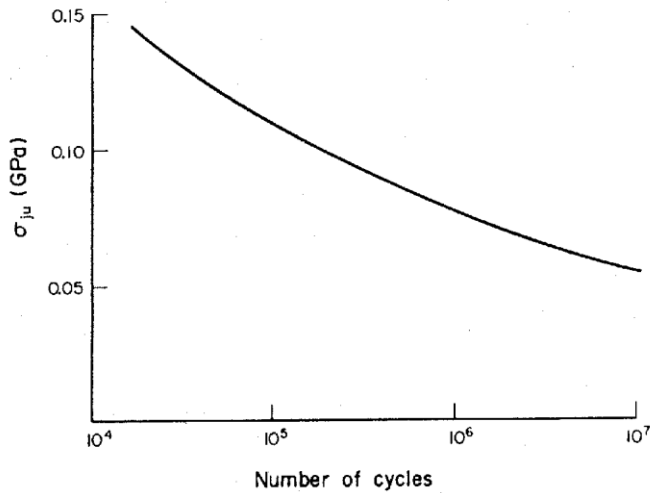


Fig. 10.46 Fatigue of unidirectional carbon-epoxy/aluminium, glued 2.5° scarf joint. (After Smith, M.A., and Hardy, R., 1977, *Composites* 8, 255-61.)

When a laminate has to be fixed to a massive support, a different type of joint is required. Some examples are shown in Fig. 10.47. The plain insert is the simplest and weakest. The divided root is much better, and the strength is greatly influenced by the number of divisions. The wrap around may be very promising, but is difficult to construct.

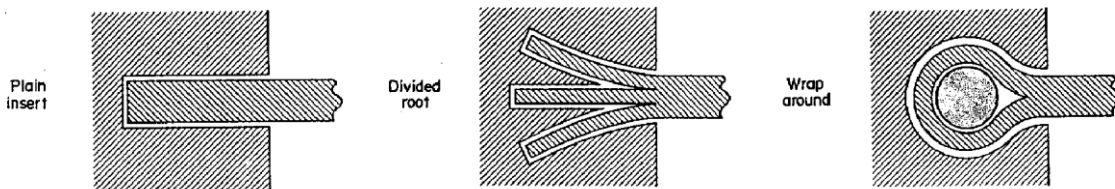


Fig. 10.47 Joints to connect laminates with massive support.

Further Reading

Gates, T.S. and Zurick, A.H., (Editors), (1997), *High Temperature and Environmental Effects on Polymeric Composites*, , ASTM STP 1302.

Grant, P. And Rousseau, C.Q., (Editors), (2000), *Composite Structures: Theory and Practice*, ASTM STP, 1383.

Chapter 10: Problems

- 10.1 Assuming that the unidirectional fibre composite in Table 10.1 does not obey the Rule of Mixtures for strength because of damage to the fibres during manufacture, calculate the size of flaws in the glass that must be present. (Neglect the matrix contribution, and assume an E-glass-epoxy, with a strength fraction calculated on the basis of data in Table 3.2.)
- 10.2 In the case of the random mat in Table 10.1, it is likely that the fibres retain only about 50% of their strength due to damage in processing. Also they cannot transfer stress efficiently due to their short lengths. Making these assumptions, estimate the aspect ratio of the fibres. Express your result as a fraction of the critical aspect ratio. (Hint: superpose the effect due to randomness, section 4.3.4, on that due to short length section 5.3.1. Neglect the matrix contribution.)
- 10.3 Calculate the compressive strength of unidirectional E-glass-epoxy, assuming that failure occurs as for glass in Fig. 6.35.
- 10.4 Calculate the ratio of effective compressive strength to effective tensile strength for Kevlar when used to reinforce epoxy, using Rule of Mixtures expressions, and the data in section 10.1.1.
- 10.5 Estimate the fibre amplitude and wavelength for a unidirectional cheap carbon-epoxy pultrusion with a compressive strength of 1.36 GPa and a modulus of 109 GPa. The fibre tows contained 1440 fibres, which retained their integrity in the pultrusion. $V_f = 0.57$ with square packing. The fibre-matrix adhesion strength was 40 MPa. Assume that the bundles consisted of fibres packed at the theoretical maximum packing density.
- 10.6 As can be seen in Fig. 3.17, in glass fibre fabrics with untwisted tows, wavelengths can be as large as 13 mm. (In the picture the rovings were about 4.2 mm wide). If the tow thickness is t , show that the compression strength equations can be adapted to this case, so that $\sigma_{fmax} = 2R_f \sigma_{my}/0.90t$ if the fibres are very densely packed in the rovings. If a composite is made with this material, together with 60% of a polyester resin which yields at 130 MPa and has a modulus of 3.5 GPa, what would its compressive strength be? Assume it fails by yielding, and make allowance for the fact that only half the fibres will be oriented in the stress direction. The fibres were E glass, the tow thickness was 1.20 mm and the amplitude of the waviness was 0.60 mm. Use R_f/t , a/t and x/t instead of R/d etc.
- 10.7 Assume the Rule of Mixtures applies to the carbon-epoxy in Table 10.3, and hence calculate V_f from S_{11} . Then determine how close the elastic constants S_{22} , S_{12} and S_{66} come to the theoretical values, expressing your answers as the ratios of theoretical to experimental values. Assume stiff carbon was used.

- 10.8 Determine the fibre strength from the data in Table 10.3, assuming $V_f = 0.54$. and also the interfacial adhesive tensile strength. Hexagonally packed stiff carbon fibres were used.
- 10.9 What would the minimum strains be in the polymer during delamination failure for T300 fibre reinforced polyetherimide and polysulphone. Assume a fibre volume fraction of 0.65 and hexagonal packing. T300 fibres have a diameter of $7.0 \mu\text{m}$, and the yield stress of the polyetherimide is 95 MPa and that of the polysulphone is 70 MPa.
- 10.10 Estimate the works of fracture from the fracture toughnesses for the first three laminates listed in Table 10.5. Assume that the laminate is made from the same material as that in question 4.15. Do the mean values obtained relate directly to the number of zero degree layers?
- 10.11 What would the effective strengths of boron, carbon, and S-glass have to be for the works of fracture in Table 10.6 to be determined by stress redistribution (G_{fb}) Assume that $\tau_i = 6.0 \text{ MPa}$ in all cases, and that the stiff carbon was used.
- 10.12 If the data in Table 10.3 is for the same material as that for the carbon-epoxy in Table 10.6, what would be the value for the fracture toughness of the material?
- 10.13 Use the data in Table 10.6 to design a Kevlar-stiff carbon hybrid epoxy with $E_I = 100 \text{ GPa}$ and $G_I = 100 \text{ kJm}^{-2}$. Determine the volume fractions of each required, neglecting any matrix contribution.
- 10.14 A $[0/90]$ carbon-epoxy laminate had a radius of curvature, after cure, of 125 mm. Each layer was 0.102 mm thick. Estimate the curing stress and strain and the curing temperature, using Rule of Mixtures type expressions for moduli based on the stiffest carbon with a volume fraction of 0.66.
- 10.15 Let $MR_T = EI$ on each half of a two ply laminate, the plies having moduli E_1 and E_2 and the same thickness $h/2$. M is developed through the action of a mean compressive stress on one side and a mean tensile stress on the other, both of magnitude σ_T . Hence develop equation (10.2).
- 10.16 Use the above result, together with the requirement that the mean strains or displacements of the two plies must be the same, to develop equation (10.3). The strains arise as a result of thermal contraction.
- 10.17 Estimate the diffusion coefficient of PEEK at 90°C and hence the activation energy for diffusion. The samples shown in Fig. 10.23 were 3 mm thick.
- 10.18 The laminate in question 10.13 absorbed water at a rate proportional to $\sqrt{\text{time}}$ until 60 seconds had elapsed, by which time it had absorbed 0.28% of its own

weight of water. Estimate the diffusion coefficient, and for an activation energy of 48kJmol^{-1} estimate the temperature at which the absorption took place if the epoxy had the same diffusion coefficient as that in Table 10.8. (Hint: use Fig. 10.34 for D_c/D_p .)

- 10.19 Design a strong carbon-E glass hybrid epoxy with a strength of 2.1 GPa and a modulus of 140 GPa. Determine the volume fractions, neglecting the matrix contribution.
- 10.20 Use Fig. 10.45 to estimate the minimum length of lap joint needed to transmit 10% of the breaking load for a continuous aligned E-glass epoxy laminate which obeys the Rule of Mixtures. Consider two cases (a) 4 layers and (b) 9 layers, where each layer has a thickness of 1.2 mm and all the fibres are parallel. $V_f = 0.47$. Would you expect such a lap joint to be able to transmit 10% of the breaking load for the nine layer laminate?
- 10.21 Estimate the fibre length which would give the modulus loss shown in Fig. 10.9 for the composite made without additive. For simplicity, assume the fibres were all reduced to the same length but remained straight and well oriented. The fibre diameter, Young's modulus and volume fraction were respectively $8\ \mu\text{m}$, 233 GPa and 0.5.

Chapter 10: Selected Answers

- 10.1 24.7 nm
- 10.3 1.8 GPa
- 10.5 0.29mm; 6.5 mm
- 10.7 0.54, 0.90, 1.06, 1.13
- 10.9 polyetherimide, 1.2; polysulphone 2.1
- 10.11 1.66 GPa, 4.8 GPa, 4.0 GPa
- 10.13 Kevlar 0.39, carbon 0.13
- 10.17 $12\ \mu\text{m}^2\text{s}^{-1}$, $32\ \text{kJm}^{-2}$
- 10.19 41% carbon and 28% glass
- 10.21 1.2 to 1.3 mm

11 OTHER FIBRE COMPOSITES

Much effort has gone into reinforcing metals, ceramics, cements and plasters with fibres such as those described in Chapter 3. Despite the expenditure of hundreds millions of dollars and thousands of person-years of work, almost no economically viable load bearing materials have emerged.

The reasons for this are as diverse as the putative matrices. For metals and ceramics major difficulties arise from thermal effects. The composites are of necessity made at a high temperature except for low melting point metals, which are of little interest in the context of load bearing materials. The high temperature causes undesirable chemical reactions between the components of the composites. These can sometimes be avoided by using barrier layers on the fibres, or extremely fast processing. However, the differential thermal shrinkage on cooling to ambient temperature, and reheating to use temperature, may cause high stresses and thermal ratcheting. These compromise the integrity of the material; see Fig 11.1.

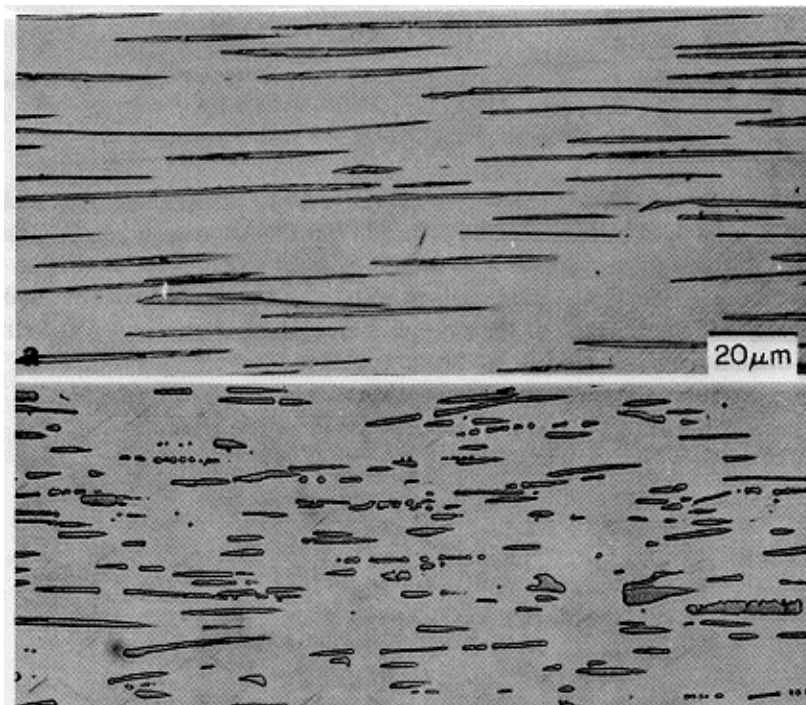


Fig. 11.1 Longitudinal microstructure of Co, Cr-NbC (a) before and (b) after about 1500 cycles between 400° and 1120°C. (After Thompson, E.R., and Lemky, F.D.,1974, *Composite Materials*, 4, 101-57, Ed. Kreider, K.G., Courtesy of Academic Press.)

A hybrid composite which is sometimes considered in conjunction with reinforced metals has the trade name Arall. This consists of laminae containing aramid fibres and a special resin, sandwiched between layers of an aluminium alloy. These laminates, which are lighter than aluminium and have improved fatigue life, do not fall into the class of reinforced metals discussed in this chapter. This is because they cannot be used at

temperatures as high as some carbon fibre reinforced polymers, whereas herein we restrict our discussion of reinforced metals and ceramics to those which are potentially useful at 500°C or more.

The acronym MMC is widely used for metal matrix composites. MMC's include metals containing small particles - the most thoroughly investigated being micron sized particles of SiC added to aluminium. This is equivalent to a metal alloy, and the SiC stiffens rather than strengthens the metal. (Also these hard particles embrittle it.) The advent of this terminology is unfortunate. With polymers it is common to add particles of various sorts: see section 9.1.1. Moreover, "filled polymers" containing glass beads which stiffen the material are rarely referred to as PMC's, i.e. polymer matrix composites. For metals "partalloy" would be better than "MMC" for a particle stiffened metal with "composite" restricted to fibre reinforced.

With cements and plasters, problems arise from chemical effects. These matrices are cheap and it makes no economic sense to reinforce them with expensive fibres. So only glass has been seriously considered as a reinforcement. Special glasses have been developed to resist the alkalinity of Portland cements. However, the resulting composites have not proven to be durable enough over the long periods expected for load bearing structures made with cements. A similar fate appears to have overtaken reinforced plasters. Low performance glass reinforced plasters are used for "water resistant" wall board in bathrooms etc. but carry no significant loads.

In this chapter we will first describe the thermal problems. Then we will describe some of the materials that have been investigated and discuss their potential usefulness for load bearing structures.

11.1 The Thermal Contraction Problem

Differences in thermal contraction between fibres and matrix can cause severe problems, and have rendered a number of potential fibre composites unserviceable. Thermal contraction can give rise to large pressures at the fibre matrix interface and even larger tensile stresses in the matrix. If the interfacial bond is good, these stresses can fracture the fibres. If bonding is poor, complete separation can take place between fibres and matrix, so that with short fibres or whiskers, reinforcement is lost. Thermal cycling is particularly damaging, and can lead to fibre break-up in many composites, including composites made by controlled crystallization of the fibres with the matrix. Figure 11.1 shows the longitudinal microstructure of Co, Cr-NbC after about 1500 cycles between 400° and 1120°C.

The thermal stresses can be calculated approximately if we consider the composite as made up of units, each consisting of one fibre surrounded by a tube of matrix, radius R_m , as shown in Fig. 11.2.

We consider continuous fibres, and Fig. 11.2a shows unit length of the composite, and the associated expansions. The longitudinal displacements per unit length of "composite" are

$$\epsilon_{cz} = \epsilon_{fz}^T + \epsilon_{fz} = \epsilon_{mz}^T + \epsilon_{mz} \quad (11.1)$$

where ϵ_{fz}^T and ϵ_{mz}^T are the displacements of fibre and matrix if free to expand thermally, and ϵ_{fz} and ϵ_{mz} are the elastic strains of the fibre and matrix, resulting from their need to expand the same amount when stuck together in the composite.

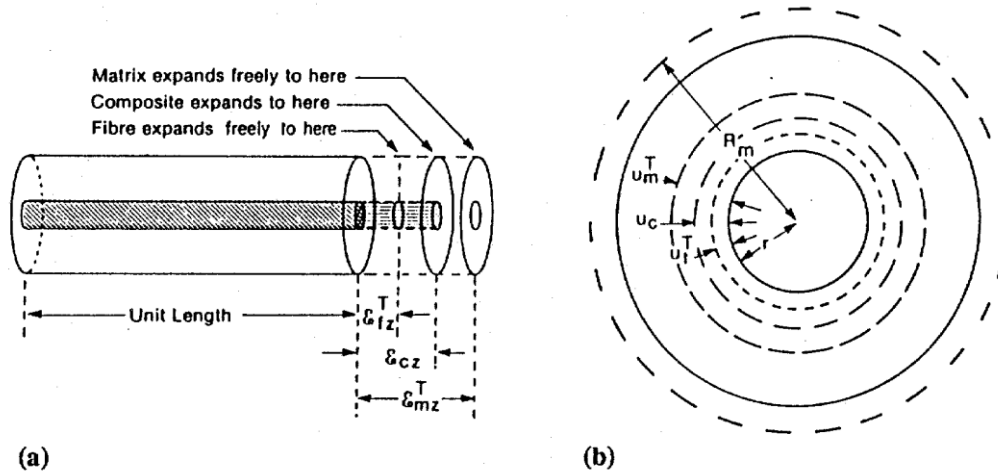


Fig. 11.2 Fibre, matrix, and composite (a) axial and (b) radial displacements.

The corresponding radial displacements are shown in Fig. 11.2b. We assume that the fibre and matrix do not separate. Thus

$$u_c = u_f^T + r\epsilon_{fr} = u_m^T + u_m \quad (11.2)$$

We assume uniform thermal expansion, so $u_f^T = r\epsilon_{fr}^T$ and $u_m^T = r\epsilon_{mr}^T$. ϵ_{fr} is the fibre elastic radial strain. u_m is the elastic matrix radial displacement, given in standard elasticity texts as

$$u_m = Pr \{ \nu_m + (1 + V_f) / V_m \} / E_m \quad (11.3)$$

where P is the internal pressure in the tube of matrix, resulting from the force exerted by the fibre expansion. V_f and V_m replace the r^2 and R_m^2 terms in the standard expression. (Note that R_m is different from R in equation 5.5; in these "composites" $V_f = r^2 / R_m^2$). In our case we must superpose a strain $-\nu_m \sigma_{mz} / E_m$ because of the axial stresses. Thus

$$u_m / r = \{ P / E_m \} \{ \nu_m + (1 + V_f) / V_m \} - \nu_m \sigma_{mz} / E_m \quad (11.4)$$

The stresses are

$$\sigma_{fr} = \sigma_{f\theta} = \sigma_{mr} = -P \quad (11.5)$$

where we are using the polar co-ordinates r and θ . Also

$$\sigma_{f\theta} = P(1 + V_f)/V_m \quad (11.6)$$

In the axial direction, with no stress applied, equilibrium of the forces requires that

$$V_f \sigma_{fz} + V_m \sigma_{mz} = 0 \quad (11.7)$$

We use three stress-strain equations of the type given in Chapter 1, i.e. 1.35-1.37:

$$\varepsilon_{fz} = [\sigma_{fz} - \nu_f(\sigma_{f\theta} + \sigma_{fr})]/E_f \quad (11.8)$$

$$\varepsilon_{mz} = [\sigma_{mz} - \nu_m(\sigma_{m\theta} + \sigma_{mr})]/E_m \quad (11.9)$$

$$\varepsilon_{fr} = [\sigma_{fr} - \nu_f(\sigma_{f\theta} + \sigma_{fz})]/E_f \quad (11.10)$$

Consider first the radial strains. Writing $\Delta\varepsilon_r$ for $\varepsilon_{fr}^T - \varepsilon_{mr}^T$ equation (11.2) gives

$$\Delta\varepsilon_r = u_m/r - \varepsilon_{fr} \quad (11.11)$$

So, substituting for u_m/r using equation (11.4) and ε_{fr} from equation (11.10) with σ_{fr} and $\sigma_{f\theta}$ given by equation (11.5) yields

$$\Delta\varepsilon_r = \{P/E_m\} \{ \nu_m + (1 + V_f)/V_m \} - \nu_m \sigma_{mz}/E_m + \{P/E_f\} \{1 - V_f\} + \nu_f \sigma_{fz}/E_f \quad (11.12)$$

Rationalizing this gives, using equation (11.7) for σ_{mz} ;

$$V_m E_m E_f \Delta\varepsilon_r = E_\lambda P + E_\nu \sigma_{fz} \quad (11.13)$$

where

$$E_\lambda = E_1 + E_f + V_m(\nu_m E_f - \nu_f E_m) \quad (11.14)$$

and

$$E_\nu \sigma_{fz} = \nu_m V_f E_f + \nu_f V_m E_m \quad (11.15)$$

with $E_1 = V_f E_f + V_m E_m$, i.e. the Rule of Mixtures (equation (4.3))

For the axial strain, we write $\Delta\varepsilon_z = \varepsilon_{fz}^T - \varepsilon_{mz}^T$, so that equation (11.1) gives

$$\Delta\varepsilon_z = \varepsilon_{mz} - \varepsilon_{fz}$$

which using equations (11.8), (11.9), (11.5) and (11.6) becomes

$$\Delta\varepsilon_z = \nu_m \{P/E_m\} \{1 - (1 + V_f)/V_m\} + \sigma_{mz}/E_m - \{\sigma_{fz} + 2\nu_f P\}/E_f \quad (11.17)$$

Again, rationalizing and using equation (11.7),

$$V_m E_m E_f \Delta\varepsilon_z = -2 E_\nu P + E_1 \sigma_{fz} \quad (11.18)$$

Finally, eliminating P between equations (11.13) and (11.18) gives

$$\sigma_{mz} = V_f E_f E_m (2E_\nu \Delta\varepsilon_r + E_\lambda \Delta\varepsilon_z) / \text{Denom} \quad (11.19)$$

where we have exchanged σ_{mz} for σ_{fz} using equation (11.7), and where

$$Denom = E_1 E_\lambda - 2 E_v^2 \tag{11.20}$$

Also, eliminating σ_{fz} between equations (11.13 and 11.18) gives

$$P = V_f E_f E_m (E_1 \Delta \epsilon_r + E_v \Delta \epsilon_z) / Denom \tag{11.21}$$

It is useful to plot the "mechanical strains", P/E_m and σ_{mz}/E_m as a function of unit thermal strain. Now $\Delta \epsilon_r = (\alpha_{fr} - \alpha_{mr})\Delta T$ and $\Delta \epsilon_z = (\alpha_{fz} - \alpha_{mz})\Delta T$ where ΔT is the temperature change and the α 's are the respective fibre and matrix thermal expansion coefficients (CTE's). Thus, we can write

$$a = (\alpha_{fz} - \alpha_{mz}) / (\alpha_{fr} - \alpha_{mr}) \tag{11.22}$$

and using dimensionless forms for our moduli, $E_f^* = E_f/E_m$, $E_1^* = E_1/E_m$ and $E_v^* = E_v/E_m$ etc. our expressions for the mechanical strains (11.21) and (11.22) reduce to

$$\frac{\sigma_{mz}}{\Delta \epsilon_r} = \frac{V_f E_f^* (2E_v^* + aE_\lambda^*)}{Denom^*} \tag{11.23}$$

and

$$\frac{P}{\Delta \epsilon_r} = \frac{V_m E_f^* (2E_1^* + aE_v^*)}{Denom^*} \tag{11.24}$$

with the asterisks denoting the dimensionless forms: thus, for example

$$Denom^* = E_1^* E_\lambda^* - 2E_v^{*2} \tag{11.25}$$

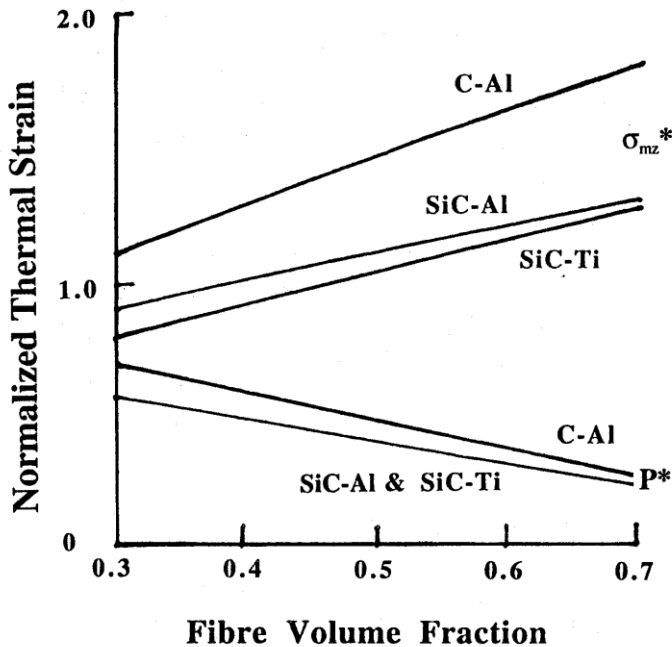


Fig. 11.3 Dimensionless plot of thermal strains estimated from the simple model shown in Fig. 11.2.

Plotting equations (11.23) and (11.24) as a function of V_f , Fig. 11.3, shows that in the practical range between $V_f = 0.3$ and 0.7 the functions are roughly linear with V_f . Carbon (e.g. Hercules AS4) gives greater values because $a = 1.57$ instead of 1.0 while for a high modulus polycrystalline silicon carbide with little preferred orientation $a \cong 1.00$. The hoop stress in the matrix, $\sigma_{m\theta}$ (equation 11.6), is always somewhat higher than σ_{mz} .

The effect of E_f^* is relatively small. Thus going from 4.0 for SiC-Ti to 6.9 for SiC-Al only affects P by about 2% and σ_{mz} by about 15% at $V_f = 0.5$. The effect of ν_m is negligible, while for a 75% change in the change in ν_f the change in P is only 2% and in σ_{mz} only 4% . Thus we can develop relatively simple approximate expressions for P and σ_{mz} good to within about 15% :

$$P^* \cong 0.40 \Delta\varepsilon_r V_m (1 + 0.8a) \quad (11.26)$$

and, somewhat less elegantly

$$\sigma_{mz}^* \cong \Delta\varepsilon_r \{10 V_f + V_m E_f^* + 2a(1 + 2V_f) - 3\} / 7$$

For $\Delta\varepsilon_r$ and a we need a knowledge of the variation of α_{fz} , α_{fr} , α_{mz} , and α_{mr} with temperature, since

$$\Delta\varepsilon_r = \int_{T_2}^{T_1} (\alpha_{fr} - \alpha_{mr}) dT \quad (11.27)$$

and similarly for $\Delta\varepsilon_z$, where T_1 and T_2 are the initial and final temperatures. Data on the thermal expansions as a function of temperature are not easy to obtain. For metals, we can estimate the thermal stresses very roughly, using the common values of α available in reference books, and assume that T_1 is the melting temperature of the matrix, and T_2 is the temperature at which we wish to estimate the stresses, so that

$$\Delta\varepsilon_r \cong (T_2 - T_1) (\alpha_{fr} - \alpha_m) \quad (11.29)$$

and

$$\Delta\varepsilon_z \cong (T_2 - T_1) (\alpha_{fz} - \alpha_m) \quad (11.30)$$

Here we are assuming a polycrystalline matrix with $\alpha_{mr} = \alpha_{mz} = \alpha_m$, and neglecting phase transformations such as the body centred cubic to tetragonal transformation that takes place as titanium cools through 883°C .

Making these assumptions, we can show that there is a potential for the development of very high stresses in reinforced metals. Thus the value 1.0 in Fig. 11.3 corresponds to a potential stress of $E_m \Delta\varepsilon_r$. For aluminium this comes to about 670MPa at room temperature when reinforced by carbon and about 800MPa when reinforced by silicon carbide. For SiC-Ti, the corresponding value is about 670MPa . Thus a reinforced aluminium alloy made from the melt (assuming this is possible) will have yielded long before cooling to room temperature. Other potentially useful metal matrix systems have the same problem.

With reinforced ceramics the strains can be large enough to promote cracking in the absence of any applied stress. We will discuss the range of allowable thermal expansion coefficients for ceramic matrix composites later.

11.2 Advantages and Drawbacks of Reinforced Metals

Reinforced metals have a number of potential advantages over reinforced polymers, apart from their generally higher temperatures of operation.

1. The ductility and higher strength of the metal matrix may give better off-axis properties and interlaminar strengths.
2. Joints are a matrix-controlled property, so the greater strength and ductility of the metal, together with the possibility of diffusion bonding of the matrix, make stronger joints possible than with reinforced polymers.
3. The modulus of the matrix is much higher than that of a polymer, so that at stresses below the matrix yield point, higher moduli are obtained than with reinforced polymers.
4. The erosion resistance, and water and organic solvent resistance of reinforced metals are greater than those of reinforced polymers. In addition metals are less permeable to gases and liquids.
5. The much greater electrical and thermal conductivity of the metal matrix can be an advantage in some applications.

There are some disadvantages, however, in addition to the severe thermal stresses.

1. The stress-strain curve has a "knee" at the matrix yield strain, see Fig. 4.2, so that the material is truly elastic only over a small range of stresses, unless a hard matrix is used. Above the knee the effective elastic modulus is not much greater than for an equivalent reinforced polymer.
2. Reinforced metals are usually less corrosion resistant than reinforced polymers.
3. Reinforced metals are difficult to make, and hence usually much more expensive than reinforced polymers.
4. Reinforced metals have higher densities than reinforced polymers.

Sections 11.3 - 11.5 will be concerned mainly with metals having improved load-bearing properties resulting from the addition of fibres (or whiskers). The description of manufacturing methods includes a brief discussion of the important properties of metals affecting manufacture. This will be followed by a description of the properties of reinforced metals and finally a brief discussion of joints.

11.3 Manufacture of Reinforced Metals

11.3.1 The Matrix

Metals are crystalline solids, and their mechanical properties depend a great deal on the perfection of the crystals. Large, nearly perfect crystals of pure metals are very soft and ductile at a small fraction of their absolute melting-temperature, T_m . (For example pure iron is easily deformed at room temperature.) They are hardened by cold working or by the presence of impurities, either as dispersed atoms or as crystals. The science of physical metallurgy is based on the control of crystal size and perfection, and the use of precipitates, in the making of alloys. A large range of properties can be achieved by this means. Some precipitates in traditional alloys behave in a way that is similar to fibre reinforcement; for example, Fe_3C precipitates in steel consist of fine platelets.

After a metal matrix composite has been put together the matrix can be extensively modified by cold work, or by heat treatment to cause precipitation of components of the metal alloy. Care has to be taken to prevent damage to the fibres, however.

Most metals are very reactive. In air they react readily with oxygen at 20°C , but some quickly form a very thin impermeable oxide film that inhibits further reaction. Good examples of this are Al, Cr, Mg, and Ni. When the oxide is permeable, reaction is slow at 20°C , unless suitable conducting paths are provided so that electrochemical processes are promoted. This happens in steel, where the presence of water and chloride ions promote rusting. At higher temperatures reaction rates are higher, but the impermeable oxide films usually maintain their effectiveness. Thus, for example, aluminium can be melted in air without much oxidation occurring.

The reactivity of metals is a serious problem in metal matrix composites, and the fibres often have to be protected by barrier layers, especially if the material is required for high temperature operation.

Other aspects of the reactivity of metals can be put to good use. For example, metals can be electrodeposited from solutions of their ions, or deposited by chemical vapour deposition from gaseous organic compounds.

Metals are also fusible, though the melting-points range from -39°C (mercury) to 3410°C (tungsten). Melting-points can be reduced by alloying, and liquid infusion from the melt is an important method of composite manufacture. However, metal alloys are quite soft and easily worked at about $0.8 T_m$. Thus, instead of melting it, the alloy can be moulded around the fibres by pressing at the appropriate temperature. Some metal properties are brought together in Table 11.1 for convenience.

Table 11.1 Selected Properties of Metals

Metal	E_m^1 (GPa)	ν_m^2	ρ_m^3 Mgm ⁻³	T_{mC}^4 (°C)	α_m^5 (MK ⁻¹)
Aluminium	71	0.345	2.70	660	24
Beryllium	315	-	1.85	1284	12
Chromium	279	0.210	7.1	1900	6.5
Copper	138	0.343	8.96	1083	17
Iron (soft)	170	0.293	7.87	1537	12
Magnesium	45	0.291	1.74	650	26
Molybdenum	325	0.293	10.2	2620	5.1
Nickel	200	0.31	8.9	1453	13.3
Tantalum	186	0.342	16.6	3010	6.5
Tin	50	0.357	7.3	232	23.5
Titanium	120	0.361	4.51	1667	8.9
Tungsten	411	0.280	19.3	3380	4.5
Zinc	105	0.249	7.1	410	31

Notes:

1) Young's modulus, 2) Poisson's ratio, 3) density, 4) melting temperature (not in Kelvins), 5) Coefficient of thermal expansion

1.3.2 General Considerations

The choice of method used for making a fibre reinforced metal is limited by the need to consider the following factors.

1. The adhesion between fibres and matrix must be adequate, so that the composite achieves the good shear and off-axis properties normally required of reinforced metals. Large numbers of wetting studies have been carried out to investigate the adhesion phenomenon. A widely used criterion is that the contact angle between a molten drop of the matrix material and the fibre material must be less than 90°. When the contact angle is greater than 90° the matrix may be modified by alloying, or the fibre may be coated with an interfacial layer that is compatible with both fibre and matrix (i.e. has a small contact angle with both fibre and matrix materials).

2. The interaction between fibres and matrix needs to be limited, so that fibres are not weakened. The reaction can result in complete decomposition of the fibre material (this happens with silica reinforced aluminium) or in the formation of brittle layers of reaction product at fibre surfaces (this happens with tungsten reinforced nickel). Partial or even slight decomposition of fibres is usually disastrous, since fibre strength is usually lost after relatively little surface attack. Brittle layers of more than about one-hundredth of the fibre diameter may have a very serious weakening effect, since they crack on cooling the composite after manufacture (or due to thermal cycling thereafter) and the cracks can easily propagate into the fibres when the composite is stressed.

3. The need to minimize mechanical damage to fibres. In hot-pressing, too much heat leads to too great an interaction, while too much pressure can cause severe mechanical damage to fibres. The temperatures and pressures used are a compromise between excessive damage of one sort or the other, and inadequate densification.

4. The volume fraction of voids must be kept as small as possible. Voids are usually concentrated at fibre-matrix interfaces, and weaken the composite by acting as stress-raisers and sites for initiation of cracking and debonding.

5. The achievement of the desired fibre geometry. It is seldom worth while to reinforce metals with randomly oriented fibres, since the small strengthening achievable (due to the relatively low volume fractions possible) is often not worth the trouble and expense. Thus, the manufacturing methods available are usually limited to those which produced aligned fibres.

Manufacturing methods can be classified according to the initial state of fibres and matrix. The fibres do not need to exist initially; they can be produced by extrusion from pellet-shaped particles within the matrix, or they can be generated by controlled precipitation from an alloy melt (this can produce either platelets or fibres depending on the volume fraction of the nascent reinforcement). The matrix in both cases is in the form of a billet or bar. When pre-existing fibres are used, the matrix can be solid, as sheets or powder, or liquid, or atomically divided, as vapour or ions. In the account that follows, these methods will be classified according to the initial state of the matrix.

11.3.3 Bar Matrix

We will first consider the co-extrusion of two phases. In this case, the matrix is the continuous phase, and the fibres result from the extrusion of a discontinuous phase of pellet-shaped particles. Both phases have to be sufficiently ductile so that they can be extruded without cracking. The method is therefore normally used to reinforce one metal with another metal. However, some oxides are ductile at high temperatures, and can be co-extruded with a metal, when hot, to produce oxide fibres in refractory metals. In this way, niobium and tantalum can be reinforced with magnesia, thoria, or zirconia. (These composites have roughly the same strength at high temperatures as the unreinforced metals, but are lighter and have higher moduli.) The reduction in cross-section during the extrusion process has to be quite large in order to produce fibres with sufficiently high aspect ratios to be efficient reinforcers.

The other method of making composites from matrix bars containing the fibre generating material is the controlled solidification and crystallization process. These are called *in situ* composites since the fibres are formed *in situ* during the solidification process. The bar can either be an off-eutectic or eutectic alloy. The discontinuous phase can either be rod shaped or plate shaped, rods usually being produced at volume fractions of 30% or less, and platelets at higher volume fractions.

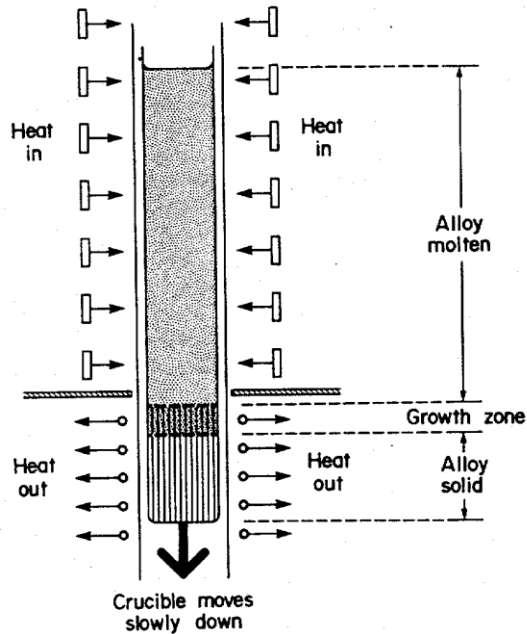


Fig. 11.4 Schematic view of a crystal growth apparatus.

Directional solidification can be achieved with a bar of the eutectic mixture by putting it in a crucible which passes slowly through a heater into a cool area. The bar is melted, and as it passes into the cool area it freezes again, as indicated in Fig. 11.4. When a nickel-chromium eutectic is used, the chromium crystallizes as rods in a matrix of nickel during the solidification.

Not all eutectics form platelet or rod-like precipitates; the phenomenon is governed to some extent by the entropy of fusion of the components. Most metals and metal alloys do so, however.

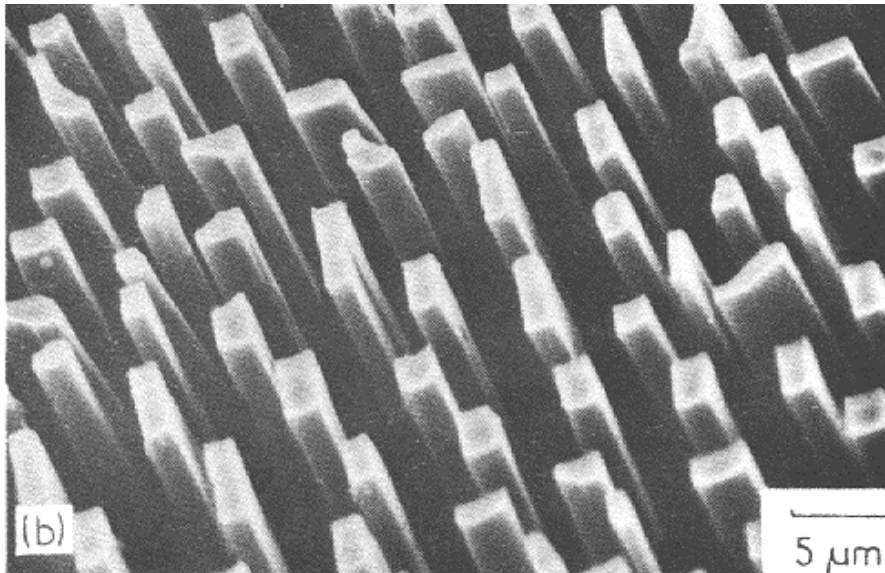


Fig. 11.5 Molybdenum fibres grown in situ in a Ni_3Al matrix. (After Sprenger, H., Richter, H. and Nickl, J.J., 1976, *J. Mater. Sci.* 11, 2075-81. Courtesy Chapman and Hall.)

With binary (and pseudobinary) eutectics, the volume fraction of the discontinuous phase is fixed, once the components of the alloy are decided upon. There are, however, many different alloy systems which can be used if pseudobinary, and certain ternary (three component) eutectics are included; for example, over 150 well-characterized alloys are available, based on nickel or cobalt. Most of these are potentially useful at high temperature, forming rod or platelet precipitates, and having volume fractions ranging from less than 10% to more than 60%. Figure 11.5 shows an in situ composite with fibres for the reinforcing phase.

Variations in volume fraction can be obtained by using off-eutectic alloys. These require much more stringent growth conditions, however, which is a great disadvantage. In addition, the matrix phase has a fixed composition, so that modifications to the matrix to improve its properties (for example, corrosion resistance) are not possible. Variation of volume fraction can be obtained with ternary and quaternary alloys which have eutectics with a wide range of compositions. The crystallization conditions do not have to be so closely controlled to get the desired results with these alloys, but the phase diagrams are very complex.

The melting is usually carried out with induction furnaces, or furnaces with large heat capacity. The alloy bar is usually held in a vertical crucible, melted, and then withdrawn from the furnace at a controlled rate, into a water-cooled region to ensure a sufficiently fast cooling rate, as shown in Fig. 11.4.

The zone-melting technique is also widely used. A molten zone is produced by induction heating, and the bar is slowly pulled through the induction heater so that the molten zone moves along the bar.

Fine structures (i.e. thin platelets or rods) are produced with fast cooling rates in the molten zone, while coarse structures are obtained with slow cooling rates. Great care is needed to keep the conditions constant; small variations can upset the crystallization process and result in the sudden termination of all the rods and platelets. (They restart further down the bar.) The regions lacking the rods or platelets are usually very weak.

11.3.4 Sheet Matrix

In this method layers of fibres are laid between thin sheets of matrix foil in a mould, and the material is then consolidated by hot pressing. The method is only suitable for relatively large diameter fibres (e.g. boron) or wires, or for composite rods (made, for example, by pre-impregnating carbon fibre tow with matrix materials by one of the methods described in 11.3.6 and 11.3.7).

The temperature and pressure have to be controlled very carefully to ensure adequate consolidation without too much chemical interaction, or mechanical damage. Tapes can be made up with sheet matrix on either side of a layer of fibres, the layers being held together by a resin binder (e.g. polystyrene) that evaporates during the first

stage of the consolidation process. The tape can be used in the same way as polymer prepeg tape, in such processes as filament winding, etc.

11.3.5 Powder Matrix

In this method the fibres and matrix powder are combined, and held together by a volatile solid binder. When the mixture is hot pressed, the binder escapes by decomposition.

Often the pressing takes place in two stages. Stage one results in removal of the binder, and sufficient consolidation to hold the matrix and fibres together. Stage two involves pressing techniques similar to those described for reinforced polymers. The temperatures and pressures used are generally much higher for metals. This process consolidates the material to the maximum practical extent consistent with acceptable chemical and mechanical damage of the fibres.

11.3.6 Liquid Matrix

The simplest method of liquid infiltration is to pour the molten matrix into a vessel containing the fibres or whiskers. Whiskers can be in the form of a felt or mat, while fibres can be aligned in a tubular mould, fitting loosely in it. The method is not suitable when the matrix reacts strongly with the fibres (e.g. aluminium with silica). In addition, difficulties may be experienced with the wetting of the fibres or whiskers, though these can often be overcome by coating them.

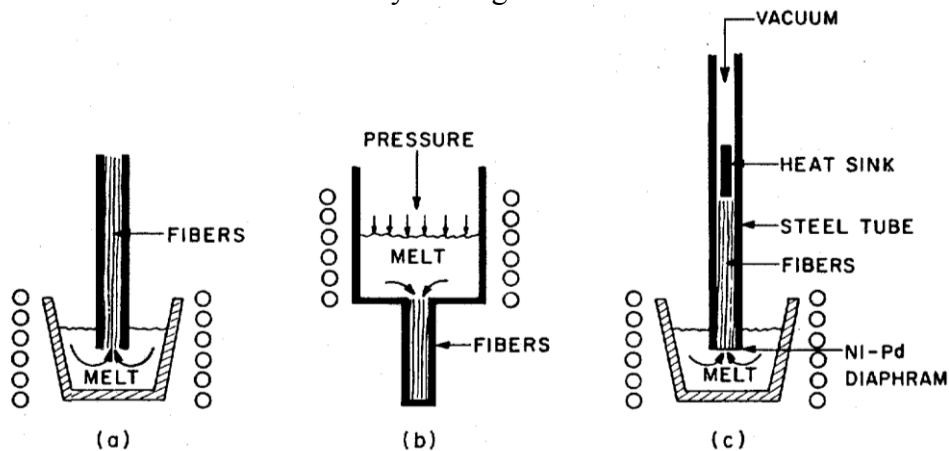


Fig. 11.6 Methods used for liquid metal infiltration. (After Mehan, R.L., and Noone, M.N., 1974, *Composite Materials*, 4, 159-227, Ed. Kreider, K.G., Courtesy of Academic Press.)

With less reactive systems (for example, carbon-aluminium) a fibre tow, which can contain as many as 10,000 individual fibres, can be drawn through a crucible containing the molten metal. The fibres enter at the top, and pass through a die at the bottom of the crucible. The fibres can be protected against attack to some degree by a suitable metallic coating (nickel was used for carbon-aluminium) or the rate of reaction can be reduced by alloying the metal to reduce its melting-point so that the process can be

carried out at lower temperature (for example, 12% silicon in the molten aluminium matrix reduces the temperature of the operation from just over 660°C to 580°C). When the reinforced rods produced by this process are not thick enough for immediate use in a structure, a large number can be combined by hot pressing to produce the cross-section desired. Figure 11.6 shows three methods of infiltration to form a solid rod, and Fig. 11.7 shows carbon tows infiltrated with aluminium.

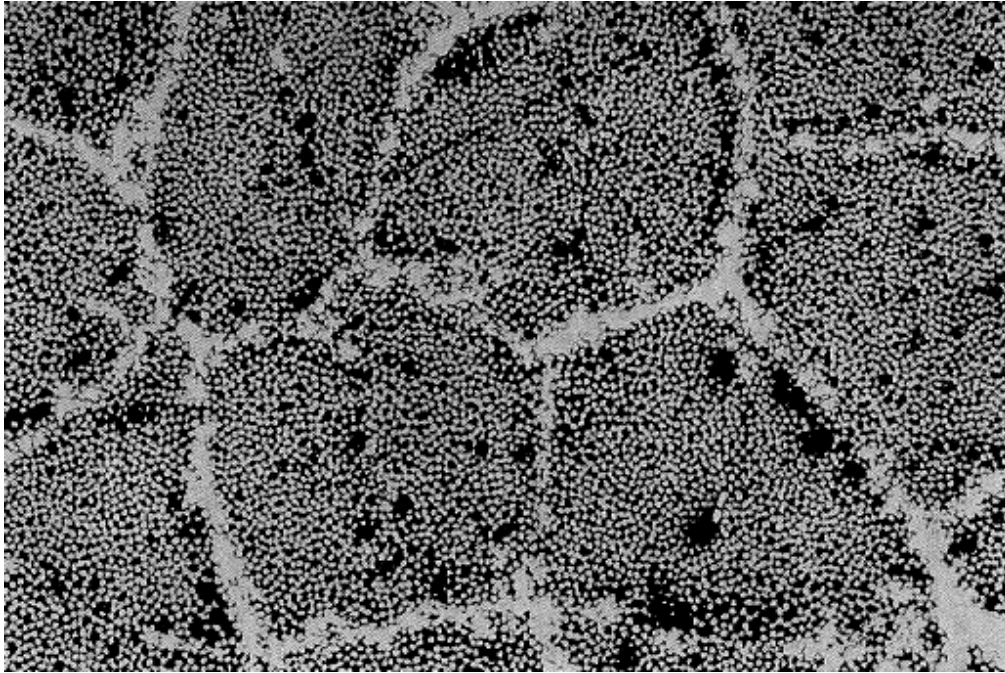


Fig. 11.7 Liquid infiltrated carbon-aluminium. (After Kendall, E.G., 1974, *Composites Materials*, 4, 319-97, Ed. Kreider, K.G., Courtesy Academic Press.)

Another method that uses the matrix in liquid form during part of the manufacturing process is plasma spraying. The matrix, melted in a gas discharge, is sprayed onto the fibres, which are supported on a foil, also made of the matrix material. The resulting tape is very porous, easily deformable, and suitable for cutting to the shape and size required for hot-pressing to the desired form. One advantage of the plasma-spraying technique is that the metal rapidly cools and freezes in contact with the fibres, thus minimizing undesirable chemical reactions.

11.3.7 Atomic and Ionic Matrix

The matrix can be deposited onto the fibres directly from the vapour, or indirectly by a vapour phase reaction. Usually referred to as CVD, this chemical vapour deposition process is used to make boron and SiC fibres; see section 3.3.3. Aluminium has been coated successfully on carbon fibres by thermal decomposition of triisobutyl aluminium, while nickel carbonyl is used for the deposition of nickel.

Electroplating, which also transports matrix ions, can be carried out on any conducting fibre or wire. Air and water must be excluded for the deposition of aluminium, so ether is used as solvent. Aqueous baths are used for the more noble metals (copper or nickel for example).

Plasma spraying, mentioned above, may involve ions instead of just liquid matrix.

The most serious difficulty with the techniques involving the matrix in these forms is that of ensuring good penetration of the matrix into fibre bundles. High rates of production are required for economic reasons, so that with carbon fibres, for example, it is necessary to plate or spray the fibres in the form of tow rather than singly. However, deposition on fibres at the centre of the tow is prevented because of shielding by the outer fibres. Consequently, the tow has to be rearranged so that all the fibres are in a plane, and none are touching. This problem is less serious with chemical vapour deposition and electroplating.

The coated fibres are hot pressed to produce the final composite. An organic binder may be used to make the coated fibres into prepreg tapes to ease subsequent production steps.

11.3.8 Laminates

Fibre reinforced metals can be made by lamination in the same way as for fibre reinforced polymers. The simplest way of doing this is to use the various tapes assembled in the desired orientation and hot press them. The pressure, temperature, and time of pressing are chosen to ensure adequate bonding within and between laminae without too much degradation of the fibres.

The sheet matrix method can be used to produce laminates directly.

11.4 Properties of Reinforced Metals

As with reinforced polymers, a wide range of properties is possible with the variety of fibres available, choice of volume fraction, and choice of metal matrix.

Many reinforced metals examined in the early days were model systems (these include sapphire-silver and tungsten-copper) fabricated to investigate the fundamentals of reinforcement, rather than with any application in mind. These will be by-passed here, and systems which might possibly have some practical applications will be discussed. Attention will be given to high temperature properties, since this is the area in which reinforced metals are most likely to make themselves useful.

11.4.1 Strength and Modulus

With reinforced metals the metal normally yields before the fibre reaches its breaking strain. Thus, the metal can be expected to contribute most of its strength to the ultimate strength of the composite. (It does not usually contribute 100% of its potential strength because the fibres have broken before it has fully work-hardened.) On these

grounds the composite may be expected to achieve a strength close to the Rule of Mixtures value. However, few do.

Table 11.2. gives some representative values for the fraction of the Rule of Mixtures strength that have been attained for reinforced metals with volume fractions close to 0.5.

Table 11.2 Reinforcement Efficiencies for Continuous Aligned Fibre Reinforced Metals, given as Fractions of the Rules of Mixtures Values (longitudinal) and of the Matrix Strength (transverse).

Matrix Fibre	Boron ¹	Aluminium Carbon ²	Silicon carbide ³	Nickel Alloy Carbon	Tungsten	Titanium Boron
Longitudinal Strength	0.93	1.05	0.88	0.63	0.90	0.78
Longitudinal Modulus	0.97	0.91	0.94	0.80	–	0.94
Transverse Strength	1.00	0.25	0.29	–	–	0.60

Notes:

1) Boron was coated with SiC; alloys used were 6061 and 2024, 2) Matrix was 0.88 Al-0.12 Si, and 3) Matrix was 6061 Al alloy.

The carbon-aluminium (the matrix is actually an aluminium-silicon alloy) achieves the high value because the silicon suppresses the reaction between carbon and aluminium. The tungsten-nickel alloy value is less than 1.0 because of internal stresses that are generated on cooling from room temperature; the efficiency of this composite increases as the temperature is raised, up to the temperature at which it was hot pressed. In the other cases the chemical reaction accounts for the low values. With in situ composites there is often some uncertainty about the "fibre" strength. However, Rule of Mixtures strengths have been obtained in some cases where the fibre strength could be determined.

Table 11.2 also gives values for the fraction of the Rule of Mixtures modulus that can be achieved in the fibre direction. Even when the strength is low, the fibres are still able to have a large stiffening effect. The elastic properties in directions oblique to the fibre direction are generally believed to obey the theoretical relationships presented in Chapter 4, although, at the time of writing, the composites community has not appreciated the need to consider wide sample testing. The transverse modulus can be higher than the inverse Rule of Mixtures, IROM, equation 4.8: see Fig. 11.8.

With in situ composites, the moduli of the phases are often not known. The moduli of nickel- and chromium-based in situ composites range from about 140 to 300GPa, as compared with a matrix modulus of 200GPa for nickel and 279GPa for chromium.

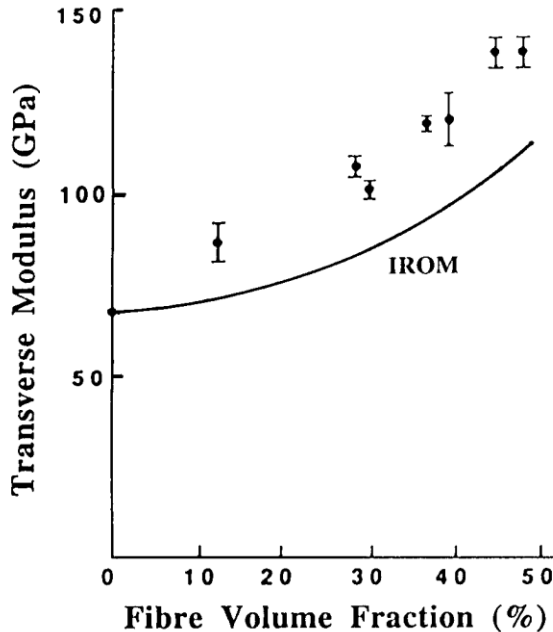


Fig. 11.8 Transverse modulus (E_2) for unidirectional boron-6061 aluminium alloy. (After Prewo, K.M. and Kreider, K.G., Metal. Trans. 13A, 1982, 1511-9.)

The best transverse strength that can be achieved is the strength of the unreinforced matrix. Table 11.2 shows that with two systems this can be achieved. With boron-aluminium the aluminium matrix fails, while with boron-titanium the boron fibres fail transversely to give the low value of 0.6. This transverse fibre failure is probably due to the high processing temperatures generating large residual stresses which, despite the subsequent annealing, weaken the fibres. The very low value of 0.25 for carbon-aluminium is the result of premature failure of the matrix caused by impurities introduced into the aluminium during the manufacturing process. This can probably be prevented by more careful control during fabrication. The low value for SiC-Al (0.29) is due to the fibres debonding and splitting. In this case the effect decreases with increasing temperature so that at 400°C, the transverse strength is about equal to the matrix strength. In situ composites should normally have the transverse strength equal to the matrix strength. However, when lamellar precipitates are obtained, the transverse strength in the plane of the lamellae can be very much greater than this, while that normal to the lamellae is then generally less.

It should be noted that the best transverse strengths can be much greater than those obtained with reinforced polymers. For the boron-aluminium described in Table 11.2. various aluminium alloys were used as matrix, and the transverse strength obtained with the strongest alloy was claimed to be 0.3GPa. (Transverse strengths of aligned fibre reinforced polymers are typically less than 0.1GPa.) However, this strength is much less than that in the fibre direction (1.8GPa), and a good non-reinforced aluminium alloy can have a strength in all directions of 0.65GPa (Table 1.1).

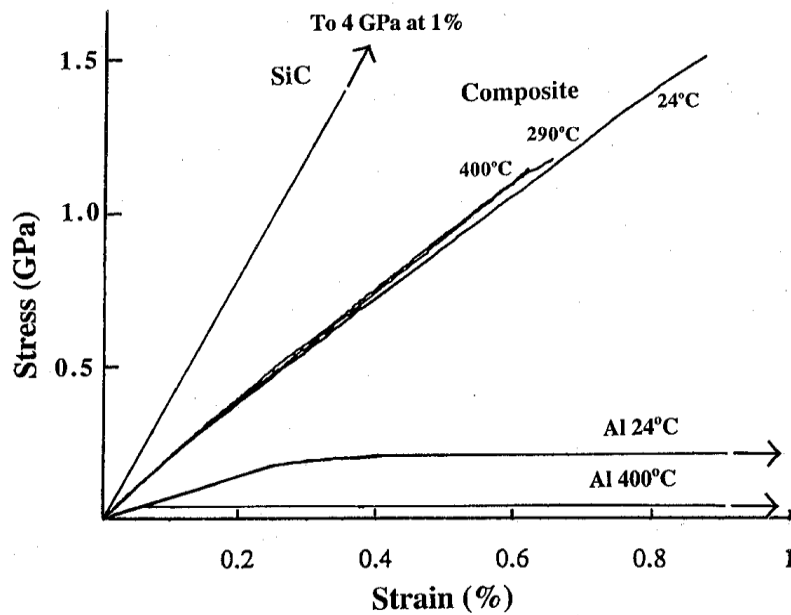


Fig. 11.9 Stress-strain curves for unidirectional silicon carbide-6061 aluminium alloy at the temperatures indicated. Also shown are curves for the fibre and the matrix. (After Daniel, I.M., Chun, H.J. and Karalekas, K., NASA CR, 195381, 1994.)

Stress-strain curves for moderate volume fraction (0.2 to 0.7) aligned continuous brittle fibre reinforced metals usually have two linear regions, the change in slope (the "knee") occurring at the matrix-yield strain. Near the breaking-stress there is sometimes a small pseudo-plastic region, during which the fibres are breaking into short lengths. Figure 11.9 shows the stress-strain curve for silicon carbide-aluminium alloy, at various temperatures. Thus there is a knee at about $\epsilon_k = 0.08\%$ and a decrease in slope just before final failure at 24°C and 290°C. Note that $\epsilon_k < \epsilon_{my}$ (about 0.23%) because of the internal stresses due to differential thermal contraction. In Fig. 11.9 the knee is not sharp. Instead there is a gradual change of slope between .08% and .15% strain.

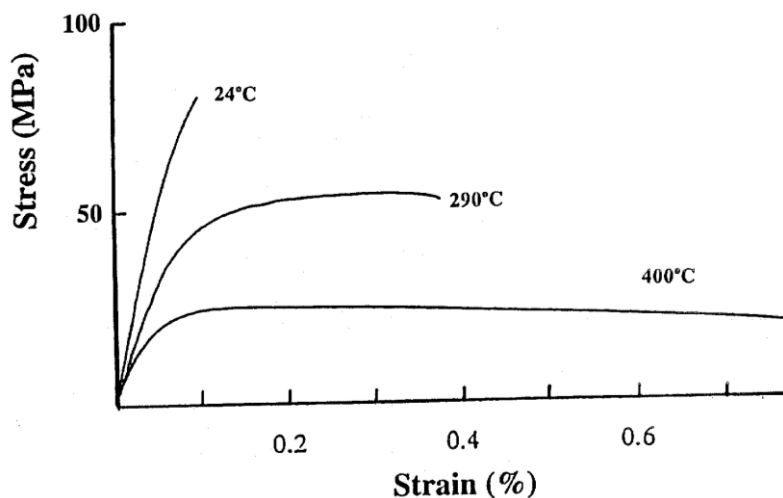


Fig. 11.10 Transverse stress-strain curves for the composite shown in Fig. 11.9.

Transverse stress-strain curves for the same SiC-Al composites are shown in Fig. 11.10. At 400°C the strength (20MPa) is still somewhat less than the matrix strength (42MPa) and the breaking strain is much reduced (1.01% compared with > 20%). For this material the transverse modulus was about $0.90 / (V_f/E_f + V_m/E_m)$.

When the fibres are ductile, there is a true plastic region, as in the case of tungsten-nickel alloy shown in Fig. 11.11. The plastic region at the highest stress is due to the tungsten deforming plastically and is extensive for 300°C and 700°C. The knee due to matrix yield is not noticeable in this case. With in situ composites stress-strain curves resembling non-reinforced metals can be obtained, due to extensive plastic deformation of the fibrous or lamellar phase. An example is shown in Fig. 11.12; this material can be heat treated to increase the yield stress of the matrix.

Little work appears to have been carried out on the compressive strength of reinforced metals. What results there are suggest that it is equal to or greater than the tensile strength. In the case of continuous aligned boron-aluminium, with $V_f = 0.6$, the compressive strength (2.14GPa) was nearly twice the tensile strength in the fibre direction, and at 30°, 60°, and 90° to the fibre direction the compressive strength was greater than the tensile strength. In the case of carbon-nickel, the tensile and compressive strengths were the same (0.69GPa) for nickel containing 50% of continuous aligned Thornel-75 graphite.

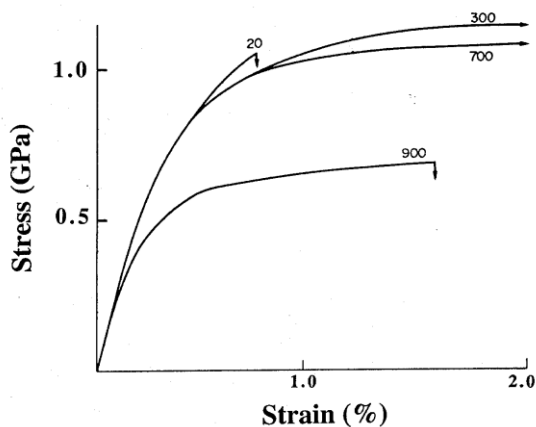


Fig. 11.11 Stress-strain curves for tungsten-nickel superalloy at temperatures (°C) indicated on the curves. (Courtesy of Westinghouse Canada Ltd.)

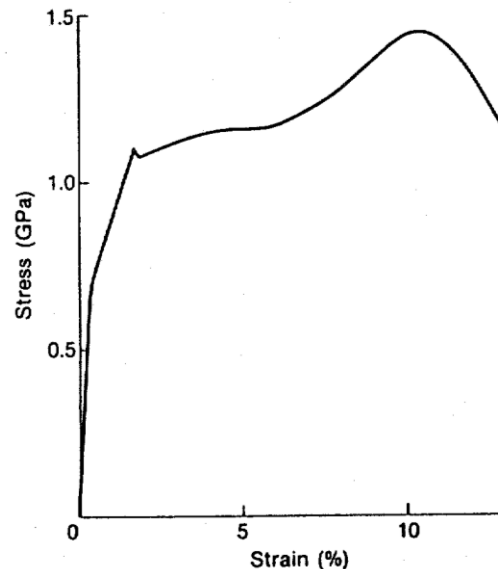


Fig. 11.12 Stress-strain curve for in situ composite (Ni-20Co-10Cr-3Al-TaC). Note the large plastic region. (After Bibring, H., Trotter, J.P., and Rabinovitch, M., and Seibel, G., 1972, Mem. Sci. Rev. Met. 68, 23-41.)

11.4.2 Toughness

The presence of the fibres usually reduces the toughness of the material. Despite this, in the case of B-Al, for fibres normal to the crack plane, the toughness increased

with increasing fibre volume fraction, in the range 0.3 to 0.5. Results from impact tests on a number of composites are given in Table 11.3, and compared with the impact toughness of the unreinforced matrix material.

Table 11.3 Work of Fracture, kJm^{-2} in the three main directions (\mathcal{G}_1 , \mathcal{G}_2 , \mathcal{G}_3) Compared with Matrix Values. Taken from Impact Tests at 20°C.

System	B-Al alloy (6061)	W-Ni ¹ alloy	NbC-Ni ¹	(CoCr) ⁻¹ (CrCo) ₇ C ₃
V_f	0.5	0.6	0.11	0.3
\mathcal{G}_1	60 ²	9 ³	340	94 ⁴
\mathcal{G}_2	15 ⁵	—	—	17 ⁴
\mathcal{G}_3	15 ⁵	—	—	14 ⁴
\mathcal{G}_m	130	240	630	—

Notes:

1) In situ composites, 2) Toughness increased with increasing V_f in range 0.3 to 0.5, 3) Toughness increased to 100kJm^{-2} at 370°C, and 500kJm^{-2} at 1100°C. Hot working the material increased the 20°C toughness to 44kJm^{-2} , 4) Slow bending tests gave much lower values (approx. 1/10), and 5) Toughness independent of V_f in the range 0.3 to 0.5.

The value for boron-aluminium is about one-third that of boron-epoxy (Table 10.6). However, it increases more than 500 fold when heated to 1100°C. The in situ alloys fare better, the value at room temperature for niobium carbide-nickel being more than twice that of Kevlar-epoxy. (Both the in situ composites included in the table have respectable tensile strengths - about 1.3GPa - and Young's moduli in the fibre direction - about 300GPa.)

The toughness of the composites is greatest when the fibres are normal to the crack plane i.e. $\mathcal{G}_1 > \mathcal{G}_2$ and \mathcal{G}_3 . When cracking occurs parallel to the fibres, boron fibres in the crack plane split, or the interfaces fail at relatively low stresses, giving much lower works of fracture.

Increasing the temperature usually increases the work of fracture, due to the decrease in the matrix yield stress. (With tungsten fibres there is also an increase in fibre toughness.) The state of consolidation and microstructure of the matrix also has a large effect on toughness; for example, hot working the tungsten-nickel alloy increased the toughness five-fold.

Fracture mechanics tests on boron-aluminium laminates with $V_f \cong 0.45$ and with varying fractions of 0° plies, together with $\pm 45^\circ$, gave \mathcal{K}_{Ic} values which depend on the specimen width. The narrowest specimens gave the lowest results; see Fig. 11.13. This composite is less likely to split than reinforced polymers, so that unidirectional composites could also be tested. These, with $V_f = 0.50$, yield and flow plastically, de-

stressing the fibres near the crack tip. Nevertheless the crack propagates transversely, as required for a meaningful test. The values for the laminates containing 50% of 0° plies were about the same as the nearly equivalent carbon-epoxy laminate: see Table 10.5 (the polymer composite has an extra 90° ply).

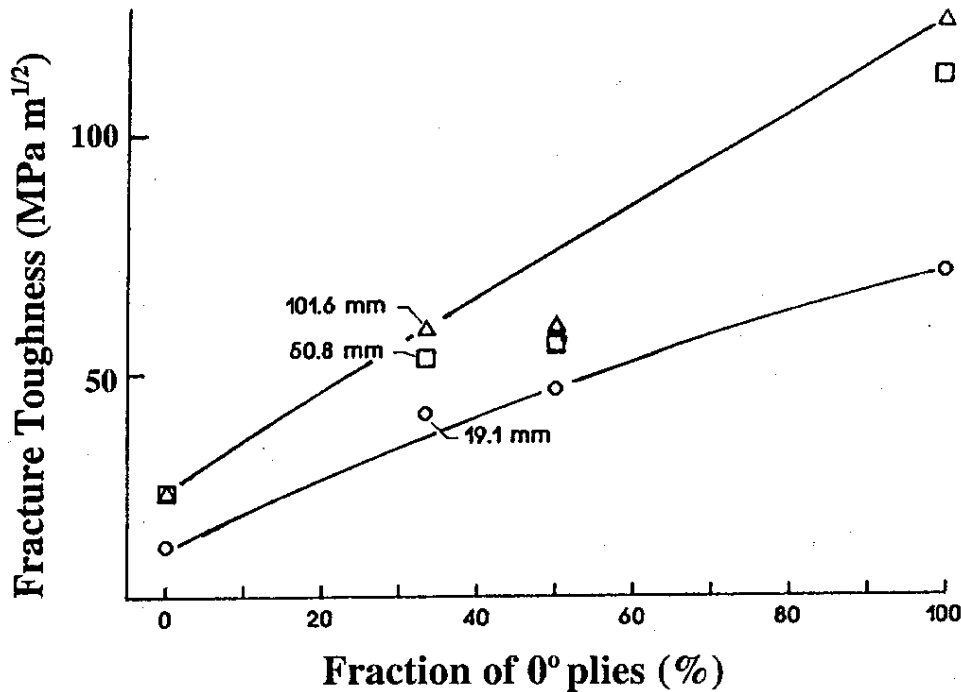


Fig. 11.13 Fracture toughness for B-Al. Laminates based on 0 ± 45 combinations as a function of the fraction of 0° plies. Specimens widths as indicated. (After Poe, C.C., Jr., 1989, ASTM STP 1032, 173-93.)

11.4.3 Fatigue

Although the fatigue resistance of fibre reinforced metals is generally not as good as that of reinforced polymers, it can be quite good. Figure 11.14 compares the fatigue resistance of unidirectional alumina-aluminium alloy with that of the unreinforced matrix (6061-T6) tested at room temperature. The fatigue resistance is mainly due to the excellent fatigue properties of the fibres, which are carrying most of the load. Excellent fatigue resistance has also been found with in situ composites containing brittle fibres.

In tension-tension fatigue the matrix can go into compression if its yield strain is exceeded during loading. The compression occurs on unloading, when the strain has decreased by an amount which exceeds the yield strain.

Fibre failure can occur at stress raisers due to imperfections at the surface, or to internal matrix cracks caused by the alternating stresses.

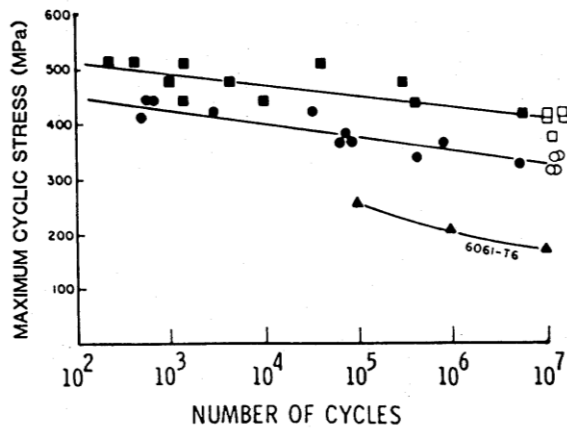


Fig. 11.14 Fatigue curves from two batches of Al_2O_3 -6061 T6 alloy samples with $V_f = 0.55$ compared with curve for matrix. The minimum stress was fixed at 0.038 GPa; open circles and squares are for samples that did not break. (After Johnson, W.S., 1989, ASTM STP 1032, 194-221.)

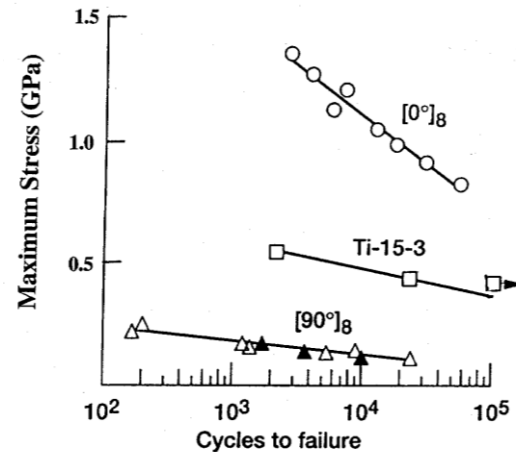


Fig. 11.15 Tension-tension fatigue of SiC-Ti alloy laminates compared with that of the matrix. (After Castelli, M., and Gayda J., 1996, NASA Reference Publication, #1361, 31-41.)

With SiC-Ti alloy laminates, tested at 430°C the apparently poor fatigue resistance, Fig. 11.15, may be due to cracks propagating from the matrix into the fibres in the $[0]_8$ case, and due to a weak fibre-matrix interface in the $[90]_8$ case. It should be noted however that the stress at failure for the $[0]_8$ laminate was always greater than that of the unreinforced matrix.

11.4.4 High-Temperature Resistance

At least three problems have to be solved before composites can be used at high temperatures: (1) the components interact chemically and react with the environment; (2) differences in thermal expansion coefficients give rise to high internal stresses; (3) most materials creep at high temperatures.

Although chemical interactions are not a problem with in situ composite (these are equilibrium systems so far as chemical potential is concerned) the large areas of interface results in high interfacial energies. Thus, at temperatures close to the melting-point, when diffusion rates become sufficiently great, the fibres tend to spheroidize, leading to progressive loss in reinforcement. This process becomes serious when the temperature exceeds $0.9 T_m$ (T_m is the melting-temperature, K) and is assisted by stress gradients.

In the case of reinforced aluminiums, although the strength at temperatures up to 500°C can be quite good in short term tests (e.g. for carbon-aluminium, 0.9 of its 20°C value) the strength falls with time at the temperature, and the maximum temperature for long term use is much lower than this. For example, Fig. 11.16 shows that the strength of boron-aluminium falls rapidly at 540°C. 300°C is probably the maximum temperature for

long term use of reinforced aluminium. This is little better than can be achieved with carbon-polyimides

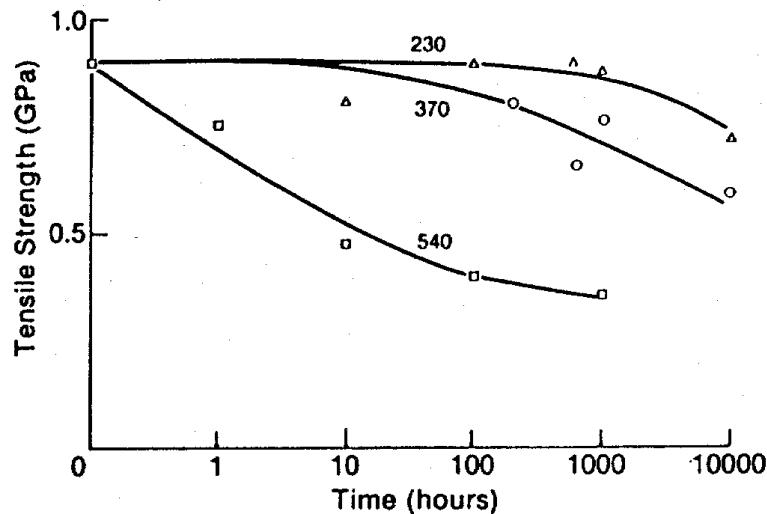


Fig. 11.16 Weakening of boron-aluminium due to exposure to temperatures ($^{\circ}\text{C}$) indicated on the curves. (After Sturke, W.F., Metal Matrix Composites, AIME, Symp. Pittsburgh, 1969.)

Reinforced titanium will operate at higher temperatures; boron-titanium will survive about 10,000 hours at 540°C before it becomes critically weakened by titanium diboride formation at the fibre surface. This time is reduced to about four hours at 760°C .

With carbon-nickel, severe degradation of the carbon occurs at temperatures above 800°C due to the nickel promoting recrystallization of the carbon. In a cobalt matrix, the carbon recrystallizes rapidly at 700°C . Tungsten can be used to reinforce nickel at temperatures above 1000°C . The nickel promotes recrystallization and loss of strength of the tungsten fibres at high temperatures. The recrystallization is inhibited by hafnium carbide; at 1200°C no significant recrystallization occurred for at least 100 hours when the fibres were coated with HfC.

Table 11.4 Maximum Temperatures for Metals Reinforced with Boron, Carbon, Silicon Carbide and Tungsten Fibres.

System	Temperature ($^{\circ}\text{C}$)	Remarks
C-Al	500	Al contains 12% Si
B-Al	540	B coated with SiC
B-Ti	650	B coated with SiC
B-Ti	540	Oxygen present; B coated
SiC-Ti	650	
C-Ni	800	
C-Ni	600	Oxygen present
W-Ni	1200	W coated with HfC

The interaction with the environment may usually be controlled by choice of matrix. For example, for high temperature operation in the presence of combustion gases (in a turbine for example) nickel alloys are normally used because of their corrosion resistance.

At temperatures above 1000°C however, oxygen readily diffuses through nickel, so oxidizable fibres have to be protected by diffusion barriers. Boron and carbon are both susceptible to attack by oxygen. Boron-titanium loses strength at 540°C due to the formation of boric oxide. (This oxide melts at 460°C.) Carbon in nickel above 600°C can oxidize rapidly and completely, to the gaseous state, leaving pores in the nickel. These results are summarized in Table 11.4.

Finally, silicon carbide whiskers reduce the creep of aluminium at 300°C: see Fig. 11.17. These whiskers had diameters of about 0.6µm and lengths of 10-80µm. They had some orientation since the material was produced by extrusion using powder matrix followed by rolling.

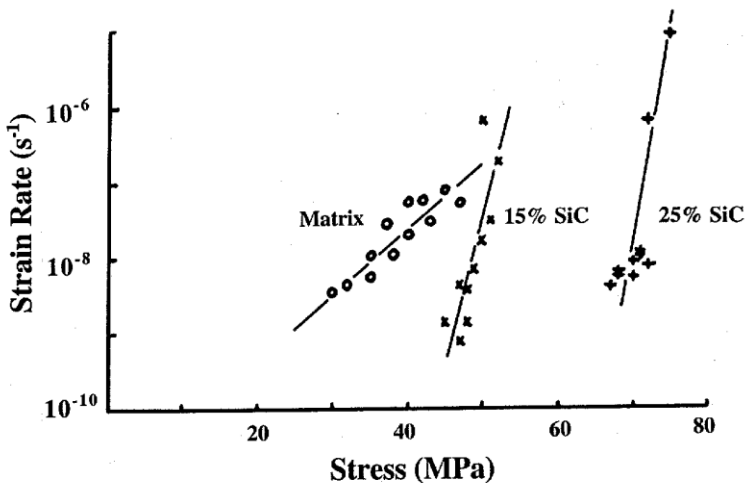


Fig. 11.17 Secondary creep rates at 300°C for the 2124 aluminium alloy matrix, and for SiC whisker reinforced alloy with $V_f = 0.15$ and 0.25 , loaded along the extrusion direction. (After Lilholt, H., and Taya, M., 1987, Proc. ICCM6-ECCM2, Elsevier, London, pp. 2.234-44.)

11.5 Joints

Joints are a problem with reinforced metals for the same reason that they are with reinforced polymers, i.e. because of the low apparent shear strength of the material compared with its tensile strength. Thus large surface areas are required with joints. For example, with aligned SiC-Al the tensile strength in the fibre direction is twenty times the apparent shear strength in planes parallel to the fibres. Thus the joint length to component thickness ratio must be at least twenty, and is usually much larger than this because of stress concentrations at the end of the joint.

Butt and scarf joints cannot be used, and brazing fluxes are inadvisable because, with the large areas involved, some flux may remain trapped in the joint and weaken it. Thus fluxless brazing and solid state diffusion are the methods recommended. Both processes require great care to ensure that the fibres are not damaged by the heat and pressures used. With these processes, joints having strengths approaching the matrix strength have been made. With boron-aluminium, for example, apparent joint shear

strengths of more than 50MPa can be achieved. Joint design follows the general outline given for reinforced polymers in section 10.6.

11.6 Reinforcement of Ceramics

11.6.1 Thermal Contraction Limitations

With reinforced metals, the matrix usually has a CTE which is greater than α_f . So even in the absence of a good bond, stress transfer can take place between fibres and matrix by friction. With all-ceramic systems this is not necessarily the case. Moreover, a large degree of relative shrinkage can cause a ceramic matrix to crack prematurely. So useful combinations of fibres and matrix have upper and lower limits for the CTE's.

To understand this situation, we use the same analysis as in section 11.1, except that now we apply a stress, σ_1 , to the "composite". Then equation (11.7) becomes

$$V_f E_{fz} + V_m E_{mz} = \sigma_1 \quad (11.7a)$$

and equation (11.19) becomes

$$\sigma_{mz} = E_m \{ V_f E_f (E_\lambda \Delta \varepsilon_z + 2E_v \Delta \varepsilon_f) + \sigma_1 (E_\lambda - 2\nu_f \varepsilon_v) \} / Denom \quad (11.19a)$$

This can be simplified, since $E_\lambda \gg E_v$. For fibres with $\alpha_{fr} = \alpha_{fz} = \alpha_f$ the equation reduces to

$$\sigma_{mz} \cong (E_m / E_1) (V_f E_f \Delta \varepsilon_z + \sigma_1) \quad (11.31)$$

To avoid premature cracking we need $\sigma_1 > \sigma_{mu}$ for $\sigma_{mz} = \sigma_{mu}$. Using equation (11.31) for σ_1 with $\sigma_1 > \sigma_{mu}$, this gives

$$E_1 \sigma_{mz} / E_m - V_f E_f \Delta \varepsilon_z > \sigma_{mu} \quad (11.32)$$

and substituting $\sigma_{mz} = \sigma_{mu}$ and rearranging yields

$$\Delta \varepsilon_z < \varepsilon_{mu} (1 - E_m / E_f) \quad (11.33)$$

Next we use equation (11.30) for $\Delta \varepsilon_z$ and writing ΔT for $T_2 - T_1$,

$$(\alpha_f - \alpha_m) \Delta T = (1 - E_m / E_f) \varepsilon_{mu} \quad (11.34)$$

so that finally, recognizing that we are considering a temperature decrease, $T_1 > T_2$ so that $\Delta T < 0$, we have

$$\alpha_f > \alpha_m - \varepsilon_{mu} (1 - E_m / E_f) / [-\Delta T] \quad (11.35)$$

Turning to the interfacial pressure, equation (11.21) becomes

$$P = V_m E_m E_f \{ E_1 \Delta \varepsilon_r + E_v \Delta \varepsilon_z + \sigma_1 (\nu_m - \nu_f) \} / Denom \quad (11.21a)$$

For friction initially (i.e. when there is no applied stress), for fibres with $\alpha_{fr} = \alpha_{fz} = \alpha_f$, we need $\alpha_f < \alpha_m$, so that our two conditions for α_f can be combined:

$$\alpha_m - \varepsilon_m (1 - E_m / E_f) / [-\Delta T] < \alpha_f < \alpha_m \quad (11.36)$$

Moreover, for frictional stress transfer to be fully effective, equation (11.21a) indicates that $\nu_m > \nu_f$.

Our condition with respect to the CTE's reduces our choice of fibre-matrix pairings rather drastically. Table 11.5 gives some expansion coefficient data, together with ΔT values for stressing at 20°C. A look at data in Table 3.3 suggests that the only pairings with a good chance of useful reinforcement are where the fibres and the matrix are the same material, i.e. C-C, SiC-SiC and Al₂O₃-Al₂O₃ when such couplings are possible with retention of the fibre properties.

In practice, it is found that a slight interfacial tension ($P < 0$) can be beneficial, since the bond between fibre and matrix (if any) is weakened, and fracture does not easily propagate from the matrix into the fibre. So fracture is accompanied by fibre pull out, which increases the fracture work and can also increase the ultimate strength. Some surface roughness of the fibres must then be involved, so that the frictional force is not zero.

Table 11.5 Matrix Data, and Range for Coefficients of Expansion for Reinforcing Fibres with Smooth Surfaces

Matrix	ΔT (°C)	σ_{mu} (GPa)	E_m (GPa)	α_m (MK ⁻¹)	α_{fmin}^1 (MK ⁻¹)	α_{fmax}^1 (MK ⁻¹)
Borosilicate glass	500	0.10	60	3.5	0.8	3.5
Glass ceramic ²	980	0.10	100	1.5	0.8	1.5
Alumina	1380	0.28	400	8.8	8.8	8.8
Silicon	580	0.45	161	4.1	3.8	4.1
Silicon nitride	1430 ³	0.3	307	2.87 ⁴	2.7	2.5 ⁵

Notes:

1) Minimum and maximum values for fibre thermal expansion coefficient, 2) lithium alumino silicate, 3) nitriding temperature, 4) a-Si₃N₄,; for b-Si₃N₄, $\sigma_m = 2.3$, the corresponding σ_f 's are 2.1 and 2.3, and 5) calculated assuming $\nu_m = 0.2$. (Poisson's ratios for fibres and matrices will be found in Table 6.1).

So let us re-examine equation (11.12) for $\alpha_{fr} > \alpha_{mr}$. When $\sigma_f = 0$, this gives

$$PE_{\lambda} / [V_m E_f] = E_m \Delta \epsilon_r + \nu_m \sigma_{mz} \quad (11.37)$$

and the matrix is just touching the fibres when

$$\sigma_{mz} = -E_m \Delta \epsilon_r / \nu_m \quad (11.38)$$

so equation (11.29) then gives our condition for stress transfer

$$(\alpha_{fr} - \alpha_m)(-\Delta T) < \nu_m \epsilon_{mu} \quad (11.39)$$

or finally

$$\sigma_{fr} < \alpha_m + \frac{v_m \varepsilon_{mu}}{-\Delta T} \quad (11.40)$$

This changes our range of values for α_f (equation (11.36)) to two conditions; the above for α_{fz} , together with equation (11.35) for α_{fz} , which is now more approximate still.

If we have surface roughness on the fibre, this relaxes equation (11.39) still further. Thus if the depth of roughness, h , obeys the condition

$$h/r > (\alpha_f - \alpha_m)(-\Delta T) - v_m \varepsilon_{mu} \quad (11.41)$$

we can still get frictional stress transfer. For example, for SiC-Si₃N₄, h only needs to be about $0.002r$, or about $0.14\mu\text{m}$ for the large SiC fibres ($140\mu\text{m}$ diameter) or about 22nm for $15\mu\text{m}$ diameter Nicalon SiC fibres.

11.6.2 The Ceramic Matrix and the Interface

High temperature ceramics are characterized by high modulus and medium strength (see Table 1.1) together with great hardness, extreme brittleness and chemical inertness. Because of these properties, it is normally the goal of the manufacturing process to produce a ceramic article in its final size and shape.

To do this economically, the high temperature treatment required must be minimized, and the use of high molding pressures avoided where possible. This may be approached in a number of ways. The new ceramic material may be prepared in a fine powder form and mixed with a fugitive binder, such as polystyrene, and then hot pressed to the desired shape and density.

Alternatively a slurry may be used. The carrier fluid is often water or an alcohol, or, rarely, a non-polar organic fluid, together with additives which act as dispersing agents, lubricants and binders. With fine ceramic particles, sintering can produce a moderately dense product, so long as the initial slurry has a high ceramic content (> 55%). Particles are normally $30\text{-}40\mu\text{m}$ for the slurry process.

Extremely fine particles can be produced using the sol-gel process. A sol is a fluid colloid (particles, $1\text{-}100\text{nm}$ diameter, suspended in a liquid or a gas) which has long term stability. In the sol-gel process, a liquid based sol is converted to a gel by removal of most or all of the fluid. The gel is a rigid solid in which the sol particles are lightly linked together. It shrinks greatly during sintering.

An example of the type of reaction is the production of silica gel:



Similarly Al₂O₃ gel can be obtained by hydrolytic decomposition of Al(OC₃H₇)₃ or Al(OC₄H₉)₃ and likewise MgO and TiO gels can be obtained.

Very fine particles and very dense gels require less heat and pressure to produce a well consolidated product. The firing or hot pressing has to be carried out at very high temperatures, above $0.8T_m$ (T_m is the absolute melting temperature in Kelvins) so that densification proceeds to the required extent in a reasonable time. Thus temperatures above 1400°C are commonplace.

Exceptions to this are glass and the glass-ceramics. They can be formed at relatively low temperature ($< 1000^\circ\text{C}$). The glass ceramics, after shaping, are then heated to crystallize the material.

In addition, ceramics can be produced directly from organics, such as polycarbosilanes by heat treatment. For example, SiC fibres are produced this way (see section 3.1): the same type of process can be used for an SiC matrix. Finally, in situ chemical reaction can be used. For example silicon can be converted to Si_3N_4 by nitridation while Al_2O_3 and AlN can be produced from molten aluminium by oxidation and nitridation respectively.

High temperature ceramics are usually the carbides, nitrides or oxides of the lighter elements (e.g. Al, Mg, Si). However, another high temperature ceramic is graphite, which is chemically reactive at high temperature, and relatively weak and very soft, in contrast with the other ceramics. It is made by hot pressing and firing, but an inert atmosphere is needed. When used as a matrix, an in situ chemical reaction, or a different process is used which is described in the next section.

The fibre-ceramic interface should normally be weak in order to prevent easy crack propagation from the matrix into the fibre, and hence take advantage of the fibre toughening effect. There are cases, however in which chemical reactions occur between the fibres and the matrix which promote adhesion. With these, care has to be taken not to allow the reaction to proceed too far and damage the fibres. For example, at 1600°C zirconia fibres react with a magnesia matrix so that bonding is good, but if the temperature is raised to 1700°C the fibres are completely destroyed. (The zirconia migrates to the grain boundaries.) Ideally the fibres should be coated to control the interface. Carbon and boron nitride have been extensively used as coatings but both have poor oxidation resistance, with carbon being particularly susceptible. With Nicalon SiC fibres it is thought that a beneficial carbon surface layer develops during manufacture of the composite.

11.6.3 Methods of Manufacture

The methods used for the manufacture of unreinforced ceramics may be used to make reinforced ceramics. Hot-pressing of the particles, together with the fibres is a method used for both random and aligned fibre composites. In the random fibre case, the chopped fibres may simply be mixed with the powdered matrix or added to a slurry or incorporated into a gel prior to hot pressing. With aligned fibres a "prepeg" tape is made, by, for example, extruding the fibre-matrix mixture with a binder, such as ammonium

alginate. (This binder hardens in an acid bath, so the extrusion is done into such a bath.) Aligned continuous fibre tapes may be made by passing the fibres through a slurry or gel containing a binder. These tapes are then cut into suitable lengths and hot-pressed.

The hot-pressing process can produce parts which are almost completely free of voids. The temperature typically exceeds 1200°C. The dies are often made of graphite, since this has a low coefficient of thermal expansion, and the part can easily be removed from the mould after cooling. However, graphite dies are brittle, are easily abraded, and are rapidly oxidized in air at these temperatures. They should be used in an inert atmosphere, and do not last long. Alternatives include molybdenum-titanium-zirconium alloys, and silicon carbide, but these have higher expansion coefficients, and other problems

Hot-pressing is time-consuming and expensive. Pressing can be carried out more economically at lower temperatures in a two-step process with some loss in mechanical properties. The first step is to press at relatively low temperatures to partly consolidate the material and give it the desired shape; the second step is to heat the partly consolidated parts at a very high temperature without pressure, to promote further densification. The density of the parts produced is lower than can be obtained by hot pressing, and the shape is much less well controlled, since the parts can warp while unrestrained at high temperature, and contraction during densification may not be uniform.

Fibres can be incorporated in glass and glass-ceramics by high-temperature casting. This can only be done with relatively low fibre volume fractions (usually < 0.1) since high volume fractions increase the viscosity of the mixture too much. Extrusion may also be used, but the fibre volume fraction is still rather restricted.

The sol-gel process has also been widely used to make reinforced ceramics. To ensure full densification, several impregnations with the gel may be employed. Hot-pressing is also used for densification of composites made by this process.

Carbon reinforced carbons are made by pyrolyzing carbon reinforced polymers (e.g. phenolics or epoxies), and then graphitizing the matrix by further heating. They are also made by coating woven fibre forms with pitch, and this is pyrolyzed in a hot isostatic press, and subsequently graphitized; several impregnation and pyrolyzation cycles are needed to complete the densification process before graphitization is carried out. The pyrolyzation step is carried out under high pressure in order to enhance the yield of carbon from the pitch. About 85% conversion can be obtained at 100MPa, while only about 50% can be achieved at 0.1MPa. The pyrolyzation takes place at 550-650°C and takes about 24 hours per cycle. Graphitization is carried out at about 2700°C for about one hour. Figure 11.18. illustrates the steps in this process.

Carbon-carbons can be made with three dimensional reinforcement using continuous fibres. This is done by special weaving processes which will produce sheets

20 mm or more in thickness. These composites can also be made by chemical vapour infiltration. Natural gas is decomposed within the fibre preform. Again three dimensional forms are usually used. Both types of process are also suitable for SiC-SiC.

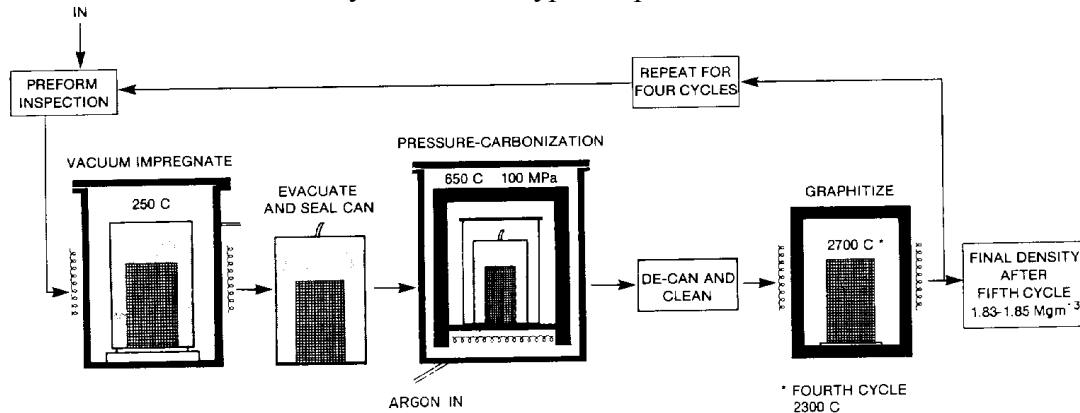


Fig. 11.18 Impregnation and densification of carbon-carbons. (Courtesy of Fiber Materials Inc.)

In situ composites can be made by controlled crystallization of molten ceramic alloys (for a discussion of this method, see section 11.3.3). The reinforcement can be in platelet or fibre form, and refractory compounds as well as elements are suitable. Tungsten reinforced zirconia, hafnia, and urania have been produced, also Mo-Gd₂O₃/GeO, and plates of BaFe₂O₄ in BaFe₁₂O₁₉. In addition, chromium and molybdenum fibres can be grown in Cr₂O₃ and (Cr,Al)₂O₃; an example is shown in Fig. 11.19.

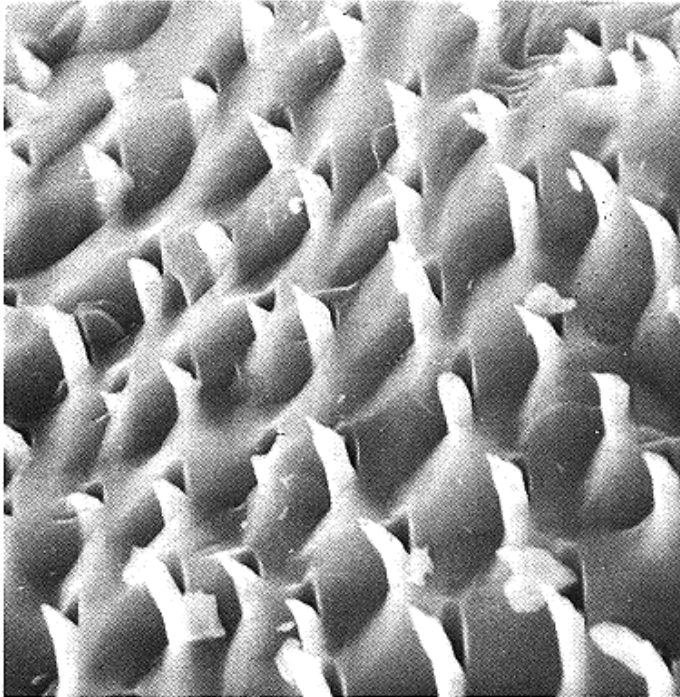


Fig. 11.19 Mo Fibres grown in (Cr, Al)₂O₃. (Courtesy of Nils Clausson, Max Planck Inst.)

The matrix has also been produced by in situ reaction. Silicon nitride matrix composites have been made by flame spraying (and plasma spraying) silicon onto a fibre form, then nitriding the silicon by heating in nitrogen to 1450°C. A carefully controlled

warm-up is required, and the whole nitriding process takes over five days. The nitride formation is accompanied by an increase in volume, which promotes densification of the composite. Fibres used for this process have to be resistant to the high temperatures involved, and unreactive. Silicon carbide, or carbon coated with silicon carbide are suitable. Silicon doughs with fugitive binders are also suitable for the production of these composites. Silicon carbide matrix has also been produced from silicon by carbonization.

Another reinforced ceramic which can be produced by in situ reaction is SiC - aluminium borate. The borate is produced by reaction with alumina, and helps consolidate the composites because the reaction is accompanied by a 14% volume increase.

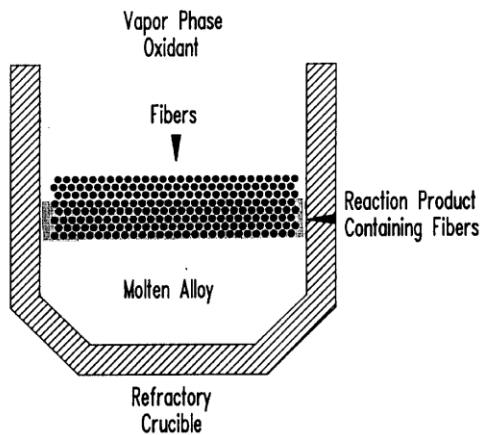


Fig. 11.20 Growth of alumina matrix composites by oxidation of a molten aluminium alloy. (Courtesy of Lanxide.)

Still another process involving chemical reaction with the fibres in place uses fibre preforms above a molten aluminium alloy: see Fig. 11.20. The aluminium is oxidized at about 1000°C and the oxide grows in the fibre form giving full densification, but with traces of free aluminium alloy. Oxidation with air produces an Al_2O_3 matrix, whereas nitrogen in the absence of oxygen produces AlN .

11.7 Reinforced Ceramic Properties

There has been a renewed interest in reinforced ceramics, so much new data is available. This, to a large degree supersedes the earlier work. So we will concentrate here on recent results.

11.7.1 Modulus and Strength

The importance of the testing in tension and compression separately, rather than flexure testing, has been stressed by some researchers. Unfortunately, this is difficult with brittle materials, so most studies still report flexure results. (In the 1960's reinforced polymers were usually flexure tested. The advent of significant use of these materials promoted the tensile testing of them using end tabs, and flexure testing was quietly phased out.) Flexure testing can be very misleading. It normally overestimates tensile

strengths. (up to 100%). Data from such tests should never be used to design components.

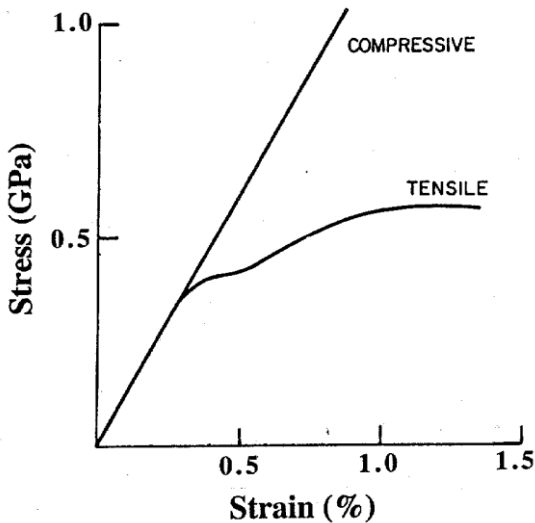


Fig. 11.21 Tensile and compressive stress-strain curves for unidirectional SiC-LAS (After Larson, D.C. and Stuchly, S.L., 1980, Fiber Reinforced Ceramic Composites, Ed., K.S. Mazdiyasm, Noyes Publications, N.J., 182-221.)

Fig. 11.21 contrasts the tensile and compressive stress-strain curves for unidirectional SiC-lithium aluminosilicate (LAS). Since this matrix is a glass-ceramic, we can expect full consolidation, so that the Young's Modulus should be given by the Rule of Mixtures. Initial slopes give a slightly higher tensile modulus (124GPa) than compressive (120GPa). These values are rather low, since $V_f = 0.40$, $E_f \cong 190\text{GPa}$ and E_m is given as 100-140 GPa for LAS. The difference between the ultimate strengths i.e. tensile of 0.58 GPa compared with 1.03GPa for compression, is striking.

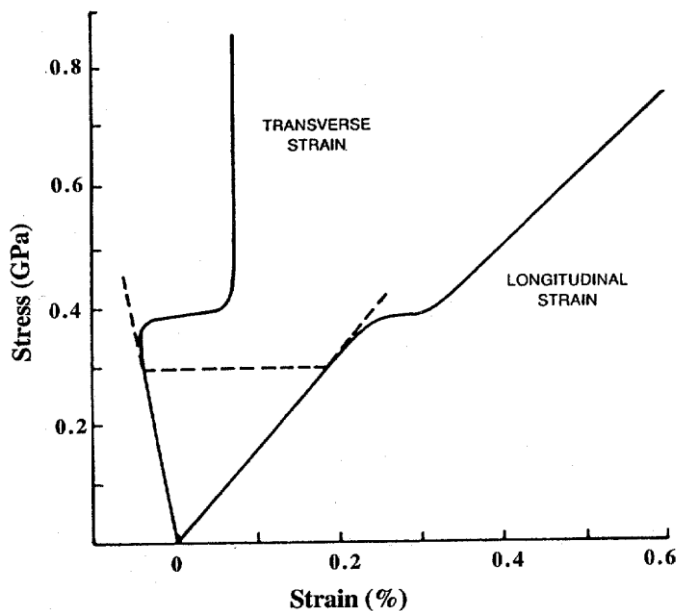


Fig. 11.22 Longitudinal and transverse strains vs stress applied to unidirectional carbon-borosilicate glass. (After Nardone, V.C. and Prewo, K.M., 1988, J. Mater. Sci. 23, 168-80.)

The change in slope of the tensile curve in Fig. 11.21 corresponds to the initiation of matrix cracking ($\epsilon_{fu} < \epsilon_{mu}$). Between about $\epsilon_1 = 0.6\%$ and 0.8% the slope, i.e. 36GPa, is about equal to $V_f E_f$, suggesting that, after splitting is completed, the matrix has broken into small pieces which are now unstressed. This matrix break-up is often

accompanied by an overall transverse expansion of the material: see Fig. 11.22, which shows longitudinal and transverse strains for carbon-glass. Clearly, the matrix is more than stress-relieved: the cracking process includes longitudinal matrix splitting ($\epsilon_2 > 0$).

Multiple matrix cracking is normally explained by the simple analysis given in section 6.3 in the first edition of this book. (It is sometimes referred to as "ACK theory" after its originators.) However, there are both experimental and theoretical difficulties with it. Experimentally, the stress-strain curve always has a moderate slope during multiple cracking while the theory requires that the slope is zero. In the theory the longitudinal splitting is ignored. Because of these shortcomings, the theory will not be reproduced here.

Furthermore, it should be borne in mind that stress-strain curves appearing in print, as in the sources quoted for Figs. 11.21 & 22, are often smoothed and "idealized". The actual experimental curves, such as shown for example in Fig. 11.23, are usually much rougher, and agreement with theory often involves a touch of faith. (It will be noted that this composite, with 30% SCS6 fibres in a Si_3N_4 matrix, which if fully dense would have a modulus of 307GPa, falls far short of the Rule of Mixtures for both modulus and strength.)

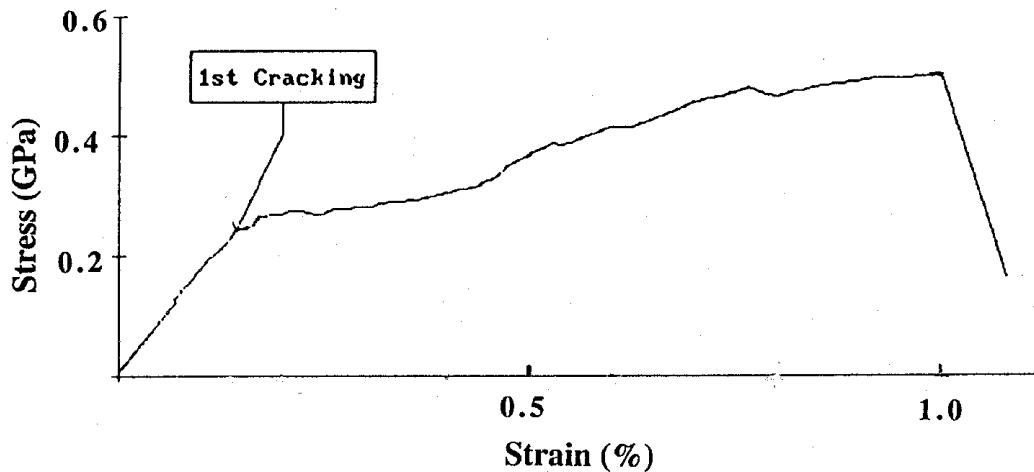


Fig. 11.23 Tensile stress-strain curve for SiC-Si₃N₄. (After Jablonski, D.A. and Bhatt, R.T., 1990, J. Comp. Tech. Res. 12, 139-46.)

In the work referenced under Fig. 11.22, $[\pm\phi]_s$ laminates were also tested, with $\phi = 10^\circ, 30^\circ, 45^\circ$ and 60° . Long narrow test coupons were used to ensure that in the central region the fibres did not go from grip to grip. Strengths could be fitted to Tsai-Hill, as is to be expected (see section 4.3.4). Remember however, that wider specimens, with polymer matrices at least, can give much higher results (section 4.4.3).

Composites which should come closest to achieving the full potential for strength and modulus are the reinforced glasses. This is because of the relatively low temperature needed for the process, and the relative fluidity of the glass. Fig. 11.24 shows an

example, with the "Rule of Mixtures" line extrapolating to 2.5GPa. This seems promising until it is remembered that these are flexural strengths, and hence could be seriously overestimating the tensile strength. With little true tensile data available we suspect that the full potential of the fibres are seldom achieved in the composite with respect to strength.

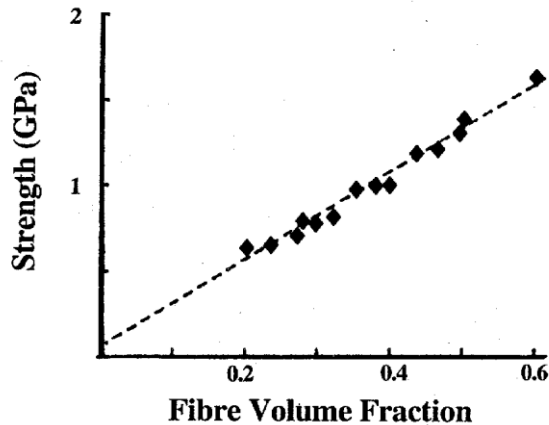


Fig. 11.24 Flexural strength of SiC-borosilicate glass vs V_f . (After Dawson, D.M., Preston, R.F., and Purser, A., 1987, Ceram. Eng. Sci. Proc. 8, 815-21.)

The same is true for composite modulus. Here, because full densification is not usually achieved, the matrix often does not contribute the expected $V_m E_m$. For example, it has been suggested that for Si_3N_4 the modulus of the matrix, when containing voids, is given by

$$E_{mv} = E_{m0} \exp(-3 V_v) \quad (11.42)$$

where E_{m0} is the void-free modulus of the matrix and V_v is the volume fraction of voids. Since it may be difficult to achieve $V_v < 0.25$, and since fibre volume fractions are generally small, < 0.4 , this can give $E_1 < E_{m0}$ unless $E_f \gg E_{m0}$.

Transverse strengths are often below those achieved in reinforced polymers. Strengths in the range 25-30MPa are commonplace with values as low as 4MPa being reported. Apparent shear strengths are often measured using the short beam test. These can be in the range 30-70MPa, again generally below these obtained with reinforced polymers.

11.7.2 Toughness

The main advantage of putting fibres into ceramics is the increase in toughness obtained thereby. Both brittle and ductile fibres can be effective, and the increase is usually very large, and greater for larger volume fractions of fibres. At low fibre volume fractions randomly oriented short ductile fibres (molybdenum and nickel) have the largest effects but for volume fractions near 0.5 aligned fibres have to be used, and brittle fibres at these concentrations can give increases in toughness of many thousand-fold over the unreinforced matrix value. Figure 11.25 illustrates some of the results obtained. Slow bend test values of 6kJm^{-2} can be obtained with reinforced ceramics. These results

should be compared with 40kJm^{-2} obtained with the same method with carbon-epoxy (Table 10.6), and the 3Jm^{-2} typical of unreinforced ceramics.

Some insight into the factors contributing to toughness in all-brittle systems can be obtained by examining the fracture surfaces and measuring fibre or whisker pull out lengths; see section 7.2.1. These indicate that weak fibre-matrix bonding is the dominant factor. However, exactly how weak to make the interface is not known, and moreover, such weakness reduces the performance of laminates such as [0,90] by promoting early cracking.

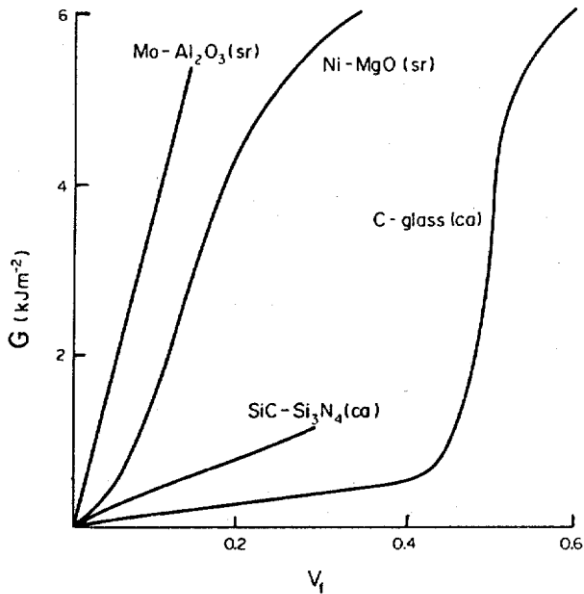


Fig. 11.25 Work of fracture of short random (sr) and continuous aligned (ca) fibre-ceramics. (After Donald, I.W., and McMillan, P.W., 1976, J. Mater. Sci., 11, 969-72.)

Very ductile fibres (e.g. Ni) are not used. Ideally they contribute a work of fracture, G_f^* , in proportion to the amount of fibre involved: see equation (7.8). In practice; they can reduce the strength rather drastically.

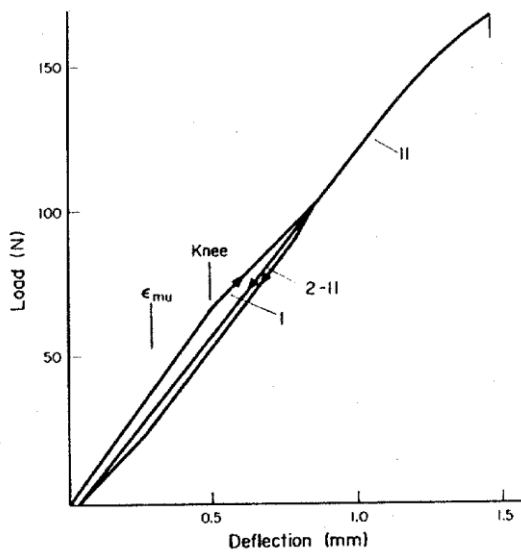


Fig. 11.26 Cyclic flexure of C-LAS. The labels on the curves indicate cycle numbers. (After Levitt, S.R., (1973), J. Mater. Sci. 8, 793-806.)

11.7.3 Fatigue, Creep and Temperature Endurance

There has been very little work on tensile fatigue: as with strength and modulus, fatigue testing is normally carried out in flexure. Unidirectional composites show hysteresis, Fig. 11.26, but little loss of strength due to this type of cyclic stressing at 20°C. Creep cracking accompanied by creep strain has been observed in flexure tests at 1100-1300°C with a commercial whisker reinforced SiC-Al₂O₃, with $V_f = 0.25$. (The whiskers increased the work of fracture from about 16Jm⁻² to about 160Jm⁻² and the flexural strength was approximately doubled to 0.64GPa. These properties were maintained up 1000°C). Fig. 11.27 shows surface strains vs time at 1100, 1200 and 1300°C. Whiskers generally reduce creep less than continuous fibres. The creep resistance of the fibres is also an important factor when the temperature is over 1000°C. The fibre creep properties, of course, depend on their melting temperature.

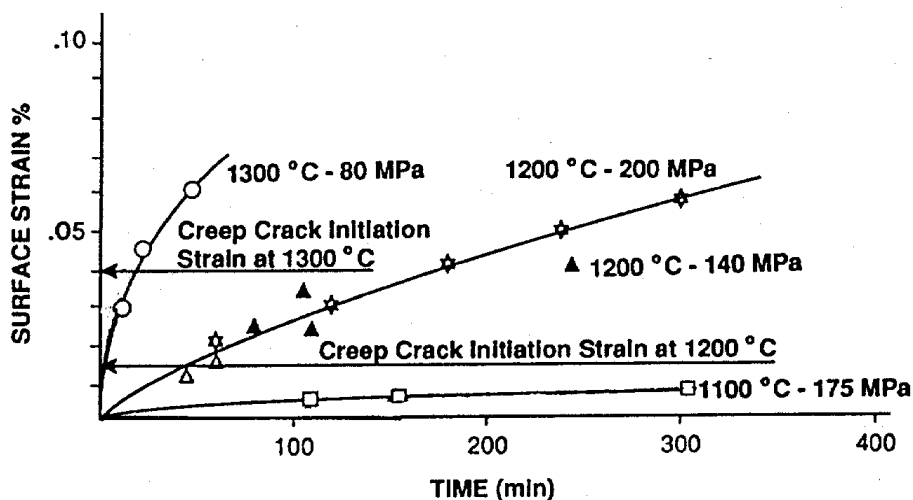


Fig. 11.27 Creep curves for a commercial SiC (whisker) - Al₂O₃ composite at high temperatures and various stress levels. (After Jakus, K., and Nair, S.V., 1990, *Comp. Sci. Tech.*, 37, 49-97 - Special Issue on Ceramic Matrix Composites.)

Heating at above 1100°C or more caused oxidation of the SiC fibres in the above composite: oxidation rates can increase an order of magnitude when these fibres are embedded in oxide matrices. This causes a severe decrease in strength. Fig. 11.28 shows some results obtained with the same fibres in LAS. At 900°C the flexural strength decreases by about 40% (it thereafter increases again). In argon the same loss occurs at about 1250°C.

The maximum temperature for the composite is often limited by oxidation or chemical interactions. Ceramic matrices are prone to developing microcracks (see section 11.6.1), and in the case of tungsten and molybdenum reinforced systems, microcracked specimens have their fibres rapidly oxidized above 700°C. Reinforced carbons, and carbon-ceramics, must be used in non-oxidizing atmospheres above about

400°C, but under the appropriate inert conditions carbon-carbon can be used up to at least 2000°C and carbon-LAS can be used at 1200°C in an inert atmosphere.

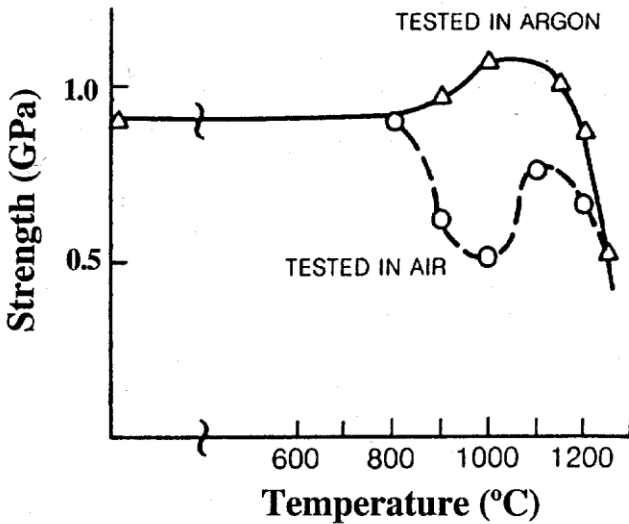


Fig. 11.28 Flexural strength of unidirectional SiC-LAS in air and argon at various temperatures. (After Prewo, K.M., Brenman, J.J., and Laydon, G.K., 1986, Am. Ceramic Soc. Bull., 65, 305-13.)

Table 11.6 gives some data for theoretical maximum temperatures based on melting or softening-points for a number of reinforced ceramics.

Another problem with the high-temperature application of reinforced ceramics is that thermal cycling can lead to destruction of the fibres or severe cracking of the matrix, or complete failure of the fibre-matrix bond. The magnitude of the effect depends on the mismatch of thermal expansion coefficients between fibres and matrix. The greater it is, the less thermal cycling the composite can withstand without severe loss of properties.

Table 11.6 Theoretical Maximum Temperatures for Some Reinforced Ceramics (Based on Melting or Softening-Points).

System	Maximum Temperature (°C)
Carbon-Pyrex glass	700-800
Carbon-glass ceramic	1300
Silicon carbide-silicon	1410
Silicon carbide-silicon nitride	1900
Carbon-carbon	3550

Note:

Carbon oxidizes in air above 400°C, and SiC oxidizes rapidly between 980 and 1150°C but is stable between 1150 and 1400°C.

11.8 Reinforced Cements and Plasters

Much effort has been devoted to producing useful and economic fibre reinforced cements and plasters. With cements (and mortar and concretes) there are two major problems.

1. Cement particles are often larger than the fibre diameter - they can be as great as 100 μm . So infiltration of fibre bundles can be a problem.

2. Cement is highly alkaline (pH as high as 13). This corrodes glass severely. Although special glass fibres have been developed (C glass) to resist corrosion, it is still not safe to use C glass fibre reinforced cement structures under significant tensile loads. (They are used, for example, for cladding of buildings, with design stresses of a few MPa) Moreover, it is not economically justifiable to reinforce cement with carbon or Kevlar or other high performance fibres, since these fibres are too expensive. So reinforced cements (and mortars and concretes) barely merit consideration as load bearing fibre composites. It should be noted, however, that fibrillated polypropylene is successfully used to increase the toughness and hence the strength of cementitious materials. Asbestos-cement has also proved to be moderately strong and durable. However, due to the toxicity of the asbestos this material is not longer widely used.

Plasters, such as plaster of paris (partly dehydrated gypsum - $\text{CaSO}_4 \cdot 1/2\text{H}_2\text{O}$) has also been reinforced with glass. However the material is seriously weakened by water, so has not proven to be useful for load bearing. Glass fibre reinforced gypsum board, reinforced with a few percent of short glass fibres, is sold as "water resistant" wall board. For a detailed discussion of these materials see section 11.2 in the First Edition.

Further Reading

Metals and Reinforced Metals

L.E. Samuels, (1988), *Metals Engineering; A. Technical Guide*, ASM Metals Park, OH.
 Clyne, T.W. and Withers, P.J., (1993), *An Introduction to Metal Matrix Composites*, (Cambridge University Press, Cambridge.)
 Taya, M. And Arseneault, R.J., (1989), *Metal Matrix Composites: Thermomechanical Behaviour*, (Pergamon Press, Oxford.)

Ceramics and Reinforced Ceramics

Musikant, S., (1991), *What Every Engineer Should Know About Ceramics*, (Marcel Dekker, New York.)
 Belitskus, D., (1993), *Fiber and Whisker Reinforced Ceramics for Structural Application*, (Marcel Dekker, New York.)
 Chawla, K.K., (1993), *Ceramic Matrix Composites*, (Chapman & Hall, London.)

Chapter 11: Problems

Unless advised otherwise, you are recommended to use the approximate expressions for thermal stresses and to assume that the matrix behaves elastically and that $T_1 = 20^\circ\text{C}$ and T_2 is the melting temperature of the matrix.

- 11.1 Compare the axial stress developed in HMS carbon reinforced Al-12% Si alloy and Nicalon silicon carbide reinforced pure aluminium. $V_f = 0.46$ in both cases.
- 11.2 Assuming that stresses start to develop when titanium cools through its transformation temperature, what would the fibre axial stress and matrix hoop stress be when reinforced with 53% SCS-6 fibres.
- 11.3 Estimate the stresses in the copper matrix for a composite with 53% of tungsten fibres.
- 11.4 Determine which carbon fibre in the following table would give (a) the smallest axial stress and (b) the smallest hoop stress in pure aluminium with a volume fraction of 50%.

Table 11.7 Thermal expansion and Other Properties of Some Carbon Fibres

Fibre	Diameter (μm)	Modulus ¹ (GPa)	Strength (GPa)	Density	Poissons Ratio	CTE (MK^{-1}) Axial	CTE (MK^{-1}) Radial
P100	11	700	2.20	2.15	-	-1.4 ²	9.7
3K100	9	520	2.50	2.12	-	-4.1	9.0
P75	10	517	2.07	2.07	-	9.0	12.9
3K75	10	400	2.20	2.12	-	7.4	9.7
P55S	10	379	1.90	2.00	0.10	0.9 ³	11.0
T300	7	230	3.50	1.78	0.22 ⁴	4.5	6.8

Notes: 1) Young's modulus, 2) taken from prior literature, 3) measured over the range 25-600°C, the others over the range 25-800°C and 4) prior literature gives 0.24 - 0.35.

Data from Villeneuve, J.A., Naslain, R., Formeaux, R. And Sevely, J., (1993), *Comp.Sci. Tech.* **49**, 89-103.

- 11.5 If the shear yield stress of an aluminium alloy matrix which melts at 643°C decreased linearly from 80 MPa at 20°C to 20 MPa at 620°C, at about what temperature would the matrix start to yield when reinforced by 50% of boron fibres. For the purpose of the calculation assume that the axial stress can be

- ignored, and use the Tresca yield criterion. (Hint: check your solutions to questions 1.13-15.
- 11.6 If the exact equations are used instead the approximate ones, what difference does this make to the maximum shear stress and the temperature at which yielding takes place in the above question.
 - 11.7 Using equations from Chapter 10, estimate the radius of curvature of a 0.42 mm thick [0/90] Si₃N₄-Al laminate with $V_f = 0.51$ after cooling to room temperature. Assume that, when not bonded together, the axial thermal contractions of each lamina are negligible and the transverse contractions are the same as the matrix shrinkage. Explain why the result is unrealistic.
 - 11.8 If the boron fibres broke into short lengths during manufacture of the reinforced aluminium, calculate the fibre length based on the modulus result given in Table 11.1. Then estimate the mean interfacial shear stress to give the strength result. Assume $V_f = 0.5$.
 - 11.9 Do the same calculation as in the above question for boron-titanium.
 - 11.10 Does the square fibre model give a better estimate for the result shown in Fig. 11.8 than IROM?
 - 11.11 What type of SiC fibres were used to give the results shown in Fig. 11.9, and what was the apparent volume fraction?
 - 11.12 The actual fibre volume fraction of the composite shown in Figs. 11.9 and 11.10 was 0.44. Compare the theoretical transverse modulus using the square model with the actual modulus.
 - 11.13 Estimate the volume fraction of tungsten from the 25°C stress-strain curve in Fig. 11.11. Hence estimate the average depth of notches developed in the fibres during the processing to account for the observed strength. The nickel had a strength of 507 MPa.
 - 11.14 Using the work of fracture given in Table 11.3, estimate the matrix strain in the worked zone at the crack faces for boron reinforced aluminium alloy. Assume that neither the fibres nor the interface contribute to the work of fracture, and do the calculation for the through thickness fracture.
 - 11.15 Do as for question 11.14 above for the work of delamination.
 - 11.16 What depth of surface roughness is required for Nextel 312 alumina fibres to be effective in reinforcing glass-ceramic.

- 11.17 Estimate the void content of the composite giving the result shown in Fig. 11.23. CVD silicon carbide fibres were used.

Chapter 11: Selected Answers

- 11.1 Carbon, 0.98 GPa; SiC, 0.57 MPa.
- 11.3 1.9 GPa
- 11.5 620°C
- 11.7 19 mm: not reasonable because yield strain ~ 0.1%
- 11.9 3.9 mm; 370 MPa
- 11.11 SCS6; 0.34
- 11.13 0.47; 1.04 μm
- 11.15 0.80
- 11.17 0.56

12 APPLICATIONS

Reinforced polymers have been available to mankind since time immemorial, in the form of wood. This can have excellent mechanical properties (see Table 1.3) and a fighter aircraft, made with wood, the Mosquito, performed well during the Second World War. Wood, however, is biodegradable, and the advent of synthetic fibre composites in the early 1940's opened up innumerable new possibilities. The use of glass-polyester for aircraft radomes, was the starting point here and glass fibre reinforced polymer was used successfully to make a small aeroplane in the 1940's. The small aeroplane use has continued, see Fig. 12.1, but the adoption of reinforced plastics was relatively limited to start with. Sports equipment, such as fishing rods, sailplanes and sailing dinghys, were early candidates, and wood was phased out quite quickly for sailplanes and small boats because glass-polyester ones performed better and were more durable.



Fig. 12.1 Fibreglass aeroplane (1970's). (Courtesy of Windeker.)

New fibres with much higher modulus, such as the carbons and polyaramids, created further possibilities. Light materials which have better load carrying capacity than aluminium became available, so military aircraft started to make extensive use of reinforced plastics and they started to capture many new markets. Today we see a wide diversity of uses which are classified herein according to the industries that use them.

Reinforced metals have not been successful. Their properties are disappointing, and rarely worth the high cost of manufacturing them.

Reinforced ceramics have not been successful for load bearing either. (They are used in cutting tools). Moreover (see section 11.6.1) we have little knowledge of their mechanical properties, since tensile testing them, using end tabs, is rare, and the customary flexural testing seriously overestimates tensile strengths.

Reinforced cements do not qualify as load bearing materials in this context: design stresses are two orders of magnitude smaller than for reinforced polymers. (There has recently been a suggestion, though, that fibres made from basalt might be sufficiently corrosion resistant to make long term reinforcement of concrete possible, so that they could safely support significant tensile stresses.)

So we will concentrate on reinforced polymers here, giving particular attention to applications that illustrate some of the unique properties of these materials. We start with aerospace, since the benefits here are self-evident.

12.1 Aerospace Structures

Initial use of reinforced polymers on commercial mid-sized aircraft followed the principle that failure must not risk loss of life. So fairings (which merely smooth the air flow) were among the first uses. Leading edges for the wings of small aircraft are also good places for composites, and de Havilland's Dash 8, Fig. 12.2, used woven Kevlar-epoxy for those, after exhaustive tests to ensure that they stood up well to bird strikes (tested using canned birds).

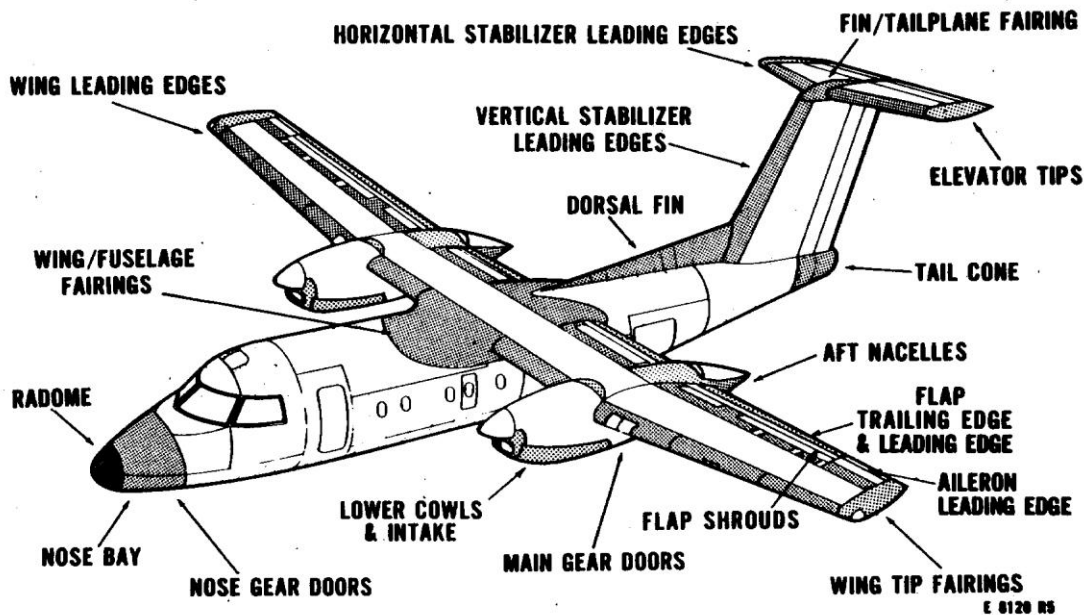


Fig. 12.2 Dash 8 reinforced plastic structures. (Courtesy of Bombardier Aerospace.)

Floors of large aircraft are made with carbon-phenolic sandwiches with polymer honeycomb between the faces. These are routinely tested for resistance to damage caused by rolling trolleys. The matrix polymer used inside the aircraft is one which produces minimal toxic fumes when on fire. Most of the other internal structures (inner walls, toilet cubicles, etc) are also made of reinforced plastics. But seat supports are still made with metal.

Nowadays some specialized small aircraft have carbon-epoxy throughout their structures: a good example is the Voyager, which made a non-stop flight round the world. Meanwhile, carbon reinforced plastics are just starting to be used for the stressed members of large civilian aircraft. Almost 20% of the dry weight of the Airbus 340 comprises composites. Load bearing members include the keel beam made from carbon-epoxy, the vertical stabilizer, ailerons, spoilers, vanes and flaps from carbon, glass- and aramid-epoxies, and the rudder and horizontal stabilizer from carbon- and glass-epoxies; see Fig. 12.3. The Boeing 777 vertical stabilizer is made from carbon-epoxy. As experience is gained, more will follow.

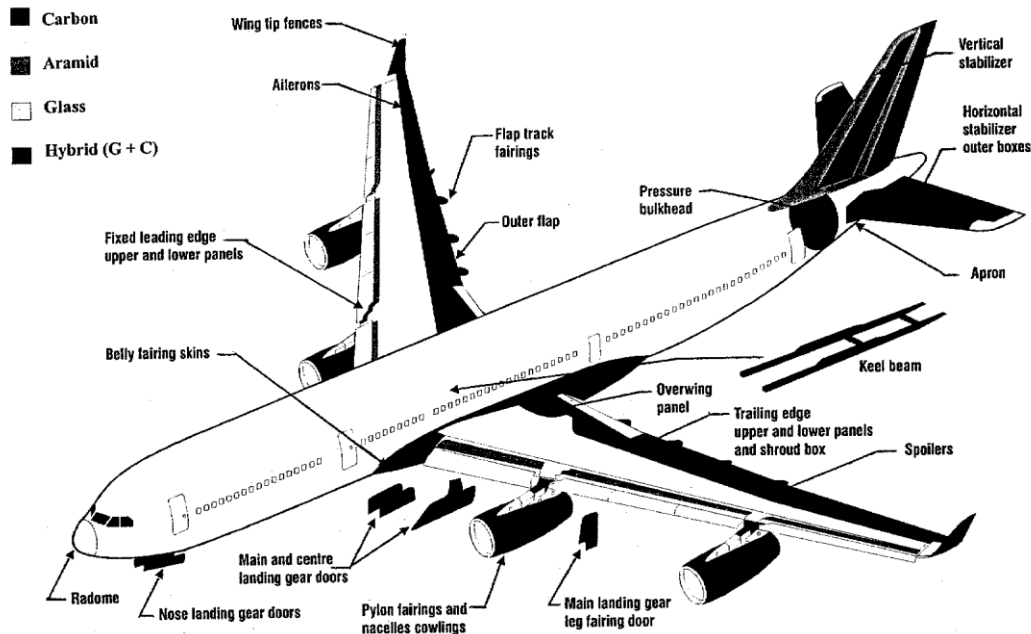


Fig. 12.3 Composite components on the Airbus A320. (Courtesy of Hexcel Composites.)

Aeroplane engines have also been made lighter and better with reinforced plastics; the Rolls Royce RB108 had glass fibre reinforced compressor rotor blades and casings in the 1950's. Nowadays these parts are made with carbon-epoxies, and for the parts experiencing higher temperatures carbon-polyimides are used. Reinforced plastics now comprise nearly one half the materials used in these engines.

Aircraft brake pads are made from carbon-carbons. These experience high compressive and shear loads, so require adequate strength to sustain the resolved tensile stresses.

Helicopters are now almost wholly made from reinforced polymers. Not only is the weight much reduced, but the use of reinforced plastics for the rotor blade and for the rotor head simplifies design, (see Fig. 12.4), and endows these parts with much longer lives as compared with metals.

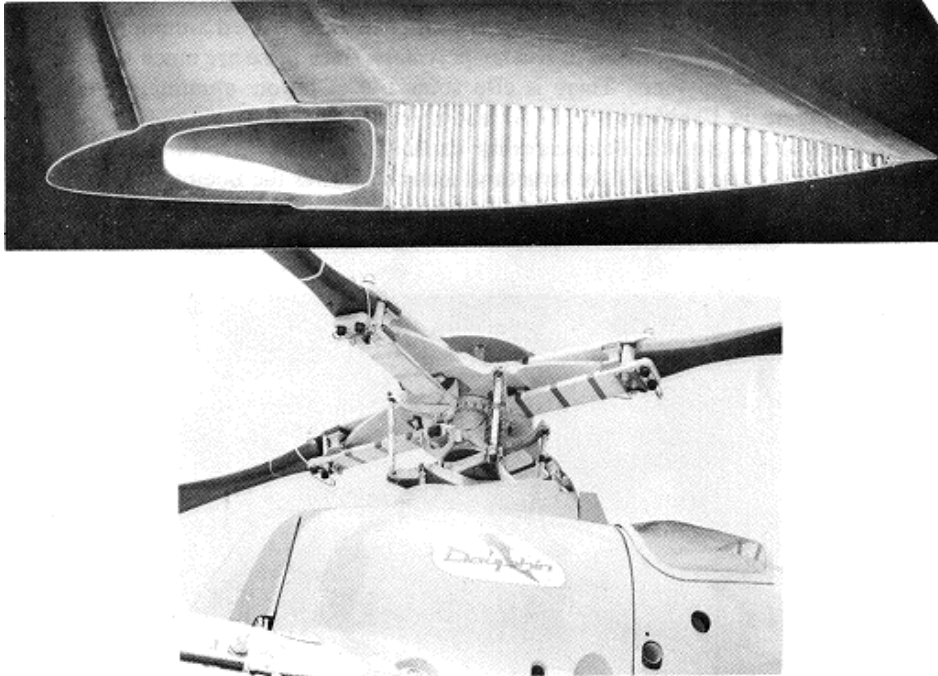


Fig. 12.4 Reinforced polymer helicopter driving parts (a) section of the rotor blade molding. (Courtesy of Westland Helicopter Ltd.,) and (b) Rotor head. (Courtesy of Societe Nationale Industrielle Aerospatiale,; note that the design has been simplified and improved since this picture.)

In space applications composites play a major role. Rockets are filament wound carbon-epoxies, or -polyimides for higher temperatures. Rocket motors too are made from carbon-epoxy: for the space shuttle, replacement of the metal reduced the motor weight by about 35% and used nearly 20 tonnes of the composite for each motor.

The low CTE of the carbon fibre is a special bonus in some space applications. Thus the use of carbon-epoxy for the structure of the Hubble space telescope gives it greatly improved thermal stability compared with other candidate materials.

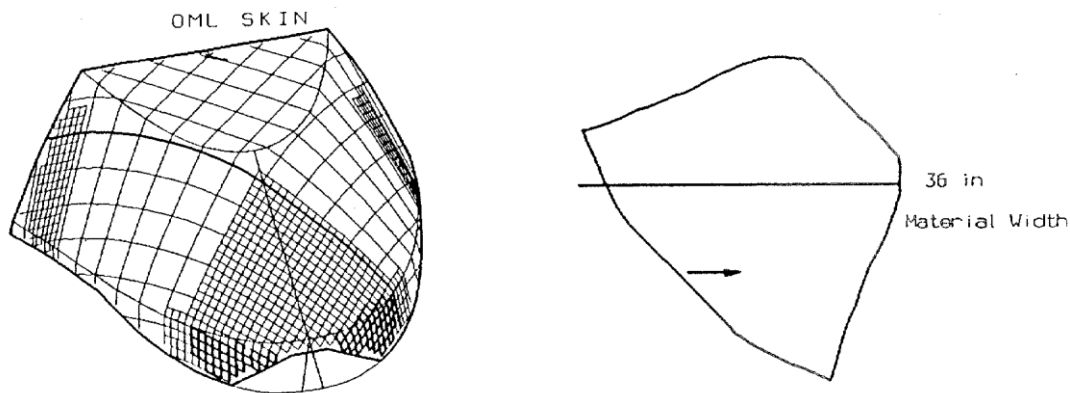


Fig. 12.5 Computer generation of a laminate surface at left, with problem areas highlighted. On the right is the resultant 2D flat pattern showing that at this stage of the design the 0.91m material width is exceeded. (Courtesy of Composite Design Technologies Inc.)

The aerospace industry has been the driving force behind numerous innovations in production techniques. For example, the design is now automated, and the software e.g. FiberSIM™ can simulate structures on the computer screen as illustrated in Fig. 12.5. This shows, at the left, how a composite material conforms over complex curvatures. The more dense grid highlights areas of moderate distortion. Here there may be some difficulty in laying up the material due to fibre orientation distortion. The more solid lines within the denser grid (near the bottom, at the front) alerts engineers to a section that cannot be manufactured as designed without causing wrinkling. At the right is shown the 2D flat pattern that Fiber SIM generates from the design. This warns the engineer that the maximum material width (36 inches, i.e. 0.91 m) has been exceeded. This information provides engineers with feedback in the early stages of design, so that they can make changes to avoid these problems.

When the design is finalized, a digitally controlled flat bed cutting machine is instructed to cut the prepreg in the most economical way, see Fig. 12.6. Another digitally controlled machine mills the honeycomb. At the lay up stage another piece of software controls a laser which outlines where each piece of prepreg is to be laid on the mould, and checks whether the positioning (done by hand) is accurate enough; see Fig. 12.7. Thus most human error is removed, and production is greatly speeded up.

The idea, much extolled in books and articles on the benefits of composites, that you can design your material, has made some headway in aerospace, an industry which has an outstanding need for using it. Designs take into account whether glass, carbon, or aramid or combinations thereof is best. Also the choice of matrix (epoxy, polyester, polyimide etc.) is a major consideration. Missing however, is much choice of fibre orientation.

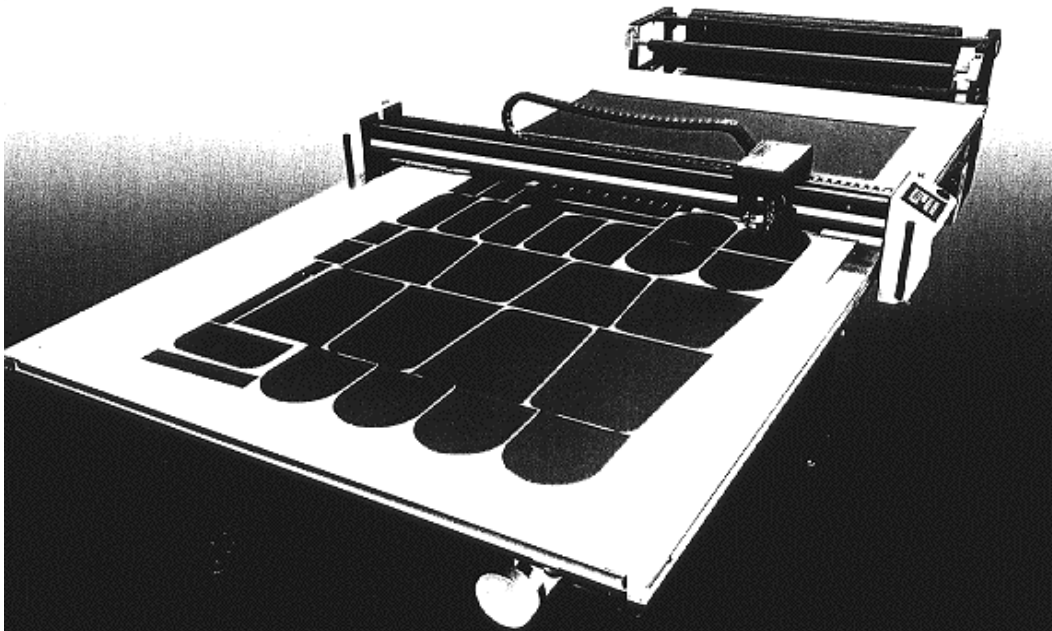


Fig. 12.6 Digital table has cutting accuracy within about $50 \mu\text{m}$ and cuts at speeds up to 1.1ms^{-1} . Can cut up to 32m long and 4.3 m wide. (Courtesy of Gerber Technology.)

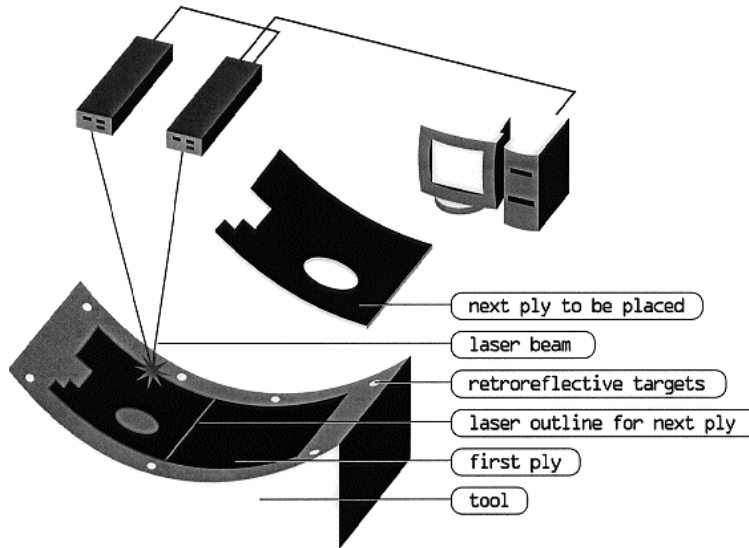


Fig. 12.7 Laser frame for positioning prepreg on mold. (Courtesy of Virtek.)

In practice, aircraft structures almost universally use 0° , 90° , $\pm 45^\circ$ arrangements in their laminates. This applies even to military aircraft. For example, a fighter aircraft used in Canada has, in one part of the wing, 28 0° plies, 6 90° plies and 34 pairs of $+45^\circ$ and -45° plies. Other parts of the wing are constructed in a similar fashion. The stated reasons are as follows:

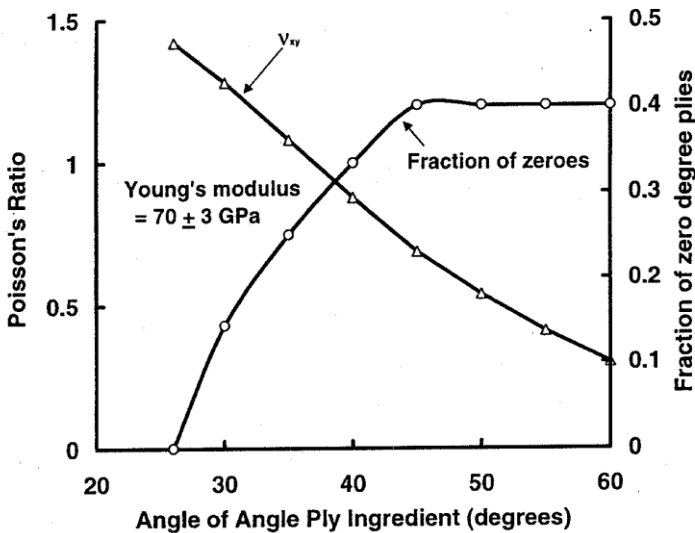


Fig. 12.8 Poisson's ratios for angle ply laminates with E_x kept approximately constant at about 70 GPa. Proportion of zero degree layers is also shown. (After Piggott, M.R., 2000, *Polymer Composites*, 21, 506-13.)

1. Load paths are variable, and not always as expected; hence the four chosen orientations ensure safety.
2. Data on such things as bearing capacity (at joints etc) are not available.
3. There is more material waste when cutting at other angles.

This might be termed the "light aluminium" approach. However, other orientations could be used with advantage. Fig. 12.8 shows how one might develop a design using angle ply arrangements together with axial fibre layers. The modulus aimed

for was 70 GPa, i.e. about the same as aluminium, and medium modulus carbon fibres were chosen for their relatively low cost. A concern to designers is that Poisson's ratio should not be excessive. If we take 0.9 as our maximum design ν_{xy} , we achieve this with $[0_2 \pm 40_3]_s$, according to Fig. 12.9. This avoids using 90° plies which tend to initiate early cracking.

Moreover, designing for some particular stiffness also takes care of the strength. If we have our main laminate direction, x , aligned with the principal stress, then as Fig. 12.9 shows, the ratio of stresses and stiffnesses are close to each other for $[\pm\phi]_{ns}$ angle ply laminates with ϕ between 15 and 45° .

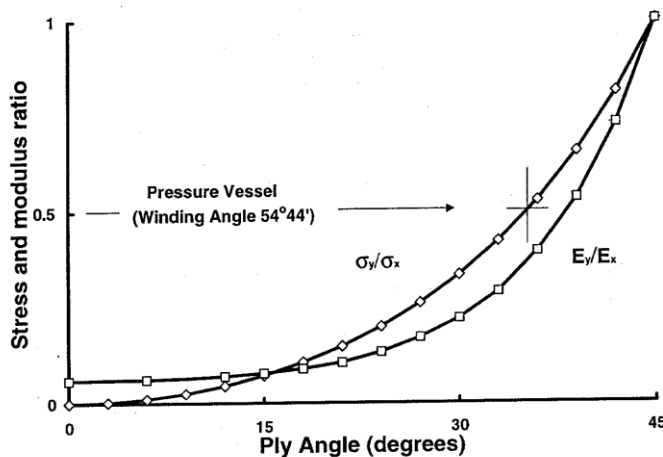


Fig. 12.9 Stress ratio and modulus ratio for balanced angle ply laminates.

It should also be remembered that pressure tests on $[\pm\phi]_n$ tubes show superior performance under biaxial stresses rather than uniaxial hoop stresses. Elimination of the crack-prone 90° layers could reduce the weight of this part of the structure by as much as 22%.

No doubt future designs will involve other angles, once fibre placement (section 9.4.4) becomes more commonplace. With this method there is very little waste. Also there is no reason why bearing capacities cannot be evaluated for angle ply laminates, and no a priori reason to expect them to be poor.

12.2 Marine Structures

Glass reinforced polymers are well established in the boat-building industry, having been used since the late 1940's. Their characteristics of light weight and high strength, design flexibility, and low thermal conductivity are very advantageous in this application. The monolithic seamless construction minimizes assembly problems and leakage, while maintenance and repair costs are reduced. The most important advantage is their excellent resistance to the marine environment.

Polyester resins are most commonly used for the matrix, being cheaper and easier to handle than epoxy resins. With glass-polyester laminates the loss in strength due to water in moderate climates is some 10-15%, increasing to a maximum of 20% in warm

climates. The strength loss occurs during the first two months, and is due to the water penetrating the resin and acting as a plasticizer. If the fibres do not have the appropriate sizing the water is absorbed on the glass, greatly weakening the fibre-matrix interface and causing a large reduction in strength. Improperly finished or under-cured resins, or laminates with excessive voids, are also more susceptible to water degradation. Thus care is needed when fibreglass is used for construction.



Fig. 12.10 Glass-polyethylene thermoformed canoe. (Courtesy of Fiberglas Canada, now Owens Corning.)

There is an increasing tendency to use epoxy resins. They have better resistance to moisture and weathering. Also, they are practically odorless when being molded, not having the troublesome styrene emission which accompanies the use of polyesters. Moreover, prepregs can be used, taking the chemistry out of the production process.

The glass employed is usually E-glass. The form of reinforcement used is random mats, spray-up, or woven cloths, according to the type of boat. The smallest boats are also made by moulding short glass fibre reinforced thermoplastics. Fig. 12.10 shows a canoe made in this way; several years of hard use in the Canadian north have proved it to be leak proof and almost dent proof. For ease of portaging, though, the best canoes are ones made with Kevlar-epoxy.

A very large fraction of small boats are now made from fibreglass, and $\pm 60^\circ$ weave has advantages for certain boat shapes. Such fabrics are available (e.g. Ahlstron Glass Fibre Oy) and can reduce weight by perhaps as much as 10% compared with the normal 0/90 weaves.

The use of fibreglass is being extended to ever larger boats using sandwich construction. A notable example is a 47 m minesweeper. Although costing more than

steel, its advantages (being non-magnetic and more corrosion resistant) were worth the extra expense.

For boat sizes larger than 50m the use of fibreglass is presently uneconomic. These are made with steel hulls. Here, improved performance is obtained by using fibre composites for decking and internal structures. As with aircraft, phenolics are used as matrix in internal structures.

Kevlar and carbon are having a big effect on high performance boat construction. The light weight and extra stiffness are the main advantages here. Kevlar is mainly used in hybrids with glass or carbon because it is otherwise prone to failure by buckling, due to its weakness in compression. Boats, such as those used for the America's Cup (see Fig. 12.11) use a lot of carbon epoxy for the hull, mast and other structures.

Reinforced plastics are starting to replace wood for shore structures such as piers and jetties. Again the reason is their superior durability.



Fig. 12.11 America's Cup boat. (Courtesy of Hexcel.)

12.3 Ground Transport

The major potential user is the private car, but this is still mostly made of steel at present because of the speed of manufacture and low cost. Specialty cars use more glass reinforced plastic - for doors, hoods, trunk lids, engine compartments etc. Sheet molding

compounds are much used for this market. Sports cars have fibreglass bodies, but there is little use of higher performance fibres such as carbons or aramid. Government sponsored efforts in North America to reduce car weights have been side stepped by people buying vans and sport utility vehicles (SUV's), but the low volume car market thrives because of the use of reinforced plastics.

Racing cars are nowadays made of carbon-epoxy. Fig. 12.12 shows the internal structure of such a car.



Fig. 12.12 Internal structure of a racing car. (Courtesy of Hexcel.)

Trucks make much use of reinforced plastics, but mainly for non load bearing parts. An important innovation here though is the fibreglass leaf spring. This is much lighter than the steel counterpart, has excellent fatigue resistance and fails in a safe, splitting mode, rather than fracturing across the thickness. A carbon-epoxy leaf spring has also been tested. This is so light that a spring for a lorry (or truck) can be replaced quite easily, since it weighs only about 7.4 kg instead of the 60 kg for a steel one. The fibreglass spring is widely used in some European cars.

Other commercial vehicles such as buses and street cars are similarly being made using larger amounts of fibreglass.

Freight containers are also being made from reinforced polymers rather than metals. Although the composite is initially more expensive than steel or aluminium, it has proved to be more durable, and hence cheaper in the long run. Glass-polyester foam sandwiches are particularly favoured for air freight, where their light weight is a great advantage. Chassis-less tanker trucks have evolved through the use of reinforced plastics.

Weight saving has driven the use of composite materials for external and internal structures in railway engines and railway coaches. These include floor panels, and internal stiffening arches, for example on the German Regio Swinger high speed trains which tilt when cornering: see Fig. 12.13. These also incorporate carbon- and glass-epoxy for leaf springs and bogie structures. Box cars make extensive use of reinforced plastics too.



Fig. 12.13 High speed tilting train uses reinforced plastics for bogies (driving wheel assemblies) and leaf springs as well as floors and side panels. (Courtesy of Adtranz.)

Weight saving is also important in some military equipment. Tanks which can be carried in planes have hulls made with glass reinforced polymer.

In all transport applications, aeroplanes included, a major advantage is the ease with which aerodynamic shapes can be produced. Moreover, the molding process makes possible excellent finish which also reduces air drag.



Fig. 12.14 Modern windmills generating electricity in a wind farm in Germany. (Courtesy of Vestas Wind Systems.)

12.4 Energy and Storage

Aeroplane engines using reinforced plastic compressor blades have already been mentioned in Section 12.1. Another important area in energy conversion is windmills for electricity generation. Wind power is the world's fastest growing energy source, using wind driven turbines up to 66m in diameter and delivering 1.65MW of power, see Fig. 12.14. The preferred structure for the blades is woven glass-epoxy faced honeycomb. In both engines and windmills, the correct aerodynamic shape is crucial for efficiency, and the smooth finish produced by the molding process is a major benefit.

Gases used as fuel require pressure resisting storage tanks. These are biaxially stressed in the ratio 2:1 so are commonly filament wound with a winding angle (relative to the tube axis) of 54.73° ; see Fig. 12.9. In the energy industry they are used for storage of natural gas, and when used to fuel buses and trucks, carbon fibres are used to reduce the dead weight. Moreover, pressure containers that permit more efficient packing are being developed, see Fig. 12.15.



Fig. 12.15 Natural gas pressure storage tank designed for efficient use of space. (Courtesy of Thiokol Propulsion, a Division of Cordent Technologies.)

Oil production and storage uses filament wound reinforced plastics. Of particular interest here is the off shore oil rig. The risers which carry oil from the sea bed need to be corrosion and fatigue resistant. Much effort is going into the development of filament wound carbon-epoxy tubes to replace steel. They do not sag as much and hence lose rigidity. So when also used as tethers they are more economical.

Electric transmission lines make much use of filament wound fibreglass poles, and insulators are also made with fibreglass. Apart from very much reduced weight, the insulator is resistant to vandalism and rifle fire, which is a major problem in the insulator industry.

Air and oxygen storage for firefighters and divers etc. require lightweight tanks which are impervious to the gas. These are often made by filament winding carbon or Kevlar onto aluminium and sometimes stainless steel liners.

12.5 Pipelines and Chemical Plant

Fibre-reinforced plastics are ideally suited to many situations where fluids have to be handled. They are very corrosion resistant, and may be used for gaseous bromine, chlorine, and carbon monoxide, and when carbon is used, for concentrated or dilute acids and alkalis. They can match the properties of Hastelloy C, and perform better than stainless steels in many cases. They are, however, limited by relatively low operating temperatures, and their susceptibility to attack by some organic liquids.

Being lighter than metals, composite structures are much easier to transport to the site, and install. They usually require less maintenance than metals, since they do not have to be checked so frequently for corrosive damage, and in some instances their low thermal conductivity reduces the amount of insulation required.

Pressure vessels and pipes made from reinforced polymers must be lined, otherwise they can start to leak at stresses which are very much less than the ultimate tensile strength of the composite. This liner can be metal (suitable for the handling of organic fluids) or polymer (generally used for inorganic fluids). They are usually made by filament winding, and chemical plants make a great deal of use of reinforced plastic pipes. Moreover, the supporting structure for the pipe system is often made with glass reinforced plastic.



Fig. 12.16 Mixing and holding tanks and associated pipework made with glass - vinyl ester.
(Courtesy of Nemato Composites Inc.)

The materials must be as fireproof as possible. Glass reinforced plastics are more fire-resistant than the plastic matrix on its own because the glass will not burn. If greater fire retardancy is required than that contributed by the glass, fire retardants such as halogenated polymers or antimony trioxide are added to the resin. Fig. 12.16 shows mixing and holding tanks. These were made with glass-vinyl ester. The inside surface uses random glass "veil" which has only 10% fibre with the rest polymer. The next layers are woven glass with 27% fibres and finally the load bearing layers on the outside are filament wound with 55-75% glass fibres.

Carbon fibres, because of their high cost, are only used in chemical plants where their superior corrosion resistance or excellent specific properties are worth the extra cost, for example in industrial centrifuges. Their electrical conductivity may also be used in applications where a vessel requires electric heat; the heating can be produced by passing an electric current through the fibres. Probably the largest use of reinforced plastics, however, is for storage vessels, where loading is relatively small.

12.6 Infrastructure

Significant load bearing use of reinforced plastics in roads and bridges etc. is a recent development. Here again, wood was the first comer, but steel and concrete are the norm. Bridging the Straits of Gibraltar cannot be done with traditional materials, but might be possible using carbon fibre suspension and light weight composite decking. But as the recent reinforced plastic footbridge across the Thames in London has shown once again, load carrying capacity is only one of many factors in the design of high aspect ratio lightweight bridges. They are prone to suffer from vibrations caused by wind and traffic movement which create instability. Nevertheless, pedestrian bridges made of glass-polyester are now quite commonplace. Mobile assault bridges to be carried on tanks have been made with carbon-epoxy. For as little as 5t weight, they can have a span of 15m.



Fig. 12.17 Bridging muddy run creek in Glasgow, DE, using glass reinforced vinyl ester. Parapets are the original concrete, refurbished. (Courtesy of University of Delaware.)

The role of reinforced plastics in bridges for heavy vehicle use has been for repair and protection: "retrofitting". For example, carbon-epoxy reinforcing rods have been

used to reinforce concrete bridge decks on motorway bridges. Steel was replaced because it was seriously weakened by corrosion. (Although the alkaline environment of the concrete was expected to protect the steel, the salt we use to disperse ice and snow on our roads seeps into the material and, with accompanying water and air, starts the corrosion process. Since the iron oxides occupy more space than the steel, the concrete cracks very severely, and breaks away allowing faster water ingress.) Glass fibres are not used directly in concrete since they are weakened also. However, glass-epoxy bars have been used successfully as dowels holding concrete paving slabs together. They have proven to be much more durable than steel used hitherto. Moreover glass-vinyl ester sandwich structures with honeycomb, or other expanded cores, are being used for bridge decks. A program of bridge replacement, starting with relatively small bridges such as shown in Fig. 12.17, has recently been initiated.



Fig. 12.18 Applying glass-epoxy to a column on a bridge on Interstate 80. (Courtesy of R.J. Watson Inc.)

Glass-Kevlar-epoxy I beams have been used to replace steel on highway bridges. The design must take account of the low shear modulus of the composite. This retrofitting has become a major business in the USA now that the Interstates are more than 30 years old.

In addition to bridge decks, the bridge supports are repaired. Carbon-epoxy is sometimes used. Special methods and machines have been developed in order to produce high quality support for columns etc. Woven fibre sheets are impregnated with resins, wound around the column and then cured; see Fig. 12.18. Another important use is repair after, and protection against future seismic damage. This is presently an important activity in Japan and California.

Old water mains are also repaired using fibreglass.

12.7 Medical Applications

The economics of the medical use of materials is quite different from that of most other applications. The major costs in medicine are the facilities: hospital, equipment,

etc. And the labour: surgeons, anaesthetists, and other highly paid specialists, together with nurses and support staff. The amount of material in a medical application is usually quite small, less than 1 kg, so the cost of even the most expensive materials is usually insignificant compared with the other costs. In addition, there is the time and suffering of the individual requiring the device, and expensive composites can often assist speedy recovery.



Fig. 12.19 Internal structure of lower limbs. Carbon-epoxy is the main component. (Courtesy Flexfoot.)

A new material cannot be accepted immediately for medical use. A device designed for internal (prosthetic) use has to be checked for unfavourable reactions, both short-term and long-term. The same is true for external (orthotic) devices, though the requirements are generally much less stringent.

Fibreglass is rapidly supplanting wood, leather, and steel for braces (or calipers) for arms and legs. The braces are stronger, lighter, more comfortable, and less noticeable. No straps are needed, and improved cuffs, having air holes, and padded with washable foam, can easily be produced.

Fibreglass is also used for artificial legs and arms. However, the advent of carbon has fostered significant design improvements. Fig. 12.19 shows the internal structure of lower limb replacements. This includes a shock absorber (non-composite) at the top, with below it, the main load support made from carbon-epoxy. The curve in it stores energy which can be released appropriately to reduce walking effort. The curved carbon-epoxy side spring adds to the stored energy. The foot itself, also carbon-epoxy, is attached using an elastomer, and restores a spring into patient's step.

An important advantage for reinforced polymers is their easy mouldability, in view of the wide range of shapes and sizes required. The outer casings of the prostheses are made from plaster moulds of the parts, using woven reinforcement with open, easily shaped weaves. These prostheses can very easily be made to mimic the appearance of human limbs. Carbon may also be used here because it imparts higher stiffness.



Fig. 12.20 Carbon-epoxy support for x-ray therapy. (After Lyons, B.R., and Molyneux, M., 1978, Proc. ICCM2, 1474-92. (Courtesy of the Metallurgical Soc. AIME.)

The combination of excellent mechanical properties and the very low X-ray absorption characteristics of carbon fibres is providing a unique opportunity for the development of better X-ray analysis and treatment devices. The angiographic technique (which involves the injection of a radio opaque fluid into the bloodstream, for the location of growths and foreign bodies) needs X-ray pictures to be taken in quick succession (up to six per second). The film has to be placed and moved on very quickly, but held precisely. The key to doing this has been the development of carbon-epoxy compression plates. These can be very precisely moulded from prepreg tape, and the plate combines excellent fatigue properties with low X-ray absorption and good elastic properties.

The computed tomography X-ray body scanning technique is used to provide a three-dimensional view of the body. This requires a support which provides great rigidity, so that a person lying on it does not deflect it significantly, and at the same time it must have low and consistent X-ray absorption for radiation passing in any direction in a plane. A carbon-epoxy foam sandwich structure has been developed for this which is highly successful, allowing X-ray resolutions that were not previously attainable. A less exacting requirement is for therapeutic X-ray table tops. These are also made with carbon-epoxy foam sandwiches, and one is shown in Fig. 12.20.

In these X-ray applications, no other material has been found which comes anywhere near the excellence of carbon-polymers.

12.8 Sports Equipment

As in the case of medical applications, materials cost is not always a major factor in sports. Boron-epoxy has been used for special golf clubs, for example, and carbon-epoxy has become commonplace in racquets for tennis, badminton, squash, etc. In fact, the advent of better materials has had a profound effect on the sports themselves. In men's tennis championships nearly all is decided on 45 ms^{-1} (100 mph) serves, thanks to the efficiency with which modern carbon-epoxy racquets can transfer energy from the arm to the ball. Pole vaulters now reach heights about 25% greater than previously attained thanks to the use of glass-epoxy poles. The key here is the glass fibres, which with a strength of 2 GPa or so, and a breaking strain of nearly 3%, can store large amounts of energy in small volumes with low weights.

Light weight is very important for many sporting applications. Modern racing bicycles are made with carbon-epoxy for this reason, and so are modern racing cars and sculling shells. Also important is the air drag, and using reinforced plastics gives the necessary smooth surface and aerodynamic design. This is supremely important in bobsleds, Fig. 12.21. Moreover, using a tough resin makes the sled more durable, so that it can withstand the bumps and the "monocoque" construction (effectively a single piece enclosure, without internal protrusions) provide better protection for the riders.



Fig. 12.21 Bobsled. Aerodynamic design and surface smoothness are overriding considerations which dictate the use of fibre reinforced polymers. Manufacturers claim a 40% reduction in drag compared with metal. (Courtesy of Dow Chemical.)

Fibreglass is still the most widely used composite. Skis usually contain fibreglass, and so do ski poles, bows for archery, gun stocks and butts, hockey sticks, and helmets and face masks. These applications all represent advances over traditional materials due to better durability and improved specific mechanical properties. Again, for the highest performance, carbon is used, and Fig. 12.22 shows some examples.

12.9 Other Uses

Fibreglass and other reinforced polymers seem destined eventually to take over nearly all uses of metal which do not require the unique properties of the more useful metals, i.e. ductility, hardness, high-temperature resistance, and conductivity. Unreinforced plastics have already supplanted metals in many applications where the low modulus and strength of the polymer are not a disadvantage. (A good reason for the use of polymers in our increasingly energy-conscious era is the low energy required to produce and process them, as compared with ferrous alloys and aluminium, the two most commonly used metals.) Now that reinforced polymers of good quality can be produced reliably and cheaply, these can be expected to take over in areas where moderate to high modulus and strength are required. In addition, the unique properties of some composites (for example the negligible thermal expansion of carbon reinforced polymers) can sometimes increase their advantages over metals at moderate temperatures.



Fig. 12.22 Carbon-epoxy sports equipment. (Courtesy of Hexcel.)

Glass fibre reinforced plastics are widely used in agriculture, home appliances, business machines, electrical and electronic hardware, and in materials handling, as well as in the areas already described in more detail above. Fig. 12.23 shows a chair in which braided sleeving was slipped over the core and pulled down tightly to conform to the chair's contour. This made for a very strong, stiff, and durable structure.

Carbon fibre reinforced plastics, being a much more recent development, are much less widely used at present. A use which takes advantage of the negligible thermal expansion of this material is a radar reflector dish used as part of an antenna. This is a sandwich structure, with an aluminium honeycomb core. The thermal stability of the carbon-polymer ensures that the antenna remains accurately tuned over a wide range of outdoor temperatures.



Fig. 12.23 Chair stiffened and strengthened using braided sleeving followed by resin impregnation. (Courtesy of A & P Technology.)

Another use of carbon fibres that takes advantage of its unique properties, this time light weight, is for moving parts in textile machinery. New machine designs using carbon pultruded bars (which can be made with greater precision than metal constructions) have increased weaving speeds by a factor of ten to twenty compared with conventional machines. The machines also contain injection moulded carbon fibre reinforced nylon. These mouldings can be made very accurately, allowing very precise alignments of the parts during machine operation. In another textile processing machine an injection moulded nylon traverse guide is used. It is shown in Fig. 12.24. The speed of operation of this machine is limited by friction and wear of this part, and the good friction and wear characteristics of the carbon-nylon are a great advantage. In addition, the carbon conducts the frictional heat away from the sliding face more efficiently than the unreinforced polyamide used previously. These advantages are also exploited in carbon-polytetrafluoroethylene (PTFE) bearings used in other machines.

Carbon-epoxy has also proven to be superior to stainless steel in industrial drive shafting due to good corrosion resistance and higher in E/ρ . They, together with glass reinforced epoxies are now widely used in marine propulsion, paper mill drives, large fans and pumps.

As mentioned earlier, aircraft brakes pads are made from carbon-carbon. This material can operate well when red hot, and is, therefore, very effective at dissipating the heat generated by the large amount of kinetic energy absorbed. Although the material can oxidize above 400°C , the time at high temperature is usually short. These brake pads are also used in racing cars.

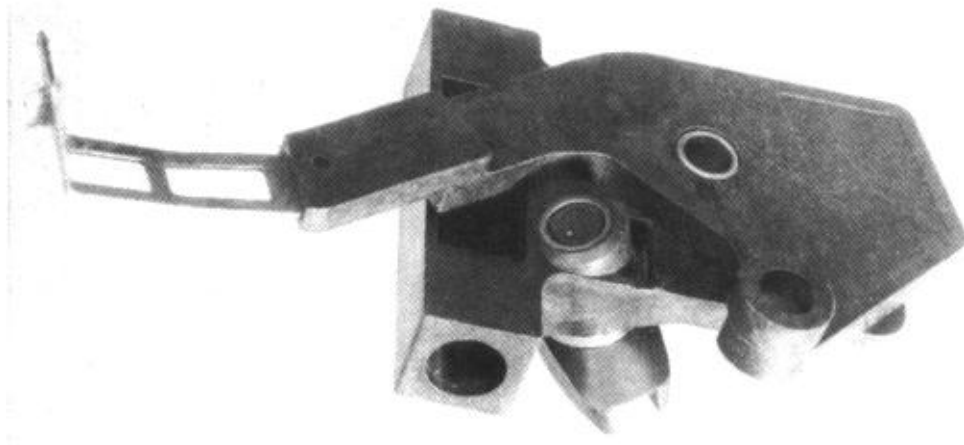


Fig. 12.24 Carbon-nylon traverse guide for textile processing. (Trewin, E.M., 1978, Proc. ICCM2, 1474 -92. (Courtesy of the Metallurgical Soc. AIME.)

Fibreglass is still used for radomes and some of these are very large nowadays: the frontispiece shows the CN Tower in Toronto, which was built primarily as a communications tower and is the first free-standing tower to exceed 550 m in height. It houses antennae for numerous microwave links, five television channels at > 1 Mw and five FM channels at 40 kw each.

The radio and TV antennae are housed inside fibreglass tubes up to 7.5 m in diameter with 4 cm wall thickness and 105 m high, shown in Fig. 12.25. Apart from its good microwave propagation properties, the material affords excellent protection from the weather at this height. This can sometimes be very severe. It is built to withstand winds of 400 km/hr^{-1} and was undamaged by 190 km/hr^{-1} winds in February 1978 which did a great deal of damage to buildings in Toronto. Another very important property is that ice and snow do not stick to this material. There is thus no danger of it icing up and the built-up ice blocks subsequently falling more than 300 m to earth, and endangering passers-by.

Although the future for reinforced polymers is assured, reinforced metals and ceramics have not yet matured. This is almost certainly only a matter of time. Technical problems, unlike human ones, always seem to be solvable.



Fig. 12.25 Glass-polyester radome atop Toronto's 550 m Communication Tower. (Courtesy CN Tower Ltd, Canada.)

Further Reading

Hazen, J. (Ed), *High Performance Composites*, published every two months. (Ray Publishing, Wheat Ridge, CO.)

Hazen, J. (Ed), *Composites Technology*, published every two months. (Ray Publishing, Wheat Ridge, CO.)

Chapter 12: Problems

- 12.1 A business man flies regularly on a 250 km non-stop journey at a height of 900 m over the sea. The plane consumes energy at a rate of $95 \text{ Js}^{-1} \text{ kg}^{-1}$ to keep it aloft and moving at its cruising speed of 210 kmh^{-1} . By calculating the fuel consumption determine which material would be better for the wings and fuselage if the choice is aluminium or fibreglass. Fibreglass has a density of 2.05 Mgm^{-3} , but more of it is needed to preserve the flexural rigidity of the structure, since its Young's modulus is only 45 GPa. When made of aluminium the volume of material needed is 0.051 m^3 . The other parts weigh 230 kg, and the business man weighs 67 kg. The heat of combustion of the kerosene fuel is 52.8 GJm^{-3} ; its weight may be neglected; the engine is 27% efficient. Calculate the amount of fuel used in each case.
- 12.2 Develop a criterion for a material to be used for floors in passenger carrying jet aircraft. The aircraft can make journeys totalling 10 million km before the floor needs replacing. The floor needs flexural rigidity, and any weight saved can be used to carry extra passengers giving an increase in income of \$0.05 per passenger km. The average weight of a passenger plus baggage and seat is 90 kg. Compare an aluminium alloy costing $\$2 \text{ kg}^{-1}$ with graphite-epoxy costing $\$50 \text{ kg}^{-1}$, and having $V_f = 0.75$. The density of the epoxy is 1.23 Mgm^{-3} .
- 12.3 Show that the elastic energy stored in a bar in tension is $1/2$ stress x strain x volume. Hence, determine whether a better material than rubber can be used to drive model aircraft. For simplicity, compare each in tension, and neglect the weight of the system needed to convert linear movement to rotation. Consider silica-, boron-, and carbon-epoxy instead of natural rubber with a density of 1.13 Mgm^{-3} ; V_f cannot exceed 0.75 without loss of properties.
- 12.4 Compressed gas is being considered as an energy store. Show that the energy stored is PdV for pressure P and change in volume dV , and hence that, with a perfect gas (for which PV is constant) the energy stored in compressing it from pressure, P_1 to P_2 is $P_2 V_2 \ln (P_2 / P_1)$ where V_2 is the volume of the container. Suppose that a gas turbine can be designed to work at 90% efficiency over a pressure range from full pressure P_2 to $P_2 / 2$. (At lower pressures its efficiency becomes negligible.) It will work at a remote site, so the gas storage vessel must be as light as possible. The vessel will be a long buried tube, so that the stress in the tube wall is $P_2 D / 2t$, and uniaxial, where D = tube diameter and t = wall thickness. Derive a figure of merit for the material, and compare the performance of the composites considered in the previous question with the aluminium alloy in Table 1.1.
- 12.5 A rotating long thin tube is under stress due to centrifugal forces. For a peripheral rotation velocity of v , and a mass M per unit tube external surface area, the forces

exert an equivalent pressure equal to $2Mv^2/D$ where D is the tube diameter. Calculate the stress in the tube, and show that the kinetic energy stored in the tube (half the tube mass, multiplied by the square of its velocity) cannot exceed the product of its ultimate tensile strength and the volume of the material in the tube. Now flywheels have been considered for energy storage in moving vehicles. Here the volume of the ring material has to be kept to a minimum. Compare the materials in the two previous questions on the basis of maximum energy stored per unit volume of material.

- 12.6 Compare the efficiency of the various forms of energy storage in questions 12.3, 12.4 and 12.5 with that of kerosene, on a volume basis. (This is important for road transport.) In your answer list the various methods in descending order of effectiveness, giving the energy stored in Jm^{-3} for the most effective in each category.
- 12.7 A cylindrical pressure vessel with hemispherical ends, unlike a long pipe, has to withstand axial stresses as well as circumferential (hoop) stresses. Show, by suitably dividing such a vessel into two halves, in two different ways, that the hoop stress is exactly twice the axial stress. Hence, making the resolved stresses along the fibres due to the axial stress equal to that due to the hoop stress, calculate the fibre winding angle, $\pm \phi$, needed for efficiently winding the cylindrical part of the vessel. Express your answer as the angle between the fibres and the hoop stress.
- 12.8 The Ford Motor Company was making a car with a carbon-polymer body, in order to reduce petrol consumption. The carbon-polymer has a density of 1.65 Mgm^{-3} . The body uses 0.035 m^3 of material. The other parts of the car weighed 420 kg. How much petrol would be used and what percentage saving could be made, compared with a steel body, using the same volume of material, in an average daily journey to work. In this average journey there is a driver weighing 72 kg, no luggage, and no passengers. The distance travelled is 10 km, and the journey takes 25 minutes, of which 30% is spent accelerating, 30% decelerating, 20% waiting at traffic lights, and 20% travelling at constant speed. Assume that the acceleration is always at a rate of 1.6 ms^{-2} up to a speed of 50 kmh^{-1} . The engine is 20% efficient when accelerating, but requires an energy input of 20 kJs^{-1} to keep it turning over when idling and 95 kJs^{-1} for travelling at 50 kmh^{-1} . The heat of combustion of petrol is 48.5 GJm^{-3} .
- 12.9 A reasonably good cross country skier can work at a rate of 230 watts for long periods. On the level he travels 3.1 m with each leg movement. If we assume that all the work goes into accelerating the ski and the leg below the knee from rest to twice and skiers average velocity, calculate and skiers speed on the level with skis made (a) from wood with $\sigma_{tu} = 34 \text{ MPa}$ and $\rho = 0.86$ and (b) strong graphite-epoxy with $V_f = 0.75$. The skier weighs 70 kg, and each foot and leg below the knee weighs 2.7 kg. The ski is 2.30 m long, and for simplicity we will assume

constant, oblong section, with a width (b) of 5.4 cm and a thickness determined by the material strength. Thus it should just support the skier when only the two ends are in contact with the ground.

- 12.10 A support for use of X-ray therapy is fixed at one end and must deflect as little as possible when a patient is on it. It must also absorb X-rays as little as possible. The bed is made as a sandwich, which can be as thick as needed to keep flexure to a minimum. The filling resists shear but does not contribute to the bending moment. Its X-ray absorption can be neglected. The surface skins take all the tensile and compressive stresses. (Consequently the stresses in them can be calculated by equating the external moments with the internal moment coming entirely from the skins). Use a Rule of Mixtures expression for the calculation of X-ray absorption, using the atomic numbers as a measure of the absorption per unit thickness. The stresses in the skins cannot exceed half the ultimate tensile strength. Derive a criterion of excellence, and determine the relative positions of silica-, boron-, and carbon-epoxy with $V_f = 0.75$, and aluminium. The atomic numbers are: boron 5, carbon 6, aluminium 13. For silica use 10 (the average for Si and two O's) and for epoxy use 3.5 (an average for hydrogen, oxygen and carbon).

Chapter 12: Selected Answers

- 12.1 Fibreglass better; 3.23; aluminium; 3.35
- 12.3 In order of excellence: silica-epoxy, 33; rubber, 25; carbon-epoxy, 24; and boron-epoxy 5, $\text{Pa m}^3\text{kg}^{-1}$.
- 12.5 In order of excellence: carbon-epoxy 4.2, boron-epoxy, 1.32; silica-epoxy, 1.30; aluminium alloy, 0.33; rubber, 0.016.
- 12.9 Wood 3.5 and carbon-epoxy 4.6 ms^{-1} .

APPENDIX A

Symbols used in text

Where possible, standard nomenclature has been used. Duplication could not be avoided entirely, but each symbol is described fully in the appropriate part of the text.

<i>A</i>	cross-sectional area: constant: with numerical subscripts, laminate extensional stiffnesses
<i>B</i>	constant
<i>C</i>	stiffness; always has subscripts indicating directions e.g. C_{16} , C_{ij}
<i>D</i>	constant: derivatives (differentials); diffusion constant; special function (Fig. 8.20): with numerical subscripts, relates moments to curvatures
<i>E</i>	Young's modulus; usually has subscripts indicating directions or materials, e.g. E_x, E_z , E_f , E_m , or shorthand for expressions, eg. E_l , (usually Rule of Mixtures modulus), E_λ , E_ν , E_R , E_r
<i>F</i>	force
<i>G</i>	shear modulus; usually has subscripts indicating directions or materials e.g. G_{xy} , G_{22} , G_f , G_m
<i>G</i>	work of fracture; usually has subscripts indicating mechanisms and directions
<i>I</i>	moment of area
<i>ID</i>	diffusion integral
<i>IR</i>	resistance integral
<i>K</i>	bulk modulus
K	fracture toughness; usually has subscripts indicating mechanisms and directions
<i>L</i>	length; fibre embedded length; fibre length is $2L$
L_m	half the mean fibre fragment length (Chapter 8)
<i>M</i>	moment of forces; has subscripts when used for laminates; proportion of water absorbed
<i>N</i>	number of fibres crossing unit area of crack face; with subscripts, forces per unit length
<i>P</i>	pressure; P_o is cure shrinkage pressure
P_f	packing factor
P_{sk}	fraction of fibres with given aspect ratio

Q	reduced stiffness; subscripts indicate directions
\bar{Q}	transformed reduced stiffness; subscripts indicate directions
\hat{Q}	$= A_{ij}/nt$: suggested for laminate stiffness (question 4.16)
R	radius; radius of curvature; distance from centre; electrical and thermal resistance of polymer
S	compliance; subscripts indicate directions
\bar{S}	lamina transformed compliance; subscripts indicate directions
\hat{S}	laminate transformed compliance; subscripts indicate directions
T	temperature
$[T]$	transformation matrix for rotation of axes
U	energy or work
V	volume fraction; subscript indicates material or form
W	dislocation width
a	amplitude, Chapter 6; constant, Chapter 8; length Fig. 10.33
a	with numerical subscripts; interatomic distances
a_c	crack length
a_o	length of unit cell side
b	Burgers vector
c	constant $(r+t)(D_i - D_p)/aD_p$
d	fibre diameter or thickness; can have numerical subscripts for distances
e	volume expansion
h	length, height, or interplanar distance
k	constant (has numerical subscripts)
l	length
l_c	critical half fibre length
m	Gruneisen constant (Chapter 2 only); fraction of fibre subject to slip
n	number of layers: Gruneisen constant (Chapter 2 only): $\{E_m/E_f(1+\nu_m)\ln(R/r)\}^{1/2}$
n_{exp}	experimentally evaluated n
q	exponent in fibre strength variation with length
r	half the fibre diameter

r_c	crack tip radius; notch radius
s	fibre aspect ratio = $2L/d = L/r$
s_c	critical fibre aspect ratio
\bar{s}	$s(1-m)$
t	specimen thickness; interphase thickness
u	displacement; subscript indicates direction or material
u_R	displacement at radial distance R from fibre axis
v	displacement in the y direction
w	displacement in the z direction; also specimen width; region widths, Fig. 10.33.
w	with subscripts; weight
x	direction
y	direction
z	direction
Δ	large change; eg. $\Delta\varepsilon$, $\Delta\alpha$, ΔT , ΔR
α	thermal expansion coefficient; subscripts indicate material
β	angle; slope of water absorption plot vs $\sqrt{\text{time}}$
γ	shear strain; subscripts indicate shear plane or material
δ	small change in a variable, e.g. σ
ε	strain; subscripts indicate directions or material, or limit
η	mutual influence coefficients; $\eta_{xyx} = \bar{S}_{16} E_x$, $\eta_{yy} = \bar{S}_{26} E_y$
θ	angle
κ	curvature; usually subscripted
λ	wavelength
μ	friction coefficient
ν	Poisson's ratio; subscripts indicate directions or material
ν_s	$\nu_f E_m / (1 + \nu_m) E_f$
ρ	density
σ	tensile stress (compressive stress is $-\sigma$); subscripts indicate direction, material, or limit
τ	shear stress; subscripts indicate directions material, or limit
ϕ	angle of axis rotation

χ_1	modulus factor for fibre misorientation
χ_2	modulus factor for fibre length
χ_3	strength factor for fibre misorientation
χ_4	strength factor for fibre length
ψ	surface energy

Subscripts

0	number, usually indicating an equilibrium or initial value
1, 2, 3, 4, 5, 6	direction or number
<i>a</i>	adhesive; also distinguishes fibre type in a hybrid composite
<i>b</i>	distinguishes fibre type in a hybrid composite
<i>c</i>	centre (σ_{fc}) or with <i>u</i> (e.g. σ_{Icu}) used for compression; also refers to cracks (a_c , b_c , r_c), and critical values (s_c)
<i>e</i>	stress near end (σ_{fe}), or elastic tensile (σ_e) or shear (τ_e)
<i>f</i>	fibre
<i>i</i>	interfacial stress (τ_i , σ_i) or work of fracture (G_i); also index
<i>ii</i>	interface interaction
<i>im</i>	mean at interface (τ_{im})
<i>j</i>	joint; also index
<i>LOM</i>	law of mixtures
<i>m</i>	matrix; also mean
<i>max</i>	maximum
<i>min</i>	minimum
<i>p</i>	gross slip (ε_{Ip} , σ_{Ip}) or pull-out (I_p)
<i>R</i>	property at radial distance <i>R</i> from fibre centre
<i>r</i>	radial
<i>s</i>	surface (τ_s , G_s) onset of slip or separation (ε_{Is} , σ_{Is}); stress in slipped region (σ_{fs}); saturated value
<i>t</i>	total
<i>th</i>	theoretical
<i>tip</i>	tip (crack tip stress)

u	ultimate (stress)
x	direction
y	direction (single subscript) yield value (second subscript)
z	direction
θ	direction
λ	for thermal shrinkage stiffness constant
ν	for thermal shrinkage stiffness constant and Van der Waals induced stress

APPENDIX B**Acronyms and Abbreviations**

ASTM	American Society for Testing and Materials
BMC	bulk moulding compound
BMI	polyimide (bismaleimide)
CBS	curved beam strength
CFRP	carbon fibre reinforced plastics
CLC	combined loading compression
CTE	coefficient of thermal expansion
CV	coefficient of variation
CVD	chemical vapour deposition
DENOM	denominator in thermal stress equations
DER	refers to a Dow Chemical epoxy resin
DGEBA	diglycidal ether of bis phenol A (an epoxy) diglycidal
DNSOC	dinorbonene spiro ortho carbonate
EPON	refers to a Shell epoxy resin
FEA	finite element analysis
GRP	glass (fibre) reinforced plastics
HDPE	high density polyethylene
ICI	Imperial Chemical Industries
IROM	inverse Rule of Mixtures
IITRI	Illinois Institute of Technology Research Institute
KFRP	Kevlar fibre reinforced plastics
LAS	Lithium alumino silicate
LDPE	Low density polyethylene
MMC	regrettably used for metal matrix composites, including particulate filled
MPS	γ -methacryloxypropyltrimethyl silane
MW	molecular weight
PA	polyamides (nylons) (III)
PAN	polyacrylonitrile
PBO	polyphenylene benzobisoxazole

PBT	polybutylene terephthalate
PBZT	poly (paraphenylene benzobisthiazole)
PC	polycarbonate (V)
PE	polyethylene (I)
PEEK	polyetherether ketone (VII)
PEI	polyether imide (X)
PES	polyether sulphone (VII)
PMC	polymer matrix composites (does not include "filled polymers")
PMMA	polymethyl methacrylate
PPO	polyphenylene oxide
PS	polystyrene
PTFE	polytetrafluoroethylene
PVC	polyvinyl chloride
PVDC	polyvinylidene chloride
PU	polyurethane (IV)
RIM	reaction injection moulding
RRIM	reinforced reaction injection moulding
RTM	resin transfer moulding
SAN	styrene acrylonitrile
SMC	sheet moulding compound
S-N curves	stress amplitude vs log (number of cycles to failure)
SRMM	structural RRIM
TETA	triethylene tetramine (XX)
TIROM	Inverse rule of mixtures with transverse fibre modulus
TMC	thick moulding compound
UHMWPE	ultra high molecular weight polyethylene
WPE	weight for epoxide

(Note: Some of these abbreviations are used in this book when otherwise there would be needless repetition of cumbersome expressions such as coefficient of thermal expansion, polyetherether ketone, etc.)

APPENDIX C***SI Units***

SI means Systeme Internationale d'Unites, and is an internationally agreed set of units. It is rapidly gaining world-wide acceptance, is replacing local systems such as the British Imperial one, and its North American cousin, and is usually called the metric system.

It is a modified form of the MKS system (Metre-Kilogram-Second) which was introduced in the late 1940's as an alternative to the cgs system (centimetre-gram-second) which had the disadvantage that electromagnetic and electrostatic secondary units (for example for potential difference and current) were many orders of magnitude different, and were inconsistent with the practical volts and amperes used everyday. (The MKS system did not have that disadvantage, nor does SI). It is fully described in ISO 1000.

In SI the basic units include metre (m), kilogram (kg), second (s), and temperature in Kelvins (K). Temperature can also be expressed in Celsius ($^{\circ}\text{C}$) To convert K to $^{\circ}\text{C}$ subtract 273.2.

Table C1. How Orders of Magnitude are Expressed in SI

Power of ten	Name	Symbol
-18	atto	a
-15	femto	f
-12	pico	p
-9	nano	n
-6	micro	μ
-3	milli	m
3	kilo	k
6	mega	M
9	giga	G
12	tera	T

SI makes a clear distinction between mass and force. For force there is a secondary unit (i.e. one that can be expressed in terms of the primary units). It is called

the Newton (N) and is the force required to accelerate 1 kg at rate of 1 ms^{-2} . Its units are therefore kgms^{-2} . The earth's gravitational field exerts a force of 9.81 N on a mass of 1 kg at the earth's surface. (The force on the kilogram at the surface of the moon is about 2 N).

When writing the units, slashes are not used for inverse units. Instead a negative power is used, e.g. ms^{-1} is used for speed, rather than m/s.

Powers of ten should not be expressed explicitly. Instead a symbol is used. These are listed in Table C1. Sometimes c is used for 10^{-2} , as in cm, but this should be avoided wherever possible. Low speeds, for example, are given in mms^{-1} (millimetres per second), higher speeds as ms^{-1} (metres per second) and very high speeds as kms^{-1} or Mms^{-1} (kilometres per second or megametres per second).

The axes of graphs should never have statements like: speed; $\text{ms}^{-1} \times 10^5$. This is confusing. Use either kms^{-1} or Mms^{-1} , whichever gives the fewer zeros.

In this text stresses and pressures are always given in Pascals (Pa). This is another secondary unit; $1 \text{ Pa} = 1 \text{ Nm}^{-2}$. It is a very small unit indeed; atmospheric pressure is about 0.1 MPa. Thus, we have normally to use MPa or GPa.

Expansion coefficients are given in MK^{-1} (i.e. micro metres of expansion, per metre original length, per degree Kelvin). Densities are given in the unfamiliar units of Mgm^{-3} , but since $1 \text{ Mgm}^{-3} = 1 \text{ gcm}^{-3}$ this should present few problems.

Table C2 lists some useful conversion factors. To make the meaning of the conversions clear, slashes separate the Imperial and SI units, and orders of magnitude are expressed as powers of 10.

Table C2. Conversion Factors Between SI and Imperial Units. To Make the Conversion Multiply by the Appropriate Factor. The Factors are Accurate to at Least One Part in 1000

Quantity	Multiplication Factor			
	SI to Imperial		Imperial to SI	
Length	3.281	ft/m	0.3048	m/ft
	39.37	in/m	0.02540	m/in
Area	10.76	ft ² /m ²	0.09290	m ² /ft ²
	1550	in ² /m ²	0.6452 x 10 ⁻³	m ² /in ²
Volume	35.31	ft ³ /m ³	0.02832	m ³ /ft ³
	61.02 x 10 ³	in ³ /m ³	16.39 x 10 ⁶	m ³ /in ³
Mass	0.9842	ton/tonne	1.016	tonne/ton
	2.205	lb/kg	0.4536	kg/lb
	35.27	oz/kg	0.2835	kg/oz
Density	62.42	lb/ft ⁻³ /Mgm ⁻³	0.01602	Mgm ⁻³ /lb/ft ⁻³
Force	0.2248	lbf/N	4.448	N/lbf
Stress and Pressure	0.1450	kpsi/MPa	6.895	MPa/kpsi
	0.06473	tons si/MPa	15.45	MPa/tons si
Fracture toughness	0.910	kpsi√in/MPa√m	1.099	MPa√m/kpsi√in
Thermal expansion	0.5556	°F ⁻¹ /K ⁻¹	1.800	K ⁻¹ /°F ⁻¹